ANL/ES-11

ANL/ES-11

PLEASE RETURN TO
MFC BRANCH LIBRARY

INL Technical Library
320903

HEATED-EFFLUENT DISPERSION IN LARGE LAKES: STATE-OF-THE-ART OF ANALYTICAL MODELING.

Part 1. Critique of Model Formulations

by

A. J. Policastro and J. V. Tokar

ARGONNE NATIONAL LABORATORY

ANL CES

CENTER FOR ENVIRONMENTAL STUDIES

RETURN TO REFERENCE FILE
TECHNICAL PUBLICATIONS
DEPARTMENT

The facilities of Argonne National Laboratory are owned by the United States Government. Under the terms of a contract (W-31-109-Eng-38) between the U. S. Atomic Energy Commission, Argonne Universities Association and The University of Chicago, the University employs the staff and operates the Laboratory in accordance with policies and programs formulated, approved and reviewed by the Association.

MEMBERS OF ARGONNE UNIVERSITIES ASSOCIATION

The University of Arizona
Carnegie-Mellon University
Case Western Reserve University
The University of Chicago
University of Cincinnati
Illinois Institute of Technology
University of Illinois
Indiana University
Iowa State University
The University of Iowa
Kansas State University
The University of Kansas
Loyola University
Marquette University
Michigan State University
The University of Michigan
University of Minnesota
University of Missouri
Northwestern University
University of Notre Dame
The Ohio State University
Ohio University
The Pennsylvania State University
Purdue University
Saint Louis University
Southern Illinois University
The University of Texas at Austin
Washington University
Wayne State University
The University of Wisconsin

NOTICE

This report was prepared as an account of work sponsored by the United States Government. Neither the United States nor the United States Atomic Energy Commission, nor any of their employees, nor any of their contractors, subcontractors, or their employees, makes any warranty, express or implied, or assumes any legal liability or responsibility for the accuracy, completeness or usefulness of any information, apparatus, product or process disclosed, or represents that its use would not infringe privately-owned rights.

Printed in the United States of America
Available from
National Technical Information Service
U.S. Department of Commerce
5285 Port Royal Road
Springfield, Virginia 22151
Price: Printed Copy $6.00; Microfiche $0.95

ANL/ES-11
Waste Heat Disposal

ARGONNE NATIONAL LABORATORY
9700 South Cass Avenue
Argonne, Illinois 60439

HEATED-EFFLUENT DISPERSION IN LARGE LAKES: STATE-OF-THE-ART OF ANALYTICAL MODELING.

Part 1. Critique of Model Formulations

by

A. J. Policastro and J. V. Tokar

Center for Environmental Studies

January 1972

TABLE OF CONTENTS

	Page
ABSTRACT	1
I. INTRODUCTION	1
A. General Discussion	1
B. The Near Field	3
C. The Far Field	5
D. Model Reviews of Recent Acquisitions	7
References	7
II. OBSERVATIONS AND RECOMMENDATIONS	8
A. Near-field Issues	8
B. Far-field Issues	10
III. MODEL SYNOPSES AND CRITICAL EVALUATIONS	14
A. Models for the Jet Regime	14
1. Heated Surface Jets in a Steady Crosscurrent, J. A. Hoopes, R. W. Zeller, and G. A. Rohlich (June 1967)	14
a. List of Symbols	14
b. Introduction	16
c. Derivation of the Mathematical Model	16
d. Application to Lake Monona and Discussion	27
e. Remarks on Major Model Assumptions	34
f. Application of Model to General Outfall Situations	36
g. Two Final Comments	38
References	39
2. A Preliminary Report on the Characteristics of a Heated Jet Discharged Horizontally into a Transverse Current: Part I. Constant Depth, H. H. Carter (November 1969)	40
a. List of Symbols	40
b. Introduction	41
c. Model Description	44
d. Determination of α_0	50
e. Determination of C_d	51

TABLE OF CONTENTS

Page

f. Centerline Trajectory 52
g. Discussion of Model Suitability 59
h. Pritchard's Application of Carter's Model 64
References 66

3. Heated Surface Jet Discharged into a Flowing Ambient Stream, Louis H. Motz and Barry A. Benedict (August 1970) 68

a. List of Symbols 68
b. Introduction. 70
c. Model Development. 70
d. Solution to Model Equation Using Similarity Assumptions on Velocity and Temperature 75
e. Flow-establishment Considerations 78
f. Evaluation of Entrainment and Drag Coefficients . . . 81
g. Model Verifications 83
h. Discussion of Model Development 86
References 89

4. An Analytical and Experimental Investigation of Surface Discharges of Heated Water, K. Stolzenbach and D. R. F. Harleman (February 1971) 90

a. List of Symbols 90
b. Introduction. 93
c. Model 1: Buoyant Jet 96
d. Model 2: Buoyant Jet in a Crossflow 117
e. Model 3: Buoyant Jet Including Bottom Slope 125
f. Application of the Theory to General Outfall Situations 126
g. Model Verifications 129
h. Final Comments. 139
References 139

B. Models for the Far Field 140

5. The Work of Akira Wada (1965-1968) 140

a. List of Symbols 140
b. Introduction. 142
c. Model 1: Thermal Diffusion of Cooling Water in Three Dimensions (1965) 145
d. Model 2: Thermal Diffusion in Two Dimensions with Variation in Flow Field Included (September 1966) . . 155

TABLE OF CONTENTS

Page

e. Model 3: Thermal Diffusion with Interaction between Flow and Heat Transfer (1968) 162
f. General Remarks Concerning Wada's Models 169
References 171

6. Initial Mixing of Thermal Discharges into a Uniform Current, J. E. Edinger and E. M. Polk, Jr. (October 1969) 173

a. List of Symbols 173
b. Introduction. 174
c. Two-dimensional Model. 175
d. Three-dimensional Model 182
e. General Comments about the Edinger-Polk Models. . 184
f. Field Verification of Models, and Discussion of Verification. 185
References 188

7. Offshore Outfall and Shoreline Surface Discharge Models for the Prediction of Thermal-plume Dispersion in the Great Lakes, G. T. Csanady (January 1970). 189

a. List of Symbols 189
b. Introduction. 190
c. Offshore Outfall Model 191
d. Shoreline Surface-discharge Model 198
References 206

8. TOPLYR-II, A Two-dimensional Thermal-energy Transport Code, D. C. Kolesar and J. C. Sonnichsen, Jr. (October 1971) 207

a. List of Symbols 207
b. Introduction. 208
c. Model Description 210
d. Model Verification 226
e. Final Comments. 229
References 231
f. Addendum 232
Addendum References 237

9. Mathematical Model for Dispersion of Heat into a Lake, Walter Wnek (to be published) 238

a. List of Symbols 238
b. The Physical Situation and Its Mathematical Simulation. 239

TABLE OF CONTENTS

Page

c. Development of the Analytical Solution 243
d. General Comments about the Model 250
References. 251

C. Complete Models. 252

10. The Work of Donald W. Pritchard (August 1969) 252

a. List of Symbols 252
b. Introduction. 254
c. Model Derivation and Discussion. 256
d. Model Predictions and Verifications. 270
e. General Discussion of the Model 272
f. Final Remarks 275
Pritchard's Papers of Interest. 276
References. 277

11. An Investigation of the Physical Effects of Thermal Discharges into Cayuga Lake--Thermal-plume Model, T. R. Sundaram, C. C. Easterbrook, K. R. Piech, and G. Rudinger (November 1969) 279

a. List of Symbols 279
b. Introduction. 281
c. The Model Derivation 284
d. Technique of Model Application. 297
e. General Discussion of the Model 298
f. Calculation of Heat Lost to the Lake beyond x_2. . . . 300
References. 302

12. Far-field Effects due to a Multiple-jet Diffuser, Y. J. Tsai (January 1970) 303

a. List of Symbols 303
b. Introduction. 304
c. Model Derivation for the Case of Zero Lake Currents 307
d. Model Derivation for the Case of Lake Currents. . . 311
e. Calculation of Surface Heat Losses to the Atmosphere for the Models in Secs. c and d Above 324
f. Some Comments about the Models 324
References. 328

TABLE OF CONTENTS

Page

IV. MODEL SUMMARIES 329

A. Near-field Regime. 329

1. Method of Approach 329

2. Dimensionality and Buoyancy Considerations 332

3. Crosscurrent and Entrainment Effects 335

4. Discharge Configuration and Discharge Angle. 339

5. Bottom Effects 339

6. Shoreline Considerations 341

7. Pressure Drag 341

8. Wind Stress 344

9. Zone of Flow Establishment 345

10. Surface Heat Transfer 347

11. Ambient Stratification 347

12. Recirculation 348

13. Field and Hydraulic Comparisons. 349

14. Computer Programs 350

15. Input Parameters for Jet Models 350

a. Hoopes, Zeller, and Rohlich 350
b. Carter 350
c. Motz and Benedict. 351
d. Stolzenbach and Harleman 351

B. Far-field Regime 351

1. Method of Approach 351

2. Dimensionality 352

3. Diffusivities and Buoyancy 353

a. Wada's Model No. 1. 354
b. Wada's Model No. 2. 354
c. Wada's Model No. 3. 354
d. Edinger and Polk Two-dimensional Model 355
e. Edinger and Polk Three-dimensional Model. 355
f. Csanady Offshore Outfall Model. 355

TABLE OF CONTENTS

Page

g. Csanady Shoreline Surface-discharge Model 355
h. Kolesar and Sonnichsen 356
i. Wnek 356
j. Pritchard 356
k. Sundaram et al. 356
l. Tsai 356

4. Surface Heat Loss 356

5. Presence of Ambient Currents. 357

6. Bottom Effects 358

7. Discharge Configuration and Angle of Discharge 358

8. Shoreline Considerations 359

9. Wind Stress 360

10. Ambient Lake Stratification. 360

11. Recirculation 360

12. Previous Comparisons with Field and Hydraulic Data . 360

13. Computer Programs 361

14. Input Parameters for Far-field Models 361

a. Wada 361
b. Edinger and Polk 363
c. Csanady 364
d. Kolesar and Sonnichsen 364
e. Wnek 365

C. Complete Models. 365

1. Discussion. 365

2. Input Parameters for Complete Models 366

a. Pritchard 366
b. Sundaram et al. 366
c. Tsai. 367

APPENDIXES

A. Typical Isotherm Sketches as Predicted by Models Reviewed 369

B. Summary of Model Characteristics. 373

ACKNOWLEDGMENTS 374

LIST OF FIGURES

No.	Title	Page
1.1.	Surface Jet Subject to a Steady Crosscurrent	16
1.2.	Prototype Situation for Two Outfalls on Lake Monona	28
1.3.	Jet Characteristics for Livingston Street Outfall; August 10, 1966	31
1.4.	Wind Stress, τ_w, vs Wind Speed	31
1.5.	Comparison of Jet Characteristics for Mathematical Models with and without Direct Wind Stress; July 17, 1966; Livingston Street	32
1.6.	Comparison of Jet Characteristics v_{sm} and T_c for Constant and Variable Entrainment Coefficients for Livingston Street Survey; July 27, 1966	33
1.7.	Comparison of Jet Characteristics b and β for Constant and Variable Entrainment Coefficients for Livingston Street Survey; July 27, 1966	34
2.1.	Schematic Drawing of a Horizontal, Two-dimensional, Bent-over Jet	42
2.2.	Definition Sketches of the Horizontal, Two-dimensional, Bent-over Jet	45
2.3.	Dilution, θ/θ_0, along the Centerline Trajectory as a Function of Downstream Distance, ξ/b_0	48
2.4.	Profiles of Eddies behind Wall and Jet	49
2.5.	Distribution of Pressure and Shear	49
2.6.	Streamline Configuration in the Slot Vicinity	49
2.7.	Plots of Eddy Profiles and Boundary Pressures	49
2.8.	Patterns of Mean Flow for $L/b_0 = 100$	49
2.9.	The Coefficient of Drag, C_d, as a Function of R	51
2.10.	Position of Orifice and Flow-establishment Region	54
2.11.	Graphical Integration of Eq. 2.11	54
2.12.	Coordinates of Point of Maximum Penetration	55
2.13.	Comparison of Theory for R = 2 and Tests 9 and 12 for the Centerline Trajectory	55
2.14.	Comparison of Theory for R = 5 and Tests 8 and 11 for the Centerline Trajectory	56

LIST OF FIGURES

No.	Title	Page
2.15.	Comparison of Theory for R = 10 and Tests 10 and 13 for the Centerline Trajectory	56
2.16.	Coordinates of the Point of Maximum Penetration	57
2.17.	Dilution, θ/θ_0, along the Centerline Trajectory Parameterized with Respect to R	57
2.18.	Horizontal Distribution of Excess Heat, θ, for $R \equiv q_0/u_a = 2.01$	58
2.19.	Horizontal Distribution of Excess Heat, θ, for $R \equiv q_0/u_a = 4.93$	58
2.20.	Horizontal Distribution of Excess Heat, θ, for $R \equiv q_0/u_a = 9.80$	58
3.1.	Definition Sketch	71
3.2.	Profiles of Eddies behind Wall and Jet	73
3.3.	Patterns of Mean Flow for $L/b_0' = 100$	74
3.4.	Volume Flux, V, and Momentum Flux, M, vs Nondimensional Jet-axis Distance, S	78
3.5.	Temperature, Velocity, and Width Ratios vs Nondimensional Jet-axis Distance, S	78
3.6.	Effect of Reduced Drag Coefficient on Location of Jet Trajectory	78
3.7.	Zone of Flow Establishment	79
3.8.	Observed Values and Fitted Curve for Length of Establishment Zone vs Velocity Ratio	80
3.9.	Observed Values and Fitted Curve for Initial Angle vs Velocity Ratio	81
3.10.	Observed Values of Reduced Drag Coefficient vs Velocity Ratio	82
3.11.	Observed Values and Fitted Curve for Drag Coefficient vs Velocity Ratio	82
3.12.	Entrainment Coefficient as a Function of Velocity Ratio	85
3.13.	Observed Field Values of Drag Coefficient vs Velocity Ratio Plotted on Laboratory Curve	85
3.14.	Observed Values of Drag Coefficient vs Reynolds Number	85

LIST OF FIGURES

No.	Title	Page
4.1.	Schematic Diagram of Heated Discharge	93
4.2.	Characteristics of Discharge Channel	97
4.3.	Geometrical Characteristics of the Jet	102
4.4.	Velocity and Temperature Characteristics of the Jet	103
4.5.	Characteristics of a Deflected Jet	118
4.6.	Crossflow Velocity in Experimental Basin	123
4.7.	Two-layer Flow in Discharge Channel	128
4.8.	Discharge-channel Schematization	129
4.9.	Theoretical Calculation of Jet Structure for Run 6	131
4.10.	Calculated Isotherms of $\Delta T_c/\Delta T_0$ for Run 6	132
4.11.	Theoretical Calculations and Experimental Data for Run 6	133
4.12.	Theoretical Calculations and Experimental Data for Run 23	134
4.13.	Theoretical Calculations and Experimental Data for Runs 17-19	135
4.14.	Dilution in the Stable Region of Buoyant Discharges	137
4.15.	Maximum Jet Depth vs $\mathbb{F}_0$ as Calculated by Theory	138
5.1.	Definition Sketch for Thermal Spread	142
5.2.	Schematic Diagram of Processes for Heat Balance	144
5.3.	Vertical Distribution of Water Temperature along the η Axis Perpendicular to the Shore: $\lambda = 0$	149
5.4.	Horizontal Distributions of Water Temperature at the Surface and Layer of $\zeta = 1.4$: $\lambda = 0$	149
5.5.	Vertical Distributions of Water Temperature at Various Sections Parallel to the Shore at $\eta = 0$, 1.6 and 4.0: $\lambda = 0$	149
5.6.	Vertical Distribution of Water Temperature along the η Axis Perpendicular to the Shore: $\lambda = 0.3$	149
5.7.	Horizontal Distributions of Water Temperature at the Surface and Layer of $\zeta = 1.4$: $\lambda = 0.3$	150
5.8.	Vertical Distributions of Water Temperature at Various Sections Parallel to the Shore at $\eta = 0$, 1.6 and 4.0: $\lambda = 0.3$	150
5.9.	Vertical Distribution of Water Temperature along the η Axis Perpendicular to the Shore	150

LIST OF FIGURES

No.	Title	Page
5.10.	Horizontal Distributions of Water Temperature at the Surface and the Layer of $\zeta = 4$	153
5.11.	Vertical Distributions of Water Temperature at Sections Parallel to the Shore at $\eta = 0$ and $\eta = 4$	153
5.12.	Establishment of Boundary Values for Semi-infinite Sea Basin	158
5.13.	Rate of Convergence of Biharmonic Type for Semi-infinite Sea Basin	158
5.14.	Rate of Convergence of Biharmonic Type for S. Bay	158
5.15.	Distribution of x Component, u, of Surface Velocity	159
5.16.	Distribution of y Component, v, of Surface Velocity	159
5.17.	Distribution of Surface Velocity	159
5.18.	Comparison of "Zero Temperature" and Constant-thermal-gradient Methods of Setting Up the Distance-boundary Condition on Temperature	161
5.19.	Distribution of Water Temperature in Surface Layer	162
5.20.	Process of Diminition of Flow and Water Temperature in Sea Basin	163
5.21.	Water-temperature Distribution along a Longitudinal Section	167
5.22.	Velocity Distribution along Longitudinal Section	167
5.23.	Profile of Water-temperature Distribution	167
5.24.	Variation of Velocity Profile	168
5.25.	Vertical Variation of Velocity Off the Outlet	169
5.26.	Vertical Distribution of Water Temperature along y Axis Perpendicular to Shore in M. Bay	169
6.1.	Two-dimensional Case	175
6.2.	Relationship of Temperature-rise Ratio to Nondimensional Surface-area Ratio for Selected Values of β	179
6.3	Two-dimensional Case in an Open-lake Situation	181
6.4.	Nondimensional Surface-area Ratio as a Function of Concentration Ratio for the Two- and Three-dimensional Cases	183
6.5.	Three-dimensional Case	184

LIST OF FIGURES

No.	Title	Page
6.6.	Surface and Typical Cross-section Temperature Contours, Holston River below John Sevier Steam Plant, October 16, 1969 .	185
6.7.	Variation in Surface Area with Temperature-rise Ratio, Holston River below John Sevier Steam Plant, October 16, 1969 .	186
6.8.	Temperature Contours at Surface, Tennessee River below Widows Creek Steam Plant, November 20, 1968.	186
6.9.	Temperature Contours in the Cross Section, Tennessee River, 200 ft below Widows Creek Steam Plant, November 20, 1968 .	187
6.10.	Temperature Contours in the Cross Section, Tennessee River, 1525 ft below Widows Creek Steam Plant, November 20, 1968 .	187
6.11.	Surface Area within a Temperature-rise Contour vs Temperature-rise Ratio with Two- and Three-dimensional Curves Superimposed, Widows Creek, November 20-21, 1968.	187
7.1.	Effluent Plume Released from Line Source of Length, b, into Uniform Lake Current of Velocity, U	191
7.2.	Isotherms as Predicted by the Offshore Outfall Model	196
7.3.	Effluent-source Model	199
7.4.	Effluent Plume Released from Line Source of Length, b, Located at Shore, into Uniform Lake Current of Velocity, U .	200
7.5.	Isotherms as Predicted by the Shoreline Surface-discharge Model	201
7.6.	Decay of Maximum Temperature due to Mixing Alone.	202
7.7.	Observed Standard Deviation of Meandering vs Distance	204
8.1.	Elemental (Nodal) Approximation to River Contours.	210
8.2.	Derivation of Energy Equation	213
8.3.	Derivation of Continuity Equation	214
8.4.	Geometry and Boundary Conditions of TOPLYR-II Model . . .	215
8.5.	TOPLYR-II Results for Various "Old" Temperatures Used for Initial Conditions	223
8.6.	TOPLYR-II Results with and without Nonphysical-value Correction with Axial-diffusion-coefficient Value of 7.0 m^2/sec .	225
8.7.	TOPLYR-II Results with and without Nonphysical-value Correction with Axial-diffusion-coefficient Value of 1.0 m^2/sec .	225

LIST OF FIGURES

No.	Title	Page
8.8.	Comparison of TOPLYR-I and II with Only Convection Mechanism Operational	226
8.9.	Comparison of TOPLYR-I and II with Diffusion Coefficient of 7.0 m^2/sec	227
8.10.	Comparison of TOPLYR-I and II with Diffusion Coefficient of 1.0 m^2/sec	227
8.11.	Comparison of Theoretical and Experimental Temperature Profiles at Output Station for Various Magnitudes of Atmospheric Energy Loss	228
8.12.	Comparison of Theoretical and Experimental Temperature Profiles at Output Station for Various Diffusion Coefficients: Time = 0020 hr	228
8.13.	Comparison of Theoretical and Experimental Temperature Profiles at Output Station for Various Diffusion Coefficients: Time = 0025 hr	228
8.14.	Geometry and Shoreline Boundary Condition of TOPLYR-II Model with Derivation of Shoreline-cell Energy Equation	232
8.15.	Comparison between Theoretical and Experimental Temperature Profiles at Output Station for Various Magnitudes of Lateral Thermal Eddy Diffusivity	233
8.16.	Effect of Source due to Energy Exchange with Atmosphere or Riverbed on Theoretical Results	234
8.17.	Effect of Reduced Thermal Diffusivity near Shoreline on Theoretical Results	234
8.18.	Improvement in Resolution by Decreasing Nodal Mesh Size	234
9.1.	Coordinate System for Lake Plume Model	243
10.1.	Horizontal Spreading of Jet	256
10.2.	Reflection Method to Calculate η_1	261
10.3.	Surface-area Correction due to Heat Loss to the Atmosphere	268
10.4.	Horizontal Distribution of Excess Temperature	272
11.1.	Schematic View of Thermal Plume	282
11.2.	Interaction of Thermal Plume with Lake Current	283
11.3.	Temperature Decay along Centerline of Plume	289

LIST OF FIGURES

No.	Title	Page
11.4.	Width of the Plume as a Function of Distance from the Origin	289
11.5.	Temperature Profiles in the Surface Plume	290
11.6.	Typical Plume Profile at a Fixed Distance from the Origin	290
11.7.	Two-step Method of Plume Analysis	291
11.8.	Velocity Distribution in a Two-dimensional, Turbulent Jet	294
11.9.	Decay of Temperature along Plume Centerline for Bell Station Discharge for "Typical" Summer Conditions	301
11.10.	Decay of Temperature along Plume Centerline for Bell Station Discharge for "Typical" Winter Conditions	301
12.1.	Intake and Discharge Arrangement	306
12.2.	Typical Flow Pattern and Temperature Distribution	307
12.3.	Cooling-water Studies, 1:81 Model, Measured Velocity Distribution, 780-cfs Cooling Water, Zero Lake Current	307
12.4.	Surface Flow Pattern and Temperature Profiles with No Natural Lake Current; Model Tests	308
12.5.	Variation of Temperature Concentration along Jet Axis at Water Surface	312
12.6.	Surface-temperature Pattern at Site with Zero Lake Current	312
12.7.	Flow Pattern and Temperature Profiles with Eastward Lake Current; Model Test	313
12.8.	Surface Flow Pattern and Temperature Profiles with Westward Lake Current; Model Tests	314
12.9.	Maximum Surface Temperature above Ambient Lake Temperature outside of Mixing Zone as a Function of Lake Current; Cooling-water Studies; 1:81 Model	315
12.10.	Surface-temperature Pattern at Site; 0.2-ft/sec Eastward Lake Current	318
12.11.	Overall Surface-temperature Pattern in Lake, 0.5-ft/sec Eastward Lake Current	319
12.12.	Overall Surface-temperature Pattern in Lake, 0.8-ft/sec Eastward Lake Current	320

LIST OF FIGURES

No.	Title	Page
12.13.	Surface-temperature Pattern at Site; 0.2-ft/sec Westward Lake Current	321
12.14.	Surface-temperature Pattern at Site; 0.5-ft/sec Westward Lake Current	322
12.15.	Surface-temperature Pattern at Site; 0.7-ft/sec Westward Lake Current	323
12.16.	Measured Values of Eddy Diffusivity in the Horizontal Direction in the Ocean, Showing Increase with Scale	327
A.1.	Hoopes, Zeller, and Rohlich Model	370
A.2.	Carter Model	370
A.3.	Motz and Benedict Model	370
A.4.	Stolzenbach and Harleman Model	370
A.5.	Wada Models	371
A.6.	Edinger and Polk Models	371
A.7.	Csanady Models	371
A.8.	Kolesar and Sonnichsen Model	371
A.9.	Wnek Model	371
A.10.	Pritchard Model	372
A.11.	Sundaram *et al*. Model	372
A.12.	Tsai Model	372

LIST OF TABLES

No.	Title	Page
2.1.	List of Parameter Values in the Hydraulic Testing Program	43
2.2.	Computation of Coordinates of Maximum Penetration	57
2.3.	Comparison of Old and New Values of 1 - f	60
3.1.	Laboratory Results Found by Varying A and β_0'	80
3.2.	Results of Statistical Tests on Parameters	83
3.3.	Relation of E to β_0'	83
3.4.	Summary of Field Results	83
3.5.	Values of Entrainment Coefficient	84
3.6.	Results of Surface-jet Analysis	86
4.1.	Integrated Equations for Buoyant Jets	111
4.2.	Integrated Equations for Deflected Buoyant Jets	120
5.1.	Main Processes of Heat Exchange at Water Surface Used in Evaluation of Q_0	144
5.2.	Maximum Range of Influence of Flow by Outfall of Warmed Cooling Water	160
5.3.	Maximum Range of Influence of Water-temperature Rise by Outfall of Warmed Cooling Water	162
8.1.	Energy-exchange Process at Water Surface	216
10.1.	Sample Area within Isotherm Calculations	271

HEATED-EFFLUENT DISPERSION IN LARGE LAKES: STATE-OF-THE-ART OF ANALYTICAL MODELING.

by

A. J. Policastro and J. V. Tokar

ABSTRACT

This report is part of a three-part literature survey to delineate the state-of-the-art of available methods for predicting heated-effluent dispersion from power-plant condenser-cooling-water discharges into large lakes. This report, which will be periodically updated, concentrates solely on mathematical predictive methods. Two companion reports assess the state-of-the-art of hydraulic modeling (E. Silberman and H. Stefan, Physical (Hydraulic) Modeling of Heat Dispersion in Large Lakes: A Review of the State of the Art, ANL/ES-2, Aug 17, 1970) and delineate existing field data (J. V. Tokar, Thermal Plumes in Lakes: Compilations of Field Experience, ANL/ES-3, Aug 1971) which could possibly be used to validate predictive methods. Essentially 16 mathematical models have been critically reviewed concerning their formational development. Criticisms have been made discussing individual model treatment of geometric, kinematic, hydrodynamic, and thermodynamic variables. The models have been categorized according to their regime of applicability, and contrasting and congruous qualities between models within each category have been summarily presented.

I. INTRODUCTION

A. General Discussion

This state-of-the-art report concerning mathematical modeling of the dispersion of heated discharges into large lakes provides information to identify and contrast available predictive models. The models reviewed here do not collectively represent all of those that may exist. We know several new models which were not included here because of their recent origin, and a number of others which were more of historical interest rather than of any practical value. There may be other models used for other siting situations as, for example, marine coastal environments, which could be adapted to lake applications. In this regard, the reader is urged to obtain the following references should he desire to obtain a state-of-the-art assessment of thermal-dispersion modeling on water bodies other than large lakes. For

estuarine modeling, see Ref. 1; coastal modeling, Ref. 2; riverine modeling, Ref. 3; cooling-pond modeling, Ref. 4; and selected modeling issues, Ref. 5.* This list is not comprehensive, but it forms a good beginning.

Subsequent discussion in this report relates mainly to heated discharges in large lakes. This report has been divided roughly into two major chapters. Chapter III deals mainly with a comprehensive review of mathematical models proposed by 12 groups of authors. Most of the material presented in Chapter III was taken from the original works cited. The sections within that chapter were sometimes supplemented by using material obtained from telephone conversations with the individual authors. Also, in most cases, the authors have had an opportunity to review their own individual sections and have suggested appropriate revisions and clarifications. Their individual reviews do not, however, imply an endorsement by them concerning our interpretation of their work. We have also attempted to delineate and criticize the problem areas within each model that have come to our attention; unfortunately, the descriptions of models were serially written, and this may have induced some biases in these criticisms. Hopefully, Chapter IV, in which the individual models were compared on an issue-by-issue basis, will resolve any inadvertent treatment as to the methodology used by the various investigators.

For convenience, Chapter III has been subdivided into three sections providing model descriptions of the jet, far-field, and integrated-flow regimes. Although all of the models reviewed are of relatively recent origin, there is an evolutionary development in their progress. Therefore, some models may seem to be more or less comprehensive on many of the important issues considered. For this reason, the models are arranged in chronological order within each section of Chapter III. From this, the reader can follow the generally increasing sophistication and complexity of the models, as knowledge in the state-of-the-art has improved. This ordering of the models is expressed in the Table of Contents in which the models are listed with their initial dates of publication. Several of them have been updated since then.

Chapter IV of this report contrasts the various models on an issue-by-issue basis. That chapter is itself divided into three sections and, like the third chapter, groups the issues by the regimes of flow. For the jet-regime flow, among the specific topics considered are:

1. Whether the models use a numerical, integral, or semi-empirical approach.
2. Whether the models are two- or three-dimensional.
3. How the models consider ambient crossflows and wind stress.
4. How the effects of buoyancy, stratification, and surface heat loss are accounted for.
5. How shoreline and bottom effects are included.

*References for each section appear at the end of that section.

6. How the position and configuration of the discharge are considered.
7. Whether models account for a flow-establishment region.
8. Whether a computer routine is available for the application of the models.
9. Whether the models have been applied to field data, hydraulic laboratory data, or both.

Fundamentally, the same issues are discussed in relation to the far-field models. The group of models that consider the whole flow field are compared as to their jet and far-field components with the other jet and far-field models. Section C of Chapter IV contrasts the method of linking of near- and far-field solutions for those complete models. Tables at the end of Chapter IV specify the needed input parameters for each model. In Appendix A the predictions of the 16 models reviewed are described schematically. Finally, Appendix B presents a chart summarizing the major characteristics of all the models.

In closing, it is the intent of Chapter IV to compare models on a point-by-point basis. No criticisms will be leveled at any model in particular within that chapter because, quite frankly, except for obvious deficiencies, no model has been sufficiently tested with field data to say whether it does or does not have merit. This issue, in fact, will be the subject of a companion report (Part 2. Model-field Verification) in which most of the models considered here will be compared with actual field data. Compilations of both laboratory and field data for lake plumes have already been published in Refs. 6 and 7. These will in part provide the necessary data for making model-field comparisons.

B. The Near Field

A heated effluent discharged into a receiving body of water may pass through several flow regimes while dispersing through the receiving media. For descriptive purposes, these flow regimes are arbitrarily visualized as belonging to either the near-field region (the region influenced by the conditions at and near the point of discharge) or the far-field region (the region primarily influenced by ambient receiving-water conditions). The distinction between the near field and far field will become clearer in the following paragraphs.

In the near field, the heated effluent can enter the receiving water at one of two locations: at the surface or at some arbitrary point below the surface. If the effluent enters the receiving water creating a tangential separation surface for velocity, the effluent is said to enter as a jet. The jet, by definition, possesses a velocity disparity with respect to the ambient fluid. Thus, as the jet enters the ambient environment, the viscous shear between the moving jet and the ambient fluid creates turbulence in the contact region. This turbulence works its way both inward toward the jet center and outward toward the ambient fluid, with a resultant net outward flux of momentum

away from the jet axis. Eventually, within some distance from the point of discharge, the turbulent mixing action reaches the jet axis, after which the jet centerline velocity begins to decrease. The region between the discharge and the point at which the centerline velocity first begins to decay is called the zone of flow establishment. Once the centerline velocity begins to decay, it is generally assumed that the jet velocity profile is established or fully developed from that point on.

For a heated discharge, the jet possesses a temperature disparity as well, which, by eddy-transport mechanisms, disperses the thermal energy away from the jet to the receiving water. It is often assumed that the zones of momentum and thermal development in turbulent jets coincide and that, once the flow becomes developed, the momentum and temperature profiles become similar and equal for any axial position. This assumption is generally made for the sake of convenience rather than for fact, because some experiments have shown the eddy thermal diffusivity to be larger than the momentum coefficient within the same flow field in free turbulent jet flows.

In the absence of doing useful work, a basic axiom of fluid mechanics requires that the kinetic energy of a jet discharge be dissipated by turbulence through viscous shear. Therefore, within a localized region about the discharge, mechanical mixing action will be expected to dominate the eddy-transport mechanisms because of the large velocity gradients present.

A jet can be further categorized as being buoyant or nonbuoyant. If the motion of a jet is partially governed by its density (temperature) disparity, it is said to be buoyant. Normally, a heated jet has positive buoyancy in an Archimedean sense; however, a heated jet can have negative buoyancy. To assess the importance of buoyancy in jet flows, one only has to compute the densimetric Froude number (F_d), which is a ratio of inertial to buoyancy forces,

$$F_d = U/\left(\frac{\Delta\rho}{\rho_0} gd\right)^{1/2},$$

where U is the velocity of the jet, $\Delta\rho$ the density disparity of the jet, ρ_0 the ambient water density, g the local acceleration of gravity, and d some suitable hydraulic diameter of the jet. For large $F_d (F_d \gg 1)$, jet flow should be considered to be inertially dominated. For densimetric Froude numbers, near-unity buoyancy becomes a dominant aspect of the flow. In fact, if the densimetric Froude number is less than unity at the point of discharge, it would be hard to characterize the discharging effluent as a jet in a practical sense. Such an effluent would merely leave the discharge and be buoyed directly to the surface, if it were not already at the surface spreading laterally like a thin sheet over the surface, due to the action of gravity and ambient turbulence. Turbulent entrainment in the vertical direction is generally limited under these circumstances, and stable stratification likely ensues. The bulk Richardson number, R, is a measure of the stability of

surface stratification. When R is greater than about 0.8, the stratified layer is said to be stable. If it is less than about 0.8, turbulent mixing in the vertical direction is possible. The bulk Richardson number is given by $B = gh\Delta\rho/(\rho_a U^2)$, where h is some average thickness of the stratified layer.

A jet may also be discharged at some arbitrary angle into a flowing ambient current. Under such circumstances, the jet can be envisioned to bend over in the direction of the crossflow. Depending on the relative velocity magnitudes of the jet, the ambient current, and other factors, this bending may involve large or small curvatures. On the upstream side of the jet, the interaction retards and partially deflects the ambient stream, creating an increased pressure at the interface; on the lee side of the jet, some separation occurs. The static pressure is therefore continuously decreased from the jet's upcurrent to leeward sides. Because the jet entrains a portion of the incoming ambient fluid, the increase in pressure on the jet's forward edge is less than what would be expected if the jet's interface were a solid body. As soon as the jet bends over and becomes aligned with the ambient current, the crosscurrent interaction ceases for all practical purposes. The behavior of the effluent may or may not be of a jetlike character once bendover is complete; however, it is more likely to be jetlike for more acute angles of introduction.

There are many other parameters and conditions that are likely to affect the dynamics of a jet. Some of these are the shape and position of the outfall, possible preexisting stratification in the ambient media, and the general topography in the vicinity of the outfall. All of these, together with those previously described, play a significant part in determining the fate of a heated effluent within the near-field zone of the discharge.

C. The Far Field

The far field, as noted earlier, is that regime of flow in which the effluent is primarily influenced by ambient receiving-water conditions. Within this regime there is no history, for example, of whether the heated effluent was introduced from a submerged round jet or from a rectangular shoreline canal. In physical extent, this regime is generally much larger than the near-field zone. The effluent within this regime of flow is generally called a plume, as contrasted to the near-field portion, which is called a jet. These title distinctions are quite arbitrary, however.

A surface plume is generally envisioned to be a passive floating sheet of heated water resting on top of the cooler receiving water. This is true for a surface plume. However, plumes can exist at submerged positions under specialized circumstances, for example, if the effluent possesses negative buoyancy. The dispersion of the plume in the far field is dominated by many factors, which are also present in the near field. Within the far field one must now additionally consider surface heat loss and the effects of ambient turbulence. Thus plume spread and dissipation in the far field are determined by ambient advective motions, lateral, longitudinal, and vertical mixing due

to ambient turbulence, buoyancy, and surface heat loss. The vertical eddy-transport mechanisms in the far field are generally considered to be much smaller than their horizontal counterparts due to the presence of vertical density gradients. The earlier comments concerning the bulk Richardson number are appropriate here.

Wind may preferentially interact with a plume to some extent. If, in fact, a preferential factor is operative, then there are sure to be some induced relative motions and/or mixing between the plume and the ambient water. Direct wind interaction in the jet regime is generally assumed to be small; however, with the far field having large plume expanses, wind interaction may be a significant factor.

In summary, the effluent dynamics in the near and far fields is influenced by many parameters some of which are included in the following listing, abstracted, in part, from Ref. 6.

1. Discharge

   a. Effluent characteristics

      (1) Temperature disparity at discharge
      (2) Velocity at discharge
      (3) Volumetric flow

   b. Outlet characteristics

      (1) Location
      (2) Submergence
      (3) Orientation
      (4) Size and shape

2. Receiving Water

   a. Flow dynamics

      (1) Ambient velocity field
      (2) Turbulence levels
      (3) Surface and internal waves

   b. Stratification

      (1) Existing ambient-water stratification

   c. Geometrical characteristics

      (1) Shoreline and bottom topography

3. Atmosphere

   a. Air

      (1) Wind velocity

(2) Air temperature
(3) Other atmospheric variables

For the model descriptions in Chapter III, it will become obvious that to keep mathematical modeling tractable it is necessary to stress or deemphasize certain of the above-outlined parameters.

D. Model Reviews of Recent Acquisitions

As previously noted, several model reviews were omitted from this report primarily because of their rather recent origin and/or discovery. It is presently anticipated that the forthcoming companion report will amend any such omissions by including critical reviews of these utilizing a format similar to that contained herein. Among those models to be reviewed in our updated report are: Koh and Fan[8a] and Koh[8b]; Wada[9]; McLay et al.[10a] and Hundal et al.[10b]; Loziuk et al.[11]; Stefan[12]; Elwin[13]; and Barry and Hoffman[14a] and Hoffman[14b]. In addition, two phenomenological models, Bryce et al.[15a] and Elliott and Harkness[15b], and Asbury and Frigo[16a] and Frigo[16b] will be discussed.

Considering the relatively recent interest in submerged outfalls for large-lake applications, we will, if time permits, include the modeling efforts of Hirst[17] and Trent[18] in the forthcoming companion report as well. The incorporation of these works should, to the best of our knowledge, update the excellent reviews of Baumgartner and Trent[2] and Fan[19] on submerged discharges.

References

1. G. H. Ward and W. H. Espey, Editors, Estuarine Modeling: An Assessment, document prepared for National Coastal Pollution Research Program, Water Quality Office, Environmental Protection Agency, Tracor, Inc., Austin, Texas (Feb 1971).

2. D. J. Baumgartner and D. S. Trent, Ocean Outfall Design, Part 1, Literature Review and Theoretical Development, U.S. Dept. of Interior Report, Federal Water Quality Administration, Pacific Northwest Water Laboratory, Corvallis, Oregon (Apr 1970).

3. F. L. Parker and P. A. Krenkel, Thermal Pollution: Status of the Art, Vanderbilt University, Dept. of Environmental and Water Resources Engineering, Nashville, Tennessee, Report No. 3 (Dec 1969).

4. D. K. Brady, W. L. Graves, and J. C. Geyer, Surface Heat Exchange at Power Plant Cooling Lakes, Johns Hopkins University, Dept. of Geography and Environmental Engineering, Report No. 5 (Nov 1969).

5. D. R. F. Harleman, Editor, Engineering Aspects of Heat Disposal From Power Generation, 1971 Summer Session, June 28-July 2, Massachusetts Institute of Technology, Dept. of Civil Engineering, Vols. 1 and 2.

6. E. Silberman and H. Stefan, Physical (Hydraulic) Modeling of Heat Dispersion in Large Lakes: A Review of the State of the Art, ANL/ES-2 (Aug 17, 1970).

7. J. V. Tokar, Thermal Plumes in Lakes: Compilations of Field Experience, ANL/ES-3 (Aug 1971).

8a. R. C. Y. Koh and Loh-Nien Fan, Mathematical Models for the Prediction of Temperature Distributions Resulting from the Discharge of Heated Water into Large Bodies of Water, National Environmental Protection Agency Report, Water Pollution Control Research Series 16130DW010/70 (Oct 1970).

8b. R. C. Y. Koh, Two-Dimensional Surface Warm Jets, American Society of Civil Engineers, Journal of the Hydraulics Division, pp. 819-836 (June 1971).

9. A. Wada, "Numerical Analysis of Distribution of Flow and Thermal Diffusion Caused by Outfall of Cooling Water," Proceedings of the Thirteenth Congress of the International Association for Hydraulic Research, pp. 335-342, August 31 to September 5, 1969.

10a. R. W. McLay, M. S. Hundal, F. Martinek, and E. B. Henson, Mathematical Modeling of Nuclear Plant Thermal Effects in Lake Champlain, American Society of Mechanical Engineers, Winter Annual Meeting, Paper No. 71-WA/Pwr-4, November 28 to December 2, 1971.

10b. M. S. Hundal, F. Martinek, E. B. Henson, and R. W. McLay, A Computer Model for Predicting Thermal Discharges in Large Lakes, Department of Mechanical Engineering, University of Vermont, Burlington, Vermont; paper presented at Fifteenth Conference on Great Lakes Research, Madison, Wisconsin, April 5-7, 1972.

11. L. A. Loziuk, J. C. Anderson, and T. Belytschko, Hydrothermal Analysis by the Finite Element Method, Sargent & Lundy Engineers, Chicago, Illinois (submitted for publication).

12. H. Stefan, Analytical Jet-Type Model of Heated Water Surface Plumes, Department of Civil and Mineral Engineering, St. Anthony Falls Hydraulic Laboratory, University of Minnesota, Minneapolis, Minnesota; paper presented at Fifteenth Conference on Great Lakes Research, Madison, Wisconsin, April 5-7, 1972.

13. E. Harvey Elwin, Uniform Flow Dispersion Model for a Thermal Source, Bechtel, Inc., San Francisco, California; paper delivered at ASCE National Environmental Engineering Meeting, St. Louis, Missouri October 18-22, 1971. (Model application: Analytical Procedures for Prediction of Temperature Distribution from Cooling Water Discharge at Rush Island, Rush Island Construction Project, Union Electric Company, Union, Missouri, 1971.)

14a. Robert E. Barry and David P. Hoffman, Computer Model for a Thermal Plume, Mechanical Division, The Detroit Edison Company, Detroit, Michigan, paper presented at ASCE National Resources Engineering Meeting, Phoenix, Arizona, January 11-15, 1971.

14b. David P. Hoffman, Thermal Plume Model, Mechanical Division, The Detroit Edison Company, Detroit, Michigan; paper presented at Fifteenth Conference on Great Lakes Research, Madison, Wisconsin, April 5-7, 1972.

15a. J. B. Bryce, W. R. Etter, and E. H. Dye, Water Environmental Studies and Water Quality Control at Ontario Hydro, The Hydro-Electric Power Commission of Ontario, Generation Projects Division, Toronto, Canada (June 16, 1971).

15b. R. V. Elliott and D. G. Harkness, A Phenomenological Model for the Prediction of Thermal Plumes in Large Lakes, The Hydro-Electric Power Commission of Ontario, Toronto, Canada; paper presented at Fifteenth Conference on Great Lakes Research, Madison, Wisconsin, April 5-7, 1972.

16a. J. G. Asbury and A. A. Frigo, A Phenomenological Relationship for Predicting the Surface Areas of Thermal Plumes in Lakes, ANL/ES-5 (Apr 1971).

16b. A. A. Frigo, Prediction of Surface Plume Areas Associated with Heated Discharges Into Large Lakes--A Phenomenological Model, Argonne National Laboratory; paper presented at Fifteenth Conference on Great Lakes Research, Madison, Wisconsin, April 5-7, 1972.

17a. E. A. Hirst, Analysis of Buoyant Jets Within the Zone of Flow Establishment, ORNL-TM-3470 (Aug 1971).

17b. E. A. Hirst, Analysis of Round, Turbulent, Buoyant Jets Discharged to Flowing Stratified Ambients, ORNL-4685 (June 1971).

18. D. S. Trent, A Numerical Model for Predicting Heat Dispersion in Thermal Plumes Issuing from Large Vertical Offshore Power Plant Outfalls in Shallow Coastal Waters, to be published as Ph.D. thesis, Oregon State University, Corvallis, Oregon.

19. Loh-Nien Fan, Turbulent Buoyant Jets into Stratified or Flowing Ambient Fluids, W. M. Keck Laboratory of Hydraulics and Water Resources, California Institute of Technology, Report No. KH-R-15 (June 1967).

II. OBSERVATIONS AND RECOMMENDATIONS

The primary objective of this work is to identify mathematical models that can be used to predict the physical extent of heated effluents discharged into large lakes. Essentially 15 of the 16 models reviewed have potential merit in this regard. Four of the models represent near-field jet flow, nine represent far-field plume flow, and two represent complete-field flow analyses. The models represent an interesting cross section of formulative assumptions and incorporative devices to achieve problem solution. Some models use rather elegant numerical schemes to solve complex sets of differential equations; others use abbreviated equations to obtain closed-form solutions. A summary and recommendations concerning these models now follow.

A. Near-field Issues

1. Most model analyses assume that the effluent leaving the discharge is uniform in both temperature and velocity or, in other words, is top-hat. The effects of this assumption should be studied.

2. In several jet analyses, the interaction of the jet with a cross-flowing current is treated as if the jet were a solid body and the resulting pressure gradients were represented by a drag force acting normal to the jet axis. Much work needs to be done to see if this is an adequate representation of the facts.

3. Most of the models that used empirical entrainment coefficients obtained these coefficients from nonbuoyant free-jet theory. A heated effluent discharging at the surface of a lake into a crossflowing current is neither nonbuoyant, free, nor symmetrical. Thus one must first establish whether the entrainment coefficient is dependent on buoyant or nonbuoyant factors; then one must determine if any influence on these coefficients is created by the presence of an interface, and finally, one must account for entrainment variability from the upcurrent to the leeward sides of the jet.

4. For most shoreline-discharge situations, the bulk Richardson number at the point of discharge is generally somewhat smaller than unity. This means that the jet will vertically entrain at a decreasing rate until buoyant forces begin to predominate at some distance from the outfall. This phenomenon is likely to be important since vertical entrainment is likely to significantly alter the jet's initial dilution rate. Only two models considered this issue by providing for vertical entrainment as a function of the Richardson number. The adequacy of the models' treatment should be verified, and other avenues of approaching this issue should be explored.

5. Most shoreline discharges generally have offshore sloping bottoms. The presence of a sloping bottom in prototype situations is likely to inhibit vertical entrainment, which in turn may significantly alter lateral jet spread. There is much controversy on this matter, and it should be resolved. Only one jet model considered bottom interaction directly, and it was not successful in doing so.

6. Most jet studies tacitly assume that when the jet becomes fully developed, the temperature and velocity profiles are Gaussian in form. For submerged buoyant or nonbuoyant jets, there is some laboratory experience suggesting this to be the case. For buoyant surface discharges, there is little evidence to substantiate these generalizations, particularly if cross-flows are present.

7. Within the same context, it is generally assumed that once jet flow is fully developed, the velocity and temperature profiles are similar and equal. Prandtl's mixing-length hypothesis suggests their equality. Reichardt presents some evidence for two-dimensional air jets indicating that the eddy-transport coefficients for heat are a factor-of-two greater than for momentum. This suggests that the velocity and temperature profiles may not be equal in the case of heated water jets. This should be investigated.

8. It is generally assumed that direct wind interaction with surface jet flow is of minimal consequence, primarily because jet surface dimensions are quite small. Only one jet model reviewed here considered this interaction; however, there is some question as to the validity of the way the model handled the wind interaction. In any event, model computations indicated a perturbation in jet flows for "moderate" wind speeds. This should be fully explored. See further comments within the far-field discussion in Sec. B below.

9. No surface jet model reviewed here treated the possible interaction of a jet with a thermally stratified ambient medium. In all cases, the ambient was assumed to have a uniform temperature. Considering the influence of stratification on submerged jets this issue should be explored.

10. Within the jet regime of a heated surface discharge, there is eventually a transition from inertially dominated flow to gravity-dominated structuring. Ideally, one would therefore have to consider the coupling between the hydrodynamic equations and the energy equation. None of the jet models described in this report considered this coupling. For submerged jets, various techniques have been evolved to perform this task. However, for layered surface flow, coupling becomes no simple matter. The importance of buoyant forces in submerged-jet dynamics is apparent; the significance in surface jets should be established.

11. Perhaps the most striking feature of jet-flow modeling, whether it be hydraulic or analytical, is that it has not been thoroughly compared against prototype field data. Those comparisons that have been made were done in a curve-fitting sense; that is, primary parameters within these models have been adjusted to fit available data. In a broad sense, however, curve fitting can be considered to be a weak form of model verification, because if a model cannot be fitted, its suitability certainly can be challenged.

Applying field data to the jet-regime models is somewhat uncertain. There is always a question as to where jet flow ceases and where the far-field data begin! This by itself is a significant issue if analytical jet models are to be tested with field data or laboratory data, for that matter.

B. Far-field Issues

1. The classic difficulty with far-field models is the inability to specify the ambient eddy-transport coefficients for heat and momentum. Experience has shown these coefficients to be nonhomogeneous. Because of temperature stratification and viscous dissipation, vertical transport coefficients are generally less than their horizontal counterparts. Further, depending on the proximity of solid boundaries or on the size of the plume, only particular scales of eddies are influential with regard to turbulent transport. For example, eddies much larger than some length scale of a plume will merely tend to advect the plume. As a plume grows in size, a continuing spectrum of eddies of increasing size can become operative to control the rates of turbulent transport. If a shoreline or lake bottom is in proximity, the length scales of the eddies will be limited in size, suggesting that the eddy-transport coefficients reach a constant value in the near-shore areas, depending on the length scale of the plume. In open-sea situations, an essentially infinite scale of eddies can appear. The Richardson 4/3-power law of diffusion is widely accepted for eddy transport in open-sea applications.

Field experiments should be performed to test the above hypothesis concerning whether a constant-value transport coefficient can be reached for a particular offshore distance in near-shore areas. If one could demonstrate this, then the next logical step would be to obtain some sort of relationship between offshore distance and the magnitude of the transport coefficient. Since these coefficients are likely to vary, depending on meteorological and seasonal conditions, it would be necessary to sample throughout the year to obtain some credible and acceptable value for model utilization.

One must not underestimate the difficulty of simply measuring these eddy-transport parameters, vertical as well as horizontal. Yet the acquisition of these coefficients is essential to obtain solutions to the far-field equations.

2. In most far-field analyses, buoyant forces are assumed to contribute little to the horizontal spread of a heated plume. In some situations, this assumption is made to decouple the hydrodynamic equations from the energy equation. Item 10 in the near-field issues has already discussed this matter. In the far-field case this is certainly a better assumption; however, nothing has come to our attention demonstrating the acceptability of this assumption. Only one far-field model considered this issue within this report. The temperature and velocity profiles for that model did indeed show a difference between density-coupled and -uncoupled flow and energy equations as a function of depth; however, the effects on lateral spread were not clearly discernible.

3. None of the far-field models considered the possible direct influence of wind stress on the plume. If a wind in some way acts in a different manner on a plume than on the surrounding ambient media, it is not unreasonable to expect that that wind could influence both the trajectory of the plume and its eddy-transport parameters, considering the relatively large fetch of the far-field plume. Some visual observations of plumes show different wave characteristics over plumes than over ambient waters, which would indicate differential behavior.

Wind may also indirectly affect plume behavior by modifying the ambient current structure or by modifying the interfacial stress at the plume/ambient-water interface.

In summary, the possible direct and indirect effects of wind on plume behavior have not been sufficiently studied to know if and how they should be incorporated into modeling efforts. This typical area should be further explored.

4. Bottom and shoreline effects have, in part, been discussed in Issue 1 within this far-field section. There are other ways in which the bottom can affect the far field. For instance, if the general plume vicinity is relatively shallow, one might expect that the so-called ambient dilution water is in part being recirculated. There is no way as yet to estimate the extent of this phenomenon. One model reviewed provided a calculational method to correct for the influence of this "background temperature."

5. Lake stratification is frequently neglected in far-field analyses for two reasons. First, this neglect uncomplicates the mathematics. Second, within the first 10-15 ft of a lake surface, the temperature is likely to be homogeneous due to the effects of wind-induced mixing. In the far-field, surface buoyant thermal plumes seldom have been measured to exceed 10 ft or so in depth; hence one would not anticipate ambient stratification to be directly influential with regard to plume dynamics or heat transfer. However, one of the reviewed models indicates that if ambient stratification is present near the surface, it will surely influence the behavior of the plume.

During certain times of the year, surface stratification is present in temperate lakes. The applicability of most far-field analyses during these periods must be questioned. Also, there seems to be more reliance on submerged offshore outfalls for condenser-cooling-water discharges into lakes and rivers. Heretofore, this form of discharge was primarily used for ocean-sewage disposal. With submerged discharges on large temperate lakes there is a greater likelihood for ambient stratification to influence far-field conditions. Future modeling should consider this issue.

6. Observations of heated surface discharges show a plume to meander with time, with parts of the plume occasionally detaching. Some investigators feel that this meandering may in part be due to changing wind patterns which initially and essentially affect the topmost surface layers of the lake; others feel that it is more characteristic of the turbulent nature of the bulk fluid. If the meandering phenomenon is primarily bulk phenomenon, then the issue suggests a possible need for stochastic analytical approaches to modeling. These points should be investigated.

Observations also show the upcurrent side of a plume to maintain a reasonably sharp vertical temperature interface with the ambient water over a significant lateral extent for heated discharges in ambient crossflows. Models either assuming or yielding "Gaussian-like" temperature profiles certainly cannot account for this phenomenon, although they may give satisfactory predictions. One hypothesis that allows for a sharp boundary in the presence of entrainment is that of a gravity-driven "head" flow. This issue should be explored.

7. The far-field plume is defined as that regime of flow for which the heated effluent is primarily influenced by ambient-receiving-water conditions. The jet-induced turbulence is thought to be sufficiently dissipated so as to be uninfluential by the time the plume reaches the far field. In reality, there exists another regime of flow between the near field and the far field which has the characteristics of both. Knowledge of this intermediate flow regime is extremely important because it establishes the limits of applicability of the near- and far-field models. These limits are the requisite boundary and initial conditions for problem solution or for near-field/far-field model matching so as to obtain a complete flow-field solution. One reviewed model interfaced its near-field analysis to its far-field analysis by equating the eddy diffusivities due to jet-induced turbulence to the eddy diffusivities of the ambient turbulence. Another full-field model assumed that the jet regime ceased and the far field began when the excess temperature of the effluent decayed to 20% to the effluent's initial excess temperature at the outfall.

The authors of the two models cited above recognized that their attempts at matching are rough approximations. Clearly, more work needs to be done in understanding this intermediate flow regime.

8. Most far-field models either assume or require a knowledge of plume depth. There is currently no a priori method of calculating this parameter when the plume becomes stably stratified. This issue is additionally of particular interest to power-plant design engineers. Many plants existing or under design use offshore submerged cooling-water intakes to take advantage of the cooler water available at the lower depths, but more importantly to avoid possible recirculation problems with heated, floating plume water originating from the plant's discharge. There is always some uncertainty as to how deep a submerged discharge must be to maintain a sufficient margin between itself and a floating plume, particularly when the plume's thickness is unknown.

Considering the cited importance of this issue, both mathematical and field investigations should be pursued to define plume depth as a function of seasonal, meteorological, or other influential factors.

9. As in the jet-model situations, there has been little field verification of the far-field analytical models, although some of the far-field models have been used in a curve-fitting sense. Antecedent to model verification is the acquisition of sufficiently comprehensive field data. In our opinion, little suitable field data exists for large-lake situations.

III. MODEL SYNOPSES AND CRITICAL EVALUATIONS

A. Models for the Jet Regime

1. Heated Surface Jets in a Steady Crosscurrent[1]

J. A. Hoopes, R. W. Zeller, and G. A. Rohlich
(The University of Wisconsin)
June 1967

a. List of Symbols

b	Jet half-width
b_0	Outfall width
C_0, C_1	Rate-of-spread coefficient
C_D	Drag coefficient
$f(n/b)$	Lateral distribution of jet velocity
$\mathbb{F}_0$	Densimetric Froude number at the outfall $= v_0/\sqrt{g(\Delta\rho_0/\rho_L)/z_0}$
$g(n/b)$	Lateral distribution of jet temperature relative to lake
g	Gravitational constant
h	x-component of dimensionless momentum flux
I_1	$\int_{-1}^{+1} f(n/b)\, d(n/b)$
I_2	$\int_{-1}^{+1} [f(n/b)]^2\, d(n/b)$
I_3	$\int_{-1}^{+1} f(n/b)\, g(n/b)\, d(n/b)$
I_4	$\int_{-1}^{+1} g(n/b)\, d(n/b)$
K	Heat-exchange coefficient
k	Vertical mixing coefficient
ℓ_x, ℓ_y	Dimensionless wind shearing stress
m	Dimensionless momentum flux
n	Natural coordinate perpendicular to jet centerline
P_x, P_y	Momentum flux in x and y directions
Q	Jet discharge at any cross section
Q_0	Outfall discharge (apparent)
Q_{0a}	Actual outfall discharge (power-plant pumping rate)

dQ	Rate of internal entrainment
s	Natural coordinate along jet centerline
s_m	Jet-centerline distance from outfall
T_c	Jet-centerline temperature
T_L	Lake temperature
T_0	Outfall temperature
T_{sm}	Jet-centerline temperature relative to the lake
u_e	Entrainment velocity
v_L	Lake-current velocity
v_0	Outfall velocity
v_s	Jet velocity
v_{sm}	Jet-centerline velocity
W	Wind speed
z_0	Jet thickness at the outfall
α	Constant entrainment coefficient
α_v	Variable entrainment coefficient
β	Jet curvature relative to y axis
γ	Dimensionless mass flux
ζ	Dimensionless x-distance function
η	Dimensionless y-distance function
θ	Wind direction relative to y axis
ν	y component of dimensionless momentum flux
ξ	Dimensionless centerline distance function
ρ	Water density
ρ_0	Density of outfall discharge water
ρ_L	Density of lake water
$\Delta\rho_0$	$\rho_L - \rho_0$
$\Delta\rho$	$\rho_L - \rho$
ρ_a	Air density
σ	Standard deviation of Gaussian distribution
τ_w	Wind-shear stress

b. Introduction

Hoopes, Zeller, and Rohlich propose a two-dimensional analysis for the surface, shoreline discharge of condenser cooling water into a large lake in the presence of wind and crosscurrent effects. The model assumes that the effect of buoyancy is to make vertical entrainment of the jet zero, the jet being fully mixed vertically and of constant depth. Based primarily upon the work of Morton[2] and Fan[3] on submerged jets, lateral entrainment is accounted for by defining an entrainment coefficient often used in submerged-buoyant-jet theory. An integral technique is then used where assumed similarity functions for velocity and temperature are introduced into the basic integrated equations of mass, momentum, and energy conservation. The jet deflection, the width, and the centerline velocity and temperature are outputs of the theory. Although the mathematical model was designed to study condenser-cooling-water discharges into a rather shallow near-shore region of Lake Monona, Wisconsin, it may be applied elsewhere under certain general conditions.

The model and its application will be discussed in three parts:

(1) Derivation of the mathematical model (Sec. c).

(2) Application of the model to two existing discharges, including a discussion of the model assumptions (Secs. d and e).

(3) Application of the model to general outfall situations (Sec. f).

c. Derivation of the Mathematical Model

(1) General Discussion. The physical situation is illustrated in Fig. 1.1. A heated jet is discharged with a volumetric flow rate Q_{0a} from a surface shoreline outfall into a steady, uniform, shore-parallel current v_L at temperature T_L. The initial jet temperature and velocity are T_0 and v_0, respectively. The outfall is assumed rectangular with width b_0 and depth z_0. The initial angle of the jet to the shoreline is β_0, and a steady wind blows at angle θ to the y axis with speed W.

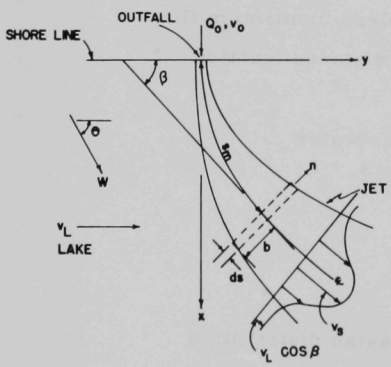

Fig. 1.1. Surface Jet Subject to a Steady Crosscurrent[1a]

The initial Froude number, defined as

$$\mathbb{F}_0 \equiv \frac{v_0}{\sqrt{g \frac{\Delta\rho_0}{\rho_L} z_0}},$$

is assumed to satisfy $\mathbb{F}_0 \gg 1$, where

$\Delta\rho_0$ = density difference between outfall discharge and lake water

and

ρ_L = ambient lake-water density

in order to ensure that the initial jet momentum is controlling the horizontal spreading. In such cases, considerable lateral entrainment will result with the jet thickness remaining approximately constant. If, however, $\mathbb{F}_0$ were much less than unity, horizontal gradients would dominate the spreading action with diminished lateral entrainment and a corresponding decrease in plume thickness would be expected. Moreover, for $\mathbb{F}_0 \ll 1$, lake water penetrates into the channel outlet itself and could effectively reduce the discharge area. To avoid these difficulties, the authors restrict their attention to initial Froude numbers $\mathbb{F}_0 \gg 1$. They assert that the range $3 \leq \mathbb{F}_0 \leq 12$* should be satisfactory in yielding a relatively constant depth momentum jet. This is based upon the work of Ellison and Turner[4] in which the stability of a surface jet, while at high Richardson numbers, causes vertical entrainment to be negligible. At larger distances from the outlet, where the far-field region of the jet has been reached, the initial buoyancy and momentum of the jet will have diminished to the point where sufficient vertical and lateral mixing result from the action of ambient turbulence. The model is to be applied only in the near-shore region, where the momentum interaction of jet and lake current govern the mixing and where the jet has an approximately constant depth. As stated above, the jet is assumed to be uniform in the vertical direction so that two-dimensionality may be presumed. All horizontal pressure and density gradients are assumed negligible, whereby the jet cools exclusively by entrainment of lake water (advection and turbulent diffusion) and surface heat loss.

Wind stress, depending upon its direction, has the effect of either increasing or decreasing the momentum flux without affecting the mass flux through any control volume. The authors use the formula for wind shear

$$\tau_W = \rho_a C_D W^2 \tag{1.1}$$

where

τ_W = wind stress,

ρ_a = density of overlying air,

C_D = drag coefficient,

W = wind speed.

Equation 1.1 is used with the assumption that the jet velocity is negligible compared to W. (If not, then W should really be replaced by $W - v_L$.)

*This range is actually too broad. Vertical entrainment initiates when $\mathbb{F}_0 \geq 1.2$.

Mass-, momentum-, and energy-conservation equations are written by analyzing a control volume of total width 2b, length ds, and depth z_0 located at centerline distance s_m from the outfall as illustrated in Fig. 1.1. First, the authors assume similarity functions for lateral velocity and temperature

$$v_s = v_{sm} f(n/b) \tag{1.2}$$

and

$$T_s - T_L = T_{sm} g(n/b), \tag{1.3}$$

where

v_s = local jet velocity,

v_{sm} = jet centerline velocity,

T_s = local jet temperature,

T_{sm} = jet centerline temperature,

n = natural coordinate perpendicular to jet centerline,

b = jet half-width,

$f(n/b)$ = lateral distribution of jet velocity,

and

$g(n/b)$ = lateral distribution of jet temperature relative to the lake.

For the application of the model to Lake Monona, the authors used the distributions

$$f(n/b) = \exp[-(n/b)^2] \qquad |n| < n_1 \tag{1.4a}$$

and

$$f(n/b) = \frac{v_L \cos \beta}{v_{sm}} \qquad |n| > n_1, \tag{1.4b}$$

where $n_1 > b$ and

$$g(n/b) = \exp[-(n/b)^2]. \tag{1.5}$$

Here f is Gaussian for $|n| < n_1$ and g is Gaussian for all lateral distances n. For $|n| > n_1$, the local velocity was assumed to be approximately equal to the lake velocity component in the lateral direction of the jet. Thus $f(n/b)$ is defined as in Eq. 1.4b.

Allowing for a variable entrainment coefficient, the authors assume that the jet half-width b grows linearly with centerline distance from the outfall,

$$b = \sqrt{2}C_1 s_m + b_0 \tag{1.6}$$

where C_1 is a "rate-of-spread" coefficient, which must be determined empirically. The authors, as will be seen later, rely predominantly upon a constant entrainment coefficient, whereby, for Gaussian assumptions of f and g,

$$b = \sqrt{2}\sigma \tag{1.7}$$

with σ the standard deviation of the normal distribution at position s_m. No linear relationship between b and s_m is assumed in the constant coefficient case. Gaussian assumptions on f and g combined with the variable entrainment assumption will imply

$$\sigma = C_1 s_m + b_0/\sqrt{2}. \tag{1.8}$$

The rate of entrainment through the lateral edges of the control volume is defined by

$$dQ = 2(u_e z\, ds) = \alpha v_{sm}(2z\, ds) \tag{1.9}$$

where

dQ = rate of lateral entrainment,

u_e = local entrainment velocity,

and

α = lateral entrainment coefficient.

The local entrainment velocity was assumed to be related to the jet centerline velocity v_{sm} by

$$u_e = \alpha v_{sm}. \tag{1.10}$$

Equations for α will be derived later. With the above assumptions the integrated mass, momentum, and energy equations can now be written.

(2) Mass Conservation. The volumetric flow rate through the control volume in Fig. 1.1 is

$$Q = z_0 \int_{-b}^{b} v_s\, dn = I_1 z_0 v_{sm} b, \tag{1.11}$$

where

$$I_1 = \int_{-1}^{1} f(n/b)\, d(n/b) \tag{1.12}$$

and f is defined by Eq. 1.2. $I_1 = 1.49$ if f is specified by Eqs. 1.4. From Eq. 1.11,

$$dQ = (I_1 z_0) \frac{d(v_{sm} b)}{ds}\, ds. \tag{1.13}$$

Equating the volume flux out of the control volume defined by Eq. 1.13 to the rate of entrainment of the colder lake water defined by Eq. 1.8, yields

$$\frac{d}{ds}(v_{sm} b) = \frac{2\alpha}{I_1} v_{sm}. \tag{1.14}$$

Equation 1.14 expresses incompressible mass or volume conservation for the jet.

(3) Momentum Flux in x Direction. The flux of momentum in the x direction is

$$P_x = z_0 \int_{-b}^{b} (\rho v_s \sin \beta) v_s\, dn = \rho z_0 \int_{-b}^{b} v_s^2 \sin \beta\, dn, \tag{1.15}$$

where ρ again is constant. The momentum flux equation in the x direction reads

$$\Sigma F_x = F_{px} + F_{sx} = \frac{\partial P_x}{\partial x}\, dx, \tag{1.16}$$

where F_{px} and F_{sx} are the net pressure and shear forces acting in the x direction, respectively. It is assumed that

(a) Horizontal pressure gradients generally present in non-buoyant jets issuing into a stagnant medium are neglected using the same assumptions of classical jet theory.

(b) Additional horizontal pressure gradients due to buoyancy effects are neglected.

(c) Horizontal pressure gradients due to the drag force on the jet arising from the crossflow are negligible.

(d) Horizontal pressure gradients arising from the jet bending and the consequent centrifugal force developed are also negligible.

(e) Lateral shear stresses are unimportant, even though there are finite velocity gradients at the jet boundary. (If an infinite-width jet was used, lateral shear stresses would not need to be considered. In that case, the distribution assumed for v_s would be invalid and there would be no easy way to handle wind forces acting on an infinite control-volume surface area.)

(f) Bottom shear stresses are negligible, due to definition of z_0 as the depth to zero shear. The inherent contradiction between this assumption and that of a fully mixed, vertically uniform plume above z_0 is considered unimportant.

(g) There is no x component of lake velocity present, implying zero entrainment of lake momentum in the x direction.

(h) The x component of the wind-shear force on the lake surface acting on the control volume is $\tau_w(2b \sin \theta \, ds)$ where τ_w is defined by Eq. 1.1.

These assumptions will be discussed in more detail later in the light of experimental data taken about two shoreline surface discharges into Lake Monona. In total, these assumptions imply that the rate of increase in x momentum, P_x, across ds at any s_m is the equal to the x component of wind shear at the lake surface; that is,

$$\tau_w 2b \sin \theta = \frac{\partial P_x}{\partial x} dx, \tag{1.17}$$

or by introducing Eq. 1.2 into Eq. 1.15, Eq. 1.17 becomes

$$\frac{d}{ds}(v_{sm}^2 b \sin \beta) = \frac{2b\tau_w}{\rho z_0 I_2} \sin \theta, \tag{1.18}$$

where

$$I_2 = \int_{-1}^{1} [f(n/b)]^2 \, d(n/b). \tag{1.19}$$

Equation 1.18 is thus the momentum-conservation equation for the x direction.

(4) <u>Momentum Flux in y Direction</u>. The flux of momentum in the y direction at any s_m is

$$P_y = z_0 \int_{-b}^{b} \rho(v_s \cos \beta) v_s \, dn = \rho I_2 v_{sm}^2 z_0 b \cos \beta, \tag{1.20}$$

where Eq. 1.2 was introduced into the above integral. Equating forces in the y direction to the rate of change of momentum in that direction yields

$$F_{py} + F_{sy} = \frac{\partial P_y}{\partial y}\, dy - \rho v_L\, dQ,$$

where F_{py} and F_{sy} are, respectively, the net pressure and shear forces in the y direction, with $\rho v_L\, dQ$ representing the momentum flux added to the control volume by the transverse lake current. Due to assumptions stated above, the rate of change of this momentum flux P_y must be balanced solely by the y component of the wind-shear force on the control volume and the momentum added by the entrainment of lake current across the lateral edges of the jet; i.e.,

$$\tau_w(2b\, ds) \cos\theta = \frac{\partial P_y}{\partial y}\, dy - \rho v_L\, dQ. \tag{1.21}$$

Inserting the form for dQ from Eq. 1.9 into Eq. 1.21 yields

$$\frac{d}{ds}(v_{sm}^2 b \cos\beta) = \frac{2v_{sm}v_L\alpha}{I_2} + \frac{2b\tau_w \cos\theta}{\rho z_0 I_2}. \tag{1.22}$$

Equation 1.22 expresses the balance between forces and momentum in the y direction.

(5) Energy-conservation Equation. In the momentum-dominated jet regime, turbulent diffusion of heat is assumed negligible so that the net convective flux of heat is balanced by the heat loss from the lake surface to the atmosphere. This can be expressed as

$$\frac{d}{ds}\left[\int_{-b}^{b} v_s(T - T_L)\, z_0\, dn\right] = -\int_{-b}^{b} K(T - T_L)\, dn, \tag{1.23}$$

where K is the coefficient of surface heat exchange. The equilibrium temperature is assumed here to be close to the lake temperature. If v_s and $T - T_L$ are replaced by their similarity forms, Eq. 1.23 becomes

$$T_c = T_{sm} + T_L = \frac{Q_0}{Q}(T_0 - T_L)\exp\left(-\frac{KI_4 t}{I_3 z_0}\right) + T_L, \tag{1.24}$$

where

T_c = jet centerline temperature

Q/Q_0 = dilution factor at distance s_m from the outfall where

$$Q = I_1 z_0 v_{sm} b_0, \tag{1.11}$$

$$Q_0 = I_1 z_0 v_0 b_0, \tag{1.11'}$$

$$I_3 = \int_{-1}^{1} f(n/b)\, g(n/b)\, d(n/b),$$

$$I_4 = \int_{-1}^{1} g(n/b)\, d(n/b),$$

and

$$t = \int_0^{s_m} \frac{ds}{v_{sm}} = \text{travel time from the outfall to position } s_m. \tag{1.25}$$

T_c may be calculated only when v_{sm} has been determined for centerline distances up to s_m. If surface heat loss is negligible, $K \approx 0$, Eq. 1.24 may be simplified to read

$$T_c = T_{sm} + T_L = (Q_0/Q)(T_0 - T_L) + T_L \tag{1.26}$$

Before Eqs. 1.14, 1.18, and 1.22 can be solved simultaneously for jet deflection β, jet half-width b, and centerline velocity v_{sm}, a form for the entrainment coefficient must be found. Once α is derived, the solution can proceed.

The authors assume that the effect of wind stress on entrainment is negligible. Upon setting $\tau_w = 0$, Eqs. 1.14, 1.18, and 1.22 reduce to

$$\frac{d}{ds}(v_{sm} b) = \frac{2\alpha}{I_1} v_{sm}, \tag{1.14'}$$

$$\frac{d}{ds}(v_{sm}^2 b \sin\beta) = 0, \tag{1.18'}$$

and

$$\frac{d}{ds}(v_{sm}^2 b \cos\beta) = \frac{2 v_{sm} v_L \alpha}{I_2}. \tag{1.22'}$$

Using Eq. 1.14' in Eqs. 1.18' and 1.22', two alternate expressions may be derived for α:

$$\alpha = \frac{I_1}{4}\left(\frac{db}{ds} - b \cot\beta \frac{d\beta}{ds}\right) \tag{1.27}$$

and

$$\alpha = -\frac{v_0 I_2 b_0^{1/2}}{2 v_L} \frac{b^{1/2}}{(\sin\beta)^{3/2}} \frac{d\beta}{ds}. \tag{1.28}$$

Thus α is described as a function of the rate of spread db/ds and the curvature $d\beta/ds$ for a jet with zero wind shear. From Eqs. 1.27 and 1.6,

$$\alpha = \frac{\sqrt{2}I_1C_1}{4} - \frac{I_1}{4} b \cot \beta \frac{d\beta}{ds}. \tag{1.29}$$

Since $d\beta/ds < 0$, α increases with distance from the outfall. In the Lake Monona application of the theoretical model, α was taken to be

$$\alpha = \frac{\sqrt{2}I_1C_1}{4} \tag{1.30}$$

as a first approximation; then α was allowed to vary as in Eq. 1.29 to ascertain the effects of a variable α, defined as α_v. The entrainment coefficient α_v, when included in the analysis, was shown to provide only insignificant improvement over use of the constant α of Eq. 1.30.

The form for the constant α is identical to the straight jet case: β = constant = 90° ($d\beta/ds = 0$) and $v_L = 0$. For a linear-spread assumption $b = \sqrt{2}C_0 s_m + b_0$,

$$\alpha = \frac{\sqrt{2}I_1C_0}{4}, \tag{1.31}$$

where C_0 is the rate-of-spread coefficient of a buoyant surface jet issuing into a stagnant lake.

Although the general problem involves solving Eqs. 1.14, 1.18, and 1.22 for the variable α, the authors focus attention on the constant-α case based upon the Lake Monona results. These equations may be written in nondimensional form for the constant α represented by Eq. 1.30 by defining

$$\gamma = \frac{z_0 v_s m b I_1}{z_0 v_0 b_0 I_1} = \text{dimensionless volume flux,} \tag{1.32}$$

$$m = \frac{z_0 v_s^2 m b}{z_0 v_0 b_0 v_L} \frac{I_2}{I_1} = \text{dimensionless momentum flux,} \tag{1.33}$$

and

$$\xi = \frac{s_m z v_L}{z_0 v_0 b_0} \frac{2\alpha}{I_2} = \text{dimensionless centerline distance.} \tag{1.34}$$

If

$$h = m \sin \beta = \text{x component of dimensionless momentum flux} \tag{1.35}$$

and

$$\nu = m \cos \beta = \text{y component of dimensionless momentum flux,} \tag{1.36}$$

Eqs. 1.14, 1.18, and 1.22 become

$$\frac{d\gamma}{d\xi} = \frac{m}{\gamma}, \tag{1.37}$$

$$\frac{dh}{d\xi} = \frac{\gamma^2}{m} \ell_x, \tag{1.38}$$

and

$$\frac{d\nu}{d\xi} = \frac{\gamma^2}{m} \ell_y + \frac{m}{\gamma}, \tag{1.39}$$

where

$$\ell_x = 2\left(\frac{I_2}{I_1}\right)^2 \frac{\tau_w \sin \theta}{\rho \alpha v_L^2} \frac{v_0 b_0}{v_L z_0} \tag{1.40}$$

and

$$\ell_y = 2\left(\frac{I_2}{I_1}\right)^2 \frac{\tau_w \cos \theta}{\rho \alpha v_L^2} \frac{v_0 b_0}{v_L z_0}. \tag{1.41}$$

The boundary conditions associated with Eqs. 1.37-1.39 are given at $s_m = 0$ ($\xi = 0$):

$$\gamma = 1, \tag{1.42}$$

$$\nu = \nu_0 = m_0 \cos \beta_0, \tag{1.43}$$

and

$$h = h_0 = m_0 \sin \beta_0, \tag{1.44}$$

where β_0 is the angle of the outfall centerline with the shoreline.

Due to the τ_w terms, the solution to Eqs. 1.37-1.39 has to be obtained numerically. If, however, the wind shear stress is negligible, τ_w may be assumed to be zero giving $\ell_x = \ell_y = 0$ whereby Eqs. 1.37-1.39 reduce to

$$\frac{d\gamma}{d\xi} = \frac{m}{\gamma}, \tag{1.37'}$$

$$\frac{dh}{d\xi} = 0, \tag{1.38'}$$

and

$$\frac{d\nu}{d\xi} = \frac{m}{\gamma}. \tag{1.39'}$$

These three nonlinear, first-order differential equations may be solved simultaneously to yield an explicit solution. For given values of v_0, b_0, z_0, T_0, T_L, v_L, K, α, and C_1, the solution for each ν may be written by the following series of calculations:

$$m_0 = \frac{I_2}{I_1}\frac{v_0}{v_L}, \tag{1.45}$$

$$\psi = \frac{2\alpha}{I_2}\frac{v_L}{v_0 b_0}, \tag{1.46}$$

$$m = (h_0^2 + \nu^2)^{1/2}, \tag{1.47}$$

$$v_{sm} = \frac{I_1}{I_2}\frac{m v_L}{\nu + 1}, \tag{1.48}$$

$$\xi = m + \ln(\nu + m) - h_0 - \ln(h_0), \tag{1.49}$$

$$\zeta = \tan^{-1}(\nu/h_0) + h_0 \ln(m/h_0), \tag{1.50}$$

$$\eta = \nu - h_0 \tan^{-1}(\nu/h_0) + \ln(m/h_0), \tag{1.51}$$

$$h = \frac{\gamma v_0 b_0}{v_{sm}}, \tag{1.52}$$

$$s_m = \frac{\xi}{\psi}, \tag{1.53}$$

$$\beta = \tan^{-1}(h_0/\nu), \tag{1.54}$$

$$x = \frac{\zeta}{\psi}, \tag{1.55}$$

$$y = \frac{\eta}{\psi}, \tag{1.56}$$

and

$$Q = I_1 b v_{sm} z_0. \tag{1.11}$$

If $K \approx 0$, then

$$T_{sm} = \frac{Q_0}{Q}(T_0 - T_L) \tag{1.26a}$$

and

$$T_c = T_{sm} + T_L. \tag{1.26b}$$

If K is not negligible, then

$$t = \int_0^{s_m} \frac{ds}{v_{sm}} \tag{1.25}$$

must be calculated by a numerical integration based upon previous values of v_{sm}. Then

$$\left.\begin{aligned} T_{sm} &= \frac{Q_0}{Q}(T_0 - T_L)\exp\left(-\frac{KI_4 t}{I_3 z_0}\right) \\ &\text{and} \\ T_c &= T_{sm} + T_L. \end{aligned}\right\} \tag{1.24}$$

d. Application to Lake Monona and Discussion

The above model was applied to the Blount Street and Livingston Street shoreline outfalls of the 190-MWe Madison Gas and Electric power plant on Lake Monona. The shoreline outfalls are 640 ft apart, with only negligible jet interference between each other. The geometry is given in Fig. 1.2. The Livingston Street intake-outfall system circulates 140 cfs through its condensers. Attention will be primarily focused on this outfall system since it is more typical of a general shoreline outfall.

The model described in Sec. c above could not be applied to either outfall without some modifications. First, no regime of flow establishment was taken into consideration in the model development during which the "top-hat" velocity and temperature distributions at the end of the discharge canal warp or change into bell-shaped forms. In general, a potential core region exists in which the effects of turbulent shear have an opportunity to work their way inward and affect the velocity distribution. Second, the average lake depth within 200 ft of the shore is 1 m or less, which stimulates

significant initial vertical mixing of the jet by bottom effects not considered in the model. Beyond 200 ft, the bottom influences were negligible and the jet spread with an approximately constant depth of 1 m. Third, the Livingston Street outfall was submerged 2 ft below the average lake level. Moreover, the outfall channel was not completely rectangular, being partly eroded and having a concrete partition down the middle. With these problems at hand, the authors found it necessary to use the above model to develop empirical correlations for the quantities v_0 and α in terms of wind-speed measurements. Uncertainties in the lake-current measurements required an empirical correlation for v_L too.

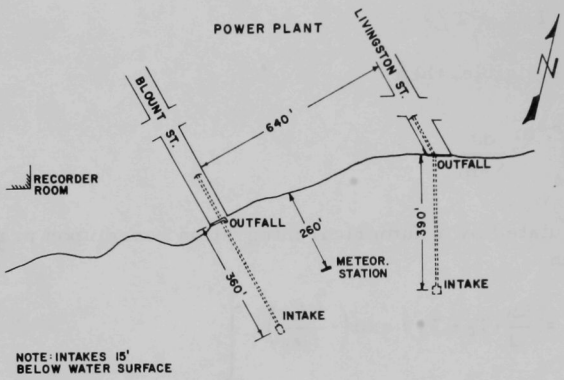

Fig. 1.2. Prototype Situation for Two Outfalls on Lake Monona[1a]

To obtain these correlations, the authors used nine of their 22 field surveys of the plume characteristics at the Blount Street and Livingston Street outfalls. In each field study, jet velocities and temperatures were measured by boat. All 22 surveys provided a wealth of data; unfortunately, none of them was fully adequate. No reliable data were taken within the first 200 ft of the outfalls. Data taken from drogue and temperature surveys were generally inadequate to completely define the axial and transverse jet-velocity profiles. It was difficult to determine whether the transverse velocity distributions were Gaussian; yet, a unique jet centerline was determined about which the field data were normally distributed. The axial and transverse temperature data were even less satisfactory. The centerline temperature decay was similar in form to that of the velocity, but transverse temperature distributions were not well defined and often appeared to be flat, probably due to data-collection techniques. Some surveys, however, did yield Gaussian-like transverse temperature distributions.

Considerable smoothing of field data had to be undertaken to provide usable curves for calculating the desired parameters. There were scatter in the data and some deviation from steady-state relationships. Field

situations were often extremely difficult. The wind was seldom steady, and the power plant did not keep an on-line steady power output during all surveys. From the observations of the investigators, the plumes were not steady in a short period of, say, 4 hr. They attempted, therefore, to confine their field measurements to a period of about 1 hr, and thus they seldom were able to extend their observations beyond 1000 ft from either outfall on any given survey.

Apart from wind speed and power-output changes, the plumes seemed to have wriggles in them that many later researchers have observed. These wriggles indicate that significant plume meandering was taking place. Erratic behavior was found from the standpoint of the temperature measurements in the measurable edges (or limits) of the plume; in fact, these measurements, more than the velocity measurements, convinced the authors that their plumes were meandering quite a bit and that all measurements were yielding more of an average picture of the plume configuration over a period of time, rather than an instantaneous or synoptic picture. This meandering phenomenon was not considered in the model development.

Wind-shear stress was not determined in any of the field surveys. Consequently, the authors had to refer to available literature to obtain relationships between wind stress and wind speed in order to estimate the effect the wind had on each plume observed in the field.

In spite of the abundant yet generally disappointing data, the authors were able to use it to yield a first-approximation judgment on the coefficients and parameters of interest for the model verification. Nine of their best surveys were reduced in detail to yield wind-speed correlations for v_0, α, and v_L to be used in applying the theoretical model. Comparisons of the model incorporating these correlations with all 22 plume surveys were then carried out.

The field data from the nine surveys were reduced as follows: First, a best-fit Gaussian velocity distribution was determined about an estimated jet centerline for each survey. Then the centerline velocity v_{sm} and jet width $b = \sqrt{2}\sigma$ (σ being the standard deviation of the fitted Gaussian distribution) were obtained at five or six positions of s_m along the centerline. The jet curvature β, and centerline temperature T_{sm} were scaled from the map of streamlines acquired from drogue studies for those locations. Using these values of b, v_{sm}, T_{sm}, and β obtained at those particular positions of s_m in addition to the measured values of Q_{0a} (power-plant pumping rate), T_0, T_L, v_L, and W, the authors used the mathematical model to define the "apparent" outfall velocity v_0 and entrainment constant α for each position s_m. These "apparent" parameters in part compensate for the strong vertical mixing near the Livingston Street outfall, for the fact that it is submerged about 2 ft and not completely of rectangular shape, and finally for the fact that no flow-establishment region was considered in the model. The

resulting values of v_0 and α for each survey were averaged and then correlated with wind speed. These correlations are, for the Livingston Street outfall,

$$v_0 = 2.0 + 9.9W \tag{1.57}$$

and

$$\alpha = 0.04 + 0.055W, \tag{1.58}$$

where W is the wind speed measured in mph and v_0 is in cm/sec. Lake-current velocities were determined directly by measuring asymptotic jet velocities and indirectly by determining apparent outfall characteristics. Correlating these characteristics with wind speed yielded

$$v_L = 0.90 + 0.60W. \tag{1.59}$$

With these empirical evaluations for parameters v_0, α, and v_L, the authors compared the mathematical model to the data obtained in the 22 surveys. Additional parameters required were

W = wind speed (for use in Eqs. 1.57-1.59),

T_L = lake temperature,

K = surface heat-loss coefficient,

z_0 = depth of discharge = depth of plume,

Q_{0a} = power-plant discharge rate,

b_0 = "apparent" outfall width determined by

$$b_0 = \frac{Q_{0a}}{I_1 v_0 z_0}, \tag{1.60}$$

C_1 = rate-of-spread coefficient evaluated from

$$\alpha = 0.528C_1,$$

and

τ_W = wind-shear stress (graph to be described later)

in the use of Eqs. 1.45-1.56, 1.11, and 1.26.

Figure 1.3 compares model predictions with data taken at the Livingston Street outfall on August 10, 1966. Negligible shear stress was assumed in addition to α = constant in the application of the model. Figure 1.3 represents one of the nine surveys used to establish the v_0, α, and v_L correlations given above. There is reasonably good agreement between predicted and observed jet characteristics here. In general, the comparisons

made with the other 21 surveys yielded model predictions of centerline velocity and temperatures within 2 cm/sec and 1°C, respectively, of field observations. Jet curvatures and widths did not compare as well with field measurements. Two facts must be noted: First, the theoretical model and field measurements were compared beyond 200 ft of the outfall, where centerline temperatures and velocities were near ambient values due to the vigorous mixing within the 200-ft region. Second, the scatter between the data and model predictions may be due to inadequate definition of the jet-velocity distributions from the data and the resultant effect of the inadequate definition on the subsequent determinations of the jet centerline, curvature, and width.

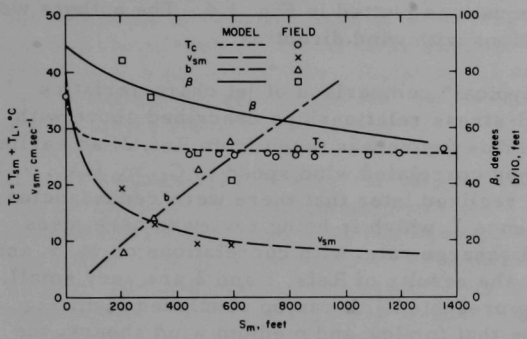

Fig. 1.3

Jet Characteristics for Livingston Street Outfall, August 10, 1966.[1a] Wind direction and speed: SE, 5 mph; Q_{0a} = 40.2 x 10^5 cm^3/sec; T_0 = 35.7°C; T_L = 24.2°C; β_0 = 90°; v_0 = 51.5 cm/sec (Eq. 1.57); v_L = 3.9 cm/sec (Eq. 1.59) and α = 0.32 (Eq. 1.58).

The above paragraph referred to comparisons made when $\tau_W = 0$ and α = constant. Similar comparisons were made with wind-shear stress given by Eq. 1.1 and α = constant. Since no wind-stress measurements were made in any of the field studies, values for τ_W and hence the drag coefficient were selected from the available literature. However, there is an extremely large range for wind-stress values for a given W, as can be seen from Fig. 1.4. Curves 1 and 2 are relationships derived from the spiral solutions of Rossby and Ekman, respectively. Curves 3 and 4, derived by Stearns, are wind-stress equations for stable and unstable conditions over Lake Mendota. All four are discussed in Ref. 5. Curves 5 and 6 are wind-stress equations of Ekman and Hellstrom, respectively, found in

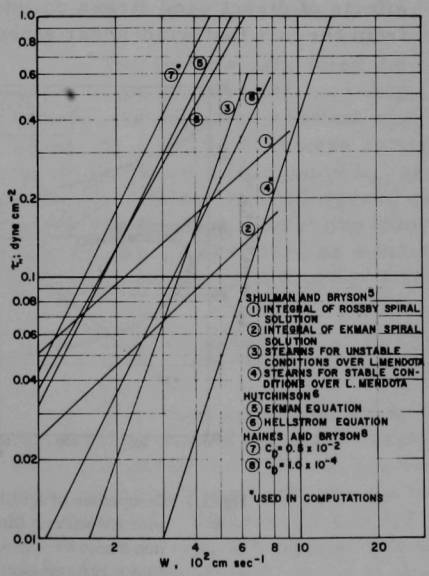

Fig. 1.4. Wind Stress, τ_W, vs Wind Speed[1b]

Ref. 6. Each of the above curves is of the form of Eq. 1.1 except that the wind speed has an arbitrary constant power for the factor W.

From the range of C_D values (0.0001-0.005) presented in Ref. 7 and the Haines and Bryson correlation formula between lake currents and wind speed for Lake Mendota,[8]

$$v_L = 1.17W - 0.045W^2, \quad (0 < W < 12) \tag{1.61}$$

curves 7 and 8 were derived. Curves 7, 8, and 4 were used to represent a range of wind-stress effects in the mathematical model. They represent high, medium, and low wind stresses at a given wind speed. These curves tend toward the mean of the equations plotted in Fig. 1.4. The authors were not able to make any correlations with wind direction.

Figure 1.5 shows a "typical" comparison of jet characteristics resulting from the three wind-stress relationships described above with the zero-wind-stress case. [This figure was taken from Ref. 2, an earlier work of the authors, where they correlated wind speed to C_1, m_0 (i.e., v_L), v_0b_0 (i.e., Q_0), and v_0. It was realized later that there were redundancies in these correlations. Reference 1, which is being reviewed here, uses Q_{0a}, the actual power-plant discharge rate, with correlations on v_0, α, and v_L. The differences between the results of Refs. 1 and 2 are very small, and hence this figure is being presented.] It can be concluded from Fig. 1.5 and from the other 21 surveys that for low and medium wind shears, the effects of direct wind stress on jet characteristics are minor. However, from the fact that wind-shear stresses were not measured and field data

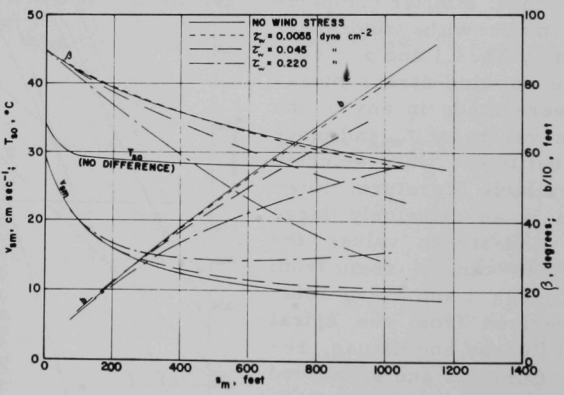

Fig. 1.5. Comparison of Jet Characteristics for Mathematical Models with and without Direct Wind Stress; July 17, 1966; Livingston Street.[1b] β_0 = 90°; Wind = NW 5-6 mph; v_0b_0 = 53.4 x 10^3 cm^2/sec; v_0 = 31.6 cm/sec; T_0 = 35.0°C; T_L = 26.9°C; v_L = 5.0 cm/sec; C_1 = 0.592; α = 0.312.

were in reasonable agreement with the theoretical model with no wind shear, the authors conclude that the effects on the jet characteristics for the near-shore region of Lake Monona are negligible.

The three-approximation method in the use of Eq. 1.1 to represent direct wind-stress effects (i.e., the use of curves 4, 7, and 8 for each field survey) represents only a simplified approach to assess whether wind stress is significant. In a zone-of-flow establishment where the jet momentum is the dominant factor and the jet is very active, Eq. 1.1 is expected to yield accurate results. Yet, far away from the outfall, well into the receiving water, more accurate relationships could perhaps have been developed if actual shear stresses had been measured in the field surveys. In reality, for distances of even 1/2 mile or so in the Lake Monona case, a small wind could be important, as far as deflecting the centerline due to its cumulative effect over a period of time. Equation 1.1 actually represents wind shear past a solid body, and its use for plumes in lakes yields only a first approximation to the actual value of τ_w.

To ascertain whether the depth of the jet was really constant, velocity and temperature measurements were taken at a depth of 1 m. The temperature distribution proved to be flat and equal to the average lake temperature and subsurface drogues indicated a jet thickness of 1 m within 400 ft of the outfall. The authors derived a coefficient k to represent the rate of vertical entrainment. Model calculations with k = 1.0 (no vertical entrainment) seemed to agree best with the available field data. Hence the authors feel justified in neglecting vertical entrainment in their relationships.

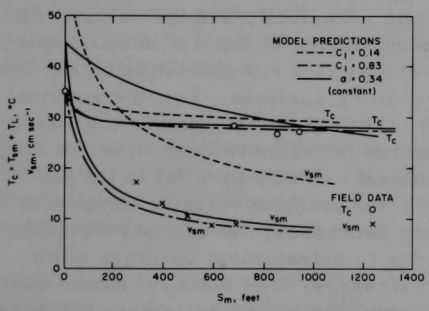

Fig. 1.6. Comparison of Jet Characteristics v_{sm} and T_c for Constant and Variable Entrainment Coefficients for Livingston Street Survey; July 27, 1966.[1b] Wind speed and direction: NW, 5–6 mph; Q_{0a} = 40.2 x 10^5 cm^3/sec; T_0 = 35.0°C; T_L = 26.9°C; β_0 = 90°; v_0 = 56.5 cm/sec (Eq. 1.57); v_L = 4.2 cm/sec (Eq. 1.59); α = 0.34 (Eq. 1.58).

The authors calculated the effect on jet characteristics using a variable-entrainment constant α_v. Equations 1.27 and 1.28 were solved for β and α_v as a function of s_m assuming the linear rate-of-spread relationship Eq. 1.6. Centerline velocity v_{sm} was also determined as a function of s_m by setting τ_w = 0 in Eq. 1.18:

$$v_{sm} = \frac{v_0 \sqrt{b_0}}{\sqrt{b \sin \beta}} \qquad (1.62)$$

With T_{sm} approximated by Eq. 1.26, predicted jet characteristics were compared for different values of C_1 in the α_v model with the model α = constant. Figures 1.6 and 1.7 represent a "typical" comparison with field data taken July 27, 1966 at the

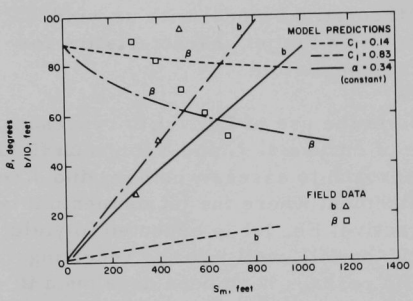

Fig. 1.7. Comparison of Jet Characteristics b and β for Constant and Variable Entrainment Coefficients for Livingston Street Survey; July 27, 1966.[1b] Same initial conditions as in Fig. 1.6.

Livingston Street outfall. The constant value of α obtained from wind correlations (i.e., Eq. 1.58) for that set of field data was $\alpha = 0.34$. The associated C_1 by Eq. 1.30 is $C_1 = 0.64$. The graphs reveal that $C_1 = 0.14$ (rate of spread for two-dimensional jet in stagnant fluid) and $C_1 = 0.83$ in the α_v case yield significantly different results from the experimental data. $C_1 = 0.64$ yields essentially identical curves to model predictions with $\alpha = 0.34$. The variable α_v model was not pursued further by the authors because it did not yield appreciably improved results in most of the field surveys.

e. Remarks on Major Model Assumptions

A weak point in the model involves the authors' analysis of entrainment. A more exact definition of entrainment than that given by Eqs. 1.9 and 1.10 is given by

$$dQ = \alpha(v_{sm} - v_L \cos \beta)\, z_0\, ds, \tag{1.63}$$

where velocity relative to the lake current is employed. Ellison and Turner,[4] Keffer and Baines,[9] Morton,[2] and Fan[3] all have defined entrainment in terms of the difference between a characteristic jet velocity and the velocity of the moving ambient current. The authors' choice of Eq. 1.9 in which entrainment is related solely to the jet velocity is a simplification of Eq. 1.63 used to reduce the complexity of the resulting analysis. Yet, the authors' definition is really applicable only when the jet is orthogonal to the shore-parallel ambient flow ($\beta = 90°$) or when the jet velocity is an order of magnitude larger than the component of ambient velocity parallel to the jet centerline. As the jet continues to bend, the ambient velocity component increases and the jet centerline velocity decreases; the velocity field becomes nearly uniform and the mixing due to entrainment becomes quite small due to the reduced lateral shear stresses. The authors' model does not take this into account, and consequently, for distances farther offshore when the jet velocities have fallen off to the same order of magnitude as the lake velocity, Eqs. 1.9 and 1.10 will not be a good approximation to Eq. 1.63 for the rate of entrainment.

The entrainment definitions of Eqs. 1.9 and 1.10 and even Eq. 1.63 had been used exclusively in the past in submerged-buoyant-jet problems. The authors tried to develop more elaborate deterministic relationships for entrainment; yet they decided to rely on Eqs. 1.9 and 1.10 more as a matter

of experience and convenience rather than theoretical judgment. In the 22 field surveys, α varied from 0.063 to 0.497, which, although considerably larger than values obtained for jets discharging into a stagnant medium [α = 0.074-0.057 (Ref. 9)], are justifiable only "in a ballpark sense." A larger α is partially due to the fact that lateral stresses were neglected and more importantly to the fact that the crossflow increases entrainment due to vortices attached to the down-current side of the jet. In spite of the somewhat surprising success in the authors' treatment of entrainment, a definition of entrainment involving relative velocity above the current would clearly be preferable.

The assumption of similar profiles for velocity and temperature in a jet with crossflow is also not strictly valid, yet was useful in the model development from the standpoint of the predictable accuracies in obtaining the general shape of the plume, its configuration, the centerline velocities, etc. The only real justification for this assumption was that the similarity assumptions proved to be good enough for at least a first approximation upon comparison of the theoretical model with the field data. Field measurements were not good enough to completely accept or refute these similarity assumptions; the measurements did, however, support their use from a statistical rather than a theoretical standpoint.

A weaker assumption of the model is that it does not handle the lack of symmetry on windward and leeward sides of the jet. This is reflected in an obvious change in entrainment coefficients on both sides of the jet. Large eddies on the down-current side cause more extensive spreading on that side. This asymmetry is easily seen from thermal imagery, where, on the upstream side of the jet, the isotherms are more closely packed together than on the down-current side. The authors' analysis does not handle that problem at all.

The linear rate of spread of the jet, although strictly valid for a non-buoyant jet in a stagnant medium, seemed to be supported quite well by the data taken at Lake Monona. This is perhaps due to the high magnitude of the turbulence involved in the measured jet region. Beyond the zone of established flow, that assumption is expected to be invalid.

Due to the predominance of jet momentum in the region of field measurements, the authors felt justified in neglecting horizontal pressure gradients due to buoyancy. In the region of flow where the jet velocities are roughly equal to the lake-current velocity, that assumption is not expected to be valid. The pressure-gradient force there could influence the lateral spreading. This force is not expected to affect the momentum balance in the direction of the jet, but rather laterally, resulting in a greater rate of increase of jet width. Although seemingly justifiable in the Lake Monona case, this assumption severely limits other applications of the model; for other outfall situations, that assumption should be weighed very carefully.

The magnitude of pressure gradients due to curvature or jet bending are impossible to verify experimentally. The authors could find no practical way of considering these gradients in the model. Jet-bending gradients were definitely not negligible because vortices within the jet were identifiable from the behavior of the drogues in the lake. Ignoring the effects of pressure gradients that exist across the jet parallel to the ambient current in predicting the deflection of the jet is a further weak point of the model.

No clear statement can be made concerning the assumption of neglecting the lateral shear stresses. Much better measurements are required to support or reject that assumption in the field. Neglecting a region of flow establishment is a more serious deficiency, which may cause difficulties in other applications away from Lake Monona.

Concerning the similarity forms for f and g, the field measurements on Lake Monona did not provide enough evidence to reveal any different rates of lateral spreading between momentum and heat. Consequently, f and g were both assumed to have a Gaussian form in the theory.

In conclusion, the authors found that neglecting the vertical-entrainment coefficient k and the variation of α_v with distance from the outfall and ignoring small and medium direct-wind-stress effects on the jet seems justified by experimental verification in the Lake Monona case, since the improvements obtained by including them in the model comparisons are minor. These conclusions have been reached with a model that ignores such things as lateral shearing stresses, a seemingly more exact definition of entrainment, a region of flow establishment, and the sundry pressure gradients involved, as was previously discussed, in addition to such other factors as unsteadiness, spatially varying lake currents, and lake-current components parallel to the outfall centerline. Expansion of the model to include all these factors is recommended by Hoopes, Zeller, and Rohlich.

f. Application of Model to General Outfall Situations

Because of the difficulties in accurately treating the first 200 ft, the Lake Monona situation was not an ideal situation from a modeling standpoint. The whole discussion of the difficulties involved in the acquisition of good field data reveals the problems that exist in checking a mathematical model with actual experimental data. The lack of an "ideal" rectangular-shaped discharge in the Lake Monona case added to the uneven bottom effects, which caused increased turbulence and vigorous vertical mixing within the vicinity of the discharge channels and required the authors to define "apparent" outfall parameters by working backwards from the region of established flow. From a general standpoint, the reliability and usability of the model are prejudiced a great deal by the behavior of the Blount Street and Livingston Street jets and the empiricisms that were used to verify the model

against the field measurements. This was the reason the authors split the field surveys into two parts: Nine were used to develop jet coefficients; all 22 were employed as test cases.

For an outfall situation where $\mathbb{F}_0 \gg 1$ and where bottom effects are expected (due generally to an area of very erratic behavior in the zone of flow establishment), the authors recommend the same method as that used for the Lake Monona case. (The authors know of no practical shoreline outfall situation in which the discharge behaves theoretically!) If no correlations of α, v_0, and v_L have been or can be made using previously determined plume data, the authors recommend that the forms for these parameters be adopted from the Livingston Street outfall case of Lake Monona (Eqs. 1.57-1.59). The "apparent" outfall width is defined from Eq. 1.60 and C_1 is determined from Eq. 1.61. With α, v_0, v_L, b_0, C_1, z_0, Q_{0a}, K, W, T_L, and T_0 as input parameters, Eqs. 1.45-1.56, 1.11, 1.24, and 1.25 are used if wind-shear stress is assumed negligible. Equations 1.37-1.41 (with boundary conditions of Eqs. 1.42-1.44) are to be solved numerically for a direct wind-shear stress taking on a medium to medium-to-high value. These two solutions should yield a range of possible effects caused by the wind.

When no bottom effects are considered, i.e., when the outfall ends in a vertical wall and $\mathbb{F}_0 \gg 1$, it is preferable to allow for an initial potential core region as an adjustment zone in which turbulent shear effects change the initial top-hat distribution into a Gaussian-like form. The length of this proposed flow-establishment region should be five to six actual outfall widths. If this adjustment region were actually employed as a flow-establishment region for the model, then the correlations developed above could not be used for the established flow region since they were not developed for that kind of situation.

Consequently, the authors recommend a less preferable alternative of using the identical method described above for the bottom interference case, except that v_0 be chosen as the actual outfall velocity rather than using its correlation formula (Eq. 1.57). Calculations in every case can proceed until the jet velocities reach 10-20% above the ambient lake current. At this location, the jet has slowed down to the point where the turbulence of the lake itself will override any effect of the jet. In any practical application of the model, the wind-speed correlations for v_L and α should be used, in keeping with the above remarks in order to account (in some empirical way, at least) for the initial flow expansion that occurs in the zone of flow establishment, the effect of any vertical mixing at the outlet, and the non-two-dimensionality of the flow right at the outlet resulting from various interfacial phenomena that occur[10] within a distance of a few feet from the outlet.

g. Two Final Comments

Concerning wind-speed correlations used to predict jet characteristics, some final remarks should be made. First, wind speed is not generally a reliable indication of the main factors affecting the plume. Ambient current and entrainment (or diffusivities) depend upon the previous history of the body of water under consideration and its motions in addition to its present environment. Surface waves, induced by winds that occurred hours before, still affect ambient entrainment and the ambient velocity. In fact, it has been observed in the field that plumes can have widely varying characteristics under seemingly identical conditions due to the time lag between a wind and its effects. Consequently, these and other simple wind-correlation formulas should be applied with caution.

Another general remark concerns the effects of wind shear on the plume. It can be argued that wind-induced stresses act not only on the plume but also on the ambient lake waters and therefore provide no incremental momentum flux to the plume. Sundaram[11] also shares this belief, recognizing the fact that wind shear affects plume dispersion by the introduction of wind-induced currents and waves. The mechanism and energy split of these two phenomena are not yet understood, but it is clear, however, that these phenomena do occur in a different manner over the plume than over the ambient lake water. Sundaram feels, however, that no methods are presently available to include the effects of these phenomena in a model. Thus the authors may be in error in their consideration of the effects of shear stress. To a certain extent this is true; however, Hoopes[12] stated that the authors envisioned the jet to be a layer approximately 1 m thick, the wind shear on the jet therefore acting over this thickness. Outside the jet, the wind effects would be felt either over the whole depth of the lake or at least down to the depth of the thermocline. Since the lake depth or thermocline is generally many times the jet thickness, it would be expected that changes in the ambient lake attributable to the wind would be smaller than the effects on the jet itself.

Sundaram also notes that the complexity involved in modeling wind effects is considerable when one recognizes that the ambient current structure will be generally nonuniform with depth. The top layers of the ambient receiving water typically travel at higher velocities and are strongly influenced by the wind and its variations. A sharp gradient in the current profile is often observed close to the surface. This makes plume dispersion essentially a three-dimensional problem where three-dimensional boundary conditions have to be supplied. Wind may also be a factor in the distribution of interfacial stress at the bottom of a stratified plume. This shear arises from the fact that momentum transfer (affected to some degree by wind) is not inhibited to the same extent as heat transfer. Most models ignore this interfacial friction.

References

1a. R. W. Zeller, J. A. Hoopes, and G. A. Rohlich, Heated Surface Jets in a Steady Crosscurrent, J. Hydraul. Div., ASCE 97, No. HY9, 1403-1426 (Sept 1971).

1b. J. A. Hoopes, R. W. Zeller, and G. A. Rohlich, Heat Dissipation and Induced Circulations from Condenser Cooling Water Discharges into Lake Monona, Report No. 35, Department of Civil Engineering, The University of Wisconsin (Feb 1968).

1c. R. W. Zeller, Cooling Water Discharges into Lake Monona, Ph.D. thesis, The University of Wisconsin, Madison, Wisconsin (June 1967).

2. B. R. Morton, On a Momentum-Flux Diagram for Turbulent Jets, Plumes, and Wakes, J. Fluid Mech. 10, 101-112 (1961).

3. Loh-Nien Fan, Turbulent Buoyant Jets into Stratified or Flowing Ambient Fluids, Tech. Report No. KH-R-15, W. M. Keck Laboratory of Hydraulics and Waters Resources, California Institute of Technology, Pasadena, California, June 1967, 196 pp.

4. T. H. Ellison and J. S. Turner, Turbulent Entrainment in Stratified Flows, J. Fluid Mech. 6, 423-448 (1959).

5. M. D. Shulman and R. A. Bryson, The Vertical Variation of Wind-Driven Currents in Lake Mendota, Limnology and Oceanography 6, 347-355 (July 1961).

6. G. E. Hutchinson, "The Effect of Wind in Generating Currents," A Treatise on Limnology, John Wiley & Sons Inc., New York, N.Y., 256-286 (1957).

7. W. S. Von Arx, Introduction to Physical Oceanography, Addison-Wesley, Redding, Massachusetts (1962).

8. D. A. Haines and R. A. Bryson, "An Empirical Study of Wind Factor in Lake Mendota," Limnology and Oceanography 6, 356-364 (June 1961).

9. G. N. Abramovich, The Theory of Turbulent Jets, The M.I.T. Press, Massachusetts Institute of Technology, Cambridge, Mass. (1963).

10. H. Stefan, Stratification of Flow from Channel into Deep Lake, J. Hydraul. Div., ASCE 96, No. HY7, Proc. Paper 7401, 1417-1434 (July 1970).

11. T. R. Sundaram, Hydronautics, Inc., private communication (1971).

12. J. A. Hoopes, private communication (1971).

2. A Preliminary Report on the Characteristics of a Heated Jet Discharged Horizontally into a Transverse Current: Part I. Constant Depth[1]

H. H. Carter
(Chesapeake Bay Institute, Johns Hopkins University)
November 1969

a. List of Symbols

A	Projected cross-sectional area normal to the crossflow
b	Lateral width of the equivalent top-hat distribution of excess temperature
b_0	Orifice width
C_d	Coefficient of drag
D	Depth of the jet
f	Fraction of a unit volume of jet fluid that is ambient fluid
f_{new}	Fraction of a unit volume of jet fluid that was water-entrained from the offshore side of the jet
g	Fraction of a unit volume of jet fluid that was water-entrained from the near-shore side of the jet
L	Length of large eddy on the lee side of the jet as measured downstream from the orifice
p	Pressure above that at $x = \infty$
dP	Drag force
q	Total velocity of jet at centerline
q_0	Initial jet velocity
Q	Initial volumetric flow rate $= b_0 D q_0$
R	Ratio of initial jet velocity to ambient velocity q_0/u_a
t	Time
u	x component of jet centerline velocity
u_0	x component of initial jet velocity
u_a	Ambient velocity
u_e	x component of velocity at the end of the zone of flow establishment
v	y component of jet centerline velocity
v_e	y component of velocity at the end of the zone of flow establishment

x	Distance measured from the orifice downcurrent along the shore
x_e	x coordinate at the end of the zone of flow establishment
y	Distance measured offshore from the orifice
y_e	y coordinate at the end of the zone of flow establishment
x_m	x coordinate of position of maximum penetration
y_m	y coordinate of position of maximum penetration
α	Angle between the jet centerline and the x axis
α_e	Value of α at the end of the zone of flow establishment
α_0	Initial value of α
ζ	Vertical distance measured downward from the surface
η	Lateral distance measured from the jet centerline
θ	Excess temperature at jet centerline
θ_b	Excess temperature of the ambient current
θ_b'	Excess temperature of water being entrained from the near-shore side
θ_i	Excess temperature of ambient fluid as it enters the intake canal
θ_j	Excess temperature of jet fluid as it leaves the discharge canal
θ_0	Excess-temperature rise across the condensers
ξ	Distance measured along the jet centerline from the orifice
ρ	Density of plume water
ρ_a	Ambient density
ψ	Streamline $= \int u\, dy$

b. Introduction

Carter has treated the problem of a jet in a transverse crosscurrent by both experimental and theoretical methods. His hydraulic experiments at the Chesapeake Bay Institute have yielded jet centerline-temperature decays and trajectories for situations in which R, the ratio of initial jet velocity q_0 to ambient current u_a, was 2, 5, and 10. Carter's centerline-temperature measurements, complemented by the experimental results of Rouse[2] on air jets, were the basis of the development of the mathematical model.

Figure 2.1 shows the physical situation treated by Carter. A heated effluent is discharged from a channel into a long, wide basin whose depth is uniformly the same as that of the discharge channel and in which a uniform crosscurrent is flowing at right angles to the discharge. The jet is assumed to be two-dimensional in which "equivalent" top-hat distributions are assumed for velocity and temperature across the width and depth of the jet. Variations are assumed to occur only with centerline coordinate. Carter envisions the jet as deflecting due to both pressure drag and entrainment of crossflow momentum. Only the jet trajectory up to the point of maximum penetration is considered.

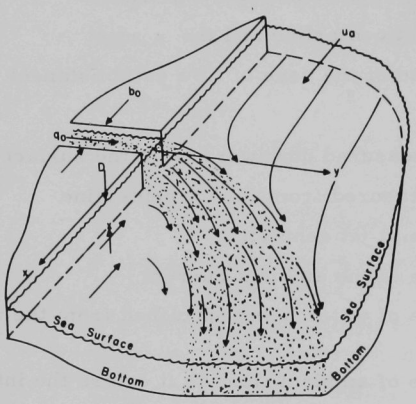

q_0 is the initial jet velocity,

u_a is the ambient velocity,

b_0 is the orifice width,

D is the depth,

R is the ratio of initial jet velocity to ambient velocity, q_0/u_a, and

Q is defined as $b_0 D q_0$

Fig. 2.1. Schematic Drawing of a Horizontal, Two-dimensional, Bent-over Jet[1]

Within the downstream limits of his measurements, Carter's laboratory experiments have shown that the centerline-temperature decay has a form apparently independent of R. This temperature distribution is then used as input to the theory to obtain predictions of the centerline trajectory, which are then compared to measured jet deflections. The scatter of the data is large, but the points are generally near the theoretical curves. Carter neglects buoyancy and surface heat loss in the model; this appears justified in his physical situation, yet the width of the jet is not measured and might readily be dependent on buoyant forces.

Carter's hydraulic experiments were carried out in a flume of effective width 2.306 ft, where the initial outfall width varied from 0.02 to 0.2 ft. Table 2.1 represents the statistics on the testing program carried out by Carter. These hydraulic tests were performed and the resulting mathematical model derived with the concern that the effective channel width (2.306 ft) was insufficient to eliminate far-shore boundary effects in the experimental setup for large values of R. Examination of temperature profiles from Tests 8-10 showed that at jet penetrations of $20b_0$ and $30b_0$, the far-shore temperature began to rise above background, indicating that the jet had spread sufficiently to cause heat to be reflected back into the

jet from the far-shore boundary. As a result, Tests 11-13 had been carried out as repeats of Tests 8-10 with respect to R, but with flume width/b_0 doubled by appropriate adjustments in Q, b_0, D, and u_a.

TABLE 2.1. List of Parameter Values in the Hydraulic Testing Program[a] (Ref. 1)

Test No.	Q, gpm	u_a, ft/sec	q_0, ft/sec	R	b_0, ft	D, ft
1	1.75	0.10	0.49	4.87	0.08	0.10
2	1.75	0.10	0.20	1.95	0.20	0.10
3	1.75	0.20	0.20	0.98	0.20	0.10
4	1.75	0.20	0.98	4.88	0.04	0.10
5	1.75	0.25	0.49	1.95	0.08	0.10
6	1.75	0.10	0.98	9.75	0.04	0.10
7	1.75	0.10	0.49	4.87	0.08	0.10
8	1.75	0.10	0.49	4.87	0.08	0.10
9	1.75	0.10	0.20	1.95	0.20	0.10
10	1.75	0.10	0.98	9.75	0.04	0.10
11	0.28	0.062	0.31	4.93	0.04	0.05
12	0.28	0.062	0.12	2.01	0.10	0.05
13	0.28	0.063	0.62	9.80	0.02	0.05

[a]All tests run with θ_0 = 10°F.

Carter has recently carried out similar hydraulic experiments in a flume approximately four times as wide, the width being 10 ft with orifice widths of about 1 in. Carter's bigger flume has a larger heat source in addition to an increased pumping rate, yet produces the same initial excess temperature. The new depth of the orifice is also somewhat different. All new parameters are the same order of magnitude as the old ones, but are not identical. Unexpected differences in the trajectories measured before were noticed, apparently because the new flume width is much larger in terms of diameters, reducing far boundary effects that were evidently significant in the smaller flume. As far as the dilutions measured, the centerline temperature decay seemed unaffected by the relative position of the far shore. These facts shed some doubt as to the efficacy of the mathematical model developed from the observations of the small flume results. Consequently, Carter emphasizes that the results he obtained and the mathematical model he developed in Ref. 1 are only preliminary. In spite of the preliminary nature of his report, he has his own interpretation of plume physics and plume modeling that is significant for inclusion in this state-of-the-art summary. Recognizing the problems involved, Carter urges caution in the applicability of his predictive model to situations in which the river or lake widths are larger than 12-60 initial outfall widths. Carter is presently carrying on additional flume experiments to ascertain

the proper relationship of the variables of the problem (including distance to the far shore) on the jet trajectory. When the laboratory experiments are completed and the data are fully analyzed, he intends to institute improvements in his present model where required. Carter's existing model will now be described, including a discussion of the assumptions made and a comparison of his model with his smaller flume data.

c. Model Description

Carter's main premise is that a jet in a crosscurrent can be considered as an obstruction in a uniform stream. This assumption has been made by others and is supported in some small degree by Carter's flume observations. Some of the ambient current is accepted by the jet, while the rest of the oncoming stream is deflected around the jet much the same as fluid reflected by a solid body. Consequently, the total pressure force normal to the jet is assumed to be given by

$$\text{drag force} = \frac{\rho_a C_d A u_a^2}{2}, \tag{2.1}$$

where C_d is the coefficient of drag, A is the cross-sectional area normal to the jet centerline, and u_a is the velocity of the flow. This form for the pressure force is analogous to the measure of total drag of solid bodies in a uniform crossflow, usually used in hydraulics or fluid mechanics. The usual drag coefficient C_d measures the relative total resistance of solid bodies of the same cross-sectional area under the same flow conditions. Employed in the liquid-jet case, Eq. 2.1 is assumed to act pointwise so that C_d is variable and defined locally as the ratio of the pressure acting on the element of area $d\xi$ D to the excess of pressure at a stagnation point over that at $x = \infty$. An incremental distance along the jet centerline trajectory is denoted as $d\xi$. The precise value of C_d must be determined experimentally and is, essentially, an added parameter which allows the measured jet trajectories to match the theoretical predictions. This drag-force formula represents a crude attempt to account for the pressure distribution set up between the offshore and near-shore sides of the jet due primarily to the flow separation on the near-shore side. A second justification for Eq. 2.1 may lie in the wind-tunnel pressure measurements of Rouse,[2] which indicated that the pressure distribution set up across an air jet is much like that across a solid body obstructing a fluid flow.

Carter develops his governing equations from the definition sketches given in Fig. 2.2. According to Rouse and Carter, the faces of the outlet exert a force downstream due to the pressure gradient across them, causing the jet to attain some x momentum at the orifice. A balance of forces and momentum in the x direction yields, from Fig. 2.2B the integral equation

$$d[\rho uqb(\xi)D] = d[\rho_a u_a fqb(\xi)D] + dP_x, \tag{2.2}$$

where the first and second terms on the right-hand side of Eq. 1.2 represent momentum changes due to entrainment and drag, respectively, f is defined as the fraction of the control volume that is ambient fluid, u_a is the uniform ambient velocity, q is the total velocity of the jet at the centerline, u is its x component, b is the lateral width of the equivalent top-hat distribution, and the drag force dP is assumed to be represented by

$$dP = \tfrac{1}{2}C_d\rho_a u_a^2\, d\xi\, D. \tag{2.3}$$

Thus

$$dP_x = dP \sin\alpha = \tfrac{1}{2}C_d\rho_a u_a^2\, dy\, D \tag{2.4}$$

and

$$dP_y = dP \cos\alpha = \tfrac{1}{2}C_d\rho_a u_a^2\, dx\, D, \tag{2.5}$$

where α is the angle between the jet centerline and the x axis.

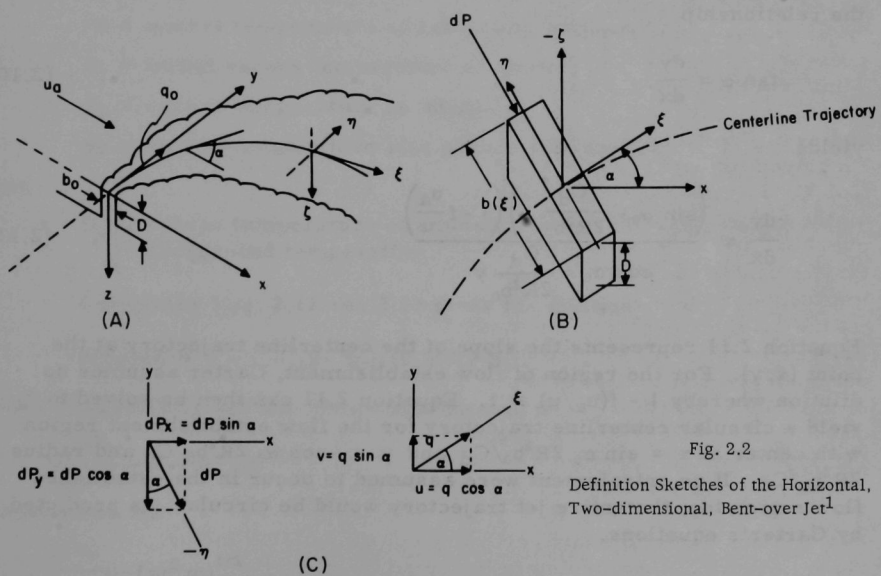

Fig. 2.2

Definition Sketches of the Horizontal, Two-dimensional, Bent-over Jet[1]

Balancing the rate of change of y momentum in the control volume with the y component of the pressure drag yields

$$d[\rho vqb(\xi)D] = -dP_y, \tag{2.6}$$

where v is the offshore component of the centerline velocity q. Substituting Eqs. 2.4 and 2.5 into Eqs. 2.2 and 2.6, respectively, and then integrating the result from the orifice $\xi = 0$ to the arbitrary centerline position ξ, yields

$$\left(\frac{q}{q_0}\right)^2 \frac{b(\xi)}{b_0} \cos\alpha \left(1 - f\frac{u_a}{u}\right) = \cos\alpha_0 + \frac{C_d}{2R^2 b_0} y \tag{2.7}$$

and

$$\left(\frac{q}{q_0}\right)^2 \frac{b(\xi)}{b_0} \sin\alpha = \sin\alpha_0 - \frac{C_d}{2R^2 b_0} x, \tag{2.8}$$

where

$$R \equiv q_0/u_a \tag{2.9}$$

and where the orifice boundary conditions $x = 0$, $y = 0$, $q = q_0$, $u = u_0$, $v = v_0$, $f = 0$, and $b = b_0$ were used. It has been implicitly assumed in the above integration that the ambient density ρ_a is approximately equal to the density ρ of the plume water. Dividing Eq. 2.8 by Eq. 2.7, with the relationship

$$\tan\alpha = \frac{dy}{dx}, \tag{2.10}$$

yields

$$\frac{dy}{dx} = \frac{\left(\sin\alpha_0 - \frac{C_d}{2R^2 b_0} x\right)\left(1 - f\frac{u_a}{u}\right)}{\cos\alpha_0 + \frac{C_d}{2R^2 b_0} y}. \tag{2.11}$$

Equation 2.11 represents the slope of the centerline trajectory at the point (x, y). For the region of flow establishment, Carter assumes no dilution whereby $1 - f(u_a/u) \equiv 1$. Equation 2.11 can then be solved to yield a circular centerline trajectory for the flow establishment region with center at $x = \sin\alpha_0\, 2R^2 b_0/C_d$ and $y = -\cos\alpha_0\, 2R^2 b_0/C_d$ and radius $2R^2 b_0/C_d$. If no entrainment were assumed to occur in the established flow region too, the entire jet trajectory would be circular, as predicted by Carter's equations.

For the region of established flow, however, Carter assumes that $u = u_a$ for all points. This assumption basically replaces the need for a continuity equation and permits a graphical integration of Eq. 2.11 in that region. Carter has no hard evidence to support that assumption, other than

his observation that the flow very rapidly turned parallel to the ambient current in the general case. The assumption will obviously be weak in the vicinity of the end of the flow-establishment region for larger R. In the zone of established flow, therefore, $1 - f(u_a/u) = 1 - f$, where f varies with centerline distance ξ. For $1 - f$ = constant, Carter states that the trajectory is an ellipse with the same center but with semimajor axis given by $2R^2b_0/C_d$ and semiminor axis given by $(1 - f)^{1/2}\, 2R^2b_0/C_d$.*

The determination of jet entrainment was obtained experimentally. Carter defines dilution as the fraction of a unit volume that was initially part of the jet discharge; the remainder was part of the ambient stream and denoted f. Neglecting surface heat transfer, Carter writes

$$\theta(\xi) = [1 - f(\xi)]\, \theta_j + f(\xi)\theta_b \tag{2.12}$$

and

$$\theta_j = \theta_0 + \theta_i, \tag{2.13}$$

where

θ = excess temperature at centerline position ξ,

θ_j = initial excess temperature of the jet,

θ_i = excess temperature at intake,

θ_0 = excess temperature rise across condensers,

and

θ_b = excess temperature of ambient current or, equivalently, the background temperature.

Combining Eqs. 2.12 and 2.13 gives the dilution

$$\text{dilution} \equiv 1 - f = (\theta - \theta_b)/(\theta_0 + \theta_i - \theta_b). \tag{2.14}$$

*Carter's integration is incorrect here. The semimajor axis should be

$$\frac{2R^2b_0}{C_d(1-f)^{1/2}}(1 - f\sin^2\alpha_0)^{1/2}$$

with semiminor axis

$$\frac{2R^2b_0}{C_d}(1 - f\sin^2\alpha_0)^{1/2}.$$

Unfortunately, the error affects his predicted theoretical trajectories obtained from the graphical integration process. The model will be discussed here as it stands without any corrections made. Any application of Carter's present model should involve the appropriate adjustments.

In Carter's model, $\theta_b = \theta_i = 0$, whereby

$$1 - f = \theta/\theta_0. \tag{2.15}$$

Figure 2.3 illustrates the measured centerline dilution θ/θ_0 for R values of 2.01, 4.93, and 9.80. The data appear to fit the straight line of slope -1/4 reasonably well. Carter's measurements were insufficiently precise to yield consistent results on the dependence of the length of the flow-establishment region on R. From his flume measurements Carter settled on the value $2.5b_0$ as the length of the temperature flow-establishment region. A survey of the available literature on the subject revealed that $3b_0$ was the right order of magnitude. Actually Carter expects that more precise measurements would shorten the length of the region of flow establishment as R increases. His more recent hydraulic tests indicate that for $R \approx 2$, say, $5b_0$ is a more accurate determination. Carter's latest experimental results in his larger flume seem to substantiate the straight-line fit of slope -1/4 to the established flow data, independent of R for $1 \leq R \leq 10$.

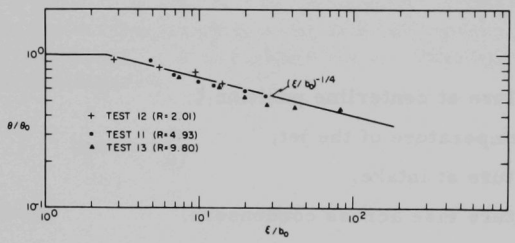

Fig. 2.3

Dilution, θ/θ_0, along the Centerline Trajectory as a Function of Downstream distance, ξ/b_0 (Ref. 1)

Carter's derivation of relationships for the determination of α_0 and C_d depend heavily on the pressure measurements made by Rouse on air jets.[2] Rouse's measurements of an air jet in an air crosscurrent were made in a wind tunnel of height 2.5 ft, where slots of fixed widths varied from 0.001 to 0.1 ft. The jet velocity was varied from 25 to 500 ft/sec, with decreasing slot width. Tunnel velocities varied from 10 to 50 ft/sec. Among other quantities, Rouse measured the pressure distribution at various sections normal to the wall (shore) from a series of piezometers. Figure 2.4 represents the geometry of the (equivalent) situation of an air jet in a crossflow with a sketch of the large eddy at the lee side of the jet. Figure 2.5 illustrates the distribution of pressure and shear at the wall. Figure 2.6 sketches the streamline configuration as expressed by Rouse. Figure 2.7 illustrates the pressure distribution along the shoreline wall for various values of R (through L/b_0). Rouse postulates the empirical relationship

$$L/b_0 = 20R^{3/2}, \tag{2.16}$$

where L is the length of the large eddy behind the jet. The pressure distribution at the wall (shoreline) as illustrated in Figs. 2.6 and 2.7 was used by Carter in estimating the values of α_0 and C_d. Figure 2.8 illustrates the detailed patterns of flow for $L/b_0 = 100$ as measured by Rouse at five downcurrent cross sections normal to the wall.

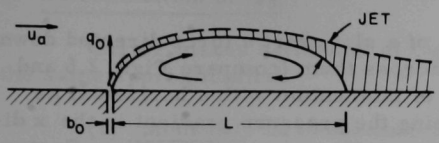

Fig. 2.4. Profiles of Eddies behind Wall and Jet[2]

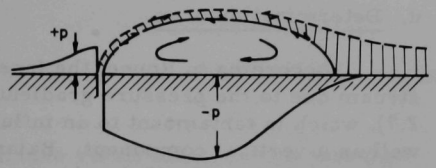

Fig. 2.5. Distribution of Pressure and Shear[2]

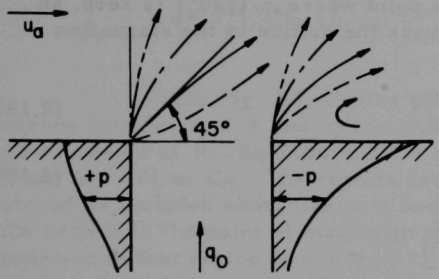

Fig. 2.6. Streamline Configuration in the Slot Vicinity[2]

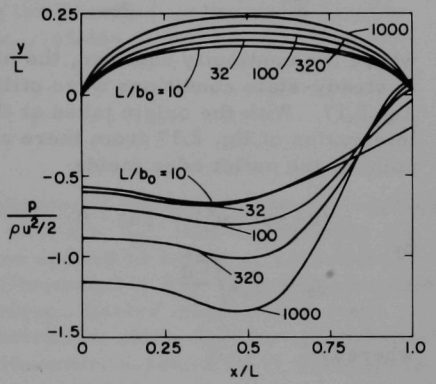

Fig. 2.7. Plots of Eddy Profiles and Boundary Pressures[2]

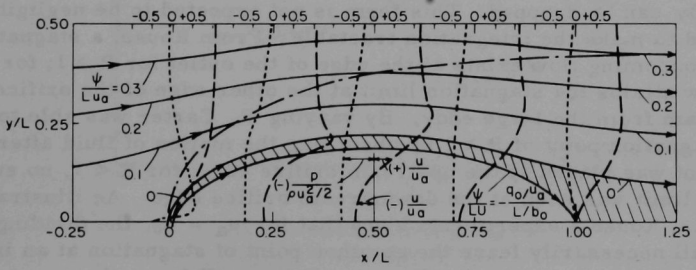

Symbols Used

b_0	Jet slot width	u_a	Ambient stream velocity
L	Eddy length	x	Longshore distance
p	Static Pressure	y	Offshore distance
q_0	Jet efflux velocity	ρ_a	Ambient density
u	Local velocity	ψ	Streamline = $\int u\, dy$

Fig. 2.8. Patterns of Mean Flow for L/b_0 = 100 (Ref. 2)

d. Determination of α_0

According to Rouse, the faces of a slot exert a force directed downstream due to the pressure gradient across them (compare Figs. 2.6 and 2.7), which is tantamount to an influx of momentum with a horizontal as well as a vertical component. Balancing the pressure gradient in the x direction with the rate of change of x momentum across the orifice, Carter achieves

$$-\frac{\partial p}{\partial x} = \rho \frac{du}{dt} = \rho \frac{\partial u^2}{\partial x}, \tag{2.17}$$

where the continuity equation, the neglect of the term $\partial(uv)/\partial y$, in addition to steady-state conditions were utilized to obtain the approximation in Eq. 2.17. With the origin taken at the point where $p/(\frac{1}{2}\rho u_a^2)$ is zero, an integration of Eq. 2.17 from there across the orifice to the stagnation point at the outlet edge yields

$$(0 - \tfrac{1}{2}\rho C_d u_a^2) = \rho u_0^2 - 0 \tag{2.18}$$

or

$$u_0 = u_a\sqrt{\frac{C_d}{2}}, \tag{2.19}$$

whereby

$$\frac{u_0}{q_0} = \cos\alpha_0 = \frac{1}{R}\sqrt{\frac{C_d}{2}}. \tag{2.20}$$

The basic assumption made in the above derivation is that the term $\partial(uv)/\partial y$ can be dropped. This term is not expected to be negligible, yet was ignored to make the integration tractable. From Rouse, a stagnation point of the oncoming flow exists at the edge of the outlet for $R \geq 1$; for $R < 1$, the jet flow attains the stagnation limit at the other edge of the orifice slightly upstream from the large eddy. By varying R, Carter was able to identify the stagnation point of $R \geq 1$ by observing the motion of fluid after a small dye spot was placed at the upstream orifice edge; for $R < 1$, no such stagnation limit was seen at the downstream orifice edge. As illustrated in Fig. 2.6, Rouse's experiments show that for $u_a = u_0$, the dividing streamline will necessarily leave the common point of stagnation at an inclination of 45°. For $u_0 > u_a$, the dividing streamline will leave the corner of the slot vertically, whereas, for $u_0 < u_a$, it will leave horizontally. These conclusions also follow from Rouse's application of the Bernoulli principle, which states that the pressure must be the same in the jet and ambient stream at every point of contact; consequently, it is possible only for the more slowly moving fluid to attain the stagnation limit at the juncture point. Recent flume measurements made by Carter when $R < 1$ reveal that the jet does not travel at right angles to its initial direction. Due to this discrepancy, Carter recommends more study for a more accurate analysis when $R < 1$.

e. Determination of C_d

Carter makes estimates of C_d by two methods, each yielding roughly the same approximation.

(1) Method 1. A momentum balance yields the condition that the pressure integral over the near-shore boundary must be equal and opposite to the y-momentum flux from the slot, $\rho q_0^2 b_0 \sin \alpha_0$. Since pressure in this warm-water-jet situation cannot presently be measured to the precision required, Carter uses Rouse's air-jet boundary pressure distribution to provide an estimate on C_d. Integrating the boundary pressure, $p/(\frac{1}{2}\rho u_a^2)$, as a function of x from the orifice to x_m, yields

$$\int_0^{x_m} p \, dx = -\rho q_0^2 b_0 \sin \alpha_0. \tag{2.21}$$

From Fig. 2.7, Carter planimetered the areas under the various curves between $x = 0$ and $x/L = 0.5$, i.e., $x \approx x_m$, thus determining C_d as a function of R. Equation 2.20 is also applied to relate α_0 determined from Eq. 2.21 to C_d. The results are illustrated in Fig. 2.9. One comment should be included about Carter's technique. Carter integrated p from the orifice to the point of maximum penetration, since C_d was approximately constant in that region (see Fig. 2.7). However, it seems more accurate to carry out the integration to $+\infty$. It is expected that C_d as presently derived may be low by approximately 30%.

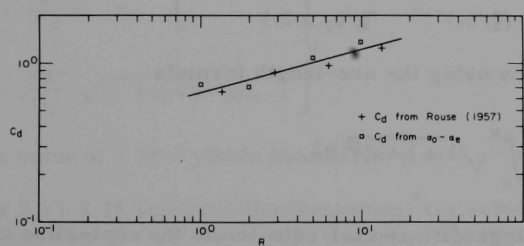

Fig. 2.9. The Coefficient of Drag, C_d, as a Function of R (Ref. 1)

(2) Method 2. An independent estimate of C_d can be obtained by a consideration of the measured length of the zone of flow establishment. Since the trajectory in the region of establishment is a circle centered at $x = \sin \alpha_0 (2R^2 b_0/C_d)$ and $y = -\cos \alpha_0 (2R^2 b_0/C_d)$ with radius $2R^2 b_0/C_d$, the arc of the circle, of length $2.5b_0$, is equal to the central angle measured in radians multiplied by the radius. That is,

$$2.5b_0 = \frac{2R^2 b_0}{C_d}\left[(\alpha_0 - \alpha_e)\frac{2\pi}{360}\right] \tag{2.22}$$

or

$$\alpha_0 - \alpha_e = \frac{225}{\pi}\frac{C_d}{R^2}, \tag{2.23}$$

where α_e is the angle at the end of the region of flow establishment with $\alpha_0 - \alpha_e$ measured in degrees. Based on the assumption that the x velocity at all points in the established flow region is equal to u_a,

$$\cos \alpha_e = u_a/q_0 = 1/R. \tag{2.24}$$

Solving Eqs. 2.20, 2.23, and 2.24 simultaneously yields an estimate on C_d. For R values of 1, 2, 5, and 10, these equations were solved numerically and the results were plotted in Fig. 2.9 for comparison with Method 1. The agreement is rather good, taking into account the uncertainties involved and the approximations made.

f. Centerline Trajectory

Carter could conceptually solve Eq. 2.11 by replacing 1 - f by the empirical formula

$$\left.\begin{aligned} 1 - f &= 1 && 0 < \xi/b_0 \le 2.5 \\ &= (\xi/b_0)^{-1/4} && \xi/b_0 > 2.5 \end{aligned}\right\} \tag{2.25}$$

and ξ in turn by using the arc-length formula

$$\xi(x) = \int_0^x \sqrt{1 + [y'(\hat{x})]^2}\, d\hat{x}, \tag{2.26}$$

yielding an integrodifferential equation on the centerline trajectory y(x). Sidestepping the associated mathematical difficulties in solving the resulting equation, he solves Eq. 2.11 graphically.*

The Carter technique involves the plotting of the family of ellipses defined by Eq. 2.11 for constant values of 1 - f and $\alpha_0 = 90°$ as functions of new variables

*As expressed in the previous footnote, Carter's analysis of the centerline trajectory is discussed as described in his report. Adjustments due to his incorrect graphical integration are not given here, yet seem quite simple to make. Equation set 2.29 in addition to the theoretical predictions given in Figs. 2.10–2.17 and Tables 2.2 and 2.3 need to be corrected. In spite of the algebraic error, Carter's methodology is of prime significance and hence is included here.

$$\left.\begin{aligned} x' &\equiv x\,\frac{C_d}{2R^2 b_0} \\ \text{and} \qquad & \\ y' &\equiv y\,\frac{C_d}{2R^2 b_0}. \end{aligned}\right\} \tag{2.27}$$

Figure 2.10 shows the position of the orifice and terminal point of the region of flow establishment. The one family of curves illustrated in Fig. 2.11 suffices for all R if all measurements are made from the end of the zone of flow establishment represented in x' coordinates as $x' = 1 - \sin\alpha_e$ and $y' = \cos\alpha_e$. Using the point as a new origin in Fig. 2.11, 1 - f of Fig. 2.3 determines a centerline distance ξ and a corresponding ξ' given by

$$\xi' \equiv \xi\,\frac{C_d}{2R^2 b_0}. \tag{2.28}$$

This value of ξ' is then marked off on Fig. 2.11 from $(1 - \sin\alpha_e, \cos\alpha_e)$ to the proper value of (1 - f) as indicated in Fig. 2.11. Repeating this procedure any number of times determines the centerline trajectory.

Carter determined the coordinates of the point of maximum penetration from Fig. 2.12 as

$$\left.\begin{aligned} x_m/b_0 &= \frac{2R^2}{C_d}\sin\alpha_0; \\ y_m/b_0 &= \frac{2R^2}{C_d}\left[\sqrt{1 - f_0} - \cos\alpha_0\right], \end{aligned}\right\} \tag{2.29}$$

where f_0 is the value of f that yields the ellipse of maximum jet penetration.

Figures 2.13-2.15 compare the theoretical trajectories for R = 2, 5, and 10 with test data for values of $x/b_0 \leq x_m/b_0$. Predicted deflections and dilutions are summarized in Fig. 2.17. Coordinates of the point of maximum penetration are given in Fig. 2.16 and in Table 2.2. Figures 2.18-2.20 sketch surface isotherms based upon hydraulic model tests 11-13. The computed jet centerline trajectories (uncorrected) are also plotted. The partial cutoff of inshore entrainment is clearly noted from the fact that the wall or shore temperature is still fairly high at significant distances downstream from the orifice.

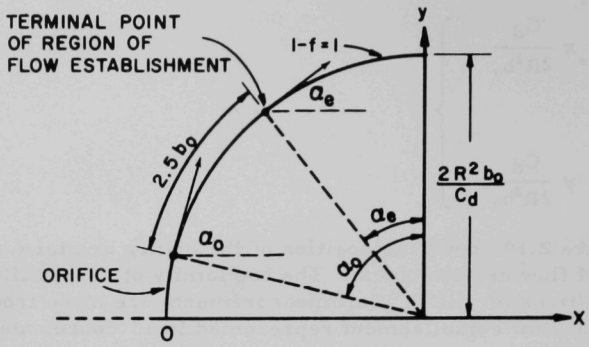

x_0 = x coordinate of orifice = $\frac{2R^2 b_0}{C_d}(1 - \sin \alpha_0)$

y_0 = y coordinate of orifice = $\frac{2R^2 b_0}{C_d} \cos \alpha_0$

x_0' = x' coordinate of orifice = $1 - \sin \alpha_0$

y_0' = y' coordinate of orifice = $\cos \alpha_0$

x_e = length of flow-establishment region in x coordinates

$= \frac{2R^2 b_0}{C_d}(\sin \alpha_0 - \sin \alpha_e)$

x_e' = length of flow-establishment region in x' coordinates

$= (1 - \sin \alpha_e) - (1 - \sin \alpha_0)$

y_e = length of flow-establishment region in y coordinates

$= \frac{2R^2 b_0}{C_d}(\cos \alpha_e - \cos \alpha_0)$

y_e' = length of flow-establishment region in y' coordinates

$= \cos \alpha_e - \cos \alpha_0$

Fig. 2.10. Position of Orifice and Flow-establishment Region

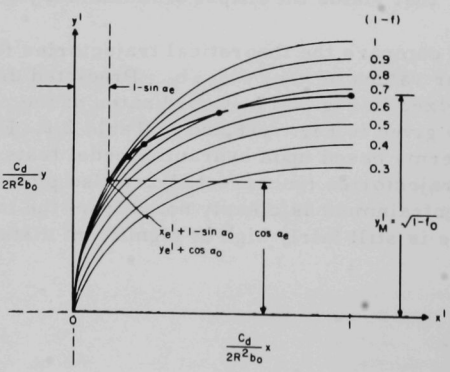

Fig. 2.11

Graphical Integration of Eq. 2.11 (Ref. 1)

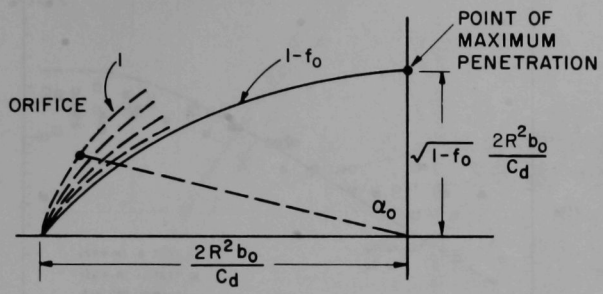

x_m = length of maximum penetration in x coordinates

$$= \frac{2R^2 b_0}{C_d} \sin \alpha_0$$

y_m = length of maximum penetration in y coordinates

$$= \frac{2R^2 b_0}{C_d} \left(\sqrt{1 - f_0} - \cos \alpha_0\right)$$

Fig. 2.12. Coordinates of Point of Maximum Penetration

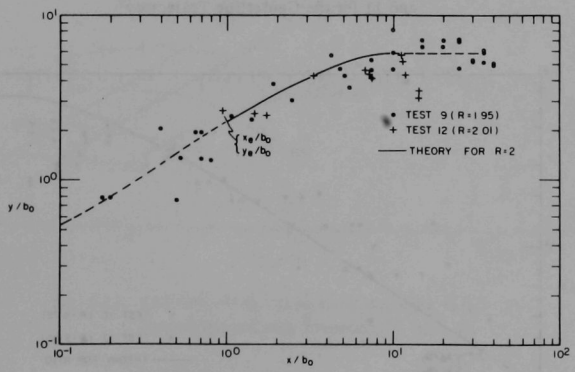

Fig. 2.13. Comparison of Theory for R = 2 and Tests 9 and 12 for the Centerline Trajectory[1]

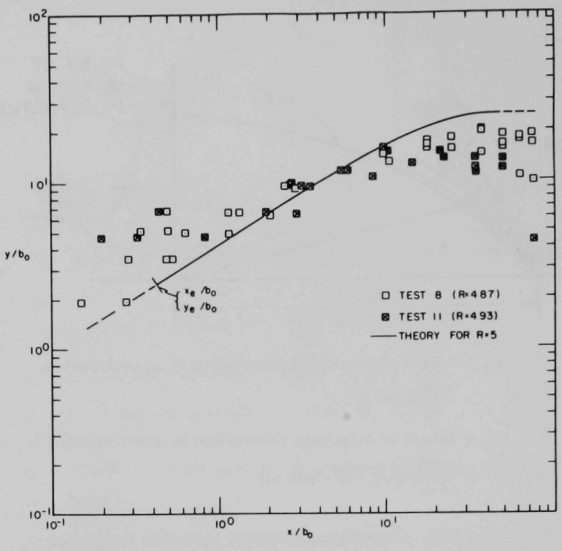

Fig. 2.14. Comparison of Theory for R = 5 and Tests 8 and 11 for the Centerline Trajectory[1]

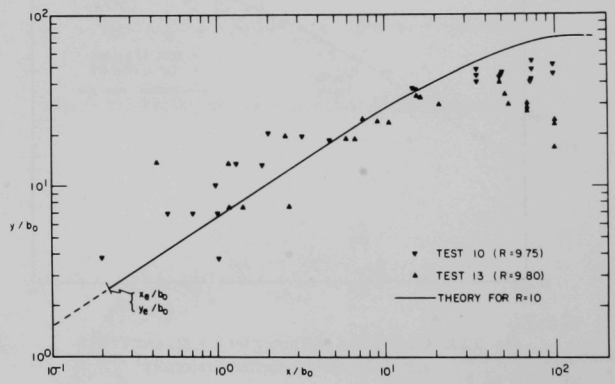

Fig. 2.15. Comparison of Theory for R = 10 and Tests 10 and 13 for the Centerline Trajectory[1]

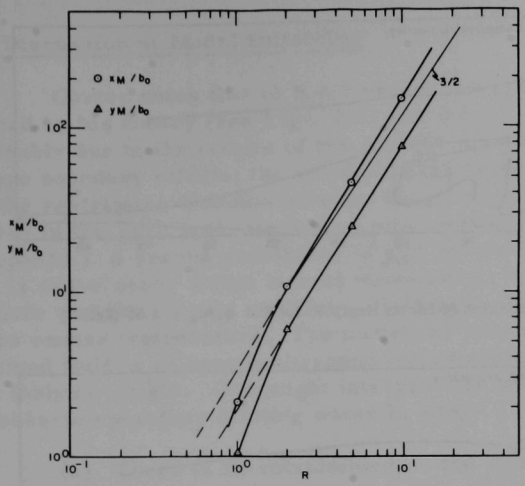

Fig. 2.16

Coordinates of the Point of Maximum Penetration[1]

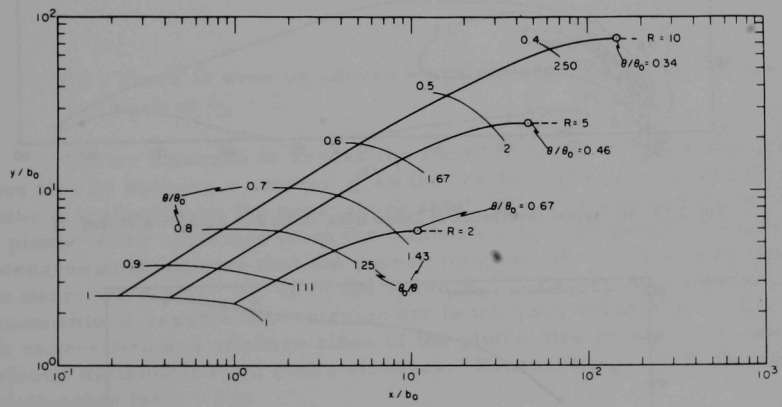

Fig. 2.17. Dilution, θ/θ_0, along the Centerline Trajectory Parameterized with Respect to R (Ref. 1)

TABLE 2.2. Computation of Coordinates of Maximum Penetration[1]

R	$\sin \alpha_0$	$\cos \alpha_0$	C_d	$\sqrt{1 - f}$	x_m/b_0	y_m/b_0
1	0.798	0.610	0.74	1.00	2.15	1.05
2	0.956	0.298	0.71	0.82	10.78	5.89
5	0.989	0.148	1.08	0.68	45.70	24.60
10	0.997	0.083	1.36	0.59	146.80	74.00

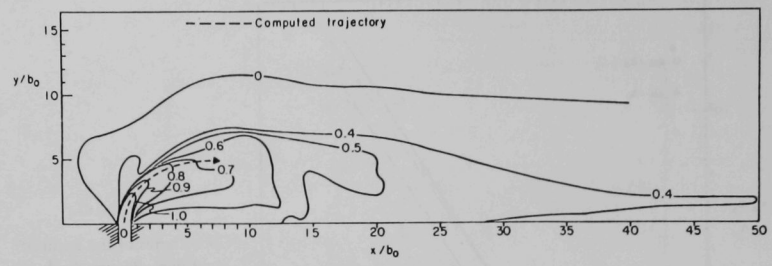

Fig. 2.18. Horizontal Distribution of Excess Heat, θ, for $R \equiv q_0/u_a = 2.01$ (Ref. 7)

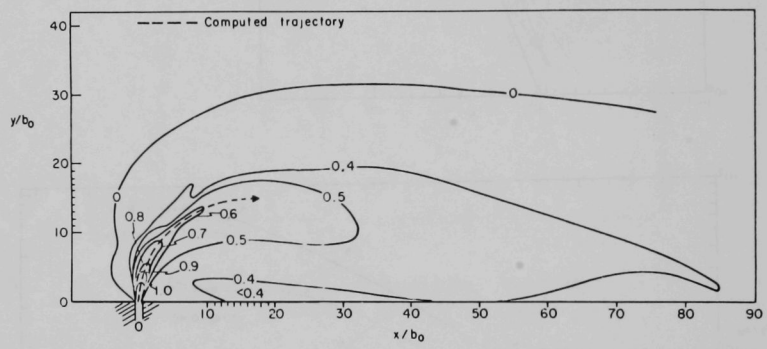

Fig. 2.19. Horizontal Distribution of Excess Heat, θ, for $R \equiv q_0/u_a = 4.93$ (Ref. 7)

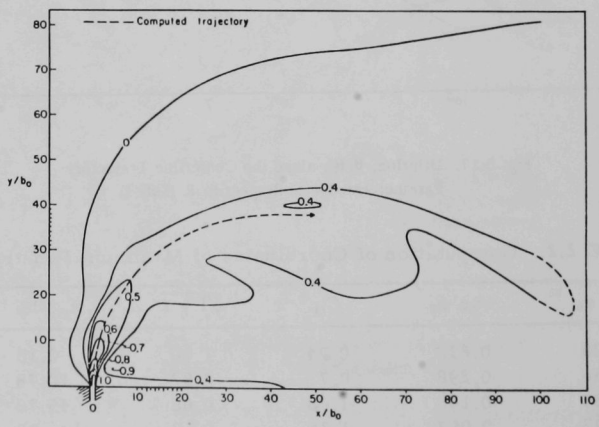

Fig. 2.20. Horizontal Distribution of Excess Heat, θ, for $R \equiv q_0/u_a = 9.80$ (Ref. 7)

g. Discussion of Model Suitability

Carter notes that at $R \geq 5$ the jet failed to penetrate as far as predicted by his theory (see Figs. 2.13 and 2.14). He speculates that this is probably due to the failure of the physical model setup to eliminate far-shore boundary effects; the effective drag coefficient becomes larger due to the restrictive distance between the jet and far shore. (The numerical error in the graphical integration procedure may contribute to this discrepancy.) A second possibility is that the background excess temperature θ_b is above zero. From lateral temperature measurements it was clear to Carter that the jet was entraining fluid on the inshore side of the jet of non-zero excess temperature. The model, as developed, assumes that all entrained fluid is at zero background temperature, independent of its offshore or inshore origin. One might interpret the indistinguishability of new zero excess-temperature diluting water in either of two ways:

(a) There is no entrainment on the inshore side of the plume with entraining water on the offshore side at $\theta_b = 0$.

or

(b) There is even or uneven entrainment on offshore and lee sides, each at $\theta_b = 0$.

Carter attempts to assess the possible error in this assumption. He does this by defining a number g as the fraction of a unit volume of plume water entrained from the near-shore side. The fraction of the unit volume of plume water entrained from the offshore side is denoted f. Experimental measurements indicate that the excess temperature of water entrained from the near-shore side, θ_b', is of the order $\theta_0/2$. Carter then considers it reasonable to assume that entrainment is unequal, volume to volume, on the near-shore and offshore sides of the plume, due primarily to unequal velocity distribution and shear stresses. Estimating $g = f/2$, the new relationship for $1 - f$ is

$$(1 - f)_{new} = (\theta/\theta_0)_{old} + g\left(1 - \frac{\theta_b'}{\theta_0}\right) \tag{2.30}$$

or

$$(1 - f)_{new} = \frac{4(\theta/\theta_0)_{old} + 1}{5}. \tag{2.31}$$

Table 2.3 compares $1 - f$ given by Eq. 2.15 with $(1 - f)_{new}$ of Eq. 2.31 with the percentage error involved. Carter notes that this effect of nonzero background excess temperatures, if real, would not be present for low values of R since the error does not become significant until small values of dilution are attained as seen in Table 2.3.

TABLE 2.3. Comparison of Old and New Values of 1 - f (Ref. 1)

θ/θ_0	1 - f (Eq. 2.15)	1 - f (Eq. 2.31)	Error, %
1.0	1.0	1.00	0
0.9	0.9	0.92	2.2
0.8	0.8	0.84	5.0
0.7	0.7	0.76	8.6
0.6	0.6	0.68	13.3
0.5	0.5	0.60	20.0

Carter noticed in his hydraulic experiments that the fluid being entrained on the near-shore side comes from a large eddy, which possesses little x momentum. Water in that eddy travels upstream along the wall, curves up, and then follows the jet downstream, creating a clockwise circulation pattern. Dropping a large number of small pieces of paper or a small dye spot in this eddy reveals only large-scale circulation with very slow clockwise motion. This fact leads Carter to assert that any modification of the x-momentum equation (Eq. 2.2) need not include a term accounting for changes in the x momentum of the large eddy on the near-shore side of the jet. Concerning the temperature of that large area, Carter has measured its extent to be nearly elliptical in shape maintaining approximately the same excess temperature.

Concerning the length of the large eddy as measured from the outlet downstream along the wall boundary, Rouse defines it as L and represents it by Eq. 2.16. Carter was unable to verify that relationship experimentally due to the difficulty in defining the precise position at which the water particles reverse direction along the wall and from the fact that only temperature-measuring equipment was utilized. Carter does not expect L to be twice x_m and suggests that it can be measured roughly by dropping dye spots along the downstream wall boundary until a position L is reached where the fluid velocity is directed upstream for distances less than L and downstream for positions greater than L.

Carter's theoretical analysis is carried out only to the point of maximum penetration of the jet into the crossflow. His flume experiments (including his most recent ones) have indicated that the plume trajectory beyond x_m tends to curve back toward the near shore. Carter reasons that the pressure distribution (gradients) set up in the receiving waters by the far boundary dissipates the initial offshore momentum and remains to return the plume to the near shore until the pressure gradient normal to the boundary is balanced by water piling up on the near shore. Carter notes that in real-world situations of a river, estuary, or moderately sized lake,

the far-shore boundary will cause a pressure gradient to be set up to return the flow to the near-shore boundary. His conclusions are supported in each of his flume experiments (far bank varied from 23 to 115 outfall widths from the outlet) and by the wind-tunnel experiments of Rouse[2] (see Figs. 2.4 and 2.5). For a large lake like Lake Michigan, the far shore is sufficiently distant to set up only feeble pressure gradients against the jet discharge; consequently, this bend-back effect might not be observed most of the time.

Carter noted that the plume return to the near shore might be a function of R. For low R, there was less tendency for the plume to come back as it evens itself out parallel to the current; as R increased, the plume curvature toward near shore was more visible and pronounced. Also, as the far-boundary distance increased, Carter noticed a deeper penetration of the jet and a longer distance downstream for the plume to initiate its near-shore return. (Unfortunately, Carter did not use identical initial parameters in the small and large flumes. Carter does feel, however, that the larger flume width is the major causative factor in jet trajectory and bend-back discrepancies. The possibility of a different type of partial cutoff of inshore entrainment could also complicate the situation. Carter can only say that he has observed the inshore region to have the same features as in the smaller flume, yet no measurements to date have been made in that region for the larger flume.) Other investigators[3] who took great care to remove far-boundary effects noted no return of the plume and, in fact, only a very slow leveling off parallel to the crosscurrent. As Carter has noted himself, more study is required to determine the precise relationship of far-bank distance and velocity ratio R on the maximum jet penetration and the plume deflection beyond that position to the near shore. However, Carter expects that only for the ocean and large lakes with a far offshore boundary, conservation of momentum in the offshore direction would be good assumption for a mathematical model. Otherwise the ambient pressure distribution set up by the far-shore boundary would be sufficient to affect the offshore momentum and consequently the jet trajectory.

Carter's form for the drag force

$$dP = \frac{\rho_a C_d A u_a^2}{2}, \tag{2.1}$$

as stated above, is an artificiality to match theoretical jet trajectories with experimental data. There is no universal form in defining dP. Fan[4] defines dP as above, except he includes a $\sin^2 \alpha$ term to cause dP to approach zero as the jet orients itself parallel to the current; Motz and Benedict[5] do the same, adding a $\sin \alpha$ term. (Any dispute over the proper form for the drag force is not of great import.) This concept of a jet being a solid-body obstruction in the flow field is fictitious and is done to obtain a free parameter to fit the theoretical model

to selected experimental data. More artificial, however, is the assumption that C_d is constant for all trajectory positions. Carter chose the form of Eq. 2.1 mainly because of its simplicity, permitting an easy solution to the problem, in addition to the fact that the x component of dP dies out as maximum penetration is reached. In addition, the values of C_d that Carter derived were close to 1.0, which is the order of magnitude of the drag coefficient in airfoil drag theory. Some other investigators like Fan,[4] Motz and Benedict,[5] and Vizel and Mostinskii[6] employ other forms for dP which yield drag coefficients at times an order of magnitude from the expected value. (Vizel and Mostinskii have values on the order of 5.0, while Fan's drag coefficients vary from 0.1 to 1.5, and Motz and Benedict have found their C_d to vary between 0.5 and 4.0.) Carter asserts that such large variances from 1.0 are hard to justify theoretically. The experimental results of Rouse on wall pressures and selected cross-sectional pressure distributions embodied in Figs. 2.7 and 2.8 were also consulted in Carter's decision not to complicate the already artificial form for dP. The approximately constant wall-pressure distribution measured for $x \leq x_m$ of Fig. 2.7 was later employed to calculate C_d from the orifice to the point of maximum penetration.* Concerning the pressure-drag formula (Eq. 2.1) once again, any such formula is a first-order attempt to account for the drag term as caused by the pressure distribution across the jet.

Carter's measurements of the lateral velocity and temperature profiles showed a complete lack of similarity in the region $x \leq x_m$. Temperature measurements revealed a bell-shaped or Gaussian-type distribution from the centerline in the offshore direction; the temperature from the centerline toward the inshore boundary dropped off continuously until it leveled off at some approximately constant value between zero and the peak temperature. The velocity appeared to start at zero at the inshore wall and increase in a bell-shaped pattern to the centerline; in the offshore direction from the centerline, the velocity was determined to be nearly constant. Consequently, the temperature and velocity profiles were almost mirror images of each other, precluding any kind of similarity. Measured velocity and temperature profiles in the vertical direction were nearly uniform. Seeing little point in postulating highly sophisticated models for velocity and temperature, Carter defined a "top-hat" distribution for both quantities and a hypothetical width, $b(\xi)$, as

$$b(\xi)\theta(\xi) = \int_{\substack{\text{jet}\\ \text{cross}\\ \text{section}}} \theta(\xi, \eta)\, d\eta.$$

*Rouse's approximately constant wall-pressure distribution for $x \leq x_m$ might have been caused to some degree by far-boundary effects. One can only speculate at this time upon how "constant" this pressure distribution would be with no far boundary present.

This b is then the width of a top-hat distribution (equivalent rectangle) with equivalent peak value $\theta(\xi)$ and area in the $\eta\zeta$ plane. Due to uncertainty in the precise form for the lateral distribution of velocity, temperature, and width, Carter side-stepped the continuity equation with his partially observed assumption that $u_a/u = 1$ in the established flow region. This simplified the problem of modeling the entrainment of ambient fluid. Carter states that jet widths defined by the above smoothing process have little physical meaning. Consequently, Carter could see no point in experimentally measuring or calculating them in the model. As a result, model information regarding the isotherm areas is lacking.

The model, in its present version, has several weak points. First, the error in integrating Eq. 2.11 throws the precise theoretical predictions of the jet trajectory as given in Figs. 2.10-2.20 including Tables 2.2 and 2.3, in doubt. The magnitude of the discrepancy has not yet been evaluated. More fundamentally, the assumption that the x velocity u in the established flow region is nothing but u_a simplifies the graphical integration of Eq. 2.11, yet does not seem physically valid for points in the general vicinity of (x_e, y_e). Only for positions beyond the point of maximum penetration (not considered in the analysis) is this truly a good assumption. Integrating the wall-pressure distribution of Rouse from $x = 0$ to $x = x_m$, instead of $x = \infty$, in the evaluation of C_d may lead to a 30% error in C_d. The lack of information on some kind of plume width and isotherm areas is a disadvantage in any predictive modeling. The extension of Carter's experimentally measured centerline decay formulas to situations where the jet is not two-dimensional, namely to problems with initial vertical entrainment, cannot readily be made. Some accounting of the additional dilution near the outfall has to be done as long as the Richardson number, say, is less than about 0.8. Carter's entrainment (dilution) curves are affected by the existence of the fixed bottom boundary. Thus, these curves may not be readily extrapolated to the case of a deep receiving basin. Another concern is whether the flat, solid bottom is causing additional lateral spreading due to the increased turbulence induced by the shear stresses at the bottom. Carter's physical situation is still two-dimensional, yet whether this kind of idealization is the "best" two-dimensional simulation of a thermal plume is still debatable. Another question is whether the magnitude of the drag coefficients will change in the presence of significant buoyant forces (large θ_0, all other parameters fixed). The answer is not clear from the experiments to date. The effect of the far-shore boundary on the jet trajectory (through the drag coefficient) and jet penetration still needs investigating. As stated above, Carter's small and large flume experiments have shown that, within the downstream limits of the measurements, the centerline temperature decay had a form apparently independent of R. Carter suspects, however, that measurements in the region in which ambient turbulence predominates would show some difference in centerline temperature decay, depending upon R.

Carter fully recognizes the limitations of this model. This is the main reason he emphasizes that his work is only preliminary. He is presently carrying on flume experiments to attempt to answer many of the above problems. Although confident of his centerline dilution formula, Carter is hesitant to predict centerline trajectories for situations in which the far bank is much greater than 60 outfall widths. Equations 2.2 and 2.6 were derived on an intuitive basis. Carter is now reevaluating the correctness of the entrainment term in Eq. 2.6. The precise method of handling a possible nonzero background temperature, especially for the lee side, is another problem to be considered. Carter's most recent measurements seem to indicate a centerline trajectory satisfying $y \propto x^{1/3}$, as seen by some other investigators. At present, he is attempting to develop the physical reasoning involved to predict that relationship. Some other researchers predict a parabolic trajectory. It seems from Carter's most recent data that something rather dramatic occurs at $R = 2$. For higher R, most of the jet trajectory data can be collapsed to a common law if the x and y coordinates are scaled by Rb_0. For $R \leq 2$, the data definitely follow a different pattern and at present do not seem to reduce under any common scaling. These facts are being investigated. Carter's main priority at this time is to develop a model that has physical reality and satisfies all his flume data.

h. Pritchard's Application of Carter's Model[8]

Pritchard applies the Carter analysis in the following manner whenever the longshore ambient current is equal to or greater than 10% of the initial jet velocity:

(1) Compute the discharge velocity q_0 from

$$q_0 = \frac{Q_c}{b_0 D}, \tag{2.32}$$

where

Q_c = volumetric flow rate of power plant,

b_0 = width of orifice,

and

D = depth of the channel discharge.

(2) Compute R from

$$R = \frac{q_0}{u_a}, \tag{2.33}$$

where u_a is the ambient current speed.

(3) Compute the trajectory of the plume centerline as described above by the graphical integration procedure on Eq. 2.11. The deflected trajectory is then plotted from the discharge orifice to the position of maximum penetration x_m, y_m as a continuously changing ellipse with initial orientation at the orifice given by α_0 and a final orientation at x_m, y_m parallel to shore.

(4) For the portion of the centerline between the orifice $\xi = 0$ and centerline distance ξ_m corresponding to position x_m, y_m, the centerline temperature decay is

$$\left.\begin{aligned} \theta/\theta_0 &= 1 & 0 \le \xi \le 2.5b_0; \\ &= (\xi/b_0)^{-1/4} & 2.5b_0 \le \xi \le \xi_m. \end{aligned}\right\} \tag{2.34}$$

(5) For the portion of the centerline between the position x_m, y_m, and the point where the excess temperature $\theta = 0.2\theta_0$, the centerline temperature decay is

$$\theta/\theta_0 = \left(\frac{nb_0}{\xi}\right)^{1/2} \tag{2.35}$$

where n is such that Eqs. 2.34 and 2.35 give the same temperature at ξ_m.

(6) For the portion of the plume centerline in which $\theta \le 0.2\theta_0$, the decay is

$$\theta/\theta_0 = \frac{kb_0}{\xi}, \tag{2.36}$$

where k is such that Eqs. 2.35 and 2.36 give the same temperature at $\xi = \xi_{0.2\theta_0}$ i.e., the same temperature at the distance in which $\theta = 0.2\theta_0$.

(7) Pritchard's inspection of the temperature data obtained in Carter's flume experiments (as expressed in Ref. 1, although not reproduced there) yielded the following criteria for calculating isotherm areas in terms of the length of the area along the plume axis to the excess temperature θ:

(a) The lateral dimension of the area contained within a fixed isotherm in an upstream and/or offshore direction from the plume axis is approximately one-eighth the length of the isotherm area, as measured along the plume axis.

(b) For excess temperatures greater than the excess temperature at x_m, y_m, the lateral dimensions of the area contained within a given isotherm in a downstream and/or inshore direction from the plume axis is approximately three-eighths of the length of the isotherm area.

(c) For excess temperatures equal to or less than that at ξ_m, the isotherms extend to shore on the inshore side of the plume.

(8) Planimeter the areas contained within the isotherms (or areas defined by the isotherms and the shoreline).

Notes

(1) This application of Carter's model assumes a completely two-dimensional situation with no vertical entrainment.

(2) Computation of the jet trajectory should involve the correction due to Carter's algebraic error in deriving his ellipse formulae (see Secs. a-f above).

(3) Carter's measurements do indicate an approximate inverse with distance centerline temperature decay when ambient turbulence predominates [see (6) above]. Carter, however, suspects that there is some dependency of this temperature decay on R. Between the point of maximum penetration and this region of dominance of ambient turbulence, Carter is unable to verify the precise form of the centerline temperature drop. There must be a region in which the temperature will decay $\approx x^{-1/2}$ as stated by Pritchard, but its precise extent is not clear to Carter from his measurements.

(4) The limitations of Carter's present model (see above discussion) should be kept in mind in any application of this procedure.

References

1. H. H. Carter, A Preliminary Report on the Characteristics of a Heated Jet Discharged Horizontally into a Transverse Current: Part I. Constant Depth, Technical Report No. 61, Chesapeake Bay Institute, the Johns Hopkins University, Baltimore, Md. (Nov 1969).

2. Hunter Rouse, Diffusion in the Lee of a Two Dimensional Jet, 9th Congress International de Mechanique Appliquee, Vol. I, pp. 307-312 (1957).

3. J. F. Keffer and W. D. Baines, The Round Turbulent Jet in a Cross-Wind, J. Fluid. Mech. 10, 481-496 (1963).

4. Loh-Nien Fan, Turbulent Buoyant Jets into Stratified or Flowing Ambient Fluids, Tech. Report No. KH-R-15, W. M. Keck Laboratory of Hydraulics and Water Resources, California Institute of Technology, Pasadena, California (June 1967).

5. Louis Motz and Barry Benedict, Heated Surface Jet Discharged Into a Flowing Ambient Stream, National Center for Research and Training in the Hydrologic and Hydraulic Aspects of Water Pollution Control, Report Number 4, Department of Environmental and Water Resources Engineering, Vanderbilt University, Nashville, Tennessee (Aug 1970).

6. Ya. M. Vizel and I. L. Mostinskii, Deflection of a Jet Injected Into a Stream, Inzhenerno-Fizicheskii Zhurual 8(2), 238-242 (1965).

7. H. H. Carter, personal communication (1971).

8. D. W. Pritchard, Modeling of Heated Discharges - A Lecture, Westinghouse School for Environmental Management, CSU, Fort Collins, Colorado (June 25, 1970).

3. Heated Surface Jet Discharged into a Flowing Ambient Stream

Louis H. Motz and Barry A. Benedict
(Vanderbilt University)
August 1970

a. List of Symbols

$_0$	Subscript denoting initial values
a	Subscript pertaining to ambient fluid
A	Ratio of ambient velocity to initial jet velocity, U_a/U_0
b	Half-width of jet
C	Circumference through which entrainment takes place
C_D	Drag coefficient
C'_D	Reduced drag coefficient
c_p	Specific heat
dA	Differential area of jet cross section
e	Subscript pertaining to establishment zone
E	Entrainment coefficient
F_D	Drag term
K	Surface heat-transfer coefficient
L	Eddy length
M	Nondimensional momentum flux
O	Origin of the coordinate system (x,y), beginning of zone of established flow
O'	Origin of the coordinate system (x',y'), point of jet discharge
p	Static pressure
s	Coordinate axis of jet, referenced to beginning of zone of established flow
s'	Coordinate axis of jet, referenced to point of jet discharge
s'_e	Length of zone of flow establishment
S	Nondimensional distance along jet axis referenced to beginning of zone of established flow
S'	Nondimensional distance along axis referenced to point of jet discharge
S'_e	Nondimensional length of zone of flow establishment

T	Centerline temperature rise, °F
T'	Temperature rise at any point in jet cross section, °F
u	Local jet velocity
U	Centerline jet velocity
U_a	Ambient velocity
U_0	Initial jet velocity
V	Nondimensional volume flux
v_i	In-flow velocity
x	Longitudinal axis, referenced to beginning of zone of established flow; long-shore distance (Fig. 3.3 only)
x'	Longitudinal axis, referenced to point of discharge
x'_e	Longitudinal length of establishment zone
X	Nondimensional longitudinal axis, referenced to beginning of zone of established flow
X'	Nondimensional longitudinal axis, referenced to point of discharge
X'_e	Nondimensional longitudinal length of establishment zone
y	Lateral axis, referenced to beginning of zone of established flow; offshore distance (Fig. 3.3 only)
y'	Lateral axis, referenced to point of discharge
y'_e	Lateral length of establishment zone
Y	Nondimensional lateral axis, referenced to beginning of zone of established flow
Y'	Nondimensional lateral axis, referenced to point of discharge
Y'_e	Nondimensional lateral length of establishment zone
z	Depth of jet, subscript pertaining to vertical coordinate
β	Angle between jet and ambient current, degrees
η	Distance along axis perpendicular to s axis
ρ	Density
ρ_a	Ambient density
σ	Standard deviation
ψ	Streamline

b. Introduction

Motz and Benedict have considered the problem of heated surface discharges to a receiving-water body in the presence of ambient long-shore currents. The authors limit their consideration only to the jet regime of the resulting thermal plume. Ambient receiving-water turbulence and surface heat exchange are assumed to be of minimal influence with regard to plume dynamics and heat transfer within this regime. Building basically upon the framework established by Morton,[2] Fan,[3] Hoopes et al.,[4] and Carter,[5] the model the authors propose is a two-dimensional analysis which eventually develops into a system of five differential equations which must be solved numerically to yield the jet trajectory, width, velocity, and temperature distributions. The only exceptional requirement for the utilization of the model is the need for the specification of drag and entrainment coefficients. As discussed in greater detail later, the specification of the drag coefficient and particularly the entrainment coefficient is a matter of much concern. For any new field situation, there is no a priori way to establish values for these parameters; so what the authors have done is to set forth reasonable ranges for them extracted from hydraulic-model studies especially for this purpose.

c. Model Development

(1) Basic Assumptions. Some of the major assumptions made in the model development were listed by the authors as:

(a) The jet is two-dimensional.

(b) Beyond a region of flow establishment, the temperature and velocity profiles are equal and similar with respect to the jet axis.

(c) The flow field is completely turbulent and is independent of the Reynolds number.

(d) Changes in density are small compared to some reference density; thus density-induced inertial forces are not considered.

(e) Turbulent mixing of the jet with the ambient waters can be represented by an inflow velocity across the jet boundary.

(f) The interaction of the jet with the ambient current is treated as if the jet were a solid body and the resulting pressure gradients were represented by a drag force.

(g) Surface heat loss from the jet regime is minimal.

(h) Steady-state conditions are applicable.

The authors reason that in many practical situations a heated surface discharge, if not initially, will soon cease to entrain vertically near the point of discharge. They qualitatively argue this point based upon the work of Ellison and Turner[6] and Hoopes et al.[4] in which it was found that the Richardson number along the jet axis changes rapidly from a number less than 1 to a value of 1 or greater. When the Richardson number of the jet is close to or greater than unity, buoyancy forces dominate over inertial forces and oppose vertical spreading. Under these conditions, the jet spreads only horizontally. Entrainment of the ambient water occurs only at the sides of the jet and not to any significant extent at the bottom.

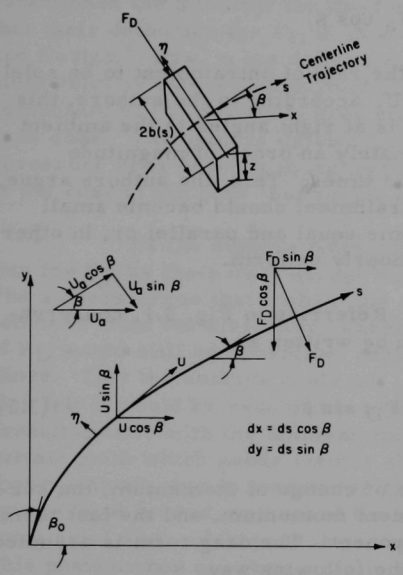

Fig. 3.1. Definition Sketch[1]

(2) Mass Conservation. Since density is assumed constant, mass conservation for a unit volume element within the jet (see Fig. 3.1) can be written as a volume continuity relationship in the following manner:

$$\frac{d}{ds}\left(\int_A u \, dA\right) = \int_C v_i \, dC, \qquad (3.1)$$

where

u = the local jet velocity directed along the s axis,

v_i = the inflow velocity (entrainment),

dA = the differential area normal to the s axis,

and

C = the circumference through which entrainment takes place.

The inflow velocity (entrainment) is assumed to be proportional to the magnitude of the difference between a characteristic velocity along the deflected jet and the parallel component of the ambient velocity. Thus,

$$v_i = E(U - U_a \cos\beta), \qquad (3.2)$$

where

U = the jet centerline velocity at s,

$U_a \cos\beta$ = the parallel component of the ambient velocity U_a at s,

β = the angle between the jet centerline and the ambient current at s,

and

E = an entrainment coefficient (assumed constant).

The form for the entrainment velocity, v_i, is nothing new; it has been used extensively in the literature. Its use is a matter of both convenience and necessity because without it, it would be literally impossible to account for the complex entrainment processes going on at the jet interface. The form of the entrainment velocity used by the authors is different from that used by Hoopes et al. in that it is referenced to the velocity disparity between the jet's centerline velocity, U, and the component of the ambient velocity along the plume axis, $U_a \cos \beta$.

Some investigators assume the rate of entrainment to be solely a function of the local jet axial velocity U; according to the authors, this definition should only apply when the jet is at right angles to the ambient flow or when the jet velocity is approximately an order of magnitude greater than the ambient velocity at other times. This, the authors argue, is because mixing due to jet-induced entrainment should become small when the jet and ambient velocities become equal and parallel or, in other words, when the velocity field becomes nearly uniform.

(3) Conservation of Momentum. Referring to Fig. 3.1, conservation of momentum in the x direction can be written as

$$\frac{d}{ds}\left[\int_A u(u \cos \beta)\, dA\right] = Cv_i U_a + F_D \sin \beta, \tag{3.3}$$

where the first term represents the rate of change of momentum, the second term the rate of entrainment of ambient momentum, and the last term the drag-force (pressure-gradient) component. The drag term is assumed to be related to the ambient velocity in the following way:

$$F_D = \frac{C_D U_a^2 z \sin \beta}{2}, \tag{3.4}$$

where C_D is an experimentally determined drag coefficient and z the jet depth. The momentum equation for the y component is therefore just

$$\frac{d}{ds}\left[\int_A u(u \sin \beta)\, dA\right] = -F_D \cos \beta. \tag{3.5}$$

According to the authors, F_D, or better $\rho F_D\, ds$, represents the drag force operating normal to the plume axis. The customary expression for the total drag, D, accounted for by a solid body in a flowing stream of velocity, V, is just

$$D = C_D\left(\rho \frac{V^2}{2}\right)(\text{area}), \tag{3.6}$$

where the area is oftentimes taken as the projected area of the solid body normal to the flowing stream. In other cases, as for airfoils aligned along the flow or slightly inclined to it, the aerodynamic force on the wing is proportional to the dynamic pressure due to the component of the stream velocity normal to the local axis of the wing as indicated by Abramovich.[7] The authors have elected the former definition, letting ds z sin β represent the projected area of the volume element normal to U_a. This also establishes the form for the drag coefficient, C_D. The authors point out that their definition for F_D is in slight variance to those chosen by Fan[3] and Carter.[5] Fan, in his definition, elected to use the square of the ambient velocity component normal to the projected area, rather than the component of the projected area normal to ambient velocity as the authors have done. The authors defend their choice based on the argument that, "pressure drag depends more on the form of the body and on separation at the rear of the body than on the conditions at the front of the body."

As the authors point out, Carter uses almost the same definition for F_D as their own, except that the sin β term is missing from Eq. 3.4. The authors argue that without the sin β term and at distances somewhat removed from the discharge, where β approaches zero, the y component of F_D would still be operative, continuing to deflect the jet towards the shore. This the authors could not intuitively accept as being correct, since they felt it would be reasonable to expect the jet axis to eventually line up asymptotically with the ambient-flow direction. This, however, is an important point which needs further clarification. Rouse[8] has experimentally shown with air jets in transverse flow that it is indeed possible for the jet axis to bend inward, or toward the shore for this present discussion, at some axial distance beyond the maximum jet penetration point, β = 0°. This phenomenon is schematically shown in Figs. 3.2 and 3.3, which were taken from Rouse. Through private correspondence, Carter revealed that he also has noticed this partial shoreward approach of the jet axis in some of his recent, yet unpublished, hydraulic-modeling studies. In these same studies, the jet-penetration distance and the distance at which the jet axis made its partial shoreward approach increased for increasing ratios of ambient width to discharge width. In Carter's experiments, these ratios ranged from approximately 12 to 120.

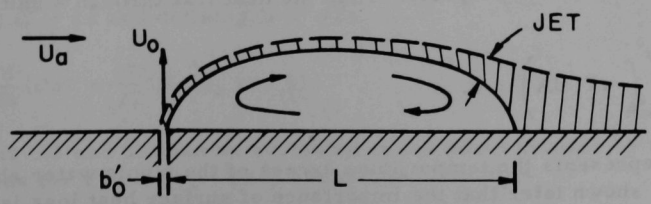

Fig. 3.2. Profiles of Eddies behind Wall and Jet[8]

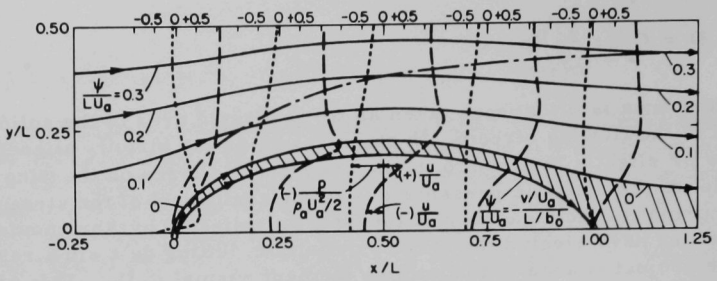

Symbols Used

b_0'	Jet slot width	U_0	Jet efflux velocity
L	Eddy length	x	Long-shore distance
p	Static pressure	y	Offshore distance
u	Local velocity	ρ_a	Ambient density
U_a	Ambient stream velocity	ψ	Streamline = $\int u\,dy$

Fig. 3.3. Patterns of Mean Flow for $L/b_0' = 100$[8]

It was not ascertained whether the ratios of channel width to jet-discharge width were varied by simply increasing or decreasing the far-bank separation, keeping everything else constant, or whether the jet width, relative velocities, and water depth had to be adjusted. It is also unknown whether the rate of change of the jet-penetration distance and the jet-axis reapproach and the magnitude of the reapproach decreased with increasing width ratios. This information would be useful in determining whether one would have to consider a far-bank phenomenon, particularly for riverine situations. In any event, the significance of these facts, with respect to the validity of Carter's, Fan's, and the authors' formulations for the drag-force term, is unknown. One thing that can safely be said is that none of the drag-force formulations will yield the pressure distribution across the y direction shown in Fig. 3.3, but again the actual significance of even this fact is unclear and therefore should not be interpreted as an indictment against the formulations. Clearly, these formulations are claimed to be no more than "handles" or artifacts to attempt to account for the pressure distribution over the jet due to flow separation.

(4) Conservation of Energy. Since the authors assumed that surface heat loss within the jet regime is minimal, they were able to treat heat as a conservative property. Thus the heat flux through a unit volume is just

$$\frac{d}{ds}\left(\int_A uT'\,dA\right) = 0, \tag{3.7}$$

where T' represents the temperature excess of the plume water above ambient. It is shown later that the importance of surface heat loss is only

meaningful when the jet's excess temperatures become small; this condition is associated with relatively large jet surface areas.

d. Solution to Model Equation Using Similarity Assumptions on Velocity and Temperature

The authors initially considered only that portion of the jet where similarity conditions were assumed to prevail. Discussion of a jet development region was deferred to later sections of their report where it was more conveniently handled; the same approach is used in this review. Since the authors chose to follow Morton's integral technique by assuming similar velocity and temperature profiles and a form for the in-flow velocity, they implicitly acknowledged a suppression of the "microscopic" knowledge of the jet in favor of obtaining a "macroscopic" view. Although any profile for the lateral distribution could have been used, the authors chose a Gaussian form, recognizing that many investigators before them had found the Gaussian form to be most suitable. Based on some limited data available, the assumption of similar velocity and temperature profiles may be inaccurate, as recognized by the authors. However, they felt justified in using similarity assumptions because of a paucity of knowledge on this matter.

The authors used the velocity distribution

$$u = U \exp(-\eta^2/2\sigma^2), \tag{3.8}$$

where

σ = the standard deviation,

and

η = distance normal to the s axis.

Substitution of Eq. 3.8 into the integral portion of Eq. 3.1 yields

$$\int_{-b}^{+b} U \exp(-\eta^2/2\sigma^2) z \, d\eta \cong Uz \int_{-\infty}^{+\infty} \exp(-\eta^2/2\sigma^2) \, d\eta = \sigma\sqrt{2\pi}, \tag{3.9}$$

where b is the jet half-width. Equation 3.1 can now be rewritten, given the fact that $C = 2z$ and defining $b = \sqrt{2}\sigma$:

$$\frac{d}{ds}(Ub) = \frac{2E}{\sqrt{\pi}}(U - U_a \cos \beta). \tag{3.10}$$

Equations 3.3 and 3.5 can be evaluated in the same manner by using the definitions for F_D and v_i. They reduce, respectively, to

$$\frac{d}{ds}(U^2 b \cos\beta) = \frac{2\sqrt{2}}{\sqrt{\pi}} E(U - U_a \cos\beta)\, U_a + \frac{C_D U_a^2 \sin^2\beta}{\sqrt{2\pi}} \tag{3.11}$$

and

$$\frac{d}{ds}(U^2 b \sin\beta) = -\frac{C_D U_a^2 \sin\beta \cos\beta}{\sqrt{2\pi}}. \tag{3.12}$$

Assuming the temperature distribution to be given by

$$T' = T \exp(-\eta^2/2\sigma^2), \tag{3.13}$$

Eq. 3.7 reduces to

$$\frac{d}{ds}(UTb) = 0. \tag{3.14}$$

Equations 3.10-3.13 now form a set of ordinary differential equations with unknowns U, T, b, and β, assuming that E and C_D are known. The independent variable, s, can be related to the x and y coordinates by the geometrical relationships

$$\left.\begin{aligned} \frac{dx}{ds} &= \cos\beta \\ &\text{and} \\ \frac{dy}{ds} &= \sin\beta. \end{aligned}\right\} \tag{3.15}$$

Thus, in all, there are six equations in six unknowns to be solved. This can be done numerically. To accomplish this, the authors rewrote the six equations in nondimensional form by defining the following relationships:

$$\left.\begin{aligned} V &= \frac{Ub}{U_0 b_0} \text{ (the nondimensional volume flux)}, \\ M &= \frac{U^2 b}{U_0^2 b_0} \text{ (the nondimensional momentum flux)}, \\ S &= (2E/\sqrt{\pi} b_0)s \text{ (the nondimensional axial distance)}, \\ A &= \frac{U_a}{U_0}, \\ C_D' &= \frac{C_D}{4E} \text{ (the reduced drag coefficient)}, \end{aligned}\right\} \tag{3.16}$$

(Contd.)

$$\left.\begin{aligned} X &= (2E/\sqrt{\pi}b_0)x \text{ (the nondimensional x distance),} \\ \text{and} \\ Y &= (2E/\sqrt{\pi}b_0)y \text{ (the nondimensional y distance).} \end{aligned}\right\} \quad \text{(Contd.)} \quad (3.16)$$

The equation for volume continuity becomes

$$\frac{dV}{dS} = \frac{M}{V} - A \cos \beta, \tag{3.17}$$

for the x component of momentum flux

$$\frac{d(M \cos \beta)}{dS} = \sqrt{2}A\left(\frac{M}{V} - A \cos \beta + AC_D' \sin^2 \beta\right), \tag{3.18}$$

for the y component

$$\frac{d(M \sin \beta)}{dS} = -\sqrt{2}A(AC_D' \sin \beta \cos \beta), \tag{3.19}$$

and the geometry equations

$$\frac{dX}{dS} = \cos \beta \text{ and } \frac{dY}{dS} = \sin \beta. \tag{3.20}$$

The energy equation can immediately be integrated to give

$$UTb = U_0 T_0 b_0. \tag{3.21}$$

Thus there are now five differential equations and five unknowns (V, M, β, X and Y), all functions of the nondimensional axial distance S.

The authors again rewrote these five equations to facilitate the use of a numerical-integration scheme which integrates a system of first-order differential equations by a fourth-order Runge-Kutta method. Details of this procedure are not reviewed here; the original work should be consulted for this information. In summary, problem solution involved the following sequence of events. First, given all the necessary input parameters, including C_D and E, the program solves for M and V for designated intervals of S. U, T, and b are then computed using the following relationships, derived from Eqs. 3.16 and 3.21:

$$\frac{U}{U_0} = \frac{M}{V}; \quad \frac{T}{T_0} = \frac{1}{V}; \quad \frac{b}{b_0} = \frac{V^2}{M}. \tag{3.22}$$

We then solve for β as a function of S. Once β is known U/U_0, T/T_0, and b/b_0 can be related to X and Y using the equations

$$X = \int_0^S \cos\beta \, dS \tag{3.23}$$

and

$$Y = \int_0^S \sin\beta \, dS. \tag{3.24}$$

The authors presented an example solution to illustrate the results of their analysis for a surface jet discharging into an ambient stream at an initial angle of $\beta_0 = 60°$. The jet velocity was assumed to be a factor of four greater than the ambient velocity, or $A = 0.25$. The reduced drag coefficient, $C_D' = C_D/4E$, was assigned values of 0.0, 0.5, and 1.0 to illustrate its effect on the jet trajectory. Since there was assumed to be no flow-establishment region, the initial coordinates were given by $X_0 = 0.0$ and $Y_0 = 0.0$. Figures 3.4-3.6 show the numerical results plotted in nondimensional form.

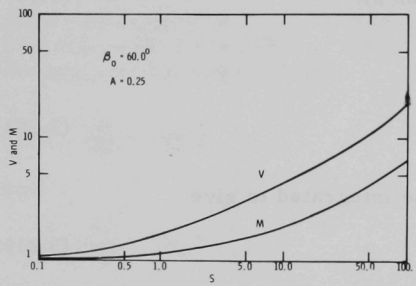

Fig. 3.4. Volume Flux, V, and Momentum Flux, M, vs Nondimensional Jet-axis Distance, S (Ref. 1)

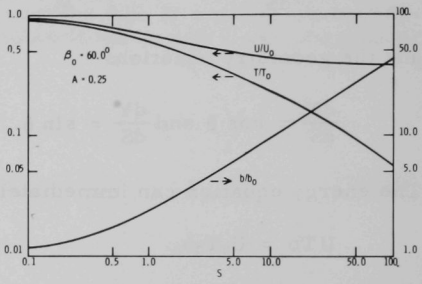

Fig. 3.5. Temperature, Velocity, and Width Ratios vs Nondimensional Jet-axis Distance, S (Ref. 1)

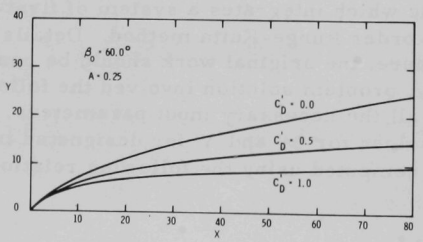

Fig. 3.6

Effect of Reduced Drag Coefficient on Location of Jet Trajectory[1]

e. Flow-establishment Considerations

The results for the hypothetical surface jet shown in Figs. 3.4-3.6 do not account for a zone of flow establishment in which the more or less

top-hat distributions of temperature and velocity at the jet origin change to fully developed profiles at some axial distance, s'_e, from the outfall, as is shown in Fig. 3.7. Figure 3.7 makes an important distinction between primed and unprimed symbols. Unprimed symbols refer to those portions of the jet for which the flow field is fully developed and the analytical development already presented applies. The prime notation applies to the portions of the jet under flow establishment.

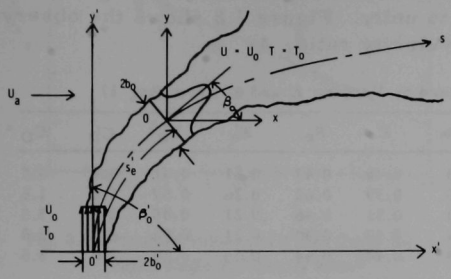

Fig. 3.7. Zone of Flow Establishment[1]

To account for the zone of flow establishment, the authors reviewed the work of Fan[3] in which he presented empirical relations for s'_e and β_0 in terms of the ratio of the ambient current speed to the initial jet velocity, that is to say, A. Fan's work accounted only for an initial discharge angle, β'_0, of 90° and for a velocity-ratio range of $0.125 \leq A \leq 0.25$. The authors felt that the range of interest for many practical situations would be more typical for $0.20 \leq A \leq 0.80$ or greater and for an arbitrary discharge angle β'_0. The authors chose to follow the example of Fan, that is to develop phenomenological relationships for s'_e and β_0 in terms of A and β'_0. Both the drag and entrainment coefficients would likely be dependent on A and β'_0. To obtain all these necessary relationships, the authors performed a series of laboratory hydraulic-model studies.

The authors presented considerable material describing the design, operation, and limitations of their laboratory experiments. While this material forms an important part of their overall effort, it cannot be discussed thoroughly here, simply because of space limitations. Only a summary of their results and conclusions will now follow.

In the laboratory experiments the velocity ratio, A, was varied from 0.18 to 0.727 while the initial discharge angle, β'_0, was fixed at 90, 60, or 45°. Table 3.1 summarizes the laboratory conditions and the experimentally determined parameters. The methods used to determine these parameters will now be discussed. Except for minor perturbations, the same methods were applied to actual field data, which will be reviewed later.

Graphical methods were used to determine s'_e and β_0 from the laboratory data in the following way: The jet trajectory for each run was estimated from the location of the maximum temperature experimentally acquired from the tank runs and plotted relative to the actual jet origin in terms of x'/b_0 and y'/b_0, where b_0 is the jet half-width at the end of the flow-establishment region or the start of the developed-flow regime. Next

the above data were replotted on log-log plots in terms of T/T_0 and s'/b_0. The length of the zone of flow establishment, s'_e/b_0, was then estimated from the log-log plot for each run by interpolating to find the largest value of s'_e/b_0 where T/T_0 was still equal to unity. Figure 3.8 shows the observed values for s'_e/b_0 plotted against the velocity ratio, A.

TABLE 3.1. Laboratory Results Found by Varying A and β'_0 (from Ref. 1)

A	β'_0	β_0	s'_e/b_0	x'_e/b_0	y'_e/b_0	E	S'_e	X'_e	Y'_e	C'_D	C_D
0.73	90.0	34.5	0.9	0.6	0.8	0.46	0.47	0.31	0.41	0.4	0.7
0.44	90.0	47.5	1.4	0.6	1.3	0.39	0.62	0.26	0.57	1.0	1.6
0.30	90.0	50.0	1.3	0.6	1.3	0.31	0.46	0.21	0.45	2.8	3.5
0.23	90.0	62.0	1.7	0.4	1.7	0.47	0.90	0.21	0.90	2.0	3.8
0.20	90.0	71.5	1.9	0.1	2.0	0.44	0.94	0.05	0.99	2.0	3.5
0.67	60.0	13.5	0.7	0.6	0.3	0.24	0.24	0.19	0.16	0.08	0.1
0.44	60.0	36.5	1.3	0.9	0.8	0.13	0.19	0.13	0.12	1.5	0.8
0.30	60.0	40.0	1.5	1.2	1.0	0.19	0.32	0.26	0.21	3.0	2.3
0.23	60.0	41.0	2.0	1.4	1.3	0.25	0.56	0.39	0.37	2.7	2.7
0.19	60.0	45.0	2.3	1.4	1.9	0.29	0.75	0.46	0.62	3.4	3.9
0.66	45.0	25.0	0.7	0.6	0.4	0.19	0.15	0.13	0.08	1.5	1.1
0.42	45.0	23.0	1.2	1.1	0.6	0.13	0.18	0.16	0.09	1.0	0.5
0.30	45.0	26.5	1.7	1.5	0.8	0.21	0.40	0.36	0.19	1.0	0.8
0.23	45.0	33.5	2.1	1.6	1.1	0.27	0.64	0.49	0.33	1.0	1.1
0.18	45.0	35.0	2.3	1.8	1.3	0.22	0.57	0.45	0.32	2.0	1.7

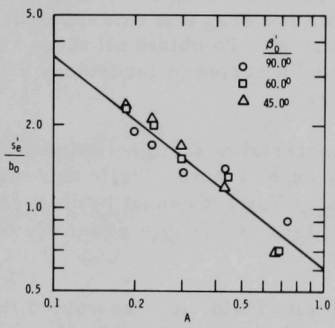

Fig. 3.8

Observed Values and Fitted Curve for Length of Establishment Zone vs Velocity Ratio[1]

The angle at the end of the zone of flow establishment was determined by first taking each previously determined value for s'_e/b_0 and locating it on the respective x'/b_0 and y'/b_0 trajectory plot that was smoothed for this purpose; β_0 the slope of the trajectory plot was then measured at that location. Values for β_0/β'_0 versus A are plotted in Fig. 3.9.

The jet half-width at the start of the established flow regime was used to form several of the nondimensionalized parameters. We can calculate b_0 by equating the heat fluxes at the immediate jet discharge and at the point, s'_e, where the jet becomes fully developed; i.e.,

$$z_0(2b'_0)U_0T_0 = z\sqrt{\pi/2}\,b_0UT, \tag{3.25}$$

where the two terms represent the integrated fluxes of heat for a top-hat and Gaussian temperature and velocity distribution, respectively. Since the excess temperature, T_0, the jet velocity, U_0, and the depth, z_0, at the outfall are equal to their respective centerline values at the start of the

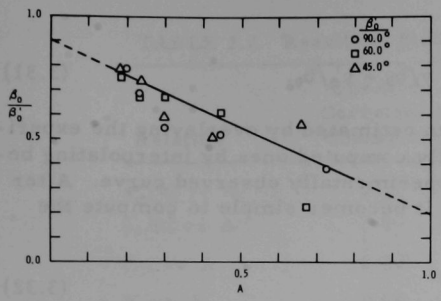

Fig. 3.9. Observed Values and Fitted Curve for Initial Angle vs Velocity Ratio[1]

established flow regime, Eq. 3.25 can be solved for b_0. Thus,

$$b_0 = \sqrt{8/\pi}\, b_0' = 1.6 b_0', \quad (3.26)$$

where b_0' is the jet half-width of the actual outfall.

f. Evaluation of Entrainment and Drag Coefficients

The laboratory studies also provided a means to determine and functionally relate the entrainment and drag coefficients to the velocity ratio and the initial angle of discharge. The entrainment coefficient, E, was obtained by first using the theoretical model to compute T/T_0 versus the nondimensional axial distance, S, for laboratory observed combinations of A and β_0' and for a range of values of the reduced drag coefficient, C_D'. An initial guess of E for each run is determined by horizontally sliding the plot of T/T_0 versus s'/b_0 over the computed curves of T/T_0 versus S until a best-fit situation arises. E can then be calculated using the following relationship obtained from Eqs. 3.16:

$$E = \sqrt{\pi}\, b_0 S/2s. \quad (3.27)$$

The nondimensional flow-establishment length, S_e', was next calculated from the observed value of s_e'/b_0 and the above preliminary value of E. A new plot of T/T_0 versus S' was then formed using the plot of T/T_0 versus S as its basis and the relationship

$$S' = S_e' + S, \quad (3.28)$$

which now references T/T_0 to the jet origin. In the same fashion as above, the plots of T/T_0 versus s' and T/T_0 versus S' were slid horizontally over each other until a best fit between the two was obtained. The final form for E was then computed from

$$E = \sqrt{\pi}\, b_0 S'/2s'. \quad (3.29)$$

The drag coefficient C_D for any run was also graphically determined. First, the mathematical model was used to calculate values for X and Y along with T/T_0 for each value of A and β_0 and several assumed values of C_D'. Each of these mathematically predicted trajectories was plotted in terms of x'/b_0 and y'/b_0, where

$$x = \sqrt{\pi}\, b_0 X/2E; \quad y = \sqrt{\pi}\, b_0 Y/2E \quad (3.30)$$

and

$$x'/b_0 = x/b_0 + x'_e/b_0; \quad y'/b_0 = y/b_0 + y'_e/b_0. \tag{3.31}$$

The actual value for C'_D is then estimated by overlaying the experimental trajectory with the theoretically computed ones by interpolating between the theoretical curves to the experimentally observed curve. After the reduced drag coefficient is found, it becomes simple to compute the drag coefficient from

$$C_D = 4EC'_D. \tag{3.32}$$

The results for C'_D and C_D are shown in Figs. 3.10 and 3.11, respectively.

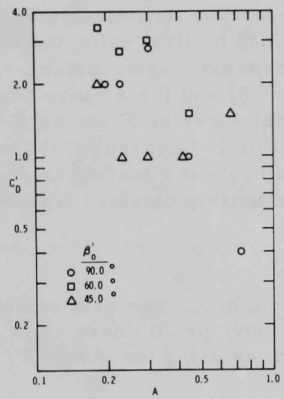

Fig. 3.10. Observed Values of Reduced Drag Coefficient vs Velocity Ratio[1]

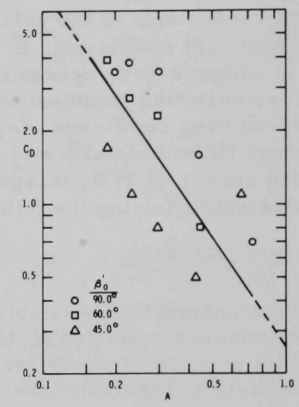

Fig. 3.11. Observed Values and Fitted Curve for Drag Coefficient vs Velocity Ratio[1]

The authors performed statistical tests on the experimentally determined parameters. Correlation coefficients were obtained (see Table 3.2) using regression methods for assumed arithmetic, semilog, and log-log relations between s'_e/b_0, β_0/β'_0, C_D, C'_D, and E versus A. The assumed relation with the highest correlation coefficient was that used for data presentation. Table 3.2 points to the fact that the entrainment coefficient was not a function of A, at least for the range of A investigated. However, some dependence of E on β'_0, was indicated by the F test, which compares the ratios of the variances; these results are shown in Table 3.3. Table 3.3 shows that the mean value of E at $\beta'_0 = 90$ is much different from the mean of the values obtained at $\beta'_0 = 60°$ or 45°. Further, Table 3.2 and Fig. 3.11 also indicate that C_D may be a function of β'_0 as well; however, because of the limited number of data points, this cannot be clearly established.

TABLE 3.2. Results of Statistical Tests on Parameters[1]

Relation	Observed Correlation Coefficient	Correlation Coefficient at 1% Level of Significance
s_e'/b_0 vs A	0.95	0.64
β_0/β_0' vs A	0.87	0.64
C_D vs A	0.72	0.64
E vs A	0.01	0.64
C_D vs A ($\beta_0' = 90.0°$)	0.98	0.96
C_D vs A ($\beta_0' = 60.0°$)	0.97	0.96
C_D vs A ($\beta_0' = 45.0°$)	0.99	0.96

TABLE 3.3. Relation of E to β_0' (Ref. 1)

β_0'	$\overline{E}$	F Ratio	Level of Significance
90°	0.41		
		23.1	0.1%
60°	0.22		
		0.20	None
45°	0.20		

g. Model Verifications

The authors compared their model to field data obtained at three locations representing a total of five independent data sets. Space limitations preclude an account of the application of the model to the field data; therefore only a discussion of the results will be given. Table 3.4 summarizes the field results.

TABLE 3.4. Summary of Field Results

	A	β_0'	Ri_0	E	C_D'	C_D
Widows Creek						
VU No. 1	0.50	85.0	0.22	0.16	1.0	0.6
VU No. 2	0.67	85.0	0.64	0.16	0.9	0.6
TVA	0.75	85.0	1.21	0.16	0.4	0.3
New Johnsonville	0.57	60.0	3.30	0.04	3.0	0.5
Waukegan	0.00	-	0.01	0.44	-	-

For the flow-establishment region the authors found it necessary to use their empirical laboratory results, because the field data were not sufficiently complete, that is, on a sufficiently fine grid, to clearly establish either the length s_e' or the angle β_0.

The entrainment coefficients for four of the five field situations were lower than anticipated. The authors argued that these situations, which were on river locations, were apparently influenced by the proximity of shoreline boundaries. The presence of shorelines would be expected to decrease the volume of colder water available for dilution on the side(s) of the jet near such boundaries. Similarly, the same effect would hold true for smaller initial discharge angles, as is indicated by a smaller E for $\beta_0' = 45$ or $60°$ when compared to a $90°$ angle, as is seen from the laboratory results.

The limited field results also indicated that the entrainment coefficient remained essentially constant at a particular location with changing values of A. This behavior is consistent with the laboratory findings, showing E to be relatively independent of A. However, in a recent progress report by Benedict and Yandell,[9] the authors have looked at some actual lake-plume data and laboratory data in which the velocity ratio A approaches zero. Under such conditions, the entrainment coefficient approached low values, <0.1, even when geometry was nonconfining. Benedict has proposed that under more normal conditions the separation of the ambient current around a jet establishes a lateral vortex in the jet which enhances mixing. As the ambient current decreases below a critical value, a point is reached at which this secondary current ceases to be important and all mixing is by "aspiration" of surrounding fluid through shearing action; this is apparently somewhat less efficient than the vortex action. Table 3.5 and Fig. 3.12 show values of the entrainment coefficient for various field situations.[9] The column labeled "k" in the table is the inverse of

TABLE 3.5. Values of Entrainment Coefficient[9]

Data Source	β_0', °	F_0	$k = \frac{U_0}{U_a}$	$W = \frac{\text{ambient-stream width}}{\text{discharge width}}$	E
Laboratory	90	3.4-6.9	1.37-5.2	24	avg = 0.4
Laboratory	45 and 60	3.1-6.3	1.53-5.2	24	avg = 0.2
Widows Creek					
VU No. 1	85	4.3	2.0	7.5	0.16
VU No. 2	85	3.7	1.5	7.5	0.16
TVA	85	3.7	1.33	7.5	0.16
New Johnsonville	60	1.3	1.75	4	0.04
Stefan (laboratory)	-	3.7-4.1	∞	34	0.06-0.09
Vandy (laboratory)	90	4.2-7.4	3-30-∞	24	0.04-0.4
Fitch[a]					
(Lake St. Croix)	60	0.25-0.55	3-19[b]	20	0.11-0.296
Ayers[a]					
(Michigan City)	90	1.2	10[b]	-	0.04
Romberg[a]					
(Waukegan)	90	5.6-6.0	1.7-5.6	-	0.046-0.059

[a]Lake field data.
[b]Estimated values.

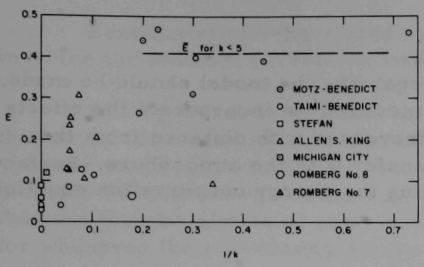

Fig. 3.12

Entrainment Coefficient as a Function of Velocity Ratio (where geometry is nonconfining)[9]

the velocity ratio A and the column "W" is the ratio of ambient-stream width to the actual outfall width.

The field values of the coefficient of drag were found to be close to the laboratory values, as is shown in Fig. 3.13. The authors point out that with the limited field data available and its apparent agreement with the laboratory curve, C_D appears to be independent of the Reynolds number. The authors at the same time caution the reader that it may not be generally possible to extrapolate the laboratory curve of C_D versus A to field situations as is done in Fig. 3.13 because prototype Reynolds numbers are two or more orders of magnitude greater than the laboratory data. Figure 3.14 shows C_D values obtained from the laboratory and field data plotted against the Reynolds number. The Reynolds number was defined as

$$Re_D = \frac{U_a z}{\nu_a}, \tag{3.33}$$

where ν_a is the ambient kinematic viscosity. This figure, according to the authors, suggests that C_D as used within the model may assume some of the characteristics normally associated with flows around solid bodies, which was one of the primary assumptions in the model.

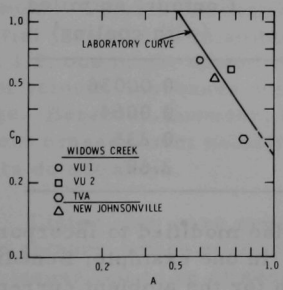

Fig. 3.13

Observed Field Values of Drag Coefficient vs Velocity Ratio Plotted on Laboratory Curve[1]

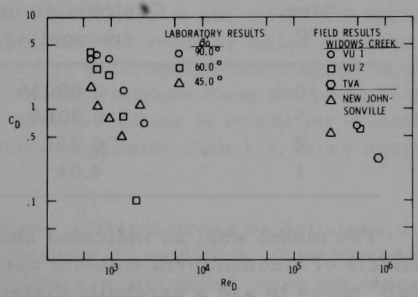

Fig. 3.14

Observed Values of Drag Coefficient vs Reynolds Number[1]

h. Discussion of Model Development

Several additional comments regarding the model should be made. The original model has recently been modified[9] to incorporate the effects of a nonuniform ambient current that increases with distance from the shore and to allow for surface heat transfer with the atmosphere. Surface heat loss was accounted for by modifying the energy conservation equation to the form

$$\frac{d}{ds}(UTb) = \frac{-\sqrt{2}\,K}{\rho c_p z_0}\,Tb, \tag{3.34}$$

where

K = surface-heat-loss coefficient

and

c_p = specific heat of water.

Equation 3.34 has been used in place of Eq. 3.7 with the results indicating that surface cooling plays no significant effect until the lower excess-temperature contours (1-2°) are reached. Benedict and Yandell[9] made an example calculation for a Lake Michigan site and for an assumed value for K of 180 Btu/ft^2-day-°F. Table 3.6 shows these results.

TABLE 3.6. Results of Surface-jet Analysis[1]

Temperature Rise, °F	Area within Contour, sq miles (no cooling)	Area within Contour, sq miles (with cooling)
10	0.00036	0.00036
5	0.0064	0.0064
2	0.255	0.235
1	4.04	2.68

The model was, as indicated above, also modified to incorporate the effects of a nonuniform ambient current. In one example, Benedict and Yandell[9] chose to use a parabolic distribution for the ambient current. Since the authors use a numerical approach, all that is done is to calculate a new ambient velocity for each incremental step in the numerical integration scheme. For the lake situation investigated and for most field cases of practical interest, they have concluded that there is little difference between predictions obtained by choosing some suitable average of the ambient current over the reach influenced by the jet when compared to the inclusion of a more refined profile. The authors indicate, however, that this generalization may not be true for values of A larger than 0.5.

Benedict et al.[10] have also modified the original model for situations in which the ambient current exceeded the initial jet velocity.

Some general comments concerning the model should be made at this point. The authors have discussed, in great length, possible sources of error with regard to their work. They recognize that the graphical methods for evaluating coefficients are somewhat subjective. They also indicate that the effects of ambient turbulent mixing should be accounted for whenever the jet velocity approaches the same direction and magnitude as the ambient current. They recognize that buoyancy-induced convective motions may be present, but they assume them to be small. Vertical entrainment is neglected; however, they indicate that it should really be considered very near the point of discharge and in the outer reaches of the jet when the jet temperature approaches that of the ambient or, in other words, when the Richardson number becomes small (<0.8).

It is also recognized that the velocity and temperature profiles at the point of discharge may not be top-hat, in which case the flow-establishment region may be smaller than predicted by their model. The authors recognized that the expression for the lateral velocity distribution, Eq. 3.8, does not approach ambient velocity conditions for large η, but rather a value of zero. The authors chose this form to obtain convenient nondimensional relationships in terms of velocity ratio A. If Eq. 3.8 were modified to account for an asymptotic approach to the ambient crosscurrent, or better, its component in the jet axial direction, the fitted values for E would differ from those specified by the authors. Much in the same vein, the authors could have chosen a top-hat lateral-velocity distribution, in which case the values for E would again be different from the above stated situations. Private correspondence with Benedict indicated that for ratios of initial jet velocity to ambient crosscurrent velocity which are less than about 1.2, one might expect the model to yield anomalous results in which the jet velocity increases with increasing distance from the point of discharge. Benedict, however, states that for ratios of initial jet velocity to ambient crosscurrent velocity which are greater than 1.5, these anomalous results do not arise.

Listed above are several of the problem areas or deficiencies noted by the authors, which need to be corrected or modified. Considered now are those issues felt to be of additional concern, but which were not stressed by Motz and Benedict. First, there seems to be some question concerning the form of the drag term, Eq. 3.4. There is some evidence pointing to the fact that the pressure term normal to the plume axis should not approach zero as β approaches zero. This issue has already been discussed. In the field work cited by the authors, the jet-development region was assumed to be governed by the laboratory modeling results because, as the authors indicate, it is difficult to obtain enough field data to delineate this development zone. This point should not be dismissed lightly. Verification of this fact

alone will shed much light on the suitability of the model and/or the applicability of laboratory modeling. If there is any portion of a thermal plume that is amenable to laboratory modeling, it is the jet regime. The failure or success of laboratory models to predict field behavior is of extreme importance, considering the amount of hydraulic modeling being performed to this end.

An inspection of Table 3.5 and Fig. 3.12 shows considerable variation in the value of the entrainment coefficient from situation to situation. Particularly for lake data, the value of E is shown to be extremely small, ~0.04, in relation to riverine situations, where E is about an order of magnitude larger. A particularly interesting contrast is afforded in Table 3.5 when the Motz and Benedict laboratory data for 90° are compared with the Romberg and Ayers lake data. Although most of the initial conditions are similar, the entrainment coefficients are different by about a factor of 10. The comments in the sixth paragraph of this section (page 87), regarding the influence of ambient crossflows on the entrainment coefficient as the velocity ratio A approaches low values, may be applicable here. Perhaps, too, part of the problem lies with the fact that the authors analyzed lake data from locations in which prominences (breakwaters, for instance) were present. Everything being about equal, it is not clear why a lake location would have a significantly lower entrainment coefficient than a river location. As soon as more lake data become available, this point can be clarified.

Regarding the application of the model to field situations, the model has as yet only been used in a "curve-fitting" sense. That is, it has been matched to existing field data by adjusting appropriate coefficients. Even so, the model has enjoyed some reasonable success. The major impediment for using this model in a predictive sense is the need for the specification of the drag and particularly the entrainment coefficients. Earlier discussions have made it clear that the value of the entrainment coefficient is highly dependent on boundary effects, the relationship being unknown except in a gross way. Confining boundaries decrease the entrainment coefficient, for the anomalous lake data, this point having been discussed earlier.

The drag coefficient was shown to be reasonably well behaved, comparing favorably with the empirically obtained laboratory data. As a first approximation, therefore, either an extrapolation of the laboratory coefficients to the prototype situation can be considered to obtain C_D, or a value of roughly 0.5 can be assumed as indicated by the field data in Fig. 3.14.

Work on this model continues to be in progress by Benedict and his co-workers at Vanderbilt University as part of an ongoing effort sponsored by the Federal Environmental Protection Agency. Therefore, as more field data become available to which this model can be compared, the proper choice for values of C_D and E may become more apparent, making this model more suitable for predictive use.

A computer program for this model is available which includes the effects of surface heat transfer and nonuniform ambient currents.

References

1. L. H. Motz and B. A. Benedict, Heated Surface Jet Discharged into a Flowing Ambient Stream, Department of Environmental and Water Resources Engineering, Vanderbilt University, Nashville, Tenn., Report No. 4 (Aug 1970).

2. B. R. Morton, On a Momentum-Mass Flux Diagram for Turbulent Jets, Plumes, and Wakes, J. Fluid Mech. 10 (1961).

3. Loh-Nien Fan, Turbulent Buoyant Jets into Stratified or Flowing Ambient Fluids, Tech. Report No. KH-R-15, W. M. Keck Lab. of Hydraulics and Water Resources, California Institute of Technology, Pasadena, Calif. (June 1967).

4. J. A. Hoopes, R. W. Zeller, and G. A. Rohlich, Heat Dissipation and Induced Circulations from Condenser Cooling Water Discharges into Lake Monona, Engineering Experiment Station Report No. 35, The University of Wisconsin, Madison, Wisc. (Feb 1968).

5. H. H. Carter, A Preliminary Report on the Characteristics of a Heated Jet Discharged Horizontally into a Transverse Current: Part 1. Constant Depth, Tech Report No. 61, Chesapeake Bay Institute, Johns Hopkins University, Baltimore, Md. (Nov 1969).

6. T. H. Ellison and J. S. Turner, Turbulent Entrainment in Stratified Flows, J. Fluid Mech. 6 (1959).

7. G. Abramovich, The Theory of Turbulent Jets, M.I.T. Press, Cambridge, Mass., p. 546 (1963).

8. H. Rouse, Diffusion in the Lee of a Two-Dimensional Jet, Iowa Institute of Hydraulics, State University of Iowa, 9th Congress International de Mechanique Appliquee, Vol. I, pp. 307-312 (1957).

9. B. A. Benedict and E. L. Yandell, Vanderbilt University, personal communication (Oct 20, 1971).

10. B. A. Benedict, E. M. Polk, E. L. Yandell, and F. L. Parker, "Surface Jet and Diffusion Models for Discharge of Heated Waters," to be published in Proceedings, 14th Congress of the International Association for Hydraulic Research.

4. An Analytical and Experimental Investigation of Surface Discharges of Heated Water[1,2]

K. Stolzenbach and D. R. F. Harleman
(Massachusetts Institute of Technology)

February 1971

a. List of Symbols

A	Discharge channel aspect ratio $= h_0/b_0$
a	Coefficient of thermal expansion $= -\frac{\partial \rho}{\partial T}$
b	Half the width of the turbulent region of the jet
b_0	Half the width of a rectangular discharge channel
c_p	Specific heat at constant pressure
D	Ratio of flow in jet to initial discharge flow = dilution
$\left(\frac{db}{dx}\right)_{NB}$	Spread of a nonbuoyant jet
E	Energy per unit mass
$\mathbb{F}$	Densimetric Froude number $= \frac{u}{\sqrt{\frac{\Delta\rho}{\rho} gh}}$
$\mathbb{F}_0$	Densimetric Froude number of discharge channel $= \frac{u_0}{\sqrt{\frac{\Delta\rho_0}{\rho_a} gh_0}}$
$\mathbb{F}_L$	Local densimetric Froude number in the jet $= \frac{u_c}{\sqrt{\frac{a\Delta T_c gh}{\rho a}}}$
f	Similarity function for velocity $= (1 - \zeta^{3/2})^2$
H	Ratio of heat flow in jet to initial discharge heat flow
h	Vertical height of turbulent region of jet
h_0	Depth of discharge channel
h_{max}	Maximum value of h obtained in heated discharge
I_1	$\int_0^1 f(\zeta)\, d\zeta = 0.4500$
I_2	$\int_0^1 f^2(\zeta)\, d\zeta = 0.3160$

I_3	$\int_0^1 t(\zeta)\, d\zeta = 0.6000$
I_4	$\int_0^1 \int_\zeta^1 t(\bar{\zeta})\, d\bar{\zeta}\, d\zeta = 0.2143$
I_5	$\int_0^1 f(\zeta)\zeta^{1/2}\, d\zeta = 0.2222$
I_6	$\int_0^1 f^2(\zeta)\zeta^{1/2}\, d\zeta = 0.1333$
I_7	$\int_0^1 f(\zeta)t(\zeta)\, d\zeta = 0.3680$
K	Surface-heat-loss coefficient
k	Thermal conductivity of water
p	Pressure
p_d	Dynamic pressure
p_h	Hydrostatic pressure
Q_0	Discharge channel flow
q_e	Entrainment flow into jet per unit length of jet
R_i	Richardson number $= \dfrac{\frac{g}{\rho}\frac{\partial \rho}{\partial z}}{\left(\frac{\partial u}{\partial z}\right)^2}$
R_H	Hydraulic radius of the discharge channel flow
r	Vertical distance from jet centerline to boundary of core region
S_x	Bottom slope
s	Horizontal distance from jet centerline to boundary of core region
t	Similarity function for temperature $= 1 - \zeta^{3/2}$
T	Temperature
T_a	Ambient temperature
T_c	Jet-surface centerline temperature
T_0	Temperature of heated flow in discharge channel
T_s	Temperature at water surface
ΔT	Temperature rise above ambient in jet $= T - T_a$

ΔT_c	Surface temperature rise above ambient at the jet centerline $= T_c - T_a$
ΔT_0	Temperature difference between the discharge and the ambient water $= T_0 - T_a$
t	Similarity function for temperature $= 1 - \zeta^{3/2}$
u, v, w	Velocity components in fixed-coordinate system
$\tilde{u}, \tilde{v}, \tilde{w}$	Velocity components in coordinate system relative to centerline of a deflected jet
u_0	Velocity in discharge channel
u_c	Surface-centerline jet velocity
V	Ambient crossflow velocity
v_e	Lateral velocity of entrained flow at jet boundary
v_b	Lateral velocity in jet at $y = s$ and $-h < z < -r$
v_s	Lateral velocity in jet at $y = s$ and $-r < z < \eta$
w_h	Vertical velocity in jet at $z = -r$ and $s < y < b + s$
w_e	Vertical velocity of entrained flow at jet boundary
w_r	Vertical velocity in jet at $z = -r$ and $0 < y < s$
x, y, z	Fixed-coordinate directions
$\tilde{x}, \tilde{y}, \tilde{z}$	Coordinate directions relative to centerline of a deflected jet
x_s	Distance from jet origin to point where $s = 0$
x_r	Distance from jet origin to point where $r = 0$
α_y	Lateral-entrainment coefficient in nonbuoyant and buoyant jets
α_z	Vertical-entrainment coefficient in a nonbuoyant jet
α_{sz}	Vertical-entrainment coefficient in a buoyant jet
ϵ	Spread, db/dx, of turbulent region in an undeflected nonbuoyant jet
η	Water-surface elevation
θ	Angle between jet centerline ($\tilde{x}$ axis) and y axis
θ_0	Angle between discharge-channel centerline and y axis
ρ	Density of water
ρ_a	Density of ambient water

ρ_0	Density of heated discharge
$\Delta\rho$	Difference between density and ambient-water density = $\rho - \rho_a$
$\Delta\rho_0$	Difference between density of heated flow in discharge channel and ambient density = $\rho_0 - \rho_a$
φ	Viscous generation of heat
ν	Kinematic viscosity of water
'	Indicates a turbulent fluctuating quantity

b. Introduction

Stolzenbach and Harleman have developed a three-dimensional mathematical model for the horizontal surface discharge of heated condenser cooling water from a rectangular open channel into a large lake. The model can handle a bottom slope and a crossflow at right angles to the discharge. Heat is dissipated by mixing discharged and ambient water and by surface heat loss to the atmosphere. The mathematical model predicts the distributions of temperature and velocity within a completely determined jet structure for a near-field region defined by the predominance of initial jet momentum over the effects of ambient lake turbulence. A heated surface discharge affected by a transverse crosscurrent and by bottom effects is illustrated in Fig. 4.1.

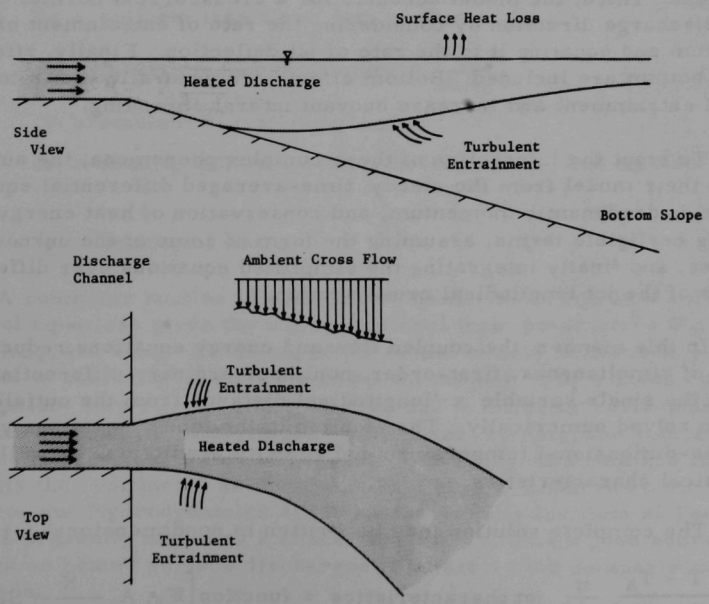

Fig. 4.1. Schematic Diagram of Heated Discharge[1]

The model synthesizes previous knowledge on buoyant and nonbuoyant jets wherever possible. The heated discharge is assumed to be structured in its physical characteristics and velocity and temperature distribution basically like a classical turbulent nonbuoyant jet. Just as for nonbuoyant jets, the authors assume an initial core region void of shear followed by the main turbulent region. Using an integral method as in most jet analyses, velocities and temperatures at each longitudinal cross section are presumed to be related to centerline values by similarity profiles. In addition, horizontal and vertical entrainment of ambient fluid is accounted for and assumed proportional to the jet centerline velocity by an entrainment coefficient. In the Stolzenbach-Harleman analysis, the lateral entrainment coefficient is determined by nonbuoyant jet theory alone; the vertical component is related to the local temperature gradient by the local Richardson number using the experimental results of Ellison and Turner[3] and is chosen to reduce to the nonbuoyant value when no density gradients exist.

The unique aspects of the model involve the incorporation of a wide range of phenomena into the theory of heated jets. First, buoyant convection is incorporated through the pressure-gradient terms in the equations of motion and through the vertical-entrainment coefficient. Buoyancy effects generally reduce vertical entrainment and enhance lateral spreading. Second, the magnitude of heat loss to the overlying air and its three-dimensional implications are investigated through a surface heat-exchange coefficient. Third, the model accounts for a crosscurrent normal to the initial discharge direction by considering the rate of entrainment of lateral momentum and equating it to the rate of jet deflection. Finally, effects of a sloping bottom are included. Bottom effects are generally known to inhibit vertical entrainment and increase buoyant lateral spreading.

To treat the interaction of these complex phenomena, the authors develop their model from the steady, time-averaged differential equations of mass, hydrodynamic momentum, and conservation of heat energy by dropping negligible terms, assuming the form of some of the unknown variables, and finally integrating the simplified equations over different portions of the jet longitudinal cross section.

In this manner, the coupled flow and energy equations reduce to a system of simultaneous, first-order, nonlinear ordinary differential equations in the single variable x (longitudinal distance from the outfall), which are then solved numerically. The solution to the model equations yields the three-dimensional temperature and velocity predictions as well as the jet physical characteristics.

The complete solution may be written in nondimensional form as

$$\frac{T - T_a}{T_0 - T_a};\ \frac{u}{u_0};\ \text{jet characteristics} = \text{function}\left[\mathbb{F}_0,\ A,\ \frac{K}{\rho c_p u_0},\ S_x,\ \frac{V}{u_0}\right],$$

where

$$\mathbb{F}_0 = \frac{u_0}{\sqrt{\frac{\Delta\rho}{\rho} g h_0}} = \text{discharge densimetric Froude number,}$$

$$A = \frac{h_0}{b_0} = \text{discharge-channel aspect ratio,}$$

$$\frac{K}{\rho c_p u_0} = \text{surface-heat-loss parameter,}$$

$$S_x = \text{bottom slope,}$$

$$\frac{V}{u_0} = \text{crossflow parameter,}$$

$$2b_0 = \text{width of discharge channel,}$$

$$c_p = \text{specific heat of water,}$$

$$g = \text{acceleration of gravity,}$$

$$h_0 = \text{depth of discharge channel,}$$

$$K = \text{surface-heat-transfer coefficient,}$$

$$Q_0 = \text{volumetric flow rate at discharge,}$$

$$T_0 = \text{initial discharge temperature,}$$

$$T_a = \text{uniform lake water temperature,}$$

$$u_0 = \text{initial discharge velocity} = \frac{Q_0}{2h_0 b_0},$$

$$V = \text{ambient crossflow velocity,}$$

$$\Delta\rho = \text{density difference between discharged, and ambient water}$$

and

$$\rho = \text{density of water.}$$

A computer routine is available to handle the numerical solution to the model equations given the nondimensional input parameters $\mathbb{F}_0$, A, $K/(\rho c_p u_0)$, S_x, and V/u_0. No fitting of the model to data is necessary since the model is basically a synthesis of known results. For a given outfall configuration, only T_a, V, and K change due to differing environmental conditions and must be determined in the field. To date, the authors have compared their model solely to hydraulic-modeling data obtained in experiments they conducted at the Ralph M. Parsons Laboratory for Water Resources and Hydrodynamics at the Massachusetts Institute of Technology. They are presently mounting a concerted effort to locate good sources of field data on heated surface discharges to affect a field comparison of their model.

c. Model 1: Buoyant Jet (no crossflow and no bottom)

(1) Outfall Geometry and Governing Equations. The outfall geometry for the model is illustrated in Fig. 4.2, where

x = longitudinal distance measured along the centerline of the plume,

y = lateral distance normal to the centerline,

z = vertical distance measured from the receiving water surface downward,

and

η = water-surface elevation in relation to the ambient lake level.

The authors begin with the basic hydrodynamic and thermodynamic equations governing compressible fluid flow with constant absolute viscosity μ (Ref. 4, pp. 36, 37, and 42).

Conservation of mass

$$\frac{\partial \rho}{\partial t} + \frac{\partial(\rho u)}{\partial x} + \frac{\partial(\rho v)}{\partial y} + \frac{\partial(\rho w)}{\partial z} = 0. \tag{4.1}$$

Conservation of x, y, z momentum

$$\left.\begin{aligned} \frac{\partial u}{\partial t} + u\frac{\partial u}{\partial x} + v\frac{\partial u}{\partial y} + w\frac{\partial u}{\partial z} &= -\frac{1}{\rho}\frac{\partial p}{\partial x} + \nu\frac{\partial}{\partial x}\left[2\frac{\partial u}{\partial x} - \frac{2}{3}\left(\frac{\partial u}{\partial x} + \frac{\partial v}{\partial y} + \frac{\partial w}{\partial z}\right)\right] \\ &+ \nu\frac{\partial}{\partial y}\left(\frac{\partial u}{\partial y} + \frac{\partial v}{\partial x}\right) + \nu\frac{\partial}{\partial z}\left(\frac{\partial w}{\partial z} + \frac{\partial u}{\partial z}\right) \end{aligned}\right\} \tag{4.2}$$

$$\left.\begin{aligned} \frac{\partial v}{\partial t} + u\frac{\partial v}{\partial x} + v\frac{\partial v}{\partial y} + w\frac{\partial v}{\partial z} &= -\frac{1}{\rho}\frac{\partial p}{\partial y} + \nu\frac{\partial}{\partial y}\left[2\frac{\partial v}{\partial y} - \frac{2}{3}\left(\frac{\partial u}{\partial x} + \frac{\partial v}{\partial y} + \frac{\partial w}{\partial z}\right)\right] \\ &+ \nu\frac{\partial}{\partial z}\left(\frac{\partial v}{\partial z} + \frac{\partial w}{\partial y}\right) + \nu\frac{\partial}{\partial x}\left(\frac{\partial u}{\partial y} + \frac{\partial v}{\partial x}\right) \end{aligned}\right\} \tag{4.3}$$

$$\left.\begin{aligned} \frac{\partial w}{\partial t} + u\frac{\partial w}{\partial x} + v\frac{\partial w}{\partial y} + w\frac{\partial w}{\partial z} &= -\frac{1}{\rho}\frac{\partial p}{\partial z} - g + \nu\left[2\frac{\partial w}{\partial z} - \frac{2}{3}\left(\frac{\partial u}{\partial x} + \frac{\partial v}{\partial y} + \frac{\partial w}{\partial z}\right)\right] \\ &+ \nu\frac{\partial}{\partial x}\left[\frac{\partial w}{\partial x} + \frac{\partial u}{\partial z}\right] + \nu\frac{\partial}{\partial y}\left[\frac{\partial v}{\partial z} + \frac{\partial w}{\partial y}\right] \end{aligned}\right\} \tag{4.4}$$

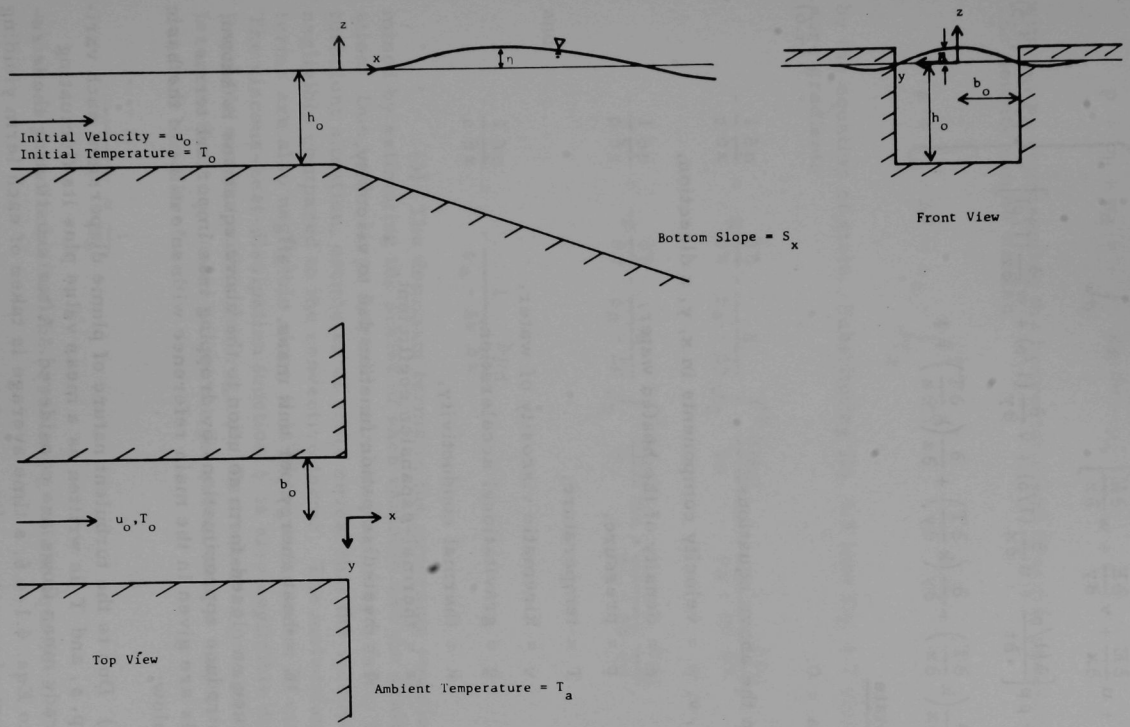

Fig. 4.2. Characteristics of Discharge Channel[1]

Conservation of energy

$$\left.\begin{aligned}&\rho\left[\frac{\partial E}{\partial t} + u\frac{\partial E}{\partial x} + v\frac{\partial E}{\partial y} + w\frac{\partial E}{\partial z}\right]\\&\quad + \rho p\left[\frac{\partial(1/\rho)}{\partial t} + u\frac{\partial}{\partial x}(1/\rho) + v\frac{\partial}{\partial y}(1/\rho) + w\frac{\partial}{\partial z}(1/\rho)\right] = \\&\quad \frac{\partial}{\partial x}\left(k\frac{\partial T}{\partial x}\right) + \frac{\partial}{\partial y}\left(k\frac{\partial T}{\partial y}\right) + \frac{\partial}{\partial z}\left(k\frac{\partial T}{\partial z}\right) + \Phi\end{aligned}\right\}. \tag{4.5}$$

Equation of state

$$\frac{\partial \rho}{\partial T} + a = 0. \tag{4.6}$$

In the above equations,

u, v, w = velocity components in x, y, z direction,

ρ = density of the heated water,

p = pressure,

T = temperature,

ν = kinematic viscosity of water,

g = gravitational acceleration,

k = thermal conductivity,

a = thermal-expansion coefficient,

Φ = heat-dissipation function due to viscosity,

and

E = heat energy per unit mass.

Since no closed-form solution to the above equations is known, the authors introduce approximations by dropping less important terms. Specific details are given in the main reference with an outline of the basic steps given below:

(1) Due to the turbulent nature of plume dispersion, each variable, u, v, w, p, ρ, and T is written as a mean value plus its fluctuating part. Only steady mean flows are considered. After substituting these relationships into Eqs. 4.1-4.6, a time average is taken of each term yielding a related system of equations. (Mean values are written without a bar for convenience with primes referring to fluctuating components.)

(2) Resolution of the pressure is affected, where

$$p = p_h + p_d = -\int_{\eta}^{z} \rho g \, dz + p_d \tag{4.7}$$

with p_h, p_d representing the hydrostatic and dynamic pressure components. The density can be written

$$\rho = \rho_a - \Delta\rho = \rho_a - \int_{T_a}^{T} a \, dT \tag{4.8}$$

by the equation of state. Substituting Eq. 4.8 into Eq. 4.7 yields the pressure gradients

$$-\frac{1}{\rho}\frac{\partial p}{\partial x} = -g\frac{\partial \eta}{\partial x} - \frac{g}{\rho_a - \Delta\rho}\int_{\eta}^{z} \frac{\partial(\Delta\rho)}{\partial x} dz - \frac{1}{\rho_a - \Delta\rho}\frac{\partial p_d}{\partial x}, \tag{4.9}$$

$$-\frac{1}{\rho}\frac{\partial p}{\partial y} = -g\frac{\partial \eta}{\partial y} - \frac{g}{\rho_a - \Delta\rho}\int_{\eta}^{z} \frac{\partial(\Delta\rho)}{\partial y} dz - \frac{1}{\rho_a - \Delta\rho}\frac{\partial p_d}{\partial y}, \tag{4.10}$$

and

$$-\frac{1}{\rho}\frac{\partial p}{\partial z} = g - \frac{1}{\rho_a - \Delta\rho}\frac{\partial p_d}{\partial z}. \tag{4.11}$$

(3) The dominant terms in the governing equations are determined by estimating the scales of each variable and the scale of its fluctuation. Due to the large Reynolds number caused by a fairly developed turbulent situation, estimates of scale reveal that the viscous terms are negligible compared to the convective terms. The molecular-heat-transfer terms are also negligible since k is of the same order of magnitude as ν. The viscous-heat-dissipation function Φ is also negligible due to a large Reynolds number within this regime. Estimates on possible density differences that may occur within the jet reveal that a may be considered constant and therefore

$$\frac{1}{\rho_a - \Delta\rho} \approx \frac{1}{\rho_a}, \tag{4.12}$$

which, in turn simplifies the pressure-gradient equations, Eqs. 4.9-4.11.

Examining the scale factors in the mass-conservation equation reveals that it reduces to the continuity equation for incompressible fluids,

$$\frac{\partial u}{\partial x} + \frac{\partial v}{\partial y} + \frac{\partial w}{\partial z} = 0. \tag{4.13}$$

Analysis of the momentum equations at large depths in z, where plume influence is nonexistent, yields a negligible scale for the free-surface change η. Due to local isotropy of turbulent shear flow, the scales of the fluctuating components u', v', and w' are the same order of magnitude, the corresponding mean values being an order of magnitude greater.

With these basic facts at hand, each term in the mass, momentum, and energy equations is estimated as to its magnitude, those negligible being dropped. This procedure is straightforward and yields the reduced system of equations,

$$\frac{\partial u}{\partial x} + \frac{\partial v}{\partial y} + \frac{\partial w}{\partial z} = 0, \tag{4.14}$$

$$\frac{\partial u^2}{\partial x} + \frac{\partial uv}{\partial y} + \frac{\partial uw}{\partial z} = \underline{\frac{ag}{\rho_a}\int_z^{-\infty} \frac{\partial \Delta T}{\partial x}\, dz} - \frac{\partial u'v'}{\partial y} - \frac{\partial u'w'}{\partial z}, \tag{4.15}$$

$$\frac{\partial uv}{\partial x} + \frac{\partial v^2}{\partial y} + \frac{\partial uv}{\partial z} = \underline{\frac{ag}{\rho_a}\int_z^{-\infty} \frac{\partial \Delta T}{\partial y}\, dz} - \frac{1}{\rho_a}\frac{\partial Pd}{\partial y} - \frac{\partial v'^2}{\partial y} - \frac{\partial v'w'}{\partial z} \tag{4.16}$$

$$0 = -\frac{1}{\rho_a}\frac{\partial Pd}{\partial z} - \frac{\partial v'w'}{\partial y} - \frac{\partial w'^2}{\partial z}, \tag{4.17}$$

and

$$\frac{\partial u\Delta T}{\partial x} + \frac{\partial v\Delta T}{\partial y} + \frac{\partial w\Delta T}{\partial z} = -\frac{\partial v'\Delta T'}{\partial y} - \frac{\partial w'\Delta T'}{\partial z}. \tag{4.18}$$

Equation 4.14 was used in the development of left-hand sides of Eqs. 4.15, 4.16, and 4.18; this was done to facilitate later integrations. The underlined terms in Eqs. 4.15 and 4.16 represent the effect of buoyancy in the flow equations and represent the mechanism that couples the momentum and energy transfer. The underlined term in Eq. 4.15 represents the buoyant force in the x direction tending to accelerate the jet; the similar term in Eq. 4.16 is the buoyant force in the y direction, which increases the lateral convection. The y-momentum equation formulates the balance between the lateral pressure gradient and the mean convective terms, which cause the lateral spreading. Equations 4.14-4.18 are similar to

relationships developed in most treatments of plane and axisymmetric turbulent jets, except that here the dynamic pressure and the turbulent terms in the x direction are not considered negligible. The longitudinal and lateral pressure gradients described above, arising from density (temperature) gradients, are usually dropped in most treatments in order to more easily obtain a solution.

(2) Simulation of Jet Structure. With the more simple set of differential equations (Eqs. 4.14-4.18) of buoyant jet flow outlined, the authors selected a particular structure for the jet from the discharge exit out to the far field. The geometrical characteristics of the jet are illustrated in Fig. 4.3. Each longitudinal cross section is assumed rectangular. The core region at any x has a half-width s and depth r. The turbulent shear region spreads horizontally with a width b at any longitudinal position x. The vertical shear region has depth h. Each cross section (see Sec. A-A of Fig. 4.3) is divided into four regions: an unsheared core region (No. 1), a vertically sheared region (No. 2), a horizontally sheared region (No. 3), and a region sheared in both directions (No. 4). The jet is assumed to be symmetric about the plane $y = 0$.

The core regions eventually disappear due to the advancing turbulent regions. The distance at which r and s become zero are defined as x_r and x_s, respectively. If $x_r < x < x_s$ or $x_s < x < x_r$, the jet will have only two regions. For $x > x_s$ and $x > x_r$, a single region (No. 4) exists, which is sheared in both directions. The entraining ambient fluid outside the four jet sections will have a second-order motion compared to that of the jet, but is not considered in the model. In reality, a jet is more trough-shaped than rectangular, and each of the above shearing characteristics may be found intermixed in all four regions represented. Moreover, some jet effects will be experienced in the ambient fluid beyond the above boundaries set by the authors. However, for mathematical simulation, some convenient scheme like the above was necessary.

(3) Similarity Assumptions on Velocity and Temperature. With the gross characteristics of the jet defined, the similarity profiles for velocity and temperature were then defined and are graphically illustrated in Fig. 4.4. Separable distributions for u and ΔT

$$\left.\begin{aligned} u &= u_c(x)F_y(y)F_z(z) \\ \text{and} \\ \Delta T &= \Delta T_c(x)T_y(y)T_z(z) \end{aligned}\right\} \qquad (4.19)$$

are assumed, where $u_c(x)$ is the velocity and $\Delta T_c(x)$ is the temperature rise at the surface centerline ($y = 0$, $z = \eta$). Similarity functions F_y, F_z, T_y, and T_z are chosen to be

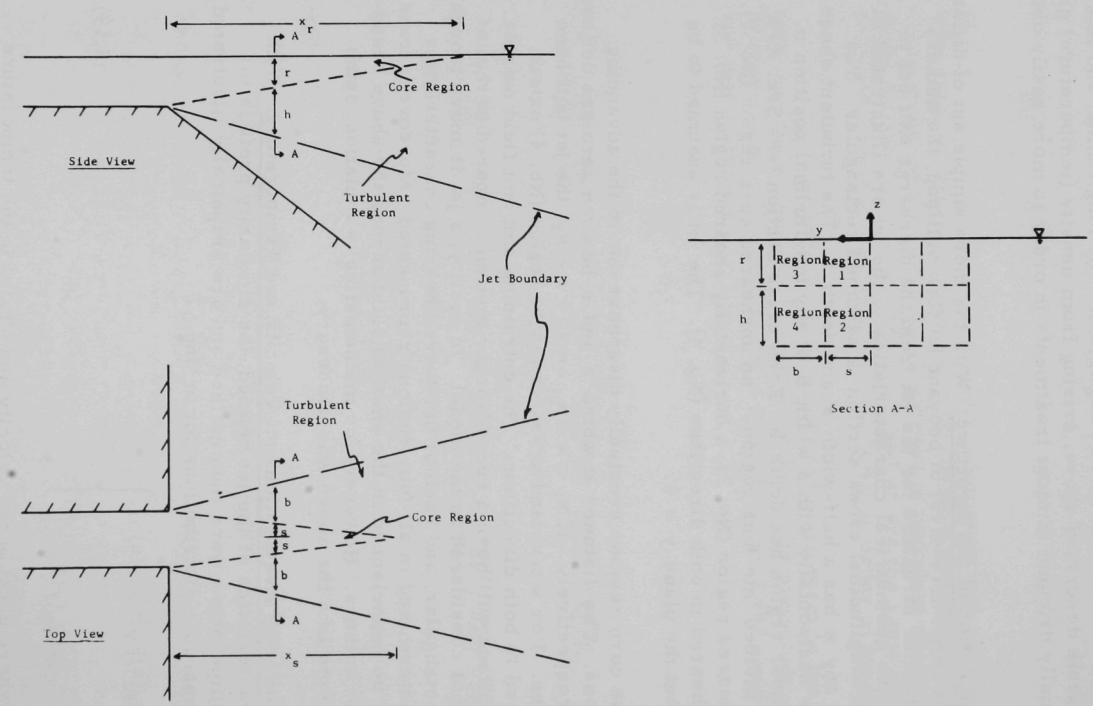

Fig. 4.3. Geometrical Characteristics of the Jet[1]

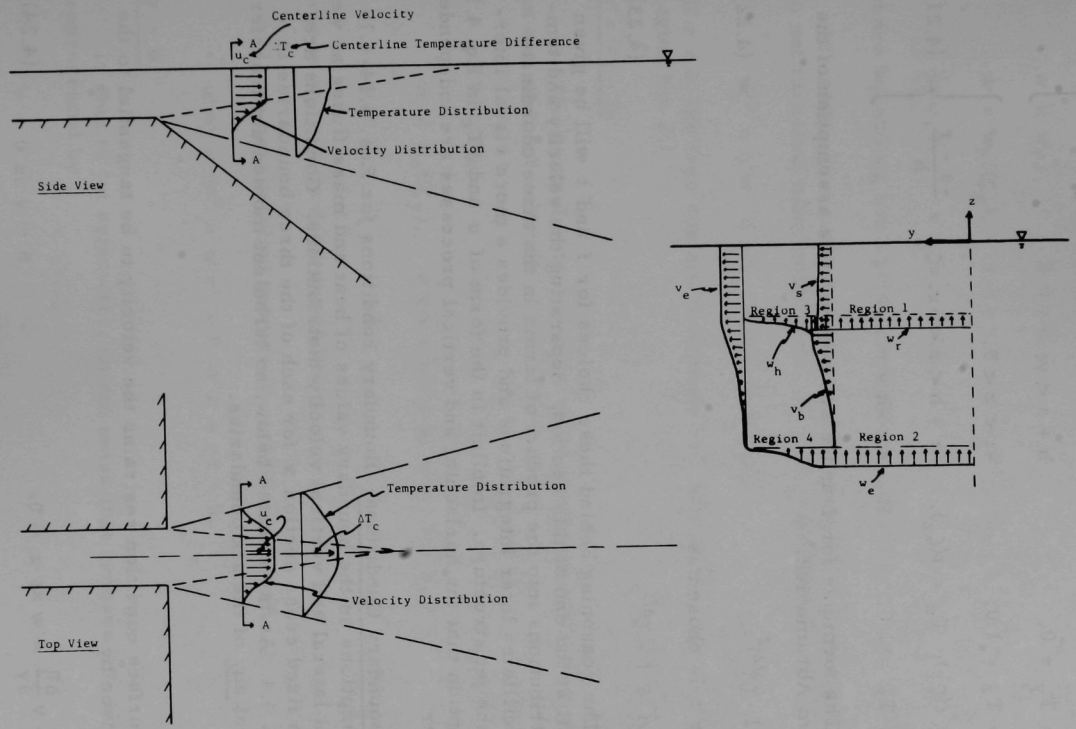

Fig. 4.4. Velocity and Temperature Characteristics of the Jet[1]

$$\left.\begin{array}{ll} F_y = T_y = 1.0 & 0 < y < s, \\ F_y = f(\zeta_y),\ T_y = t(\zeta_y), & s < y < b + s,\ \zeta_y = \dfrac{y - s}{b}, \\ F_y = T_y = 0, & b + s < y; \end{array}\right\} \quad (4.20)$$

$$\left.\begin{array}{ll} F_z = T_z = 1.0, & -r < z < \eta, \\ F_z = f(\zeta_z),\ T_z = t(\zeta_z), & -r - h < z < -r,\ \zeta_z = \dfrac{-z - r}{h}, \\ F_z = T_z = 1.0, & z < -h - r. \end{array}\right\} \quad (4.21)$$

The formulas for f and t are a very basic assumption of the theory. From Abramovich,[5]

$$f = (1 - \zeta^{3/2})^2. \quad (4.22)$$

The form for t is chosen as

$$t = \sqrt{f} = 1 - \zeta^{3/2}. \quad (4.23)$$

The reasoning behind these choices for f and t will be given in more detail at the end of this section. Separating the velocity and temperature distributions into the product of terms in the three coordinate directions facilitates later integrations and provides a more visual interpretation of the jet structure. Implicit in the form of u and ΔT_c in Eq. 4.19 is the assumption that the horizontal and vertical processes are independent of one another.

(4) Boundary Conditions. Boundary conditions for Eqs. 4.14-4.18 require assumptions on the boundary values of heat and mass fluxes as well as on internal lateral and vertical velocity distributions. Conditions are specified at a fixed cross section x for each of the three boundaries in y and z in Fig. 4.4. As is indicated below, no turbulent momentum transfer is permitted at any of the six boundaries.

$z = \eta$:

1. The surface condition restrains the velocity to be tangential to the surface, as given by

$$u \frac{\partial \eta}{\partial x} + v \frac{\partial \eta}{\partial y} = w \text{ at } z = \eta. \quad (4.24)$$

2. No net turbulent momentum transfer occurs across the free surface, as given by

$$w'^2 = u'w' = v'w' = 0 \text{ at } z = \eta. \quad (4.25)$$

$z = -r$:

1. Vertical velocity is assumed to be

$$\left.\begin{aligned} w &= w_r, & 0 < y < s, \\ w &= w_h f(\zeta_y), & s < y < b + s \text{ at } z = -r, \\ w &= 0, & s + b < y, \end{aligned}\right\} \tag{4.26}$$

where w_r and w_h are variables yet to be determined from theory.

2. Although momentum does transfer across this nonrigid boundary, no net turbulent momentum does, as is represented by

$$w'^2 = u'w' = v'w' = 0 \text{ at } z = -r. \tag{4.27}$$

(If $r = 0$, the free surface conditions will hold at the upper boundary of region No. 2.)

$z = -r - h$:

1. The normal velocity is assumed specified at this outer boundary as an entrainment velocity,

$$\left.\begin{aligned} w &= w_e, & 0 < y < s, \\ w &= w_e f(\zeta_y), & s < y < b + s \text{ at } z = -r - h, \\ w &= 0, & s + b < y, \end{aligned}\right\} \tag{4.28}$$

where w_e will be determined below.

2. No net turbulent momentum transfer implies

$$u'w' = w'^2 = w'v' = 0 \text{ at } z = -r - h. \tag{4.29}$$

$y = 0$:

1. Due to jet symmetry, no net mass flux crosses this boundary, as represented by

$$v = 0 \text{ at } y = 0. \tag{4.30}$$

2. No net flux of turbulent momentum crosses the boundary, as given by

$$v'^2 = u'v' = v'w' = 0 \text{ at } y = 0. \tag{4.31}$$

<u>$y = s$</u>: Conditions here are analogous to those at boundary $z = -r$. Therefore,

$$\left.\begin{aligned} &1.\ v = v_s, && -r < z < \eta, \\ &\quad v = v_b f(\zeta_z), && -r - h < z < -r \text{ at } y = s, \\ &\quad v = 0, && -h - r < z, \end{aligned}\right\} \tag{4.32}$$

where again v_s and v_b are variables yet to be determined from theory.

$$2.\ u'v' = v'w' = v'^2 = 0. \tag{4.33}$$

(If $s = 0$, these conditions are replaced by those for $y = 0$.)

<u>$y = s + b$</u>: Conditions here are analogous to those at $z = -r - h$. Therefore,

$$\left.\begin{aligned} &1.\ v = v_e, && -r < z < \eta, \\ &\quad v = v_e f(\zeta_z), && -r - h < z < -r \text{ at } y = s + b, \\ &\quad v = 0, && z < -h - r. \end{aligned}\right\} \tag{4.34}$$

$$2.\ v'^2 = u'v' = v'w' = 0. \tag{4.35}$$

As indicated earlier, the variables v_b, v_s, w_r, and w_h are unknown functions of x and must be determined by the theory; v_e and w_e are entrainment velocities to be described below.

The boundary conditions on the turbulent heat flux are

$$\left.\begin{aligned} &w'T' = 0, \quad z = -r - h, \\ &v'T' = 0, \quad y = 0 \text{ and } y = s + b, \end{aligned}\right\} \tag{4.36}$$

which specify no heat transfer from jet into ambient fluid. Surface heat transfer to the atmosphere is represented by

$$w'T' = K(T - T_a) \text{ at } z = \eta, \tag{4.37}$$

where K is the surface-heat-transfer coefficient and T_a is the ambient temperature. The use of Eq. 4.37 implies that the equilibrium temperature is sufficiently close to the ambient temperature.

Finally, the boundary conditions at $x = 0$ are assumed to be

$$\left.\begin{aligned} r &= h_0, \\ s &= b_0, \\ b &= h = 0, \\ u_c &= u_0, \\ \text{and} \quad \Delta T &= \Delta T_0. \end{aligned}\right\} \tag{4.38}$$

Equations 4.14-4.18 are solved by integrating the equations over portions of the yz plane such that the contribution of the turbulent fluctuation terms u', v', and w', about which no lateral and vertical distribution has been assumed, is zero. The choices for the boundary functions given above will be discussed briefly toward the end of this section.

(5) Evaluation of Entrainment Velocities v_e and w_e. To evaluate the entrainment velocities v_e and w_e, the authors apply nonbuoyant jet theory. Their philosophy is that lateral entrainment is unchanged by buoyancy effects; also, vertical entrainment may be determined from the theory of Phillips[6] and from the experimental results of Ellison and Turner with a vertical-entrainment coefficient chosen to reduce to the nonbuoyant value when no temperature differences exist. Consequently, they solve Eqs. 4.14-4.18 with the identical outfall conditions, similarity assumptions, boundary conditions, and jet structure as given above for the buoyant case, except that $\Delta T = 0$; i.e.,

$$\frac{\partial u}{\partial x} + \frac{\partial v}{\partial y} + \frac{\partial w}{\partial z} = 0, \tag{4.14'}$$

$$\frac{\partial u^2}{\partial x} + \frac{\partial uv}{\partial y} + \frac{\partial uw}{\partial z} = -\frac{\partial u'v'}{\partial y} - \frac{\partial u'w'}{\partial z}, \tag{4.15'}$$

$$0 = -g\frac{\partial \eta}{\partial y} - \frac{1}{\rho_a}\frac{\partial p_d}{\partial y} - \frac{\partial v'^2}{\partial y} - \frac{\partial v'w'}{\partial z}, \tag{4.16'}$$

and

$$0 = -\frac{1}{\rho_a}\frac{\partial p_d}{\partial z} - \frac{\partial v'w'}{\partial y} - \frac{\partial w'^2}{\partial z}. \tag{4.17'}$$

These are the so-called turbulent shear-flow equations for nonbuoyant jets. The authors also use the well-known experimental relationships for nonbuoyant jets,

$$\frac{dr}{dx} = \frac{ds}{dx} \tag{4.39}$$

and

$$\frac{dh}{dx} = \frac{db}{dx} = \epsilon = 0.22. \tag{4.40}$$

To solve these nonbuoyant equations, the authors integrate Eqs. 4.16' and 4.17' over the entire yz plane of the half-jet to yield equations on the nonbuoyant dynamic pressure p_d from which the total pressure within the jet is shown to be constant. Applying Bernoulli's theorem along a streamline followed by ambient entraining fluid, the authors conclude that the entrainment velocities v_e and w_e for the nonbuoyant case are proportional to the local longitudinal velocity scale and are an order of magnitude less. Consequently, they define entrainment coefficients,

$$\left.\begin{aligned} v_e &= \alpha_y(x)u_c(x) \\ &\text{and} \\ w_e &= \alpha_z(x)u_c(x) \end{aligned}\right\}, \tag{4.41}$$

where α_y and α_z are determined by the solution to Eqs. 4.14'-4.17'. The x-momentum and continuity equations are then integrated over the four regions of the jet using the similarity for the velocity, the boundary conditions, and the entrainment definitions. Including Eqs. 4.39 and 4.40, this yields 11 equations with 11 variables: u_c, v_b, v_s, w_r, w_h, b, r, s, h, α_y, and α_z. The solution for nonbuoyant jets can be written in closed form and is given by the following:

<u>For all x</u>

$$\left.\begin{aligned} v_s &= v_b = w_r = w_h = 0, \\ &\text{and} \\ h &= b = \epsilon x. \end{aligned}\right\} \tag{4.42}$$

<u>Initial Region</u> $\quad x < \frac{h_0}{\epsilon I_2}, \quad x < \frac{b_0}{\epsilon I_2}$

$$\left.\begin{aligned} u_c &= u_0, \\ r &= h_0 - \epsilon I_2 x, \\ s &= b_0 - \epsilon I_2 x, \\ &\text{and} \\ -\alpha_y &= \alpha_z = \epsilon(I_1 - I_2). \end{aligned}\right\} \tag{4.43}$$

For $h_0 < b_0$ $\quad \frac{h_0}{\epsilon I_2} < x < \frac{b_0}{\epsilon I_2}$,

$$\left.\begin{aligned} u_c &= u_0\sqrt{\frac{h_0}{x\epsilon I_2}}, \\ r &= 0, \\ s &= b_0 - \epsilon I_2 x, \\ \alpha_y &= -\epsilon(I_1 - I_2), \\ &\text{and} \\ \alpha_z &= \frac{I_1\epsilon}{2}. \end{aligned}\right\} \tag{4.44}$$

For $b_0 < h_0$ $\quad \frac{b_0}{\epsilon I_2} < x < \frac{h_0}{\epsilon I_2}$,

$$\left.\begin{aligned} u_c &= u_0\sqrt{\frac{b_0}{x\epsilon I_2}}, \\ s &= 0, \\ r &= h_0 - \epsilon I_2 x, \\ \alpha_y &= \frac{-I_1\epsilon}{2}, \\ &\text{and} \\ \alpha_z &= \epsilon(I_1 - I_2). \end{aligned}\right\} \tag{4.45}$$

For $x > \frac{b_0}{\epsilon I_2}$ and $x > \frac{h_0}{\epsilon I_2}$,

$$\left.\begin{aligned} u_c &= \frac{u_0\sqrt{h_0 b_0}}{I_2\epsilon x}, \\ r &= s = 0, \\ &\text{and} \\ -\alpha_y &= \alpha_z = \frac{I_1\epsilon}{2}. \end{aligned}\right\} \tag{4.46}$$

In the above equations, $I_1 = 0.450$ and $I_2 = 0.316$. Note that the nonbuoyant centerline velocity remains constant in the core region, drops off as $x^{-1/2}$ for the next range of x, and finally decays as x^{-1}. More

important, however, are the forms for the entrainment coefficients. Although there is a discontinuity in the entrainment constants α_y and α_z in the above formulas as r or s becomes zero, which obviously cannot occur physically, the authors are confident that these values are close to the correct behavior for nonbuoyant jets and that the actual observed transition region in the values for α_y and α_z is small enough to safely be neglected. Note also that the specific rates of growth of b, h, r, and s were assumed which allowed the calculation of the entrainment coefficients.

In the buoyant case, no such growth rates are known, necessitating some new kind of assumption on the entrainment. The mechanisms that cause lateral entrainment in the nonbuoyant case are assumed to be unchanged in the presence of buoyancy. Hence, the lateral-entrainment coefficient $\alpha_y(x)$ derived above is used in the buoyant jet case also. Vertical density gradients, however, will definitely reduce vertical entrainment.

To account for this reduction, Stolzenbach and Harleman define a vertical entrainment coefficient in the case of a buoyant jet as

$$\alpha_{sz}(x) = \alpha_z(x) \exp\left[-5.0 \frac{agh(x)\Delta T_c(x)}{\rho_a u_c^2(x)}\right]. \tag{4.47}$$

This formula is based on the theory of Phillips,[6] which relates the effect of density gradients on the flow by the local Richardson number ($R_i = 1/F^2$). Equation 4.47 represents the reduction of entrainment as a function of R_i, where entrainment for zero density gradient is taken as α_z derived above for nonbuoyant jets. The equation was calibrated with the data of Ellison and Turner,[3] which yielded 5.0 as the constant in the exponent of Eq. 4.47. The form of Eq. 4.47 is not unique with this study. It was independently proposed in its simple empirical form earlier by Mamayev.[7] In addition to the derivation given in Refs. 1 and 2, the choice of Eq. 4.47 to represent the vertical diffusivity is a logical one, if one analyzes the available data that provide a clue to the shape of the curve (exponential) and the dependencies involved. It may well represent a state-of-art form for the vertical eddy thermal diffusivity.

(6) Solution to Governing Equations. The buoyant equation set (Eqs. 4.14-4.18) can now be integrated over the plume cross section. The continuity and x-momentum equations are integrated over each of the four regions defined in Fig. 4.4 to yield the first eight equations in Table 4.1. The y-momentum equation requires additional attention.

The y-momentum equation in the nonbuoyant case, Eq. 4.16', states physically that a balance between the dynamic pressure and the turbulent velocities exists and that these are the only kinds of momentum transfers that occur. The authors interpreted that equation as an entrainment relationship. Also, none of the terms in that equation are, in order of

TABLE 4.1. Integrated Equations for Buoyant Jets[1]

Region No. 1 continuity:

$$rs\frac{du_c}{dx} + rv_s - sw_r = 0.$$

Region No. 2 continuity:

$$I_1 s\frac{du_c h}{dx} + su_c\frac{dr}{dx} + v_b h I_1 + s(w_r - \alpha_{sz}u_c) = 0.$$

Region No. 3 continuity:

$$I_1 r\frac{du_c b}{dx} + ru_c\frac{ds}{dx} - w_h b I_1 - r(v_s - \alpha_y u_c) = 0.$$

Region No. 4 continuity:

$$I_1^2\frac{du_c hb}{dx} + u_c I_1\left(b\frac{dr}{dx} + h\frac{ds}{dx}\right) + (w_h - \alpha_{sz}u_c)\, I_1 b - (v_b - \alpha_y u_c)\, I_1 h = 0.$$

Region No. 1 momentum:

$$u_c\left(2rs\frac{du_c}{dx} + rv_s - sw_r\right) + \frac{ags}{\rho_a}\left(\frac{d}{dx}\Delta T_c\frac{r^2}{2} + I_3 r\frac{d}{dx}\Delta T_c h\right) = 0.$$

Region No. 2 momentum:

$$sI_2\frac{du_c^2 h}{dx} + su_c^2\frac{dr}{dx} + u_c v_b h I_2 + u_c s w_r + \frac{ags}{\rho_a}\left(I_4\frac{d\Delta T_c h^2}{dx} + I_3\Delta T_c h\frac{dr}{dx}\right) = 0.$$

Region No. 3 momentum:

$$rI_2\frac{du_c^2 b}{dx} + ru_c^2\frac{ds}{dx} - u_c w_h b I_2 - u_c r v_s$$
$$+ \frac{ag}{\rho_a}\left[\frac{I_3}{2}\frac{d\Delta T_c b r^2}{dx} + I_3^2 r\frac{d\Delta T_c bh}{dx} + \Delta T_c\left(\frac{r^2}{2} + I_3 hr\right)\frac{ds}{dx}\right] = 0.$$

Region No. 4 momentum:

$$I_2^2\frac{du_c^2 hb}{dx} + u_c^2 I_2\left(h\frac{ds}{dx} + b\frac{dr}{dx}\right) + u_c I_2(w_h b - v_b h)$$
$$+ \frac{ag}{\rho_a}\left(I_3 I_4\frac{d\Delta T_c h^2 b}{dx} + I_4\Delta T_c h^2\frac{ds}{dx} + I_3^2\Delta T_c hb\frac{dr}{dx}\right) = 0.$$

TABLE 4.1 (Contd.)

y momentum:

$$\frac{d}{dx}\left[\frac{db}{dx} - \left(\frac{db}{dx}\right)_{NB}\right][u_c^2 b I_6(r + hI_2)] - \frac{ag}{\rho_a}\Delta T_c\left(\frac{r^2}{2} + I_3 rh + I_4 h^2\right) = 0.$$

Heat:

$$\frac{d}{dx}[u_c \Delta T_c(r + hI_7)(s + bI_7)] + K\Delta T_c(s + bI_3) = 0.$$

In the above equations,

$$I_1 = \int_0^1 f(\zeta)\, d\zeta = \int_0^1 (1 - \zeta^{3/2})^2\, d\zeta = 0.4500,$$

$$I_2 = \int_0^1 f^2(\zeta)\, d\zeta = \int_0^1 (1 - \zeta^{3/2})^4\, d\zeta = 0.3160,$$

$$I_3 = \int_0^1 t(\zeta)\, d\zeta = \int_0^1 (1 - \zeta^{3/2})\, d\zeta = 0.6000,$$

$$I_4 = \int_0^1 \int_\zeta^1 t(\bar{\zeta})\, d\bar{\zeta}\, d\zeta = \int_0^1 \int_\zeta^1 (1 - \bar{\zeta}^{3/2})\, d\bar{\zeta}\, d\zeta = 0.2143,$$

$$I_5 = \int_0^1 F(\zeta)\zeta^{1/2}\, d\zeta = \int_0^1 (1 - \zeta^{3/2})^2\, \zeta^{1/2}\, d\zeta = 0.2222,$$

$$I_6 = \int_0^1 f^2(\zeta)\zeta^{1/2}\, d\zeta = \int_0^1 (1 - \zeta^{3/2})^4\, \zeta^{1/2}\, d\zeta = 0.1333,$$

$$I_7 = \int_0^1 f(\zeta)t(\zeta)\, d\zeta = \int_0^1 (1 - \zeta^{3/2})^3\, d\zeta = 0.3680,$$

$\left(\frac{db}{dx}\right)_{NB}$ = nonbuoyant spreading rate calculated from the above equation set with $\Delta T = 0$,

$$\alpha_y = \begin{cases} -(I_1 - I_2)\,\epsilon, & s > 0, \\ -\dfrac{I_1 \epsilon}{2}, & s = 0, \end{cases}$$

$$\alpha_z = \begin{cases} (I_1 - I_2)\,\epsilon, & r > 0, \\ \dfrac{I_1 \epsilon}{2}, & r = 0, \end{cases} \qquad \alpha_{sz} = \alpha_z \exp\left(-5.0\,\frac{ag\Delta T_c h}{\rho_a u_c^2}\right),$$

TABLE 4.1 (Contd.)

ε = spreading rate of a free turbulent region = 0.22,

and

$$\left.\begin{aligned} r &= h_0 \\ s &= b_0 \\ h &= b = 0 \\ \frac{db}{dx} &= \varepsilon \\ u &= u_0 \\ \Delta T &= \Delta T_0 \end{aligned}\right\} \quad x = 0$$

magnitude, as large as the terms in the x equation (Eq. 4.15'). The y-momentum equation in the case of buoyancy now contains lateral convective terms and a pressure gradient resulting from a lateral temperature gradient. The balance between the lateral entrainment and the dynamic pressure in the nonbuoyant problem is assumed to hold in the buoyant case too as second-order terms compared to the new buoyancy-generated terms. The authors' philosophy is that the entrainment process is a microscale turbulent process and is not affected by the gross convection induced by lateral gravitational spreading. Local conditions at the interface between turbulent and nonturbulent regions are therefore considered to be unaffected by buoyancy. Thus Eq. 4.16' is also held to be valid for the buoyant case with the identical lateral-entrainment function used. Subtracting 4.16' from Eq. 4.16 yields

$$\frac{\partial uv}{\partial x} + \frac{\partial v^2}{\partial y} + \frac{\partial vw}{\partial z} = \frac{ag}{\rho_a} \int_z^{-\infty} \frac{\partial \Delta T}{\partial y}\, dz, \tag{4.48}$$

after dropping the negligible η term. Integrated over the entire yz plane of the half-jet yields

$$\frac{d}{dx} \int_0^{b+s} \int_{-h-r}^{0} uv\, dz\, dy = \frac{ag}{\rho_a} \int_0^{s+b} \int_{-(r+h)}^{0} \int_z^{-\infty} \frac{\partial \Delta T}{\partial y}\, d\zeta\, dz\, dy, \tag{4.49}$$

where the lateral velocity v is understood to be only the "spreading part" of the total velocity v, which causes the additional lateral spreading beyond the nonbuoyant linear spread. Since no previously defined distribution has been given for this v, the authors assume v to be proportional to the difference between the buoyant and nonbuoyant spreading,

$$v \sim \left[\frac{db}{dx} - \left(\frac{db}{dx}\right)_{NB}\right] u. \tag{4.50}$$

The proportionality factor is assumed to be the y dependent part of the temperature gradient in the y direction, derived from Eq. 4.19 as

$$\left.\begin{aligned} \frac{\partial \Delta T}{\partial y} &= 0, & 0 < y < s, \\ \frac{\partial \Delta T}{\partial y} &= -\frac{\Delta T_c}{b}\left(1 - \zeta_z^{3/2}\right)\frac{3}{2}\zeta_y^{1/2}, & s < y < b + s, \\ \frac{\partial \Delta T}{\partial y} &= 0, & s + b < y, \end{aligned}\right\} \tag{4.51}$$

with the rationale that the additional spreading caused by the buoyancy is actually induced by the lateral temperature difference in the jet. So

$$\left.\begin{aligned} v &= 0, & 0 < y < s, \\ v &= \left[\frac{db}{dx} - \left(\frac{db}{dx}\right)_{NB}\right]\left[u_c\left(1 - \zeta_z^{3/2}\right)^2\left(1 - \zeta_y^{3/2}\right)^2 \zeta_y^{1/2}\right], & s < y < b + s, \\ v &= 0, & s + b < y. \end{aligned}\right\} \tag{4.52}$$

Equations 4.50 and 4.52 are pure assumptions on the part of the authors. They are based upon physical hunches, due to the lack of concrete information, which permit the analysis to proceed. The choice of $\zeta_y^{1/2}$ rather than say $\frac{3}{2}\zeta_y^{1/2}$ in Eq. 4.51 was done as follows: The lateral spreading velocity at a given point is assumed to be proportional to the local longitudinal velocity u, with the tangent of the streamline angle from the centerline as a proportionality factor. Consequently, v/u is proportional to the tangent of that streamline angle at the point of interest. The authors next consider the distribution of that angle from the centerline out to the edge of the jet. The properties of the velocity ratio v/u can be determined from that analysis. First, at the centerline, v = 0, yielding a zero streamline angle. At the edge of the jet now, the tangent of that angle should be the difference between the buoyant and nonbuoyant spreading rates of the jet as expressed in Eq. 4.50. Consequently,

$$\frac{v}{u\left[\frac{db}{dx} - \left(\frac{db}{dx}\right)_{NB}\right]}$$

varies from zero at the centerline to unity at the jet edge. Since $\zeta_y^{1/2}$ also has such a range, the authors felt confident in their choice of unity as the

proportionality factor in the incorporation of Eq. 4.51 into Eq. 4.50. Extracting a structure for v was more important to them than extracting a particular value for the constant. Substituting this assumed distribution for v in Eq. 4.52, the integrated y-momentum equation results as the ninth equation of Table 4.1.

Integrating the z-momentum equation over the entire half-jet reveals a relationship on η that permits it to be neglected in all integrations. The energy equation is integrated over the entire jet, and the resulting relationship may be seen as the heat equation of Table 4.1. These 10 equations are coupled, nonlinear first-order differential equations in x on the variables u_c, ΔT_c, v_b, v_s, w_r, w_h, b, r, s, and h. A numerical solution has been carried out and a computer program written. The output is given in dimensionless form in which u_0, ΔT_0, and $\sqrt{h_0 b_0}$ are normalization factors for velocity, temperature, and length, respectively.

(7) Discussion of Model. A few remarks should be made here as to some of the assumptions made by Stolzenbach and Harleman in their model. The main assumption in this work is in the form of the similarity functions

$$f = (1 - \zeta^{3/2})^2 \tag{4.53}$$

and

$$t = \sqrt{f} = 1 - \zeta^{3/2}, \tag{4.54}$$

which describe the off-axis decay of velocity and temperature. The choice of the function f is somewhat arbitrary, yet cannot be avoided. One may derive an f by defining a form for the turbulent terms in the equations for submerged nonbuoyant plane or axisymmetric jets and then solving for it. This becomes quite complicated, the result being generally inconvenient to use. The authors' choice of f was taken from Abramovich's work on plane, submerged, nonbuoyant jets. The function f does compare well with nonbuoyant data in the situation for which it is derived. An implicit assumption made in its use is that a surface jet is equivalent to half a submerged jet.

Abramovich uses a different value of the similarity function f and jet rate of growth ϵ for the main and core regions of a jet and matches the inner and outer regions by allowing h and b to change over a transition zone. The authors, however, use only Abramovich's main-region results for their entire jet. The authors assert that the error incurred by this approximation in the inner region will be small. The different jet width and similarity function used in this inner core region, will, however, merge correctly in the outer region to Abramovich's results. Since the authors are mainly interested in the location of the core region rather than its

exact properties, they consider this convenient assumption satisfactory. Hence ϵ and f given by Eqs. 4.40 and 4.53 are used for all x.

The choice of $t = \sqrt{f}$ has its theoretical base in the Taylor free-turbulence theory for a plane or axially symmetric submerged jet and describes physically that heat is being diffused laterally faster than momentum. This assumption is in general agreement with experimental data. The above choices of f and t have two additional advantages. First, these similarity functions are zero outside of a finite region, yielding a clearly defined jet boundary. Second, there is the added convenience in that all integrations would not have to be carried out to ∞, as would be the case with the more popular choice of Gaussian distributions for f and t. The authors feel, and perhaps rightly so, that the Gaussian form for the lateral velocity distribution has not been looked at hard enough in its applications.

Many of the assumptions concerning jet structure and the assumed forms for some of the variables are frankly open to argument, considering the present state of knowledge of buoyant and nonbuoyant jets. All choices of treatment for the buoyant-jet problem were based on the philosophy that the theory should reduce as correctly as possible to known results for nonbuoyant jets when no density differences exist. That the buoyancy results come close to giving the length of the core region correctly, in giving the velocity and temperature distributions correctly when the model was limitedly tested hydraulically, is its justification. The assumptions, however, all had the common purpose of developing a workable numerical scheme that gives satisfactory results for the nonbuoyant case.

Concerning the internal velocities defined above as part of the boundary conditions, the assumptions as to their precise forms are impossible to test or measure due to the fictitious structure of the jet. Yet they had to be specified in order to carry out the integrations. The computer program available for this model does not solve for them. They are intermediate variables, and the only test of their validity is in the analysis of the final results. There is no other justification as to their correct form. They are the authors' assumptions in setting up a structure for the jet and in specifying the variables of interest.

The assumptions made on the ambient fluid were simply that it has a uniform temperature, that it is semi-infinite in extent, and that far from the outfall it has a constant water level. The nonstratified nature of the receiving water is expected to permit greater vertical entrainment and dilutions than one would expect for a typical stably stratified situation of most large lakes during summer. In short, application of this model to such stratified situations is expected to yield optimistic results, and this should be kept in mind in any use. Truly three-dimensional situations are indeed rare in practice, except possibly for unstratified situations where the bottom depth drops off very rapidly.

d. Model 2: Buoyant Jet in a Crossflow (no bottom slope)

(1) Introduction. A lateral crossflow deflects a buoyant jet in the direction of the current due to the incorporation of increased lateral momentum and to the addition of new net pressure forces. These additional lateral pressure forces are caused first by the eddying motion of the ambient fluid in the lee of the jet and second by the distortion of the jet boundaries. The assumption of a small crossflow velocity (compared to the initial jet velocity) implies small deflections from which the authors assume negligible effects of any net pressure force. The only force then deflecting the jet is entrainment of lateral momentum. The actual deflection of the jet in the ambient crosscurrent is calculated by balancing the rate of entrainment of the lateral momentum by the rate of jet deflection.

(2) Development of Model Equations. A natural coordinate system is chosen for the deflected jet were $\tilde{x}$ is the distance measured along the deflected centerline, and $\tilde{y}$ is normal to $\tilde{x}$ and considered positive in the downstream direction where θ is defined as the angle of the tangent line to the plume centerline measured from the y axis. Characteristics of the deflected jet are illustrated in Fig. 4.5. With these new variables, Eqs. 4.14-4.18 become

$$\frac{\partial \tilde{u}}{\partial \tilde{x}} + \frac{\partial \tilde{v}}{\partial \tilde{y}} + \frac{\partial \tilde{w}}{\partial \tilde{z}} + \tilde{v}\frac{\partial \theta}{\partial \tilde{x}} = 0, \tag{4.55}$$

$$\frac{\partial \tilde{u}^2}{\partial \tilde{x}} + \frac{\partial \tilde{u}\tilde{v}}{\partial \tilde{y}} + \frac{\partial \tilde{u}\tilde{w}}{\partial \tilde{z}} + 2\tilde{u}\tilde{v}\frac{\partial \theta}{\partial \tilde{x}} = \frac{ag}{\rho_a}\int_{\tilde{z}}^{-\infty} \frac{\partial \Delta T}{\partial \tilde{x}}\, d\tilde{z} - \frac{\partial \tilde{u}'\tilde{v}'}{\partial \tilde{y}}$$

$$- \frac{\partial \tilde{u}'\tilde{w}'}{\partial \tilde{z}} - 2\tilde{u}'\tilde{v}'\frac{\partial \theta}{\partial \tilde{x}}, \tag{4.56}$$

$$\frac{\partial \tilde{u}\tilde{v}}{\partial \tilde{x}} + \frac{\partial \tilde{v}^2}{\partial \tilde{y}} + \frac{\partial \tilde{v}\tilde{w}}{\partial \tilde{z}} - \tilde{u}^2\frac{\partial \theta}{\partial \tilde{x}} + \tilde{v}^2\frac{\partial \theta}{\partial \tilde{x}} = \frac{ag}{\rho_a}\int_{\tilde{z}}^{-\infty} \frac{\partial \Delta T}{\partial \tilde{y}}\, d\tilde{z} - \frac{1}{\rho_a}\frac{\partial pd}{\partial \tilde{y}}$$

$$- \frac{\partial \tilde{v}'^2}{\partial \tilde{y}} - \frac{\partial \tilde{v}'w'}{\partial \tilde{z}} + \tilde{u}'^2\frac{\partial \theta}{\partial \tilde{x}} - \tilde{v}'^2\frac{\partial \theta}{\partial \tilde{x}}, \tag{4.57}$$

$$0 = \frac{-\partial pd}{\partial \tilde{z}} - \frac{\partial \tilde{v}'\tilde{w}'}{\partial \tilde{y}} - \frac{\partial \tilde{w}'^2}{\partial \tilde{z}}, \tag{4.58}$$

and

$$\frac{\partial \tilde{u}\Delta T}{\partial \tilde{x}} + \frac{\partial \tilde{v}\Delta T}{\partial \tilde{y}} + \frac{\partial \tilde{w}\Delta T}{\partial \tilde{z}} = - \frac{\partial \tilde{v}'\Delta T'}{\partial \tilde{y}} - \frac{\partial \tilde{w}'\Delta T'}{\partial \tilde{z}}. \tag{4.59}$$

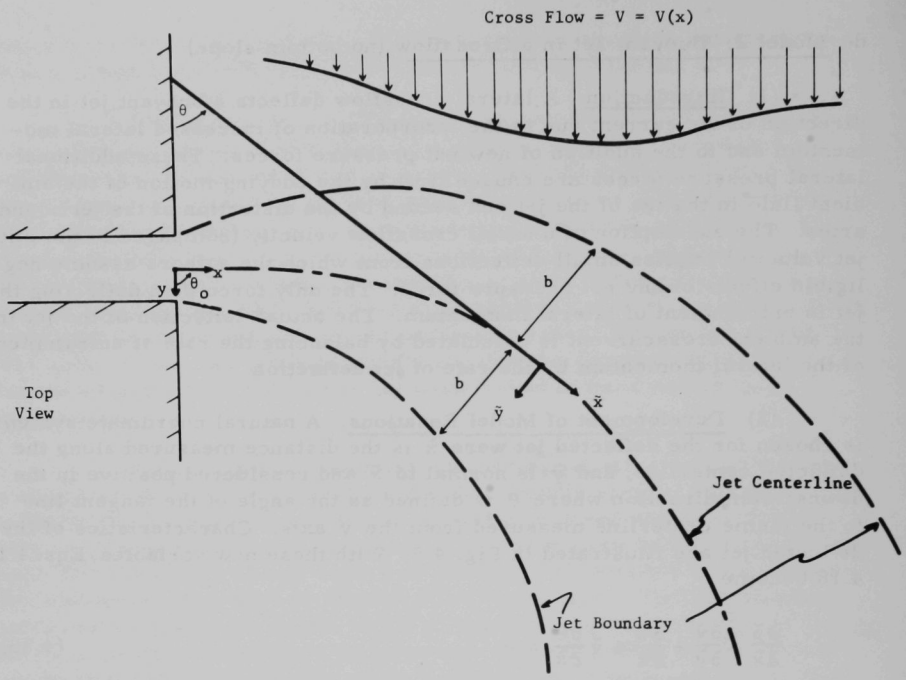

Fig. 4.5. Characteristics of a Deflected Jet[1]

The crossflow adds two additional terms to the $\tilde{x}$-momentum equation: one accounts for entrained $\tilde{x}$ crossflow momentum; the other is the bending term in the $\tilde{y}$ momentum equation, which balances the entrainment of $\tilde{y}$ crossflow momentum. A small crossflow velocity (as compared to jet centerline velocities) permits the dropping of certain negligible terms from these equations.

To derive the model equations, the authors first integrate the $\tilde{x}$ and $\tilde{y}$ momentum equations (Eqs. 4.56 and 4.57) over the entire jet which yields

$$\frac{d}{d\tilde{x}} \int_{-(r+h)}^{0} \int_{-(s+b)}^{s+b} \tilde{u}^2 \, d\tilde{y} \, d\tilde{z} =$$

$$\frac{ag}{\rho_a} \int_{-(r+h)}^{0} \int_{-(s+b)}^{(s+b)} \int_{z}^{-\infty} \cdot \frac{d\Delta T}{d\tilde{x}} \, d\tilde{z}' \, d\tilde{y} \, d\tilde{z} + q_e V \cos\theta \qquad (4.60)$$

and

$$\frac{d\theta}{d\tilde{x}} \int_{-(r+h)}^{0} \int_{-(s+b)}^{s+b} \tilde{u}^2 \, d\tilde{y} \, d\tilde{z} = -q_e V \sin\theta, \tag{4.61}$$

where q_e is the total mass flux of ambient fluid entrained into the jet per unit distance along $\tilde{x}$. The derivation of Eqs. 4.60 and 4.61 assumes approximate symmetry of the jet about the $\tilde{y} = 0$ plane with the assumption of no pressure drag force on the jet. Due to the uneven entrainment on either side of the jet, the deflected jet will in reality be unsymmetrical. The distortion, however, is assumed small with the symmetrical distribution in the nondeflected buoyant case assumed to hold to a first approximation.

The authors then assume that Eq. 4.60 holds for <u>each</u> of the four regions. The results are represented in Table 4.2 as the $\tilde{x}$-momentum equations. The same similarity functions as defined for the nondeflected buoyant case were used, except for u, which was replaced by

$$\tilde{u} = \tilde{u}_c F_y F_z + V \cos\theta, \tag{4.62}$$

where F_y and F_z are defined by Eqs. 4.20 and 4.21. All boundary conditions were assumed identical, except for the entrainment conditions

$$\left.\begin{array}{lll} \left.\begin{array}{lll} \tilde{w}_e = w_e - V\cos\theta \dfrac{dh}{d\tilde{x}}, & & 0 < \tilde{y} < s, \\ \tilde{w}_e = w_e f(\tilde{\zeta}_y) - V\cos\theta \dfrac{dh}{d\tilde{x}}, & & s < \tilde{y} < b + s, \\ \tilde{w}_e = 0, & & b + s < \tilde{y}, \end{array}\right\} & \text{at } \tilde{z} = -r - h; \\ \text{and} & & \\ \left.\begin{array}{lll} \tilde{v}_e = v_e + V\cos\theta \dfrac{db}{d\tilde{x}}, & & -r < \tilde{z} < \eta, \\ \tilde{v}_e = v_e f(\tilde{\zeta}_z) + V\cos\theta \dfrac{db}{d\tilde{x}}, & & -r - h < \tilde{z} < -r, \\ \tilde{v}_e = 0, & & -r - h > \tilde{z}, \end{array}\right\} & \text{at } \tilde{y} = s + b. \end{array}\right\} \tag{4.63}$$

The relations established by Eqs. 4.63 represent kinematic boundary conditions similar in form to the condition used on the surface boundary. Equations 4.63 recognize two components to the total velocities $\tilde{w}_e$ and $\tilde{v}_e$: the first due to entrainment, and the second due to the angle of the jet. If the "control volume" method of setting up the differential equations

TABLE 4.2. Integrated Equations for Deflected Buoyant Jets[1]

Region 1 continuity:

$$rs\frac{d}{d\tilde{x}}(u_c + V\cos\theta) + rv_s - sw_r = 0.$$

Region 2 continuity:

$$s\left\{\frac{d}{d\tilde{x}}[h(u_cI_1 + V\cos\theta)] + (u_c + V\cos\theta)\frac{dr}{d\tilde{x}} + w_r - \alpha_{sz}u_c\right\} + v_bhI_1 = 0.$$

Region 3 continuity:

$$r\left\{\frac{d}{d\tilde{x}}[b(u_cI_1 + V\cos\theta)] + (u_c + V\cos\theta)\frac{ds}{d\tilde{x}} - v_s + \alpha_y u_c\right\} - w_rbI_1 = 0.$$

Region 4 continuity:

$$\frac{d}{d\tilde{x}}[hb(u_cI_1^2 + V\cos\theta)] + (u_cI_1 + V\cos\theta)\left(b\frac{dr}{d\tilde{x}} + h\frac{ds}{d\tilde{x}}\right) + (w_h - \alpha_{sz}u_c)I_1b - (v_b - \alpha_y u_c)I_1h = 0.$$

Region 1 $\tilde{x}$ momentum:

$$(u_c + V\cos\theta)\left[2rs\frac{d}{d\tilde{x}}(u_c + V\cos\theta) + rv_s - sw_r\right] + \frac{ag}{\rho_a}s\left[\frac{d}{d\tilde{x}}\left(\Delta T_c\frac{r^2}{2}\right) + I_3r\frac{d}{d\tilde{x}}(\Delta T_ch)\right] = 0.$$

Region 2 $\tilde{x}$ momentum:

$$s\left\{\frac{d}{d\tilde{x}}[h(u_c^2I_2 + 2V\cos\theta\, u_cI_1 + V^2\cos^2\theta)] + (u_c + V\cos\theta)^2\frac{dr}{d\tilde{x}} + w_r(u_c + V\cos\theta) - \alpha_{sz}u_cV\cos\theta\right.$$
$$\left. + \frac{ag}{\rho_a}\left(I_4\frac{d\Delta T_ch^2}{d\tilde{x}} + I_3\Delta T_ch\frac{dr}{d\tilde{x}}\right)\right\} + v_bh(u_cI_2 + V\cos\theta\, I_1) = 0.$$

Region 3 $\tilde{x}$ momentum:

$$r\left\{\frac{d}{d\tilde{x}}[b(u_c^2I_2 + 2V\cos\theta\, u_cI_1 + V^2\cos^2\theta)] + (u_c + V\cos\theta)^2\frac{ds}{d\tilde{x}} - v_s(u_c + V\cos\theta) + \alpha_y u_cV\cos\theta\right\}$$
$$- w_hb(u_cI_2 + V\cos\theta\, I_1) + \frac{ag}{\rho_a}\left[\frac{I_3}{2}\frac{d\Delta T_cbr^2}{d\tilde{x}} + I_3^2r\frac{d\Delta T_cbh}{d\tilde{x}} + \Delta T_c\left(\frac{r^2}{2} + I_3hr\right)\frac{ds}{d\tilde{x}}\right] = 0.$$

Region 4 $\tilde{x}$ momentum:

$$\frac{d}{d\tilde{x}}[hb(u_c^2I_2^2 + 2V\cos\theta\, u_cI_1^2 + V^2\cos^2\theta)] + [u_c^2I_2 + 2V\cos\theta\, u_cI_1 + V^2\cos^2\theta]\left(b\frac{dr}{d\tilde{x}} + h\frac{ds}{d\tilde{x}}\right)$$
$$+ (w_hb - v_bh)(u_cI_2 + V\cos\theta\, I_1) - u_cI_1[\alpha_{sz}b - \alpha_y h]V\cos\theta$$
$$+ \frac{ag}{\rho_a}\left[I_3I_4\frac{d\Delta T_ch^2b}{d\tilde{x}} + I_4\Delta T_ch^2\frac{ds}{d\tilde{x}} + I_3^2\Delta T_chb\frac{dr}{d\tilde{x}}\right] = 0.$$

Jet $\tilde{y}$ momentum:

$$\frac{d}{d\tilde{x}}\left[\frac{db}{d\tilde{x}} - \left(\frac{db}{d\tilde{x}}\right)_{NB}\right][u_c^2bI_6(r + hI_2) + 2V\cos\theta\, u_cbI_5(r + hI_1) + V^2\cos^2\theta\, b(r + h)]$$
$$- \frac{ag}{\rho_a}\Delta T_c\left(\frac{r^2}{2} + I_3rh + I_4h^2\right) = 0.$$

Jet heat:

$$\frac{d}{d\tilde{x}}[u_c\Delta T_c(s + bI_7)(r + hI_7) + V\cos\theta\,\Delta T_c(s + bI_3)(r + hI_3)] + K\Delta T_c(s + bI_3) = 0.$$

TABLE 4.2 (Contd.)

Jet bending:

$$[u_c^2(s+bI_2)(r+hI_2) + 2V\cos\theta\, u_c(s+bI_1)(r+hI_1) + V^2\cos^2\theta(s+b)(r+h)]\frac{d\theta}{d\tilde{x}}$$

$$- u_c V \sin\theta[-\alpha_{sz}(s+bI_1) + \alpha_y(r+hI_1)] = 0.$$

Jet x position:

$$\frac{dx}{d\tilde{x}} - \sin\theta = 0.$$

Jet y position:

$$\frac{dy}{d\tilde{x}} - \cos\theta = 0.$$

In the above equations I_1, I_2, I_3, I_4, I_5, I_6, and I_7 are as defined in Table 4.1.

$\left(\frac{db}{d\tilde{x}}\right)_{NB}$ = nonbuoyant spreading rate calculated from above equations with $\Delta T = 0$,

$$\alpha_y = \begin{cases} -(I_1 - I_2)\,\epsilon, & s > 0, \\ -\dfrac{I_1\epsilon}{2}, & s = 0, \end{cases}$$

$$\alpha_z = \begin{cases} (I_1 - I_2)\,\epsilon, & r > 0, \\ \dfrac{I_1\epsilon}{2}, & r = 0, \end{cases} \qquad \alpha_{sz} = \alpha_z \exp\left(-5.0\,\frac{ag\Delta T_c h}{\rho_a u_c^2}\right),$$

ϵ = spreading rate of a free turbulent region = 0.22,

$$\left.\begin{array}{ll} r = h_0, & \dfrac{db}{d\tilde{x}} = \epsilon, \\ s = b_0, & u = u_0, \\ x = y = h = b = 0, & \Delta T = \Delta T_0, \\ & \theta = \theta_0, \end{array}\right\} \tilde{x} = 0.$$

is used, only the entrainment velocities of ambient water inflow need be considered. Developing the final equations by integrating the differential equations of conservation, as used here by the authors, requires the specification of the Eulerian or spatial velocities, not the relative velocities. The additional components involving $V\cos\theta$ account for the slant or slope of the jet boundary which contains jet fluid at a nonzero velocity due to the crosscurrent. Thus, the extra terms are kinematic velocities to ensure that the net velocity is parallel to the jet surface; i.e., if one subtracts the normal entrainment velocity from the total velocity at any jet edge, the remaining velocity vector should be parallel to the jet boundary. This is handled by the kinematic boundary condition applied to each jet edge. These extra terms did not arise in the nondeflected jet case because the velocity was zero at those edges, the kinematic condition degenerating to a single-term entrainment relationship. Of special interest is the relationship of $\tilde{v}_e$ given in Eq. 4.63; the lateral entrainment is presumed equal on either

side of the deflected jet. This assumption will be discussed in more detail later. For this crossflow situation, the authors assume the entrainment coefficients α_y and α_{sz} to be identical to the previous undeflected case and relate $\tilde{w}_e$ and $\tilde{v}_e$ to $\tilde{u}_c$ in the same manner.

The $\tilde{y}$-momentum equation is used to yield two separate equations in Table 4.2. The first equation, denoted "jet bending," is supplementary and is derived in a similar manner to the y-momentum equation for the situation of a buoyant nondeflected jet as described by Model 1. This is done by first assuming that Eq. 4.61 holds on each half of the surface $\tilde{y} = 0$. From it a lateral-spreading equation similar to Eq. 4.52 results. The lateral-spreading velocity is for $s < \tilde{y} < b + s$, chosen as

$$\tilde{v} = \left[\frac{db}{d\tilde{x}} - \left(\frac{db}{d\tilde{x}}\right)_{NB}\right] \tilde{\zeta}_y^{1/2}\left[\tilde{u}_c(1 - \tilde{\zeta}_z^{3/2})^2(1 - \tilde{\zeta}_y^{3/2}) + V \cos\theta\right] \tag{4.64}$$

and zero otherwise. The different distribution for $\tilde{u}$ has been incorporated into this formula. The final equation that results from this $\tilde{v}$ is the jet-bending equation of Table 4.2. This equation balances the rate of deflection with the entrainment of lateral momentum. The second equation derived is denoted as the $\tilde{y}$-momentum equation in Table 4.2 and is simply Eq. 4.61 for region $\tilde{y} > 0$ with the application of the above similarity assumptions. The nonbuoyant spreading rate $(db/d\tilde{x})_{NB}$ is calculated by setting $\Delta T \equiv 0$ in the equations of Table 4.2 to find $b(\tilde{x})$. This step clearly involves a good deal of calculation and is done during the numerical calculations in the computer program. The calculation is done step-by-step with the calculations for the deflected jet by setting $\Delta T \equiv 0$ at each grid point and making the appropriate evaluation of the nonbuoyant spreading rate at that position.

Continuity equation 4.55 is integrated over regions 1-4 to yield the first four equations of Table 4.2. The curvature term in Eq. 4.55 is negligible since it can be shown to be proportional to the ratio of the jet velocity to the current velocity. (The $\tilde{z}$-momentum equation, as before, simply states that η may be neglected in all integrations.) Energy equation 4.59 is integrated over the entire jet to yield the heat equation. The complete system of equations is given in Table 4.2 and must be solved numerically.

(3) Discussion of Crossflow Model. A few comments will now be made about the Stolzenbach-Harleman crossflow model. First, it is derived and assumed valid only for small ambient currents in relation to the initial discharge velocity. Although the actual velocity and temperature profiles are really not similar, as assumed by the authors, due to uneven entrainment, similarity profiles may be a good approximation for slightly perturbed jets. Of more concern, however, is the fact that for significant crossflows the actual entrainment mechanisms implied by nonbuoyant

noncrossflow jet theory used here may not be present or may be changed completely. The authors employ a constant lateral-entrainment coefficient; however, the entrainment coefficient is most likely not constant for velocities of the ambient fluid comparable to centerline velocities.

The authors used a parabolic-shaped crossflow velocity (see Fig. 4.6) in the application of their theoretical model and in their hydraulic-model verifications. This meant that the ambient velocity was small near the outfall, where the jet velocity is high, and increased as the jet velocity decreased. Stolzenbach indicated that upon matching at each centerline position of the jet the relative magnitudes of the jet centerline velocity and ambient crosscurrent almost always revealed small relative crossflow velocities. Measurements ceased when the ambient velocity became equal

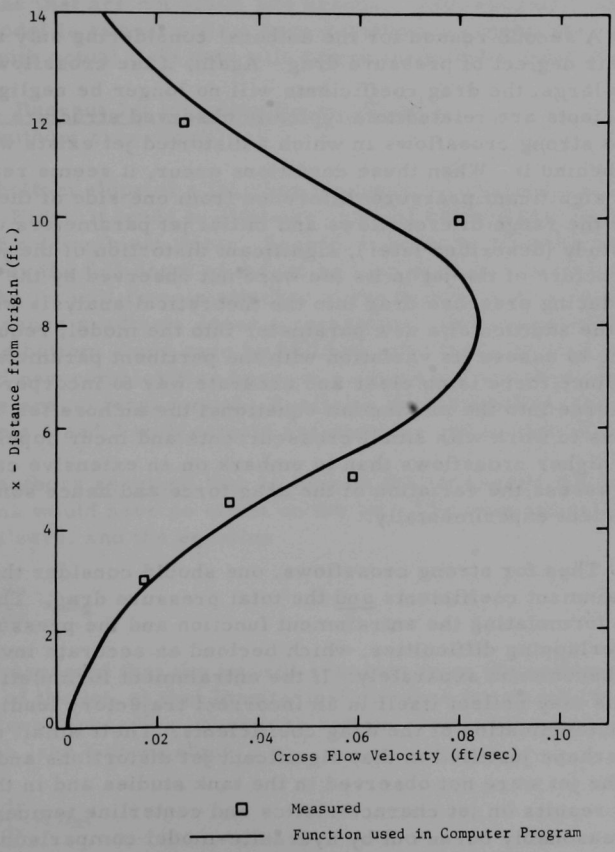

Fig. 4.6. Crossflow Velocity in Experimental Basin[1]

to the jet centerline velocity. The centerline temperature decay matched fairly well with theoretical predictions, apparently because none of the undesirable effects that result from crossflows were able to appear before the jet reached its "stable region" (the downstream region of jet in which vertical stability inhibits vertical entrainment and jet depth decreases due to lateral spreading, discussed later). The authors expect their model to yield satisfactory results as long as the maximum velocity of their parabolic distribution V_{max} is smaller than about $0.4u_0$ or $0.5u_0$. If, however, a constant ambient velocity is used, its magnitude should seemingly be quite small to satisfy the small crossflow requirements for distances reaching into the stable region. No mathematical or hydraulic studies were carried out with constant crossflows, so no firm conclusions can be made for that case.

A second reason for the authors' considering only small crossflows is their neglect of pressure drag. Again, if the crossflow velocity is sufficiently large, the drag coefficients will no longer be negligible. These drag coefficients are related to a typically observed structure for jets in moderate to strong crossflows in which a distorted jet exists with a region of eddying behind it. When these conditions occur, it seems reasonable to postulate a significant pressure difference from one side of the jet to the other. For the range of crossflows and initial jet parameters used in their hydraulic study (described later), significant distortion of the jet and the eddying structure of the jet in its lee were not observed by the authors. Also, introducing pressure drag into the theoretical analysis would generally imply the addition of a new parameter into the model, requiring some curve fitting to assess its variation with the pertinent parameters of the problem. Since there is no clear and accurate way to incorporate this additional force into the momentum equations, the authors felt it more advantageous to work with small crosscurrents and incur hopefully small errors for higher crossflows than to embark on an extensive campaign to accurately assess the variation of the drag force and hence some kind of drag coefficient experimentally.

Thus for strong crossflows, one should consider the variation in the entrainment coefficients and the total pressure drag. The complexity involved in formulating the entrainment function and the pressure force leads to overlapping difficulties, which becloud an accurate investigation into each phenomenon separately. If the entrainment formulation is incorrect, this may reflect itself in an incorrect trajectory leading to an incorrect determination of the drag coefficients. Their small crossflow model is perhaps justified in that significant jet distortions and eddying in the lee of the jet were not observed in the tank studies and in that their theoretical results on jet characteristics and centerline temperature decay were reasonably borne out by hydraulic-model comparisons.

Finally, the Stolzenbach-Harleman model has the trait that entrainment becomes less important downstream due to the density effects and the small vertical projected lateral area. The phenomenon will not generally occur for a submerged buoyant jet. Entrainment in such circumstances occurs practically over the entire extent of vertical spreading and would not get suppressed by any other considerations such as buoyancy or the presence of a free surface. This die-off of entrainment for a surface jet apparently mitigates the effect of the constant assumed entrainment coefficient and perhaps "saves" the authors' model. In short, the question of similarity of velocity and temperature distributions for slightly bent jets is expected not to be nearly as sensitive a question as crossflow entrainment as long as a reasonable choice of similarity functions is made. Neglecting the additional pressure forces due to the crossflow may also be significant for deflections that are not small and gradual. Consequently, the authors' crossflow model is at best a first approximation for moderate crossflows, and testing with actual field data will determine how accurate it is.

e. Model 3: Buoyant Jet Including Bottom Slope (with or without crossflows)

The bottom slope of a lake has two general effects on a discharged surface jet: First, it tends to diminish vertical entrainment by reducing the supply of cold ambient water. Second, it tends to promote lateral entrainment over the full depth of the jet as long as it is attached to the bottom. Generally, the jet will remain attached to the bottom until buoyancy forces or negative pressure gradients cause a separation. Deriving a mathematical model for the bottom slope case by building upon facts learned from Models 1 and 2 yielded new complexities because a number of assumptions made in those models are no longer valid. Realizing the difficulties, the authors applied Models 1 and 2 with certain assumptions and modifications.

The authors assumed that as long as the jet hugged the bottom, all buoyant terms would have no effect on the jet. The vertical entrainment, w_e, was then zero, and the equation

$$\frac{dh}{dx} + \frac{dr}{dx} = S_x \tag{4.65}$$

holds. They assumed that the jet will separate from the bottom, over the entire width of the jet, at that longitudinal distance for which the buoyant effects of lateral spreading caused the bottom slope of the jet to be less than the given lake bottom slope; i.e.,

$$\frac{dh}{dx} + \frac{dr}{dx} < S_x. \tag{4.66}$$

In the preseparation region, the use of Eq. 4.65 required the dropping of one of the other governing equations. The x-momentum equation was still valid if one assumed that the additional frictional losses incurred by a sloping bottom are negligible. The y-momentum equation was chosen to be relaxed mainly because of the difficulty in determining the bottom wall pressures now required in that equation and from the fact that the nonbuoyant y-momentum equation (used in conjunction with the buoyant y-momentum equation for the no-slope case) led to the condition $db/dx = dh/dx$, which is known to be invalid for sloping conditions.

The authors calculated the solution to the bottom slope problem by testing at each x whether Inequality 4.66 would hold if the bottom were not present. If so, the calculation proceeds as if the bottom were not there. This assumes identical entrainment to the no-slope case. If, however, the jet (no-slope conditions) would have spread more rapidly than the actual lake-bottom slope allows, Eq. 4.65 replaces the y-momentum equation and the calculation proceeds with the restricted-slope set of equations. The two sets of governing equations must be solved numerically; the program for the calculations is included in the main work.

The authors note that in comparing the above bottom slope theory to their hydraulic model tests, the theory fails to reproduce the significant lateral spreading that is observed. They conclude, therefore, that their assumption of a jet not exhibiting buoyant spreading when attached to the bottom is clearly not valid. They concluded that the jet must actually be spreading laterally at its edges while remaining attached near its centerline with a resultant distortion of the jet, which their theory could not predict with simple similarity functions. The mass balance is not violated by the authors' model, but clearly the y-momentum equation should not have been dropped completely, in spite of the apparent impossibility to calculate the unknown pressure at the bottom wall. These facts should be kept in mind in any application of the sloping-bottom model.

f. Application of the Theory to General Outfall Situations

The three-dimensional temperature and velocity distributions and jet characteristics for the general case of a buoyant jet in a crossflow in the presence of bottom slope are predicted by a single computer program developed from the above models. Input requirements for that computer routine are, as stated before, the five nondimensional parameters $\mathbb{F}_0$, A, S_x, $K/(\rho c_p u_0)$, and V/u_0. Their calculation in any application requires the specification of the ambient temperature T_a, the initial temperature rise ΔT_0, the discharge-channel geometry, the initial-discharge velocity u_0, the bottom slope S_x, the surface-heat-loss coefficient K, and the crossflow velocity V, where V is a function only of distance normal to the ambient current or shoreline. The ambient temperature is assumed constant in

space and time throughout the model development. In reality, variations do generally occur due to stratification and variable atmospheric conditions. The authors state that their model may be applied by using an "average" ambient temperature for T_a, provided variations do not differ by more than a few degrees Fahrenheit.

The initial-discharge temperature excess, ΔT_0, is determined as the difference between the discharge temperature T_0 and the ambient temperature T_a. The value of ΔT_0 will equal the temperature rise across the condensers only when the intake temperature is T_a.

The discharge-channel geometry affects the value of the initial densimetric Froude number $\mathbb{F}_0$ through the specification of the initial depth h_0 and the aspect ratio A by the values of both h_0 and b_0. Because actual outfall geometries are rarely perfectly rectangular, the authors suggest a method for determining an "equivalent" b_0 and h_0 given <u>any</u> channel shape. First, h_0 is defined as the actual maximum discharge channel depth. Second, b_0 is defined from the channel area as

$$b_0 = \frac{\text{actual channel area}}{2h_0}. \tag{4.67}$$

The definitions of $\mathbb{F}_0$ and A remain unchanged, but where the above choices of b_0 and h_0 are used, the use of this "equivalent" rectangular shape is expected to yield somewhat distorted results near the outfall, accuracy being improved with increasing longitudinal distance downstream.

The initial-discharge velocity u_0 can generally be calculated from the power-plant pumping rate and the actual discharge-channel area.

The surface-heat-loss coefficient K is assumed to be constant and may be calculated from atmospheric data by a number of formulas available in the literature.

The crossflow velocity is assumed to be a function of distance normal to the ambient current and/or shoreline and can be measured from drogue surveys or current meters.

A slight complication arises if the discharge densimetric Froude number is less than unity. In this case, a stagnant wedge of ambient water extends upstream into the discharge channel beneath the flow of the heated water. The situation is illustrated in Fig. 4.7. The cold-water wedge will require the heated effluent to obtain a densimetric Froude number of unity at the discharge point. The depth of the heated flow in the presence of this wedge is given by[8]

$$h_0^* = h_0 \mathbb{F}_0^{2/3}, \tag{4.68}$$

where h_0 and $\mathbb{F}_0$ are based on channel dimensions. The new initial velocity is derived from

$$\frac{u_0^*}{\sqrt{\frac{\Delta\rho}{\rho} gh_0^*}} = 1.0. \tag{4.69}$$

These values of h_0^* and u_0^* should be used in all theoretical calculations in place of h_0 and u_0.

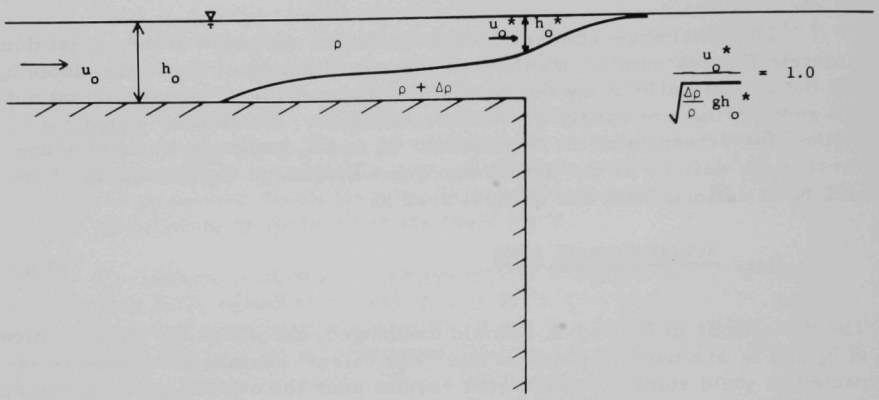

Fig. 4.7. Two-layer Flow in Discharge Channel[1]

The outfall situations described above may be complicated even further by the existence of additional boundaries obstructing free spreading of the jet. The authors assert that their model can still be used if proper schematization is possible. The more common situations are illustrated in Fig. 4.8. Discharges with entrainment on both sides are handled with no alterations. A discharge directed parallel to shore, however, restricts entrainment to only one side of the jet. The authors schematize this situation by considering the shoreline as the jet centerline and the initial channel width used for theoretical calculations to be twice the width calculated by the above procedure due to shoreline reflection. For the situation of a jet impinging at right angles to a straight solid body located just offshore, the schematization illustrated in Fig. 4.8 may be used. New values of u_0 and T_0 may need to be determined depending on the level of initial dilution that occurs as the jet changes direction by 90°. Once the discharge is moving parallel to shore, the previous schematization of a jet moving parallel to shore is then used. For more complicated solid-boundary arrangements causing uneven jet entrainment or distortions of jet boundaries, no schematization is readily possible.

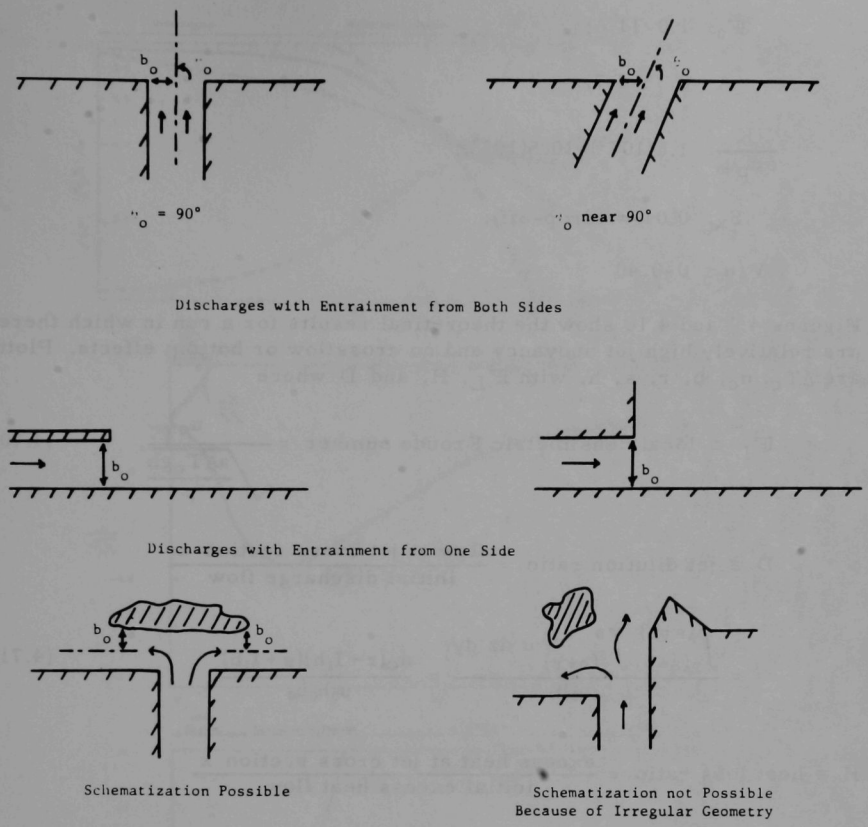

Fig. 4.8. Discharge-channel Schematization[1]

Finally, when a meaningful schematization of an actual outfall situation has been made, a theoretical analysis can be performed using the computer routine developed by the authors for their model. With inputs $\mathbb{F}_0$, A, S_x, $K/(\rho c_p u_0)$, and V/u_0 (as a function of $x/\sqrt{h_0 b_0}$), the program prints out $\Delta T_c/\Delta T_0$, u_c/u_0, $b/\sqrt{h_0 b_0}$, $h/\sqrt{h_0 b_0}$, $r/\sqrt{h_0 b_0}$, $s/\sqrt{h_0 b_0}$, and the position of the jet centerline as a function of longitudinal distances along the centerline. The computer program is listed in Ref. 1.

g. Model Verification

The authors carried out 25 hydraulic-modeling experiments under a range of input conditions in an attempt to verify the mathematical models. The chosen ranges of the five nondimensional input parameters were

$\mathbb{F}_0$: 1.0-11.6;

A: 0.35-5.7;

$\frac{K}{\rho c_p u_0}$: $1.6(10^{-5})$-$10.5(10^{-5})$;

S_x: 0.01-∞ (drop-off);

V/u_0: 0-0.40.

Figures 4.9 and 4.10 show the theoretical results for a run in which there are relatively high jet buoyancy and no crossflow or bottom effects. Plotted are ΔT_c, u_c, b, r, s, h, with $\mathbb{F}_L$, H, and D where

$$\mathbb{F}_L \equiv \text{local densimetric Froude number} = \frac{u_c}{\sqrt{\frac{a\Delta T_c g h}{\rho}}}, \tag{4.70}$$

$$D \equiv \text{jet dilution ratio} = \frac{\text{flow at jet cross section } x}{\text{initial discharge flow}}$$

$$= \frac{\int_{-(s+b)}^{(s+b)} \int_{-(h+r)}^{0} u \, dz \, dy}{u_0 h_0 b_0} = \frac{u_c(r + I_1 h)(s + I_1 b)}{u_0 h_0 b_0}, \tag{4.71}$$

$$H \equiv \text{heat loss ratio} = \frac{\text{excess heat at jet cross section } x}{\text{initial excess heat flow}}$$

$$= \frac{\rho c_p \int_{-(s+b)}^{(s+b)} \int_{-(h+r)}^{0} u\Delta T \, dz \, dy}{\rho c_p \Delta T_0 u_0 h_0 (2b_0)} = \frac{u_c \Delta T_c (r + I_7 h)(s + I_7 b)}{\Delta T_0 u_0 h_0 b_0}. \tag{4.72}$$

These theoretical results are compared to experimental results in Fig. 4.11 with respect to centerline temperature ΔT_c, jet half-depth $h_{1/2}$ and jet half-width $b_{1/2}$. The variables $h_{1/2}(x)$ and $b_{1/2}(x)$ are defined to be the vertical and horizontal distances, respectively, measured from the jet centerline to the point where the jet surface temperature is half the centerline value. Variables $h_{1/2}$ and $b_{1/2}$ were defined to facilitate experimental data acquisition. Only T_c, $h_{1/2}$, and $b_{1/2}$ were measured in the hydraulic experiments. Figure 4.12 compares these three quantities with theory for a crossflow but no bottom. The crossflow velocity distribution used in the experimental basin and the function used in the computer program are both plotted in Fig. 4.6. Figure 4.13 represents the comparison of model and hydraulic data for the condition of bottom slope (S_x = 1/100, 1/50, 1/25, ∞) when no crosscurrent interferes.

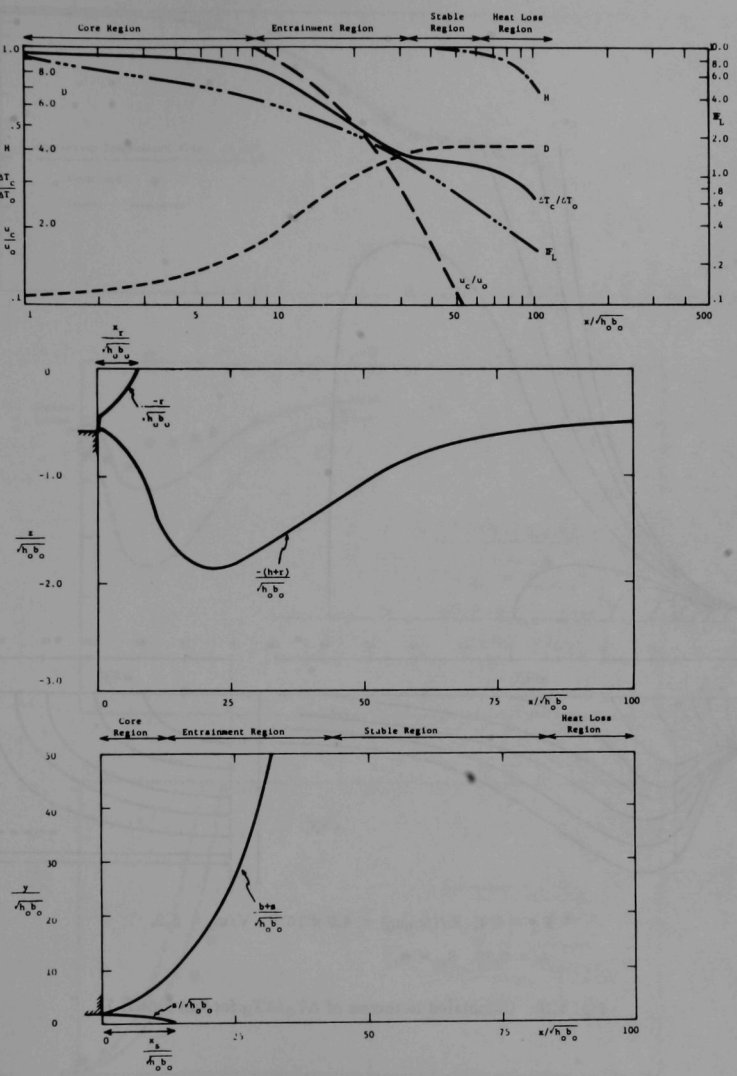

$\mathbb{F}_0 = 4.4$, $K/(\rho c_p u_0) = 4.2 \times 10^{-5}$, $V/u_0 = 0$,

$A = 0.35$, $S_x = \infty$.

Fig. 4.9. Theoretical Calculation of Jet Structure for Run 6 (Ref. 1)

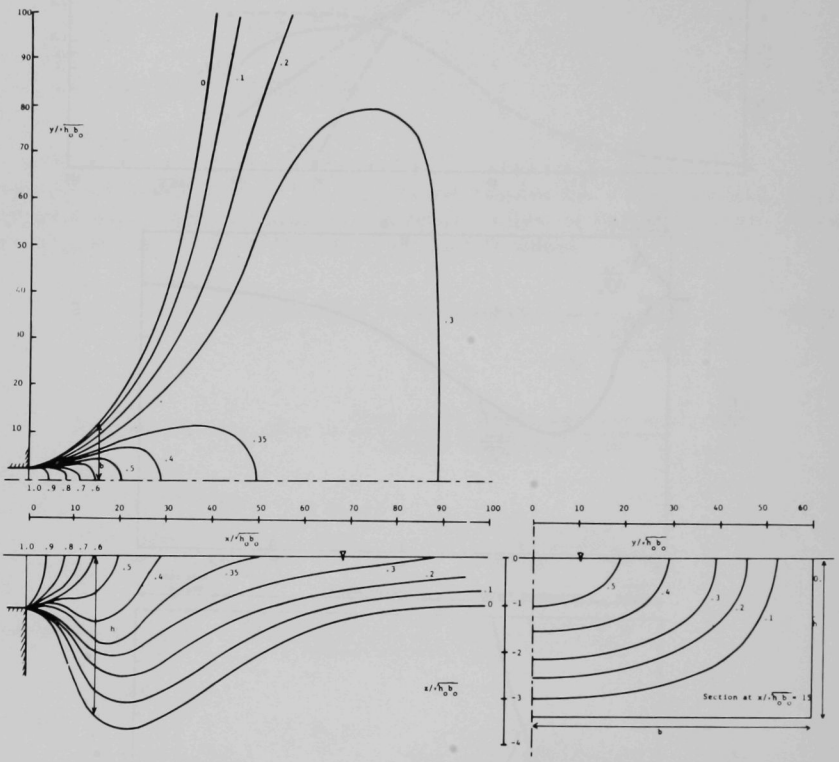

$\mathbb{F}_0 = 4.4$, $K/(\rho c_p u_0) = 4.2 \times 10^{-5}$, $V/u_0 = 0.0$,

$A = 0.35$, $S_x = \infty$.

Fig. 4.10. Calculated Isotherms of $\Delta T_c/\Delta T_0$ for Run 6 (Ref. 1)

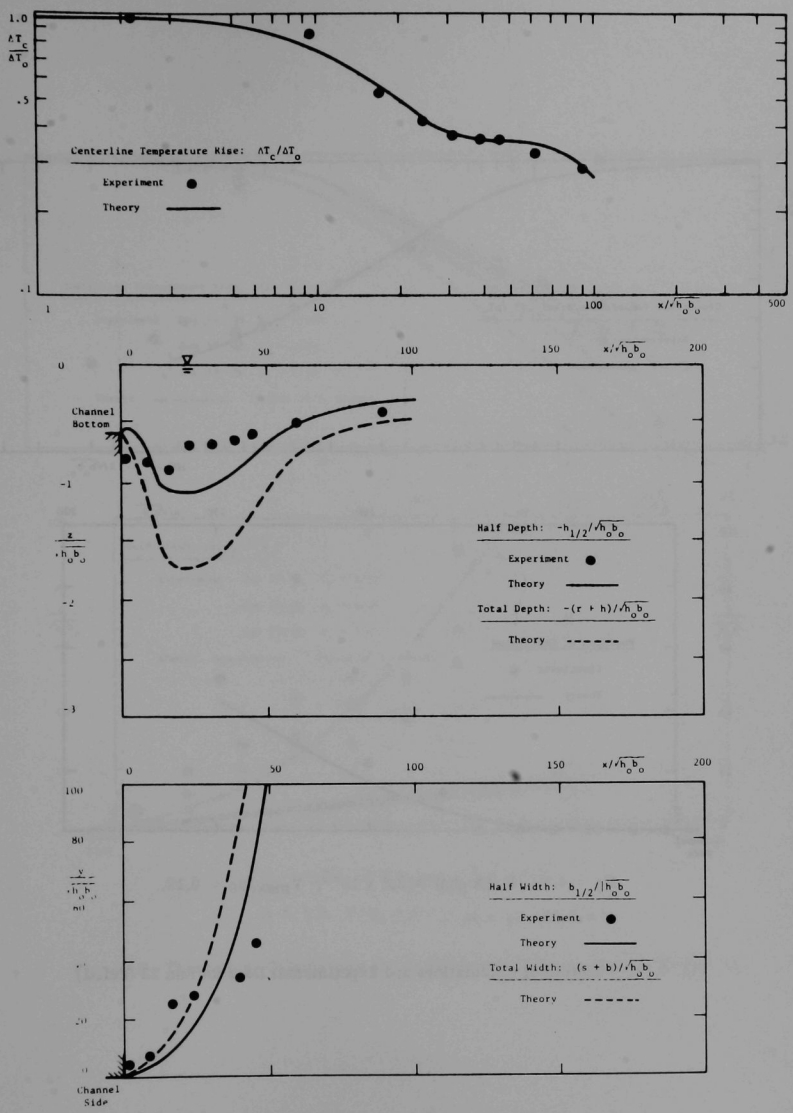

$F_0 = 4.4$, $K/(\rho c_p u_0) = 4.2 \times 10^{-5}$, $V/u_0 = 0$,

$A = 0.35$, $S_x = \infty$.

Fig. 4.11. Theoretical Calculations and Experimental Data for Run 6 (Ref. 1)

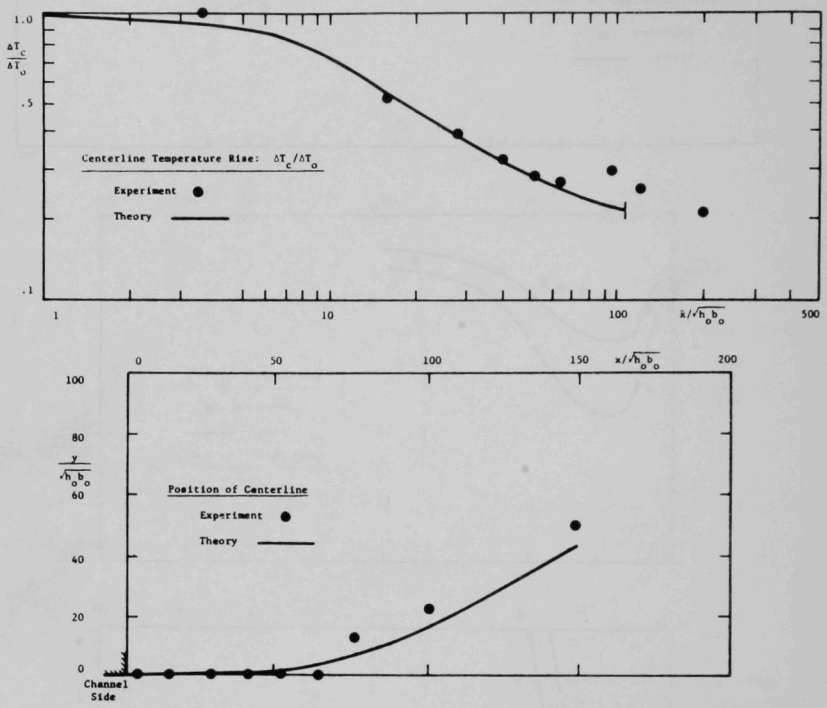

$\mathbb{F}_0 = 4.10$, $K/(\rho c_p u_0) = 2.8 \times 10^{-5}$, $V_{max}/u_0 = 0.12$,

$A = 3.95$, $S_x = \infty$.

Fig. 4.12. Theoretical Calculations and Experimental Data for Run 23 (Ref. 1)

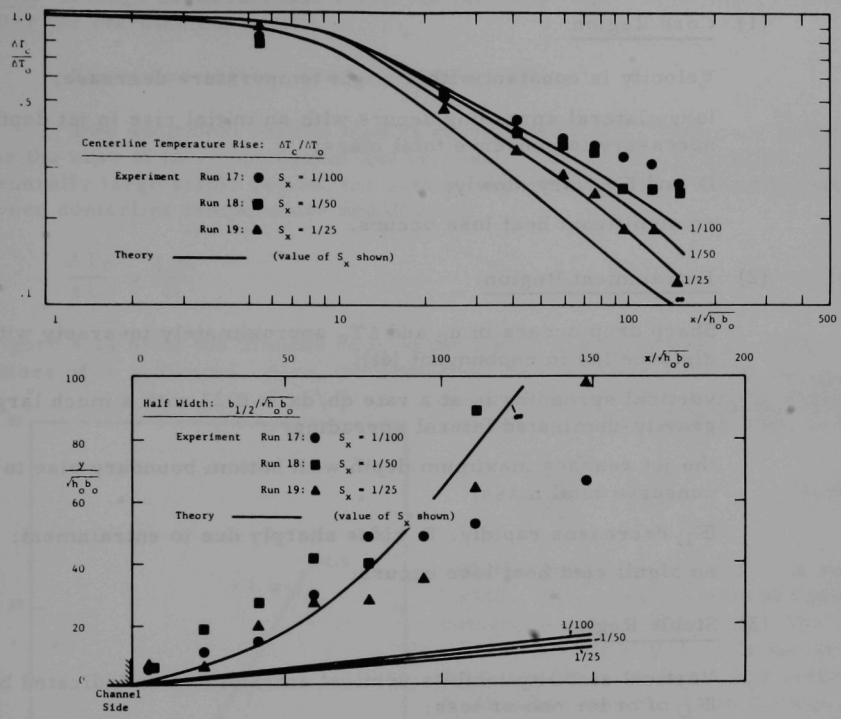

$F_0 = 11.6$, $K/(\rho c_p u_0) = 1.6 \times 10^{-5}$,

$A = 1.9$, $V/u_0 = 0$.

Fig. 4.13. Theoretical Calculations and Experimental Data for Runs 17–19 (Ref. 1)

Theoretical and experimental results obtained in the 25 surveys led the authors to divide the jet into five regions where different phenomena take precedence over others. In turn, they are, with their specific characteristics, as follows:

(1) Core Region

Velocity is constant with a slight temperature decrease;

large lateral spreading occurs with an initial rise in jet depth necessary to conserve total mass;

D and $\mathbb{F}_L$ vary slowly;

no significant heat loss occurs.

(2) Entrainment Region

Sharp drop occurs in u_c and ΔT_c approximately inversely with distance (as in nonbuoyant jet);

vertical spreading is at a rate $dh/dx \approx 0.22$ with a much larger gravity-dominated lateral spreading;

the jet reaches maximum depth with bottom boundary rise to conserve total mass;

$\mathbb{F}_L$ decreases rapidly, D rises sharply due to entrainment;

no significant heat loss occurs.

(3) Stable Region

Vertical stability inhibits vertical entrainment as indicated by $\mathbb{F}_L$ of order one or less;

jet depth decreases due to lateral spreading causing D and ΔT_c to be relatively constant;

wide surface-temperature isotherms are apparent.

(4) Heat-loss Region

Significant surface heat transfer occurs due to large plume area;

ΔT drops again;

centerline velocity is low;

discharge may no longer be considered a jet.

(5) Far-field Region

Ambient convective and diffusive processes dominate.

Note: If large crosscurrents exist, the far-field region may begin directly after the entrainment region.

These five regions are noted in Fig. 4.9.

Two additional results may be derived from the theoretical model for the case of no crosscurrent and no slope. Due to the importance of the generally large stable region, the authors derive a useful relationship between centerline temperature and dilution

$$\frac{\Delta T_c}{\Delta T_0} = \frac{1.5}{D}. \tag{4.73}$$

Figure 4.14 plots the dilution ratio in the stable region against $\mathbb{F}_0$ with values of A indicated. Also, the maximum depth of the discharge, h_{max}, is located in the entrainment region and was derived approximately to be

$$\frac{h_{max}}{\sqrt{h_0 b_0}} = \frac{1}{2}\mathbb{F}_0 \tag{4.74}$$

with the small dependence on A neglected. This result is plotted against numerical data in Fig. 4.15. The scatter seen in Fig. 4.15 is due to the dependence on the aspect ratio A. A straight line was drawn through the calculated data for convenience; no reasonable alternatives could be seen that were simple and yet yielded such an easily applicable result.

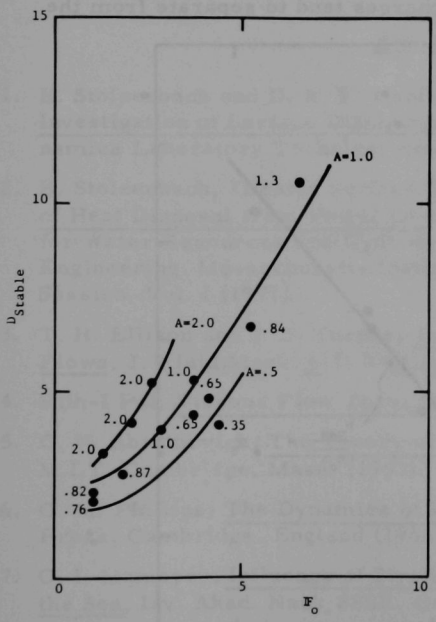

Fig. 4.14. Dilution in the Stable Region of Buoyant Discharges.[1] (Points are calculated by the theoretical model. Values of A are indicated.)

In general, the theoretical model does fit the hydraulic data satisfactorily for those situations considered (except for lateral spreading in the presence of a bottom slope). A close analysis of all the model results and experimental data yielded the following general conclusions:

(1) Buoyant jets ($1 < \mathbb{F}_0 < 10$) consist of the five regions where the

heat-loss region marks the end of the jet and the beginning of the far-field region dominated by ambient processes.

(2) Entrainment increases with initial densimetric Froude number $\mathbb{F}_0$ and aspect ratio A.

(3) Buoyancy inhibits the vertical spread of the jet, but increases lateral spreading. Decreasing $\mathbb{F}_0$ increases the buoyancy effects and consequent lateral spreading.

(4) Surface-heat loss has generally an insignificant effect in the first four regions described above, except possibly for low-$\mathbb{F}_0$, high-aspect-ratio discharges.

(5) Small crosscurrent velocities (as compared to initial discharge velocity) deflect the jet centerline, yet do not greatly change the temperature distribution.

(6) Bottom slopes tend to inhibit vertical entrainment and result in higher centerline temperatures than for a no-slope case whenever $\mathbb{F}_0$ is greater than about 5. Smaller $\mathbb{F}_0$ discharges tend to separate from the

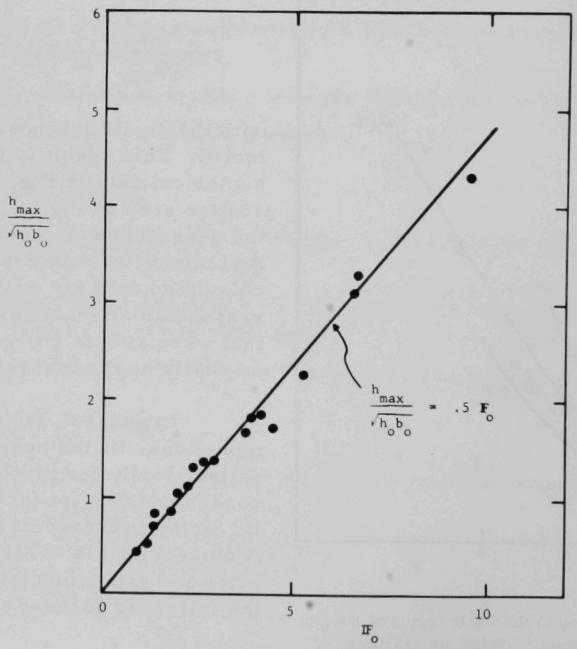

Fig. 4.15. Maximum Jet Depth vs $\mathbb{F}_0$ as Calculated by Theory[1]

bottom close to the outfall exit and show little dependence on the actual value of the slope S_x. The authors found evidence to indicate that in low-$\mathbb{F}_0$ discharges there is increased entrainment over the region in which the jet is attached to the bottom due to the increased lateral area.

h. Final Comments

The advantages of the Stolzenbach-Harleman model lie in its careful technical development and its easy application. Its considerations of all the major factors (initial mixing, buoyancy, discharge-channel geometry, bottom slope, surface heat loss, and ambient crossflow) make it unique among jet models. The model compares satisfactorily with limited hydraulic modeling data, except for lateral spreading in the presence of a sloping bottom. The model simply synthesizes the results of previous investigations concerning turbulent jets and stratified flows into one complete model. Of special significance is its simplicity of application where the theory requires only five nondimensional parameters and does not require any fitting of the theory to the data for their determination. As stated above, one should be wary in any model application due to the nonstratified lake assumption and the expected greater vertical entrainment and dilutions that will be predicted.

References

1. K. Stolzenbach and D. R. F. Harleman, An Analytical and Experimental Investigation of Surface Discharges of Heated Water, M.I.T. Hydrodynamics Laboratory Technical Report No. 135 (Feb 1971).

2. K. Stolzenbach, "Heated Surface Discharges," in Engineering Aspects of Heat Disposal from Power Generation, Ralph M. Parsons Laboratory for Water Resources and Hydrodynamics and Department of Civil Engineering, Massachusetts Institute of Technology 1971 Summer Session, Vol. I (1971).

3. T. H. Ellison and J. S. Turner, Turbulent Entrainment in Stratified Flows, J. Fluid Mech. 6(3) (Oct 1969).

4. Shih-I Pai, Viscous Flow Theory, D. Van Nostrand Company, Inc. (1956).

5. G. N. Abramovich, The Theory of Turbulent Jets, The M.I.T. Press, M.I.T. Cambridge, Mass. (1963).

6. O. M. Phillips, The Dynamics of the Upper Ocean, Cambridge University Press, Cambridge, England (1966).

7. O. I. Mamayev, Influence of Stratification on Vertical Turbulent Mixing in the Sea, Izv. Akad. Nauk SSSR, Geofiz 7 (English Translation).

8. D. R. F. Harleman, "Stratified Flow," in Handbook of Fluid Dynamics, V. L. Streeter, Ed., McGraw-Hill Book Company, Inc., New York (1961).

B. Models for the Far Field

5. The Work of Akira Wada[1-9]
(Central Research Institute of the Electric Power Industry)
1965-1968

a. List of Symbols

a	Thermal-expansion coefficient
A_0, A_1	Empirical coefficients in the Mamayev form for A_z
A_p	Overrelaxation factor
A_{opt}	Optimum value of A_p
A	Surface area of bay
A_h	Horizontal coefficient of eddy momentum
A_x, A_y, A_z	Eddy-viscosity components in x, y, and z directions
$2B$	Breadth of outlet
b_0, b_1	Coefficients dependent upon meteorological conditions
B_0	$b_0/(C_w H_w)$
B_1	$b_1/(C_w H_w)$
a, b	Constants
c_p	Specific heat of water (lake, bay, or sea)
$e(T)$	Saturation pressure for water temperature
f	Specific humidity
g	Acceleration of gravity
h	Distance between grid points
h_a	Heat-transfer coefficient
H	Height of outlet
H_w	Thickness of plume or depth to thermocline
K_0, K_1	Empirical coefficients in the Mamayev form for K_z
K_x, K_y, K_z	Eddy-thermal diffusivities
K	Coefficient depending on cloud height
k	Mass-transfer coefficient
M	Empirical coefficient in exponent for the Mamayev form of A_z

n	Cloudiness on the scale 1-10 (also empirical coefficient in exponent of K_z according to Mamayev)
P	Stream function
p	Pressure
Q_i	Flow rate of intake of cooling water
Q_0	Heat gain or loss for surface layer of sea basin
Q_s	Radiation energy from sun and sky
Q_b	Effective back-radiation energy from sea surface
Q_e	Heat-exchange rate by evaporation
Q_h	Convection energy of sensible heat
Q_c	Heat energy added by outfall of cooling water from power plant
R	Residuals
R_i	Richardson number
R_n	Maximum of absolute value of all residuals at nth iteration
r_1	Mixing ratio from upper layer
T	Water temperature
T_2	Apparent water temperature defined by Eq. 5.36
T_a	Atmospheric pressure
T_b	Water temperature in bottom layer
T_c	Rise of water temperature added by condenser of power plant
T_0	Water temperature of discharged water
u, v, w	Velocity components in x, y, and z directions
U	Steady uniform crosscurrent velocity parallel to shore
U_0, V_0	Initial velocity components at outlet
V	Wind velocity
W	Resultant velocity
x	Lateral distance, measured parallel to shore
y	Longitudinal distance, measured perpendicular to shore
z	Vertical distance, measured downward from the surface

α, β	Coefficients indicating node spacing in η, ζ directions of finite-difference mesh
ρ	Density of sea water $[\approx\rho_0(1 - aT)]$
λ_k	Unit vector in z direction
λ	$u/\sqrt{K_x}$
ξ	$x/\sqrt{K_x}$; also vorticity in Model 3
η	$y/\sqrt{K_y}$
ζ	$z/\sqrt{K_z}$
σ	Stefan-Boltzmann's constant for black-body radiation

b. Introduction

For the past several years, Akira Wada and his colleagues have studied the phenomena of flow and thermal diffusion resulting from the discharge of heated condenser cooling water from power plants sited on various bays in Japan. Their purpose was to develop criteria for the hydraulic design of intake and outlet structures for some of Japan's larger power plants. This involved, among other things, a study of the problem of cooling-water recirculation, which in turn required predictive knowledge of the extent and spreading behavior of warm water discharged from an outfall. Comprehensive field studies were undertaken investigating tidal action, wind stress, the heat budget of the bay, the configuration and bottom contours of the bay, the stratified condition of the ambient waters in the vicinity of the outfall, etc. The effects of these factors were analyzed separately, and the results were synthesized in the development of design criteria for the hydraulic structures of the power-plant cooling system.

Of particular interest here are the three diffusion models developed by Wada and his colleagues. Although developed for outfalls placed on the coast lines of bays, the techniques used, if not the complete models themselves, may be applied under certain general conditions to outfalls on large lakes. To date, the models are untested with lake data; this is due mostly to the previous inaccessibility of the complete details of the models to the general user.

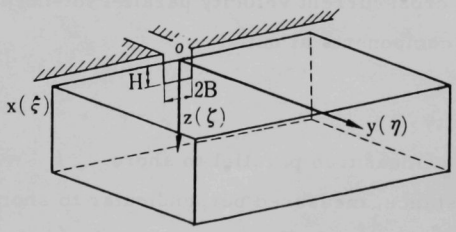

Fig. 5.1. Definition Sketch for Thermal Spread[5]

The three diffusion models compute flow and temperature data resulting from a rectangular shoreline outfall discharging heated water at the surface of a bay. Figure 5.1 is a sketch of the outfall and the Cartesian coordinate system used in the mathematical

simulation. The outlet is of width 2B and height H. The effluent is initially at constant temperature T_0 and is discharged at constant velocity U_0. The equations of mass, momentum, and heat-energy conservation are

$$\frac{\partial(\rho u_i)}{\partial x_i} = 0, \tag{5.1}$$

$$u_j \frac{\partial u_i}{\partial x_j} = -\frac{\partial p}{\partial x_i} + \rho g \lambda_k + \frac{\partial}{\partial x_j}\left(A_j \frac{\partial u_i}{\partial x_j}\right), \tag{5.2}$$

and

$$u_j \frac{\partial T}{\partial x_j} = \frac{\partial}{\partial x_j}\left(\frac{K_j}{\rho}\frac{\partial T}{\partial x_j}\right) + \frac{Q_0}{\rho c_p H_w}, \tag{5.3}$$

where j = 1, 2, 3 refer to the x, y, z directions, respectively, λ_k is a unit vector along the z axis, u_i (i = 1, 2, 3) are the velocity components along the x, y, z directions, and the eddy momentum diffusivities corresponding to these directions are A_x, A_y, and A_z. Also, eddy thermal diffusivities for i = 1, 2, 3 are K_x, K_y, and K_z, p is the pressure, ρ is the density, and T the temperature. Q_0 represents the net heat transfer at the surface of the bay (or lake), c_p is the specific heat of water, and H_w is the depth of the thermal plume. Wada uses the approximate relationship between density and temperature given by

$$\rho = \rho_0(1 - aT), \tag{5.4}$$

where ρ_0 is a reference density and a is the coefficient of thermal expansion. The three diffusion models attempt to solve Eqs. 5.1-5.4 numerically under differing assumptions. Wada lists in Table 5.1 the main processes of heat exchange at the water surface used in the evaluation of Q_0. The form of the expression for the addition of waste heat from the power plant Q_c as a factor in heating the sea basin is standard. It assumes, as is widely accepted, that this waste is ultimately spread equally over the bay surface as an aftermath of mixing. Figure 5.2 is a schematic diagram of the processes for heat balance. Q_0 then becomes

$$Q_0 = Q_s - Q_b + Q_h + Q_c \approx b_0 - b_1 T, \tag{5.5}$$

where b_0 and b_1 are constants depending upon the meteorological parameters.

Although Q_0, the surface heat-transfer term described above, is written in Eq. 5.3 as a source term, it must be considered solely as a boundary condition for three-dimensional dispersion. Although not explicitly

stated in Wada's papers, it is assumed he is using Q_0 in this manner whenever he is considering heat loss in a three-dimensional problem. For two-dimensional dispersion, the Q_0 term in Eq. 5.3 can justifiably be introduced in the differential equation.

TABLE 5.1. Main Processes of Heat Exchange at Water Surface Used in Evaluation of Q_0 (from Ref. 7)

Process of Heating the Sea Basin	Process of Cooling the Sea Basin
1. Absorption of radiation from the sun and the sky, $Q_s = Q_s^{\downarrow}(1 - \bar{r})$	1. Back radiation from the sea surface, $Q_b = \sigma(T + 273)\left[1 - a - b\sqrt{e(T_a)}\right](1 - Kn)$
2. Convection of sensible heat from atmosphere, Q_h	2. Convection of sensible heat to atmosphere, $Q_h = h_a(T_a - T)$
3. Condensation of vapor, Q_e	3. Evaporation, $Q_e = k[e(T_a) - e(T)]$
4. Addition of waste heat from power plant, $Q_c = \frac{Q_i}{A}[(1 - r)T_b + T_c - (1 - r)T]$	

$Q_s^{\downarrow}$ = radiation energy from sun and sky.
$\bar{r}$ = average reflectance over integration period.
T = water temperature in surface layer.
σ = Stefan-Boltzmann's constant for black-body radiation.
a, b = constants.
$e(T_a)$ = the saturation vapor pressure at the sea surface in mbars.
K = coefficient depending on the cloud height.
n = cloudiness on scale 1-10.
T_a = atmospheric temperature.
$e(T)$ = saturation pressure for water temperature.
h_a = heat-transfer coefficient [$= 2.77 \times 10^{-4}(0.48 + 0.272\,V)$].
k = mass-transfer coefficient ($k \simeq 2h$).
Q_i = intake discharge of cooling water.
A = surface area of bay.
r = mixing ratio from upper layer.
T_c = rise of water temperature added by condenser of power plant.
T_b = water temperature in bottom layer.

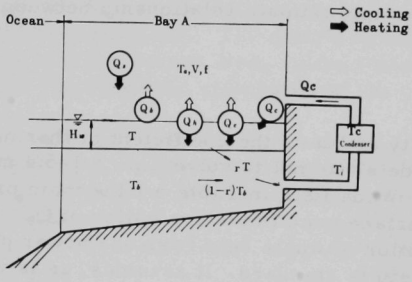

Fig. 5.2

Schematic Diagram of Processes for Heat Balance[7]

The second term (diffusion term) in Eq. 5.3 is in a nonstandard, unrecognizable form. The usual expression for that term in kinematic units is given in standard texts as

$$\frac{1}{\rho c_p}\frac{\partial}{\partial x_j}\left(\rho c_p K_j \frac{\partial T}{\partial x_j}\right).$$

The rationale for that form is unclear to us.*

*One can only speculate (this is pure speculation) that the use of Eq. 5.3 by Wada is a method of linearization to achieve stability for his numerical schemes.

Each of the three models predicts the temperature distribution of a heated shoreline surface discharge from a rectangular outlet using finite-difference methods. Model 1 predicts the three-dimensional temperature dispersion of a thermal plume in the presence of a steady, uniform shore-parallel current allowing for bottom effects. Model 2 is two-dimensional with no vertical variations considered. The flow is established first from the uncoupled hydrodynamic equations (Eqs. 5.1 and 5.2), and the resulting velocity distribution is fed into the energy equation (Eq. 5.3) to calculate the thermal diffusion. Model 3 is two-dimensional but considers longitudinal and vertical motion only. Interaction of flow and temperature is handled by the treatment of the entire coupled set of equations (Eqs. 5.1-5.4).

Unfortunately, the full details in the development of these models is not given in Wada's papers. The careful reader is generally more satisfied with Wada's formulation of his problems and his discussion of the predicted results than in the precise form and manipulation of his differential equations. One gets the vague feeling that Wada somehow has done correct solutions, although at times his work may seem incorrect or hard to follow.

Each of Wada's models will now be discussed in more detail. General comments applicable to the three models appear at the end of the model descriptions.

c. Model 1: Thermal Diffusion of Cooling Water in Three Dimensions (1965)

(1) The Physical Situation and Basic Equation. Wada considers the problem of three-dimensional thermal diffusion of power-plant heated-water discharges for homogeneous and stratified bays (or lakes). The outfall configuration is illustrated in Fig. 5.1. A steady uniform current is assumed to be shore-parallel and tends to advect the warm-water downcurrent. The other processes affecting heat dissipation are assumed to be thermal diffusion governed by the ambient lake turbulence and heat loss to the atmosphere. Any effects resulting from a possible jet-like effluent flow near the discharge are neglected. The heated water is assumed to act like a surface plume from the point of discharge with ambient turbulence primarily dominant in the field of flow. The equation to be solved then is (see previous footnote).

$$U\frac{\partial T}{\partial x} = \frac{\partial}{\partial x}\left(\frac{K_x}{\rho}\frac{\partial T}{\partial x}\right) + \frac{\partial}{\partial y}\left(\frac{K_y}{\rho}\frac{\partial T}{\partial y}\right) + \frac{\partial}{\partial z}\left(\frac{K_z}{\rho}\frac{\partial T}{\partial z}\right) + \frac{Q_0}{\rho c_p H_w}, \qquad (5.6)$$

where

T = temperature of the bay water,

U = constant velocity of the crosscurrent parallel to shoreline (x axis),

K_x, K_y, K_z = eddy thermal diffusivities in x, y, z directions, respectively,

ρ = density of the plume water,

Q_0 = heat loss from the bay surface,

H_w = depth of plume,

and

c_p = specific heat of water.

Although Wada includes the net-surface-heat-loss term in the differential equation, the Q_0 term is a boundary condition and is treated as such. The coefficients of thermal diffusion K_x, K_y, and K_z are assumed constant in the entire region of interest; Wada justifies this assumption by referring to field observations made of the temperature and velocity of flow issuing from the Mizushima Steam Power Plant located on Mizushima Bay in 1964, which yielded essentially constant thermal diffusivities when the temperature and velocity distributions were analyzed using a diffusion equation. The tongue-like shape of the observed vertical and horizontal temperature profiles was a second indication to Wada that those coefficients might be treated as approximately uniform.

(2) The Homogeneous-lake Case. Wada first investigates the problem for a nonstratified, single-layer bay whose temperature is uniformly T_b. Within the plume itself the author neglects vertical and horizontal density differences indicating a fully-mixed plume assumption. Equation 5.6 reduces to

$$U\frac{\partial T}{\partial x} = K_x\frac{\partial^2 T}{\partial x^2} + K_y\frac{\partial^2 T}{\partial y^2} + K_z\frac{\partial^2 T}{\partial z^2} + \frac{Q_0}{\rho c_p H_w}. \tag{5.7}$$

Boundary conditions associated with Eq. 5.7 are

$$T = T_0 \text{ at } y = 0,\ -B \le x \le B, \text{ and } 0 \le z \le H_w; \tag{5.8}$$

$$\frac{\partial T}{\partial y} = 0 \text{ at } y = 0, \text{ and } -B > x > B \text{ (no heat flux at shore boundary);} \tag{5.9}$$

$$\left.\begin{aligned} &\frac{\partial^2 T}{\partial z^2} = 0 \quad \text{at } z = 0, \text{ and } y > 0 \text{ (gradient of temperature as a function of depth is vertical at the surface),} \\ &T = T_b \quad \text{as a distribution of vertical temperature at all longitudinal and lateral positions "infinitely far" from the outlet,} \\ &\text{and} \\ &\frac{\partial T}{\partial z} = 0 \quad \text{at } z = H_w \text{ (no heat flux below the plume bottom).} \end{aligned}\right\} \tag{5.10}$$

Wada solves the elliptic differential equation (Eq. 5.7) by the method of finite differences. He first makes the transformations

$$\lambda = \frac{U}{\sqrt{K_x}}, \quad \xi = \frac{x}{\sqrt{K_x}}, \quad \eta = \frac{y}{\sqrt{K_y}}, \text{ and } \zeta = \frac{z}{\sqrt{K_z}} \tag{5.11}$$

to give

$$\lambda \frac{\partial T}{\partial \xi} = \frac{\partial^2 T}{\partial \xi^2} + \frac{\partial^2 T}{\partial \eta^2} + \frac{\partial^2 T}{\partial \zeta^2}. \tag{5.12}$$

This transformation will yield a solution independent of diffusivities, where the scale factors were chosen to permit stability for the subsequent numerical scheme. The $\{\xi, \eta, \zeta\}$ space is subdivided as usual by a mesh with node points $\xi = mh$, $\eta = n\alpha h$, $\zeta = p\beta h$ (h is the mesh width in the ξ direction, and α, β are coefficients indicating node spacing in η, ζ directions, where $m, n, p = 0, \pm 1, \pm 2, \ldots$).

Using central-difference approximations for the derivatives

$$\left.\begin{aligned}
\frac{\partial T}{\partial \xi} &\rightarrow \frac{T(\xi+1, \eta, \zeta) - T(\xi-1, \eta, \zeta)}{2h}, \\
\frac{\partial^2 T}{\partial \xi^2} &\rightarrow \frac{T(\xi+1, \eta, \zeta) - 2T(\xi, \eta, \zeta) + T(\xi-1, \eta, \zeta)}{h^2}, \\
\frac{\partial^2 T}{\partial \eta^2} &\rightarrow \frac{T(\xi, \eta+1, \zeta) - 2T(\xi, \eta, \zeta) + T(\xi, \eta-1, \zeta)}{\alpha^2 h^2}, \\
\text{and} \quad & \\
\frac{\partial^2 T}{\partial \zeta^2} &\rightarrow \frac{T(\xi, \eta, \zeta+1) - 2T(\xi, \eta, \zeta) + T(\xi, \eta, \zeta-1)}{\beta^2 h^2},
\end{aligned}\right\} \tag{5.13}$$

Eq. 5.12 yields the solution for $T(\xi, \eta, \zeta)$ as a weighted average of its four neighboring nodal points,

$$\begin{aligned}
T(\xi, \eta, \zeta) = \frac{1}{2\left(1 + \frac{1}{\alpha^2} + \frac{1}{\beta^2}\right)} \Bigg\{ & \left(1 - \frac{\lambda h}{2}\right) T(\xi+1, \eta, \zeta) + \left(1 + \frac{\lambda h}{2}\right) T(\xi-1, \eta, \zeta) \\
& + \frac{1}{\alpha^2}[T(\xi, \eta+1, \zeta) + T(\xi, \eta-1, \zeta)] \\
& + \frac{1}{\beta^2}[T(\xi, \eta, \zeta+1) + T(\xi, \eta, \zeta+1)] \Bigg\}.
\end{aligned} \tag{5.14}$$

Wada solves Eq. 5.14 by the method of successive overrelaxation. According to this technique, a first guess is made for the solution

$T(\xi, \eta, \zeta)$ at each nodal point. The second and all subsequent approximations can be made by substituting the values determined at the previous step into the right-hand side of Eq. 5.14 to yield the next improved approximation. An overrelaxation factor A is used to speed up the convergence. If $T^{(k)}(\xi, \eta, \zeta)$ denotes the kth approximation to the solution, the method is represented by

$$R^{(k)}(\xi, \eta, \zeta) = \frac{1}{2\left(1 + \frac{1}{\alpha^2} + \frac{1}{\beta^2}\right)} \left\{\left(1 - \frac{\lambda h}{2}\right) T^{(k)}(\xi + 1, \eta, \zeta) + \left(1 + \frac{\lambda h}{2}\right) T^{(k+1)}(\xi - 1, \eta, \zeta)\right.$$

$$+ \frac{1}{\alpha^2}\left[T^{(k+1)}(\xi, \eta + 1, \zeta) + T^{(k)}(\xi, \eta - 1, \zeta)\right]$$

$$\left. + \frac{1}{\beta^2}\left[T^{(k+1)}(\xi, \eta, \zeta + 1) + T^{(k)}(\xi, \eta, \zeta - 1)\right]\right\} - T^{(k)}(\xi, \eta, \zeta) \quad (5.15)$$

and

$$T^{(k+1)}(\xi, \eta, \zeta) = T^{(k)}(\xi, \eta, \zeta) + A \times R^{(k)}(\xi, \eta, \zeta) \quad (5.16)$$

with $1 < A < 2$. $R^{(k)}(\xi, \eta, \zeta)$ is the residual at the kth step, where, as can be seen from Eq. 5.15, only the latest values at the node points are used. This method of successive overrelaxation converges faster than the well-known Gauss-Seidel method ($A = 1$), often used for elliptic partial differential equations. The proper choice of the relaxation factor A determines the rate of convergence of the method. Wada found that a suitable approximation to the optimum value was $A_{opt} = 1.80$ for both two- and three-dimensional applications. This choice yielded 0.89×10^{-7} as the sum of the squares of the residuals after 100 iterations (for the three-dimensional case to be described). More details on the determination of A_{opt} are given in Ref. 5.

Iterations by the above method should be continued until

$$R_n = \max_{\text{all nodes}}\left|R^{(k)}\right| = \frac{1}{A}\max\left|T^{(n)} - T^{(n-1)}\right| \quad (5.17)$$

is less than some prescribed tolerance.

Results of the numerical computations are illustrated in Figs. 5.3-5.8 for $\lambda = 0.3$ and $\lambda = 0$ (no crosscurrent). The outlet size in ξ-ζ coordinates is $\xi_0 = 4.0$, $\zeta_0 = 1.0$. The outlet temperature is 35°C with an ambient temperature of 30°C. For this sample situation, no surface heat loss is assumed ($Q_0 = 0$). Figure 5.3 ($\lambda = 0$) and Fig. 5.6 ($\lambda = 0.3$) give vertical temperature distributions along the η axis perpendicular to the shoreline. Figure 5.4 ($\lambda = 0$) and Fig. 5.7 ($\lambda = 0.3$) represent the horizontal distribution at the surface and at a depth $\zeta = 1.4$. Finally, Fig. 5.5 ($\lambda = 0$) and Fig. 5.8 ($\lambda = 0.3$) show vertical temperature profiles for $\eta = 0, 1.6$, and 4.0 parallel to the shore.

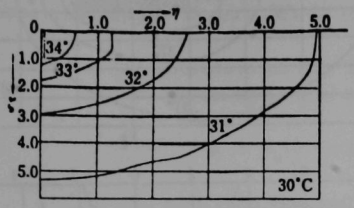

Fig. 5.3

Vertical Distribution of Water Temperature along the η Axis Perpendicular to the Shore: $\lambda = 0$ (Ref. 1)

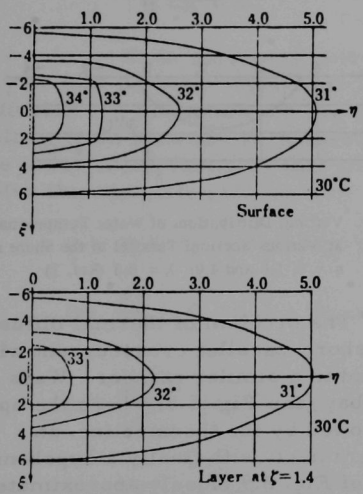

Fig. 5.4. Horizontal Distributions of Water Temperature at the Surface and Layer of $\zeta = 1.4$: $\lambda = 0$ (Ref. 1)

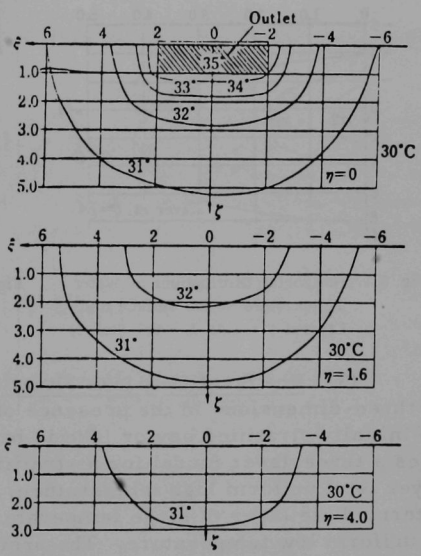

Fig. 5.5. Vertical Distributions of Water Temperature at Various Sections Parallel to the Shore at $\eta = 0$, 1.6 and 4.0: $\lambda = 0$ (Ref. 1)

Fig. 5.6

Vertical Distribution of Water Temperature along the η Axis Perpendicular to the Shore: $\lambda = 0.3$ (Ref. 1)

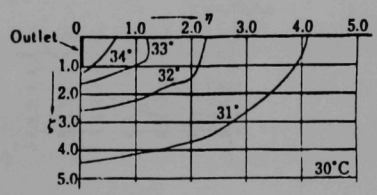

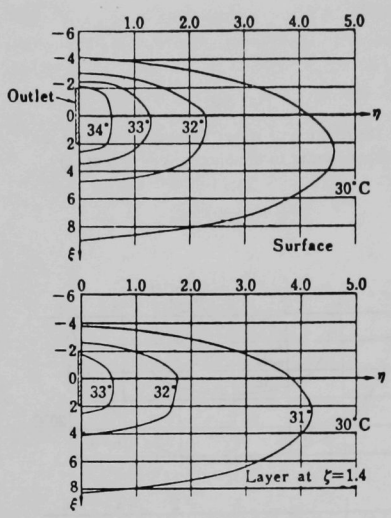

Fig. 5.7. Horizontal Distributions of Water Temperature at the Surface and Layer of ζ = 1.4: λ = 0.3 (Ref. 1)

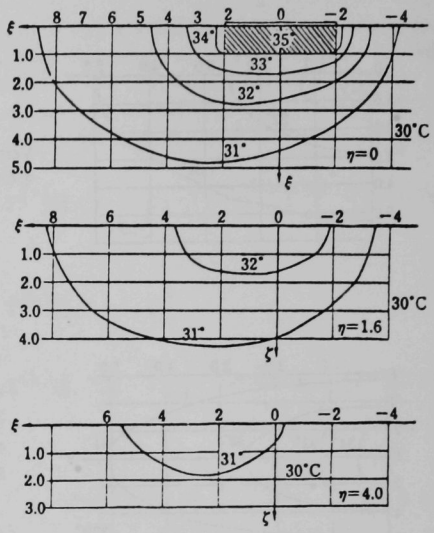

Fig. 5.8. Vertical Distributions of Water Temperature at Various Sections Parallel to the Shore at η = 0, 1.6 and 4.0: λ = 0.3 (Ref. 1)

(3) The Stratified-lake Situation. The problem of thermal diffusion in three-dimensions in the presence of a shore-parallel crosscurrent within an initially stratified bay or lake is handled in a similar manner. Wada uses a three-layer model for a stratified bay (see Fig. 5.9) where the upper layer is of uniform high temperature, followed by the thermocline, an intermediate layer of large temperature gradient, with finally a hypolimnion of uniform low temperature. The profile of Fig. 5.9 closely approximates the summer thermal gradient found in field observations of the near-shore ambient region of Mizushima Bay close to the Mizushima Power Plant. For a stratified bay (or lake), Wada considers density variations in the upper layer $z < H_W$ of the plume. H_W is defined as the depth of the upper

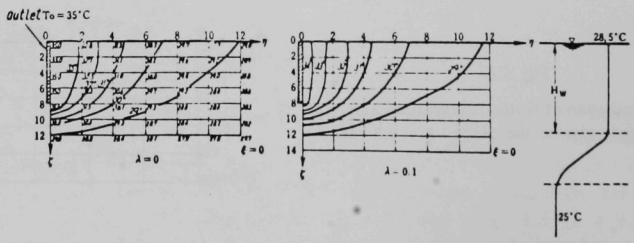

Fig. 5.9. Vertical Distribution of Water Temperature along the η Axis Perpendicular to the Shore[1]

limit of the thermocline layer and measures the thickness of the initially isothermal upper layer. Wada divides the problem solution into two parts:

(a) Solution of Eq. 5.6 with density related to temperature given approximately as

$$\rho = \rho_0(1 - aT)$$

and with the surface heat loss term Q_0 included for the upper layer of the lake $z < H_w$.

(b) Solution of Eq. 5.7 for the two <u>lower</u> layers $z > H_w$ with $Q_0 = 0$.

Wada considers there to be a natural division at $z = H_w$ in the bay or lake between physical processes. Surface heat inputs and turbulent diffusion are important for the upper layer. Simple internal diffusion resulting from nonuniform temperature conditions at different boundaries for the lower layer dominate that lower region. Boundary conditions used to solve the complete problem are:

(a) $T = T_0$ at $y = 0$, $-B \leq x \leq B$ and $0 \leq z \leq H$.

(b) $\frac{\partial T}{\partial y} = 0$ at $y = 0$, and $-B > x > B$ (no heat flux at shore boundary).

(c) $\frac{\partial^2 T}{\partial z^2} = 0$ at $z = 0$ and $y > 0$ (vertical temperature gradient at the surface).

(d) Vertical distribution of ambient water temperature similar to that shown in Fig. 5.6 is specified for the bay or lake region "infinitely far" from the outlet.

(e) $T = T_b$ (constant bottom layer water temperature) at $z = z_b$ (bay or lake bottom).

(Wada's papers do not give details on the precise method of the matching of the two solutions at $z = H_w$.)

To solve Eq. 5.6 with ρ variable, the transformations (Eq. 5.11) are made once again after the form for the density variation has been substituted to yield

$$\rho_0(1 - aT)\,\lambda\frac{\partial T}{\partial \xi} = \frac{\partial^2 T}{\partial \xi^2} + \frac{\partial^2 T}{\partial \eta^2} + \frac{\partial^2 T}{\xi \zeta^2}$$

$$+ \frac{a}{1 - aT}\left[\left(\frac{\partial T}{\partial \xi}\right)^2 + \left(\frac{\partial T}{\partial \eta}\right)^2 + \left(\frac{\partial T}{\partial \zeta}\right)^2\right] + B_0 + B_1 T, \qquad (5.18)$$

where

$$B_0 = \frac{b_0}{c_p H_w}, \; B_1 = \frac{b_1}{c_p H_w}. \tag{5.19}$$

This semilinear, elliptic partial differential equation is solved in the same manner as the linear one derived above for constant ρ. Using the same form for the centered first and second differences, the solution $T(\xi, \eta, \zeta)$ to the resulting difference equation may be written implicitly, when $\alpha = \beta = 1$, as

$$\left.\begin{aligned} T(\xi, \eta, \zeta) = \Big(& F1 \times T(\xi+1, \eta, \zeta) + F2 \times T(\xi-1, \eta, \zeta) \\ & + F4[T(\xi, \eta+1, \zeta) + T(\xi, \eta-1, \zeta) + T(\xi, \eta, \zeta+1) \\ & + T(\xi, \eta, \zeta-1)] + F5 \times B_0 + F6\{[T(\xi+1, \eta, \zeta) \\ & - T(\xi-1, \eta, \zeta)]^2 + [T(\xi, \eta+1, \zeta) - T(\xi, \eta-1, \zeta)]^2 \\ & + [T(\xi, \eta, \zeta+1) - T(\xi, \eta, \zeta-1)]^2\}[1.0 - a \times T(\xi, \eta, \zeta)]^{-1}\Big) \\ & \div \{1.0 - F3[T(\xi+1, \eta, \zeta) - T(\xi-1, \eta, \zeta)]\} \end{aligned}\right\} \tag{5.20}$$

where

$$\left.\begin{aligned} F1 &= (1.0 - \rho_0 \lambda h/2.0)/(6.0 + B_1 h^2), \\ F2 &= (1.0 + \rho_0 \lambda h/2.0)/(6.0 + B_1 h^2), \\ F3 &= (\rho_0 a \lambda h/2.0)/(6.0 + B_1 h^2), \\ F4 &= 1.0/(6.0 + B_1 h^2), \\ F5 &= h^2/(6.0 + B_1 h^2), \\ \text{and} \quad & \\ F6 &= a/4.0(6.0 + B_1 h^2). \end{aligned}\right\} \tag{5.21}$$

The successive overrelaxation method as described above is used again, where

$$T^{(k+1)}(\xi, \eta, \zeta) = T^{(k)}(\xi, \eta, \zeta) + A \times R^{(k)}(\xi, \eta, \zeta), \tag{5.22}$$

with $R^{(k)}(\xi, \eta, \zeta)$ equal as usual to the difference between the right- and left-hand sides of Eq. 5.20; and where $T(\xi+1, \eta, \zeta)$, $T(\xi, \eta-1, \zeta)$, $T(\xi, \eta, \zeta-1)$, and $T(\xi, \eta, \zeta)$ are evaluated at time k; and $T(\xi-1, \eta, \zeta)$, $T(\xi, \eta+1, \zeta)$, and $T(\xi, \eta, \zeta+1)$ are evaluated at time k + 1. The optimum value for A was again found to be 1.80. The iterations are carried out from an initial guess of the temperature solution until all the residuals are sufficiently small.

Results of the numerical solution are given in Figs. 5.9-5.11 in nondimensional coordinates for $\lambda = 0.1$ and $\lambda = 0$ (no crossflow). In ξ, η, ζ coordinates, the outfall width is 4.0 with depth 8.0. The temperature of the outlet is 35°C, and the ambient bay temperature is 28.5°C. Although not stated in Wada's papers, it is surmised that surface heat loss was considered in the boundary conditions for this test case. Figure 5.9 ($\lambda = 0$ and $\lambda = 0.1$) illustrates the vertical temperature profile along the η axis perpendicular to shore. Figure 5.10 ($\lambda = 0$ and $\lambda = 0.1$) gives the horizontal water temperatures at the surface $z = \zeta = 0$ and at depth $\zeta = 4$. Finally, Fig. 5.11 shows the vertical profiles at sections $\eta = 0$ and $\eta = 4$ parallel to the shoreline. The effect of the current given by $\lambda = 0.1$ is small, while the effects of thermal stratification are quite significant as can be seen from Fig. 5.11. Based on the Mizushima field studies, the horizontal thermal diffusivity was found to be about 50 times as great as the vertical, which itself was of the order 0.01 m^2/sec. If the longitudinal and lateral diffusivities are each equal to 0.5 m^2/sec (in kinematic units), then $\lambda = 0.1$ corresponds to U = 0.23 ft/sec. As before, turbulent diffusion predominates well above current advection.

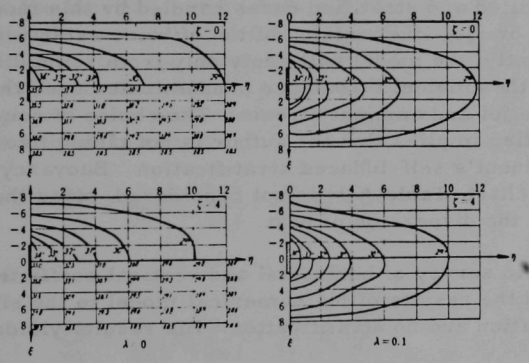

Fig. 5.10

Horizontal Distributions of Water Temperature at the Surface and the Layer of $\zeta = 4$ (Ref. 1)

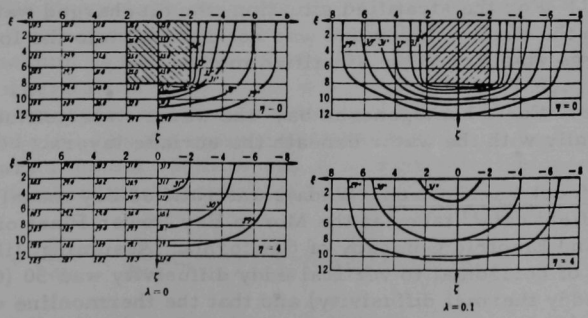

Fig. 5.11. Vertical Distributions of Water Temperature at Sections Parallel to the Shore at $\eta = 0$ and $\eta = 4$ (Ref. 1)

(4) Some General Comments. It appears from Figs. 5.9-5.11 that Wada's numerical results in the stratified situation do not seem to depend on the nonstandard form of Eq. 5.6 (or equivalently Eq. 5.3), assuming, of course, that Eq. 5.6 is indeed correct. Density variation in the standard form of the energy equation is, in general, not expected to yield any significant difference in the prediction of dilutions as long as no flow-energy coupling is apparent. Basically, there should be no direct effect of density variation, except through the gravity term, ρg, in the vertical equation of motion. In our experience, there is no field situation in which this statement does not hold. This essentially is the meaning of the Boussinesq approximation. Before variation in ρ becomes significant in the convective-diffusion equation, it will have importance in the inertial terms on the left-hand side of the x, y, and z momentum equations. Most investigators realize the unimportance of variations in ρ in the energy equation and consequently work immediately with ρ constant and with kinematic quantities. In short, if Eq. 5.6 is correct, the ρ variation introduced there should not affect the numerical results.

Both the unstratified and stratified cases handled by this model do not consider any inertial or "jet-like" mixing of the effluent water with the ambient lake. Consequently, the model will apply only from some distance downcurrent at which the ambient turbulence predominates over the momentum interaction of the jet and ambient stream. The choice of constant eddy thermal diffusivities implies that the author is not taking into account the warm-water effluent's self-induced stratification. Buoyancy (as defined in the summary chart, Table A.1) is not considered, since the flow is here uncoupled from the dispersion of heat.

Based upon a field survey of horizontal and vertical coefficients of diffusion, Wada compared the results of his numerical model to the situations of significant stratification and no stratification. His results yielded the following facts:

(1) For the stratified situation, the discharged water tended to mix only with the surface layer and was not diffused into the lower layers due to the large stability of the stratified media.

(2) For a homogeneous bay, the warm-water effluent seemed to mix uniformly with the water beneath the surface layers.

(5) Model Verification. Wada's unstratified bay model has been compared to field data[19] taken at the Morro Bay Power Plant of the Pacific Gas and Electric Company of California. Assuming, like Wada, that the ratio of horizontal to vertical eddy diffusivity was 50 (0.01 m^2/sec for vertical eddy thermal diffusivity) and that the thermocline was sufficiently strong to prevent mixing between the surface and bottom water layers, Tamai et al. compared Wada's model to the data of Cheney and Richards.[20] The precise details of the comparison were not given in Ref. 19,

and the theoretical curve fell within the large scatter of the data. Since details concerning the precise application of this model to the Morro Plant situation are not known, no further comments regarding the suitability of the model to that situation can reasonably be assessed. No other comparisons of Wada's models (1, 2, and 3) to actual thermal-plume data are known to exist.

d. Model 2: Thermal Diffusion in Two Dimensions with Variation in Flow Field Included (September 1966)

(1) The Physical Situation and Basic Equations. The second model developed by Wada treats the surface shoreline discharge of heated water from a rectangular outlet into a quiescent body of water. The geometry of the situation is again illustrated by Fig. 5.1. A two-layer model is assumed with a warm, vertically uniform layer of water resting upon a colder layer. Motion is assumed to be a two-dimensional lateral flow restricted to the upper region (i.e., warmer water above the thermocline). The technique of solution is first to obtain the flow pattern by ignoring density differences and the inertial terms in the hydrodynamic equations. These assumptions uncouple momentum and heat transfer. Then the temperature distribution is deduced from the known flow pattern. With the inertia of the fluid ignored, the temperature will be a result only of turbulent diffusion, advection and heat loss. No buoyant convective motions can be present. The flow equations to be solved are

$$\frac{\partial p}{\partial x} = \frac{\partial}{\partial x}\left(A_x \frac{\partial u}{\partial x}\right) + \frac{\partial}{\partial y}\left(A_y \frac{\partial u}{\partial y}\right) \tag{5.23}$$

and

$$\frac{\partial p}{\partial y} = \frac{\partial}{\partial x}\left(A_x \frac{\partial v}{\partial x}\right) + \frac{\partial}{\partial y}\left(A_y \frac{\partial v}{\partial y}\right), \tag{5.24}$$

where p is the pressure, and A_x and A_y are eddy momentum diffusivities in the x and y directions, respectively. Equations 5.23 and 5.24 are the x and y momentum equations for steady flow, where density differences are ignored and where all inertial terms were assumed very small compared to the turbulent transport and pressure terms. Wada solves these equations for u(x, y) and v(x, y) by the method of finite differences under the assumption that A_x, A_y are constant. With u and v as advective inputs, the two-dimensional temperature distribution becomes the solution of

$$u\frac{\partial T}{\partial x} + v\frac{\partial T}{\partial y} = \frac{\partial}{\partial x}\left(K_x \frac{\partial T}{\partial x}\right) + \frac{\partial}{\partial y}\left(K_y \frac{\partial T}{\partial y}\right) + \frac{Q_0}{\rho c_p H_w}, \tag{5.25}$$

where K_x and K_y are the eddy thermal diffusivities in the x and y directions, T is temperature, Q_0 is the surface heat loss to the atmosphere ($= b_0 - b_1 T$), and H_w is the depth to the thermocline. The above solution method implicity

assumes that the eddy viscosities of momentum and heat prevail in the entire field of flow. In such a case, the shape of the coastal boundary is expected to be a strong influence on the flow pattern near the outlet. Wada solves the problem for an ideal semi-infinite bay and then for the irregular coast of Seto Bay.

It appears that the model can handle a situation of a lake with a shore-parallel current as well as that of a stagnant lake in its prediction of the far-field velocity and temperature distribution. The method of solution will now be summarized below.

(2) Derivation of Flow Pattern. Wada solves Eqs. 5.23 and 5.24 by introducing the stream function P defined by

$$u = \frac{\partial P}{\partial y}, \quad v = -\frac{\partial P}{\partial x}, \tag{5.26}$$

which automatically satisfies the continuity equation

$$\frac{\partial u}{\partial x} + \frac{\partial v}{\partial y} = 0. \tag{5.27}$$

(Neglecting density differences in the calculation of the flow pattern allows the application of Boussinesq approximation to Eq. 5.1 simplifying it to the usual continuity equation, Eq. 5.27). Assuming the eddy momentum diffusivities A_x and A_y to be constant, cross-differentiation on Eqs. 5.23 and 5.24 yields

$$\frac{\partial^2 p}{\partial x \partial y} = A_x \frac{\partial}{\partial y}\left(\frac{\partial^2 u}{\partial x^2}\right) + A_y \frac{\partial}{\partial y}\left(\frac{\partial^2 u}{\partial y^2}\right) \tag{5.28}$$

and

$$\frac{\partial^2 p}{\partial x \partial y} = A_x \frac{\partial}{\partial x}\left(\frac{\partial^2 v}{\partial x^2}\right) + A_y \frac{\partial}{\partial x}\left(\frac{\partial^2 v}{\partial y^2}\right). \tag{5.29}$$

Subtracting Eq. 5.29 from Eq. 5.28 eliminates the pressure terms. Replacing u and v by Eqs. 5.26 and 5.27, the horizontal motion may be written entirely in terms of the stream function P as the biharmonic equation,

$$\frac{\partial^4 P}{\partial x^4} + (1+\delta)\frac{\partial^4 P}{\partial x^2 y^2} + \frac{\partial^4 P}{\partial y^4} = 0, \tag{5.30}$$

where δ in Eq. 5.30 is A_y/A_x. Once P(x, y) is determined, the flow distribution in a bay is established from Eq. 5.26. The solution to Eq. 5.30 is calculated by the method of finite differences, again using the successive

overrelaxation technique. Dividing the x-y plane into a two-dimensional mesh with $\alpha = 1$ and using the same central-difference formulas as in the previous model, an expression is easily derived for $P(\zeta, \eta)$ (Wada assumes $\delta = 1$):

$$P(\xi, \eta) = 0.40[P(\xi+1, \eta) + P(\xi, \eta+1) + P(\xi-1, \eta) + P(\xi, \eta-1)]$$

$$- 0.10[P(\xi+1, \eta+1) + P(\xi-1, \eta+1) + P(\xi-1, \eta-1) + P(\xi+1, \eta-1)]$$

$$- 0.05[P(\xi+2, \eta) + P(\xi, \eta+2) + P(\xi-2, \eta) + P(\xi, \eta-2)]. \qquad (5.31)$$

The procedure of solution is identical to that in the previous model. If $P^{(k)}(\xi, \eta)$ denotes the kth approximation of the solution, the following equation is obtained:

$$P^{(k+1)}(\xi, \eta) = P^{(k)}(\xi, \eta) + A_p \times R^{(k)}(\xi, \eta), \qquad (5.32)$$

where A_p is the overrelaxation factor and $R^{(k)}(\xi, \eta)$ is the residual at the kth step.

The boundary conditions on the stream function P are defined from

$$P(x, y) = \int dP = \frac{\partial P}{\partial x} dx + \frac{\partial P}{\partial y} dy \qquad (5.33)$$

and Eq. 5.26. For points on a straight shoreline,

$$P = -V_0 \int dx + U_0 \int dy \qquad (5.34)$$

or

$$P = -V_0 H, \quad x > H;$$

$$P = V_0 H, \quad x < -H;$$

$$P = V_0 x, \quad |x| \leq H;$$

due to the no-slip condition at the solid coastal boundary, where U_0 and V_0 are the initial velocity components in the x and y directions, respectively. The boundary conditions for P are illustrated for the straight shoreline, semi-infinite bay case illustrated in Fig. 5.12. (Wada does not provide the complete details of his choice of boundary values for P at the other three sides of the mesh boundary in any of his papers.)

Using the iterative technique as set down by the overrelaxation method to solve difference Eq. 5.31 under boundary conditions determined by Eq. 5.32, a solution for $P(\xi, \eta)$ may be obtained for any irregular shoreline configuration. Figures 5.13 and 5.14 compare the rates of convergence of this iterative method for a semi-infinite sea basin and an

irregular shoreline contour. The convergence is seen to be slow in both cases, but even slower for irregularly shaped Seto Bay.

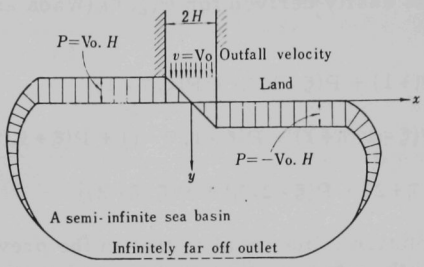

Fig. 5.12

Establishment of Boundary Values for Semi-infinite Sea Basin[5]

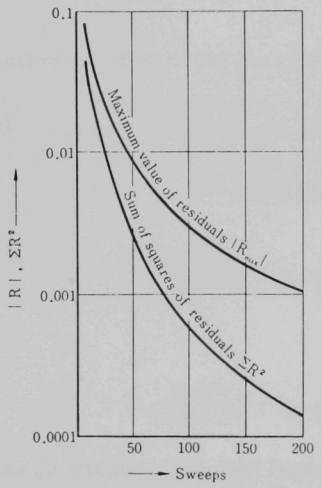

Fig. 5.13. Rate of Convergence of Biharmonic Type for Semi-infinite Sea Basin[5]

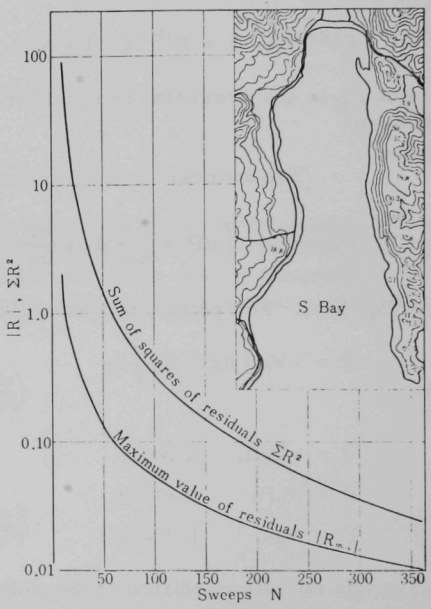

Fig. 5.14. Rate of Convergence of Biharmonic Type for S. Bay[5]

Figures 5.15-5.17 plot isolines of constant u and v velocities, and total velocity W under input conditions $U_0 = 0$, $V_0 = 1$ m/sec, B = 20 m, H = 1 m for a straight shoreline and a semi-infinite lake. The initial discharge rate is $Q = V_0BH = 20\ m^3/sec$. (Wada does not state whether a shore-parallel ambient current is being considered in this sample calculation.) Sixty-five equidistant lattice points were taken in each of the ξ and η directions for the finite-difference net. Under these conditions, it

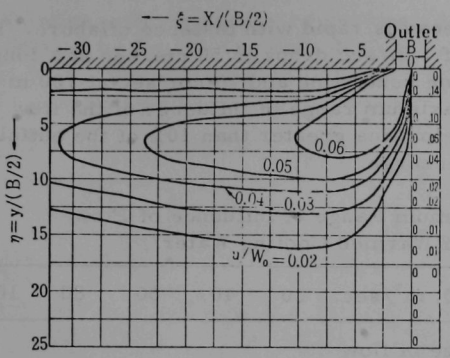

Fig. 5.15

Distribution of x Component, u, of Surface Velocity (W_0 = 1 m/sec, W_0: outfall velocity)[5]

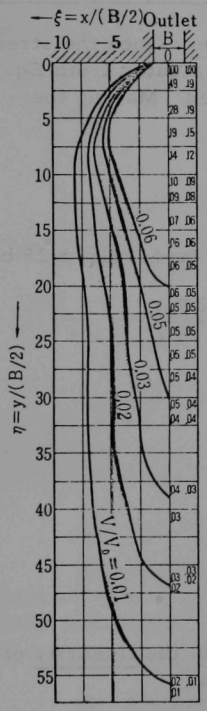

Fig. 5.16

Distribution of y Component, v, of Surface Velocity (W_0 = 1 m/sec, W_0: outfall velocity)[5]

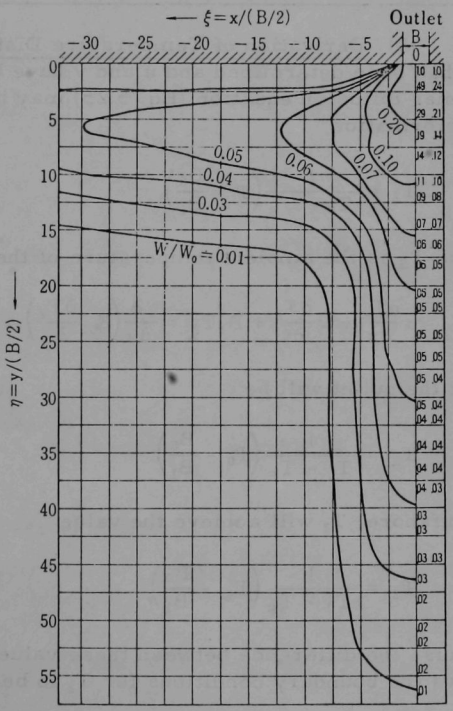

Fig. 5.17

Distribution of Surface Velocity (W_0 = 1 m/sec, W_0: outfall velocity)[5]

can be seen that the velocity decay is rapid with distance offshore. From Fig. 5.16, the initial velocity of 1 m/sec drops to 50 cm/sec at a longitudinal distance of 25 m along the plume centerline and 10 cm/sec at 100 m downstream. Table 5.2 lists the maximum range of influence of the flow (defined as the area of the basin with velocities greater than 10% of the outfall velocity) versus the rate of discharge.

TABLE 5.2. Maximum Range of Influence of Flow by Outfall of Warmed Cooling Water[5]

Cooling-water Flow Q, m^3/sec:	20	40	60	80	100
Maximum range of influence of flow (distance from outlet: m)	60	120	180	240	300

(3) Derivation of Temperature Distribution. Once the stream function has been determined and u and v have been evaluated from Eq. 5.26, the thermal-diffusion equation (Eq. 5.25) may be solved. Making the transformation

$$T_2 = \frac{1}{T_0 - T_s}\left(T - \frac{B_0}{B_1}\right), \tag{5.36}$$

where T_s is the ambient temperature of the upper layer, Eq. 5.25 becomes

$$u\frac{\partial T_2}{\partial x} + v\frac{\partial T_2}{\partial y} + B_1 T_2 = \frac{\partial}{\partial x}\left(K_x \frac{\partial T_2}{\partial x}\right) + \frac{\partial}{\partial y}\left(K_y \frac{\partial T_2}{\partial y}\right). \tag{5.37}$$

T_2 at the outlet will be

$$T_2 = \frac{1}{T_0 - T_s}\left(T_0 - \frac{B_0}{B_1}\right); \tag{5.38}$$

far offshore, T_2 will achieve the value

$$T_2 = \frac{1}{T_0 - T_s}\left(T_s - \frac{B_0}{B_1}\right). \tag{5.39}$$

Because the difference between these values is 1.0, the linearity of Eq. 5.37 allows the boundary conditions for T_2 to be taken as

(a) $T_2 = 1.0$ at the outlet.

(b) $T_2 = 0.0$ sufficiently far offshore where the ambient lake water will be unaffected by the heated discharge.

(c) $(\partial T_2/\partial n)(x, y) = 0$ for all shoreline points, where n represents the direction normal to the shore at a given (x, y).

The solution under boundary conditions a and b is then added to the expression defined by Eq. 5.39 to yield the old T_2 temperature distribution defined in Eq. 5.36. The complete solution for T is determined by solving Eq. 5.36 for T in terms of the T_2 just evaluated.

Equation 5.37 is written in finite-difference form and solved by overrelaxation as described before using boundary conditions a-c. The details are not described in Wada's papers. This method may also be applied for an arbitrarily shaped shoreline. Boundary condition b assumes that the discharged water does not influence the most distant lake points. Wada introduces an alternate boundary condition for condition b, which states that the thermal gradient remains constant at "infinite" distances from the outfall. Figure 5.18 compares the two methods of setting up the boundary conditions. Wada asserts that the two methods approach each other when there is a good deal of surface heat loss or when the temperature gradient near the surface is small.

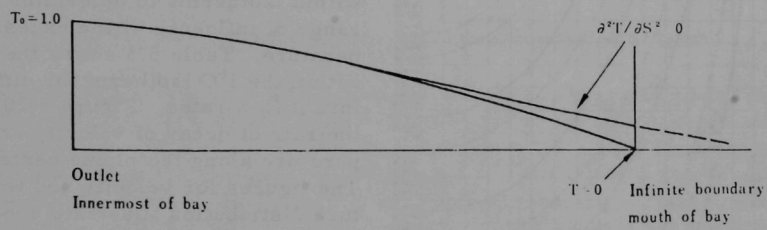

Fig. 5.18. Comparison of "Zero Temperature" and Constant-thermal-gradient Methods of Setting Up the Distance-boundary Condition on Temperature[5]

Wada derives the two-dimensional temperature distribution predicted by the above method using the initial conditions in the sample program described above and the calculated flow pattern. The boundary conditions for the numerical solution are:

(a) The discharge temperature T_2 is 1.0.

(b) The limit of calculations established by the three lines is $\xi = -32.5$, $\zeta = 32.5$, $\eta = 65$. These boundaries represent infinity in the numerical simulation. The thermal gradient is taken as constant here.

(c) Thermal flux is zero normal to the shore boundary.

(d) Meteorological data are taken as (typical summertime conditions for Mizushima Bay in Japan):

Average atmospheric temperature:	$T_a = 28.5°C$
Average wind speed:	$V = 3.3$ m/sec
Relative humidity:	$f = 79\%$
Cloud cover:	$n = 6.3$
Coefficient depending on cloud height:	$K = 0.083$

Rise of water temperature added by condenser power plant: $T_c = 8°C$
Ambient lake temperature (upper layer): $T_s = 28.5°C$
Hypolimnion temperature (lower layer): $T_b = 25°C$
Thermocline depth: $H = 3$ m

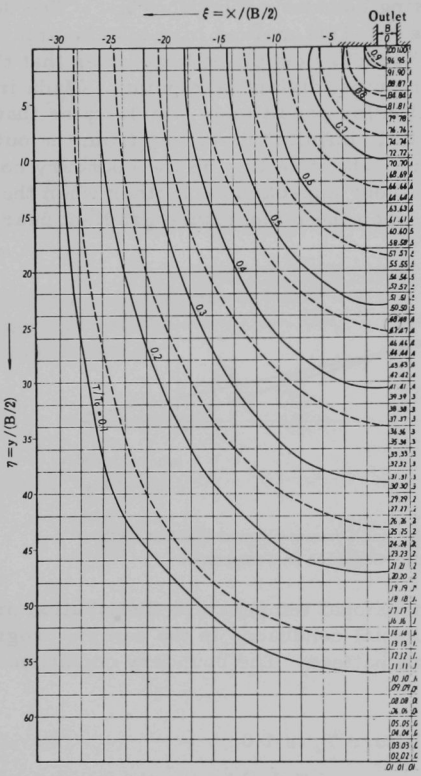

Fig. 5.19. Distribution of Water Temperature in Surface Layer[5]

Isotherms of the resulting numerical solution corresponding to the velocity distributions given in Figs. 5.15-5.17 are plotted in Fig. 5.19. The dotted isotherms refer to the corresponding solution when the boundary condition $T_2 = 0.0$ is used for the "infinite" basin boundaries. In terms of the actual temperature T, Wada calculated areas within isotherms to determine the range of influence of the excess temperature. Table 5.3 shows the areas within the 1°C isotherm for different initial flow rates. Figure 5.20 shows the rate of decay of velocity and temperature along the plume centerline. The figures for velocity and temperature distribution illustrate the difference between the phenomenon investigated by Wada (eddy viscosities predominant in the entire flow region) and that of jet flow that usually prevails in the vicinity of an outfall.

(4) Some General Comments. The hydraulics of the flow may be oversimplified with the assumption of a fully mixed layer above the thermocline. For a region close to the source, at least, the flow is generally three-dimensional. Obtaining the flow

TABLE 5.3. Maximum Range of Influence of Water-temperature Rise by Outfall of Warmed Cooling Water[5]

Cooling Water Flow Q, m^3/sec:	20	40	60	80	100
Maximum range of influence in which water temperature of sea basin rises 1°C	460	920	1380	1840	2300
Its influenced area: m^2	17.8×10^4	71.3×10^4	160.5×10^4	285.4×10^4	446.0×10^4

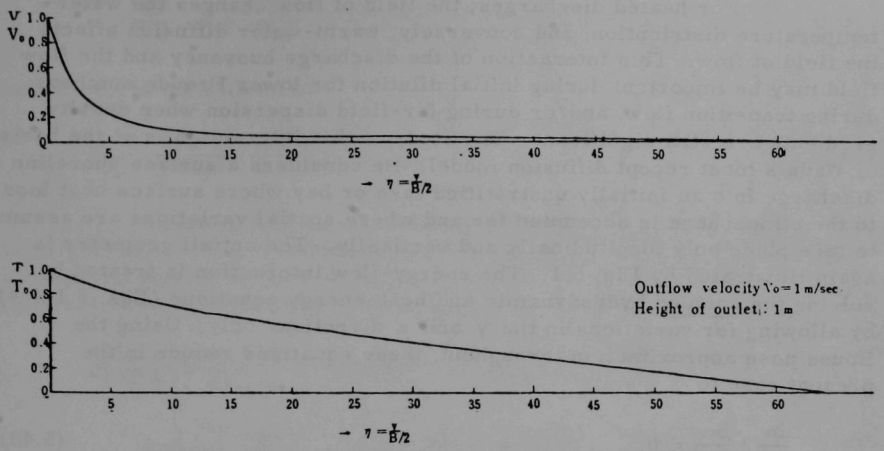

Fig. 5.20. Process of Diminition of Flow and Water Temperature in Sea Basin[5]

pattern by neglecting any density variations implies that the model may be applied only for very small density differences. Furthermore, jet entrainment was not considered; thereby the analysis will become less accurate for larger Froude numbers. As with Model 1, Model 2 is suitable solely in the far field due to the neglect of inertial (jet) mixing. Finally, the model is strictly applicable only when an ambient crosscurrent does not affect the flow and no bottom slope interferes with dispersion. The fact that no ambient crosscurrent is assumed may be a limiting factor in the model's application.

e. Model 3: Thermal Diffusion with Interaction between Flow and Heat Transfer (1968)

(1) Physical Situation and Basic Equations. The model equations of Wada Model 3 represent a total-field description upon proper formulation of diffusivities in the various regions of flow. The inertial terms are included in the equations of motion of the heated effluent, which allows for a description of momentum flow; yet a far-field form for vertical eddy diffusivities is suggested in Wada's papers. While this model may appear to be universal it is not because, in general, it neglects lateral spreading and possible crosscurrent interactions. Thus this model can only be qualitative and should be used only for obtaining physical insight.

Wada applies his model to a jet situation in a sample problem. However, for continuity of presentation of Wada's work, we have taken the liberty to discuss and relate to Wada Model 3 as a far-field description.

For heated discharges, the field of flow changes the water-temperature distribution, and conversely, warm-water diffusion affects the field of flow. This interaction of the discharge buoyancy and the flow field may be important during initial dilution for lower Froude numbers, during transition flow, and/or during far-field dispersion when density gradients are still significant. The study of this interaction is at the basis of Wada's most recent diffusion model. He considers a surface shoreline discharge into an initially unstratified lake or bay where surface heat loss to the atmosphere is accounted for and where spatial variations are assumed to take place only longitudinally and vertically. The outfall geometry is again illustrated by Fig. 5.1. The energy-flow interaction is treated by solving the coupled hydrodynamic and heat-energy equations (Eqs. 5.1-5.4) by allowing for variations in the y and z directions only. Using the Boussinesq approximation throughout, these equations reduce in the present case to

$$\frac{\partial v}{\partial y} + \frac{\partial w}{\partial z} = 0, \tag{5.40}$$

$$v\frac{\partial v}{\partial y} + w\frac{\partial v}{\partial z} = -\frac{\partial p}{\partial y} + \frac{\partial}{\partial y}\left(A_h\frac{\partial v}{\partial y}\right) + \frac{\partial}{\partial z}\left(A_z\frac{\partial v}{\partial z}\right) \tag{5.41}$$

$$v\frac{\partial w}{\partial y} + w\frac{\partial w}{\partial z} = -\frac{\partial p}{\partial z} + \rho g + \frac{\partial}{\partial y}\left(A_h\frac{\partial w}{\partial y}\right) + \frac{\partial}{\partial z}\left(A_z\frac{\partial w}{\partial z}\right) \tag{5.42}$$

and

$$v\frac{\partial T}{\partial y} + w\frac{\partial T}{\partial z} = \frac{\partial}{\partial y}\left(\frac{K_h}{\rho}\frac{\partial T}{\partial y}\right) + \frac{\partial}{\partial z}\left(\frac{K_z}{\rho}\frac{\partial T}{\partial z}\right) \tag{5.43}$$

with ρ given approximately by

$$\rho = \rho_0(1 - aT) \tag{5.44}$$

and where

A_h, A_z = horizontal and vertical eddy momentum diffusivities,

K_h, K_z = horizontal and vertical eddy thermal diffusivities,

v, w = velocity in y, z directions, respectively,

and

y, z = longitudinal and vertical directions, respectively.

(2) Model Derivation. From the Boussinesq approximation, density variations in the inertial terms of the equations of motion were neglected, but the ρg term in the vertical equation of motion was retained due to the relative size of g. Wada solves Eqs. 5.1-5.4 with Eq. 5.5 in terms of the stream function P defined by

$$v = \frac{\partial P}{\partial z}, \; w = -\frac{\partial P}{\partial y} \tag{5.45}$$

and the vorticity defined as

$$\xi = -\frac{1}{2}\left(\frac{\partial^2 P}{\partial y^2} + \frac{\partial^2 P}{\partial z^2}\right). \tag{5.46}$$

Equation 5.40 is satisfied from the definition of P. Equations 5.41 and 5.42 are combined to yield the one equation for the vorticity transfer ξ; this is done by cross-differentiation of Eqs. 5.41 and 5.42 and subtraction to eliminate the pressure p. The result becomes

$$2\left(\frac{\partial p}{\partial z}\frac{\partial \xi}{\partial y} - \frac{\partial p}{\partial y}\frac{\partial \xi}{\partial z}\right) = -g\alpha\rho_0\frac{\partial T}{\partial y} + 2\left(A_h\frac{\partial^2 \xi}{\partial y^2} + A_z\frac{\partial^2 \xi}{\partial z^2}\right)$$

$$+ \frac{\partial}{\partial y}\left(\frac{\partial A_z}{\partial z}\frac{\partial w}{\partial z}\right) - \frac{\partial}{\partial z}\left(\frac{\partial A_z}{\partial z}\frac{\partial v}{\partial z}\right) + \frac{\partial A_z}{\partial y}\frac{\partial^2 w}{\partial z^2} - \frac{\partial A_z}{\partial z}\frac{\partial^2 v}{\partial z^2} \tag{5.47}$$

using the definitions of ξ and P, Eq. 5.44 for ρ, in addition to $A_h \approx$ constant and $A_z = A_z(y, z)$. Replacing v and w by the corresponding directional derivative of P, Eq. 5.43 becomes

$$\frac{\partial P}{\partial z}\frac{\partial T}{\partial y} - \frac{\partial P}{\partial y}\frac{\partial T}{\partial z} = \frac{\partial}{\partial y}\left(\frac{K_h}{\rho}\frac{\partial T}{\partial y}\right) + \frac{\partial}{\partial z}\left(\frac{K_z}{\rho}\frac{\partial T}{\partial z}\right) \tag{5.48}$$

Equations 5.46-5.48 are then to be solved simultaneously for P, ξ, and T. The temperature-gradient term in the vorticity-transfer equation (Eq. 5.47) binds the flow to the thermal diffusion.

Wada assumes the vertical eddy coefficients of momentum and heat energy to be of the form

$$\left.\begin{aligned} A_z &= A_1 + A_0 e^{-mR_i} \\ &\text{and} \\ K_z &= K_1 + K_0 e^{-nR_i} \end{aligned}\right\} \tag{5.49}$$

following the work of Mamayev[21] on diffusion in the sea, where A_1, A_0, K_1, K_0, m, and n are empirical coefficients and R_i is the local Richardson number. These vertical eddy coefficients are the factors that relate heat and momentum diffusion to the velocity shear and the vertical density gradient, and represent the influence of stability on the vertical mixing process due to turbulence. Considering the lack of an all-inclusive theory relating turbulent transfers to mean gradients at all scales and Richardson numbers, the semiempirical results of Mamayev were used and represent perhaps as good a first approximation to these coefficients <u>for the sea</u> as

can be found in the literature. As Wada notes, these eddy coefficients were obtained under a considerable amount of empiricism and cannot be expected to be valid for all physical frameworks.

Wada chooses A_1, A_0, K_1, K_0, m, and n to be constant in space, implying that he is assuming ambient turbulence to control the diffusion process from the outlet. This applies to the specific form of the total model capability Wada presents in his papers. Using the data of Jacobsen (no reference given), he uses n = 0.8 and m = 0.4. "Typical" values of the other empirical coefficients are of the order $K_0 = 0.01$, $K_1 = 0.1$, $A_0 = 0.01$, and $A_1 = 0.1$.

Wada chooses A_x and K_x by specifying the ratios A_z/A_x and K_z/K_x; in a calculation for a sample case, he specifies them as 0.1. (Although not stated explicitly, it is assumed that Wada was taking a constant "average" value for A_x and K_x in light of the predominance of the constants A_1 and K_1 in the forms for A_z and K_z and in light of the assumption of the approximate constancy of A_h in the derivation of Eq. 5.47.)

With the diffusion coefficients of momentum and heat defined above, Wada derives a numerical solution to Eqs. 5.46-5.48 by an iterative technique. In the first approximation, the equations are solved neglecting the thermal-gradient term in Eq. 5.47. Wada states that this solution itself can be applied to a bay with a negligible stratification or to a heated effluent having very small gravitational convective motions. A second approximation is obtained by combining Eqs. 5.46-5.48 and using the first-order solution of flow and temperature just obtained. The process is repeated until a satisfactory approximation is reached. The details of Wada's numerical scheme are not given in his papers. Wada does say that he uses an alternating-direction implicit method (the accelerated Liebman method) in the calculations. Moreover, the results of only one sample calculation were shown. That special case yields physically reasonable results and illustrates the nature of the interaction phenomenon between flow and temperature.

The special problem considered has its geometry given by Fig. 5.1, where the initial effluent temperature T_0 is 33°C, the (constant) ambient temperature is T_a = 25.0°C, the depth of discharge H = 2m, the initial velocity U_0 = 0.5 m/sec, and the lake bottom depth is 14 m. The Froude number of the discharge is 2.3, implying that the physical problem is basically that of a jet. Heat transfer to the atmosphere was considered, but the specific meteorological data used were not given. Horizontal diffusivities were defined by $A_z/A_x = K_z/K_x = 0.1$, and vertical diffusivities defined by the Mamayev forms given above with $K_0 = 0.01$, $K_1 = 0.1$, $A_0 = 0.01$, and $A_1 = 0.1$. The two-dimensional temperature and velocity distribution along a vertical section containing the outlet were calculated numerically and are illustrated in Figs. 5.21 and 5.22.

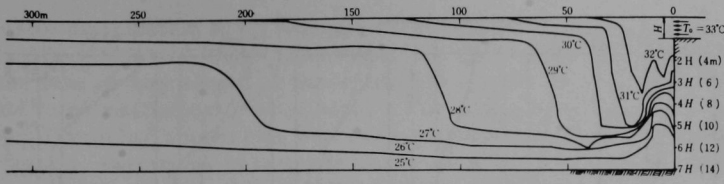

Fig. 5.21. Water-temperature Distribution along Longitudinal Section[9]

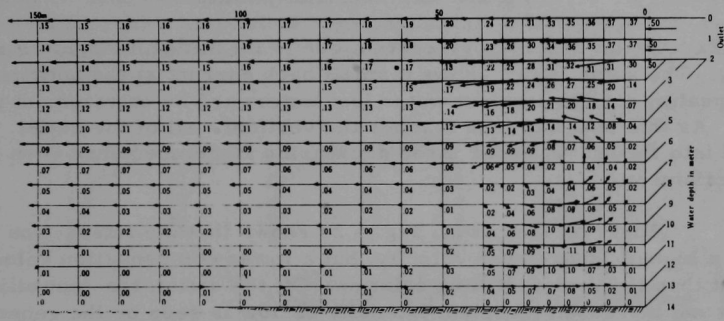

Fig. 5.22. Velocity Distribution along Longitudinal Section[9]

Specific vertical temperature and velocity profiles are illustrated in Figs. 5.23 and 5.24, where the first approximation (no interaction of flow and heat energy) and the fourth approximation (interaction solution) are plotted. From the set of figures, a region of initial entrainment can be seen near the discharge with a stable two-layer system developed farther from the outlet. The discharged heated water can be seen from

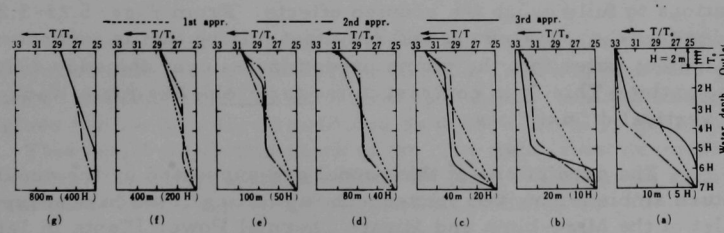

Fig. 5.23. Profile of Water-temperature Distribution
($K_z = K_1 + K_0 e^{-nR_i}$, $A_z = A_1 + A_0 e^{-mR_i}$)[9]

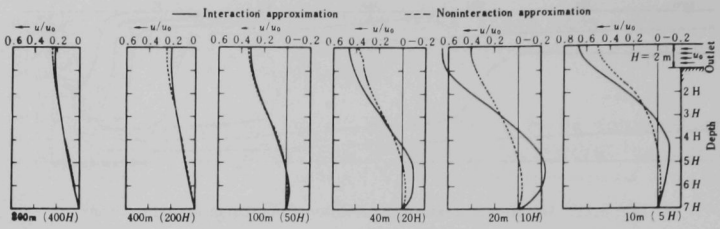

Fig. 5.24. Variation of Velocity Profile[9]

Fig. 5.22 to be an upper-layer current due to its initial momentum and lower density. The same figure shows a small back current at the bottom layer, compensating for the ambient water lost waterward by entrainment near the outlet. As this back current reaches the vertical wall of the outlet, it is sucked into the heated upper layer decreasing its temperature even more by entrainment.

Right off the outlet, Fig. 5.23 shows that the interaction solution yields a higher upper-layer velocity, but a lower compensation velocity current than the noninteracting solution. Off the outlet, the "upwelling" motion and increased turbulent intensity of flow is seen by the general upward movement of isotherms in Figs. 5.21 and 5.23. Here, the different levels of advection between the two counter-directional flows develops a density instability reflected by the Richardson number being below its critical value, yielding much increased vertical diffusivities (Eqs. 5.49).

At distances of 40H or more from the outlet, the differences between the first and later approximations are relatively small. Only near the outlet, where a high-temperature, high-velocity effluent is mixing with the colder lake water will the interaction be significant, requiring a number of iterations to fully gauge the coupled effects. From Figs. 5.21-5.24 Wada concludes that the entrainment and resultant mixing that is incorporating lower ambient water into the plume predominates over the eddy diffusion near the outlet. This is in contrast to the far-field-like form Wada chose for his vertical diffusivities.

The predictions of this model are supported by the occurrence of a return ambient flow and consequent "upwelling" motion observed near the outlet of the Mizushima and Minato Thermal Power Plants in Japan. Vertical velocity and temperature profiles representing these experimental observations are plotted in Figs. 5.25 and 5.26.

(3) Some General Comments. Although Wada's interaction model yields physically reasonable results and successfully predicts a number of observed phenomena, it is doubtful that many field situations correspond to Wada's problem. First, in spite of the fact that the analysis demonstrated significant differences in the flow and temperature fields between the cases of interaction and no interaction, the interactions between the flow field and

the density distribution are generally three-dimensional, especially during initial dilution. A two-dimensional analysis as done by Wada may be applied when the lake or bay situation has sufficient symmetry to allow one space variable to be realistically eliminated. For general shoreline situations, however, irregular boundaries and currents preclude such symmetry and, consequently, variations parallel to shore must be considered. Neglecting lateral entrainment of ambient fluid seems unrealistic for most discharge situations. If the discharge channel is sufficiently wide, the warm-water effluent may behave initially like a two-dimensional flow with small lateral variations in temperature and velocity; yet, the turbulent structure of the flow would generally be jet-like near the outlet, which would invalidate the constant-space assumption of the parameters A_1, A_0, K_1, and K_0 in the form for the diffusivities.

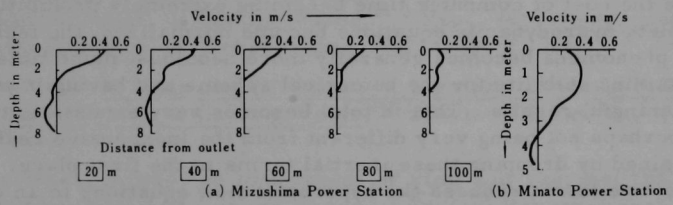

Fig. 5.25. Vertical Variation of Velocity off the Outlet[9]

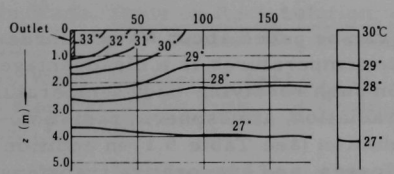

Fig. 5.26

Vertical Distribution of Water Temperature along y Axis Perpendicular to Shore in M. Bay[9]

From Wada's papers, one gets the impression that this model can be applied only for an arbitrary vertical section which passes through the orifice. Evidence for this statement is deduced from the information Wada gives for the boundary conditions he uses, especially the one for the shore. This would imply that much of the flow field is not described by the model, unless the outlet width is extremely large. Thus, with such a situation, the model results have mainly qualitative benefits.

In spite of the fact that the inclusion of the inertial terms in the equations of motion implies that momentum flow can be accounted for, Wada uses the constant-coefficient form for the vertical diffusivities, which indicates that ambient turbulence predominates the dispersion process. Again, proper selections for A_h, A_z, K_h, and K_z in the different regions of flow can make Wada Model 3 a complete-flow-regime model. The neglect of lateral spreading in this model is its major detriment. Also, the effect of an ambient crosscurrent is not considered.

f. General Remarks Concerning Wada's Models

Although Wada's approach in modeling is reasonable, it has some limitations. First, any application of his Models 1 and 2 should be with the understanding that they do not simulate any kind of jet flow near the outlet due to the neglecting of the inertial terms in the equations of motion. For most lake-field conditions, the turbulent structure close to the discharge is jet-like and ambient turbulence only controls the diffusion process later at some distance downstream. Moreover, it is not clear that all the inertial terms in the equations of motion can be neglected, especially near the source of the warm-water discharge. If Wada had included the convective terms in the equations of motion, the complexity of the numerical solution would have increased to a great degree, due mostly to stability problems, with the increase in the cost of computer time becoming extremely prohibitive. Once the complete hydrodynamic equations become normalized, the feeling for the physical phenomena becomes generally more nebulous, much time being spent obtaining stability for the numerical scheme and having it yield physically meaningful results. This in total becomes very expensive, the final results perhaps not being very different from the inexpensive realistic results obtained by dropping these inertial terms in the first place. Neglecting the convective terms reduces the hyperbolic flow equations to an elliptic form, which is considerably simpler to solve by finite differences. Following this simplified approach, Wada sacrifices any accurate representation of the initial-jet flow region.

Two additional comments can be added about Wada's three diffusion models. First, the use of absolute temperatures is a disadvantage. Each model must now have input data on such receiving-body temperature-independent phenomena as solar radiation, atmospheric radiation, and reflected solar and atmospheric radiation (see Table 5.1) in addition to back radiation, conduction/convection losses, and evaporative transfers. If excess temperatures above ambient were employed, surface heat transfer from the plume (i.e., relative to the ambient body of water) would only need be considered, simplifying the data required to be taken from the field to ambient temperature, excess temperature, and wind speed. Second, Wada does not compare any of his models to either field or hydraulic data for verification of his theory in any of his translated papers. Wada may well have done so in Japan, but, to our knowledge, he has not reported such comparisons. At present, the models have to be considered as unverified.

As was indicated at several points throughout the discussion of the three models, much of the detail concerning Wada's work is not contained within the references cited below. Undoubtedly more comprehensive coverage of this work may be available. An attempt will be made to acquire additional reference material along with a request for the computer program listings for the three models.

References

Pertinent Works of Akira Wada:

1. S. Senshu and A. Wada, "Thermal Diffusion of Cooling Water into the Stratified Sea Basin,"[1] Proc. 11th Congress of the International Association for Hydraulic Research, Leningrad, 1965 (also additional comments presented at IAHR Congress, pp. 286-293).

2. Kyohei Manabe, Yoshio Watanabe, and Akira Wada, Study on Recirculation of Cooling Water of Tsuruga Nuclear Power Station Sited on Urayoke Bay,[2] Coastal Engineering in Japan 9 (1966).

3. Akira Wada, "A Study on Phenomena of Flow and Thermal Diffusion Caused by Outfall of Cooling Water,"[1,2] Proc. 10th Conference on Coastal Engineering, Tokyo, Japan, Vol. II (Sept 1966).

4. Akira Wada, A Study on Phenomena of Flow and Thermal Diffusion Caused by Outfall of Cooling Water,[1-3] Coastal Engineering in Japan 10 (1966).

5. Akira Wada, A Study on Phenomena of Flow and Thermal Diffusion Caused by Outfall of Cooling Water,[1,2] Central Research Institute of Electric Power Industry, Abiko-cho, Japan, Technical Report C:66006 (Jan 1967).

6. Akira Wada, Study on Recirculation of Cooling Water of Power Stations Sited on a Bay,[1,2] Coastal Engineering in Japan 10 (Dec 1967).

7. Akira Wada, Numerical Analysis of Distribution of Flow and Thermal Diffusion Caused by Outfall of Cooling Water,[3] Coastal Engineering in Japan 11 (1968).

8. Akira Wada, "Studies of Prediction of Recirculation of Cooling Water in a Bay,"[3] Proc. 11th Conf. on Coastal Engineering, London (Sept 1968).

9. Akira Wada, Numerical Analysis of Distribution of Flow and Thermal Diffusion Caused by Outfall of Cooling Water,[3] Central Research Institute of Electric Power Industry, Abiko-cho, Japan, Technical Report C:67004 (Jan 1969).

Some of Wada's other relevant papers are:

10. Akira Wada, On the Disturbed Waves in a Bay Sheltered by Breakwater, Coastal Engineering in Japan 7 (1964).

11. S. Senshu and A. Wada, Study on Bottom Water Intake for Condenser Cooling System of Power Station Sited on a Bay, Central Research Institute of Electric Power Industry (1964).

12. Akira Wada, On a Method of Solution of Diffraction Problems, Coastal Engineering in Japan 8 (1965).

13. Akira Wada, Effect of Winds on a Two-layered Bay, Central Research Institute of Electric Power Industry, Technical Report C:66002, Abiko-cho, Japan (Sept 1966).

Wada's recent works not reviewed are:

14. Akira Wada and Naoaki Katano, Problems of Intake and Outfall of Industrial Water for Use (in Japanese) (1968).

15. Akira Wada, Numerical Analysis of Distribution of Flow and Thermal Diffusion Caused by Outfall of Cooling Water, International Association for Hydraulic Research (1969).

16. Akira Wada, Development of Simulation for Diffusion of Industrial Wastewater by Tidal Model with Two Layer Sea, Coastal Engineering in Japan (in Japanese) (1969).

17. Akira Wada, Development of Simulation Method for Diffusion Phenomena of Industrial Waste Water in the Sea (in Japanese) (1970).

18. Akira Wada, Prediction of Water Pollution in the Sea Caused by Outfall of Industrial Waste Water, Bulletin on Coastal Oceanography (in Japanese) (1970).

Note: The numbers written as superscripts after the title of a paper refer to the number of the model described in this discussion.

Additional Reference for Present Discussion:

19. Nobuyuki Tamai, Robert Wiegel, and Gordon Tornberg, "Horizontal Surface Discharge of Warm Water Jets," Proceedings ASCE PO2 (Oct 1969).

20. W. O. Cheney and Gordon Richards, Ocean Temperature Measurements for Power Plant Design, Coastal Engineering, Santa Barbara Conference, October 1965, ASCE, pp. 955-989 (1966).

21. O. I. Mamayev, The Influence of Stratification on Vertical Turbulent Mixing in the Sea, Izv. Acad. Nauk. USSR, Geofiz., No. 7 (1958).

6. Initial Mixing of Thermal Discharges into a Uniform Current

J. E. Edinger and E. M. Polk, Jr.[1]
(Vanderbilt University)
October 1969

a. List of Symbols

A_n	Scaling area defined by Eq. 6.26
c_p	Specific heat of water
d	Depth of plume
D_x	Longitudinal dispersion coefficient at a point and for a given time
D_y	Lateral dispersion coefficient at a point and for a given time
D_z	Vertical dispersion coefficient at a point and for a given time
K	Coefficient of surface heat exchange
Q_p	Power-plant pumping rate
Q_R	Volumetric flow rate of a river
s	Conservative temperature-distribution function
s_p	Source concentration or, equivalently, the initial excess temperature at discharge
s_c	Temperature rise at a fixed arbitrary isotherm
S	Strength of point source of heat
W	Width of a river
x	Longitudinal distance (along shoreline)
x_c	Downstream distance to point of intersection of shoreline with isotherm $s = s_c$
x_s	x coordinate position of source
y	Lateral distance (perpendicular to shore)
z	Vertical distance (measured from surface)
α	Nondimensional parameter related to K and defined by Eq. 6.5
β	Nondimensional parameter related to K and defined by Eq. 6.22
η	Nondimensional variable of integration defined by Eq. 6.22
θ	Temperature rise
θ_c	Temperature rise at a fixed arbitrary isotherm
θ_p	Initial excess temperature of thermal discharge

ξ Nondimensional variable related to x defined by Eq. 6.4

ξ_s ξ-coordinate position of source

σ_0 Standard deviation of initial Gaussian temperature distribution

σ Standard deviation of Gaussian temperature distribution for any distance $x > x_s$ downstream $[\sigma(x_s) = \sigma_0]$

σ_y 4x times the square of the standard deviation in the lateral direction y of the three-dimensional Gaussian temperature distribution (defined by Eq. 6.27)

σ_z 4x times the square of the standard deviation in the vertical direction z of the three-dimensional Gaussian temperature distribution (defined by Eq. 6.27)

ρ Specific weight of water

b. Introduction

Edinger and Polk have treated the problem of the surface discharge of a heated effluent by considering it as a continuous point source of heat on the boundary of a uniform flowing stream which is infinitely wide and deep. The philosophy behind the model is their conviction that certain simplified analytical solutions to the basic heat-conservation equation might apply to warm-water discharges. They derive a closed form expression for a two- and three-dimensional temperature field, together with an analytical expression for the "area" contained within the resulting isotherms.

This "contour area" description of the temperature field has the advantage that its formulas are arranged in a form having parameters of the velocity and dispersive fields grouped as ratios and multipliers which can be evaluated from field data. Moreover, working with areas within isotherms sidesteps the usual difficulties associated to a pointwise comparison of experimental data. Also, state thermal-effluent standards are sometimes written with the option of a heated discharge satisfying an equivalent area-mixing-zone criterion in which the area within a specified isotherm is restricted by some predetermined upper bound. This fact also encourages a contour-area description of the thermal plume.

The Edinger and Polk analysis is based on a simplification of the general three-dimensional conservation equation written for a unit mass within a body of water:

$$\frac{\partial\theta}{\partial t} + u\frac{\partial\theta}{\partial x} + v\frac{\partial\theta}{\partial y} + w\frac{\partial\theta}{\partial z} = \frac{\partial}{\partial x}\left(D_x\frac{\partial\theta}{\partial x}\right) + \frac{\partial}{\partial y}\left(D_y\frac{\partial\theta}{\partial y}\right) + \frac{\partial}{\partial z}\left(D_z\frac{\partial\theta}{\partial z}\right) + \frac{h}{\rho c_p}, \tag{6.1}$$

where

θ = temperature rise above ambient,

u, v, w = longitudinal, lateral, and vertical velocity components at a point x, y, z and time t,

D_x, D_y, D_z = longitudinal, lateral, and vertical dispersion coefficients at a point and for a given time,

and

h = internal source or sink term denoting the net rate of heat input or output due to outside effects.

c. Two-dimensional Model

(1) Model Description and Discussion. In seeking analytical solutions to Eq. 6.1, the authors first focus attention on a simplified, two-dimensional, steady-state situation (see Fig. 6.1) of a heat source located along a shoreline parallel to the direction of a uniform longitudinal current. No influence of any far bank is considered.

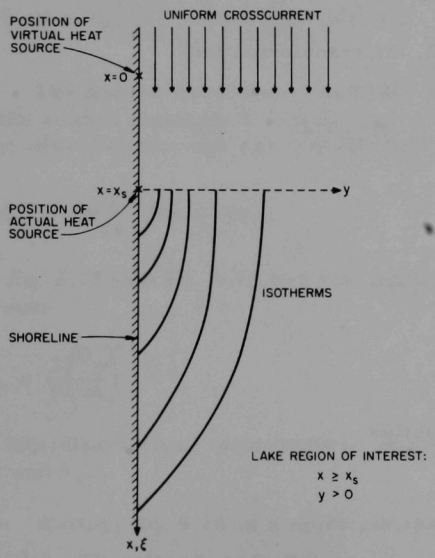

Fig. 6.1

Two-dimensional Case

Equation 6.1 reduces to

$$u\frac{\partial\theta}{\partial x} = \frac{\partial}{\partial y}\left(D_y\frac{\partial\theta}{\partial y}\right) - \frac{K}{\rho c_p d}\,\theta, \tag{6.2}$$

where

θ = temperature rise above ambient,

x = distance downstream (measured from a virtual origin to be determined later),

y = lateral distance measured from the shoreline,

D_y = lateral diffusivity (assumed constant),

K = coefficient of surface heat exchange (assumed constant),

and

d = depth of plume (assumed constant).

Equation 6.2 states that the rate of change in longitudinal advection is balanced by the rate of lateral dispersion and surface heat loss. No longitudinal or vertical convection is assumed to occur, and no buoyant effects are considered. The temperature distribution is being determined entirely by a constant lateral eddy diffusivity, by an assumed plume depth, and by a surface-heat-exchange coefficient. The authors' development of Eq. 6.2 is summarized below.

To solve Eq. 6.2, the transformation

$$\theta = [s(\xi, y)]e^{-\alpha\xi} \tag{6.3}$$

is made with

$$\xi = \frac{xD_y}{u} \tag{6.4}$$

and

$$\alpha = \frac{K}{\rho c_p D_y d}. \tag{6.5}$$

The function $s(\xi, y)$ now satisfies

$$\frac{\partial s}{\partial \xi} = \frac{\partial^2 s}{\partial y^2}. \tag{6.6}$$

The solution to the two-dimensional diffusion equation (Eq. 6.6) for a point source is the exact Gaussian

$$s(\xi, y) = \frac{C}{2\sqrt{\xi}} \exp\left(-\frac{y^2}{4\xi}\right) \tag{6.7}$$

where C is a constant of integration. Therefore,

$$\theta(\xi, y) = \frac{C}{2\sqrt{\xi}} \exp\left(-\frac{y^2}{4\xi}\right) e^{-\alpha\xi}. \tag{6.8}$$

From Eq. 6.8,

$$\frac{\partial\theta}{\partial y}(\xi, y)\bigg|_{y=0} = 0 \tag{6.9}$$

automatically satisfies the desired boundary condition of zero heat flux at the shoreline. Also, θ tends to zero as $y \to \infty$ for all $\xi > 0$ as desired; for $\xi = 0$ it vanishes everywhere except at $y = 0$ where it becomes infinite. Since $\theta(\xi, 0)$ decreases from ∞ to zero as ξ increases from 0, the integration constant C can be determined at the source position $\xi = \xi_s$, $y = 0$, where θ will equal the initial excess temperature θ_p. With C determined, θ becomes

$$\theta(\xi, y) = \theta_p\left(\frac{\xi_s}{\xi}\right)^{1/2} \exp\left(-\frac{y^2}{4\xi}\right) \exp[-\alpha(\xi - \xi_s)], \qquad \xi \geq \xi_s. \tag{6.10}$$

The source coordinate position ξ_s is uniquely determined by equating the source strength $S = \theta_p Q_p$ (Q_p = volumetric discharge rate) to the rate of advection through any downstream cross section

$$\theta_0 Q_p = ud\int_0^\infty \theta(x, y)\, dy. \tag{6.11}$$

Inserting Eq. 6.10 into Eq. 6.11 and evaluating the definite integral at $\xi = \xi_s$ yields

$$\xi_s = \frac{1}{\pi}\left(\frac{Q_p}{ud}\right)^2. \tag{6.12}$$

The final two-dimensional temperature distribution is represented by Eqs. 6.10 and 6.12.

Writing Eq. 6.10 in a more recognizable Gaussian format gives

$$\frac{\theta(\xi, y)}{\theta_0} = \frac{\sigma_s}{\sigma} \exp\left(-\frac{y^2}{2\sigma^2}\right) \exp[-\alpha(\xi - \xi_s)], \qquad \xi > \xi_s, \tag{6.13}$$

with

$$\sigma^2 = 2\xi, \quad \sigma_s = \sqrt{2}\,\xi_s, \tag{6.14}$$

where σ and σ_s represent the standard deviations of the Gaussian factor of the solution (Eq. 6.10) at downstream distances ξ and ξ_s, respectively.

Note also that, for $y = 0$,

$$\frac{\theta}{\theta_0} = \frac{\sigma_s}{\sigma} \exp[-\alpha(\xi - \xi_s)] = \sqrt{\frac{x_s}{x}} \exp\left[-\left(\frac{\alpha D_y}{u}\right)(x - x_s)\right] \tag{6.15}$$

where x_s is the source position (in x, y coordinates)

$$x_s = \frac{u\xi_s}{D_y} = \frac{1}{\pi} \frac{Q_p^2}{ud^2 D_y}. \tag{6.16}$$

Equation 6.15 states that the temperature along the shore is inversely proportional to the square root of x with an additional dieoff factor of $\exp[-(\alpha D_y/u)(x - x_s)]$ due to surface heat dissipation.

The Gaussian solution (Eq. 6.10) is especially suited to calculation of surface areas within isotherms. The equation for the isotherm $\theta = \theta_c$ is, from Eq. 6.10,

$$y = 2\xi^{1/2}\left\{\ln\left[\frac{\theta_p}{\theta_c}\left(\frac{\xi_s}{\xi}\right)^{1/2}\right] - \alpha(\xi - \xi_s)\right\}^{1/2}. \tag{6.17}$$

The surface area within the isotherm is

$$A = \int_{x_s}^{x_c} y\,dx = \frac{2u}{D_y}\int_{\xi_s}^{\xi_c} \xi^{1/2}\left\{\ln\left[\frac{\theta_p}{\theta_c}\left(\frac{\xi_s}{\xi}\right)^{1/2}\right] - \alpha(\xi - \xi_s)\right\}^{1/2} d\xi, \tag{6.18}$$

where x_s is the source location and where x_c is the longitudinal position where the isotherm $\theta = \theta_c$ intersects $y = 0$. From Eq. 6.10, ξ_c satisfies the nonlinear equation

$$\sqrt{\xi_c}\, e^{\alpha\xi_c} = \frac{\theta_p}{\theta_c}\sqrt{\xi_s}\, e^{\alpha\xi_s}, \tag{6.19}$$

which must be solved numerically. The integral in Eq. 6.17 can be made nondimensional and dependent only on the ratio θ_p/θ_c by the substitution

$$\eta = \frac{\theta_c}{\theta_p}\left(\frac{\xi}{\xi_s}\right)^{1/2} \tag{6.20}$$

so that Eq. 6.18 becomes

$$A = A_n\left(\frac{\theta_c}{\theta_p}\right)^{-3} \int_{\theta_c/\theta_p}^{\eta_c} \eta^2 \left\{ \ln\left(\frac{1}{\eta}\right) - \beta\left[\left(\frac{\theta_p}{\theta_c}\right)\eta^2 - 1\right]\right\}^{1/2} d\eta. \tag{6.21}$$

We define β above from

$$\beta = \alpha\xi_s = \frac{1}{\pi}\frac{KQ_p^2}{\rho c_p D_y d^3 u^2}, \tag{6.22}$$

and the scaling area A_n is

$$A_n = \frac{4}{\pi^{3/2}}\frac{Q_p^3}{D_y u^2 d^3}. \tag{6.23}$$

The nondimensional integral in Eq. 6.21 must be evaluated numerically once β, θ_c/θ_p, and η_c have been determined.

The ratio A/A_n is plotted in Fig. 6.2 as a function of the ratio θ_c/θ_p for selected values of β. The case $\beta = 0$ represents the conservative case with no surface heat loss ($K = 0$). The authors noted from the graph that surface cooling has little influence until θ_c/θ_p reaches 0.60 by mixing.

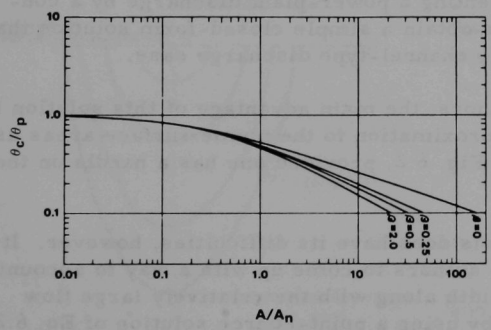

Fig. 6.2

Relationship of Temperature-rise Ratio to Nondimensional Surface-area Ratio for Selected Values of β

Comparison of Eq. 6.21 with field data is straightforward. Isotherms are constructed from the surface-temperature data, and the actual areas within isotherms are plotted against θ_c/θ_p on log-log paper with the same grid size as in Fig. 6.2. The data plot is then superimposed on Fig. 6.2 and slid along the abscissa until a best fit is obtained. The ratio of the actual to the nondimensional area will be a constant for every point along the abscissa, and the constant will be the scaling area A_n.

From Eqs. 6.22 and 6.23,

$$\beta = \frac{\sqrt{\pi}}{4} \frac{KA_n}{\rho c_p Q_p}. \tag{6.24}$$

Consequently, if K and Q_p are known, the value of A_n found from matching the abscissas must agree with the value of β along which the data falls.

A few observations can be made from the expression defining the areas within specific isotherms:

(1) The surface area varies inversely with the cubic power of the ratio θ_c/θ_p (two-dimensional case only).

(2) For a fixed temperature ratio θ_c/θ_p, the area varies directly with the cubic power of the plant pumping rate. Consequently, the area within specific isotherms may be related for different power plants, depending upon size.

(3) From Fig. 6.2, surface cooling can be important in determining the size of the plume areas for low θ_c/θ_p ratios, as can be seen by the continuous changing in the slope of the relation of θ_c/θ_p versus A/A_n in Fig. 6.2 due to the surface heat exchange.

At this point, a few general remarks should be made concerning the above model. By representing a power-plant discharge by a continuous point source, the authors obtain a simple closed-form solution that may be applied to practically any channel-type discharge case.

According to the authors, the main advantage of this solution is that it provides a reasonable approximation to the plume surface areas using the simple generalized curve of Fig. 6.2, provided one has a handle on the diffusion coefficient.

Such a simple analysis does have its difficulties, however. It was virtually impossible for the authors to come up with a way to account for a finite discharge-channel width along with the relatively large flow input of a power plant to a lake by using a point-source solution of Eq. 6.2. To account for this in some way, Edinger and Polk positioned a "phantom" point source at a shoreline position some distance upstream. The solution to Eq. 6.2 thus yielded a half-Gaussian distribution ($0 \leq y < \infty$ only) at the true source.

A second difficulty comes from the fact that, although the derived temperature distribution given in Eq. 6.8 is defined for $0 < \xi < \xi_s$ also, the authors do not consider any of the derived upstream temperature values as being part of the final solution. They give two arguments. First, for a downstream current, the plume does not penetrate upstream any

significant amount. Second, and more generally, the flow region near (above or below) the true source is jet-like and cannot be represented solely by Eq. 6.2. Consequently, the point-source solution given by Eq. 6.8 would not be expected to give a true representation of plume dispersion near the discharge. The authors expect the accuracy of their solution to improve at larger downstream distances since the effluent field will then behave essentially like a buoyant floating plume, being convected along by the ambient current and simultaneously spreading laterally due to the ambient turbulence.

In reality, to account for the effects of initial jet momentum and the secondary velocity currents set up due to buoyancy differences and the interaction between the jet and the transverse current in the near-field region, a more complicated model is required demanding more boundary conditions and possibly defying any type of closed-form solution. Thus Edinger and Polk have employed a point-source solution, using a "phantom" source, to make it applicable to a finite discharge width with anticipated fair approximate results downstream. The model is therefore strictly a far-field one.

(2) Application of Theory to Surface Discharges into Uniform Currents. The applicability of the Edinger-Polk procedure is not limited to shoreline discharges into shore-parallel currents. It can be applied, for example, to offshore surface discharges into uniform currents (see Fig. 6.3). For this case, the integral in Eq. 6.11 would start at $-\infty$ rather than zero. The change in the limits of integration modifies the parameters ξ_s, x_s, and σ_0, as follows:

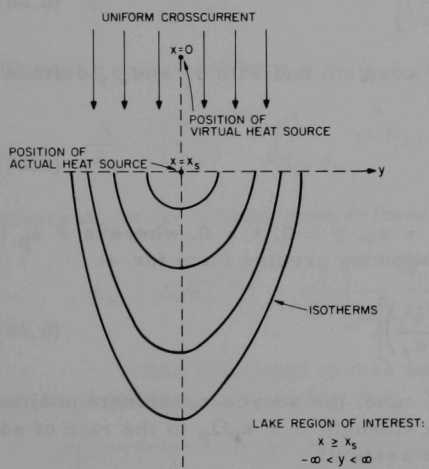

Fig. 6.3. Two-dimensional Case in an Open-lake Situation

$$\xi_s = \frac{1}{4\pi}\left(\frac{Q}{ud}\right)^2,$$

$$x_s = \frac{1}{4\pi}\,\frac{Q^2}{D_y u d^2},$$

and

$$\sigma_0 = \frac{1}{\sqrt{2\pi}}\,\frac{Q}{ud}.$$

Equations 6.10 and 6.12 keep the same form, except that A_n is now

$$A_n = \frac{Q^3}{\pi^{3/2} D_y u^2 d^3}.$$

d. Three-dimensional Model

(1) Model Description. Edinger and Polk next extend their point-source Gaussian model to three dimensions, representing the vertical-diffusion process by a Gaussian distribution. With the same shoreline-discharge problem considered, the energy-conservation equation for lateral and vertical dispersion of heat becomes

$$u\frac{\partial s}{\partial x} = \frac{\partial}{\partial y}\left(D_y\frac{\partial s}{\partial y}\right) + \frac{\partial}{\partial z}\left(D_z\frac{\partial s}{\partial z}\right), \tag{6.25}$$

where s now represents the temperature excess above ambient at longitudinal, lateral, and vertical positions x, y, and z, respectively. D_y and D_z are assumed to be constant. No surface heat loss is considered. The three-dimensional distribution does not have a simple analytical solution in the nonconservative case.

The function

$$s(x, y, z) = \frac{c}{x}\exp\left[-\frac{1}{4x}\left(\frac{y^2}{\sigma_y} + \frac{z^2}{\sigma_z}\right)\right] \tag{6.26}$$

satisfies Eq. 6.25 with c an arbitrary constant and with σ_y and σ_z defined by

$$\sigma_y = \frac{D_y}{u}, \quad \sigma_z = \frac{D_z}{u}. \tag{6.27}$$

Evaluating c at the source loaction $x = x_s$, $y = 0$, $z = 0$, where $s = s_p$ is the source concentration, yields the following precise form for s:

$$\frac{s(x, y, z)}{s_p} = \frac{x_s}{x}\exp\left[-\frac{1}{4x}\left(\frac{y^2}{\sigma_y} + \frac{z^2}{\sigma_z}\right)\right]. \tag{6.28}$$

As in the two-dimensional case, the source-coordinate position x_s is evaluated by equating the source strength $S = s_pQ_p$ to the rate of advection through any downstream cross section:

$$s_pQ_p = u\int_0^\infty\int_0^\infty s(x, y, z)\,dy\,dz. \tag{6.29}$$

The double integral is independent of x and has the value $\pi x_s s_p\sqrt{\sigma_y\sigma_z}$. Solving Eq. 6.29 for x_s yields

$$x_s = \frac{Q_p}{\pi\sqrt{D_yD_z}}. \tag{6.30}$$

As the authors note, the source position x_s is independent of the uniform current, depending solely on the product of the lateral and vertical diffusivities.

The areas within surface isotherms are calculated as before. The equation of the isotherm $s = s_c$ on the surface $z = 0$ has the form

$$y = 2\sqrt{\sigma_y}\, x^{1/2}\left\{\ln\left[\frac{s_p}{s_c}\frac{x_s}{x}\right]\right\}^{1/2} \tag{6.31}$$

as derived from Eq. 6.28. The area within that isotherm is given by

$$A = \int_{x_s}^{x_c} y\, dx = 2\sqrt{\sigma_y}\int_{x_s}^{x_c} x^{1/2}\left[\ln\left(\frac{s_p}{s_c}\frac{x_s}{x}\right)\right]^{1/2} dx, \tag{6.32}$$

where x_c is found from Eq. 6.28 for $y = 0$, $z = 0$, to be

$$x_c = \frac{s_p}{s_c}\, x_s. \tag{6.33}$$

Changing variables from x to $\eta = (s_c/s_p)(x/x_s)$ in Eq. 6.32 yields

$$\frac{A}{A_n} = \left(\frac{s_c}{s_p}\right)^{-3/2}\int_{s_c/s_p}^{1} \eta^{1/2}[\ln(1/\eta)]^{1/2}\, d\eta, \tag{6.34}$$

where A_n is the scaling area defined by

$$A_n = 2\sqrt{\sigma_y}\, x_s^{3/2} = \frac{2}{\pi^{3/2}}\left[\frac{Q_p^3}{u(D_y D_z^3)^{1/2}}\right]^{1/2}. \tag{6.35}$$

The fractional excess temperature s_c/s_p is plotted as a function of the area ratio A/A_n in Fig. 6.4. The two-dimensional conservative case

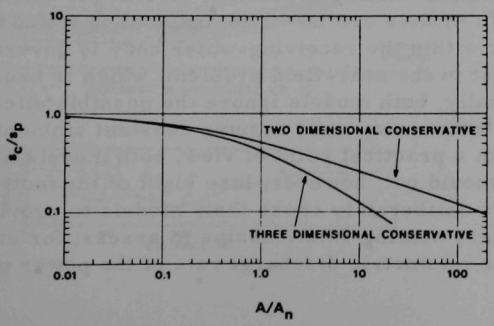

Fig. 6.4

Nondimensional Surface-area Ratio as a Function of Concentration Ratio for the Two- and Three-dimensional Cases[1]

is also shown in Fig. 6.4. A comparison of Eqs. 6.21 and 6.34 show that the area increases inversely with the 3/2 power of the fractional excess-temperature ratio as compared with the cubic power for the two-dimensional case. Moreover, the three-dimensional scaling area A_n increases with the 3/2 power of the plant pumping rate as compared to the cubic power for the two-dimensional case. Figure 6.4 indicates the expected result that for a given fractional excess temperature, more area is enclosed within that isotherm in two-dimensional mixing and dispersion than for three-dimensional mixing. Surface isotherms as predicted by the model are again illustrated in Fig. 6.1. Vertical isotherms are depicted in Fig. 6.5a.

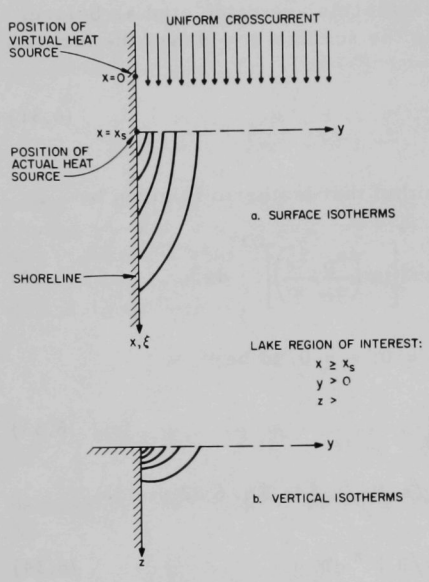

Fig. 6.5. Three-dimensional Case

(2) Application of Theory to Surface Discharge into Uniform Currents. The applicability of the Edinger-Polk procedure for three-dimensional dispersion is again not limited to shoreline discharges into shore-parallel currents. Following the procedure established in Sec. c(2) above, a three-dimensional (conservative) temperature distribution may be derived with areas within surface isotherms for the problem of an offshore discharge into a uniform current. Again, the integrals of Eq. 6.29 would start at $-\infty$. Surface and vertical isotherms are predicted in Fig. 6.5.

e. General Comments about the Edinger-Polk Models

Several general comments need to be made concerning the two models proposed by the authors. First, the title of their work is somewhat misleading, stating that it concerns the initial mixing of thermal discharges into a uniform current. In reality, both models are far-field analyses in which the dispersion of the heated effluent within the receiving-water body is governed by ambient turbulence in contrast to the near-field problem, which is usually dictated by jet mixing. Additionally, both models ignore the possible effects of buoyancy, stratification, and bottom slope and assume constant ambient thermal diffusivities. Thus from a practical point of view, both models have some severe limitations. One should not, however, lose sight of the motivation for their work. The authors deliberately chose their models to provide a design engineer with preliminary scaling relationships to assess, for example, the effects of doubling the volumetric discharge rate of the power plant

or to assess the relative size of a power plant in relation to a water body. A recent publication by Asbury and Frigo[2] attests to the usefulness of Edinger and Polk's methodology.

The Edinger-Polk models are applicable for the far field and may be applied when turbulent diffusion is the dominating factor in the distribution of temperature. Such a situation occurs when the initial densimetric Froude number exceeds 1.0 by a significant amount and the discharge velocity does not have a large vector difference from the ambient velocity. Any jet interaction with the ambient stream should then be minimized, and consequently the authors expect their analytical diffusion models to yield satisfactory results. The authors have compared their models to river and coastal plume data, but only in a curve-fitting sense; i.e., diffusivities were determined by matching as close as possible the theoretical curves of Figs. 6.2 and 6.4 to the field data on isotherm areas.

f. Field Verification of Models, and Discussion of Verification

The authors attempted to verify their two-dimensional model by fitting a theoretical curve to the field data taken during surveys of the Tennessee Valley Authority's John Sevier Steam Plant on the Holston River near Rogersville, Tennessee. This 800-MW plant operated at 75% capacity throughout the survey. The heated effluent was discharged into a relatively shallow wide portion of the Holston River with average depth 4.5 ft and average width 500 ft. The initial excess temperature (above ambient) of the effluent was 13.7°F; the initial discharge velocity was about twice that of the ambient stream. Lateral and vertical temperature measurements were taken at seven cross sections downcurrent from the power plant. From those data, temperature contours were drawn for the surface and for various cross sections. Figure 6.6 illustrates the surface isotherms and typical cross-sectional temperature contours. From meteorological data, the decay coefficient β was determined to be 0.0032, indicating that atmospheric cooling played an insignificant role in mixing during the field survey. Thus the

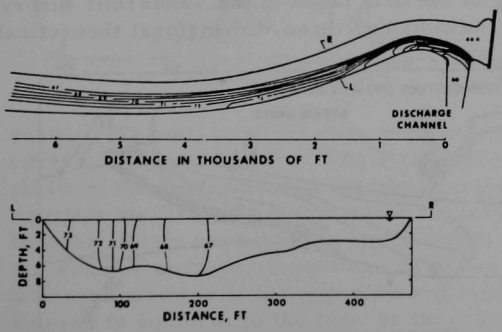

Fig. 6.6

Surface and Typical Cross-section Temperature Contours, Holston River below John Sevier Steam Plant, October 16, 1969[3]

two-dimensional conservative solution was used as a theoretical comparison with the surface area data. The river velocity in Eq. 6.23 was determined from

$$u = \frac{Q_R}{Wd}, \tag{6.36}$$

where Q_R is the total river flow and W the width. Figure 6.7 compares the theoretical solution with the measured surface area within each temperature contour. From the graph, the scaling area A_n was determined from which the lateral diffusion coefficient $D_y = 3.7\ ft^2/sec$ was evaluated.

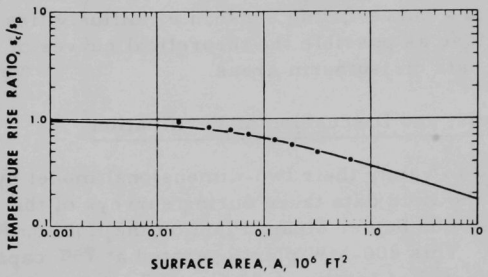

Fig. 6.7

Variation in Surface Area with Temperature-rise Ratio, Holston River below John Sevier Steam Plant, October 16, 1969[3]

The authors attempted to verify their three-dimensional diffusion model with data taken at the TVA's 1750-MW Widows Creek Steam Plant near Stevenson, Alabama. The plant discharges into the Tennessee River where the average width of the stream is 1200 ft and the average depth is about 20 ft. The heated effluent is discharged from a 6-ft-deep embayment at one bank. Figure 6.8 illustrates surface isotherms, and Figs. 6.9 and 6.10 sketch typical cross-sectional temperature contours obtained from the vertical and lateral temperatures measurements of November 20, 1968 at seven downstream cross sections. The measurements were taken over a distance of slightly greater than 1 mile downcurrent from the discharge. Figure 6.11 illustrates the fitting of the data taken in the Vanderbilt surveys of November 20 and 21, 1968, to the two- and three-dimensional theoretical

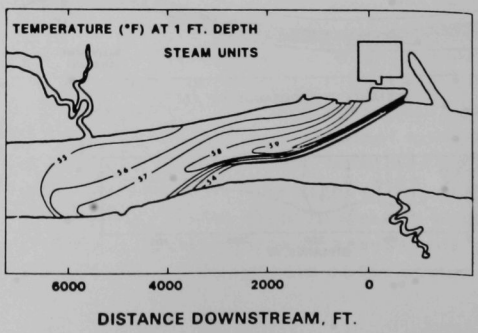

Fig. 6.8

Temperature Contours at Surface, Tennessee River below Widows Creek Steam Plant, November 20, 1968[3]

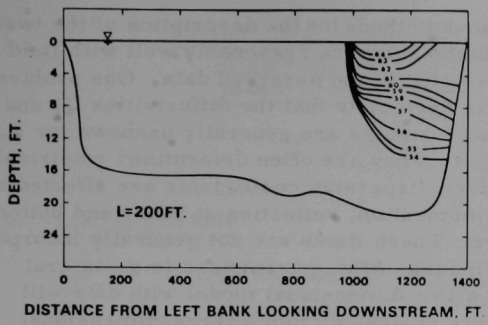

Fig. 6.9

Temperature Contours in the Cross Section, Tennessee River, 200 ft below Widows Creek Steam Plant, November 20, 1968[3]

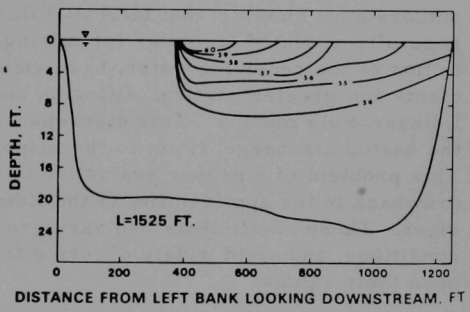

Fig. 6.10

Temperature Contours in the Cross Section, Tennessee River, 1525 ft below Widows Creek Steam Plant, November 20, 1968[3]

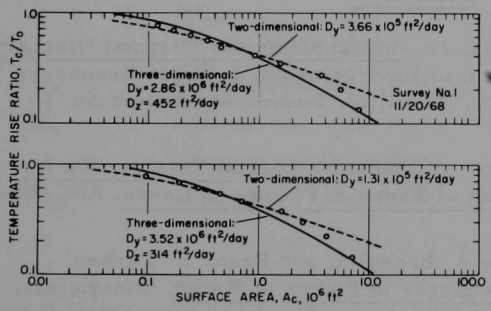

Fig. 6.11

Surface Area within a Temperature-rise Contour vs Temperature-rise Ratio with Two- and Three-dimensional Curves Superimposed, Widows Creek, November 20-21, 1968[3]

curves. The diffusivities were determined from the superposition of these curves to the data points. The three-dimensional curve gives the best overall fit to the data, although the two-dimensional curve (conservation case) matches the first few points more accurately. Polk et al.[3] assert that initial buoyant effects tended to prevent vertical mixing, after which complete mixing with the ambient stream was achieved some distance downstream. Thus different portions of the experimental temperature distribution could be considered to conform to the two- or three-dimensional models.

Edinger and Polk's analytical methods for the description of the two- and three-dimensional diffusion plume compare reasonably well with field data when the theoretical model is fitted to the observed data. One problem with using the models as predictive devices is that the diffusivities D_y and D_z required to evaluate the various formulas are generally unknown for conditions near power-plant discharges. They are often determined empirically from field data. Empirically derived dispersion coefficients are affected by such considerations as initial jet momentum, reflection at banks and bottom, and angle of plume axis with shore. These items are not generally incorporated in any far-field theoretical model. Also, parameters (e.g., lateral diffusivity) evaluated from fitting a two-dimensional model with data will differ from the identical parameters evaluated from a three-dimensional model and moreover will reflect any defects these models may have. The authors have shown[1,3] that lateral-diffusion coefficients, as predicted from generally accepted formulas for mixing of discharges having densities equal to that of the receiving water, have yielded smaller lateral-diffusion coefficients and greater vertical-diffusion coefficients than determined from the Edinger-Polk models. This discrepancy may be due to buoyancy effects of the heated discharge, if not to the inapplicability of the models themselves. This problem of a proper evaluation of the diffusivities is still a severe drawback in the applicability of the Edinger-Polk models as predictive devices. These coefficients can vary greatly, depending upon environmental conditions, and yield widely differing temperature distributions depending upon their values.

References

1. J. E. Edinger and E. M. Polk, Jr., Initial Mixing of Thermal Discharges into a Uniform Current, Dept. of Environmental & Water Resources Engr., Vanderbilt University, Nashville, Tennessee, Report No. 1 (Oct 1969).

2. J. G. Asbury and A. A. Frigo, A Phenomenological Relationship for Predicting the Surface Areas of Thermal Plumes in Lakes, ANL/ES-5 (Apr 1971).

3. Edward M. Polk, Jr., Barry A. Benedict, and Frank L. Parker, Dispersion of Thermal Discharges in Bodies of Water, Commercial Power Generation, Chemical Engineering Progress Symposium Series, No. 119, Vol. 67 (Sept 1971).

7. Offshore Outfall and Shoreline Surface Discharge Models for the Prediction of Thermal-plume Dispersion in the Great Lakes

G. T. Csanady
(University of Waterloo)
January 1970

a. List of Symbols

A_e	Cross-sectional area of outlet
b	Length of line source
B	Bowen ratio defined by Eq. 7.4
c_p, c_{pw}	Specific heat of water
c_{pa}	Specific heat of air
C_{10}	Drag coefficient at reference height of 10 m
h	Depth of plume
K	Surface heat-transfer coefficient
K_y	Lateral eddy diffusivity
m_y	Standard deviation of meandering
p	Relative intensity of horizontal lake turbulence
q	Magnitude of point source of equivalent strength to the line source of length b in current U
Q_s	Upward heat flux from the plume surface
Q_y	Average heat-flux component in the y direction
U	Uniform steady-current velocity
U_{10}	Wind speed at reference height of 10 m
v'	Fluctuating turbulent velocity in the y direction
V_e	Exit velocity of discharge
W	Width of plume
x	Longitudinal distance measured along plume centerline
x_c	Longitudinal distance at which surface cooling factor in θ solution drops off to half its initial value
x_m	Longitudinal distance at which turbulent mixing factor (Shoreline Surface Discharge Model) reduces to half its initial value
y	Lateral distance measured perpendicular to plume centerline

α	Heat-loss parameter related to K by Eq. 7.14
θ	Excess temperature of plume above ambient
θ_0	Excess temperature of plume at line source
$\bar{\theta}_0$	Initial excess temperature at outlet position
θ_s	Shoreline temperature-decay formula for Shoreline Surface Discharge Model
ρ, ρ_w	Density of water
ρ_a	Density of air
σ_y	Standard deviation of relative diffusion for the continuous-point-source solution
χ	Two-dimensional, conservative temperature field solution (i.e., turbulent mixing solution)
χ_{max}	Centerline temperature decay of χ
χ_0	Value of χ at the line source ($= \theta_0$)
χ_p	χ solution to a continuous point source defined by Eq. 7.19
χ_s	Shoreline temperature decay of χ

b. Introduction

In the past 10 years, G. T. Csanady of the University of Waterloo, Ontario, Canada, has investigated the disposal of pollutants in the Great Lakes, mainly Lakes Huron and Erie, by experimental methods. Data obtained from aerial photography, drogue, and dye-plume studies plus the acquisition of lake-temperature and current-structure data have led the author to specific conclusions concerning the parameters governing small- and large-scale mixing processes involved in plume dissipation. In his most recent works,[1,2] the author has used his experimental results in the development of two far-field predictive models for thermal-plume dispersion in large lakes.

The first mathematical model analyzes the situation of plume dispersion resulting from an offshore outfall or diffuser after the plume has attained a moderately large size and is drifting at the surface with the prevailing current. The second model considers the situation resulting when a warm-water effluent is discharged at the shoreline into a uniform transverse current. Both models apply only after the initial momentum of the discharging jet has been dissipated and the plume is convected along by the shore-parallel current; each involves a two-dimensional steady-state situation. The models will now be considered in more detail.

c. Offshore Outfall Model

(1) Model Development. Csanady has developed a two-dimensional mathematical model to treat the problem of dispersion of a heated effluent discharged from an outfall, perhaps 2-3 miles offshore. Any method of effluent introduction can be considered as long as it results in an initial plume of considerable size, fully mixed throughout the available depth of discharge and retaining no initial momentum. A prototype situation could easily be the discharge through a submerged multiport diffuser. It is assumed that the effluent plume remains thoroughly mixed at its initial depth and drifts along with the prevailing lake currents (generally shore-parallel) while it disperses horizontally. No bottom effects are considered, and any possible interference with any remote bank is ignored. The lake current is assumed uniform spatially over the depth and distance range involved. A steady-state situation is examined. As is done in Brooks,[3] the author treats the problem as diffusion into a steady current from a line-source of finite length b. The situation is illustrated in Fig. 7.1.

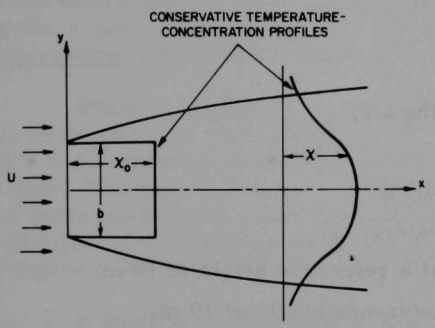

Fig. 7.1

Effluent Plume Released from Line Source of Length, b, into Uniform Lake Current of Velocity, U (Ref. 1)

Csanady considers the two-dimensional energy equation

$$U\frac{\partial\theta}{\partial x} = -\frac{Q_s}{\rho c_p h} - \frac{1}{\rho c_p}\frac{\partial Q_y}{\partial y} \tag{7.1}$$

to be appropriate to the nonconservative temperature field produced by the line source where

x = longitudinal distance downstream,

y = lateral distance measured normal to x,

θ = excess temperature above ambient,

h = depth of plume,

U = constant ambient velocity,

ρ = specific weight of water,

c_p = specific heat at constant pressure,

Q_s = upward heat flux from the free surface,

and

Q_y = average heat flux component in y direction.

The surface heat flux Q_s arising from convection, evaporation, and conduction may be written, neglecting the assumed small contribution of back radiation, as

$$Q_s = K\theta, \tag{7.2}$$

where

$$K = \left(1 + \frac{1}{B}\right) \frac{\rho_a}{\rho_w} \frac{c_{pa}}{c_{pw}} C_{10} U_{10}, \tag{7.3}$$

and

ρ_a = density of overlying air,

ρ_w = density of plume,

c_{pa} = specific heat of air,

c_{pw} = specific heat of water,

C_{10} = drag coefficient at a reference height of 10 m,

U_{10} = wind speed at a reference height of 10 m,

θ = excess temperature of plume over ambient lake,

and

B = Bowen ratio defined by

$$B = 0.66 \frac{\theta}{\Delta p_v}, \tag{7.4}$$

where

Δp_v = vapor pressure difference between the plume surface and air at 10 m above.

For a water-air temperature difference of 8°C, $B \approx 0.8$.

Equation 7.1 can now be written

$$U\frac{\partial\theta}{\partial x} = -\frac{K}{\rho c_p h}\theta - \frac{1}{\rho c_p}\frac{\partial Q_y}{\partial y}. \tag{7.5}$$

If

$$\theta = \chi \exp\left(-\frac{K}{\rho c_p h U}x\right), \tag{7.6}$$

then χ satisfies

$$U\frac{\partial\chi}{\partial x} = -\frac{1}{\rho c_p}\frac{\partial Q_y}{\partial y}. \tag{7.7}$$

Equation 7.7 may be interpreted as a two-dimensional diffusion equation for $\chi(x, y)$ in a turbulent field. Predicting the temperature or concentration distribution of some <u>conservative</u> effluent is equivalent to predicting the χ field. Introducing the "decay factor" given in Eq. 7.6, the <u>nonconservative</u> temperature field is also described.

While accepting the line-source model for the temperature field as in Brooks, the author diverges from the Brooks analysis by assuming a constant horizontal diffusivity instead of one increasing with plume size. The author's empirical investigations have yielded the result that for moderately sized plumes on the Great Lakes, the assumption of a constant diffusivity gives a more accurate approximation than the Richardson 4/3-power law used by Brooks.

If longitudinal diffusion is neglected, the two-dimensional heat-conservation equation becomes the simple diffusion equation for the conservative temperature field χ,

$$U\frac{\partial\chi}{\partial x} = K_y\frac{\partial^2\chi}{\partial y^2}. \tag{7.8}$$

The technique of solution is to consider each element of the line source as a "continuous point source" which generates a Gaussian plume.

A continuous point source in a uniform steady current yields a "slender" plume in which longitudinal diffusion is negligible. Due to the unimportance of diffusion along x, the plume dimension in this direction is irrelevant to the problem solution, thus justifying an idealized line source of length b to be placed perpendicular to the current and equal to the initial plume width.

If x is replaced by

$$\sigma_y = \left(2K_y \frac{x}{U}\right)^{1/2}, \tag{7.9}$$

the standard deviation of the point-source solution, the appropriate solution to Eq. 7.8 is

$$\left.\begin{aligned} \chi(x, y) &= \frac{\chi_0}{\sqrt{2\pi}\sigma_y} \int_{-b/2}^{b/2} \exp\left[-\frac{(y - y')^2}{2\sigma_y^2}\right] dy' \\ &= \frac{\chi_0}{2}\left(\operatorname{erf} \frac{b/2 + y}{\sqrt{2}\,\sigma_y} + \operatorname{erf} \frac{b/2 - y}{\sqrt{2}\,\sigma_y}\right) \end{aligned}\right\}, \tag{7.10}$$

where

$$\operatorname{erf} \lambda = \frac{2}{\sqrt{\pi}} \int_0^{\lambda} e^{-t^2}\, dt \tag{7.11}$$

and $\chi_0 = \theta_0$.

The complete solution for θ is then easily obtained from Eq. 7.6. Along the centerline, this yields

$$\theta_{max} = \chi(x, 0) \exp\left(-\frac{K}{\rho c_p h U} x\right). \tag{7.12}$$

These relationships show that at any downstream distance x, the excess temperature θ (or θ_{max} for centerline positions) is equal to θ_0 multiplied by two decay factors, one resulting from surface heat loss, the other due to mixing.

The form of the surface-heat-loss factor

$$\exp\left(-\frac{Kx}{\rho c_p h U}\right) \tag{7.13}$$

indicates that it is negligible for distances near the source and has significance only for far-downstream distances. This is due to the fact that a typical value of the parameter

$$\alpha = \frac{K}{\rho c_p h U} \tag{7.14}$$

is 1.16×10^{-5} for $K = 150$ Btu/ft^2-day-°F, $h = 5$ ft, $U = 0.5$ ft/sec.

Analyzing the turbulent mixing factor, i.e., the function $\chi(x, y)$, requires deeper analysis. This factor is of particular interest when:

(1) $y = 0$, which yields the conservative centerline temperature-decay formula;

(2) x is large, allowing an asymptotic form for χ to be developed;

(3) x is small, which gives information on dilution close to the source.

Setting $y = 0$ in Eq. 7.10 gives the decay of the maximum temperature at each cross section x,

$$\chi_{max}(x) = \chi_0 \operatorname{erf} \frac{b}{2\sqrt{2}\sigma_y}. \tag{7.15}$$

For large x, the exponential in the integrand of Eq. 7.11 may be written

$$\exp\left[-\frac{(y - y')^2}{2\sigma_y^2}\right] \cong \exp\left[-\frac{y^2}{2\sigma_y^2} + \frac{yy'}{\sigma_y^2}\right] \quad (y' \ll \sigma_y) \tag{7.16}$$

whereby

$$\chi(x, y) = \chi_0 \frac{b}{\sqrt{2\pi}\sigma_y} \exp\left(-\frac{y^2}{2\sigma_y^2}\right)\left[\frac{2\sigma_y^2}{by} \sinh \frac{by}{2\sigma_y^2}\right] \quad (b \ll \sigma_y) \tag{7.17}$$

Thus, if y/σ_y is not large compared to 1, the bracketed term in Eq. 7.17 is seen using Taylor's expansion to be approximately unity, which gives the following asymptotic formula for χ_{max}:

$$\chi_{max}(x) = \chi_0 \frac{b}{\sqrt{2\pi}\sigma_y} \quad (x \to \infty). \tag{7.18}$$

This last form is the identical formula for the centerline temperature rise resulting from a point source of strength $q = b\chi_0 U$ (per unit depth) placed at the center position of the line source. Csanady considers the point-source formula

$$\chi_p(x, y) = \chi_0 \frac{b}{\sqrt{2\pi}\sigma_y} \exp\left(-\frac{y^2}{2\sigma_y^2}\right) \tag{7.19}$$

to be a sufficiently good approximation when

$$\sigma_y > 3b \tag{7.20}$$

because the bracketed term in Eq. 7.17 is close to unity.

For small x, both error functions in Eq. 7.13 tend to unity i.e., $\chi \to \chi_0$ at $y = 0$. From Eq. 7.13, the centerline temperature rise is 1% of the initial temperature rise when

$$\frac{b}{2\sqrt{2}\,\sigma_y} \geq 2 \tag{7.21}$$

or, approximately,

$$\sigma_y \leq b/6. \tag{7.22}$$

In terms of longitudinal distance downstream, $\chi \approx \chi_0$ up to a distance

$$x \approx \frac{b^2 U}{64 K_y}. \tag{7.23}$$

Csanady substitutes "typical" values of the parameters involved to estimate the expected dilution at downstream distances. When U = 20 cm/sec, b = 100 m and K_y = 500 cm^2/sec. Equation 7.23 yields x = 625 m, implying that the model predicts negligible dilution for distances even up to 1 km. This is due to the fact that the initial plume width is large, requiring some distance before the ambient fluid can penetrate its way to the centerline. The distance x to which this holds is given by Eq. 7.23 and is proportional to b^2, which can be rather large for initially broad plumes. The "point source" formula, Eq. 7.20, will hold for x > 11.25 km for the above situation; however, by the time the effluent reaches that distance, the validity of the formula is questionable due to relatively frequent current reversals. Isotherms for the "Offshore Outfall Model" are sketched in Fig. 7.2.

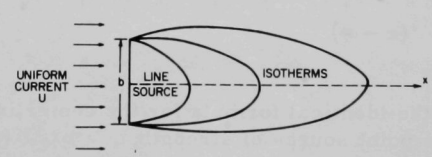

Fig. 7.2

Isotherms as Predicted by the Offshore Outfall Model

(2) Discussion of the Constant-diffusivity Model. At this point a few comments need to be made concerning the author's choice of a constant-diffusivity model. First, the horizontal eddy diffusivity is generally defined as

$$K_y = \text{const}\ U \frac{d(W^2)}{dx}, \tag{7.24}$$

where W is the observable width (under any reasonable definition) of a steady plume. If a constant K_y is assumed, then, from Eq. 7.24,

$$W = \text{const } x^{1/2}. \tag{7.25}$$

For the 4/3-power law,

$$K_y = \text{const } W^{4/3}, \tag{7.26}$$

and consequently, from Eq. 7.24,

$$K_y = \text{const } x^{3/2}, \tag{7.27}$$

implying that the plume grows faster than linearly and much faster than a constant-K_y model.

From Csanady's experiments in Lakes Huron and Erie with drift bottles and point discharges of fluorescent dye, it was concluded that a rapid phase of lateral plume growth indeed exists. However, this occurs at downstream distances x of 300-500 m from the point source producing a typical plume width of 20-50 m. Also, at distances of order 1 mile and beyond, a constant diffusivity was encountered. Csanady found that an appropriately chosen constant K_y would predict the growth of the plume width quite satisfactorily for $W > 50$ m or so. Consequently, Csanady concludes that for downstream distances of order 1-2 miles, a constant-K_y model is preferable to a more elaborate model. Errors may occur, but these are not usually significant in practice, according to Csanady.

How the plume sizes and longitudinal distances quoted above apply to a large-scale plume emitted by a power plant is still not clear. Csanady recommends a constant K_y for large-scale plumes only after the plume has reached a moderate size (roughly 100 m wide) and up to several kilometers in downstream distance. These are rough estimates, considering the kinds of complexities involved and the present state-of-the-art. Some investigators have recently collected field data that suggest that the plume width grows greater than a rate suggested by a constant K_y for larger downstream distances than several kilometers. Due to the present uncertainty involved, Csanady employs a constant-diffusivity model for extended longitudinal distances x.

The 4/3-power law used by Brooks is basically a theoretical result. If the turbulence field is homogeneous in the horizontal, the theoretical results of Batchelor[4] are applicable; in particular, during some stage of horizontal plume growth the Richardson's "4/3-power law" for diffusivity is approximately valid. The 4/3-power law can also be deduced theoretically from the Weizsacher-Heisenberg or Kolmogoroff theories.[5]

The derivation is based on the similarity of the diffusion of mass and momentum. The law does seem to compare well with field data on ocean diffusion. Many least-squares fittings have indicated that the "4/3-power law" is a good description of lateral plume growth with an associated increase in the scale of diffusion. In fact, the results of over 40 independent studies of turbulent dispersion seem to support the "4/3-power law" for the ranges (10 m to 100 km) applicable to oceanic turbulence.[6]

A good deal of recent experimental evidence by Csanady, Okubo, and others does not really support the 4/3-power law for large lakes. It appears that a constant diffusivity is satisfactory as long as the flow is homogeneous. Trouble can occur at dye patches or in large-scale diffusion where some kind of discontinuity in the flow field, such as a sudden change in current, occurs; this type of phenomenon would destroy the simple diffusivity model, where now the size of the plume becomes a critical factor. Much research is still necessary to determine which of these laws or perhaps some other law is most accurate in representing lateral diffusivities.

(3) General Comments about the Offshore Model. In addition to the uncertainty in specifying the precise functional form for the eddy thermal diffusivity, the model has other limitations. First, buoyant lateral spreading due to density differences within the plume and between the plume and ambient water is not considered. The flow field is defined to be ambient and unaffected by any temperature differences. Consequently, the model may be used only for a relatively small temperature differential between the plume and receiving water. This may not be a strict limitation, since any initial jet mixing has been assumed to occur before the applicability of this model.

Second, the plume depth is generally unknown, yet has to be specified in this model as a known constant.

Third, the constant diffusivity used in the model can vary up to several orders of magnitude with different sites and environmental conditions. Previous field measurements would be required to best analyze the variation in different circumstances. Such a requisite adversely affects the predictive nature of the model. At present, the model has not been verified with actual field data.

d. Shoreline Surface-discharge Model

(1) Model Development. Csanady employs the energy conservation equation to model a power station cooling water outfall located on a shoreline and discharging to the surface of a large lake. Empirical information on the surface heat flux and turbulent diffusion is included in the model, which was obtained during the author's investigations of the Great Lakes.

The situation is illustrated in Fig. 7.3. The condenser cooling water enters the lake at the shoreline into a transverse current. Any initial momentum is assumed to be quickly dissipated in an adjustment zone located between the outlet and a short distance downcurrent. At that point, the plume is assumed to drift along with the current and spread laterally by turbulent mixing. The author neglects bottom effects and assumes that the plume does not change in vertical size as its width grows. Diffusion along the current direction is once again ignored, and the plume is regarded as if it had been discharged from a line source of length b perpendicular to shore.

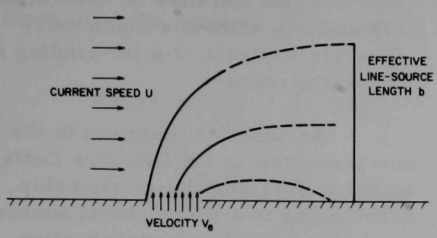

Fig. 7.3. Effluent-source Model[2]

The width of the line source b may be crudely estimated from a simple heat balance between the actual outlet and the line source:

$$V_e A_e \bar{\theta}_0 = bUh\theta_0, \tag{7.28}$$

where

V_e = exit velocity of the discharge,

A_e = cross-sectional area of the outlet,

U = current velocity,

h = depth of the plume,

$\bar{\theta}_0$ = initial excess temperature,

and

θ_0 = temperature excess at the line source (assumed constant).

Csanady recommends use of the empirical relationship

$$\bar{\theta}_0 = 3\theta_0 \tag{7.29}$$

as a crude estimate of the dilution factor encountered as a result of the initial mixing. In practice, this factor is clearly a complicated function of the ratio between exit and current velocity, discharge geometry, and lake-bottom contours. Equation 7.29 is based on the author's experimental investigations on the Great Lakes and particularly on his studies of the Douglas Point Nuclear Power Station on Lake Huron. Substituting Eq. 7.29 into Eq. 7.28 yields

$$b = \frac{3V_e A_e}{Uh} \tag{7.30}$$

as a rough approximation for b. The line source may be placed directly at the outlet or perhaps up to 100 yards downcurrent, as illustrated in Fig. 7.4. Estimates on the length, b, the constant temperature excess at the line source, and its proper position are quite difficult and may be determined only crudely without a much more elaborate analysis of a jet bending in a crosscurrent.

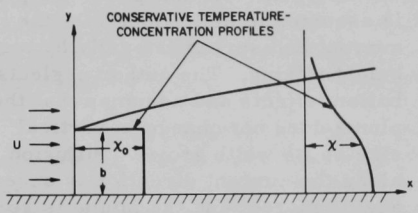

Fig. 7.4. Effluent Plume Released from Line Source of Length, b, Located at Shore, into Uniform Lake Current of Velocity, U (Ref. 1)

An analysis identical to the one presented in the Offshore Outfall Model concerning the relationship between the two-dimensional nonconservative θ field and conservative X field implies that

$$\theta(x, y) = X(x, y) \exp\left(- \frac{K}{\rho c_p h U} x\right). \tag{7.6}$$

$X(x, y)$ as before satisfies

$$U \frac{\partial X}{\partial x} = - \frac{1}{\rho c_p} \frac{\partial Q_y}{\partial y} \tag{7.7}$$

with the same notation as used above. Attention will thus be focused, as before, upon constructing a solution for the X field for the present physical problem.

Of prime importance in this problem, according to Csanady, is the calculation of nonconservative temperatures at fixed points along the shore. This interest is due to the "coastal-entrapment" phenomenon observed by Csanady for large-scale effluent plumes discharged at or near the shore of lakes in which the plume closely hugs the shore for considerable distances. This was observed, for instance, at Douglas Point by tagging the entire plant flow with a fluorescent tracer. Visual and photographic evidence available from other discharges on the Great Lakes confirms this to be a fairly universal phenomenon. Since temperatures at specific shoreline distances are desired, <u>absolute</u> diffusion of the plume must be considered.

From Csanady's experimental analyses, the standard deviation for a point-source plume located near shore grows more rapidly than would follow from a constant-diffusivity model. Eddies generated by the shore boundary are more efficient mixers than those 2-3 miles offshore. As a crude approximation, Csanady uses

$$S_y = px, \tag{7.31}$$

where p is the nondimensional relative intensity of horizontal lake turbulence. This form for S_y will be discussed in greater detail later.

Arranging point-source plumes, each with a Gaussian format, at all points of $-b < y < b$ (the segment $-b < y < 0$ allows for shoreline reflection of the plumes), the conservative temperature distribution becomes

$$\left.\begin{aligned} \chi(x, y) &= \frac{\chi_0}{\sqrt{2\pi}\, S_y} \int_{-b}^{b} \exp\left[-\frac{(y - y')^2}{2S_y^2}\right] dy' \\ &= \frac{\chi_0}{2}\left(\operatorname{erf}\frac{b - y}{\sqrt{2}\, S_y} + \operatorname{erf}\frac{b + y}{\sqrt{2}\, S_y}\right) \end{aligned}\right\}, \tag{7.32}$$

where $\chi_0 (= \theta_0)$ is the temperature at the line source. This result may also be obtained by solving the diffusion equation with a variable diffusivity. Equation 7.32 gives the solution for the χ field in terms of two nondimensional numbers; i.e.,

$$\chi/\chi_0 = f\left(\frac{y}{px}, \frac{px}{b}\right). \tag{7.33}$$

The total solution given for the θ field is

$$\theta(x, y) = \chi(x, y) \exp\left(-\frac{K}{\rho c_p h U} x\right). \tag{7.34}$$

Isotherms for $\theta(x, y)$ are sketched in Fig. 7.5.

Along the axis of the plume, i.e., at the shoreline,

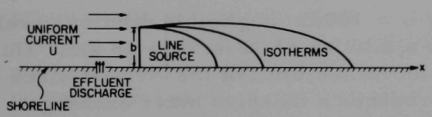

Fig. 7.5. Isotherms as Predicted by the Shoreline Surface-discharge Model

$$\theta_s(x) = \theta_0 \exp\left(-\frac{K}{\rho c_p h U} x\right) \operatorname{erf}\frac{b}{\sqrt{2}\, px}. \tag{7.35}$$

This relationship shows, as before, that at any downstream distance, x, the excess temperature θ_s is equal to θ_0 multiplied by two decay factors, one resulting from surface heat loss, the other due to mixing. The decay of the mixing factor along the plume centerline is plotted in Fig. 7.6.

As explained in the Offshore Outfall Model, the heat-loss factor is negligible for distances near the shore and has significance only for far-downcurrent distances.

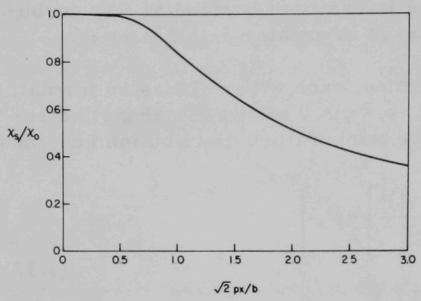

Fig. 7.6. Decay of Maximum Temperature due to Mixing Alone[2]

Analyzing the turbulent-mixing factor is again more complicated. For large longitudinal distances along shore, the error function may be approximated by a linear term. Consequently,

$$\chi_s/\chi_0 = \sqrt{\frac{2}{\pi}}\,\frac{b}{px} \qquad (x \to \infty) \tag{7.36}$$

This is equivalent to placing a point source of strength $q = Ub\chi_0$ at the center of the line source. For small x, $\chi_s = 0.99\,\chi_0$ when

$$\frac{b}{\sqrt{2}\,px} \geq 2 \tag{7.37}$$

and

$$x \leq \frac{b}{2\sqrt{2}\,p} \approx 3b, \tag{7.38}$$

where a typical value of p (= 0.1) was used above. This relatively large distance, 3b, implies that it takes a while for ambient entrainment to penetrate to the centerline. Csanady notes that at 3-4 times this x, the point-source formula (Eq. 7.36) may be used with minimal error. For p = 0.1,

$$\chi_s/\chi_0 \approx 8b/x \qquad (x \to \infty,\ p = 0.1). \tag{7.39}$$

For typical conditions, say b = 100 m, negligible dilution results up to distances of about 1 km, and only a dilution of 30 for x = 25 km. This latter distance may well represent the influence limit of the effluent since by then a current reversal generally produces a massive mass exchange between the shore zone and the main lake mass.

Csanady provides a final insight into his surface-heat-loss and turbulent-mixing factors in the centerline temperature-decay formula by comparing the longitudinal distances required for each factor to drop to half its initial value. The distance at which θ drops off to $\frac{1}{2}\theta_0$ is

$$x_m = 1.47b/p \quad \text{(mixing only)} \tag{7.40}$$

and

$$x_c = 0.694\,\frac{U}{K} \quad \text{(cooling only).} \tag{7.41}$$

For typical input parameters $B = 0.8$, $\rho_w/\rho_a = 800$, $c_{pw}/c_{pa} = 4$, $C = 0.002$, and $U/U_{10} = 0.02$,

$$x_c = 10^4 h. \tag{7.42}$$

Note that x_m and x_c are directly proportional to b and h, respectively. For h = 10 m and b = 100 m, x_c and x_m are calculated to be 100 and 1.5 km, respectively. This implies negligible surface cooling within the region of the plume of greatest interest. The author concludes that his model predicts that turbulent mixing predominates over any surface cooling that may occur to a good degree of approximation over the entire plume. This is expected to be true for moderately deep plumes with a more or less steady current of moderate to high velocity (10-50 cm/sec). Csanady also states that the total dilution predicted by his model is insufficient for most practical applications.

The temperature field θ represents <u>mean</u> values of that quantity amidst turbulent fluctuations superimposed upon it, as generally occurs in turbulent diffusion. However, two methods present themselves for the measurement of such mean temperatures:

(1) A fixed-point mean, implying that temperatures are averaged at a fixed position over a suitably long period of time.

(2) A mean temperature, defined in a frame of reference moving with the center of gravity of a plume.

The second method of measurement ignores any meandering of a plume and considers only diffusion about the center of gravity. The difference lies in that a fixed-point mean may be including zero excess temperatures for periods of time due to the irregular meandering that may occur within the neighborhood of the plume's average path. Temperature profiles measured by either method for a plume following a shoreline turn out quite similar since meandering perpendicular to the shore is less important. However, the period of averaging should be chosen long enough to include several cycles of large eddies contributing to the meandering; in practice, this requires several hours.

(2) <u>The Functional Form S_y</u>. A brief discussion (based on Refs. 1 and 2) will now attempt to describe Csanady's thinking in his use and choice of the functional form for S_y for the present problem of a large-scale plume dispersion from a shoreline outfall in the presence of shore-parallel currents. This discussion will be followed by some general comments on the model itself and its use.

For a fixed frame of reference, horizontal plume dispersion is produced by both relative diffusion and meandering. If S_y is the standard

deviation at a downstream distance x from a continuous point source, then S_y may, in general, be written[4]

$$S_y^2 = \sigma_y^2 + m_y^2 \tag{7.43}$$

where σ_y and m_y are the standard deviations of relative diffusion and meandering, respectively. For $0 < x < 6$ km or so, $m_y \gg \sigma_y$ so that S_y is approximately m_y. From pilot plume data taken by the author (see Fig. 7.7), m_y is approximately linear with a range

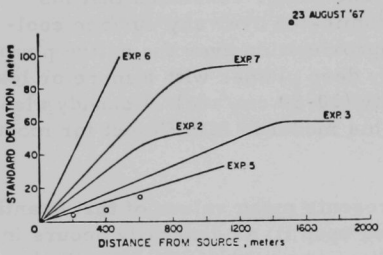

Fig. 7.7. Observed Standard Deviation of Meandering vs Distance (1966 and 1967)[1]

$$0.03x \le m_y \le 0.25x. \tag{7.44}$$

(The experimental data shown in Fig. 7.7 were obtained by aerial photography of apparently steady currents.) Consequently, S_y may be written

$$S_y = px, \tag{7.45}$$

where p is expected to range from 0.03 to 0.25 (from Fig. 7.7). The parameter p is defined as the lateral turbulent intensity in the current regime and may be determined from

$$p = \frac{\sqrt{\overline{v'^2}}}{U}, \tag{7.46}$$

where

v' = the fluctuating turbulent velocity in the lateral direction y

and

U = mean current speed.

A typical value of p is about 0.1.

To properly determine p, direct turbulence measurements need be made for each situation. Moreover, certain parts of the spectrum of velocity fluctuations are irrelevant for the diffusion process at our considered scale of interest. To calculate m_y, the low-frequency end of the spectrum is required since the corresponding eddies contribute to the plume meandering rather than relative diffusion or fluid-particle shape distortions, which are essentially nonvortical (Ref. 1, pp. 84-85).

Equation 7.45 is accurate with a <u>constant</u> p only in the initial phase as the plume from a point source (or equivalently from an infinitesimal element of a line source, as is used here in the Shoreline Surface Discharge Model) grows in essentially a conical shape. Equation 7.45 is roughly valid

when S_y is less than about 2 km. For p = 0.1, this gives a region of validity of Eq. 7.45 for $x < 20$ km. For distances beyond this a diffusivity may be defined or the same Eq. 7.45 used with p allowed to decrease slowly with x to take into account the fact that the linear relationship no longer applies.

In atmospheric diffusion problems, an empirically determined form for S_y is generally introduced. In certain specific cases, S_y grows as x^n with n = 0.85-0.90. To date, lake-diffusion data are inadequate to distinguish between n = 0.85 or 1.0. In lake situations, there have been only scant data available to properly define p for different situations. For this reason, the author uses only a "typical" value of p in his analysis. The parameter p depends on such qualitative phenomena as large-scale lake-flow regimes, shoreline irregularities, and the supply and magnitude of large eddies. At present, the scant experimental results that do exist predict that a linear growth S_y = const.x is acceptable as a very rough approximation where the above proportionality constant may be taken as 0.1 and may vary by a factor of two above or below that value, depending upon the influencing factors previously described.

In addition to the experimental support for Eq. 7.45, there are also possible theoretical justifications. The Taylor theory of turbulence for homogeneous fluids predicts the variation of width by Eq. 7.45 along the initial stages of spreading for an effluent from a continuous point source. Although the existence of a lake plume precludes a completely homogeneous medium, the assumptions of Taylor's theory may be applied as an approximate means is generally supported by empirical data.

Due to the above uncertainties in the formula for $S_y = 0.1x$, Csanady suggests that field data be taken at different downstream distances to more accurately determine p. If p changes downstream, this should be included in the model solution. If no experimental data on S_y can be obtained, fitting the model to the plume-temperature data is the only alternative to the roughly approximate assumption of $S_y = 0.1x$.

(3) General Comments about the Surface-discharge Model. The simplifications and limitations of the present model are several. First, buoyant convective motions are not considered, implying that the model should be applied only when relatively small temperature differences exist. Second, variable bottom effects are not included. A shallow bottom generally creates additional vertical turbulence and smaller-scale eddies, which is an additional aid to mixing and heat dissipation. Csanady's chosen form for S_y attempts, in a rough approximate manner, to account for additional eddies generated by the shore boundary. Third, the validity of the S_y functional form itself has not really been verified for water systems. The variation of p with distance needs a great deal of further study. The measurements for p and, consequently, S_y with distance are difficult

and considerably complicate model verification. This uncertainty with the plume's lateral-diffusion characteristics adversely affects the model's predictive capability. Fourth, the rule of thumb handling the jet mixing is extremely crude, as is Csanady's advice on the proper placement of the line source. One should understand that these crude approximations are really secondary in the model development and that they represent an uncomplicated method to initiate the far-field analysis. Finally, the plume depth is generally unknown, yet required as input to the far-field model. Csanady's Shoreline Surface Discharge Model as well as his Offshore Outfall Model are presently untested with field data.

(4) Csanady's Conclusions Based upon His Models. Each of the two models discussed above predicts a small dilution, even at large distances from the line source. Csanady proposes that the best way to dilute the initial discharge is to mix it before it goes out into the lake or mix at very close to the discharge. For large initial temperatures, an efficiently designed diffuser with a number of high-velocity jets may well be satisfactory, since it produces its own turbulence in addition to using the natural lake turbulence for mixing. Also, discharging effluents at lake bottom and beyond the influence of the coastal jets at distances of about 5 miles offshore may also prevent a shoreward return of the heated effluent.

For shoreline discharges, Csanady suggests that large rocks or even sunken wrecks in the path of the effluent jet will cause additional artificial turbulence to increase the dilution.

(5) Final Comment. Keep in mind, in applying Csanady's models, that phenomena such as stagnation periods of the ambient current where $U \approx 0$, density stratification which inhibits plume spreading, and recirculation affecting the flow field, cause these models to be oversimplified and should be supplemented by other considerations.

References

1. G. T. Csanady, Dispersal of Effluents in the Great Lakes, Water Research 4, 79-114 (Jan 1970).

2. G. T. Csanady, Waste Heat Disposal in the Great Lakes, University of Waterloo (1970).

3. N. H. Brooks, "Diffusion of Sewage Effluent in an Ocean Current," Proc. 1st Int. Conf. Waste Disposal in the Marine Environment, Pergamon Press, Oxford (1960).

4. G. K. Batchelor, "Diffusion in a Field of Homogeneous Turbulence," Proc. Camb. Phil. Soc. 48, 345-362 (1952).

5. Henry Stommel, Horizontal Diffusion due to Oceanic Turbulence, J. Marine Research VIII, 199-225 (1949).

6. Jerry Yudelson, A Survey of Ocean Diffusion Studies and Data, W. M. Keck Laboratory of Hydraulics and Water Resources, California Institute of Technology, Pasadena, Calif. (1967).

8. TOPLYR-II, A Two-dimensional Thermal-energy Transport Code[1]

D. C. Kolesar and J. C. Sonnichsen, Jr.
Hanford Engineering Development Laboratory
October 1971

a. List of Symbols

BR	$6.1 \times 10^{-4} P(T_a - T_w)/(e_0 - e_a)$
c_p	Water-heat capacity at constant pressure
E	Error vector
e_a	Partial vapor pressure of air
e_0	Vapor pressure of water
h	Depth of river
L	Longitudinal length of flow field
L_0	Latent heat of vaporization of water
ℓ_t, ℓ_x, ℓ_y	Finite-difference increments
N	Conversion factor = 1.164×10^{-9} m/hr-mbar
P	Average atmospheric pressure on water surface
q	Effective air-water surface energy flux
Q	$2\ell_t q/\rho c_p h$
Q_b	Back radiation
Q_e	Evaporative heat exchange
Q_h	BRQ_e
Q_r	Reflected radiation from the water surface
Q_s	Short-wave radiation measured by a radiometer
q_z	$\sum(Q_s - Q_r) - Q_b - Q_e \pm Q_h$
r_x, r_y	$\ell_t/\ell_x^2, \ell_t/\ell_y^2$
s_x, s_y	$\ell_t/\ell_x, \ell_t/\ell_y$
t	Time variable
T	Temperature
T*	Temperature at end of half time-step
T_a	Mean absolute air temperature
T_w	Absolute temperature of water surface
u	Longitudinal velocity

U	Wind velocity (meters/hr)
v	Lateral velocity
w	Lateral width of flow field
x	Longitudinal distance, independent variable
y	Lateral distance, independent variable
α_x, α_y	Longitudinal and lateral thermal diffusivities
β, γ	Finite-difference splitting parameters
β_0	Atmospheric radiation factor derived from the cloud cover
δ	Central-difference operator
ρ	Density of plume water
σ	Stefan-Boltzmann radiation constant

Subscripts and superscripts

A	Identification on purely convective temperature distribution, which specifies that a second law like correction has been made
C	Identification on purely convective temperature distribution
I	Value of i at exit section
i, j, k	Row, column, and time mesh-point identification
j_*	Value of j along plume centerline
t, x, y	Time and distance (longitudinal and lateral) association

b. Introduction

The numerical model developed by Kolesar and Sonnichsen treats the problem of the far-field dispersion of a heated effluent in bodies of water in which the initial momentum of the source and the plume buoyancy no longer affect the flow. This far-field model yields a two-dimensional transient temperature distribution upon input of the two-dimensional, time-independent velocity distribution and horizontal eddy thermal diffusivities. Model computations begin at a far-field cross section, at which the temperature distribution is specified as a function of time, and extend to a further downstream cross section, at which only the initial temperature distribution is given. The model handles a variable bottom contour, but assumes no vertical variation in velocity and temperature below the surface. Atmospheric heat loss from the plume is also included. An alternating-direction implicit algorithm is used to solve the finite-difference relationships written for the energy-conservation equation. The HEDL numerical model is coded for a river situation, yet has built-in options to handle a given lake-plume problem.

TOPLYR-II is a modification of the TOPLYR* code[2] in which second-order accurate difference equations are used rather than first-order relationships to reduce the numerical errors resulting from the TOPLYR finite-difference scheme. The ultimate goal of the HEDL investigators is to develop a complete numerical plume model which is valid for the jet, transition, and far-field regions. An accurate numerical simulation of such phenomena as the momentum interaction of the jet and ambient current, buoyant spreading, and drift-zone dispersion involves numerous complexities. The authors, consequently, embarked on a stepwise procedure in the development of their total-model concept. TOPLYR-I and -II treat the far-field region in which buoyancy effects and initial jet momentum are assumed negligible. The next step in their program will be the development of TOPLYR-III, which will handle the buoyancy mechanism that will involve the treatment of the transition zone between the jet and far-field regimes. This anticipated pseudo three-dimensional model would incorporate momentum balances in the horizontal and vertical directions, maintaining essentially the same principles as in TOPLYR-II for the horizontal axial direction. This new model would still exclude other effects that would be important in the jet regime. When TOPLYR-III is completed, a jet model would be developed to treat the initial jet interaction with the receiving water.

The advantages of this model development procedure (far field to near field) are several. First, each improvement can be added to the basic model with much of the previous code being salvaged. Second, most of the field data presently available for model verification was obtained in the far field, which encourages model development from that end. Third, the far-field or drift zone is simplest to model since lateral density gradients are generally small. It is typical in that region to neglect the interaction between buoyancy and flow and thus analyze the hydraulic problem separate from the heat diffusion. Velocity distributions then calculated from hydraulic analyses or estimated from field measurements may then be used as known input to compute the convective terms in the heat-transport equation. This latter procedure was used in TOPLYR-I and -II.

The major disadvantage of this approach, at least in the development of TOPLYR-II, is the severely limited applicability of the resulting far-field code as a predictive device. The input conditions required for TOPLYR-II are:

(1) Problem geometry.

(2) Time-dependent meteorological parameters.

(3) Horizontal eddy-thermal diffusivities.

---

*The original TOPLYR code[2] will be denoted TOPLYR-I in the present discussion.

(4) Initial temperature distribution at the inlet and outlet far-field cross sections bounding the lake or river region of interest.

(5) Inlet and outlet axial velocity distributions.

(6) Time-dependent inlet temperature distribution.

(7) Convergence criteria.

(8) Alternating-direction implicit (A.D.I.) splitting parameters β and γ (to be discussed later).

Items 3-6 are not usually known in advance, requiring estimates from field data previously taken at the site in question, if available. Even with estimates on the diffusivities, the time-dependent temperature distribution at the far-field source cross section and the far-field axial velocity distribution are generally unknown for lake situations. In spite of this limitation on the present version of TOPLYR, the authors consider the code as a first step toward a useful and complete predictive numerical model. The authors point out that their present code was originally designed to test certain existing experimental data and it could have taken a different and apparently more useful form had the original purpose for the development of the model been more general.

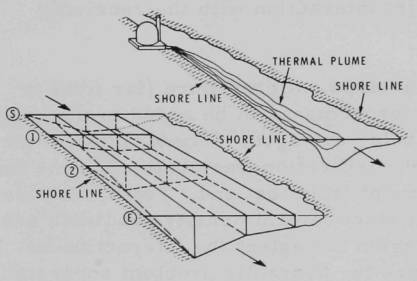

Fig. 8.1. Elemental (Nodal) Approximation to River Contours[1a]

c. Model Description

(1) The Physical System and Main Assumptions. The physical system being analyzed is represented in Fig. 8.1. One shoreline is assumed straight (denoted "left bank"); the opposite shoreline changes depending upon the river width or lake breadth. The thermal plume is assumed to be well within these shore boundaries. In a lake situation, a code option permits the transformation of the left bank into a line of symmetry when a symmetrical plume is expected within some infinite medium. The region between two plume cross sections in the far field is analyzed, these sections denoted source (inlet) and exit (outlet). The bottom depth and a time-independent mean axial velocity is assumed to be specified at each of these two cross sections.

The source cross section is assumed to be sufficiently downcurrent so that the initial momentum of the discharge and any residual buoyant spreading of the actual heat source is negligible. The plume is assumed to be fully mixed vertically with no variation in plume properties below the water surface. TOPLYR-II would hence be applicable to relatively shallow rivers or lakes when no stratification exists and where the plume

extends down to the entire receiving-body depth. For deeper bodies of water with or without stratification, the bottom contours should be replaced by the bottom of the thermal plume or the bottom of the epilimnetic region, depending upon which is more applicable in a given situation. If no field data are available to provide an estimate of plume depth, the authors recommend the choice of a constant depth of 10 ft, based mainly upon the observations of a wide variety of lake-plume data made by Pritchard.[3]

The actual heat source is introduced as a time-dependent boundary condition on the source cross section. If a thermal plume exists in the river or lake initially, the temperature distribution over the inlet (as a function of time) and outlet (initial time only) sections must be specified. Optionally, the inlet temperature may be given as a function of time, with the outlet section being equated initially to ambient temperature.

The computer code superimposes a given model mesh on the river (or lake region) and approximates the river's (or plume's) intermediate bottom contour, initial temperature, and axial speed by linear interpolation carried out by a subroutine applied on the initial data. The "right side" of the nodal mesh is terminated in the river or lake, thereby maintaining rectangular cells. The numerical simulation assumes that the region beyond the neighborhood of the plume does not affect the analysis and may be removed from the problem domain and replaced by a zero-heat-flux condition at those grid edges. This will be valid for a large river or a large lake or in situations with two straight shoreline boundaries.

A subroutine (CHANL) computes lateral velocities based upon continuity requirements at each grid cell, thereby establishing mass transport across each longitudinal cross section determined by the grid. Due to inaccuracies in data collection, it may occur that the net mass entering the inlet section is not equal to the net mass as measured exiting the outlet section. A 15% discrepancy in net mass through these sections is permitted by the code. If discrepancies exist, it is arbitrarily assumed that the axial velocities inputted in the source section are accurate; the outlet axial velocities are each adjusted by the ratio of net outlet mass to net inlet mass to maintain mass conservation.

The main assumptions in the model are:

(1) Steady-state situation with regard to turbulent fluctuations.

(2) Two-dimensional flow and energy transfer.

(3) No buoyant spread included in diffusion mechanism.

(4) Depth, velocity, and initial temperature profiles varying linearly between inlet and outlet sections.

(5) Incompressible plume water.

(6) Straight shoreline or line of symmetry.

(7) Zero heat flux at shore and right grid boundary.

Variation in river depth causes a relocation of the thermal plume due to the resulting transverse flow. The changing cross-sectional area at each station yields a variation in the thermal-energy flux. The variable volume of fluid between cross sections affects the heat contained and consequently alters the atmospheric-heat-loss term. Energy is transported solely by advection due to the mean current, turbulent diffusion, and atmospheric heat loss. (The inclusion of buoyancy effects would necessarily involve a three-dimensional structure, which would require a description of the additional lateral-convective motion expected.)

(2) Derivation of Equations and Boundary Conditions. The authors derive the equations to be solved by making an energy and mass balance on a typical cell of the grid. Depths and temperatures are specified in the center of each cell with longitudinal and lateral velocities specified on the edges of the cell.

An energy balance carried out on the central cell is shown in Fig. 8.2, where

c_p = specific heat (constant),

ρ = density (assumed constant),

x = distance measured longitudinally downcurrent,

y = lateral distance,

q_z = heat loss to the atmosphere,

q_x, q_y = heat flux in x, y directions given by the Fourier law of energy transport,

$$q_x = \rho c_p \alpha_x \frac{\partial T}{\partial x},$$

$$q_y = \rho c_p \alpha_y \frac{\partial T}{\partial y},$$

α_x, α_y = eddy thermal diffusivities (assumed constant) in x, y directions,

and

T = temperature at (x, y).

Equation A in Fig. 8.2 represents this energy balance, and if that expression is divided by $(\Delta x \Delta y h_{i,j} \rho c_p)$ and the limit is taken as $\Delta x, \Delta y \to 0$, Eq. B results, where the following approximations were used:

$$\left.\begin{aligned} h_{i,j} &= \tfrac{1}{2}\left(h_{i,j+\frac{1}{2}} + h_{i,j-\frac{1}{2}}\right) \\ \text{and} \qquad & \\ h_{i,j} &= \tfrac{1}{2}\left(h_{i-\frac{1}{2},j} + h_{i+\frac{1}{2},j}\right) \end{aligned}\right\}. \tag{8.1}$$

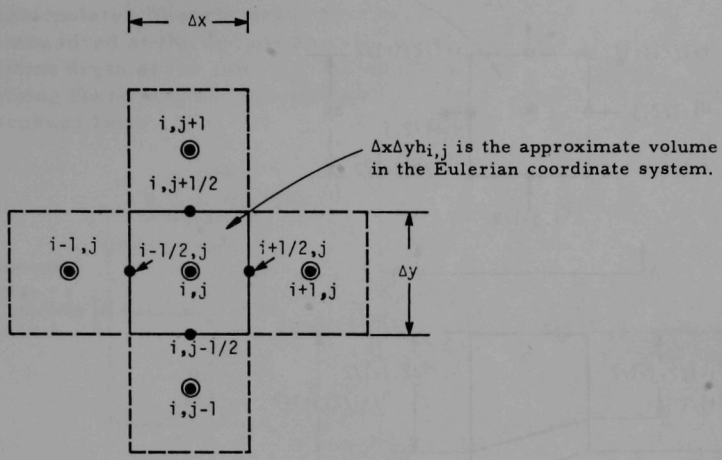

Energy Balance

$$\begin{aligned} \Delta x\Delta y h_{i,j}\left[\frac{\partial}{\partial t}(\rho c_p T)\right]_{i,j} = {} & \Delta y h_{i-\frac{1}{2},j}(\rho u c_p T)_{i-\frac{1}{2},j} - \Delta y h_{i+\frac{1}{2},j}(\rho u c_p T)_{i+\frac{1}{2},j} \\ & + \Delta x h_{i,j-\frac{1}{2}}(\rho v c_p T)_{i,j-\frac{1}{2}} - \Delta x h_{i,j+\frac{1}{2}}(\rho v c_p T)_{i,j+\frac{1}{2}} \\ & - \Delta y h_{i-\frac{1}{2},j}(q_x)_{i-\frac{1}{2},j} + \Delta y h_{i+\frac{1}{2},j}(q_x)_{i+\frac{1}{2},j} \\ & - \Delta x h_{i,j-\frac{1}{2}}(q_y)_{i,j-\frac{1}{2}} + \Delta x h_{i,j+\frac{1}{2}}(q_x)_{i,j+\frac{1}{2}} \\ & + \Delta x\Delta y (q_z)_{i,j}. \end{aligned} \tag{A}$$

Dividing by $\rho c_p \Delta x \Delta y h_{i,j}$ and using Eqs. 8.1-8.4 when Δx, $\Delta y \to 0$ yields

$$\frac{\partial T}{\partial t} = -\frac{1}{h}\frac{\partial}{\partial x}(huT) - \frac{1}{h}\frac{\partial}{\partial y}(hvT) + \frac{\alpha_x}{h}\frac{\partial}{\partial x}\left(h\frac{\partial T}{\partial x}\right) + \frac{\alpha_y}{h}\frac{\partial}{\partial y}\left(h\frac{\partial T}{\partial y}\right) + \frac{q_z}{\rho c_p h}. \tag{B}$$

Fig. 8.2. Derivation of Energy Equation[1]

A mass balance is carried out in Fig. 8.3. The resulting relationship (Eq. C) is used to evaluate the lateral velocities v at each cell. This is done cell by cell, starting from the source cells using the boundary

conditions on u and v (to be described later). For each cell, $u_{i-\frac{1}{2},j}$, $v_{i+\frac{1}{2},j}$, and $v_{i,j-\frac{1}{2}}$ are known, whereby $v_{i,j+\frac{1}{2}}$ can be calculated.

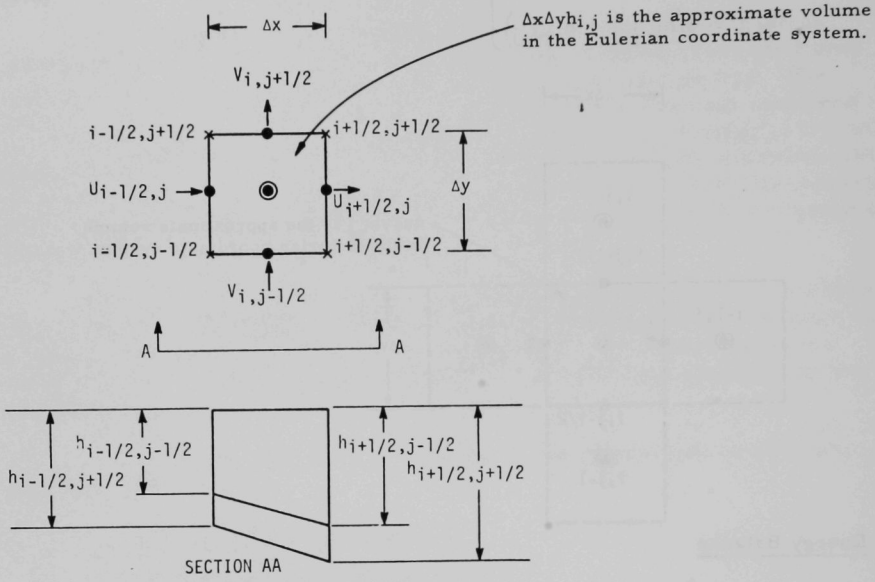

NOTE: $u_{i-\frac{1}{2},j}$, $u_{i+\frac{1}{2},j}$, $v_{i,j-\frac{1}{2}}$ ARE KNOWN

Mass Balance

$$\Delta y\left[h_{i-\frac{1}{2},j-\frac{1}{2}} + \tfrac{1}{2}\left(h_{i-\frac{1}{2},j+\frac{1}{2}} - h_{i-\frac{1}{2},j-\frac{1}{2}}\right)\right] u_{i-\frac{1}{2},j} + \Delta x\left[h_{i-\frac{1}{2},j-\frac{1}{2}} + \tfrac{1}{2}\left(h_{i+\frac{1}{2},j-\frac{1}{2}} - h_{i-\frac{1}{2},j-\frac{1}{2}}\right)\right] v_{i,j-\frac{1}{2}} =$$

$$\Delta y\left[h_{i+\frac{1}{2},j-\frac{1}{2}} + \tfrac{1}{2}\left(h_{i+\frac{1}{2},j+\frac{1}{2}} - h_{i+\frac{1}{2},j-\frac{1}{2}}\right)\right] u_{i+\frac{1}{2},j} + \Delta x\left[h_{i-\frac{1}{2},j+\frac{1}{2}} + \tfrac{1}{2}\left(h_{i+\frac{1}{2},j+\frac{1}{2}} - h_{i-\frac{1}{2},j+\frac{1}{2}}\right)\right] v_{i,j+\frac{1}{2}}. \qquad \text{(C)}$$

Dividing by $\Delta x\Delta y$ and using Eqs. 8.3 and 8.4 as Δx, $\Delta y \to 0$ yields

$$\frac{\partial(hu)}{\partial x} + \frac{\partial(hv)}{\partial y} = 0. \qquad \text{(D)}$$

Fig. 8.3. Derivation of Continuity Equation[1]

Figure 8.4 illustrates the boundary conditions specialized to a nonsymmetrical river or lake situation. The situation of a completely symmetrical plume in essentially an infinite medium will be discussed shortly. The shoreline and bottom are assumed to maintain zero heat flux in the normal direction. The "right side" of the two-dimensional mesh is assumed to be sufficiently far removed from the plume to be unaffected by it; the authors assume zero heat flux across that fictitious boundary there also. Longitudinal velocities at that grid boundary are determined from linear interpolation of the inlet and outlet velocities u. The lateral velocities v

are derived from the mass balance. The shoreline is regarded as a no-slip surface in which the depth is assumed to be uniform. For the line-of-symmetry option, when a plume is flowing with the ambient current unrestricted by boundaries, the zero-heat-flux condition still holds at the centerline due to symmetry, yet the u must be specified as a function of longitudinal distance (v = 0 by symmetry) in order to apply the code. At present, the code interpolates linearly using the values of u at the input and outlet boundaries measured at the endpoints of the line of symmetry. For this option, the bottom depth at the line of symmetry may vary arbitrarily. The method of applying these boundary conditions to the finite-difference scheme will be discussed later.

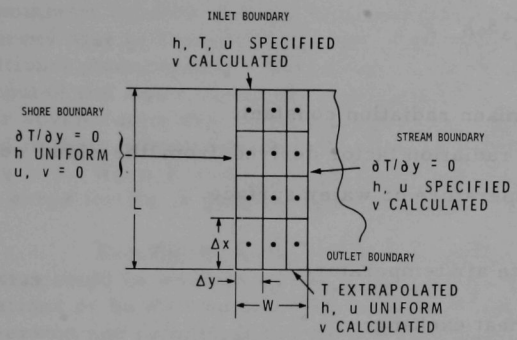

Fig. 8.4

Geometry and Boundary Conditions of TOPLYR-II Model[1a]

Table 8.1 describes the quantities and equations used to calculate the heat exchange at the surface. The determination of q_z follows primarily the Lake Hefner heat-budget calculations[4] as employed by Sonnichsen and Oster,[5] except that the convective loss was based upon the Bowen ratio.[6] According to the authors, their heat-exchange model is applied to river situations, even though the rivers and lakes have different internal motions and will consequently have different heat-exchange rates. They assert that at present, no suitable surface exchange model for rivers exists. Moreover, the Lake Hefner results apply to a lake in an arid region; applying it to a lake in a humid area might yield a significant error. This potential difficulty should be realized in any model application.

(3) Complexities of the Numerical Solution. The solution of Eq. B by finite differences must handle a number of difficulties that arise in the numerical simulation of convective diffusion equations. Equation B will behave like a parabolic equation when diffusion dominates, and like a hyperbolic problem when convection predominates. In the general situation, hyperbolic and parabolic effects will both be present. Due to the convective terms in Eq. B, any numerical scheme will yield some "numerical dispersion." This is defined as the discrepancy that results between the exact solution to the differential equations and that of the finite-difference numerical scheme. Since hyperbolic equations involve the propagation of waves,

TABLE 8.1. Energy-exchange Process at Water Surface

$$q_z = \sum(Q_s - Q_r) - Q_b - Q_e \pm Q_h,$$

where

Q_s = short-wave radiation measued by a radiometer,

Q_r = reflected radiation from water surface,

and

Q_b = back radiation.

$$Q_b = 0.970\sigma(T_w^4 - T_a^4\beta_0),$$

where

σ = Stefan-Boltzmann radiation constant,

β_0 = atmospheric radiation factor derived from the cloud cover,

T_w = absolute temperature of water surface,

and

T_a = mean absolute air temperature.

Q_e = evaporative heat exchange

$$= \rho L_0 NU(e_0 - e_a),$$

where

ρ = density of water,

L_0 = latent heat of vaporization of water,

N = conversion factor = 1.164×10^{-9} m/hr-mbar,

U = wind velocity (meters/hr),

e_0 = vapor pressure of water (mbars),

and

e_a = partial vapor pressure of air (mbars).

Q_h = conduction/convection heat loss

$$= BRQ_e,$$

where

$$BR = 6.1 \times 10^{-4}P(T_a - T_w)/(e_0 - e_a).$$

(P = average atmospheric pressure on water surface.)

such numerical errors in the finite-difference approximation will propagate at a different speed than the theoretical solution and may be amplified, depending upon the nature of the numerical scheme. The numerical method used by Kolesar and Sonnichsen uses a time centering with a three-time-level approximation for the temperature at a given node for the convective and diffusive terms. This technique greatly diminishes numerical dispersion, but does not completely eliminate it. Only in higher-order-differences approximations would one achieve more satisfactory success.

A second effect, known as "numerical diffusion," occurs due to the accumulation of truncation error in the numerical approximation. This phenomenon depends strictly on the numerical scheme. The errors thereby incurred may be thought of as possessing their own "diffusivity," causing an additional plume spread. This produces a second discrepancy between the computed and exact solutions. The authors reduce numerical diffusion by their specification that the two arbitrary splitting parameters β and γ defined in their alternating-direction implicit (A.D.I.) technique satisfy $\beta + \gamma = 1$. When β and γ are so chosen, the principal part of the truncation error for Eq. B yields a better than second-order correction.

For Eq. B, further reduction of numerical diffusion and dispersion could be attained by employing higher-order-accuracy difference equations or be eliminated by the method of characteristics. Numerical dispersion and numerical diffusion will occur in some form for <u>all</u> numerical methods for <u>every</u> differential equation. Although never completely eliminated, these errors may be reduced depending upon the scheme used and the differential equation involved. Moreover, one cannot, in general, distinguish between the contributions of each in the total numerical discrepancy between computed and exact values. The authors disagree with statements made by other investigators of hyperbolic and convective-diffusion problems that time centering and the use of three time levels, as accomplished in TOPLYR-II, <u>completely</u> eliminate numerical diffusion.

A third complexity handled in TOPLYR-II is the problem of "nonphysical values." This occurs when the temperature at a given node is calculated as being higher than the values used to compute it, clearly violating the second law of thermodynamics. There is not much literature on this subject. The investigations previously made indicate that nonphysical values are potentially possible in all purely hyperbolic problems. Also, remarks made by some investigators seem to indicate that nonphysical values may also be found in convective-diffusion problems. Indeed, certain problems not solely involving convection but including some diffusion, i.e., problems in which heat is readily diffused, have been known to produce nonphysical values in certain numerical routines. For a purely hyperbolic problem or a purely convective situation in Eq. B, these nonphysical values tend to be periodic in character. If these periodic oscillations superimposed on the solution grew in an unbounded way, the solution would be unstable.

There have been problems in which bounded nonphysical value oscillations do occur. This follows from the hyperbolic nature of the problems since, for a hyperbolic equation, the solution may be broken down into a sum of wave modes. When diffusion is also present, these ripples in the solution become damped out with time. Potential nonphysical values that may occur are handled in TOPLYR-II by an implementation of the Hain scheme. This method requires that any newly computed value of the dependent variable will be within the range of the values of the dependent variable used to compute it. In applications of TOPLYR-II to actual river situations, no actual nonphysical values have yet occurred; only in a contrived one-dimensional problem were they observed, requiring the utilization of the Hain method.

(4) The TOPLYR-II Numerical Scheme. The actual numerical scheme used in TOPLYR-II will now be described. If δ_x, δ_y refer to central difference operators in the x, y directions, respectively, Eq. B in difference form becomes

$$\frac{h_{i,j}}{2\ell_t}\left(T_{i,j}^{k+1} - T_{i,j}^{k-1}\right) = -\frac{1}{\ell_x}\,\delta_x(huT)_{i,j}^{k} - \frac{1}{\ell_y}\,\delta_y(hvT)_{i,j}^{k}$$

$$+ \frac{\alpha_x}{\ell_x^2}\,\delta_x h_{i,j}\delta_x T_{i,j}^{k} + \frac{\alpha_y}{\ell_y^2}\,\delta_y h_{i,j}\delta_y T_{i,j}^{k} + \frac{q_{i,j}^{k}}{\rho c_p}, \quad (8.2)$$

where ℓ_x, ℓ_y, and ℓ_t are the finite-difference increments in x, y, and t, and i, j, and k refer to row x, column y, and time-mesh identification, respectively. Multiplying Eq. 8.2 by $2\ell_t/h_{i,j}$, and replacing $T_{i,j}^{k}$ on the right-hand side of Eq. 8.2 by the time-centered, three-time-level approximation

$$T_{i,j}^{k} \rightarrow \frac{1}{3}\left(T_{i,j}^{k+1} + T_{i,j}^{k} + T_{i,j}^{k-1}\right), \quad (8.3)$$

yields

$$T_{i,j}^{k+1} + \frac{2}{3}\,\frac{s_x}{h_{i,j}}\,\delta_x(huT)_{i,j}^{k+1} + \frac{2}{3}\,\frac{s_y}{h_{i,j}}\,\delta_y(hvT)_{i,j}^{k+1} - \frac{2}{3}\,\frac{\alpha_x r_x}{h_{i,j}}\,\delta_x h_{i,j}\left(\delta_x T_{i,j}^{k+1}\right)$$

$$- \frac{2}{3}\,\frac{\alpha_y r_y}{h_{i,j}}\,\delta_y h_{i,j}\delta_y T_{i,j}^{k+1} = f\left(T_{i,j}^{k}, T_{i,j}^{k-1}, q_{i,j}^{k}\right), \quad (8.4)$$

where

$$r_x = \ell_t/\ell_x^2, \quad r_y = \ell_t/\ell_y^2, \text{ and } s_x = \ell_t/\ell_x, \quad s_y = \ell_t/\ell_y.$$

This may be written in operator notation as

$$(1 + A_x + A_y - B_x - B_y)\, T_{i,j}^{k+1} = (-A_x - A_y + B_x + B_y)\, T_{i,j}^{k+1} + Q_{i,j}^{k}$$

$$+ (1 - A_x - A_y + B_x + B_y)\, T_{i,j}^{k-1}, \qquad (8.5)$$

where the operators 1, A_x, A_y, $-B_x$, and $-B_y$ applied to $T_{i,j}^{k+1}$ are given by the first five terms of Eq. 8.4. The operator $Q_{i,j}^{k}$ is given by

$$Q_{i,j}^{k} = \frac{q_{i,j}^{k}}{\rho c_p}.$$

Following the usual technique when handling convective-diffusion problems, the authors complete the square on the left-hand side of Eq. 8.5 and introduce two arbitrary parameters β and γ:

$$(1 + A_x - B_x)(1 + A_y - B_y)\, T_{i,j}^{k+1} =$$

$$[-A_x - A_y + B_x + B_y + (A_xA_y - A_xB_y - A_yB_x + B_xB_y)\,\beta]\, T_{i,j}^{k} + Q_{i,j}^{k}$$

$$+ [1 - A_x - A_y + B_x + B_y + (A_xA_y - A_xB_y - A_yB_x + B_xB_y)\,\gamma]\, T_{i,j}^{k-1}. \qquad (8.6)$$

These parameters define the character of the A.D.I. splitting and affect the stability of the solution. From Eq. 8.6, temperatures at times k and k + 1 are operated on to yield the system of temperatures at time k + 1. In the A.D.I. method, one works with two time steps as one unit. In the authors' application, information is known at times k - 1 and k, whereby difference equations are defined for times k + 1* and k + 1. Each of the two sets of equations is in tridiagonal form and may be readily solved; the first set is solved row by row, the second column by column. In operator notation, the authors divide Eq. 8.6 into

$$(1 + A_x - B_x)\, T_{i,j}^{k+1} = [-A_x - A_y + B_x + B_y + (-A_y + B_y)\,\beta]\, T_{i,j}^{k}$$

$$+ [-A_x - A_y + B_x + B_y + (-A_y + B_y)\,\gamma]\, T_{i,j}^{k-1} + Q_{i,j}^{k} \qquad (8.7)$$

and

$$(1 + A_y - B_y)\, T_{i,j}^{k+1} = T_{i,j}^{k+1*} + (A_y - B_y)\left(\beta T_{i,j}^{k} + \gamma T_{i,j}^{k-1}\right). \qquad (8.8)$$

Equation 8.6 involves variation in time k + 1* only within rows; Eq. 8.7 has variation at time k + 1 only within columns. The method of splitting up Eq. 8.6 is not unique. The choice made was based upon the

experience of other investigators and simple intuition. The authors wanted their most difficult terms in the first half-time step; the expression involving the second time step would then alleviate the difficulties built up on the first half-time step. In nodal notation, Eqs. 8.7 and 8.8 become

$$\left(\frac{s_x}{3} u_{i+1,j} \frac{h_{i+1,j}}{h_{i,j}} - \frac{2\alpha_x r_x}{3} \frac{h_{i+\frac{1}{2},j}}{h_{i,j}}\right) T^{k+1*}_{i+1,j} + \left(1 + \frac{2\alpha_x r_x}{3} \frac{h_{i+\frac{1}{2},j} + h_{i-\frac{1}{2},j}}{h_{i,j}}\right) T^{k+1*}_{i,j}$$

$$- \left(\frac{s_x}{3} u_{i-1,j} \frac{h_{i-1,j}}{h_{i,j}} + \frac{2\alpha_x r_x}{3} \frac{h_{i-\frac{1}{2},j}}{h_{i,j}}\right) T^{k+1*}_{i-1,j} = \left(- \frac{s_x}{3} u_{i+1,j} \frac{h_{i+1,j}}{h_{i,j}}\right.$$

$$\left. + \frac{2\alpha_x r_x}{3} \frac{h_{i+\frac{1}{2},j}}{h_{i,j}}\right)\left(T^{k}_{i+1,j} + T^{k-1}_{i+1,j}\right) - \left[\frac{4\alpha_x r_x}{3} \frac{h_{i+\frac{1}{2},j} + h_{i-\frac{1}{2},j}}{h_{i,j}}\right.$$

$$\left. + \frac{2\alpha_y r_y}{3} (1+\beta) \frac{h_{i,j+\frac{1}{2}} + h_{i,j-\frac{1}{2}}}{h_{i,j}}\right] T^{k}_{i,j} + \left(\frac{s_x}{3} u_{i-1,j} \frac{h_{i-1,j}}{h_{i,j}} + \frac{2\alpha_x r_x}{3} \frac{h_{i-\frac{1}{2},j}}{h_{i,j}}\right)\left(T^{k}_{i-1,j} + T^{k-1}_{i-1,j}\right)$$

$$+ \left[- \frac{s_y}{3} (1+\beta) v_{i,j+1} \frac{h_{i,j+1}}{h_{i,j}} + \frac{2\alpha_y r_y}{3} (1+\beta) \frac{h_{i,j+\frac{1}{2}}}{h_{i,j}}\right] T^{k}_{i,j+1} + \left[\frac{s_y}{3} (1+\beta) v_{i,j-1} \frac{h_{i,j-1}}{h_{i,j}}\right.$$

$$\left. + \frac{2\alpha_y r_y}{3} (1+\beta) \frac{h_{i,j-\frac{1}{2}}}{h_{i,j}}\right] T^{k}_{i,j-1} + \left[1 - \frac{2\alpha_x r_x}{3} \frac{h_{i+\frac{1}{2},j} + h_{i-\frac{1}{2},j}}{h_{i,j}}\right.$$

$$\left. - \frac{2\alpha_y r_y}{3} (1+\gamma) \frac{h_{i,j+\frac{1}{2}} + h_{i,j-\frac{1}{2}}}{h_{i,j}}\right] T^{k-1}_{i,j} + \left[- \frac{s_y}{3} (1+\gamma) v_{i,j+1} \frac{h_{i,j+1}}{h_{i,j}}\right.$$

$$\left. + \frac{2\alpha_y r_y}{3} (1+\gamma) \frac{h_{i,j+\frac{1}{2}}}{h_{i,j}}\right] T^{k}_{i,j+1} + \left[\frac{s_y}{3} (1+\gamma) v_{i,j-1} \frac{h_{i,j-1}}{h_{i,j}}\right.$$

$$\left. + \frac{2\alpha_y r_y}{3} (1+\gamma) \frac{h_{i,j-\frac{1}{2}}}{h_{i,j}}\right] T^{k}_{i,j-1} + Q^{k}_{i,j} \tag{8.9}$$

and

$$\left(\frac{s_y}{3} v_{i,j+1} \frac{h_{i,j+1}}{h_{i,j}} - \frac{2\alpha_y r_y}{3} \frac{h_{i,j+\frac{1}{2}}}{h_{i,j}}\right) T^{k+1}_{i,j+1} + \left(1 + \frac{2\alpha_y r_y}{3} \frac{h_{i,j+\frac{1}{2}} + h_{i,j-\frac{1}{2}}}{h_{i,j}}\right) T^{k+1}_{i,j}$$

$$- \left(\frac{s_y}{3} v_{i,j-1} \frac{h_{i,j-1}}{h_{i,j}} + \frac{2\alpha_y r_y}{3} \frac{h_{i,j-\frac{1}{2}}}{h_{i,j}}\right) T^{k+1}_{i,j} = T^{k+1*}_{i,j} + \left(\frac{\beta s_y}{3} v_{i,j+1} \frac{h_{i,j+1}}{h_{i,j}}\right.$$

$$\left. - \frac{2\beta\alpha_y r_y}{3} \frac{h_{i,j+\frac{1}{2}}}{h_{i,j}}\right) T^{k}_{i,j+1} + \left(\frac{2\beta\alpha_y r_y}{3} \frac{h_{i,j+\frac{1}{2}} + h_{i,j-\frac{1}{2}}}{h_{i,j}}\right) T^{k}_{i,j}$$

$$- \left(\frac{\beta s_y}{3} v_{i,j-1} \frac{h_{i,j-1}}{h_{i,j}} + \frac{2\beta\alpha_y r_y}{3} \frac{h_{i,j-\frac{1}{2}}}{h_{i,j}}\right) T^{k}_{i,j-1} + \left(\frac{\gamma s_y}{3} v_{i,j+1} \frac{h_{i,j+1}}{h_{i,j}}\right.$$

$$\left. - \frac{2\gamma\alpha_y r_y}{3} \frac{h_{i,j+\frac{1}{2}}}{h_{i,j}}\right) T^{k-1}_{i,j+1} + \left(\frac{2\gamma\alpha_y r_y}{3} \frac{h_{i,j+\frac{1}{2}} + h_{i,j-\frac{1}{2}}}{h_{i,j}}\right) T^{k-1}_{i,j}$$

$$- \left(\frac{\gamma s_y}{3} v_{i,j-1} \frac{h_{i,j-1}}{h_{i,j}} + \frac{2\gamma\alpha_y r_y}{3} \frac{h_{i,j-\frac{1}{2}}}{h_{i,j}}\right) T^{k-1}_{i,j-1}, \tag{8.10}$$

using the linear approximations given by Eq. 8.1. Equation 8.9 limits transport to an x-direction mode, and Eq. 8.10 limits transport to a y-direction mode.

Among the variety of algorithms available, Kolesar and Sonnichsen use a Gaussian elimination (implicit technique to solve the tridiagonal system of linear equations generated by the splitting. The solution technique proceeds as follows: First, since the temperatures are assumed known at all nodal points at times k - 1 and k, the right-hand side of Eq. 8.9 for all points is easily calculated. Hence, for any given row j in the planar grid, a simultaneous tridiagonal system of linear equations exists with unknowns $T^{k+1*}_{i_1}$, $T^{k+1*}_{i_2}$, ... This system is readily solved, since each equation is coupled only to its two adjacent neighbors (one if it is the first or last equation). Each column is solved in succession. Once $T^{k+1*}_{i,j}$ is obtained for all grid points, Eq. 8.10 is used to yield temperatures at time k + 1. The procedure is identical, except that the temperatures $T^{k+1}_{j_1}$, $T^{k+1}_{j_2}$, ..., are obtained for each row i. The entire process is repeated for each full-time

increment until maximum-time or steady-state conditions are reached. The method is simply an alternate solution for temperature by columns and then a solution by rows.

Generally, the above A.D.I. method has advantages over the two more classical numerical schemes. Explicit difference methods lead to equations which are simple to solve, but which require an uneconomically large number of time steps of limited size. Stability questions must generally be handled. For implicit difference schemes, there is no limit on the time step used, but each step requires the solution by iteration of large sets of simultaneous equations. Instability seldom affects implicit methods. The A.D.I. method usually requires a relatively small increase in computer storage capacity over most implicit techniques, but reduces considerably the number of total calculations required. The above A.D.I. numerical approximation appears stable from the results of its applications to date, but no proof of general stability of the code has been given. The standard conclusion reached for problems with an implicit numerical method is that there may be possible inaccuracies in the solution due to the finite-difference approximations; yet no instability, as defined in the classical sense by the usual stability parameters, occurs.

Restrictions on the size of the time increment in convective-diffusion equations to minimize possible accuracy losses are represented in TOPLYR-II by a convection and a diffusion criterion. The usual explicit stability parameter is satisfied in TOPLYR-II with a relationship between ℓ_x and ℓ_t such that a fluid particle can pass only into an adjacent cell in one time step. If these criteria are not satisfied, a loss of accuracy results.

In the applications of TOPLYR-II to one-dimensional problems and various two-dimensional river situations, the solution has been found to be relatively insensitive to the choice of the A.D.I. splitting parameters β and γ.

(5) The "Initial" Old-temperature Distribution. To start the problem, the initial temperature and "initial" old-temperature distribution (k - 1 step, k = 1) must be specified. This is equivalent to specifying an initial value and initial time derivative for the temperature distribution. The initial temperature (k step, k = 1) is part of the initial data. The program code provides several options, including the separate input of the "initial" old temperatures. According to the authors, the choice of an initial old-temperature distribution is not critical and its importance diminishes with time. However, the choice of a sufficiently large nonphysical initial time derivative (i.e., $T^k - T^{k-1}$ large, for k = 1) can lead to irregularities in the solution. Figure 8.5 illustrates the effect of the choice of two possible, yet widely different, initial "old" temperatures. The first choice assumes that the temperature for $t < 0$ is equal to the distribution at $t = 0$. The second assumes that for $t < 0$, the temperature at all nodes

was equal to ambient temperature. Conditions for the problem illustrated in Fig. 8.5 are:

$u = 0.018$ m/sec (assumed constant and equal to river speed),

$v = 0$,

$\alpha_x = 7.0$ m^2/sec,

$\alpha_y = 0$,

mean air temperature = 15.6°C,

dewpoint temperature = 10°C,

wind speed = 10 mph,

amount of solar radiation = 230 langleys/day,

constant plume depth,

ambient river temperature = 16°C,

and

initial plume temperature at inlet section = 27.1°C.

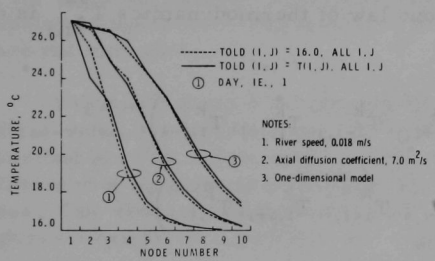

Fig. 8.5

TOPLYR-II Results for Various "Old" Temperatures Used for Initial Conditions[1a]

The authors set up an artificial boundary condition at the outlet section to permit later time iterations. Following Fromm,[7] the authors calculate temperatures out to the exit section where $i = I$. Two fictitious nodes are defined at $I + 1$ and $I + 2$. Axial velocity and depth are assumed constant and equal to the value at node I. $T^k_{I+1,j}$ is calculated from the zero-heat-flux condition,

$$T^k_{I+1,j} - T^k_{I,j} = T^k_{I,j} - T^k_{I-1,j}.$$

This value, calculated as an extrapolation of conditions prevailing at the end code, is used in place of $T^k_{i,j}$ at later time steps.

One problem arises in the actual form and position of the data when provided as input. According to the numerical scheme, velocities are

to be provided on the cell edges, while the depth and plume temperature are to be specified at the cell centers. Field data are seldom measured at the precise positions required by the grid; experimental data of velocity, temperature, and depth are given typically at common locations. The present version of TOPLYR-II assigns inlet and outlet experimental data to the element surface or element center as required by the grid, without interpolation. There will obviously be an error incurred in the final temperature solution. This error will decrease either as the grid becomes finer or more data points are taken for cross sections at, and in the vicinity of, the inlet and outlet stations, allowing a satisfactory interpolation between data points taken at different positions and time. The error introduced in the TOPLYR-II procedure approaches zero as the number of elements in the axial and transverse directions becomes large.

(6) Nonphysical Values. The possibility of nonphysical values occurring in the finite-difference approximation of Eq. B was discussed earlier. To handle this potential difficulty, the authors use a special implementation of the Hain principle as described below:

First a purely convective solution $T_{c_{i,j}}^{k+1}$ is calculated. Then a solution that satisfies the second law of thermodynamics $T_{A_{i,j}}^{k+1}$ is determined from

$$T_{max} = \max\left(T_{i,j}^{k-1}, T_{i+1,j}^{k}, T_{i-1,j}^{k}, T_{i,j+1}^{k}, T_{i,j-1}^{k}\right), \tag{8.11}$$

$$T_{min} = \min\left(T_{i,j}^{k-1}, T_{i+1,j}^{k}, T_{i-1,j}^{k}, T_{i,j+1}^{k}, T_{i,j-1}^{k}\right), \tag{8.12}$$

and

$$T_{A_{i,j}}^{k+1} = \max\left[T_{min}, \min\left(T_{max}, T_{c_{i,j}}^{k+1}\right)\right]. \tag{8.13}$$

An error vector $E_{i,j}^{k+1}$ is then defined from

$$T_{c_{i,j}}^{k+1} = T_{A_{i,j}}^{k+1} + E_{i,j}^{k+1} \tag{8.14}$$

and represents the incremental temperature that one must remove from a purely convective solution to have it just satisfy the Hain principle. Next the complete Eq. B is analyzed, including the diffusion and source terms. The error function defined from Eq. 8.14 is introduced there as an additional pseudomechanism for the transfer of heat energy, which, when subtracted

from $T_{i,j}^{k+1}$ (all convective, diffusive, and source terms included), results in a temperature that will satisfy the Hain principle for Eq. B. Essentially, one is thereby computing a pseudomechanism of energy transfer, which, when applied to the purely convective problem, gives a solution that just does satisfy the Hain principle. This mechanism is simply retained when the full equation is solved. This is done for each half-step in time. It is physically plausible for a system with a large source term to have an energy buildup. For example, if the whole system experienced a compression, the second law would permit an energy buildup and the Hain convective principle (a statement of the thermodynamics of the problem) must not exclude such a phenomenon. As implemented in TOPLYR-II, this Hain principle would allow that heat buildup.

The method of preventing nonphysical values by the Hain principle is not unique. Moreover, the literature in this area does not disclose any explicit statements about how nonphysical values or the Hain principle should be handled in general. As stated by the authors, the Hain principle is strictly valid only when pure convection occurs. Other investigators have used it, as done here, to yield a solution when all mechanisms are present. No method presently available is completely satisfactory. The authors' approach, for instance, yields a correction that serves only to place limits on the computed temperature. Physically improbable variations within those limits are not excluded.

Figures 8.6 and 8.7 compare results before and after the nonphysical-value correction is made. The identical one-dimensional problem described for Fig. 8.5 is used. As the contribution of the diffusion terms in the differential equation is increased, the nonphysical-value correction decreases. The diffusion contribution acts as a viscous term, which dampens these spurious nonphysical oscillations. Again one may envision the solution

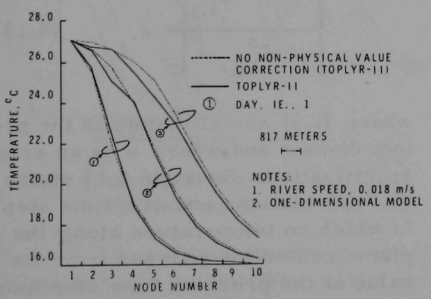

Fig. 8.6. TOPLYR-II Results with and without Nonphysical-value Correction with Axial-diffusion-coefficient Value of 7.0 m^2/sec (from preliminary draft of Ref. 1a)

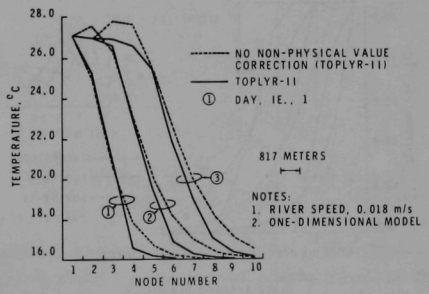

Fig. 8.7. TOPLYR-II Results with and without Nonphysical-value Correction with Axial-diffusion-coefficient Value of 1.0 m^2/sec[1a]

as being a sum of waves in which some of them are causing these nonphysical difficulties. Introduction of viscous dissipation (diffusion terms) overpowers and depresses these spurious waves, which are due solely to the approximate nature of the mathematics. In fact, in the one-dimensional applications of TOPLYR-II (see Figs. 8.6 and 8.7), nonphysical values, when occurring, build up with time, then reach equilibrium, and then decrease due to the dissipation present. Even for a purely convective problem, the pseudodiffusion due to the approximations made in the difference equations yield a fictitious diffusion to help dampen the nonphysical-value ripples or oscillations. Figure 8.7 indicates that the temperature may locally (in the domain behind the wavefront) exceed the boundary value. The hump appears right at the wavefront, grows a little bit right at the start, and then remains approximately constant while riding in back of the thermal wave as it moves downstream. The authors assert that, for problems with a sufficiently large axial-diffusion coefficient or moderate temperature gradients, no Hain-type correction is required.

(7) The A.D.I. Splitting Parameters. Concerning the A.D.I. splitting parameters, the authors derive the fact that for depth and velocity constant, the truncation error associated to Eqs. 8.4 and 8.5, when $\beta + \gamma = 1$, is proportional to the squares of the increments ℓ_t, ℓ_x, and ℓ_y. For arbitrary depths and velocities with $\beta + \gamma \neq 1$, the authors expect the truncation error to be proportional to ℓ_t. In the one- and two-dimensional applications of TOPLYR-II to date, the solutions seemed relatively insensitive to different choices of β and γ, including situations when $\beta + \gamma \neq 1$.

To halt the computations, either a specific value of t is inputted or, for steady state, convergence criteria are specified in the form of an incremental temperature. The computations cease in the code when

$$\left| \frac{T^{n+1}_{i,j} - T^{n}_{i,j}}{T^{n}_{i,j}} \right| < \varepsilon, \qquad (8.15)$$

where (i, j) are all points in the problem domain and where ε is an error specification. Equation 8.15 states that calculations end at a time step in which no temperature along the plume centerline changes from its value at the previous time step more than the specified ε value.

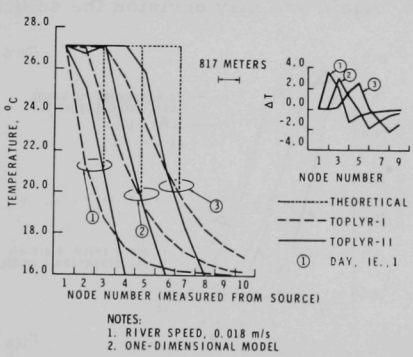

Fig. 8.8

Comparison of TOPLYR-I and II with Only Convection Mechanism Operational[1a]

d. Model Verification

Figure 8.8 compares TOPLYR-II with a one-dimensional theoretical

result. The initial parameters are identical to those used for Fig. 8.5, except that only the convection mechanism is operational. The thermal pulse results from a continuous source and travels at constant speed, maintaining all points it reaches at 27.1°C. This is the simplest one-dimensional problem that one may analyze. Also included are the predicted results from TOPLYR-I, an earlier version of the model. TOPLYR-I involved only first-order accurate difference approximations and led to significant inaccuracies for certain applications. As can be seen from Fig. 8.8, TOPLYR-I leads to significant numerical dispersion. (For this problem, both TOPLYR codes solve a hyperbolic system of equations.) The thermal pulse extends beyond the theoretical limit for both sets of TOPLYR results, and for TOPLYR-I the temperature is nonzero, even for early times. TOPLYR-II here exhibits reduced numerical dispersion. Straight-line interpolation was used between nodes in TOPLYR-I and -II in Fig. 8.8. Figures 8.9 and 8.10 illustrate both TOPLYR codes when convection and diffusion is operational. The equations involved possess properties of hyperbolic and parabolic differential equations. Due to the significant improvement of TOPLYR-II over TOPLYR-I in one-dimensional problems and two-dimensional river problems, the authors recommend the exclusive use of TOPLYR-II in terms of improved accuracies. It is of interest to note that TOPLYR-I did not produce any nonphysical values due to the Lelevier approximation made to the convective terms, yet at a sacrifice in accuracy.

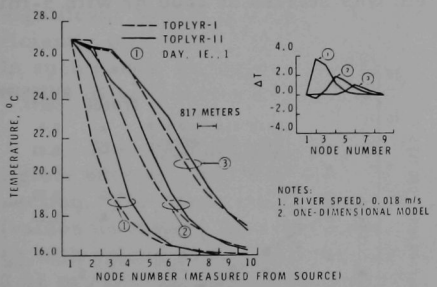

Fig. 8.9. Comparison of TOPLYR-I and II with Diffusion Coefficient of 7.0 m^2/sec[1a]

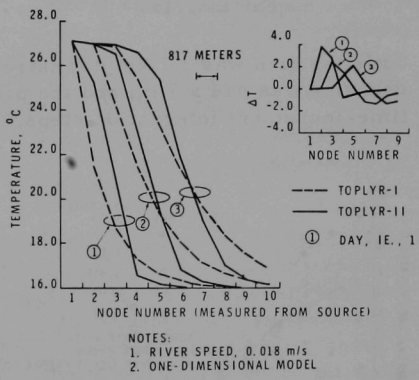

Fig. 8.10. Comparison of TOPLYR-I and II with Diffusion Coefficient of 1.0 m^2/sec[1a]

The authors assume constant diffusivities for river and lake applications of their model. For a lake situation they recommend no method at this point for the calculation of the longitudinal and lateral diffusivities for the far-field region of the lake to employ in their model. Yet they suggest that, in the absence of secondary currents due to buoyancy, some of the work of Csanady[8] might be helpful in lake modeling. For rivers, the lateral diffusivity is estimated from the initial data on inlet and outlet sections. Using

the tables in the U.S. Geological Survey,[9] they estimate a friction factor for the river under consideration. They then employ a standard technique to compute the lateral diffusivity. They make a guess as to the value of the longitudinal diffusivity. For the rivers so far considered, axial diffusion has been negligible and the solution insensitive to the value of longitudinal diffusivity has been chosen. So far, the method of choosing the lateral diffusivity has yielded satisfactory results when the model is fitted with river data.[10] Using diffusivity values from zero to four times the calculated transverse diffusivity has yielded an envelope within which the experimental data were well contained. The code has, however, been sensitive to values of transverse diffusivity. The problems analyzed so far have yielded solutions that were relatively insensitive to atmospheric conditions.

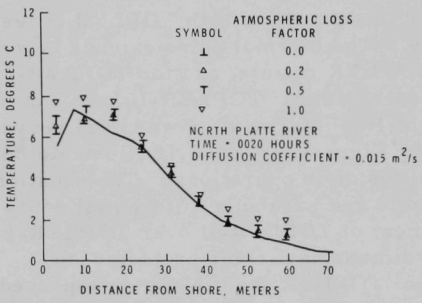

Fig. 8.11. Comparison of Theoretical and Experimental Temperature Profiles at Output Station for Various Magnitudes of Atmospheric Energy Loss[1a]

Figures 8.11-8.13 represent comparisons of TOPLYR-II to data taken at the North Platte River in Wyoming by the U.S. Geological Survey[10] on January 28-29, 1970. The initial section was 0.2 km downstream from a 420-MWt power plant. The outlet section was 3.1 km downstream from the discharge point. The mesh cell size was 414 x 7 m, and the problem was started at 2200 hr with 5-min time-increment integration steps.

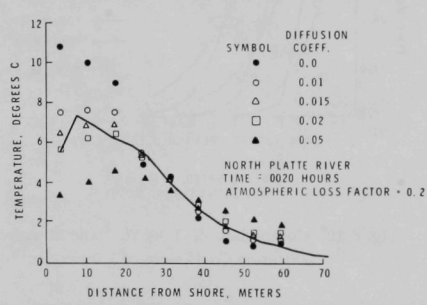

Fig. 8.12. Comparison of Theoretical and Experimental Temperature Profiles at Output Station for Various Diffusion Coefficients:[1a] Time = 0020 hr

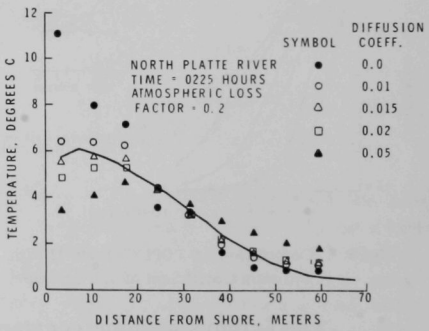

Fig. 8.13. Comparison of Theoretical and Experimental Temperature Profiles at Output Station for Various Diffusion Coefficients:[1a] Time = 0225 hr

The code was fit to the data in a semiempirical manner. Constant longitudinal and lateral river diffusivities and the relative magnitude of the atmospheric energy loss were taken as free parameters. (Meteorological parameters were taken by the U.S.G.S., but not in as complete a form as needed by the authors; consequently, the Lake Hefner source-sink model was assumed to be functionally correct, but a multiplicative coefficient associated with the source term was assumed sufficient to extend the Lake Hefner model to the local environmental conditions.) The authors calculated the lateral-diffusion coefficient of the North Platte River to be of the order of magnitude of 0.01 m^2/sec by the methods described above. The spread of results of Figs. 8.11-8.13 indicates that lateral-diffusion coefficients between 0.01 and 0.02 m^2/sec with an atmospheric loss factor of 0.2 simulate the field data satisfactorily. Variation in the longitudinal-diffusion coefficient from 0.0 to 1.0 m^2/sec did not yield significant changes in the temperature distribution. For any period of time in excess of several hours, the authors expect these values to yield satisfactory predictive results for this river at those input-output stations. The authors hypothesize that the differences between numerical and field results in that case might be due to the boundaries being nonadiabatic, the spatial variation of the lateral diffusion coefficient, and the nonexact placement of initial data to the mesh nodal points.

A disadvantage of TOPLYR-II (at least for river situations) is the fact that previous field data have to be available for fitting purposes to obtain diffusivities and an atmospheric loss parameter before they can be reasonably applied as a predictive device. If a situation is analyzed in which significant buoyancy occurs, the transverse diffusivity will have to be sufficiently increased to be able to predict the increased lateral spreading. In such cases, the model will have to be fit to the data since the proper choice of an "effective diffusivity" will be unknown.

The other river applications considered so far have also had negligible buoyancy and negligible initial momentum remaining at the inlet section. For these cases, there was insensitivity to the axial diffusivity (values used were between 1 and 10 m^2/sec) and a generally satisfactory fit with values of the transverse diffusivity (values employed were about 0.01 m^2/sec) as calculated from Ref. 10. The only difficulties so far in the model application to rivers has occurred for deep rivers with significant stratification (e.g., Potomac River data[10]). The authors hypothesize that the choice of the bottom of the plume or epilimnion would have been a better choice for the $h_{i,j}$ values than the river bottom. At this point, it should be emphasized that the model adequacy for river situations is still being tested. Comparisons with lake data have not yet been attempted.

e. Final Comments

A disadvantage of the present version of TOPLYR-II is its use of absolute temperatures. TOPLYR-II now must have input data on such

receiving-body temperature-independent phenomena as solar radiation, atmospheric radiation, and reflected solar and atmospheric radiation in addition to back radiation, conduction/convection losses, and evaporative transfers. If excess temperatures above ambient were used, surface-heat transfer from the plume (i.e., relative to the ambient lake) would only need be considered. This simplifies the data required to be taken from the field to be only ambient temperature, excess temperature, and wind speed. A third alternative, though not as advantageous as the latter method, involves using the difference between actual and equilibrium temperatures as the dependent variable in the thermal-energy balance. Use of this equilibrium temperature method would simplify the source term, base the source-term computation on the current temperature, and provide intermediate results that would possess unique debugging properties, since the use of a differential would give indications of positive or negative trends in the results. However, the use of a constant thermal-exchange coefficient is a generally employed approximation that may limit the validity of the energy budget. Also, computation of the equilibrium temperature, which requires the same input data as used in the absolute-temperature method, increases the running time of the problem by requiring a trial-and-error calculation. The authors regret not using some type of temperature increment in their integration.

A second disadvantage involves the treatment of the potential nonphysical values that may occur by using the Hain Scheme. As stated before, the correction made serves only to place limits on the computed temperature, and physically improbable variations within those limits are not excluded. Furthermore, at the edges of the grid, a slight deflection in temperature is generally noted in model applications, perhaps attributed to the adiabatic assumptions. This difficulty is presently being investigated. Some small problems have also occurred at the corners of the grid when poor choices of input parameters are made. This latter difficulty is currently being remedied. The main criticism that may be made of the present version of the code is the difficulty in its applicability for the majority of lake situations. As stated above, one generally does not know the input conditions necessary to apply it. On the other hand, one should recognize that this code is a first step in the development of a complete jet and far-field model. One may, however, use a suitable jet model to yield temperatures and velocities at some arbitrary cross section downstream and then follow with this version of the TOPLYR series. TOPLYR-II may be used to treat the transient effects involved with the starting up of a power plant or the effects of variable meteorological conditions on a thermal plume. A computer program for TOPLYR-II is presently available.

References

1a. D. C. Kolesar and J. C. Sonnichsen, Jr., TOPLYR-II--A Two-Dimensional Thermal-Energy Transport Code, Hanford Engineering Development Laboratory, Richland, Washington (Oct 1971).

1b. D. C. Kolesar, Mathematical Modeling of Thermal Plume Dispersion in a Receiving Water Body, paper presented at the Combined 2nd Annual Thermal Power Conference and 8th Biennial Hydraulics Conference at Washington State University, Pullman, Washington (Oct 5-8, 1971).

2. J. C. Sonnichsen, Jr. and D. C. Kolesar, TOPLYR--A Two-Dimensional Thermal-Energy Transport Code, HEDL-TME 71-39, Hanford Engineering Development Laboratory, Richland, Washington (Jan 1971).

3. D. W. Pritchard, Modeling of Heated Discharges--A Lecture, Westinghouse School for Environmental Management, CSU, Fort Collins, Colorado (June 25, 1970).

4. Water-Loss Investigations: Lake Hefner Studies, Technical Report, Geological Survey Professional Paper 269 (1954).

5. J. C. Sonnichsen, Jr. and C. A. Oster, Examination of the Thermocline, Proc. of ASCE, SA-2 (Apr 1970).

6. R. J. Callaway, K. V. Byram, and G. R. Ditsworth, Mathematical Model of the Columbia River from the Pacific Ocean to Bonneville Dam. Part I, Theory, Program Notes and Programs, Federal Water Pollution Control Administration Northwest Region, Pacific Northwest Water Laboratory, Corvallis, Oregon (Nov 1969).

7. J. E. Fromm, Practical Investigation of Convective Difference Approximations of Reduced Dispersion, RJ 531, IBM, Thomas J. Watson Research Center, Yorktown Heights, New York (Oct 28, 1968).

8. G. T. Csanady, Accelerated Diffusion in the Skewed Shear Flow of Lake Currents, J. Geophys. Res. 71(2), 411-420 (Jan 15, 1966).

9. U.S. Geological Survey, Roughness Characteristics of Natural Channels, U.S. Government Printing Office, Washington, D.C. (1967).

10. U.S. Geological Survey, data on thermal plumes in eight rivers released to the authors through the courtesy of R. Schneider (report to be published).

f. Addendum

The synopsis and discussion of the Kolesar-Sonnichsen Model given above were based upon a semifinal draft of their model. The additional changes in the code which became part of the final draft will now be described.

First, heat transfer through the river shoreline and bottom was additionally included in the analysis by assuming that the rate of such heat loss is given by Newton's law of cooling. The proper inclusion of this extra term in the heat balance of a typical cell is illustrated in Fig. 8.14B for the special case of a shoreline nodal cell. That specific case is described here since the new code employs a second change, a triangular (rather than trapezoidal) cell at the boundary. in the figure, H is the coefficient of convective heat transfer and T_∞ is the ambient (bottom) temperature. The term $(\Delta x \Delta y/2)(1/\cos\theta)[H(T_\infty - T)]$ represents the rate of heat transfer through the river bottom. Both H and T_∞ are experimentally determined constants. The authors have found that by introducing this extra term, the output results are improved near the shoreline. Figure 8.14A describes the precise treatment of the boundary cells. The authors reason that since the ambient current speed is zero along the shoreline, the tangential component of velocity is zero on the boundary nodal cells. The normal component of velocity is

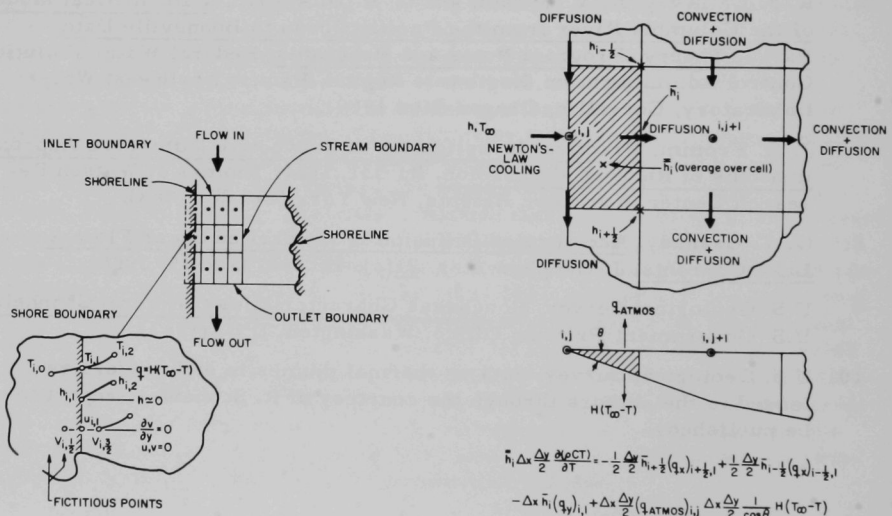

A. Geometry and Shoreline Boundary Condition of TOPLYR-II Model

B. Derivation of Energy Equation for Shoreline Cell

Fig. 8.14. Geometry and Shoreline Boundary Condition of TOPLYR-II Model with Derivation of Shoreline-cell Energy Equation

defined at a distance $\Delta y/2$ from the shoreline (see Fig. 8.14A). The authors approximate a zero value for that quantity in order to conserve mass over each boundary cell.

A third change the authors made in their final version of TOPLYR-II involves the inclusion of a code option to reduce the longitudinal and lateral diffusivities from positive values in the flow field to zero at the boundary. The authors use nonzero diffusivities of lesser magnitude than the constant uniform stream values in order to compensate for reduced turbulent transport at the shoreline. The code permits that option to alter the boundary mode only. The correction factor was estimated from the grid size and what was considered to be the correct physical adjustment that equates diffusivity to local velocity and local depth. For the North Platte River data, the authors derived the factor of 1/16.

The authors amplify on their method of calculating the lateral diffusivity in their final TOPLYR-II manuscript. First, the Manning roughness coefficient is estimated from the character of the river.[A1] Then the mean velocity calculated using the Manning formula is used to compute the friction velocity.[A2] Finally, the lateral diffusivity is computed, based on the empirical formula of Elder.[A3] This algorithm is used for river situations only. The authors' experience has shown that their analysis is relatively insensitive to the longitudinal diffusivity. The authors follow Elder in calculating longitudinal and lateral diffusivities by having them proportional to the local mean velocity and river depth.

Figures 8.15-8.18 illustrate the updated comparison of TOPLYR-II with the North Platte field data. The initial conditions of the numerical results are also illustrated in the figures. The field data are joined by the solid line. With the procedure described above, the lateral eddy diffusivity

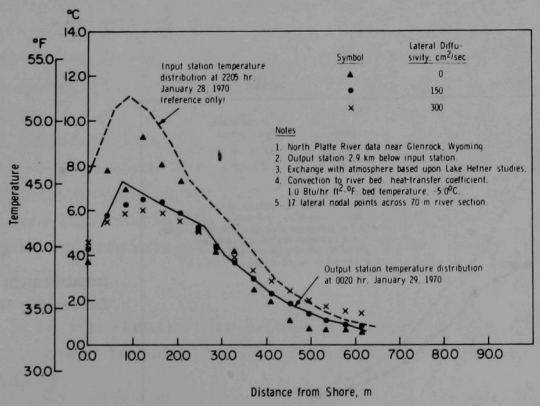

Fig. 8.15. Comparison between Theoretical and Experimental Temperature Profiles at Output Station for Various Magnitudes of Lateral Thermal Eddy Diffusivity

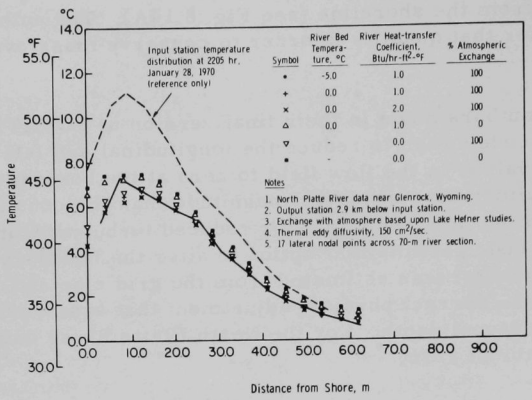

Fig. 8.16

Effect of Source due to Energy Exchange with Atmosphere or Riverbed on Theoretical Results

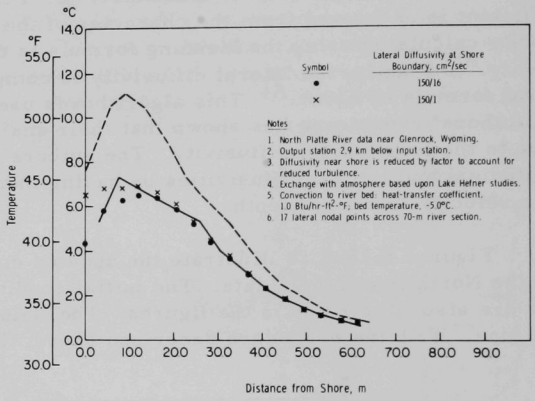

Fig. 8.17

Effect of Reduced Thermal Diffusivity near Shoreline on Theoretical Results

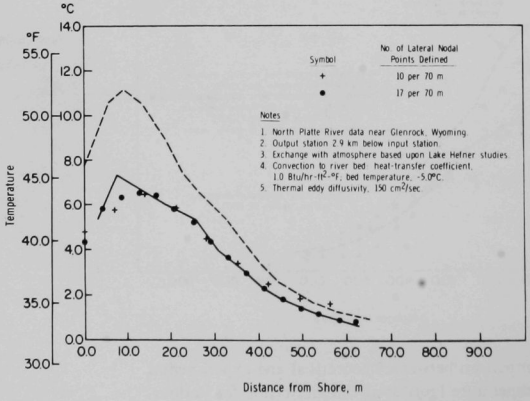

Fig. 8.18

Improvement in Resolution by Decreasing Nodal Mesh Size

was computed to be of order 100 cm^2/sec (based on river geometry and flow conditions using the standard methods[A1,A2] and Ref. A3). Figure 8.15 implies a good comparison with field data when the lateral eddy-thermal diffusivity is 150 cm^2/sec. Again, the results were relatively insensitive to longitudinal diffusivities as large as 1 m^2/sec. What the authors regarded as reasonable assumptions for H and T_∞ were made in that comparison. Figure 8.16 compares the relative importance of the Newton cooling and surface-heat-loss terms in the model. The average heat-transfer coefficient, H, used in the calculations was 1 Btu/ft^2-hr-°F, which was in line with the recommendations of Dynatech,[A4] as used by the authors. Interpreting that reference led to an expected range of 0.5-2.5 in the coefficient. Figure 8.16 shows only little changes in prediction upon such variation in H. The results are, however, sensitive to T_∞. Estimates on "riverbed" temperature (not provided in the data) still left a 5-10°C uncertainty. As the authors note, the uncertainties in the weather data have a much greater impact on the solution than ground-loss uncertainties. The authors assert that adjustment in T_∞ and the lateral diffusivity within their range of uncertainty is sufficient to yield nearly perfect agreement. The authors cannot say that introducing Newton's law of cooling improves the results uniquely because there is at least one other phenomenon (gradation in diffusivities near the shore) that makes a correction in a similar way. From the authors' experience in comparing their model to the North Platte River data, they conclude that inclusion of the Newton law does affect the results to some extent. However, juggling the weather conditions within a possible slight experimental error or introducing an altered or variable diffusivity could provide the same results. If one does not allow for this uncertainty in the weather data or in Newton's law, the results are still not altered significantly <u>for the North Platte</u>.

Figure 8.17 illustrates the effect of choosing the code option that allows a reduction in diffusivity near the shoreline. The authors presume a reduced level of turbulence consistent with source-cell average rather than the zero level expected at the shoreline mode position. Kolesar and Sonnichsen are basically following the work of Elder[A3] here. It is not clear to us; a reduction in turbulence does actually occur in the proximity of the shore. Eddies generated by the shore boundary may well be more efficient mixers than those significantly offshore. The computer code can handle the reduced-turbulence option as well as the model having constant diffusivities. Figure 8.17 shows that variation in local diffusivity near the shore plays an important role in determining the proper shape of the temperature distribution near the shore.

Figure 8.18 illustrates the effect of using a finer grid on the code results. Improvement by employing a finer grid is seen to be mostly at the shore boundary.

In the authors' study of the river data they analyzed, they noted consistent deficiencies in the determination of such quantities as weather

parameters, shoreline-slope considerations, environmental conditions (ice, snow, etc.), existence of thermal springs (in the immediate vicinity of measurements), and local ground temperature and heat-flux coefficient. This is in addition to the generally accurate determination of plume velocities, temperatures, and depth at a particular cross section. Note that in Fig. 8.16 a riverbed temperature of -5°C does not imply ice in the river. In that North Platte situation, the wet- and dry-bulb temperatures were about -10°C. The authors claim that, for a variety of reasonable circumstances, the bottom temperature can be as low as the wet-bulb temperature, with the river current having temperatures above (generally slightly above) 0°C.

The TOPLYR-II code as the option that allows the user to assign a nonzero value for boundary points and points at which the bottom depth is zero. The value 0.01 m was used for the North Platte River comparison. Some such number should be assigned considering the form of difference Eqs. 8.9 and 8.10. No attempt has yet been made to determine if that assignment is in any way a critical one.

The authors have added an additional option in handling the outlet boundary condition. Originally the conditions

$$T^{k}_{i+1,j} = 2T^{k}_{i,j} - T^{k}_{i-1,j}$$

and

$$T^{k+1*}_{i+1,j} = 2T^{k+1*}_{i,j} - T^{k+1*}_{i-1,j}$$

were used to terminate the computation at a finite number of nodes by means of a simple extrapolation. Now the option to use

$$T^{k+1*}_{i+1,j} = T^{k}_{i+1,j}$$

is provided whenever the original extrapolation fails to provide a plausible temperature based upon newly computed temperatures in the problem domain. The authors expect this option to be useful only in problems with little real physical meaning.

Kolesar and Sonnichsen feel that their model can be applied when bends of moderate curvature occur in the river. The model is applied as described, downstream distance along the shore being identified with downstream centerline distance as used by the computer code.

Our final comment involves the alteration of the final draft of TOPLYR-II to account for local changes in the eddy-thermal diffusivities.

This change is not included in Ref. 1a, but will be described in a future quarterly report of the Hanford Engineering Development Laboratory. The difficulty in including a variable diffusivity was only in writing the code, not a conceptual one involved in the character of the equations. Defining a variable depth as the authors have done has enabled them to introduce variable diffusivities into the model quite simply. Kolesar and Sonnichsen anticipate introducing buoyancy into the model next as an outgrowth of TOPLYR-II. Their goal is to develop equations that will hopefully lead to success for lake applications.

Addendum References

A1. U.S. Geological Survey, Roughness Characteristics of National Channels, U.S. Government Printing Office, Washington, D.C. (1967).

A2. V. T. Chow, Open-Channel Hydraulics, McGraw-Hill, New York (1959).

A3. J. W. Elder, The Dispersion of Marked Fluid in Turbulent Shear Flow, J. Fluid Mech. 5, 544-560 (1959).

A4. Dynatech R/D Company, A Survey of Alternate Methods for Cooling Condenser Discharge Water--Large-Scale Heat Rejection Equipment, Report to Water Quality Office, EPA, Project No. 16130 DHS (July 1969).

9. Mathematical Model for Dispersion of Heat into a Lake

Walter Wnek
(Illinois Institute of Technology Research Institute)
(to be published)

a. List of Symbols

f	Function related to initial temperature defined by Eq. 9.8
G_1, G_2, G_3	Green's function satisfying conditions of Eqs. 9.34, 9.35, and 9.36, respectively
$\overline{G}_1$, $\overline{G}_2$, $\overline{G}_3$	Green's function satisfying same conditions as G_1, G_2, and G_3, except that distant boundary conditions are applied at infinity
G	$G_1G_2G_3$
$\overline{G}$	$\overline{G}_1\overline{G}_2\overline{G}_3$
h	Heat-transfer coefficient
k_1	Parameter defined by Eq. 9.19
k_2	Parameter defined by Eq. 9.20
K_x, K_y, K_z	Thermal diffusivities in x, y, and z directions, respectively
L	Length of continuous line source
M	Arbitrarily large and fixed positive number
M_1, M_2, M_3	Large fixed positive numbers defined by Eq. 9.16
n	Outward-drawn normal
Q_p	Volumetric discharge rate
S	Distributed heat source or sink
S_0	Bounding surface to volume V
t	Time
T	Variable temperature
T_0	Initial temperature distribution
T_E	Equilibrium temperature function
$\hat{T}$	Temperature function related to T and defined by Eq. 9.9
v_x, v_y, v_z	Velocities in x, y, and z directions, respectively
x	Coordinate measured in direction of the shore

x_0	x coordinate of outfall point-source position (or center of line source parallel to shore)
y_0	y coordinate of outfall point-source position (or line source parallel to shore)
y	Coordinate measured across the lake
z	Coordinate measured vertically downward
z_0	z coordinate of outfall point-source position (or line source parallel to shore)
x'	x coordinate of point-source position
y'	y coordinate of point-source position
z'	z coordinate of point-source position
$\hat{x}$	$x/\sqrt{K_x}$
$\hat{y}$	$y/\sqrt{K_y}$
$\hat{z}$	$z/\sqrt{K_z}$
$\hat{x}'$	$\hat{x}$ coordinate of point-source position
$\hat{y}'$	$\hat{y}$ coordinate of point-source position
$\hat{z}'$	$\hat{z}$ coordinate of point-source position
$\hat{x}_0$	$x_0/\sqrt{K_x}$
$\hat{y}_0$	$y_0/\sqrt{K_y}$
$\hat{z}_0$	$z_0/\sqrt{K_z}$
θ_0	Initial excess temperature

b. The Physical Situation and Its Mathematical Simulation

Walter Wnek of the Illinois Institute of Technology Research Institute has developed a three-dimensional mathematical model for the dispersion of heat in the near-shore waters of a large lake. The model represents the origin of the excess heat by an arbitrary distributed source in space and time $S(x, y, z, t)$. With this consideration, he develops a time-dependent exact analytical solution to the heat conservation equation with constant coefficients using Green's function techniques. Later in this discussion, the solution will be described when the source S takes on the two specific forms:

(1) A continuous point source.

(2) A continuous line source.

Bottom effects and any reflections due to any remote bank are neglected in the model.

The author's analysis is based upon the three-dimensional convective/diffusion conservation equation,

$$\frac{\partial T}{\partial t} + v_x(x, y, z, t)\frac{\partial T}{\partial x} + v_y(x, y, z, t)\frac{\partial T}{\partial y} + v_z(x, y, z, t)\frac{\partial T}{\partial z} =$$

$$\frac{\partial}{\partial x}\left[K_x(x, y, z, t)\frac{\partial T}{\partial x}\right] + \frac{\partial}{\partial y}\left[K_y(x, y, z, t)\frac{\partial T}{\partial y}\right]$$

$$+ \frac{\partial}{\partial z}\left[K_z(x, y, z, t)\frac{\partial T}{\partial z}\right] + S(x, y, z, t), \qquad (9.1)$$

where

T = temperature,

x, y, z = coordinates measured in the direction along the shore, normal to the shore, and vertically downward, respectively,

t = time,

v_x, v_y, v_z = velocities in the x, y, and z directions, respectively,

K_x, K_y, K_z = turbulent eddy diffusivities for the x, y, and z directions, respectively,

and

S = heat source or sink.

Equation 9.1 is derived by making a heat balance on a differential element of volume in the lake. The first term represents the local time rate of change of temperature within the volume element; the next three terms account for changes due to advection; the first three terms on the right-hand side of the equation define turbulent dispersion of heat; the last term represents a heat source or sink.

For power-plant thermal discharges, $S(x, y, z, t)$ describes the rate of heat input to the lake system from the condenser cooling water. For a continous-point-source representation of the outfall,

$$S(x, y, z, t) = \theta_0 Q_p, \qquad x = x_0\delta(x - x_0), \quad y = y_0\delta(y - y_0),$$

$$z = z_0\delta(z - z_0), \quad t \geq t_0, \qquad (9.2)$$

where θ_0 is the initial excess temperature, Q_p is the volumetric flow rate of discharge, and (x_0, y_0, z_0) is the source position. If the outfall is to be given by a continuous line source of length L parallel to shore, then S may be taken as

$$S(x, y, z, t) = \frac{\theta_0 Q_p}{L}, \qquad |x - x_0| \le L/2, \quad y = y_0 \delta(y - y_0),$$

$$z = z_0 \delta(z - z_0), \quad t \ge t_0,$$

$$= 0, \qquad |x - x_0| > L/2, \text{ and } t < t_0, \tag{9.3}$$

where θ_0, Q_p, and L are defined above with (x_0, y_0, z_0) being the center position of the line source. Again, the analysis to be described can treat any arbitrary $S(x, y, z, t)$.

The solution to Eq. 9.1 is derived under the assumption of constant velocities v_x, v_y, and v_z and constant diffusivities K_x, K_y, and K_z. Rationale for these assumptions follows later.

Initial and boundary conditions associated with Eq. 9.1 are:

Initial Condition:

$$T(x, y, z, 0) = T_0(x, y, z). \tag{9.4}$$

Boundary Condition 1: No heat flux across the shore,

$$\left.\frac{\partial T(x, y, z, t)}{\partial y}\right|_{y=0} = 0. \tag{9.5}$$

Boundary Condition 2: Heat transfer from the lake's surface to the atmosphere:

$$\left.\frac{\partial T(x, y, z, t)}{\partial z}\right|_{z=0} = h\left[T - T_E(x, y, t)\right], \tag{9.6}$$

where h is the heat-transfer coefficient (assumed constant) and T_E is the equilibrium temperature.

Boundary Condition Set 3: No heat flux in any coordinate direction infinitely far from the heat source,

$$\left.\begin{aligned} &\lim_{x\to\infty} \frac{\partial T(x, y, z, t)}{\partial x} = \lim_{x\to-\infty} \frac{\partial T(x, y, z, t)}{\partial x} = 0; \\ &\lim_{y\to\infty} \frac{\partial T(x, y, z, t)}{\partial y} = 0; \\ &\lim_{z\to\infty} \frac{\partial T(x, y, z, t)}{\partial z} = 0. \end{aligned}\right\} \tag{9.7}$$

For most applications to plumes in large lakes, the above assumption of no reflection at remote shore boundaries is generally justified. The author also states that the more accurate boundary condition concerning the lake bottom boundary,

$$\left.\frac{\partial T(x, y, z, t)}{\partial z}\right|_{\text{lake bottom}} = 0,$$

can, in most cases, be replaced by the assumption of infinite lake depth with the concomitant specification,

$$\lim_{z \to \infty} \frac{\partial T(x, y, z, t)}{\partial z} = 0.$$

This assertion is based on the fact that when the plume is still quite warm it does not disperse greatly in the z direction due to stratification. Also, after stratification breaks down, the plume dissipates in deep water, resulting in a greatly decreased temperature, with little chance then of reaching the bottom.

The use of the heat-conservation equation (Eq. 9.1) with an input of a constant dispersive and velocity field implies that the resulting solution is valid for a far-field region of the plume. First, the turbulent structure close to the discharge is jet-like and cannot be represented by Eq. 9.1 by itself. An investigation of the jet regime requires analysis of both the momentum- and energy-conservation equations. Second, specific assumptions on the form of S may lead to a temperature-distribution error in a region close to the source. For example, if S represents a continuous point source, $T(x_0, y_0, z_0, t_0)$ must necessarily be infinite. At distances sufficiently downstream from the discharge and for sufficiently later times, however, the temperature will be independent of the type of initial source distribution chosen and, consequently, the model is expected to yield more accurate predictions. Finally, constant velocity and dispersive fields may generally be found only at some distance from the source. Actually, this assumption was made here mainly to make the mathematics of the problem tractable. Wnek, however, has noted that from correlations of field data taken in Lake Michigan (Ref. 2, p. 281) that the horizontal dispersion coefficients do not vary much for radial and vertical distances from the heat source greater than about 1000 ft and that constant values for these parameters may be taken as a first approximation. Also, from studies of the near-shore currents of Lake Michigan, the author feels confident that v_x, v_y, v_z may also be assumed constant for a first approximation. Actually v_x will be much larger than v_y or v_z with v_y, v_z nearly zero. In Ref. 1, pp. 14-19, Wnek treats the variable velocity and dispersive field case by an iterative technique where the solution is obtained by perturbing a related constant-coefficient case. The method is cumbersome to apply and will not be discussed here.

c. Development of the Analytical Solution

The method of solution of Eq. 9.1 with constant parameters,

$$\frac{\partial T}{\partial t} + v_x \frac{\partial T}{\partial x} + v_y \frac{\partial T}{\partial y} + v_z \frac{\partial T}{\partial z} = K_x \frac{\partial^2 T}{\partial x^2} + K_y \frac{\partial^2 T}{\partial y^2} + K_z \frac{\partial^2 T}{\partial z^2} + S, \qquad (9.8)$$

with auxiliary conditions given by Eqs. 9.4-9.7, will now be summarized. First, to facilitate later analysis, the infinite lake volume defined in Fig. 9.1 is replaced (temporarily) by the closed finite region $-M \le x \le M$, $0 \le y \le M$, $0 \le z \le M$, where M is any fixed arbitrarily large positive number. Boundary Condition Set 3 is consequently replaced by

$$\frac{\partial T}{\partial x}(x, y, z, t)\Big|_{x=M} = \frac{\partial T}{\partial x}(x, y, z, t)\Big|_{x=-M} = \frac{\partial T}{\partial y}(x, y, z, t)\Big|_{y=M} =$$

$$\frac{\partial T}{\partial z}(x, y, z, t)\Big|_{z=M} = 0. \qquad (9.7')$$

This adjustment permits a subsequent integration over a finite volume of fluid.

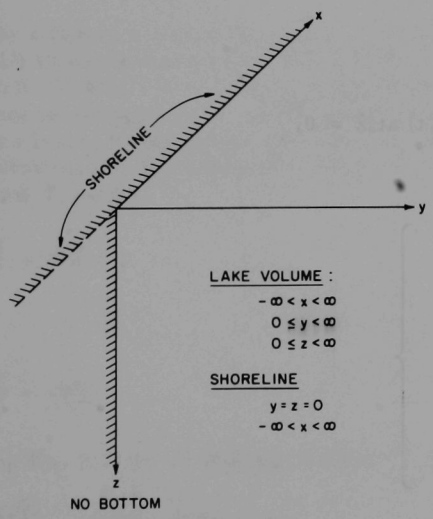

Fig. 9.1

Coordinate System for Lake Plume Model

Equation 9.8 will now be simplified by removing the convection terms. This is done by making the transformation

$$T(x, y, z, t) = \hat{T}(\hat{x}, \hat{y}, \hat{z}, t) \exp\left[\frac{1}{2}\frac{v_x}{(K_x)^{1/2}}\hat{x} + \frac{1}{2}\frac{v_y}{(K_y)^{1/2}}\hat{y} + \frac{1}{2}\frac{v_z}{(K_z)^{1/2}}\hat{z} - \sum_{i=1}^{3}\frac{v_i}{4K_i}t\right], \qquad (9.9)$$

where

$$\hat{x} = \frac{x}{\sqrt{K_x}}, \quad \hat{y} = \frac{y}{\sqrt{K_y}}, \quad \hat{z} = \frac{z}{\sqrt{K_z}}. \tag{9.10}$$

Inserting Eq. 9.9 into Eq. 9.8 and transforming conditions 9.4, 9.5, 9.6, and 9.7' yields the initial-value problem in $\hat{T}$ defined by

differential equation:

$$\frac{\partial \hat{T}}{\partial t} = \sum_{i=1}^{3} \frac{\partial^2 \hat{T}}{\partial \hat{x}_i^2} - \psi(\hat{x}, \hat{y}, \hat{z}, t), \tag{9.11}$$

initial condition:

$$\hat{T}(\hat{x}, \hat{y}, \hat{z}, 0) = f(\hat{x}, \hat{y}, \hat{z}), \tag{9.12}$$

boundary condition 1:

$$\frac{\partial \hat{T}}{\partial \hat{y}} = k_1 \hat{T} \text{ at } \hat{y} = 0, \tag{9.13}$$

boundary condition 2:

$$\frac{\partial \hat{T}}{\partial \hat{z}} = k_2 \hat{T} - \varphi(\hat{x}, \hat{y}, 0, t) \text{ at } \hat{z} = 0, \tag{9.14}$$

boundary condition set 3:

$$\left.\begin{aligned} &\frac{\partial \hat{T}}{\partial \hat{x}} = 0 \text{ at } \hat{x} = \pm M_1, \\ &\frac{\partial \hat{T}}{\partial \hat{y}} = 0 \text{ at } \hat{y} = M_2, \\ &\text{and} \\ &\frac{\partial \hat{T}}{\partial \hat{z}} = 0 \text{ at } \hat{z} = M_3, \end{aligned}\right\} \tag{9.15}$$

where

$$M_1 = \frac{M}{\sqrt{K_x}}, \quad M_2 = \frac{M}{\sqrt{K_y}}, \quad M_3 = \frac{M}{\sqrt{K_z}} \tag{9.16}$$

and

$$\psi = S \exp\left(-\frac{1}{2}\sum_{j=1}^{3} \frac{v_j}{\sqrt{K_j}}\hat{x}_j + t\sum_{j=1}^{3}\frac{v_j^2}{4K_j}\right), \tag{9.17}$$

$$f = T_0 \exp\left(-\frac{1}{2}\sum_{j=1}^{3} \frac{v_j}{\sqrt{K_j}}\hat{x}_j\right), \tag{9.18}$$

$$k_1 = -\frac{v_y}{2\sqrt{K_y}}, \tag{9.19}$$

$$k_2 = h\sqrt{K_z} - \frac{v_z}{2\sqrt{K_z}}, \tag{9.20}$$

and

$$\varphi = h\sqrt{K_z}T_E \exp\left[-\frac{1}{2}\left(\frac{v_x\hat{x}}{\sqrt{K_x}} + \frac{v_y\hat{y}}{\sqrt{K_y}}\right) + t\sum_{j=1}^{3}\frac{v_j^2}{4K_j}\right]. \tag{9.21}$$

The solution to the above linear parabolic problem for $\hat{T}$ is obtained by using the Green's function for that problem. The Green's function $G(\hat{x}, \hat{y}, \hat{z}, t; \hat{x}', \hat{y}', \hat{z}', t')$ is defined as the temperature due to an instantaneous point source of strength unity placed at the point $(\hat{x}', \hat{y}', \hat{z}')$ at time t' subject to zero initial temperature and boundary conditions to be determined later. Following the development of Carslaw and Jaeger (Ref. 3, pp. 353-365), G and $\hat{T}$ satisfy

$$\frac{\partial \hat{T}}{\partial t'} = \nabla^2\hat{T} + \psi \tag{9.22}$$

and

$$\frac{\partial G}{\partial t'} = -\nabla^2 G. \tag{9.23}$$

Multiplying Eq. 9.22 by G and Eq. 9.23 by $\hat{T}$ and subtracting yields

$$\frac{\partial(G\hat{T})}{\partial t'} = G\nabla^2\hat{T} - \hat{T}\nabla^2 G + G\psi. \tag{9.24}$$

Since G is discontinuous at $t' = t$, Eq. 9.24 is integrated in time from 0 to $t - \epsilon$, where ϵ is an arbitrarily small positive number and over the finite volume V of lake fluid defined by

$$V: \; -M_1 \le x \le M_1;$$
$$0 \le y \le M_2;$$
$$0 \le z \le M_3.$$

This implies (using Green's Theorem)

$$\int_0^{t-\varepsilon} dt' \left[\iiint_V \frac{\partial(G\hat{T})}{\partial t'} \, dV' \right] = \int_0^{t-\varepsilon} dt' \left[\iiint_V (G\nabla^2\hat{T} - \hat{T}\nabla^2 G + G\psi) \, dV' \right] \tag{9.25}$$

or

$$\iiint_V G\hat{T}\Big|_{t'=t-\varepsilon} dV' - \iiint_V G\hat{T}\Big|_{t'=0} dV' =$$

$$\int_0^{t-\varepsilon} dt' \left[\iint_{S_0} \left(G\frac{\partial \hat{T}}{\partial n} - \hat{T}\frac{\partial G}{\partial n} \right) dS' \right] + \int_0^{t-\varepsilon} dt' \iiint_V G\psi \, dV', \tag{9.26}$$

where

n = the outward drawn normal,

and

S_0 = the bounding surface.

Now if G is defined by

$$\frac{\partial G}{\partial t} = \nabla^2 G, \tag{9.27}$$

initial condition:

$$G(\hat{x}, \hat{y}, \hat{z}, 0) = 0, \tag{9.28}$$

boundary condition 1:

$$\frac{\partial G}{\partial \hat{y}} = k_1 G \text{ at } \hat{y} = 0, \tag{9.29}$$

boundary condition 2:

$$\frac{\partial G}{\partial \hat{z}} = k_2 G \text{ at } \hat{z} = 0, \tag{9.30}$$

boundary condition set 3:

$$\left.\begin{aligned} \frac{\partial G}{\partial \hat{x}} &= 0 \text{ at } \hat{x} = \pm M_1; \\ \frac{\partial G}{\partial \hat{y}} &= 0 \text{ at } \hat{y} = M_2; \\ \frac{\partial G}{\partial \hat{z}} &= 0 \text{ at } \hat{z} = M_3; \end{aligned}\right\} \tag{9.31}$$

for an instantaneous point source, then

$$\int_0^{t-\varepsilon} dt' \iint_{S_0} \left(G \frac{\partial \hat{T}}{\partial n} - \hat{T} \frac{\partial G}{\partial n} \right) dS = \int_0^{t-\varepsilon} dt' \iint_{S_0} G\varphi \, dS. \tag{9.32}$$

Finally, by taking the limit as $\varepsilon \to 0$ in Eq. 9.28, and using the filtering property of Green's functions, the solution for T becomes

$$\begin{aligned} \hat{T}(\hat{x}, \hat{y}, \hat{z}, t) = & \iiint_V G(\hat{x}, \hat{y}, \hat{z}, t; \hat{x}', \hat{y}', \hat{z}', t') \, f(\hat{x}', \hat{y}', \hat{z}') \, dV' \\ & + \int_0^t dt' \iint_{S_0} (G\varphi)\Big|_{S_0} dS \\ & + \int_0^t dt' \iiint_V G(\hat{x}, \hat{y}, \hat{z}, t; \hat{x}', \hat{y}', \hat{z}', t') \, \psi(\hat{x}', \hat{y}', \hat{z}', t') \, dV'. \end{aligned} \tag{9.33}$$

The final step in the solution is the construction of G. Let $G_1(\hat{x}, t; \hat{x}', t')$, $G_2(\hat{y}, t; \hat{y}', t')$, and $G_3(\hat{z}, t; \hat{z}', t')$ be the instantaneous point-source solution to the associated problems:

$$\left.\begin{aligned} G_1: \quad & \frac{\partial G_1}{\partial t} = \frac{\partial^2 G_1}{\partial \hat{x}^2} \text{ for an instantaneous source at } (\hat{x}', t'), \\ & \frac{\partial G}{\partial \hat{x}}\bigg|_{\hat{x}=M_1} = \frac{\partial G}{\partial \hat{x}}\bigg|_{\hat{x}=-M_1} = 0; \end{aligned}\right\} \tag{9.34}$$

$$\left.\begin{aligned} G_2: \quad & \frac{\partial G_1}{\partial t} = \frac{\partial^2 G_1}{\partial \hat{y}^2} \text{ for an instantaneous source at } (\hat{y}', t'), \\ & \frac{\partial G_2}{\partial \hat{y}}\bigg|_{\hat{y}=0} = k_1 G_2(0, t); \ \frac{\partial G}{\partial \hat{y}}\bigg|_{\hat{y}=M_2} = 0, \end{aligned}\right\} \tag{9.35}$$

$$\left.\begin{aligned} &G_3\colon\ \frac{\partial G_3}{\partial t} = \frac{\partial^2 G_3}{\partial \hat{z}^2} \text{ for an instantaneous source at } (\hat{z}', t'), \\ &\left.\frac{\partial G_3}{\partial \hat{z}}\right|_{\hat{z}=0} = k_2\, G_3(0, t); \quad \left.\frac{\partial G_3}{\partial \hat{z}}\right|_{\hat{z}=M_3} = 0. \end{aligned}\right\} \tag{9.36}$$

It is easily seen then that $G \equiv G_1 G_2 G_3$ satisfies differential equation 9.23 and all auxiliary conditions 9.28-9.31 on the Green's function. Furthermore, since M_1, M_2, and M_3 are arbitrarily large numbers, it may be shown that G_1, G_2, and G_3 will approach the corresponding functions $\overline{G}_1$, $\overline{G}_2$, and $\overline{G}_3$ when boundary conditions are applied at infinity. From Ref. 3, p. 358,

$$\overline{G}_1(\hat{x}, t; \hat{x}', t') = \frac{1}{2\sqrt{\pi(t - t')}} \exp\left[-\frac{(\hat{x} - \hat{x}')^2}{4(t - t')}\right], \tag{9.37}$$

$$\begin{aligned} \overline{G}_2(\hat{y}, t; \hat{y}', t') = {} & \frac{1}{2\sqrt{\pi(t - t')}} \left\{\exp\left[-\frac{(\hat{y} - \hat{y}')^2}{4(t - t')}\right] + \exp\left[-\frac{(\hat{y} + \hat{y}')^2}{4(t - t')}\right]\right\} \\ & - k_1 \exp[(t - t') k_1^2 + k_1(\hat{y} + \hat{y}')] \operatorname{erfc}\left[\frac{\hat{y} + \hat{y}'}{2\sqrt{t - t'}} + k_1\sqrt{t - t'}\right], \end{aligned} \tag{9.38}$$

and

$$\begin{aligned} \overline{G}_3(\hat{z}, t; \hat{z}', t') = {} & \frac{1}{2\sqrt{\pi(t - t')}} \left\{\exp\left[-\frac{(\hat{z} - \hat{z}')^2}{4(t - t')}\right] + \exp\left[-\frac{(\hat{z} + \hat{z}')^2}{4(t - t')}\right]\right\} \\ & - k_2 \exp[(t - t') k_2^2 + k_2(\hat{z} + \hat{z}')] \operatorname{erfc}\left[\frac{\hat{z} + \hat{z}'}{2\sqrt{t - t'}} + k_2\sqrt{t - t'}\right]. \end{aligned} \tag{9.39}$$

Hence the final solution is Eq. 9.33 with G defined by $\overline{G}_1\overline{G}_2\overline{G}_3$. For the present problem, Eq. 9.29 becomes

$$\begin{aligned} \hat{T}(\hat{x}, \hat{y}, \hat{z}, t) = {} & \int_0^\infty \int_0^\infty \int_{-\infty}^\infty f(\hat{x}', \hat{y}', \hat{z}')\, G(\hat{x}, \hat{y}, \hat{z}, t; \hat{x}', \hat{y}', \hat{z}', 0)\, d\hat{x}'\, d\hat{y}'\, d\hat{z}' \\ & + \int_0^t dt' \int_0^\infty \int_{-\infty}^\infty \varphi(\hat{x}', \hat{y}', 0)\, G(\hat{x}, \hat{y}, \hat{z}, t; \hat{x}', \hat{y}', 0, t')\, d\hat{x}'\, d\hat{y}' \\ & + \int_0^t dt' \int_0^\infty \int_0^\infty \int_{-\infty}^\infty \psi(\hat{x}', \hat{y}', \hat{z}', t')\, G(\hat{x}, \hat{y}, \hat{z}, t; \hat{x}', \hat{y}', \hat{z}', t') \\ & \cdot\, d\hat{x}'\, d\hat{y}'\, d\hat{z}'. \end{aligned} \tag{9.40}$$

The original temperature profile $T(x, y, z, t)$ is obtained from Eq. 9.9.

In Eq. 9.40, the first integral is the contribution of the initial temperature distribution, the second integral accounts for the effect of heat transfer to the atmosphere, and the third integral represents the contribution of the heat source. This last term is easily evaluated for many cases of interest.

If a continuous point source is assumed to represent the outfall, S is given by Eq. 9.2 and ψ becomes, from Eq. 9.17

$$\left.\begin{aligned} \psi(\hat{x},\hat{y},\hat{z},t) &= \theta_0 Q_p \exp\left(-\frac{1}{2}\frac{v_x}{\sqrt{K_x}}\hat{x}_0 - \frac{1}{2}\frac{v_y}{\sqrt{K_y}}\hat{y}_0 \right. \\ &\quad \left. -\frac{1}{2}\frac{v_z}{\sqrt{K_z}}\hat{z}_0 + t\sum_{j=1}^{3}\frac{v_j^2}{4K_j}\right) \\ &\quad \text{for } \hat{x} = \hat{x}_0\delta(\hat{x}-\hat{x}_0),\ \hat{y} = \hat{y}_0\delta(\hat{y}-\hat{y}_0), \\ &\quad \hat{z} = \hat{z}_0\delta(\hat{z}-\hat{z}_0),\ t \geq t_0. \end{aligned}\right\} \tag{9.41}$$

Finally, integrating the product of ψ and the Green's function G over the lake volume, the third integral in Eq. 9.40 reduces to

$$\theta_0 Q_p \int_0^t \overline{G}(\hat{x},\hat{y},\hat{z},t;\hat{x}_0,\hat{y}_0,\hat{z}_0,t')$$

$$\cdot \exp\left(-\frac{1}{2}\frac{v_x}{\sqrt{K_x}}\hat{x}_0 - \frac{1}{2}\frac{v_y}{\sqrt{K_y}}\hat{y}_0 - \frac{1}{2}\frac{v_z}{\sqrt{K_z}}\hat{z}_0 + t'\sum_{j=1}^{3}\frac{v_j^2}{4K_j}\right)dt'. \tag{9.42}$$

For a continuous line source, if S is described by Eq. 9.3, ψ becomes

$$\left.\begin{aligned} \psi(x,y,z,t) &= \theta_0 Q_p \exp\left[-\frac{1}{2}\frac{v_x}{\sqrt{K_x}}\hat{x} - \frac{1}{2}\frac{v_y}{\sqrt{K_y}}\hat{y} \right. \\ &\quad \left. -\frac{1}{2}\frac{v_z}{\sqrt{K_z}}\hat{z} + t\sum_{j=1}^{3}\frac{v_j^2}{4K_j}\right] \\ &\quad \text{for } |\hat{x}-\hat{x}_0| \leq \frac{L}{2\sqrt{K_x}},\ \hat{y} = \hat{y}_0\delta(\hat{y}-\hat{y}_0), \\ &\quad \hat{z} = \hat{z}_0\delta(\hat{z}-\hat{z}_0),\ t \geq t_0, \\ &\quad = 0 \text{ for } |\hat{x}-\hat{x}_0| > \frac{L}{2\sqrt{K_x}} \text{ and } t < t_0. \end{aligned}\right\} \tag{9.43}$$

Consequently, the third integral in Eq. 9.40 reduces to

$$\theta_0 Q_p \exp\left(-\frac{1}{2}\frac{v_y}{\sqrt{K_y}}\hat{y}_0 - \frac{1}{2}\frac{v_z}{\sqrt{K_z}}\hat{z}_0\right)\int_0^t dt' \int_{\hat{x}_0 - L/2\sqrt{K_x}}^{\hat{x}_0 + L/2\sqrt{K_x}}$$

$$\exp\left[-\frac{v_x}{2\sqrt{K_x}}\hat{x}' + t'\sum_{j=1}^{3}\frac{v_j^2}{4K_j}\right]\bar{G}(\hat{x}, \hat{y}, \hat{z}, t; \hat{x}', \hat{y}_0, \hat{z}_0, t')\, d\hat{x}'. \qquad (9.44)$$

Note that the first two integrals in Eq. 9.40 and the Green's function $G \equiv \bar{G}_1\bar{G}_2\bar{G}_3$ are all independent of the choice of the source distribution.

d. General Comments about the Model

Several general observations are needed at this point. This model is only applicable in the far field, because jet-induced inertial mixing is neglected at the point of discharge. Bottom effects are not considered in the model; however, lake stratification can be accounted for in the initial condition, Eq. 9.4. From a practical point of view the inclusion of stratification in Eq. 9.4, rather than assuming an initially uniform ambient temperature, is sure to greatly complicate later integrations.

Wnek, as was noted earlier, can treat a variable-velocity and dispersive-field case by iterative techniques, but the method is extremely cumbersome and only the constant-parameter situation, Eq. 9.8, was considered here. Using the constant-parameter case, the author has carried out all the volume integrations in Eq. 9.40 in closed form for a continuous point source assuming constant ambient and equilibrium temperatures. He was not, however, able to evaluate the time integrals in closed form. The integrations with time are currently being programmed. One difficulty that may arise in the evaluation of the steady-state temperature distribution is taking the limit as $t \to \infty$ of solution equation 9.40. This raises the possibility of computer overflows with large t. From past experience, however, the author expects that with similar mathematical models a steady state should be reached within only 24 hr.

The main advantage of this model over other far-field models using a finite-difference approach lies, according to Wnek, in the expected reduction of computer time, since the various integrals involved in Eq. 9.40 can hopefully be evaluated using available integration subroutines. In addition, there is theoretically no conceptual difficulty in representing the heat source $S(x, y, z, t)$ as three-dimensional and time-variant. Any outfall shape can be considered; only the integration capabilities are limiting.

In summary, once input parameters and input functions

K_x, K_y, K_z = constant turbulent eddy diffusivities,

v_x, v_y, v_z = constant velocity field,

h = heat-transfer parameter,

$T_0(x, y, z)$ = initial temperature distribution,

$T_E(x, y, t)$ = equilibrium temperature,

and

$S(x, y, z, t)$ = source-distribution function

are given for a particular problem, Eqs. 9.40 and 9.9 may then be used to yield the time-dependent temperature distribution $T(x, y, z, t)$ for the physical situation described in Fig. 9.1.

References

1. Walter Wnek, Mathematical Model For the Dispersion of Heat into a Lake, Illinois Institute of Technology Research Institute (to be published).
2. Lake Michigan Currents, Federal Water Pollution Control Administration (Nov 1967).
3. H. S. Carslaw and J. C. Jaeger, Conduction of Heat in Solids, Oxford University Press (1959).

C. Complete Models

10. The Work of Donald W. Pritchard
(Chesapeake Bay Institute)
August 1969

a. List of Symbols

A_θ	Surface area with excess temperature equal to or greater than θ
b	Local width of jet distribution of velocity and temperature
b_0	Width of outfall
b_θ	Mean width of area within θ isotherm
$\bar{b}_\theta$	Maximum width of area within θ isotherm
c_p	Specific heat at constant pressure
D	Characteristic "critical" mixing depth of receiving body of water
D_0	Equivalent diameter of a rectangular outfall
D_θ	Thickness of plume at a distance ξ_θ where $\xi_\theta < \eta_1$ (when vertical mixing occurs)
h_0	Outfall depth
K	Surface-heat-transfer coefficient (a function of excess temperature θ)
n	Inverse-spreading rate
n_1	θ_0/θ_1
n_2	θ_0/θ_2
Q_H	Excess heat-rejection rate of power plant based on θ_0 $(= \rho c_p u_0 b_0 h_0 \theta_0)$
Q_0	Volumetric flow rate of power plant at discharge
R_i	Local Richardson number
u	Centerline velocity, a function of ξ
u_a	Velocity of transverse crosscurrent (assumed constant)
u_0	Initial velocity of the jet at discharge
$\Gamma(1°)$	Rate of heat loss from the area contained within the 1° isotherm
$\Delta\Gamma_{\overline{\theta_n}}$	Rate of heat loss from the area contained between the θ_n, θ_{n-1} isotherms
$\Delta A_{\overline{\theta_n}}$	Incremental area between θ_n and θ_{n-1} isotherms

$\Delta A_{0.5}$	Area having <u>mean</u> excess temperature 0.5°F
η_1	Longitudinal distance at which vertical entrainment ceases
θ	Local excess temperature
θ_0	Initial excess temperature at discharge
$\bar{\theta}$	Local excess temperature correction of the horizontal temperature distribution due to additional dilution resulting from vertical entrainment
$\theta_{\varphi'}$	Corrected excess temperature corresponding to the distance ξ_θ along the plume axis due to nonzero background temperature
$\bar{\theta}_n$	Mean excess temperature between the nth and (n-1)st isotherm
θ_1	Excess temperature at a given position resulting from thermal plume No. 1
θ_2	Excess temperature at a given position resulting from plume No. 2
θ'	Superposed excess temperature at a given position resulting from plume No. 1 and 2
ξ	Longitudinal distance measured along plume centerline
ξ_θ	Centerline distance out to a given excess temperature θ
ξ_v	Distance from the virtual source of the jet to the end of the region of flow establishment
ρ	Density of plume water (assumed constant)
φ	Background excess temperature

Notation

$(\ )_m$	Denotes that the parameter inside the parentheses has been determined assuming dilution (mixing) alone
$(\ )_{m,c}$	Denotes conditions after correction of the excess temperature distribution for surface cooling

b. Introduction

The thermal-plume model developed by Pritchard predicts the dispersion of a heated discharge from a rectangular outfall at the surface of a large receiving body of water. The model is basically a synthesis of previous theoretical and physical modeling results for buoyant and nonbuoyant jets, complemented with results the author has gleaned from field data obtained from existing power plants sited on bays, estuaries, and large lakes.

The model is simple and considers plume dispersion to be governed solely by momentum-jet entrainment, turbulent diffusion, and surface heat loss. An integral technique is used in which the plume velocity and excess temperature (above ambient) are assumed to have at each longitudinal position a "top-hat" distribution laterally and vertically. Buoyancy-induced convective motions are not considered. No ambient crosscurrent is assumed to exist in the theoretical development; yet, the author expects that the predicted centerline temperature decay and areas within isotherms are still accurate in the presence of a shore-parallel current less than 10% of the initial discharge velocity. In the model, environmental changes are reflected solely in the surface-heat-transfer coefficient K. Entrainment is accounted for by the specification of a fixed "inverse spreading rate" parameter $n = 6$. The lake bottom is assumed to have no effect other than upon the author's choice of a plume depth and, when necessary, upon the length and depth of an initial region of vertical entrainment.

The model handles both the jet and far-field regions; it predicts a two-dimensional temperature field and areas within isotherms down to a 1°F temperature excess. The parameters required for the application of this model are:

b_0 = width of rectangular outfall,

h_0 = depth of rectangular outfall,

Q_H* = excess heat-rejection rate of power plant based on θ_0,

θ_0 = initial excess temperature of the jet,

and

K = surface-heat-loss coefficient.

In spite of the simplifications made in the model development, the author claims the model to be conservative in many respects and simple to apply.

*Q_H would be identically equal to the total condenser heat-rejection rate if the condenser intake temperature were identically equal to the ambient temperature.

The author's theoretical development is carried out in four consecutive stages:

(1) Horizontal spreading is considered, neglecting vertical diffusion and surface heat loss to the atmosphere. A two-dimensional temperature field is determined for the jet and far-field regions.

(2) Vertical entrainment is then considered independent of horizontal spreading and surface heat loss. The depth is assumed constant, except possibly for a small region in the vicinity of the outfall where the depth grows slowly in a linear fashion. When vertical spreading is assumed to occur, a correction of the two-dimensional temperature field is made to account for the additional dilution.

(3) A second correction of the temperature field may be needed, depending upon the temperature of the water entrained into the plume. Due to possible recirculation of condenser cooling water, the diluting water mixed into the plume may have an excess temperature above 0.0°F. Once this additional correction on the temperature field is made, the areas within isotherms are calculated for the condition of mixing alone.

(4) Surface heat losses are then included in the analysis as a correction to the areas derived in stage 3. This surface-heat-loss correction yields the final two-dimensional temperature field and the isotherm areas.

Separating dispersion into distinct vertical and horizontal processes is common and facilitates the model development. Each of the four steps will be considered in some detail. First, a brief discussion of the dominant processes involving plume dispersion will be given as conceptualized by the author.

The author distinguishes between three primary processes, which lead to a decrease in excess temperature in a thermal plume. First, there is the initial dilution, which occurs through mechanical mixing of the heated water with the receiving water as a result of the excess momentum in the discharge stream. The second process involves natural mixing or turbulent diffusion of the heated effluent into the cooler ambient water. The third process is a loss of heat with a consequent reduction in excess temperature from the water body to the atmosphere.

According to the author, mechanical dilution is the primary process within the range between the plume's initial excess temperature θ_0 down to a value corresponding to about $0.2\theta_0$. This value is based mainly upon flume experiments done at the Chesapeake Bay Institute, where it was found that, when the centerline temperature decays to about $0.2\theta_0$, the temperature distribution begins to act like the asymptotic temperature spread from

a point source in a stagnant medium. Thus the temperature reduction beyond $0.2\theta_0$ would decay essentially inversely with distance. Pritchard found this relationship to be generally valid in the field when ambient turbulence dominates the dispersion.

Due to the large volume of the source, natural turbulent diffusion is a secondary process in the jet regime, initially acting only at the edges of the plume with only little cooling until the transverse distribution of temperature has been altered from an initial "top-hat" form to a bell-shaped form. Also in these initial regions, surface cooling contributed only a second-order correction to the distribution of excess temperature for temperatures greater than about 10% of the excess temperature at discharge. Surface heat loss seems to become increasingly more important compared to the other two processes when the excess temperature has decreased considerably and becomes the dominant process for excess temperatures less than about 1°F due to the relatively large plume areas involved at these low excess temperatures. The above conclusions concerning the loss of heat to the atmosphere were reached from comparisons of flume experimental data (no surface losses) and with actual field data obtained when surface heat exchange was significant.

c. Model Derivation and Discussion

(1) Horizontal Dispersion (no vertical spreading or surface heat loss). Pritchard considers horizontal dispersion due to a mechanical dilution and turbulent diffusion first. Vertical effects of this dilution are considered in Sec. d below as a correction. Surface heat loss is considered separately in Sec. f as a final correction.

The geometry illustrating horizontal spreading is shown in Fig. 10.1. The author assumes the spreading of the jet to be given by

$$b = \xi/n, \qquad \xi > \xi_V = nb_0, \tag{10.1}$$

where b is the width of the jet, ξ is the distance measured along the jet centerline, n is the inverse spreading rate of the jet taken as 6, and ξ_V is the length of the flow-establishment region in which no spreading is assumed to occur and where the jet maintains its initially top-hat profiles of velocity and temperature. For $\xi > \xi_V$, the jet begins to spread horizontally. The author assumes for simplicity that the excess temperature has a top-hat profile laterally at each longitudinal position downstream with the realization that in the established flow region the

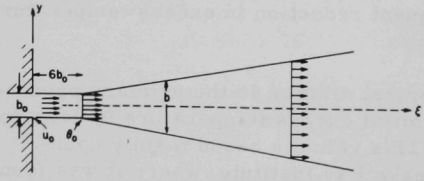

Fig. 10.1. Horizontal Spreading of Jet (mixing but no surface cooling)

profiles are more bell-shaped. Integral equations of momentum and heat-energy conservation are

$$\rho \int_{-b/2}^{b/2} u^2 \, dy = \rho u_0^2 b_0, \qquad \xi > \xi_v, \tag{10.2}$$

and

$$\rho c_p \int_{-b/2}^{b/2} u\theta \, dy = \rho c_p u_0 \theta_0 b_0, \qquad \xi > \xi_v. \tag{10.3}$$

Since $u = u(\xi)$, $\theta = \theta(\xi)$, for any position (ξ, y) within the jet, Eqs. 10.2 and 10.3 may be solved to yield

$$u(\xi) = u_0 \left(\frac{\xi_v}{\xi}\right)^{1/2} \tag{10.4}$$

and

$$\theta_\xi \equiv \theta(\xi) = \theta_0 \left(\frac{\xi_v}{\xi}\right)^{1/2}. \tag{10.5}$$

The equation of mass conservation is replaced essentially by Eq. 10.1, which gives the rate of spreading of the jet or, equivalently, the rate of ambient fluid entrainment. This is equivalent to a similarity assumption on entrainment.

The author's choice of $n = 6$ as the inverse spreading rate is based upon values found in the literature for the spreading of two-dimensional jets and upon plume experiments carried out by the Chesapeake Bay Institute. From the tank studies of Jen, Wiegel, and Mobarek,[1,2] an inverse spreading rate of one on seven was obtained. Their study involved the horizontal discharge of a heated jet at the surface of a large body of water at uniform density with no bottom interferences. For that situation, the jet experienced <u>three-dimensional</u> entrainment. The slope of the vertical spreading was one on seven, as was the horizontal spreading coefficient. The relationship between excess temperature and distance along the plume axis was

$$\frac{\theta}{\theta_0} = 7.0 \frac{D_0}{x}, \qquad x/D_0 < 100, \tag{10.6}$$

where $D_0 = \frac{1}{\pi}\sqrt{b_0 h_0}$ for a rectangular slot orifice. Other papers (Refs. 3-5 for example) have found inverse spreading rates ranging from five to seven for various submerged and surface buoyant and nonbuoyant jets. The author

states that when a bottom inhibits vertical mixing and/or when naturally existing thermal stratification is present, vertical mixing and vertical entrainment are generally inhibited to the point that entrainment appears to be primarily horizontal. For this reason, Pritchard assumes a two-dimensional jet. The number $n = 6$ was found in the literature to be most prevalent for two-dimensional nonbuoyant jets. The spreading rate $n = 6$ was also seen in flume experiments at the Chesapeake Bay Institute. It will be shown later that this two-dimensional assumption for plume dispersion yields more conservative results with respect to isotherm areas and centerline temperature decay than the assumption of three-dimensional dispersion.

The integral approach used above to derive the temperature distribution follows the technique first employed by Albertson et al.[6] for submerged jets. Albertson et al. used Gaussian, rather than top-hat, profiles and considered horizontal entrainment to occur right from the outfall, rather than from the downstream longitudinal distance ξ_V.

The determination of $\xi_V = 6b_0$ comes from the choice of the inverse spreading rate $n = 6$ and from the author's decision to allow the "virtual" source to coincide with the mouth of the orifice. In the literature, the point of intersection of the two diverging lines representing the spread of the jet defines the position of a "virtual" source. The length of the zone of flow establishment ξ_V would then be the distance from that virtual source to the point where the two diverging lines become separated by a distance equal to the width of the actual orifice. At present there is no clear agreement among experimenters as to the actual location of the virtual source. If the virtual source is located inside the actual orifice, part of the region of flow establishment would be within the outfall; if the diverging lines intersect outside the orifice, then there would be a longer region of flow establishment entirely within the receiving body of water. As stated, Pritchard assumes the virtual source to be coincident with the mouth of the actual orifice. Since the spreading rate of the jet width is one on six, $\xi_V = 6b_0$; thereby the region of flow establishment will initiate at the orifice and continue for six outfall widths downstream.

Clearly, the actual location of the virtual source is not critical. However, upon comparison of his model with data, Pritchard has found that his model predicts higher temperatures than is generally observed near the outlet, indicating that there is entrainment closer to the source than he has allowed for in his model. The discrepancy may be due in part or, in total, to the meandering of the jet as it issues from the outfall, creating difficulties in measuring the centerline temperature excess accurately, especially for a narrow orifice. The choice of the actual position of the virtual source and the neglecting of any spreading or entrainment in the flow-establishment region are not expected to lead to significant differences for temperatures at distances remote from the orifice.

The temperature distribution given by Eq. 10.5 is assumed to be valid for longitudinal distances ξ_θ where $0.2\theta_0 \le \theta \le \theta_0$. From Eq. 10.5,

$$\xi_\theta = \left(\frac{\theta_0}{\theta}\right)^2 nb_0, \qquad 0.2\theta_0 \le \theta \le \theta_0. \tag{10.7}$$

Now, beyond the point where $\theta = 0.2\theta_0$, the author assumes that dilution of the excess heat in the plume is primarily the result of natural mixing processes. In this region of the plume, the excess temperature along the centerline (uncorrected for surface cooling) would, as somewhat expected, decrease as the inverse first power of distance (natural diffusion from a continuous point source); thus,

$$\frac{\theta}{\theta_0} = 30b_0\left(\frac{1}{\xi}\right), \qquad \theta \le 0.2\theta_0. \tag{10.8}$$

The choice of the constant $30b_0$ (for $n = 6$) was made so that Eqs. 10.5 and 10.8 would match for $\theta = 0.2\theta_0$. A top-hat lateral distribution for temperature is assumed again for simplicity with the plume width defined by Eq. 10.1. In terms of θ, the distance ξ_θ may be written from Eq. 10.8 as

$$\xi_\theta = \frac{30b_0\theta_0}{\theta}. \tag{10.9}$$

Plume studies at Cape Kennedy[7] have shown that, in a truly three-dimensional situation, natural diffusion will cause an initial concentration to decay as ξ^{-2}; for pseudo two-dimensional motion, the concentration drops as $\xi^{-5/2}$. Again the assumption of two-dimensional dispersion would yield conservative results for his temperature field.

Equations 10.1, 10.5, and 10.8 now represent the two-dimensional temperature distribution considering horizontal dilution alone (no vertical mixing or surface cooling).

(2) The Vertical-spreading Correction. A major assumption made by the author is that for each body of water there is a "critical depth of mixing" peculiar to the natural processes of dispersion for that body. If the depth of the shoreline discharge (initial depth of the thermal plume) is less than this mixing depth, Pritchard states that the plume will entrain vertically from its initial depth to that mixing depth. The plume depth will then remain constant from that point on. The author assumes a linear growth of plume depth during vertical entrainment. If the initial depth is equal to or greater than the critical mixing depth, the plume thickness will remain constant from the discharge exit to the far-field position, where the plume is sufficiently diluted to mix into the deeper layers of the lake or bay.

This plume depth model was developed by the author upon examining plume data from large water bodies in the midwest and east. The author recommends that the critical depth be determined by examining data taken from existing thermal plumes on the lake or bay of interest. For Lake Michigan, Pritchard uses the value of 10 ft mainly surmised from the data taken at the Waukegan Power Station[8] on that lake. By examination of plume data taken on Lake Michigan and similar water bodies, the author found that the excess heat is generally contained in a depth of between 10 and 15 ft. The plume temperature changes slowly with depth down to a point where it begins to decrease sharply to a vertical depth where the temperatures are not measurably larger than ambient temperature.

The author chooses the critical depth as the midpoint of that region of rapid temperature decline. A plume with a critical depth of 10 ft may well contain measurable heat down to 15 ft. In general, according to the author, natural stratification in a lake or bay combines with a sloping bottom to maintain a certain stability, which keeps the plume at its critical depth. Even for cases void of a great deal of stratification, the author asserts that his field evidence indicates only a small variation in vertical thickness of the jet. If no evidence is available for a particular body of water, the author suggests the use of 10 ft for that critical depth. In the author's model application to the Zion Nuclear Power Plant on Lake Michigan, the vertical thickness at the discharge was a sheet 3 ft thick, whereby vertical entrainment was assumed in the model until the jet occupied a layer 10 ft thick. No further vertical entrainment was included.

In the author's model for the Waukegan Power Station on Lake Michigan, a bar confined the initial jet thickness to about 5 ft out to a distance of approximately 500 ft offshore. As the bottom then dropped off at the end of the bar, the model allowed for an additional 5-ft growth of the jet to a total 10-ft thickness. For Lake Erie, however, the author used 6 ft for the critical depth in modeling the Davis-Bessie Power Plant discharge because of previous plume studies on Lake Erie and because at the location of the plant the lake water is about 6 ft deep with a shelving bottom that does not increase in depth very rapidly.

These examples should indicate that each lake and outfall situation should be considered separately whenever possible. It will become apparent later that the value of the mixing depth chosen is not a critical parameter in the model, except for a small initial jet thickness requiring vertical entrainment for its depth to reach that critical value.

Assuming an essentially constant depth plume and a two-dimensional temperature field is a conservative approach. If a three-dimensional or a quasi-two-dimensional distribution were assumed, a remarkably smaller area would be affected by the plume with a more rapid temperature decay with distance. This will be discussed in more detail later.

Once the critical mixing depth has been determined for a given outfall situation, vertical entrainment will then occur if $h_0 < D$, where D is the critical depth. When $h_0 \geq D$, the plume will maintain a constant depth of h_0, according to the author.

Two situations are distinguished by the author. The first is the case, such as for Waukegan (beyond the 500-ft bar) and for some shoreline conditions off the California coast, where the bottom slopes off quite rapidly. From field evidence, the author suggests the use of a linear growth rate for the vertical plume thickness of 0.2 ft for every 100 ft measured longitudinally along the plume centerline.

The other situation of a slowly sloping bottom is more difficult to handle and is treated theoretically as described below. As before, the plume thickness is assumed to grow linearly but at a rate to be determined by the method of reflection. The distance between the outfall of depth h_0 and the first longitudinal position of the plume at which the plume thickness is the critical depth D is denoted η_1. The quantity η_1 is calculated first. Both the water surface and the bottom act as reflecting boundaries for the vertical spread of the jet. For this derivation, Pritchard assumes a fairly small slope in the lake bottom which may be approximated to be constant. He places a pseudosource of height h_0 above the water surface to cancel the flux there and a second pseudosource at an equal distance below the lake bottom to cancel the flux of the surface sources at the bottom. The geometry of the source placements is illustrated in Fig. 10.2. Assuming a spreading rate of one on six as in horizontal spreading, the author calculates the superposition of the temperature fields of the actual source and the two pseudosources. The distance η_1 is calculated as that distance at which the superimposed temperature fields yield a temperature equivalent to completely mixing the actual source over a layer of depth D.

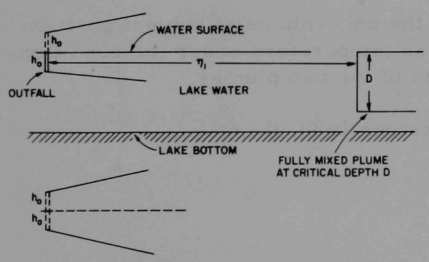

Fig. 10.2. Reflection Method to Calculate η_1

The author superimposes his plumes in a unique manner. In general, the derivation is as follows: If

θ_1 = excess temperature at a given position resulting from one thermal plume

and

θ_2 = excess temperature at the same position resulting from the other thermal plume,

and if θ_0 is the initial temperature at each of the two sources, then

$$\theta_1 = n_1\theta_0; \qquad \theta_2 = n_2\theta_0, \tag{10.10}$$

where

n_1 = the fraction of the unit volume at the subject position which is heated water from the first source

and

n_2 = the fraction of the unit volume at the subject position which is heated water from the second plume.

Then

$1 - n_1$ = the fraction of the unit volume at the subject position that has zero excess heat under the conditions of the first source

and

$1 - n_2$ = the fraction of the unit volume at the subject position that has zero excess heat under the conditions of the second source.

The product

$(1 - n_1)(1 - n_2)$ = the fraction of the unit volume at subject position with zero excess temperature under the conditions of superposition of the two plumes.

Thus, if the superposed excess temperature is θ', then

$$\theta' = \left[1 - (1 - n_1)(1 - n_2)\right]\theta_0$$

or

$$\theta' = \left[\theta_1 + \theta_2 - \frac{\theta_1\theta_2}{\theta_0}\right]. \tag{10.11}$$

For large distances from each source, the superposition formula reduces approximately to the simple sum of the two plume temperatures, which is the case for the superposed plume from point sources. Using this formula and the top-hat horizontal temperature field derived in Sec. (1) above and applying it vertically, the condition on η_1 is given by

$$\left(\frac{h_0}{D}\right)\theta_0 = \theta_0\left[\frac{6(2h_0)}{\eta_1}\right]^{1/2} + \theta_0\left[\frac{6(2h_0)}{\eta_1}\right]^{1/2} - \frac{\theta_0\left[\frac{6(2h_0)}{\eta_1}\right]^{1/2}\theta_0\left[\frac{6(2h_0)}{\eta_1}\right]^{1/2}}{\theta_0}. \tag{10.12}$$

The solution of the above quadratic equation for η_1 is

$$\eta_1 = \frac{12h_0}{(1 - \sqrt{1 - h_0/D})^2}. \tag{10.13}$$

Now, assuming that the jet thickens by vertical entrainment in a linear manner from h_0 feet at the source to D feet at a distance η_1, the vertical thickness D_θ of the plume at a point where the excess temperature is θ is

$$\left.\begin{aligned} D_\theta &= h_0 + \frac{D - h_0}{\eta_1}\xi_\theta, & \xi_\theta \le \eta_1, \\ &= D, & \xi_\theta > \eta_1, \end{aligned}\right\} \tag{10.14}$$

where ξ_θ is the distance along the axis of the plume to the excess temperature θ. If the plume is assumed to be uniformly mixed at each cross section, the dilution ratio of the plume, which is also spreading by horizontal entrainment, is assumed to be augmented by the factor h_0/D_θ.

Once the dilution ratio h_0/D_θ is determined, the two-dimensional temperature distribution obtained for horizontal entrainment and mixing only

$$\left.\begin{aligned} \xi_\theta &= 6b_0\left(\frac{\theta_0}{\theta}\right)^2, & \theta \ge 0.2\theta_0, \\ &\text{and} \\ \xi_\theta &= 30b_0\frac{\theta_0}{\theta}, & \theta < 0.2\theta_0, \end{aligned}\right\} \tag{10.15}$$

can now be corrected. For each θ used to compute ξ_θ, a corrected value $\bar{\theta}$ is found from

$$\bar{\theta} = \frac{h_0}{D_\theta}\theta. \tag{10.16}$$

The values $\bar{\theta}$ versus ξ_θ are interpolated to find ξ'_θ, the corrected distance along the plume axis to the excess temperature θ. The values ξ'_θ for each θ now represent the two-dimensional temperature field due to horizontal and vertical mixing neglecting surface cooling.

At this point, a few comments should be made concerning the correction for vertical mixing. First, the reflection method used to calculate η_1 removes heat flux from the bottom surface by the placement of the two pseudosources, but does not remove the heat flux at the surface from the bottom pseudosource. The heat flux can be removed from the surface

and the bottom only by the usual technique of positioning an infinite number of sources above the surface and below the lake bottom at equal distances from one another. It can only be surmised that the author assumed the contribution of these terms to be of second order and therefore negligible. The use of the spreading rate of one on six for the vertical spreading is an assumption here. For three-dimensional diffusion at the surface of a large body of water, Wiegel, Mobarek, and Jen[2] found a vertical spreading rate of one on seven with no bottom interference. Pritchard is thus assuming that his jet entrains vertically at the same rate it entrains laterally. Concerning his general method of superposition of overlapping thermal plumes, the method is purely analytical. It was not derived with any experimental data at hand, nor has it since been compared with any field or hydraulic data. Until that is done, the method must be considered unverified. The above superposition technique was employed by Pritchard in his analysis and prediction of the temperature distribution resulting from the Zion discharge,[8] where two offshore discharges have been constructed which yield intersecting plumes.

The author's model for vertical diffusion is approximate at best. The author does not have a three-dimensional model that includes a diffusion term or a vertical entrainment term that results in a solution for the vertical thickness. He asserts, however, that no three-dimensional model now available can predict vertical plume thickness that matches his observational data.

Any accurate model of vertical spreading should involve some assessment of the effects of vertical shear in the velocity field and vertical density gradients which control vertical entrainment. A well-known criterion for vertical entrainment is the so-called Richardson number R_i. Vertical spreading will be initiated when R_i is less than about 0.8 and will cease when $R_i \geq 0.8$. The use of this criterion would probably have led to a more accurate determination of η_1.

(3) Background Temperature Correction. The model as previously discussed implicitly assumes that the receiving body of water is an infinite sink from the standpoint of dilution and surface cooling. In some practical situations, the lake or bay is not sufficiently large or the natural exchange mechanisms within the body do not adequately supply a sufficient quantity of "new" dilution water to the inshore region at which the plant is sited. Under such circumstances, the author determines a "background temperature" and considers the entraining water to have some excess temperature rather than 0.0°F. This "background temperature" is estimated by calculating the excess temperature that would exist if the heated effluent were completely mixed into the available rate of supply of diluting water to the inshore area where the heated effluent is being discharged.

For a discharge into a unidirectional flowing stream such as a large river, the available supply of dilution water would simply be the volumetric flow rate of the river. In an estuary, the ocean and river inflow provide two sources of new water. For an estuary system, the author uses a mathematical model of circulation with the known distribution of salinity as a conservative tracer to compute how much new water is available. The background temperature there is essentially the excess temperature that is derived from assuming that the total heat flux of the plant is mixed into the available new river and ocean water. The value obtained is then corrected for surface cooling. The author has used this procedure for the Surry Plant discharge on the James River[9] and the Calvert Cliffs Nuclear Power Plant on the Chesapeake Bay.[10] At Calvert Cliffs, for example, the author found that the total volumetric flow of new water was about 90,000 cfs throughout the year due to the relative balancing between the river outflow and sea water coming in upstream at different times of the year. From that discharge, the excess temperature of the entraining water was calculated as 0.6°F from mixing alone and adjusted to 0.4°F by allowing for surface cooling over the area of the tidal segment. This latter value was used as the background temperature of the new water mixed into the plume for that site.

For a lake or bay situation, the calculation is not so straightforward. Short of building a hydraulic model or undertaking an extensive field program, the author knows of no general method for calculating or estimating the background temperature. At the Davis-Bessie Nuclear Power Station on Lake Erie, recirculation of heated water was expected due to the presence of islands and shoals found in the relatively sheltered and limited western basin of Lake Erie where the heated discharge would enter. There, the author estimated the background temperature as 0.5°F, based upon what he concluded to be the volume rate of flow of water through the entire western basin of that lake and the rate of heat discharge of the power plant.* For power plants on Lake Michigan, the author recommends no background temperature correction due to the open and fairly straight shoreline and the expected abundant supply of dilution water predicted from flume tests and from the examination of lake circulation and bottom topography data. Although no method for estimating the background temperature is singly recommended by Pritchard, an estimate should, however, be made when required. Once the background temperature is determined, the two-dimensional temperature distribution is corrected as follows. For a given ξ_θ, θ is replaced by

$$\theta'_\varphi = \left(\frac{\theta}{\theta_0}\right)\theta_0 + \left(1 - \frac{\theta}{\theta_0}\right)\varphi, \tag{10.17}$$

*The Davis-Bessie Plant design presently calls for the use of a natural-draft evaporative cooling tower in place of a once-through cooling system.

where

φ = background temperature (above ambient),

$\frac{\theta}{\theta_0}$ = fraction of mixture that is condenser cooling water,

$1 - \frac{\theta}{\theta_0}$ = fraction of mixture that is diluting water

and

θ'_φ = corrected excess temperature corresponding to the distance ξ_θ along the plume axis.

For a fixed θ, a corrected distance corresponding to θ, denoted ℓ_θ, may be determined by interpolating values of ξ_θ.

With corrections made for possible vertical entrainment and background temperature, the areas within isotherms (mixing alone, no cooling) may now be calculated. The theoretical width of the top-hat distribution was assumed to have the form of Eq. 10.1. Because the actual lateral distribution of temperature is more bell-shaped, the author uses some empirical results in his calculation of areas within isotherms. After examining a great deal of experimental data, both from physical modeling and in the field (with $K \approx 0$), Pritchard developed an empirical formula for calculating areas within isotherms and a series of guidelines for the schematic representation of the horizontal distribution of excess temperature in the thermal plume.

(a) The maximum width of the area having an excess temperature equal to or greater than θ is

$$\bar{b}_\theta = \tfrac{1}{4}\xi_\theta. \tag{10.18}$$

The area within the θ isotherm, A_θ, is

$$A_\theta = 0.86\bar{b}_\theta\xi_\theta = 0.215\xi_\theta^2. \tag{10.19}$$

(b) The area within a given isotherm θ increases smoothly in width from the outfall, attaining a maximum width, $\bar{b}_\theta$, at a distance along the plume axis equal to $0.33\xi_\theta$.

(c) The area defined by isotherm θ has a constant width b_θ from longitudinal distance $0.33\xi_\theta$ to the point $0.75\xi_\theta$.

(d) The shape of the isotherm between longitudinal distance $0.75\xi_\theta$ and the maximum distance ξ_θ is "tongue"- or "bullet"-shaped.

These approximate formulas and guidelines were developed from examination of the results of flume studies at the Chesapeake Bay Institute, from model studies done for the Pilgrim Nuclear Power Station on Cape Cod Bay, and from data taken at small existing plants in the Chesapeake Bay region such as the Chalk Point Plant and the Chesterfield Plant on the James River. The hydraulic modeling done at Vicksburg and the experimental data obtained from the Waukegan Plumes[8] were also included. The author found that these plume relationships were approximately valid, even for the case of a nonnegligible cooling coefficient since the effect of surface heat transfer seemed to be a nearly uniform shrinking in plume dimensions and areas.

(4) The Surface-cooling Correction. To correct the areas within isotherms calculated from mixing processes above, the author defines

A_{θ_n} = area of the plume inside isotherm θ_n (i.e., area with excess temperature $> \theta_n$).

Then

$\Delta A_{\overline{\theta_n}} = A_{\theta_n} - A_{\theta_{n-1}}$ = area between two adjacent isotherms,

where

$\overline{\theta_n} = \dfrac{\theta_n + \theta_{n-1}}{2}$ = mean excess temperature for that incremental area

The rate of loss of excess heat from the area between two isotherms is given by

$$\left(\Delta\Gamma_{\overline{\theta_n}}\right)_m = K\overline{\theta}_n\left(\Delta A_{\overline{\theta_n}}\right)_m \tag{10.20}$$

or

$$\left(\Delta\Gamma_{\overline{\theta_n}}\right)_{m,c} = K\,\overline{\theta}_n\left(\Delta A_{\overline{\theta_n}}\right)_{m,c} \tag{10.21}$$

where the subscript m refers to the value of the parameter determined from mixing only and m,c refers to the parameter value after the correction for surface cooling has been made. The quantities $\left(\Delta\Gamma_{\overline{\theta_n}}\right)_m$ are known and are used to derive $\left(\Delta\Gamma_{\overline{\theta_n}}\right)_{m,c}$ and $\left(\Delta A_{\overline{\theta_n}}\right)_{m,c}$.

Pritchard considers the rate of excess heat loss to the atmosphere as a decrease in source strength of the heated effluent. Thus heated water distributed at a given isotherm responds as if the cooling process were equivalent to reducing the source strength by the amount of heat that has been lost between the source and that isoline of excess temperature. This is represented by

$$\left(\Delta A_{\overline{\theta}_n}\right)_{m,c} = \left(\Delta A_{\overline{\theta}_n}\right)_m \left[\frac{Q_h - \sum_{i=1}^{n} \left(\Delta\Gamma_{\overline{\theta}_i}\right)_{m,c}}{Q_h}\right], \tag{10.22}$$

where the numerator of the bracketed term represents the effective source strength applicable to the θ_n isotherm. The bracketed correction factors are illustrated in Fig. 10.3 for the first four isotherms. Using the relationship

$$\left(\Delta\Gamma_{\overline{\theta}_n}\right)_{m,c} = \frac{\left(\Delta A_{\overline{\theta}_n}\right)_{m,c}}{\left(\Delta A_{\overline{\theta}_n}\right)_m} \left(\Delta\Gamma_{\overline{\theta}_n}\right)_m \tag{10.23}$$

derived from Eqs. 10.20 and 10.21, the simultaneous linear equation set 10.22 may be solved to yield

$$\left(\Delta A_{\overline{\theta}_n}\right)_{m,c} = \left(\Delta A_{\overline{\theta}_n}\right)_m \frac{Q_h - \sum_{i=1}^{n-1} \left(\Delta\Gamma_{\overline{\theta}_i}\right)_{m,c}}{Q_h + \left(\Delta\Gamma_{\overline{\theta}_n}\right)_m}. \tag{10.24}$$

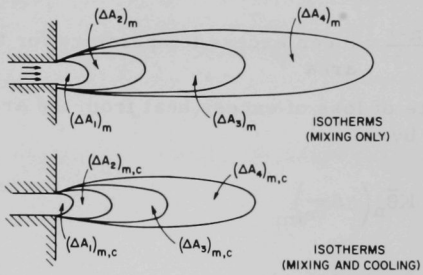

$$(\Delta A_1)_{m,c} = (\Delta A_1)_m \left[\frac{Q_h - (\Delta\Gamma_1)_{m,c}}{Q_h}\right]$$

$$(\Delta A_2)_{m,c} = (\Delta A_2)_m \left[\frac{Q_h - (\Delta\Gamma_1)_{m,c} - (\Delta\Gamma_2)_{m,c}}{Q_h}\right]$$

$$(\Delta A_3)_{m,c} = (\Delta A_3)_m \left[\frac{Q_h - (\Delta\Gamma_1)_{m,c} - (\Delta\Gamma_2)_{m,c} - (\Delta\Gamma_3)_{m,c}}{Q_h}\right]$$

$$(\Delta A_4)_{m,c} = (\Delta A_4)_m \left[\frac{Q_h - (\Delta\Gamma_1)_{m,c} - (\Delta\Gamma_2)_{m,c} - (\Delta\Gamma_3)_{m,c} - (\Delta\Gamma_4)_{m,c}}{Q_h}\right]$$

$$(\Delta\Gamma_i)_{m,c} = \frac{(\Delta A_i)_{m,c}}{(\Delta A_i)_m} (\Delta\Gamma_i)_m, \quad i = 1, \ldots, 4.$$

Fig. 10.3. Surface-area Correction due to Heat Loss to the Atmosphere

Equation 10.24 is applied in steps starting with n = 1. Here the summation term is zero and hence the corrected incremental area for n = 1 is obtained immediately from Eq. 10.24 using $\left(\Delta\Gamma_{\overline{\theta}_1}\right)_m$ computed from Eq. 10.20. The corrected rate of heat loss within that innermost isotherm is calculated from Eq. 10.23 setting n = 1. Now, for n = 2, the value of $\left(\Delta\Gamma_{\overline{\theta}_1}\right)_{m,c}$ is used in the summation term of Eq. 10.22 to allow the computation of the incremental area bounded between the first two isotherms. Equation 10.23 is again used to calculate $\left(\Delta\Gamma_{\overline{\theta}_2}\right)_{m,c}$. The first two corrected heat-loss terms are used in Eq. 10.22 to yield $\left(\Delta A_{\overline{\theta}_3}\right)_{m,c}$, from which the corresponding heat-loss term is calculated from Eq. 10.23. In this manner, all corrected incremental areas and heat-loss terms are calculated. Once this is accomplished, the total corrected areas $\left(A_{\theta_n}\right)_{m,c}$ may be calculated by summing the incremental areas

$$\left(A_{\theta_n}\right)_{m,c} = \sum_{i=1}^{n} \left(\Delta A_{\overline{\theta}_i}\right)_{m,c} .$$

Using Eqs. 10.18 and 10.19 for the surface-cooling corrected parameters $\left(A_{\theta_n}\right)_{m,c}$, $\left(\xi_\theta\right)_{m,c}$, and $\left(\overline{b}_{\theta_n}\right)_{m,c}$ yields

$$\left(\xi_{\theta_n}\right)_{m,c} = \left(\xi_{\theta_n}\right)_m \left[\frac{\left(A_{\theta_n}\right)_{m,c}}{\left(A_{\theta_n}\right)_m}\right]^{1/2} \tag{10.25}$$

and

$$\left(\overline{b}_{\theta_n}\right)_{m,c} = \left(\overline{b}_{\theta_n}\right)_m \left[\frac{\left(A_{\theta_n}\right)_{m,c}}{\left(A_{\theta_n}\right)_m}\right]^{1/2} . \tag{10.26}$$

From these relationships the final areas within isotherms and the final two-dimensional top-hat temperature distribution has been determined.

Reflecting upon the argument just presented for the surface-cooling correction to the areas within isotherms, it would seem that the correction between uncorrected and corrected isotherm areas would more accurately be written

$$\left(\Delta A_{\overline{\theta}_n}\right)_{m,c} = \left(\Delta A_{\overline{\theta}_n}\right)_m \left[\frac{Q_h - \sum_{i=1}^{n} \left(\Delta\Gamma_{\overline{\theta}_i}\right)_{m,c}}{Q_h}\right]^2$$

rather than as postulated by the author in Eq. 10.22. The temperature excess at a given distance is directly proportional to the source strength. Consequently, the area (length squared) within a given isotherm should be proportional to the square of the source strength. At this point, it would

seem that this may be a correction that should be applied to Pritchard's model. This modification of the model increases the cooling correction; as it stands, the author's model is conservative in this respect.

In general, for lake situations the author carries out his predictions based upon the above model to excess temperatures equal to or above 1°F above ambient. This is due to the fact that one seldom can determine the ambient temperature to within 0.5°F. Consequently, any predictions of the temperature distribution would be purely speculative and unverified. In fact, temperatures in the natural environment can vary on the order of several degrees in space and in time, and to select the ambient temperature within 0.5°F from the field data would be extremely difficult. A purely theoretical estimate of the area having a <u>mean</u> excess temperature of 0.5°F can be computed from

$$\Gamma(1°) = \sum_{i=1}^{n} \left(\Delta\Gamma_{\overline{\theta}_i}\right)_{m,c} = \sum_{i=1}^{n} K\overline{\theta}_i \left(\Delta A_{\overline{\theta}_i}\right)_{m,c}$$

and

$$Q_h - \Gamma(1°) = K(0.5°F)0.5\ \Delta A_{0.5°},$$

where

$\Gamma(1°)$ = the total heat lost to the atmosphere from areas having excess temperature equal to or greater than 1°F,

$Q_h - \Gamma(1°)$ = amount of surface heat loss from areas having excess temperatures less than 1°F,

and

$\Delta A_{0.5°}$ = the area having <u>mean</u> excess temperature of 0.5°F.

The above analysis assumes that the flux of excess heat from the water to the atmosphere must ultimately be equal to the flux of heat rejected to the lake in the heated discharge. In the above analysis, the heat beyond the 1°F isotherm is thought of as being lost entirely at the 0.5°F isotherm. The area beyond the 1°F isotherm is, in reality, infinite for a semi-infinite lake acting as heat sink. The quantity $\Delta A_{0.5}$ is thus only a fictional quantity, defined by the above equation, to assess the relative size of the area influenced by the heated discharge beyond the 1°F isotherm.

d. <u>Model Predictions and Verifications</u>

The above-described model developed by Pritchard has been applied to various outfall and field situations; it has been compared to several existing thermal plumes and also has been used as a predictive model for the design of a number of discharge structures. Actual comparisons with field

data are either presently unavailable, or the comparison is made with data that are really not of the quality or quantity that can actually validate a model of that nature.

Three sample theoretical computations carried out by the author[11] are given in Table 10.1 with the predicted isotherms plotted in Fig. 10.4. In each case it is assumed that the rate of heat rejection from a power plant is 6.8×10^9 Btu/hr and that this heat is rejected at the surface of a large lake from a rectangular outfall. The initial temperature rise is assumed to be 20°F, and hence the required volumetric flow rate is 1520 ft^3/sec. It is also assumed that outfall height is 10 ft in a lake whose "critical depth" is also 10 ft, requiring no initial vertical mixing. Moreover, the receiving body of water is assumed to continually provide new diluting water, so that the background temperature is 0.0°F. Pritchard assumes that no long-shore currents are present, or else the discharge structure is located sufficiently far offshore so that free passage of dilution water can occur on both sides of the plume in the presence of a small long-shore current (less than 10% the initial outfall velocity, according to Pritchard). (These assumptions prevent the possibility of the plume bending toward the shore with a cutoff of entrainment on the inshore side of the plume.)

Case I (see Table 10.1) represents a discharge structure for which dilution of the heated effluent by the cooler ambient water is minimized. A wide discharge orifice was chosen with a small initial jet velocity. Case II

Table 10.1. Sample Area within Isotherm Calculations[11]

The area, in acres, contained within specified isotherms of excess temperature in the thermal plume resulting from the discharge of the condenser cooling water from a steam-electric generating plant, rejecting 6.8×10^9 Btu/hr of excess heat at the condensers, for three different discharge structure designs as described in the text. (This rate of heat rejection corresponds to a nominal 1000-MWe nuclear power plant or to a nominal 1700-MWe fossil fuel plant at present efficiency levels.)

	Case I	Case II	Case III
θ_0, °F	20	20	20
Q_c, $ft^3\ sec^{-1}$	1520	1520	1520
b_0, ft	500	50	15
u_j, ft sec^{-1}	0.30	3.0	10.1
θ, °F	Area, in acres, for:		
0.14	1.66×10^2	1.9	0.2
10	5.42×10^2	7.1	0.6
5	2.57×10^3	1.11×10^2	10
3	3.19×10^3	4.65×10^2	44
2	3.26×10^3	1.00×10^3	99
1	3.29×10^3	3.47×10^3	3.91×10^2

represents a discharge structure designed to promote rapid mixing and dilution. A small discharge width was chosen with a resultant high initial jet velocity. The author states that a number of power plants under construction or in the planning stage on lakes, bays, or estuaries are adopting the design principles of Case III. Among them are the Surry Nuclear Power Station on the James River Estuary, the Morgantown Power Plant on the Potomac River Estuary, the Calvert Cliffs Nuclear Power Plant on Chesapeake Bay, the Pilgrim Nuclear Power Station on Cape Cod Bay, and the Zion Nuclear Power Station on Lake Michigan. The results of the model computations are illustrated in terms of areas within isotherms and a plot of these contours in Table 10.1 and Fig. 10.4, respectively. Clearly, Case III represents the greatest dilution with area of the heated effluent.

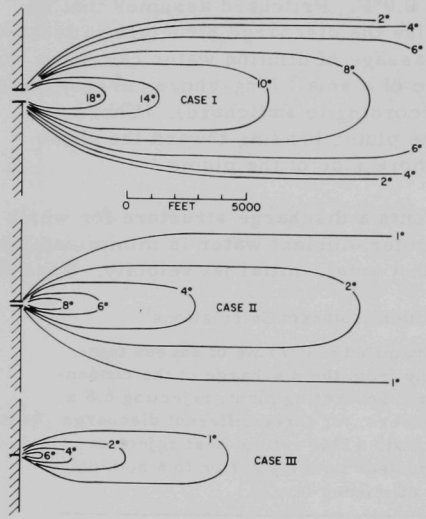

Fig. 10.4. Horizontal Distribution of Excess Temperature[11]

Pritchard's model predicts that the heat lost to the atmosphere beyond the 1°F isotherm, Q_h - $\Gamma(1°)$, will be on the order of magnitude of 80-98% of the initial heat discharged by the power plant for the outfall conditions described in Cases I-III above. This result is indeed realistic, even though derived with the concept of a two-dimensional model.

e. General Discussion of the Model

Pritchard's model implicitly assumes zero ambient current. If, however, the shore-parallel current is sufficiently large compared to the initial jet velocity, a number of complexities arise which cannot be handled by the author's model. First, the trajectory of the jet will be bent over into a direction parallel to the current. Second, the entrainment and consequent dilution may be significantly reduced on the inshore side of the plume. Application of the author's model to that case is expected to yield significantly smaller areas and centerline temperatures than would actually occur. Carter[12] and Pritchard have concluded from experimental evidence in the laboratory and in the field that, for an ambient current velocity greater than approximately 10% of the initial jet velocity, these complexities will be significant enough to require new analysis. If the outfall structure is located at the end of a long discharge canal formed by jetties which extend above the water surface between the shoreline and the discharge orifice, the same difficulties occur in the restriction of the supply of new dilution water. In such cases, Pritchard uses the theoretical model of Carter[12] in predicting the temperature field and plume areal characteristics (see Sec. III.A.2).

Reference 13 compares the Carter model* with the Pritchard results for a "typical" shoreline situation where the transverse ambient current is equal to 20% of the initial discharge velocity of the jets and where lateral entrainment is significantly decreased on the inshore side. Carter's model predicts a fourfold increase in plume areas and a twofold increase in centerline temperature over Pritchard's results. From an examination of field and flume data, Pritchard suggests that for a current velocity u_a greater than 10% of the initial jet velocity u_0, Carter's model should be used. For $u_a < 0.1\ u_0$, the author asserts from the data he has seen that his model yields satisfactory predictions for centerline temperatures and isotherm areas. (The actual plume trajectory will, however, be altered by the current.) Hydraulic-model studies carried out for the Pilgrim Power Station on Cape Cod Bay support his conclusion. In spite of the small long-shore current present in that case, the discharge traveled far enough offshore to allow new water to be brought in along the shore on the downstream side to continually provide new dilution water; the predictions, the dilution and isotherm areas were characteristic of the Pritchard model, which assumes no long-shore current.

The adverse effects of a shore-parallel current are reduced if the discharge structure is located offshore and if the enclosed discharge pipes are buried below the bottom of the lake, between the shoreline and the discharge orifice, thus allowing a free flow of the ambient current inshore of the discharge. Presently, studies are being made at the Chesapeake Bay Institute to find a relationship between the strength of a long-shore current and the distance offshore that the jet should be discharged at which the plume behaves, irrespective of its bending, as if there were no long-shore currents. At present, due to purely analytical arguments, the author suggests that a significant reduction in the adverse effects of a transverse current would result if the outfall were located offshore a distance of 100 times the initial discharge width. In any case, even for the critical case of a long-shore current from a shoreline discharge cutting off inshore entrainment, the isotherm areas will be much smaller for a high-speed discharge than for a low-speed discharge.[13]

A few additional remarks will now be made about Pritchard's two-dimensionality assumption. First, a true three-dimensional (3D) jet seldom occurs in nature. Only on a coastline whose bottom drops off very rapidly with depth with no natural vertical density gradient present could three-dimensional spreading occur for a discharged surface jet. In most field conditions, either the natural bottom or the natural thermal stability prevents three-dimensional jet entrainment over the entire flow field. The assumption of a two-dimensional (2D) solution is safer and probably more conservative with respect to the temperature field and isotherm areas.

---

*As stated in the discussion of Carter's work (Sec. III.A.1.), there is an algebraic error in Carter's graphical solution for the centerline trajectory. Pritchard has compared his model with the uncorrected Carter model; the effect of any correction has not yet been determined.

Three-dimensionality yields more rapid mixing and much smaller areas and volumes affected by the discharge. In Ref. 14, the author compares his model to the results of the laboratory studies of Jen, Wiegel, and Mobarek.[1,2] The latter found Eq. 10.6 to represent the three-dimensional temperature distribution due to a surface discharge of heated water into a uniform-density, very deep flume (compared to orifice dimensions).

For input parameters

b_0 = 14 ft,

h_0 = 10 ft,

Q_H = 7.5 x 10^9 Btu/hr,

θ_0 = 20°F,

and

Q_0 = 1670 ft^3/sec (volumetric flow rate),

the comparison between Pritchard's results and that of Jen et al. with respect to areas within surface isotherms is given in the following table:

	Areas, acres	
Isotherm	Pritchard (2D)	Jen, Wiegel, and Mobarek (3D)
14°	0.2	-
10°	0.6	0.2
5°	10.0	0.7
3°	44.0	2.1
2°	99.0	4.6
1°	339.1	18.4

Clearly, from this comparison, conditions that allow for vertical mixing yield smaller isotherm areas and, consequently, a greater dilution with distance. However, for the same outfall conditions, a three-dimensional jet has a greater vertical spread of heat and temperatures than the corresponding two-dimensional jet. Finite, though relatively small, temperatures can be found at larger subsurface depths when three-dimensional entrainment occurs. Consequently, Pritchard's model is conservative in these respects. This will also be true for a more likely pseudo two-dimensional-type field situation with respect to vertical entrainment and dilution.

The critical parameter in the determination of the size of the areas within isotherms is not the depth of the discharge or the "critical lake depth," but the width of the orifice b_0. If the depth of the jet at discharge

were 5 ft and remained at 5 ft, the jet velocity would have to be twice as great as for a constant 10-ft plume depth with the same orifice width. Consequently, the resulting entrainment will be almost the same in both cases. The depth selection is not so critical, except for an initial plume thickness smaller than 10 ft whereby the jet is assumed to entrain, where depth allows it, to 10 ft and from then on will not entrain. Pritchard states that differences of the order of ±50% or even numbers twice as large as a chosen plume depth would not seriously change the predicted isotherm area results of his model, due to the compensating effect of changing the velocity when the thickness is altered.

f. Final Remarks

At this point a few general comments can be made about the Pritchard model. It is simple to apply, and it represents a limiting case in its conservative treatment of a few major phenomena; one such is vertical mixing, which has already been discussed in great detail. It may or may not be conservative with respect to the background temperature, depending upon how it is handled in an individual case. If it is assumed to be zero, the model results may not be conservative but optimistic. Concerning transverse currents, the model is not expected to be conservative if a portion of the inshore boundary is prevented from receiving new dilution water.

Buoyancy effects are completely neglected. There is no dependence of the temperature distribution on the initial Froude number. If the initial discharge velocity is not high, the additional lateral spreading due to buoyant convective motions would be expected to distort the simple linear spread assumed in the model. Also, the lateral temperature distribution at a given longitudinal position is really not top-hat; it is more bell-shaped and vertically probably somewhat J-shaped. The specific value of the bottom slope in inhibiting vertical mixing of the plume in the lake or bay is not handled analytically. More complex models do handle some of these features in a reasonably satisfactory manner; yet these same models tend to have other deficiencies of their own. The main criticism of the Pritchard model is that it is too simplistic to be all-encompassing. There is no inclusion of some of the major complications that may well be important in certain field cases.

In short, the Pritchard analysis is by no means a complete model. As recognized by the author, there are three main areas in which additional improvements would be useful. The first involves vertical mixing, which hopefully would remove the arbitrary choice of a constant mixed layer. More conclusive information on the dependence of vertical entrainment and vertical mixing on the Richardson number or on some measure of the vertical stability, such as vertical shear in the velocity field and vertical density gradients, would be instructive as a way to predict vertical spreading. Second, a better treatment of the transition zone between the

region of dominance of momentum jet entrainment and natural mixing should be made. This zone is not fixed as is assumed in the model. A better understanding of the changeover from the plume being controlled by its own velocity field to the plume being controlled by the large-scale natural mixing processes is needed. Third, more data are needed to be able to provide for an ambient temperature correction due to the lack of an infinite amount of new water available for dilution. This point, however, is weak in most models. Finally, more information is needed to accurately assess the cross-current value at which transverse flow becomes sufficiently small to be unimportant. According to Pritchard's present understanding of the evidence, plume bending is not important with respect to areas and centerline temperature decay for small currents, yet is important to determine the precise jet shape and trajectory. Thus, aside from stagnant-lake situations, the Pritchard model cannot be used to determine the precise location of the thermal plume, only its isotherm areas and centerline temperature decay. Again, Pritchard uses the Carter model when $u_a > 0.1u_0$. Also, the model should be applied only for larger Froude numbers (greater than about 2, say) due to the numerous assumptions in the model requiring a jet-like behavior of the discharge.

Pritchard's model, in its present form, does not handle the question of the partition of heat between that lost to the atmosphere and that retained by the deeper layers of the lake. According to the Pritchard model, all the heat discharged by the power plant is lost to the atmosphere. This assumption in effect was probably made to yield a conservative estimate of the area within the low-temperature isotherms. In reality, some of the heat will always be retained by the lake for eventual release to the atmosphere during other portions of the year. The model of Sundaram et al. (see Sec. III.C.11) has addressed this issue analytically.

In summary, Pritchard's model is basically an intuitive one based upon the observation of lake, river, and estuary plumes. He has forgotten about more field data than most researchers have ever seen. His model, however, represents a culmination of experience which would have been lost if he had not taken the trouble to formulate it. It has the advantage of being one of the very few that can be used to predict the complete plume-temperature field, that is, from the point of effluent discharge all the way to near-ambient conditions. As stated above, the model remains relatively unverified with quality lake field data; i.e., its application to surface-discharge situations for a large range of initial Froude numbers is still unknown. The reason for this is simply that good quality field data are difficult to obtain and only recently are becoming available.

The author is presently conducting studies to improve the model from the standpoint of shoreline interference in the presence of a crosscurrent and on the precise effect of a specific bottom slope on jet dispersion. When more precise data and information on the complex physical processes are available, model improvements will be instituted.

References

1. Y. Jen, R. L. Wiegel, and I. Mobarek, Surface Discharge of Horizontal Warm Water Jet, HEL No. 3-3, Hydraulic Engineering Laboratory, University of California (Dec 1964).

2. R. L. Wiegel, I. Mobarek, and Y. Jen, Discharge of Warm Water Jet Over Sloping Bottom, Hydraulic Engineering Laboratory, University of California (1966).

3. Loh-Nien Fan, Turbulent Buoyant Jets into Stratified or Flowing Ambient Fluids, Report No. KH-R-15, W. M. Keck Laboratory of Hydraulics and Water Resources, California Institute of Technology (June 1967).

4. Gerritt Abraham, Horizontal Jets in Stagnant Fluid of Other Density, Proc. Amer. Soc. Civ. Engineering Jour. Hyd. Division 92, HY2, 423-429 (Mar 1966).

5. T. Hayashi, Diffusion of Warm Water Jets Discharged Horizontally at the Water Surface, Proc. IAHR 4, Colorado (1967).

6. M. L. Albertson, Y. B. Dai, R. A. Jensen, and H. Rouse, Diffusion of Submerged Jets, Trans. Am. Soc. Civ. Eng. 115, Paper No. 2407, 689-697 (1950).

7. H. H. Carter and Akira Okubo, The Study of the Physical Processes of Movement and Dispersion in the Cape Kennedy Area, AEC Report No. NYO 2973-1, Reference 65-2, The Chesapeake Bay Institute, the Johns Hopkins University (Mar 1965).

8. L. P. Beer and W. O. Pipes, A Practical Approach: Environmental Effects of Condenser Water Discharge in Southwest Lake Michigan, Industrial BIOTEST Lab., Inc. (no date given).

9. Pritchard-Carpenter Consultants, Surry Plant Studies on the James River, completed for the Virginia Electric and Power Company (proprietary report) (not reviewed).

10. Public testimony by Pritchard before the State of Maryland Hearing Board on Water Use Permit Work; also appears in the Governor's (Maryland) Task Force Report (not reviewed).

11. D. W. Pritchard, Design and Siting Criteria for Once-Through Cooling Systems, American Institute of Chemical Engineers, 68th Annual Meeting, Houston, Texas (Mar 2, 1971).

12. H. H. Carter, "A Preliminary Report on the Characteristics of Heated Jet Discharged Horizontally Into a Transverse Current Part I--Constant Depth," Chesapeake Bay Institute, the Johns Hopkins University, Reference 69-14, Technical Report 61 (Nov 1969).

13. D. W. Pritchard, Modeling of Heated Discharges--A Lecture, Westinghouse School for Environmental Management, CSU, Fort Collins, Col. (June 25, 1970).

14. Public hearings, Illinois Pollution Control Board, R-70, Chicago, Ill. (Sept 26 and Nov 5, 1971).

11. An Investigation of the Physical Effects of Thermal Discharges into Cayuga Lake--Thermal-plume Model[1]

T. R. Sundaram, C. C. Easterbrook, K. R. Piech, and G. Rudinger
(Cornell Aeronautical Laboratory)
November 1969

a. List of Symbols

A_T, A_q	Eddy coefficients of momentum and heat transfer
b_0	Width of outfall (virtual, unless otherwise specified)
b	Width of plume defined by Eq. 11.12
$b_{1/2}$	Half-width of jet at half-depth of velocity profile
$\overline{b}$	Width of mixing zone in jet-diffusion region
B	Bulk Richardson number
d	Depth of plume
g	Acceleration of gravity
h	Thickness of a general plume averaged over depth at longitudinal distance x
h_e	Value of effective source height at any downstream shoreline distance x in the Bosanquet centerline formula
$h_{e_{max}}$	Maximum value of h_e
J	Momentum per unit length of a two-dimensional jet
k_H	Constant of proportionality in the Richardson 4/3-power law
$K_{M_{jet}}$	Eddy diffusivity of self-induced jet turbulence
K	Coefficient of surface heat loss
K_1	Constant of proportionality in formula for jet eddy diffusivity, in Eq. 11.31
K_0	J/ρ
K_H	Eddy diffusivity of heat
K_M	Eddy diffusivity of momentum for far-field region
ℓ	Length scale of lake diffusion
m	Arbitrary constant in the general power law, $K_H = k_H b^m$
P_1	Peclet number
P_2	Nondimensional parameter related to surface heat loss

q_L	Total rate of heat loss from the plume to the atmosphere
q_R	Rate of heat input to the lake by the power plant
R	Length of far-field region considered in the model
s	Fixed characteristic distance at the outfall
T	Two-dimensional excess-temperature function
T_0	Initial temperature at virtual outfall
u	Velocity in x direction (above ambient)
u_a	Ambient current velocity
u_0	Initial velocity at virtual outfall
U	Centerline velocity of jet
U_s	Centerline velocity at outfall
v	Velocity in y direction (above ambient)
x	Distance measured along the shore from the outfall in the application of the Bosanquet et al.[8] formulas (Eqs. 11.25 and 11.26 for the plume centerline, or
	Distance measured along the centerline from the actual outfall in the jet regime, or
	Distance measured along the centerline from the virtual outfall in the far-field region
$\hat{x}$	Distance along centerline measured from virtual outfall in jet region
x_0	Centerline distance from actual outfall to the virtual outfall
x_1	Downstream distance measured along centerline to the point where vertical entrainment ceases in a general surface plume (see Fig. 11.1)
x_2	Downstream distance along centerline where vertical entrainment reinitiates for a general surface plume (see Fig. 11.1)
y	Distance normal to the centerline
α, β, γ	Empirical constants in evaluation of jet centerline position
η	Nondimensional variable defined by Eq. 11.34
θ	Two-dimensional temperature function defined by Eq. 11.8
ρ	Density of fully mixed plume
ρ_a	Density of ambient receiving water
σ	Empirical constant defined by Eq. 11.34
τ	Turbulent shear stress

Superscript ~ denotes the quotient of that variable with b_0

Subscript 0a denotes the value of a particular variable at the actual outfall

Subscript 0v denotes the value of a particular variable at the virtual outfall

Notation $\Big|_s$ denotes evaluation at the orifice

b. Introduction

The thermal-plume model developed by Sundaram et al. treats the problem of the dispersion of a heated effluent discharged from a rectangular open channel at the shoreline of a large stratified lake in the presence of a shore-parallel crosscurrent. The model is two-dimensional in its analysis of both the initial jet phase and the subsequent phase where ambient lake turbulence is the controlling factor. The mathematical model is an extension of an earlier one used by Brooks[2] for the diffusion of sewage effluent in an ocean current.

As suggested by the experimental work of Ellison and Turner,[3] the plume is divided into three separate and distinct regions based upon its vertical diffusion characteristics. In general, the vertical spread of the plume is dependent on the nature of the entrainment process at the interface of the plume and the underlying colder lake water. The rate of vertical entrainment at any axial location x downstream is proportional to the bulk Richardson number B, defined as

$$B \equiv \frac{gh}{V^2} \frac{\rho_a - \rho}{\rho_a},$$

where

g = acceleration of gravity,

h = plume average thickness,

ρ = depth-averaged value of the density at x,

ρ_a = ambient water density,

and

V = jet velocity (relative to the ambient fluid) averaged over depth.

Vertical entrainment and vertical plume spreading will cease when B reaches a critical value of about 0.8. Using the Richardson number criterion, Sundaram et al. divide the surface plume into three regions. The first lasts for a short distance downcurrent. Here the initial jet causes

rapid vertical entrainment until the decaying jet velocity and increased jet depth combine to cause B to attain its critical value of about 0.8 at some downstream axial location, say x_1. This point marks the boundary between the first and second regions. Beyond this point, the value of B becomes greater than the critical value due to the decreasing relative velocity of the plume. The plume changes little in depth in this second region, since there is no vertical entrainment. As the velocity V approaches that of the ambient current, B begins to decrease due to the diminishing density difference $(\rho_a - \rho)$. At some further location downcurrent, x_2, the value of B will again attain its critical value. Beyond this point, B continues to fall and vertical entrainment again takes place. The plume now grows fairly rapidly in depth and will ultimately be mixed into the deeper layers of the lake. The division of a plume into three regions based upon vertical diffusion is illustrated in Fig. 11.1 for a hypothetical surface plume spreading in a stagnant lake. The phenomenon of heat being lost to the deeper layers of the lake beyond x_2 is illustrated in Fig. 11.2.

If the value of the bulk Richardson number is calculated for the conditions at the outfall and found to be greater than the critical value, the second region will start at the outfall and a constant-depth plume will result for all distances up to x_2. Moreover, for many practical conditions, the effect of the first region on the temperatures at sufficiently large distances from the outfall are small and, according to the authors, can be neglected. From these facts, the authors assume in their analysis a constant-depth plume extending from the outfall to the far-field distance x_2, where the plume sinks to the deeper layers of the lake. In short, they assume an outflow that is "supercritical" right from the point of discharge, the

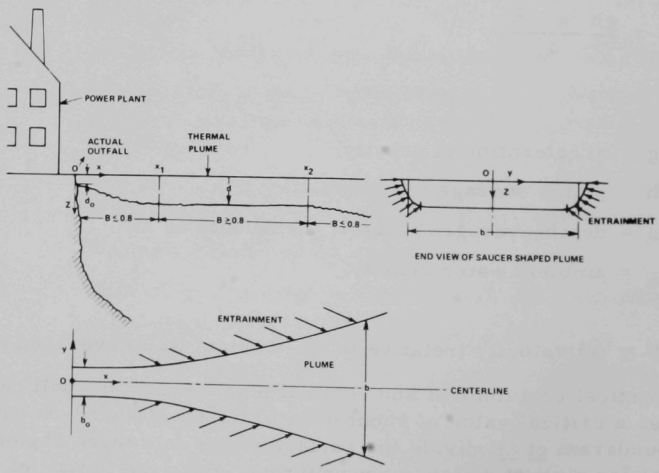

Fig. 11.1. Schematic View of Thermal Plume[1a]

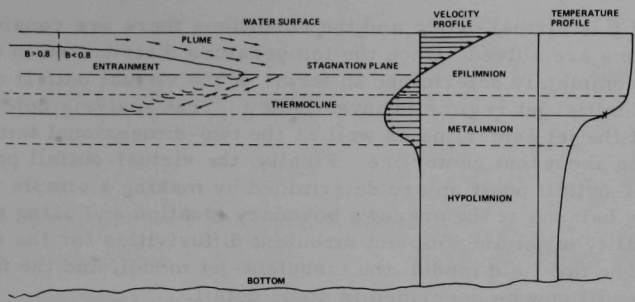

Fig. 11.2. Interaction of Thermal Plume with Lake Current[1a]

stratification being so intense that there is no initial vertical mixing. For the outfall conditions at the Bell Power Station for which the authors developed this model, this was indeed the situation and no assumption was involved. This permits a two-dimensionality assumption of a constant-depth, completely vertically mixed plume.

In addition to the classification of various regions of the plume by their vertical-diffusion characteristics, the authors also subdivide the horizontal-diffusion characteristics by separating an initial jet-diffusion phase from a later, more extensive phase where ambient lake turbulence is the controlling feature. The initial phase of horizontal plume spreading is governed primarily by self-induced turbulence within the jet itself and by the interaction of the jet momentum with the transverse crossflow. The jet is bent over by the crosscurrent until the initial momentum of the jet is nearly dissipated. After the bending of the jet is nearly complete, it acts as a passive plume. In the second region of horizontal diffusion, the plume is convected in the direction of the steady current and is dispersed laterally by the turbulent-diffusion mechanisms of the ambient lake. The boundary between the jet phase and the ambient-turbulence-controlled phase cannot be clearly defined. The authors argue that this boundary can be assumed to be at the plume centerline position, where the eddy diffusivities due to jet-induced turbulence and ambient turbulence are equal. As will be seen later, this criterion is used to calculate the plume centerline distance at which a jet solution and a separate far-field solution are joined together. This boundary position of the two horizontal phases of dispersion is completely independent of x_1, defined to be point of demarcation of the first two vertical-entrainment regions.

At this point, the mathematical model for horizontal dispersion within the jet and far-field regions will be described. The analysis of the authors is done in three parts. The region dominated by ambient turbulence is considered first, using the development of Brooks.[2] To simplify the problem, the authors assume that the initial conditions for this second region are not those of the actual outfall, but those of a virtual outfall. The

position of this virtual origin and the conditions there are considered after the equations are solved. Once the temperature distribution in the second region is completely determined in terms of the virtual outfall characteristics, the initial jet regime is investigated. That analysis determines the position of the jet centerline as well as the two-dimensional temperature distribution about that centerline. Finally, the virtual-outfall parameters and virtual-outfall position are determined by making a simple momentum and energy balance at the unknown boundary location and using the condition of the equality of jet and ambient turbulent diffusivities for the cross section. The far-field model, the turbulent-jet model, and the matching procedure will now be described in some detail.

c. The Model Derivation

(1) The Far-field Model. The analysis given by the authors for the excess temperature $T(x, y)$ above ambient closely follows that developed by Brooks.[2] The coordinate system for the analysis is given in Fig. 11.1 where the bottom diagram has a new interpretation. The x axis is taken along the plume centerline and the y axis normal to it with the origin at the center of the virtual outfall. The ambient fluid is assumed to be moving in a steady current u_a parallel to the x axis. The plume is assumed to be issuing from a virtual outfall of width b_0, representing a source at constant temperature T_0 and velocity u_0 (b_0, T_0, u_0 will be determined later). The plume is assumed to be moving along with the current, losing and transferring heat simultaneously by advection in the direction of the current, lateral turbulent diffusion, and surface heat loss to the atmosphere. The plume depth is, as stated above, assumed constant, precluding any vertical mixing, and is denoted by d. Steady flow is assumed which, by its very nature, precludes meandering of the plume often seen in actual plume observations. (This limitation has been pointed out by the authors; indeed, meandering can be treated separately and then superimposed on the present solution. According to the authors, meandering will alter the steady plume profile to be described below, but it is not likely to influence significantly the rate of temperature decay or areas enclosed within specific isotherms.)

Due to the long, thin nature of most plumes, the "boundary-layer" approximations usually made in analyses of plumes and jets are assumed, including: negligible pressure gradients, lateral velocities small compared to longitudinal ones, lateral derivatives much larger than longitudinal ones, and transport by advection predominating over turbulent mixing in the direction of the current. With these assumptions, the incompressible-flow and energy-conservation equations reduce to

$$\frac{\partial u}{\partial x} + \frac{\partial v}{\partial y} = 0, \tag{11.1}$$

$$(u + u_a)\frac{\partial u}{\partial x} + v\frac{\partial u}{\partial y} = \frac{\partial}{\partial y}\left(K_M \frac{\partial u}{\partial y}\right), \tag{11.2}$$

and

$$(u+u_a)\frac{\partial T}{\partial x} + v\frac{\partial T}{\partial y} = \frac{\partial}{\partial y}\left(K_H\frac{\partial T}{\partial y}\right) - \frac{K}{\rho c_p d}T, \tag{11.3}$$

where

u = velocity in x direction (above ambient),

v = velocity in y direction,

u_a = ambient current velocity (assumed constant),

T = excess temperature of plume above ambient,

K = coefficient of surface heat loss,

ρ = density of the fully mixed plume ($\approx\rho_a$),

d = depth of plume,

K_M = eddy diffusivity of momentum,

and

K_H = eddy diffusivity of heat.

Equations 11.1-11.3 are valid for all regions of the plume if it can be assumed that the curvature of the plume is small. They are valid in <u>all</u> regions for discharges into a co-flowing or counter-flowing current. The associated boundary conditions to Eqs. 11.1-11.3 are:

$$\left.\begin{aligned} &u = u_0, \quad T = T_0, \quad \text{at } x = 0, \quad -b_0/2 < y < b_0/2; \\ &u = 0, \quad T = 0, \quad \text{at } x = 0, \quad |y| > b_0/2; \end{aligned}\right\} \tag{11.4}$$

$$\lim_{x\to\infty} u(x,y) = \lim_{x\to\infty} v(x,y) = \lim_{x\to\infty} T(x,y) = 0 \text{ for all } y, \tag{11.5}$$

and

$$\lim_{y\to\pm\infty} u(x,y) = \lim_{y\to\pm\infty} v(x,y) = \lim_{y\to\pm\infty} T(x,y) = 0 \text{ for all } x. \tag{11.6}$$

Since u and v are very small in the far-field region (jet-induced effects on diffusion are neglected in this region), Eq. 11.6 may be uncoupled from Eqs. 11.4 and 11.5 and written as

$$u_a\frac{\partial T}{\partial x} = \frac{\partial}{\partial y}\left(K_H\frac{\partial T}{\partial y}\right) - \frac{KT}{\rho c_p d} \tag{11.7}$$

with the same boundary conditions on T as given above. Conditions now refer to the virtual origin, and x should be measured from this origin.

Equation 11.7 states that the advection of heat in the direction of the current is balanced by the heat transferred due to lateral turbulent diffusion and dissipation from the lake surface (above ambient). One can remove the atmospheric-heat-loss term from the equation with the transformation

$$T = \theta \exp\left(-\frac{Kx}{\rho c_p u_a d}\right), \tag{11.8}$$

which yields the following equation for θ

$$u_a \frac{\partial \theta}{\partial x} = \frac{\partial}{\partial y}\left(K_H \frac{\partial \theta}{\partial y}\right). \tag{11.9}$$

The significance of θ is that it is proportional to the concentration of any contaminant that is uniformly suspended or dissolved in the effluent. The problem of finding the distribution of such contaminants in the lake is automatically solved along with the problem for the temperature distribution if one makes the reasonable assumption that the eddy diffusivities for heat and matter are equal.

The difficulty in solving Eq. 11.9 lies in the fact that K_H is not really known. Following Brooks, the authors assume Richardson's 4/3-power law as a model for the diffusivity K_H,

$$K_H = k_H \ell^{4/3}, \tag{11.10}$$

where ℓ is an appropriate-length scale and k_H is a constant. The authors support the use of this law by referring to the array of existing data available on horizontal diffusion in the ocean that fit that law.[4] The authors also refer to the dye-dispersion studies made by Gunnerson[5] in Santa Monica Bay, which agreed well with Eq. 11.10. Also mentioned were estuary studies made by Harleman and Ippen.[6] The constant k_H has, however, been found to vary by up to three orders of magnitude. It is expected that k_H depends upon the prevalent environmental conditions above the lake. Based on the work of Ziltinkevich,[7] the authors assert that k_H should at least depend on the wind speed above the lake, the thermal stability of the overlying air, and the fetch and direction of the wind. It is also expected that k_H depends on the level of ambient turbulent-energy dissipation. Due to the complexities involved and the wide range of values of k_H possible, some kind of measurement has to be made to determine k_H for each set of meteorological conditions. This will be discussed in more detail later. Thus, with the 4/3-power law representing K_H, the uncertainty in the diffusivity is transferred to k_H, whose functional dependence on the environmental condition is not known.

Following Brooks again, ℓ is chosen to be b(x), the width of the plume at x, whereby from Eq. 11.10,

$$K_H = k_H b^{4/3}. \tag{11.11}$$

Recognizing that there are many ways to define plume width, the authors follow Brooks and define it as $2\sqrt{3}$ times the standard derivation of the temperature solution,

$$b(x) = 2\sqrt{3}\left\{\frac{1}{b_0\theta_0}\int_{-\infty}^{\infty} y^2\theta(x, y)\, dy\right\}^{1/2}. \tag{11.12}$$

The reason for using the factor $2\sqrt{3}$, instead of the more commonly used factor of 4, was to make $b = b_0$ at $x = 0$. Equation 11.9 can be solved analytically, in spite of the fact that k_H is in terms of θ itself.

If x' is defined by the ordinary differential equation

$$\frac{dx'}{dx} = \left[\frac{b(x)}{b_0}\right]^{4/3}, \tag{11.13}$$

Eq. 11.9 reduces to

$$u_a\frac{\partial\theta}{\partial x'} = [k_H b_0^{4/3}]\frac{\partial^2\theta}{\partial y^2}. \tag{11.14}$$

This is the classical heat-conduction equation and if

$$\tilde{x} = \frac{x}{b_0},\ \tilde{x}' = \frac{x'}{b_0}, \tag{11.15}$$

$$\tilde{y} = \frac{y}{b_0}, \tag{11.16}$$

$$\tilde{\theta} = \frac{\theta}{\theta_0} = \frac{\theta}{T_0},\ \tilde{T} = \frac{T}{T_0}, \tag{11.17}$$

and

$$P_1 = \frac{u_a}{k_H b_0^{1/3}}, \tag{11.18}$$

the solution can be written

$$\tilde{\theta}(\tilde{x}, \tilde{y}) = \frac{1}{2}\left(\operatorname{erf}\frac{2\tilde{y} + 1}{4\sqrt{\tilde{x}'/P_1}} - \operatorname{erf}\frac{2\tilde{y} - 1}{4\sqrt{\tilde{x}'/P_1}}\right). \tag{11.19}$$

Representing θ in Eq. 11.12 by the derived result of Eq. 11.19, the ordinary differential equation defining x' may be solved to yield

$$\tilde{x}' = \frac{P_1}{24}\left[\left(1 + \frac{8}{P_1}\tilde{x}\right)^3 - 1\right]. \tag{11.20}$$

If P_2 is defined by

$$P_2 = \frac{K}{\rho c_p u_a}\frac{b_0}{d}, \tag{11.21}$$

then

$$\tilde{T}(\tilde{x}, \tilde{y}) = \frac{1}{2}\exp(-P_2\tilde{x})\left(\operatorname{erf}\frac{2\tilde{y} + 1}{4\sqrt{\tilde{x}'/P_1}} - \operatorname{erf}\frac{2\tilde{y} - 1}{4\sqrt{\tilde{x}'/P_1}}\right). \tag{11.22}$$

The nondimensional parameter P_1 is the Peclet number for the flow. It denotes the ratio of the inertia forces to the heat-conduction forces. The nondimensional parameter P_2 is a measure of the ratio of the rate of heat loss to the atmosphere to the rate of loss to the colder lake water through the plume sides. The ratio can be shown[1a] to be directly proportional to b/b_0 with P_2 as one proportionality factor. Since b increases with increasing longitudinal distance, the heat loss to the atmosphere becomes increasingly more important relative to heat loss to the colder ambient lake water. Introducing "typical" values of the basic parameters into the definitions of P_1 and P_2 reveals a wide spread of numbers due to the large variation or uncertainty in k_H.

Two results of particular interest in the above solution are first the reduction of excess temperature with distance along the plume centerline and the growth of the plumes width from its initial value. From Eq. 11.22, the centerline temperature decay is

$$\tilde{T}(\tilde{x}, 0) = \exp(-P_2\tilde{x})\operatorname{erf}\left[\frac{1.5}{\left(1 + \frac{8}{P_1}\tilde{x}\right)^3 - 1}\right]^{1/2}, \tag{11.23}$$

which again indicates that the dilution factor is a separable function with distinct heat loss and turbulent mixing factors, as was shown in Eq. 11.8. Figure 11.3 illustrates the temperature decay along the centerline of the plume for four sets of values of P_1 and P_2. The origin of coordinates in that figure is at the virtual outfall, unless the initial jet regime is unimportant whereby b_0, T_0, and u_0 correspond to the actual outfall conditions.

The growth of the plume width is obtained from Eqs. 11.19 and 11.12 and is

$$\frac{b(\tilde{x})}{b_0} = \left(1 + \frac{8}{P_1}\tilde{x}\right)^{3/2}. \tag{11.24}$$

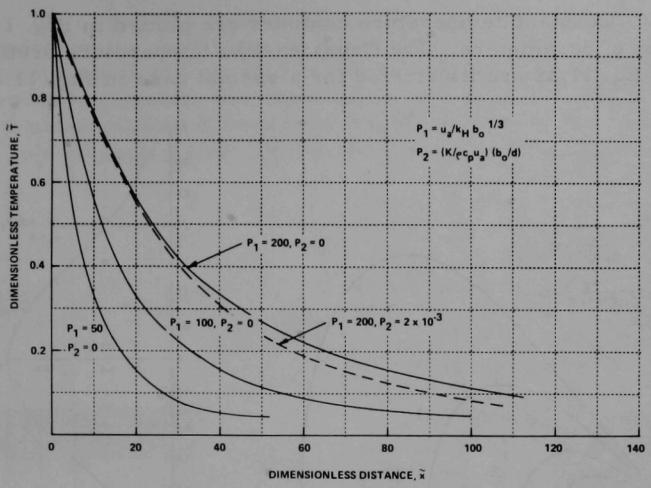

Fig. 11.3. Temperature Decay along Centerline of Plume[1a]

This result is illustrated in Fig. 11.4 for two values of the parameter P_1. As noted by the authors, b is independent of the heat-loss parameter P_2 that resulted from the uncoupling of flow and energy equations. The growth rate for the plume shows a convex nominal boundary, indicating that the plume spreads at an increasing rate.

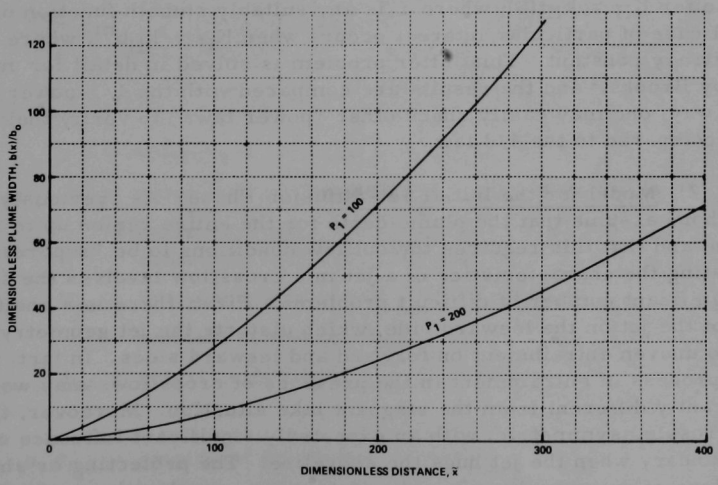

Fig. 11.4. Width of the Plume as a Function of Distance from the Origin[1a]

Constant-temperature contours are plotted in Fig. 11.5 for a typical set of parameters. The Gaussian-like temperature profiles predicted by Eq. 11.22 are illustrated for a special case in Fig. 11.6.

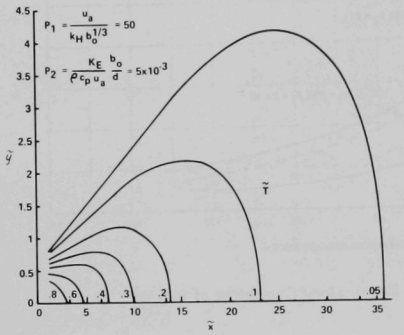

Fig. 11.5

Temperature Profiles in the Surface Plume[1a]

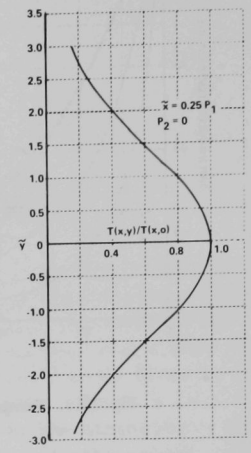

Fig. 11.6

Typical Plume Profile at a Fixed Distance from the Origin[1a]

Equation 11.9 can be easily solved not only when $K_H = k_H b^{4/3}$ but also for $K_H = k_H f(b)$, where f is any suitably smooth function of b. A special case of particular interest occurs when $K_H = k_H b^m$, where m is an arbitrary constant. This latter problem is solved in detail for m = 0 and 1 by Brooks,[2] and the results are compared with the 4/3-power law. In this way, one may easily check other "power laws" to verify their precision compared to the 4/3 law.

(2) Model for the Initial Jet-diffusion Phase. As previously stated, the authors assume that the plume depth for the entire region up to x_2 is constant and that this requires the outflow conditions to be "supercritical." Calculating the characteristics of a jet in a crossflow involves the solution of a significant number of difficult problems. First, there is a sheltering effect of the jet on the leeward side, which distorts the jet geometry and leads to uneven entrainment on forward and leeward sides. In fact, the entire process of entrainment in the presence of crossflows may well be significantly different from the stagnant lake situation. Moreover, the jet is grossly asymmetric, with an expectedly significant influence on the flow boundary when the jet hugs the shoreline. The protecting or sheltering of portions of an irregular shore leads to many complications. Since no theoretical model is available to handle all the problems arising with a jet in a crossflow, the authors embarked on a simplified approach.

They applied a modification of the two-step procedure commonly used in predicting the dispersion of gaseous stack effluents. First, they applied a semiempirical formula frequently used for chimney-stack effluents in a crosswind to calculate the warm-water-jet centerline position. Second, they used a classical two-dimensional turbulent-jet analysis derived for a heated jet in a stagnant receiving fluid to specify the lateral temperature and velocity distributions about that curved centerline; this method is illustrated in Fig. 11.7. This clearly is a highly simplified analysis, but, as stated by the authors, it is the best that could be done according to the state-of-the-art at the time of the model development.

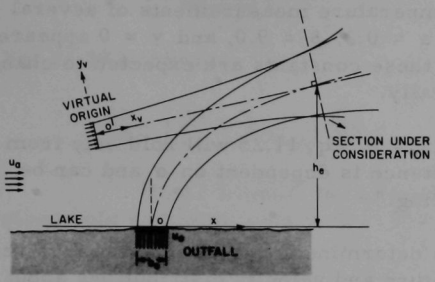

Fig. 11.7. Two-step Method of Plume Analysis[1a]

The centerline formulas chosen by the authors are the semi-empirical relations of Bosanquet, Carey, and Halton[8] frequently used to predict the dispersion of chimney-stack effluents into the atmosphere. The formulas are of the form

$$\frac{h_e(x)}{h_{e_{max}}} = 1 - \alpha \frac{h_{e_{max}}}{x} \tag{11.25}$$

and

$$\frac{h_{e_{max}}}{b_0} = \frac{\beta}{1 + \gamma(u_a/U_{0a})} \frac{U_{0a}}{u_a}, \tag{11.26}$$

where

x = distance measured from the outfall along the shore,

h_e = value of the effective source height at any point x,

$h_{e_{max}}$ = maximum value of h_e (maximum penetration of the jet centerline into the crossflow),

U_{0a} = initial velocity of the jet at the outlet,

u_a = ambient current velocity,

b_{0a} = actual outfall width,

and

α, β, γ = empirical constants.

The above formulas take into account the initial momentum of the effluent, but not its initial buoyancy at the source position. For a lake-plume situation this is a reasonable assumption. According to the authors,

the parameters α, β, and γ are not functions of environmental conditions, and therefore they are assumed to be independent of the characteristics of the ambient turbulence. These parameters are actually dependent on outfall geometry, shoreline and bottom topography, etc. The authors found this last assumption to be satisfactory and were able to determine the empirical constants for the Milliken Station plume on Lake Cayuga by comparison of Eqs. 11.25 and 11.26 with surface-temperature measurements of several bent plumes. The parameter values $\alpha = 0.2$, $\beta = 9.0$, and $\gamma = 0$ appeared to fit the data best. For other sites, these constants are expected to change and should be determined experimentally.

Due to the singularity at $x = 0$, Eq. 11.25 will hold only from some distance downstream. That distance is dependent on α and can be determined satisfactorily by "eyeballing."

Once the jet centerline is determined, the second step involves the calculation of the lateral temperature and velocity distributions about that centerline. The authors apply a classical two-dimensional jet analysis[9] for a free turbulent jet in a stagnant medium; this analysis of Schlicting is summarized below.

The steady incompressible-flow equations for a free turbulent jet are

$$\frac{\partial u}{\partial \hat{x}} + \frac{\partial v}{\partial y} = 0 \tag{11.27}$$

and

$$u\frac{\partial u}{\partial \hat{x}} + v\frac{\partial u}{\partial y} = \frac{1}{\rho}\frac{\partial \tau}{\partial y}, \tag{11.28}$$

where

$\hat{x}$ = distance along a straight plume centerline measured from some <u>virtual</u> jet outlet,

y = lateral distance normal to $\hat{x}$,

u = actual velocity in $\hat{x}$ direction,

v = actual velocity in y direction,

τ = turbulent shear stress,

and

ρ = jet fluid density.

"Boundary-layer" approximations have been used in the derivation of Eqs. 11.27 and 11.28. The pressure remains constant at least to a first approximation, so the pressure gradient term has been dropped. Using Prandtl's second mixing-length hypothesis

$$\tau = \rho K_{M_{jet}} \frac{\partial u}{\partial y}, \tag{11.29}$$

Eq. 11.29 becomes

$$u \frac{\partial u}{\partial \hat{x}} + v \frac{\partial u}{\partial y} = K_{M_{jet}} \frac{\partial^2 u}{\partial y^2}. \tag{11.30}$$

Other Prandtl hypotheses yield results that differ from each other only comparatively little. The virtual kinematic viscosity is given as

$$K_{M_{jet}} = K_1 \bar{b} U, \tag{11.31}$$

where

K_1 = constant to be determined,

$\bar{b}$ = width of mixing zone of the jet,

and

U = centerline velocity.

Using Schlicting's notation, if s is the fixed characteristic distance at the orifice, and U_s and $\bar{b}_s$ are the orifice centerline velocity and jet width, respectively, then from dimensional analysis and by assuming b is proportional to $\hat{x}$,

$$U = U_s \left(\frac{\hat{x}}{s}\right)^{-1/2}, \quad \bar{b} = \bar{b}_s \left(\frac{\hat{x}}{s}\right), \tag{11.32}$$

and

$$K_{M_{jet}} = K_{M_{jet}}\Big|_s \left(\frac{\hat{x}}{s}\right)^{1/2} \text{ with } K_{M_{jet}}\Big|_s = K_1 \bar{b}_s U_s. \tag{11.33}$$

Further, if

$$\eta = \sigma \frac{y}{\hat{x}}, \tag{11.34}$$

where σ is an experimental constant to be determined, Eqs. 11.27 and 11.30 may be solved to yield

$$u = \frac{\sqrt{3}}{2} \sqrt{\frac{K_0 \sigma}{\hat{x}}} \left(1 - \tanh^2 \eta\right) \tag{11.35}$$

and

$$v = \frac{\sqrt{3}}{4}\sqrt{\frac{K_0}{\hat{x}\sigma}}\,[2\eta(1 - \tanh^2\eta) - \tanh\eta], \tag{11.36}$$

where $K_0 = J/\rho$ and

$$J = \rho\int_{-\infty}^{\infty} u^2\,dy = \frac{(4/3)U_s^2 s\rho}{\sigma} \tag{11.37}$$

is the constant momentum per unit length. Reichardt determined σ by experiment to be 7.67. The lateral velocity distribution is plotted in terms of u/u_{max} versus $y/b_{1/2}$ in Fig. 11.8. Curve 1 refers to Tollmein's solution using Prandtl's first mixing-length hypothesis; Curve 2 uses the above solution, Eq. 11.35. The experimental data plotted are from the measurements of E. Foerthmann.[9] From the above value of σ, K_1, and $\bar{b}_s/s$ may be determined as 0.02445 and 0.174, respectively. Consequently,

$$K_{M_{jet}} = 0.02445\bar{b}U \tag{11.38}$$

and

$$\bar{b} = 0.174\hat{x} \tag{11.39}$$

If $b_{1/2}(\hat{x})$ is defined as the lateral distance y such that $u/u_{max} = 1/2$, then

$$K_{M_{jet}} = 0.037b_{1/2}U, \tag{11.40}$$

where $b_{1/2}(\hat{x})$ may be determined from Eq. 11.35 to be

$$b_{1/2}(\hat{x}) = 0.1147\hat{x}. \tag{11.41}$$

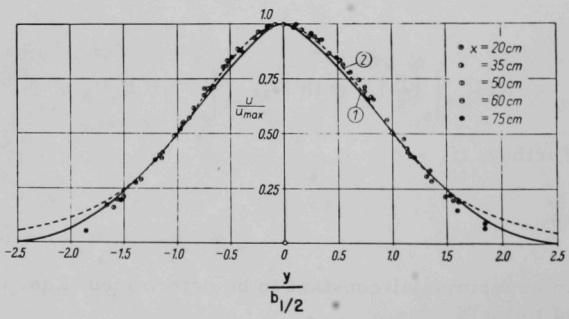

Fig. 11.8. Velocity Distribution in a Two-dimensional, Turbulent Jet. Measurements due to Foerthmann.[9] Theory: Curve 1 due to Tollmien; Curve 2 from Eq. 11.35.

Due to the analogy or similarity between heat and momentum transfer for horizontal dispersion in a turbulent medium,

$$\frac{u}{u_{max}} = \frac{T}{T_{max}}, \tag{11.42}$$

where, for any longitudinal distance $\hat{x}$,

T = excess temperature of the jet at $(\hat{x}, y)$

and

T_{max} = excess temperature of the centerline distance $\hat{x}$.

If x is the longitudinal distance measured from the actual outfall then, using Eq. 11.39,

$$x = \hat{x} - 5.75 b_{0a}, \tag{11.43}$$

where b_{0a} $(= \bar{b}_s)$ is the actual outfall width. Equation 11.42 follows from Prandtl's mixing-length theory and from Reynolds analogy.

The velocity and temperature distributions determined above are independent of the definition of the jet width. By using Eqs. 11.35 and 11.41, $b_{1/2}$ may be related to the Brooks definition of b, Eq. 11.12. This yields

$$b = b_{0a} + 0.2x \tag{11.44}$$

and

$$KM_{jet} = 0.008bU, \tag{11.45}$$

where

b = width of jet defined by Eq. 11.12

and

U = centerline velocity.

From Eqs. 11.32, 11.42, and 11.44, the centerline temperature decay for the jet is

$$\frac{T}{T_{0a}} = \left(\frac{b_{0a} + 0.2x}{b_{0a}}\right)^{-1/2}, \tag{11.46}$$

where T_{0a} is the temperature excess at the actual outfall.

Consequently, the velocity distribution (in the x direction), the plume width, the temperature distribution, and the eddy viscosity for a turbulent two-dimensional jet issuing into a stagnant medium are given by Eqs. 11.35, 11.44, 11.46, and 11.45, respectively. The characteristics of a heated jet in a crossflow are thus determined by applying these equations, with x now identified as the actual arc distance along the bent centerline.

The method described above for calculating the temperature and velocity distributions for a jet in a crossflow is essentially a patching of two solutions. The first step in the solution involves the incorporation of all the crosscurrent effects into the formula for obtaining the centerline axis. The second step of the solution involves the derivation of the temperature and velocity fields with no crosscurrent interference. These two distributions are assumed to hold laterally about the bent jet centerline and represent dispersion about the centerline.

(3) Matching of the Jet and Far-field Solutions. The spatial extent of the initial horizontal jet-diffusion phase is governed by the criterion that this region has an eddy diffusivity arising from jet-induced turbulence greater than or equal to the eddy diffusivity due to ambient turbulence. Since the eddy diffusivities of heat and momentum are assumed equal in horizontal turbulent flow, the relationship

$$K_{M_{jet}} = K_H \tag{11.47}$$

marks the end of the jet phase. From Eq. 11.45 and 11.11, this is equivalent to

$$0.008\, b_{0v} U_{0v} = k_H b_{0v}^{4/3}, \tag{11.48}$$

where the subscript 0v denotes values at the virtual outfall. Equating momenta at the virtual and actual outfalls yields

$$b_{0v} U_{0v}^2 = b_{0a} U_{0a}^2, \tag{11.49}$$

where the subscript 0a denotes values at the actual outfall. Combining Eqs. 11.48 and 11.49 leads to a relationship of the virtual and actual outfall widths

$$\frac{b_{0v}}{b_{0a}} = \left(0.008 \frac{U_{0a}}{k_H b_{0a}^{1/3}}\right)^{1.2}. \tag{11.50}$$

The distance of the outer extremity of the jet region is determined from Eq. 11.44 as

$$x_0 = 5(b_{0v} - b_{0a}), \tag{11.51}$$

where x_0 is measured along the bent jet centerline.

T_0, the temperature at the virtual source, is calculated by conservation of heat flux at the boundary of the jet and far-field regions,

$$T_0 U_{0v} b_{0v} = \int_{-\infty}^{\infty} u(x_0, y) T(x_0, y) b(x_0)\, dy. \tag{11.52}$$

If the right-hand side of Eq. 11.49 is less than unity, the jet-diffusion phase can be neglected. The virtual outfall then coincides with the actual outfall. For this situation, the mean path of the plume is first calculated, as before, using the Bosanquet formulas 11.25 and 11.26. The far-field solution is then applied from the outfall with $b_{0v} = b_{0a}$ and $T_0 = T_{0a}$, identifying x in that solution with the arc distance along the bent centerline.

d. Technique of Model Application

As described above, three distinct aspects of the solution are specified in the model. The first involves the calculation of the mean path of the plume. This is done completely separate from the plume-diffusion characteristics. The plume path is bent and is solely a function of the ambient current or, more precisely, u_0/u_a. Over this mean path is superimposed two distinct regions: the jet-diffusion region and the ambient turbulent region as previously described. The dividing line between the two is arbitrary and was chosen in the model to be at the point at which the eddy diffusion due to the jet itself is equal to the ambient turbulence. If the jet diffusion is sufficiently slow at the outlet, the eddy coefficient of ambient turbulence is equal to or greater than that for jet diffusion, and thereby the far-field solution will apply right from the outfall and be superimposed over the entire bent centerline. In the author's application of the model to Lake Cayuga, the exit velocity was never low enough to cause the jet diffusion to be completely negligible.

To apply the overall model for given parameters b_{0a}, U_{0a}, T_{0a}, u_a, K, and d, it is necessary to first evaluate the empirical constants α, β, γ, and k_H. Since a purely theoretical analysis for a jet in a crossflow does not exist, it is not advisable to apply one set of parameter values to other field situations. Consequently, α, β, and γ must be measured by comparing Eqs. 11.25 and 11.26 to actual surface-temperature data in the initial jet regime. The values of k_H as a function of meteorological conditions above the lake can be determined by comparing actual observations of thermal plumes from the existing outfall with Eq. 11.22. This is done by matching the centerline of an observed plume with Eq. 11.23. P_2 is calculated using the heat-exchange coefficient K and the measured value of the ambient current u_a. P_1 is evaluated by matching the theoretical and observed plume centerline, and k_H is then determined from P_1. The determination of the virtual-outfall parameters requires a value of k_H. Thus this technique

would generally require some iteration; an initially guessed value of k_H may need to be corrected if the fitting is not sufficiently accurate. As noted by the authors, plume characteristics at large distances from the virtual outfall are not very sensitive to the precision of evaluation of the virtual-outfall characteristics.

In applying this to the Milliken Power Station on Lake Cayuga, the authors found a good correlation between experimental data for the plume centerline and the mathematical model. They calculated k_H for six "typical" sets of environmental conditions and felt justified to use those values again in plume situations when similar environmental conditions prevailed.

In the general case, with these parameters evaluated, Eqs. 11.25 and 11.26 give the complete trajectory of the plume. Equations 11.35, 11.46, and 11.42 yield the temperature and velocity distribution in the jet regime. Equation 11.22 specifies the temperature distribution in the far field. Each of these distributions is centered about the appropriate portion of the deflected plume centerline.

e. General Discussion of the Model

At this point, some general comments about the model would be useful. Two major simplifications are knowingly employed by the authors. The first involves the assumption of a constant-depth, stably stratified plume from the outfall out to centerline distance x_2. Clearly, this puts limitations on the outfall conditions; if the Richardson number at the outfall is not greater than about 0.8, there will be vertical entrainment, which will increase the depth of the jet, in which case many new complications arise. The authors could find no way a priori to incorporate initial vertical entrainment into a model. The implied two-dimensionality assumption permitted the application of the Brooks model for the far-field region and the classical two-dimensional jet analysis for the initial horizontal-diffusion zone. The classical two-dimensional jet theory can be applied with confidence to an actual jet of depth d as long as it is assumed to be fully mixed in the vertical direction and thus two-dimensional.

The second major assumption involved the very simplified model for the effect of the crossflow on the jet characteristics. In the two-step technique used, there is an idealization which is an obvious simplification considering the complex phenomena involved, yet it is expected to lead to some useful approximate results. Clearly, the effect of the crossflow is felt, not only with the bending of the centerline but also in the temperature and velocity distributions centered about it, and may be accurately determined only by careful consideration of the differential equations involved with an accurate representation of the entrainment phenomenon. Moreover, the fully mixed constant-depth-plume assumption precludes consideration of buoyant forces, which lead to convective motions that increase lateral entrainment of the jet while the plume touches the bottom and the expected increased lateral spreading due to the bottom constraints.

These deficiencies of the model were well recognized by the authors in Ref. 1. The model is, however, a reasonable and plausible one within the state-of-the-art that existed at the time that model was developed (1968). Due to the increased knowledge and understanding recently gained in several important areas (such as vertical entrainment, the "bending-over" phenomenon, sheltering, and the transition between near- and far-field regions), there is room for considerable improvement in the model. To date, there is no model to our knowledge that handles all these phenomena successfully.

The supposed similarity between heat and momentum transfer for horizontal dispersion in a turbulent medium (with no horizontal stratification) as expressed by Eq. 11.42 in the author's jet analysis is not universally accepted (Ref. 9, pp. 703-705). According to the Prandtl mixing-length theory, the mechanisms of the transfer of momentum and heat in free turbulent flows are identical, supporting the use of Eq. 11.42. However, the Taylor theory of turbulent mixing predicts a temperature profile at some developed axial position to be wider than the velocity profile satisfying.

$$\frac{T}{T_{max}} = \left(\frac{u}{u_{max}}\right)^{1/2}. \tag{11.53}$$

H. Reichardt derived the relationship

$$\frac{T}{T_{max}} = \left(\frac{u}{u_{max}}\right)^{A_\tau/A_q}, \tag{11.54}$$

using empirical relationships rather than hypotheses on turbulent flow. Here A_τ and A_q are, respectively, coefficients of momentum and heat transfer defined from

$$\tau = A_\tau \frac{du}{dy}; \quad q = c_p A_q \frac{dT}{dy}. \tag{11.55}$$

Reichardt's experimental results for a two-dimensional jet showed good agreement with Eq. 11.53. Using $A_\tau/A_q = 1$ rather than $A_\tau/A_q = 1/2$ results in flatter isotherms for the jet regime in the Sundaram _et al_. model. Only further experimental studies into the relative rates of lateral spreading of momentum and energy will reveal which of Eqs. 11.42 and 11.53 is more adequate.

Most investigators consider a flow-establishment region in which the initially top-hat profiles for velocity and temperature become approximately bell-shaped in character. This is done to reflect the influence of adjacent boundaries as well as the initially flat profiles of velocity and temperature. The two-dimensional, _free_ turbulent-jet analysis applied here considers similarity profiles initiating from the actual orifice. The effect of the neglect of a flow-establishment region is expected to be insignificant for sufficiently large distances downstream.

The authors in Ref. 1 emphasized that, although gross simplifications are made, the hypotheses were chosen to be self-consistent, at the same level of rigor, and, wherever possible, in agreement with the experimental data that existed at the time of model development. A prime example is the choice of the 4/3-power law to represent the diffusivity in which well-verified ocean and estuary data were used. The authors found satisfactory agreement with this law in fitting their model to Lake Cayuga data. In addition, the patching of jet and far-field solutions was done with conservation equations to minimize the impact of that discontinuity at larger downstream distances. Although a "top-hat" profile does exist at the virtual origin, this profile immediately becomes Gaussian-like beyond that point where heat energy is conserved.

f. Calculation of Heat Lost to the Lake beyond x_2

Finally, the authors have investigated heat loss to the atmosphere in order to determine the heat lost to the lake beyond x_2. Due to the small spatial extent of the jet regime and the expected predominance of turbulent mixing in that region, heat loss to the overlying air was neglected in their jet model. This is a very reasonable assumption for moderately sized jet regimes. The total heat loss to the atmosphere (relative to the ambient lake) is thus

$$q_L = \int_{-\infty}^{\infty} \int_{0}^{x_2 - x_0} KT(x, y)\, dx\, dy, \tag{11.56}$$

where T is given by Eq. 11.22. If the heat rejected by the power plant is

$$q_R = \rho c_p T_{0a} U_{0a} b_{0a} d, \tag{11.57}$$

then

$$\frac{q_L}{q_R} = \frac{u_a}{U_{0v}} [1 - \exp(-P_2 \tilde{R})], \tag{11.58}$$

where

$$\tilde{R} = \frac{x_2 - x_0}{b_{0v}}. \tag{11.59}$$

For an epilimnetic intake, $q_R = q_P$, where q_P is the total rate of heat rejected by the power plant. Thus, for an epilimnetic intake, the heat lost to the deeper layers of the lake beyond x_2 is just $q_R - q_L$, according to the model. For a hypolimnetic intake, the total heat rejected by the power plant does not participate in surface heat transfer as far as the plume is concerned, since part of this heat is used to increase the hypolimnetic-cooling-water temperature to an epilimnetic value. Thus for a deep-water intake, the equivalent heat loss to the deeper layers of the lake is

$$(q_R - q_L) + (q_P - q_R) = q_P - q_L. \tag{11.60}$$

For an epilimnetic intake, the heat loss to the lake is also $q_P - q_L$, since $q_P = q_R$; however, the magnitude of q_L would be greater than q_L for a hypolimnetic intake, because the epilimnetic intake would result in a higher effluent discharge temperature relative to the ambient water.

Figures 11.9 and 11.10 give model predictions for plume surface-temperature decay for "typical" summer and winter conditions on Cayuga Lake. Outfall parameters are based on the proposed Bell Station outfall geometry, i.e., for an outfall width of 100 ft and depth of 10 ft.

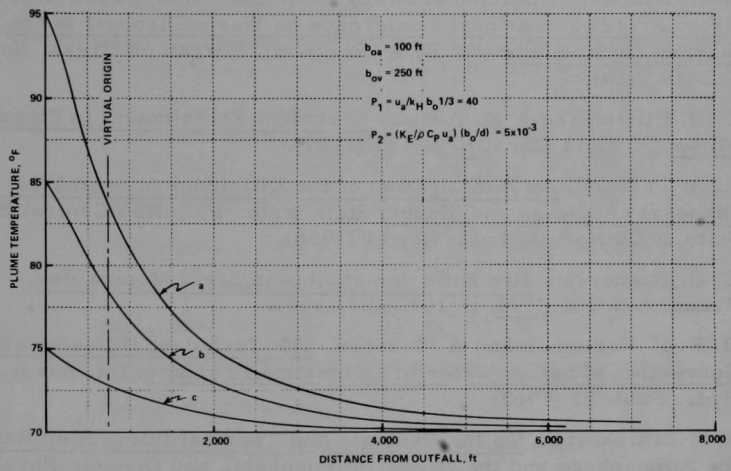

Fig. 11.9. Decay of Temperature along Plume Centerline for Bell Station Discharge for "Typical" Summer Conditions. Lake surface temperature = 70°F; discharge temperature = 75, 85, or 95°F.[1a]

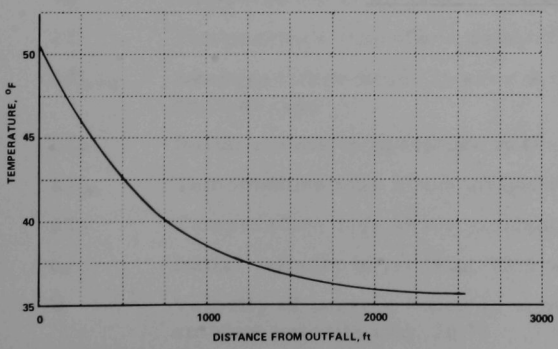

Fig. 11.10

Decay of Temperature along Plume Centerline for Bell Station Discharge for "Typical" Winter Conditions. Lake surface temperature = 36°F; discharge temperature = 51°F.[1a]

References

1a. T. R. Sundaram, C. C. Easterbrook, K. R. Piech, and G. Rudinger, An Investigation of the Physical Effects of Thermal Discharges into Cayuga Lake (Analytical Study), CAL No. VT-2616-0-2, Cornell Aeronautical Laboratory, Inc. (Nov 1969).

1b. T. R. Sundaram, C. C. Easterbrook, K. R. Piech, G. Rudinger, An Investigation of Heat Release Patterns Associated with Present and Planned Electric Power Plants on Cayuga Lake, Final Report Summary, CAL No. VT-2616-0-1 (Nov 1969).

2. N. H. Brooks, "Diffusion of Sewage Effluents in an Ocean Current," Proc. First International Conference on Waste Disposal in the Marine Environment (ed. E. A. Pearson), Pergamon Press, New York, p. 246 (1960).

3. T. H. Ellison and J. S. Turner, Turbulent Entrainment in Stratified Flows, J. Fluid Mech. 6, p. 423 (1959).

4. E. A. Pearson, An Investigation of the Efficiency of Submarine Outfall Disposal of Sewage and Sludge, State Water Pollution Control Board, State of California, Publ. No. 14 (1956).

5. C. G. Gunnerson, Dye Diffusion Studies in Santa Monica Bay, Trans. A.S.C.E. HY4, p. 101 (Apr 1960).

6. D. R. F. Harleman and A. T. Ippen, The Turbulent Diffusion and Convection of Saline Water in an Idealized Estuary, Int. Assoc. Sci. Hydr. Publ. 51 (1960).

7. S. S. Ziltinkevich, On the Dynamic and Thermal Interaction Between the Atmosphere and the Ocean, Atmospheric and Oceanic Physics 627 (1968).

8. C. H. Bosanquet, W. H. Carey, and E. M. Halton, Dust Deposition from Chimney Stacks, Proc. Inst. Mech. Engrs. (London) 162, p. 355 (1950).

9. H. Schlicting, Boundary Layer Theory, McGraw-Hill Co., New York (1968).

12. Far-field Effects due to a Multiple-jet Diffuser

Y. J. Tsai
Consultant, Environmental Engineering
(Stone and Webster Engineering Corporation)
January 1970

a. List of Symbols

A	Area of plume cross section, 300 ft in a lakeward direction of the diffuser
B	Constant determined by Eq. 12.11
d	Equivalent diameter of hypothetical jet used to predict plume characteristics in the lake-current case
D_0	Equivalent diameter of hypothetical jet before mixing, used to predict plume characteristics in the zero-lake-current case; inside diameter of nozzle (Fig. 12.5 only)
E_0	Initial eddy diffusivity (at $x = 0$)
F_0	Densimetric Froude number defined by Eq. 12.3
g	Acceleration of gravity
Δh_p	Heat-loss factor in (Btu/sq ft)/hr
L	Width of flow field at distance x downstream
L_0	Initial plume width
Q_0	Volumetric discharge rate of power plant
R_0	Reynolds number
T_m	Centerline temperature of jet (Fig. 12.5 only)
T_w	Temperature of receiving water (Fig. 12.5 only)
T_0	Temperature of jet before mixing (Fig. 12.5 only)
ΔT	Temperature rise above ambient of surface water in mixing jet
ΔT_{ave}	Average temperature in area A for the zero-lake-current case
ΔT_c	Initial excess temperature at the diffuser
ΔT_m	Temperature rise above ambient along axis of jet
ΔT_0	Temperature rise above ambient of the jet before mixing
u_0	Initial velocity of jet (Fig. 12.5 only)
U	Velocity of surface water in x direction (Eq. 12.1) or ambient velocity (Eq. 12.7)

U_0	Initial jet velocity (zero-lake-current case)
U_m	Velocity of jet along axis
V_0	Initial jet velocity (lake-current case)
V_h	Vapor pressure of saturated air at plume temperature, in. Hg
V_n	Vapor pressure of saturated air at ambient lake temperature, in. Hg
W	Wind speed, mph
x	Horizontal coordinate along the jet centerline measured from the origin of the hypothetical surface jet (zero-lake-current case);
	Downcurrent coordinate of centerline measured from the initial position of the hypothetical jet (lake-current case)
x_0	Distance from the hydraulically measured profiles back to the origin of the hypothetical jet (zero-lake-current case)
y	Horizontal coordinate normal to the jet axis, measured from the centerline (zero-lake-current case);
	Offshore coordinate of centerline measured normal to x from the initial position of the hypothetical jet (lake-current case)
α	Angle between initial jet axis and current
ε	Eddy thermal diffusivity
ρ	Density of ambient fluid
ρ_0	Density of jet
$\rho(T_a)$	Density evaluated at ambient lake temperature
$\rho(T_0)$	Plume density at either edge of flow field, defined 300 ft lakeward of the diffuser
σ	Standard deviation of Gaussian distribution defined by Eq. 12.12

b. Introduction

In the past, the major application of jet-induced dilution has been for sewage disposal in the ocean. The use of jet-diffuser structures for thermal power-plant discharges is a more recent application. The mathematical treatment to be described is part of a combined hydraulic and analytic modeling scheme used for predicting plume dispersion from the James A. FitzPatrick Nuclear Power Plant of the Power Authority of the State of New York, located seven miles east of Oswego, New York, on Lake Ontario, scheduled for completion in 1973.

Because of the New York State thermal criterion that requires no greater than a 3°F surface temperature rise above ambient water conditions outside a 300-ft radius (or equivalent area) from the discharge, a multiport jet-diffuser system was selected to meet the requirements. The use of a multioutlet submerged jet discharge for the FitzPatrick Plant is more effective than a single-orifice design since greater dilution can be achieved by using a series of properly spaced orifices. This is particularly important in the FitzPatrick Plant vicinity, because the lake currents are usually small and sometimes nonexistent, and hence greater reliance on dilution by jet entrainment must be sought. Hence, the basic concept of the FitzPatrick discharge structure is to achieve very rapid dilution of condenser water with the colder lake water and corresponding decrease in temperatures at the surface by means of a number of submerged high-velocity jets.

Analytical and hydraulic model studies were used to develop the hydraulic design of the structure and to ensure that the temperature patterns produced by the plant operation under widely varying environmental conditions would comply with New York State thermal standards. Four basic discharge directions were investigated using a distorted-scale hydraulic model. The design of the diffuser was complicated by the fact that the direction of the warm surface flow has to be determined in order to locate an intake in a region unaffected by the warm water. Also, the existence of the Nine Mile Point Power Plant 3200 ft to the west was a factor, since the cumulative effects of both plants had to be considered. The most desirable scheme turned out to be a single line of submerged jets essentially parallel to the shore with the jets discharging horizontally toward the lake.

The temperature rise through the condenser and the circulating water flow used for design of the diffuser are 32.4°F and 785 cfs, respectively. The diffuser design is illustrated in Fig. 12.1. Twelve jets are discharged in pairs from six diffuser heads at an initial velocity of 14 ft/sec at 5-6 ft above lake bottom. The direction of discharge is lakeward and essentially normal to the local bottom contours. The diffuser heads are located on 150-ft centers on two tunnels branching off the main discharge tunnel at a point approximately 1100 ft offshore. The branch tunnels run almost parallel to shore. The intake is located 270 ft shoreward of the branch tunnels in an area that is expected to be relatively uninfluenced by the warm water from the FitzPatrick jets with its sector-shaped opening oriented toward the shore. Further details concerning the discharge and intake structures including the preliminary lake studies and design modeling are documented in Ref. 1. The hydrothermal analyses and design concepts were developed in the Environmental Engineering Division of The Stone and Webster Engineering Corporation, Boston, Mass. The hydraulic-model tests were conducted by the Alden Research Laboratories, Holden, Mass.

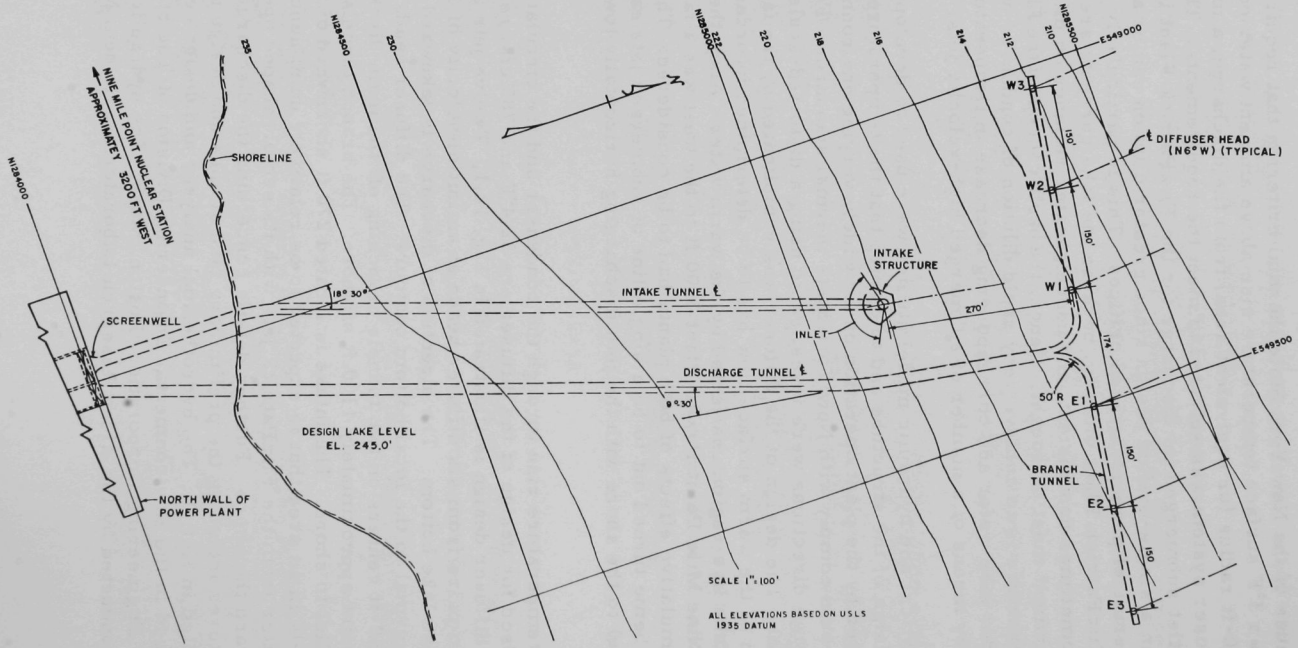

Fig. 12.1. Intake and Discharge Arrangement[1]

The combined hydraulic and analytical modeling scheme used for the FitzPatrick discharge will now be discussed for the two situations in which shoreline currents are and are not present.

c. Model Derivation for the Case of Zero Lake Currents

Figure 12.2 represents a typical flow pattern and temperature distribution resulting from the diffuser under hydraulic-model testing. The tests indicated that the diffuser jets induced sufficient ambient lake flow for dilution to the point where the maximum surface temperature rise, 300 ft lakeward from the line of discharge, was approximately 2.5°F above ambient at its centerline position. The excess temperature 500 ft to either side of the centerline was found to be roughly 2°F. The corresponding centerline velocity 300 ft away from the line of discharge was 1.0 fps; the velocity 500 ft on either side of the centerline was only 0.1 fps directed inward towards the diffuser, as is shown in Fig. 12.3. The surface-flow pattern and temperature profiles as determined from the hydraulic model tests are illustrated in Fig. 12.4.

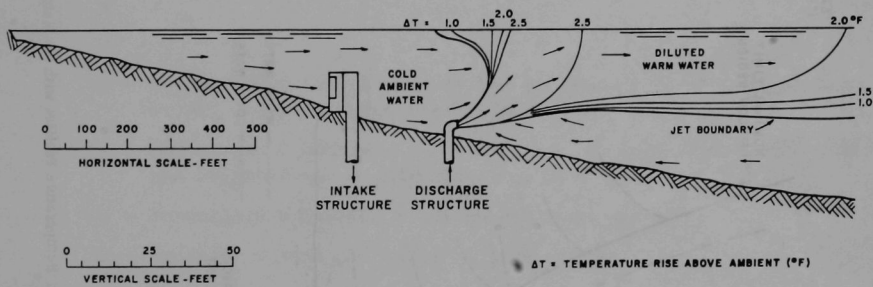

Fig. 12.2. Typical Flow Pattern and Temperature Distribution[1]

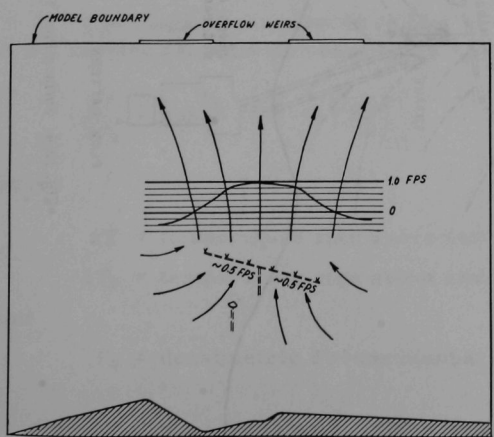

Fig. 12.3

Cooling-water Studies, 1:81 Model, Measured Velocity Distribution, 780-cfs Cooling Water, Zero Lake Current[1]

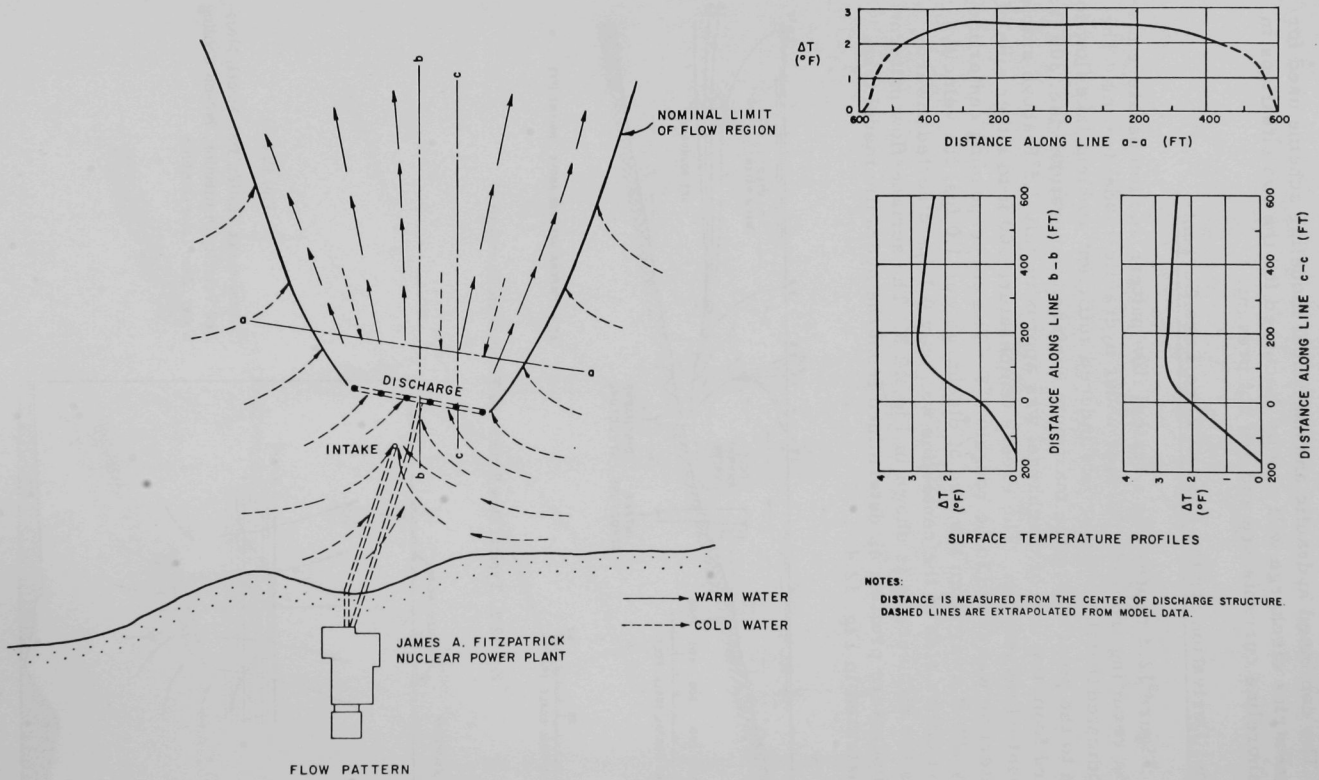

Fig. 12.4. Surface Flow Pattern and Temperature Profiles with No Natural Lake Current; Model Tests[1]

From the results of the hydraulic-model tests it was observed that at about 300 ft lakeward of the diffuser the flow field was well established and could be characterized as surface flow. Therefore, beyond 300 ft lakeward from the diffuser, the mathematical model discussed hereafter was used. First, it was assumed that the end-point velocities at 300 ft of 0.1 fps were directed lakeward rather than inward towards the diffuser. The temperature and the modified velocity profiles were then assumed to be Gaussian in form. The temperature and flow field established by the actual diffuser could now be envisioned to arise from a single hypothetical buoyant surface jet located some distance shoreward of the actual line of discharge. The work of Tamai, Wiegel, and Tornberg[2] and Jen, Wiegel, and Mobarek[3] were then used to obtain the characteristics of the hypothetical jet. From Ref. 2, the distribution of the horizontal component of velocity in the axial direction of a nonbuoyant jet, and assumed valid by Tsai for a buoyant jet as well, is given by

$$\frac{U}{U_0} = 6.2\frac{D_0}{x}\exp\left[-76\left(\frac{y}{x}\right)^2\right], \tag{12.1}$$

where

x = horizontal coordinate along the jet axis, measured from the origin of the hypothetical surface jet,

y = horizontal coordinate normal to the jet axis, measured from the origin of the hypothetical surface jet,

D_0 = equivalent diameter of jet before mixing,

U = velocity of surface water in x direction,

and

U_0 = initial velocity of the jet.

The formula established by Ref. 3 for the temperature concentration at the surface for a jet discharging horizontally at the water surface is

$$\frac{\Delta T}{\Delta T_0} = 7.0\frac{D_0}{x}\exp\left[-3F_0^{1/2}\left(\frac{y}{x}\right)^2\right], \tag{12.2}$$

where

ΔT = temperature rise above ambient of surface water in mixing jet,

ΔT_0 = temperature rise above ambient of the jet before mixing,

and

F_0 = densimetric Froude number, defined by

$$F_0 = \frac{U_0}{\sqrt{\frac{\Delta\rho}{\rho} g D_0}}, \tag{12.3}$$

where

ρ = mass density

and

g = acceleration of gravity.

Along the centerline, the velocity and temperature become

$$\frac{U_m}{U_0} = 6.2 \frac{D_0}{x} \tag{12.4}$$

and

$$\frac{\Delta T_m}{\Delta T_0} = 7.0 \frac{D_0}{x}, \tag{12.5}$$

where

U_m = velocity of jet along axis

and

ΔT_m = temperature rise above ambient along axis of jet.

The problem solution next required the calculation of D_0, F_0, U_0, and x_0, the distance from the hydraulically measured profiles back to the origin of the hypothetical jet. A trial-and-error process was set up to evaluate these parameters. First, dividing Eq. 12.4 by Eq. 12.5 yielded a relationship between ΔT_0 and U_0. Next, a table was generated matching corresponding likely values of ΔT_0 and U_0. For y = ±500 ft, D_0 is calculated from Eq. 12.1 and F_0 is evaluated from Eq. 12.2. Next, F_0 is checked from its definition

$$F_0 = \frac{U_0}{\sqrt{\frac{\rho(T_a) - \rho(T_0)}{\rho(T_a)} g D_0}}, \tag{12.6}$$

where

$\rho(T_0)$ = density of hypothetical jet before mixing

and

$\rho(T_a)$ = density evaluated at ambient lake temperature.

If F_0 does not check, a new corrected pair of values U_0 and ΔT_0 is chosen. A number of such iterations yielded the parameters D_0, U_0, and F_0 within sufficient accuracy. Then, x_0 was calculated from Eq. 12.4 or 12.5. In the present case, the calculated values turned out to be U_0 = 13 ft/sec, ΔT_0 = 28.9°F, D_0 = 38 ft, F = 6, and x_0 = 2870 ft. The resulting temperature distribution downstream was plotted using Eq. 12.2 when $x/D_0 \leq 100$; the graph given in Fig. 12.5 (from Ref. 3) was used to derive the temperature distribution for $x/D_0 > 100$. Surface isotherms were then drawn. The results of the analysis are given in Fig. 12.6 which includes the flow-field isotherms, the temperature decay along the plume centerline, and the area enclosed by consecutive isotherms. Some smoothing of the isotherms was done here to permit them to close at the diffuser rather than at the position of the hypothetical surface jet.

A separate analysis was made of the role of surface heat loss in calculating plume temperatures and areas within isotherms, which proved that the heat-loss effect was negligible. The investigation is described more fully for the case of currents and zero currents in Sec. e below.

d. Model Derivation for the Case of Lake Currents

Lake currents affect the FitzPatrick discharge by deflecting it in the direction of the prevailing current in an increased manner as the jet velocity decreases for increasing distances away from the line of discharge.

Hydraulic modeling was again used to predict the temperature profiles (velocity profiles were not measured) within 300 ft of the diffuser in the lakeward direction. As in the zero-current situation, the diffuser jets again produced an approximate line source at the 300-ft lakeward distance.

Figure 12.7 shows the model flow pattern and surface-temperature rises produced with a current of 0.8 ft/sec to the east, and Fig. 12.8 shows the model flow pattern and surface-temperature rises for a current of 0.7 ft/sec to the west. The maximum surface temperatures measured in the hydraulic model for the above current conditions are seen to be 3.2 and 3.5°F, respectively. Figure 12.9 plots the excess temperature against eastward lake current 300 ft lakeward of the diffuser. Hydraulic modeling for eastward currents of 0.2, 0.5, and 0.8 and westward currents of 0.2, 0.5, and 0.7 ft/sec had shown the temperature profile for each set of conditions to be near Gaussian in form 300 ft lakeward of the diffuser. The profiles were similar to the zero-lake-current case, probably due to the large initial jet-diffuser velocities and the relatively small lake currents involved.

With the temperature profile fully determined up to 300 ft by hydraulic modeling, an analytical procedure was then used to yield the overall temperature distribution. As with the zero-current case, the flow field at 300 ft is again considered to be a line source and to have resulted from a single hypothetical jet placed upstream.

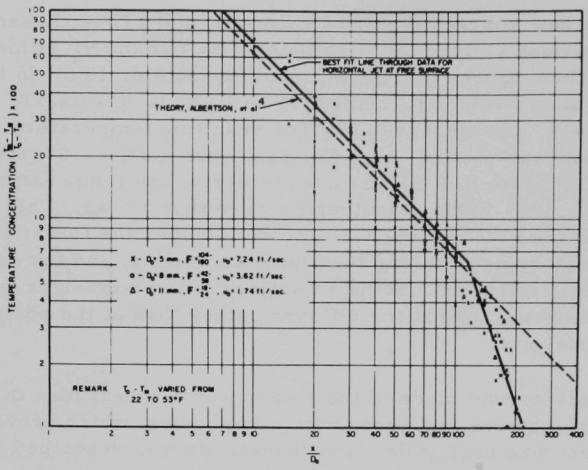

Fig. 12.5

Variation of Temperature Concentration along Jet Axis at Water Surface[3]

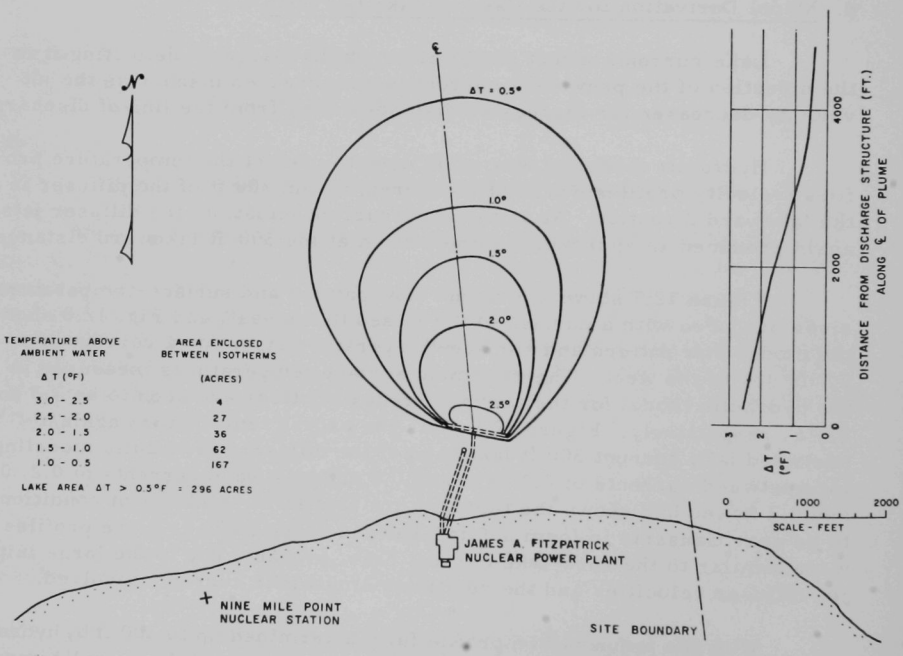

Fig. 12.6. Surface-temperature Pattern at Site with Zero Lake Current[1]

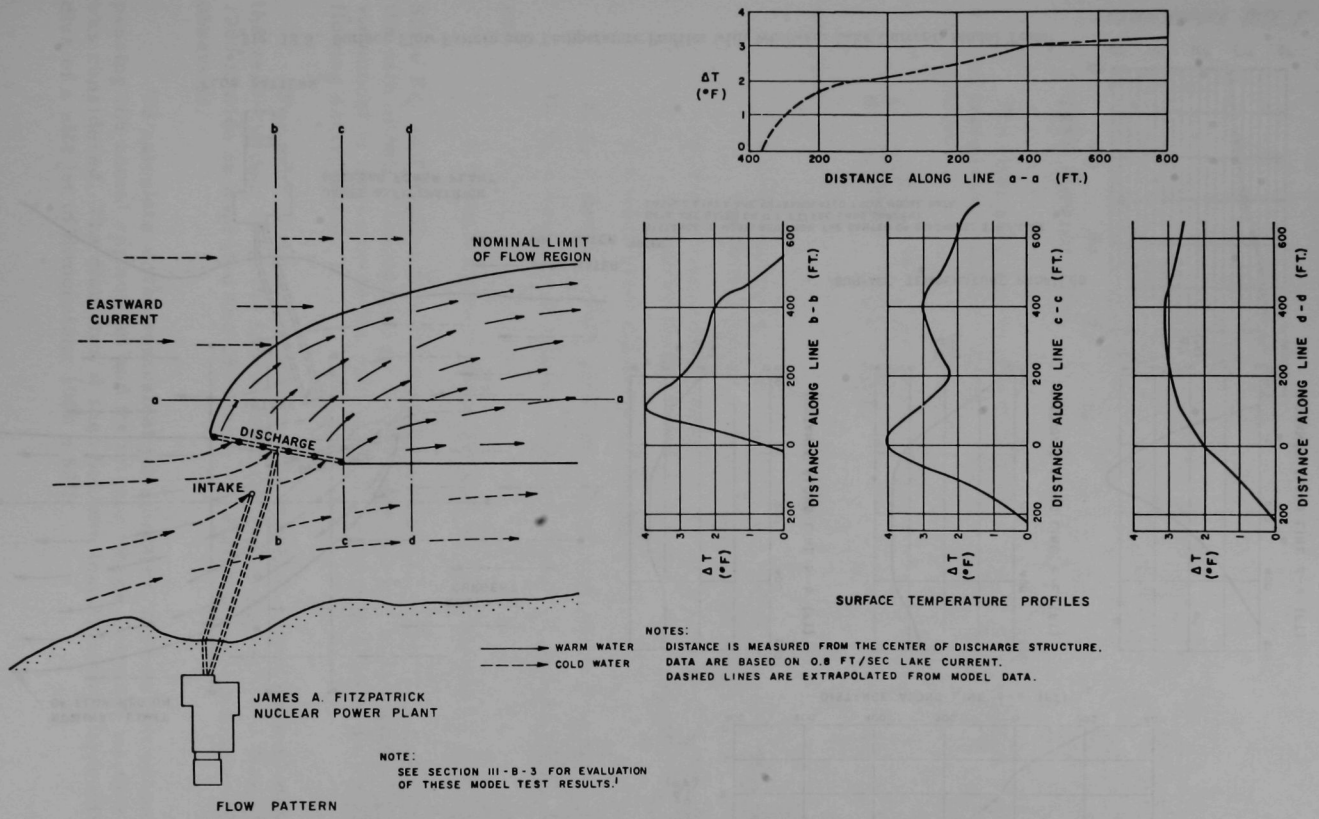

Fig. 12.7. Flow Pattern and Temperature Profiles with Eastward Lake Current; Model Test[1]

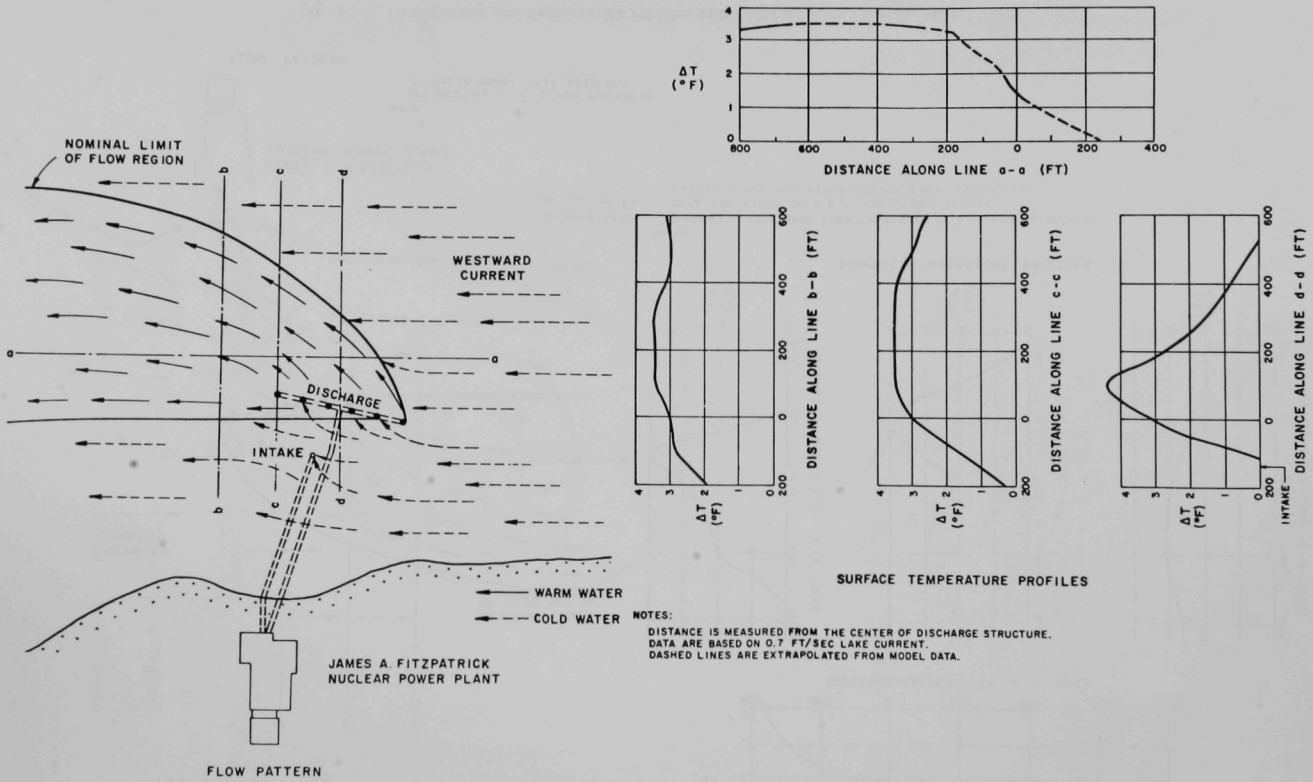

Fig. 12.8. Surface Flow Pattern and Temperature Profiles with Westward Lake Current; Model Tests[1]

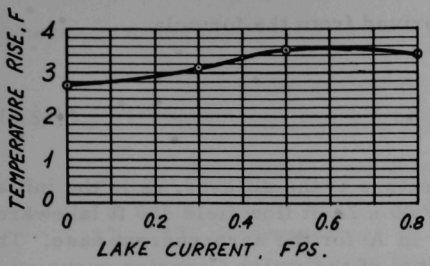

Fig. 12.9

Maximum Surface Temperature above Ambient Lake Temperature outside of Mixing Zone as a Function of Lake Current; Cooling-water Studies; 1:81 Model[1]

The first step was to determine the centerline of the flow field for a fixed transverse current. This was done by using the Shandorov empirical equation[5]

$$\frac{x}{d} = \frac{\rho U^2}{\rho_0 V_0^2}\left(\frac{y}{d}\right)^{2.55} + \frac{y}{d}\left(1 + \frac{\rho U^2}{\rho_0 V_0^2}\right)\cot\alpha, \tag{12.7}$$

where

x = downcurrent coordinate of the centerline, measured from the initial position of the hypothetical jet,

y = offshore coordinate of the centerline, normal to x and measured from the initial position of the hypothetical jet,

d = equivalent diameter of the jet,

ρ, ρ_0 = density of the ambient fluid and jet, respectively,

U, V_0 = velocity of lake current and initial jet velocity, respectively,

and

α = angle between initial jet axis and the current.

Since Eq. 12.7 applies to a completely submerged jet, it was assumed that the path of half a submerged jet (here, a surface jet) in half a flowing environment is the same as the path of a fully submerged jet in an infinite flowing environment.

For each of the above-mentioned six lake-current values, including the zero-current case, the flow field at the 300-ft distance was found to be 1000 ft wide as expected and 25 ft thick. A distinct two-layer flow was observed.

To calculate d, the equivalent jet diameter, the total jet encompassing the actual surface jet and its mirror image above the water surface was considered. The diameter d then became four times the hydraulic radius of a slot jet of dimensions 1000 x 50 ft.

The initial jet velocity V_0 is derived from the formula

$$V_0 = \frac{Q_0 \dfrac{\Delta T_c}{\Delta T_{ave}}}{A}, \tag{12.8}$$

where ΔT_c is the initial excess temperature at the diffuser, Q_0 is the initial discharge rate, A is the area of the 1000 x 25-ft flow field 300 ft lakeward, and ΔT_{ave} is the average temperature in A for the zero-current case. The temperature ΔT_{ave} is a weighted average of the entire Gaussian curve expressing temperature rise with lateral distance. The temperature excess curve for zero current is used so as not to define the initial hypothetical jet velocity with numbers depending upon a given fixed-crosscurrent value. The effect of the crosscurrent should only be felt at distances downstream of the initial hypothetical jet cross section. Consequently, V_0 is determined as the average velocity at the 300-ft-distant flow-field cross section.

The angle α between the initial jet axis and the deflecting flow is exactly 90°. Although the diffuser is oriented slightly eastward, the jets are directed due north, normal to any eastward or westward currents.

Consequently, for <u>each</u> crosscurrent case, d = 95.2 ft, V_0 = 0.466 ft/sec, and $\alpha = \pi/2$. With these three parameters evaluated, the path of the deflected jet for any eastward or westward current velocity is completely determined. The initial position of the hypothetical jet is at the 300-ft lakeward distance mark.

Now that the jet centerline position is specified, the second step involves the determination of the overall temperature distribution about that centerline. The lateral spread of the flow field was computed by considering the dispersion of a continuous line source in a flowing environment following the Brooks analysis.[6] Following the same assumptions as in the Brooks model, where eddy diffusivity is a sole function of flow-field width, with lateral diffusion the only means of dispersion, and where steady-state conditions are assumed to prevail, application of the model predicts a centerline temperature decay of

$$\frac{\Delta T_m}{\Delta T_0} = \operatorname{erf} \sqrt{\frac{3/2}{[1 + (2/3)Bx/L_0]^3 - 1}} \tag{12.9}$$

and lateral flow-field dimension of

$$L/L_0 = \left[1 + (2/3)B\frac{x}{L}\right]^{3/2}, \tag{12.10}$$

where

L = width of flow field at distance x downstream,

L_0 = initial plume width,

x = longitudinal distance measured along the plume centerline,

ΔT_m, ΔT_0 = temperature rise along plume axis at distance x downstream, and initial temperature excess, respectively,

and

$$B = \frac{12E_0}{UL_0}, \tag{12.11}$$

where

E_0 = initial eddy diffusivity (at $x = 0$).

The temperature rise at distances perpendicular to the jet axis were assumed to be normally distributed with standard deviation defined as in Brooks by

$$L(x) = 2\sqrt{3}\sigma(x). \tag{12.12}$$

The initial eddy diffusivity was chosen as 10 ft^2/sec. This value was obtained from Ref. 6, p. 249, where measured values of eddy diffusivity in the horizontal direction in the ocean are plotted against the length scale of a thermal plume. The value E_0 = 10 ft^2/sec corresponds to a plume length scale of 1000 ft using the plotted relationship $\epsilon = 0.01\ L^{4/3}$ representing the four-thirds-power law for eddy diffusivities. The above two-dimensional temperature analysis implies the prevalence of eddy diffusion in lateral spreading and a distinct two-layer flow with no mixing below the depth of 25 ft.

Flow patterns and constant-temperature contours are shown plotted for eastward currents of 0.2, 0.5, and 0.8 ft/sec in Figs. 12.10-12.12; results of westward currents of 0.2, 0.5, and 0.7 ft/sec are plotted in Figs. 12.13-12.15. It is generally concluded from the figures that as the current velocity increases, there appears to be less dilution at a given distance and more area within a fixed isotherm. Generally, higher current speeds produce a more elongated plume with more total area within the 0.5°F isotherm, say, than is the case for lower currents. The only difference that appears between westward and eastward currents occurs in the vicinity of the discharge structure as was determined by the hydraulic-model tests.

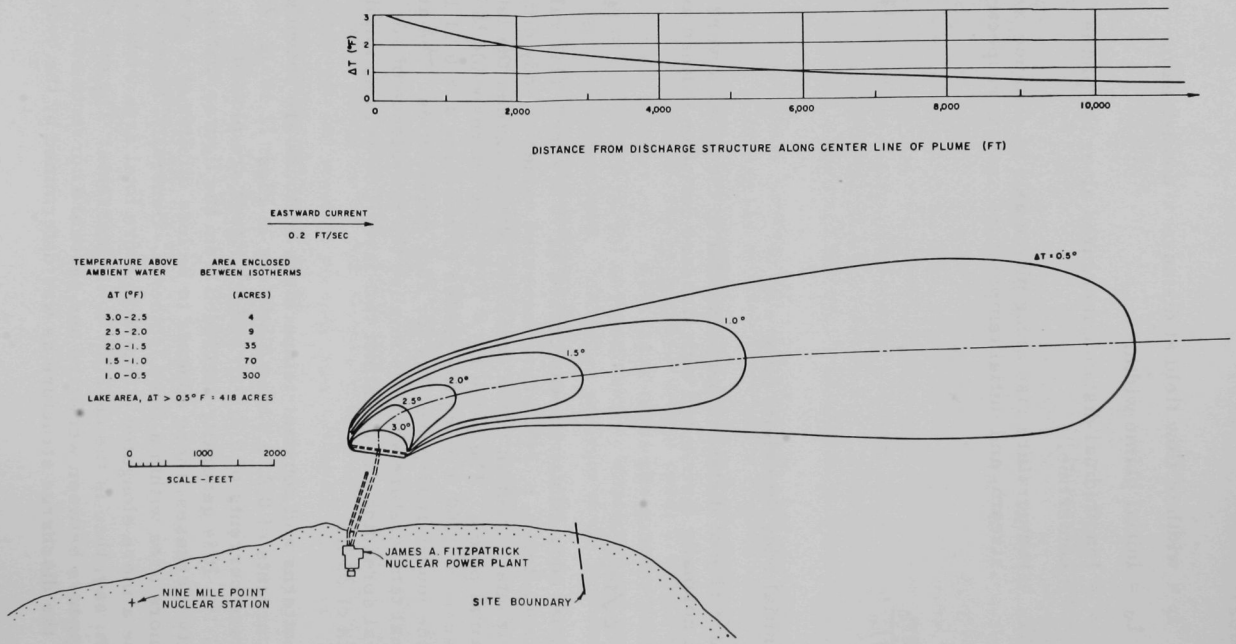

Fig. 12.10. Surface-temperature Pattern at Site; 0.2-ft/sec Eastward Lake Current[1]

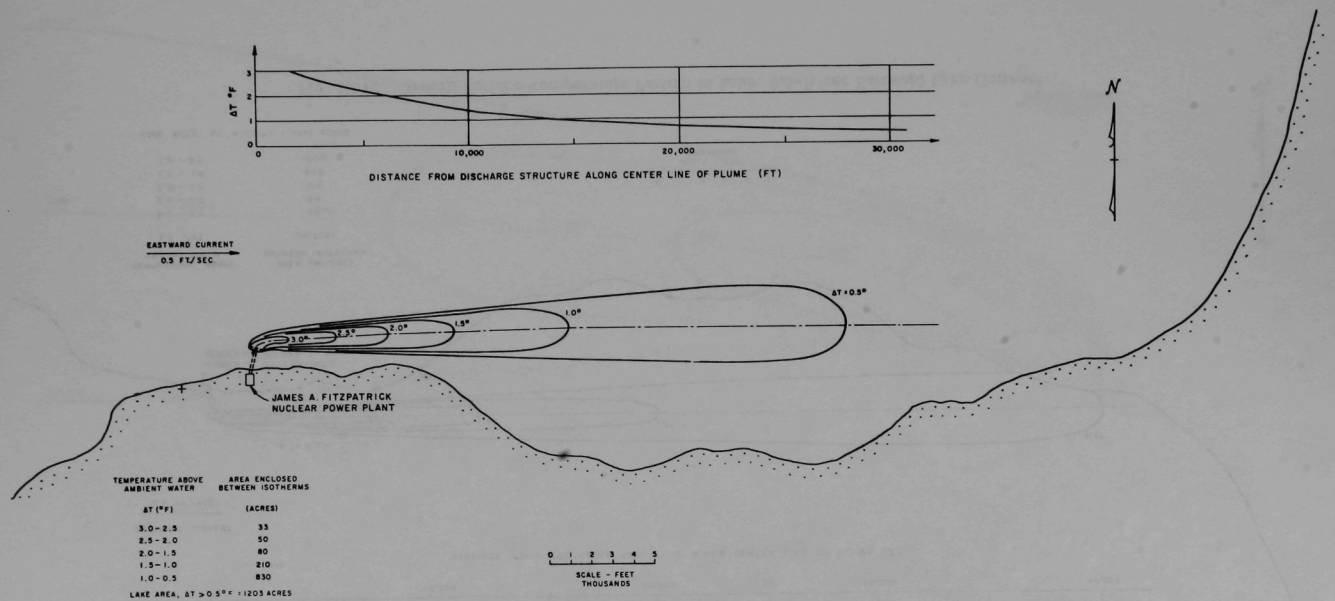

Fig. 12.11. Overall Surface-temperature Pattern in Lake, 0.5-ft/sec Eastward Lake Current[1]

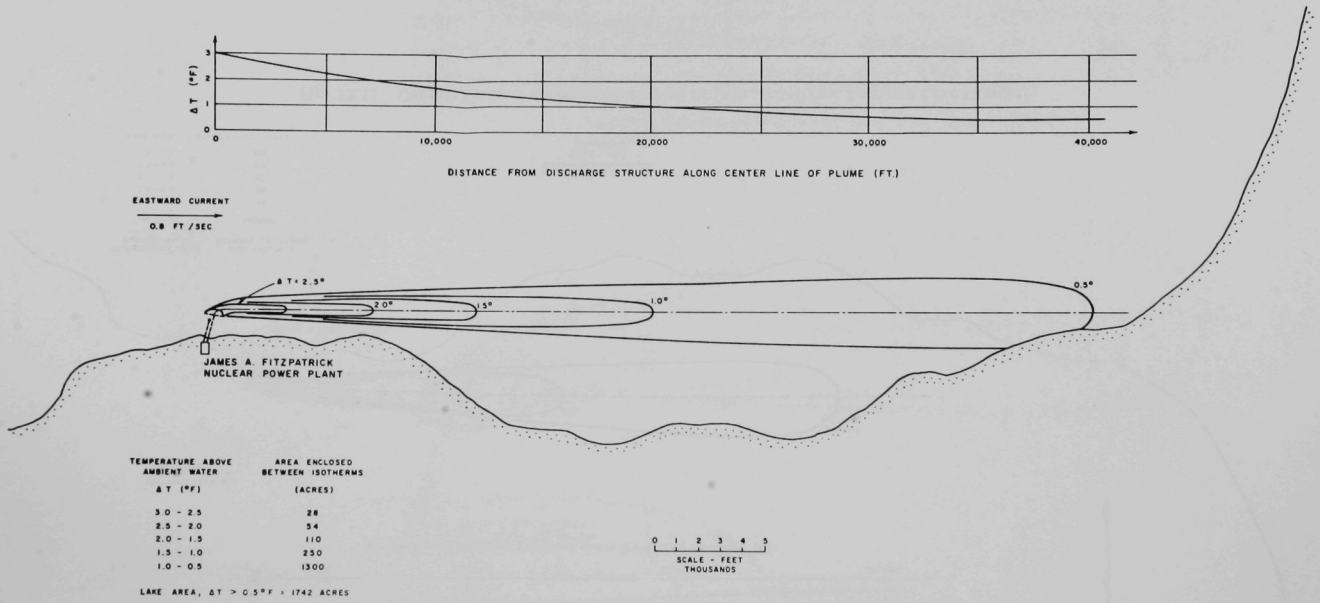

TEMPERATURE ABOVE AMBIENT WATER ΔT (°F)	AREA ENCLOSED BETWEEN ISOTHERMS (ACRES)
3.0 - 2.5	28
2.5 - 2.0	54
2.0 - 1.5	110
1.5 - 1.0	230
1.0 - 0.5	1300

LAKE AREA, ΔT > 0.5°F = 1742 ACRES

Fig. 12.12. Overall Surface-temperature Pattern in Lake, 0.8-ft/sec Eastward Lake Current[1]

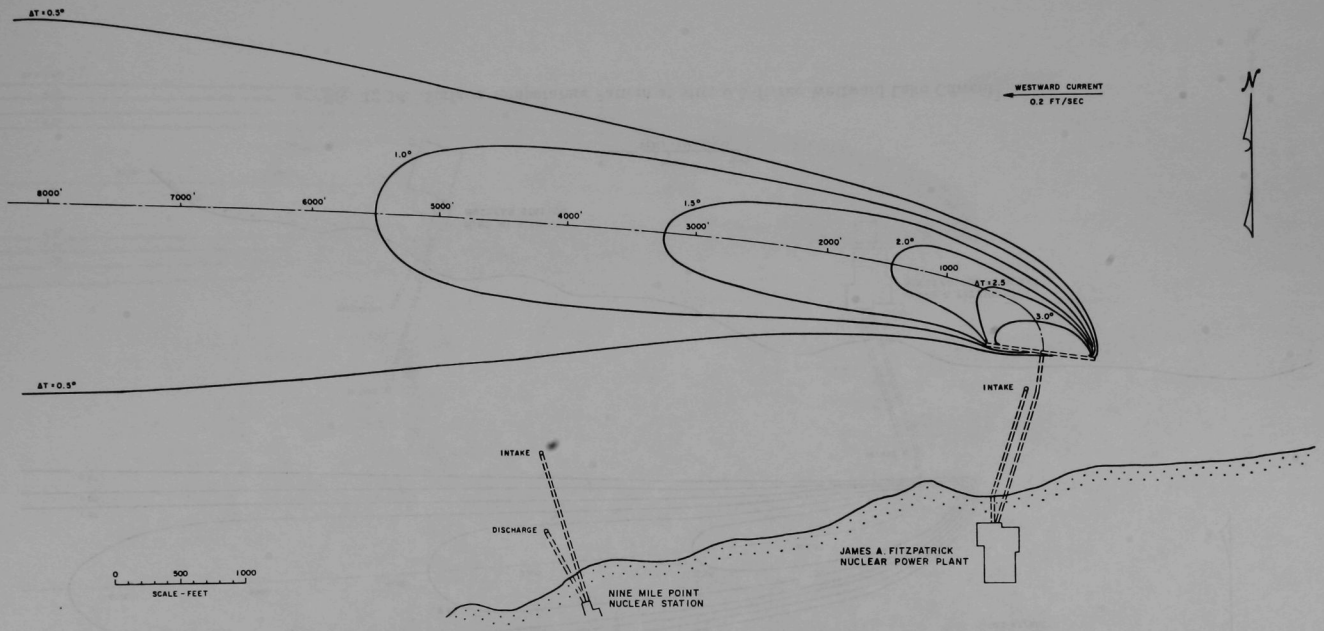

Fig. 12.13. Surface-temperature Pattern at Site; 0.2-ft/sec Westward Lake Current[1]

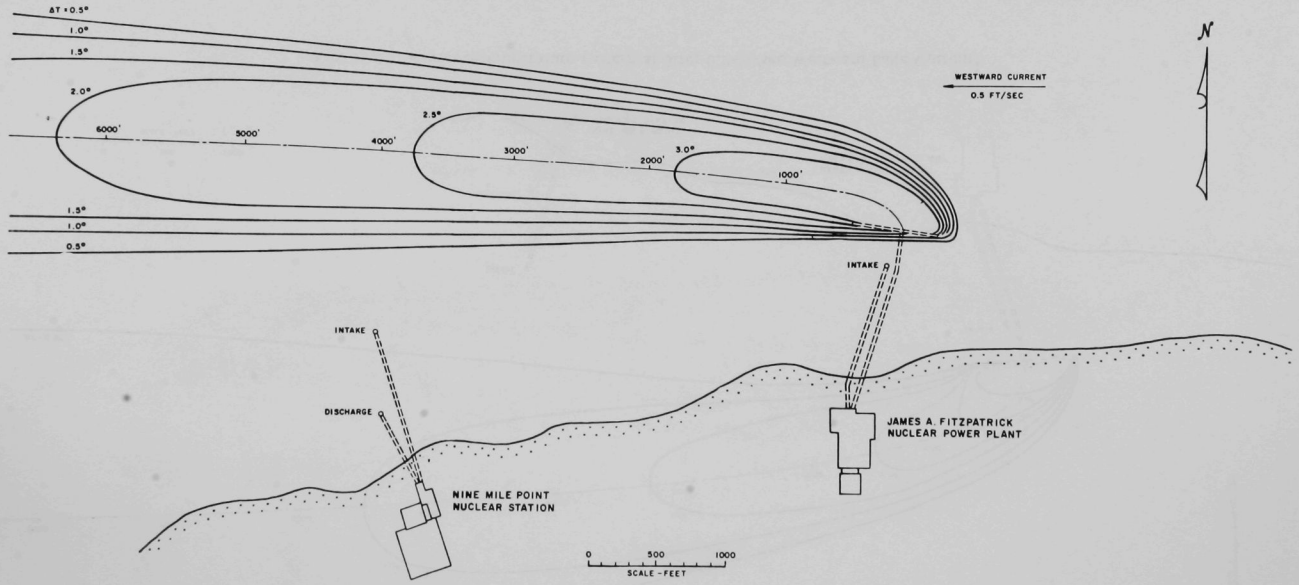

Fig. 12.14. Surface-temperature Pattern at Site; 0.5-ft/sec Westward Lake Current[1]

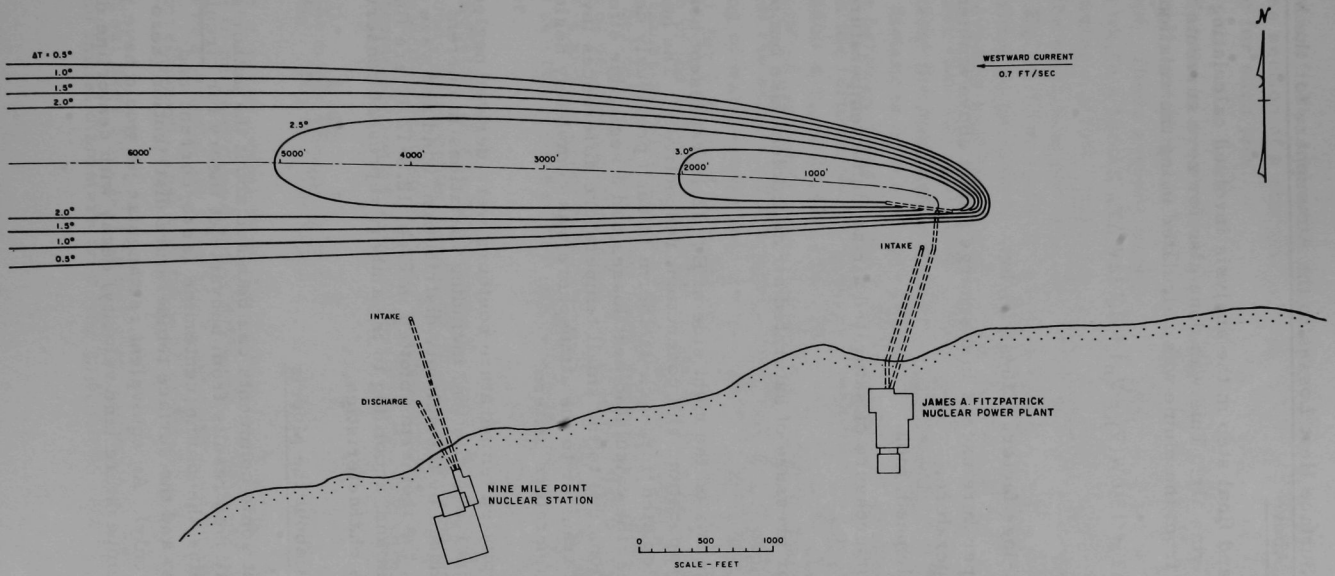

Fig. 12.15. Surface-temperature Pattern at Site; 0.7-ft/sec Westward Lake Current[1]

e. Calculation of Surface Heat Losses to the Atmosphere for the Models in Secs. c and d Above

The third and final step in the analysis involved calculating heat losses to the overlying air. This was done also for zero currents. The relative heat loss from the plume was calculated using the relationship

$$\Delta h_p = 1.1\Delta T + 13.0W(V_h - V_n) + 0.132W\,\Delta T, \qquad (12.13)$$

where

Δh_p = heat-loss factor, (Btu/sq ft)/hr,

ΔT = temperature excess in discharge plume above ambient lake temperature,

W = wind speed, mph,

V_h = vapor pressure of saturated air at plume temperature, in. Hg,

and

V_n = vapor pressure of saturated air at ambient lake temperature, in. Hg.

The three terms on the right side of Eq. 12.13 represent heat loss due to radiation, evaporation, and conduction, respectively. The heat-loss factor Δh_p was calculated for each isotherm in each previously described plume. In all cases, the calculated heat losses had a negligible effect on the isotherm locations due to the small temperature differences involved. Consequently, heat transfer to the atmosphere was completely neglected in predicting each temperature pattern.

The above-plotted temperature contours were derived neglecting other factors that increase dilution, including variations in current direction, shear produced by the velocity distribution, wind and wave effects, etc. Consequently, the isotherms plotted in Figs. 12.8-12.13 are final results of the analysis and, according to the author, represent conservative estimates on plume characteristics.

f. Some Comments about the Models

At this point some comments can be made about the author's diffuser models. Tsai used results from buoyant-jet theory for circular orifices to determine the plume centerline (zero-current and crosscurrent cases) and the surface temperature distribution (zero-crosscurrent case only). An equivalent rectangular jet would have yielded a greater rate of temperature (and velocity) decay with centerline distance.[7]

Tsai chose to fit the hydraulic data taken 300 ft offshore from the diffuser to a cross section of a circular jet mainly due to the abundant information available for such jets.

For the zero-crosscurrent situation, the experimental results of Jen, Wiegel, and Mobarek[3] as extended by Tamai, Wiegel, and Tornberg[2] were used. These authors conducted hydraulic experiments in a long, deep flume in which a heated jet was discharged at the surface of a body of receiving water. A fully three-dimensional jet resulted, which was found to satisfy the empirical formula (Eq. 12.2) for surface-temperature distribution and Eq. 12.5 for surface centerline decay. Jen et al. found those relationships to be valid for initial Froude numbers between 18 and 180, initial Reynolds numbers between 8300 and 21,000, and downstream distances less than 100 diameters. The curve in Fig. 12.5 was determined to represent the measurements of the centerline temperature decay at greater distances downstream. Tamai et al. found that for initial Froude numbers between 3 and 11, the jet axial-temperature decay agreed fairly well with the formula of Jen et al. within the range of Reynolds numbers tested ($6600 \leq R_0 \leq 21{,}300$) for $x/D_0 < 60$. No measurements were taken for $x/D_0 > 60$, in order to ensure negligible wall effects. Tamai et al. found that the empirically determined curves describing the surface spreading of warm-water jets were a little different than reported by Jen et al. for $3 < F_0 < 11$ and $6600 < R_0 < 21{,}300$. The lateral distribution of the surface temperature was found not to be described by the normal Gaussian distribution as measured by Jen et al. The initial Froude number derived by Tsai for the hypothetical jet was 6. Therefore, due to the lack of definite information on the lateral distribution of temperature for $F_0 = 6$ and the proper jet centerline decay beyond $x/D_0 = 60$, Tsai decided to use the results of Jen et al., hoping that any discrepancies would be minor.

Equation 12.1 is referenced in the work of Jen et al.[3] and originated in the submerged nonbuoyant air-jet theory of Albertson et al.[4] Equation 12.1 is the velocity distribution at the surface if one considers a surface jet as half a completely submerged jet. The complete formula is

$$\frac{U}{U_0} = \frac{1}{2C_2}\frac{D_0}{x}\exp\left(-\frac{1}{2C_2^2}\frac{r^2}{x^2}\right),$$

in which r is the radius in an axisymmetric flow and C_2 is a dimensionless constant to be determined empirically ($C_2 \approx 0.08$). The application of this formula to a buoyant-jet situation is not clear. Again, at the time of the model development, Tsai considered this formula the best one available.

Tsai uses Eqs. 12.1 and 12.2 for a total distance of about 8000 ft or about 200 initial diameters from the hypothetical jet source. It is doubtful

that the effluent is still a jet, even for 60-100 diameters, due to the increasing importance of ambient turbulence with increasing downstream distance. This receiving-body turbulence was not physically modeled in the experiments referred to above due to lack of knowledge on the scale of the eddies involved, the degree of lake turbulence, and the capability of reproducing this turbulence in the laboratory. Another area of concern involves the use of the experimental results of Jen et al. and Tamai et al. in a general lake situation. The laboratory results applied were carried out with no ambient-stratification effects and no bottom-boundary influences. Rarely does a jet discharge spreading along the surface act as a fully three-dimensional jet. The vertical spreading, as allowed for in the use of the results of Jen et al., Tamai et al., and Albertson et al. will eventually be inhibited by the lake bottom. This fact is not considered in Tsai's application of Eqs. 12.1-12.5. The smaller extent of the isotherms in the zero-current case, as compared to the crosscurrent problem, is due to the three-dimensional dilution allowed for by that model.

Tsai's crosscurrent model, on the other hand, considers a stably stratified two-dimensional plume of constant depth for the region beyond 300 ft of the diffuser. The temperature is assumed to be vertically uniform from the surface to a depth of 25 ft.

Tsai uses the Shandorov empirical equation to determine the position of the deflected centerline of the spreading heated discharge for distances greater than 300 ft from the diffuser. The formula was developed from experiments on air jets in crosscurrents from a circular nozzle. The Shandorov formula accounts for differing densities of the jet and ambient fluid. Tsai verified the Shandorov formula for a limited number of experiments on high- and low-velocity stack releases (the ratio of exit velocity to ambient velocity varied from 1 to 20) with residual buoyancy included. Tsai found the formula applicable for those cases. The Brooks analysis of the dispersion of a heated effluent in a uniform stream is used to give the temperature distribution about that centerline. The philosophy behind this patching technique has an inherent contradiction. The Shandorov relationship is developed from dispersion of a heated jet, in which the jet's self-induced turbulence predominates in the jet motion and temperature decay. The Brooks formulas are developed theoretically under the assumption that ambient turbulence dominates in plume dispersion. The Brooks model also assumes a uniform line source from which the effluent is discharged into the far field. The direction of the current is the same as the direction of the discharge. Tsai, however, uses Brooks' results for an assumed line source discharging normally into a flowing stream. He is thereby assuming a negligible zone of adjustment on temperature, in which the actual diffuser effluent interacts with the ambient flow and disperses downcurrent. Tsai made these assumptions with the thought that they were the best that could be done with the present state-of-the-art and the time he had available to develop a model.

As Brooks did, Tsai uses the "four-thirds-power law" as a form for the lateral eddy thermal diffusivity. This form has been validated for dispersion in the open sea. Tsai notes that for the larger currents considered, the plume is sufficiently far from the shore boundaries to allow a nearly unrestricted eddy size in dispersing the plume. From this argument, Tsai justifies the use of the four-thirds-power law. However, for the lower ambient velocities, the plume will approach or intersect the shoreline because of its wider spread. In that case, the four-thirds-power law will yield optimistic results. A different form for the diffusivity would need to be used to account for the restricted eddy sizes caused by a bottom and shoreline influence.

Tsai uses $E_0 = 10\ ft^2/sec$ to represent the constant in the four-thirds-power law. This value corresponds to an eddy size of 1000 ft (the initial width of the flow field). Figure 12.16, taken from Brooks,[6] was used in this calculation. Brooks found that a four-thirds-power-law approximation fit numerous data on diffusivities in the ocean, the diffusivity being related to the four-thirds power of an appropriate length scale by $\epsilon = 0.01L^{4/3}$. The value of the constant can, however, vary up to two orders of magnitude. If a smaller value of E_0 were used, the plume would extend a greater distance and the order of spread would be much smaller. A higher value would shorten the plume's longitudinal expanse, but cause it to spread wider. Tsai's solutions are clearly a function of E_0. No sensitivity analyses were done to ascertain the change in plume characteristics with the E_0 chosen.

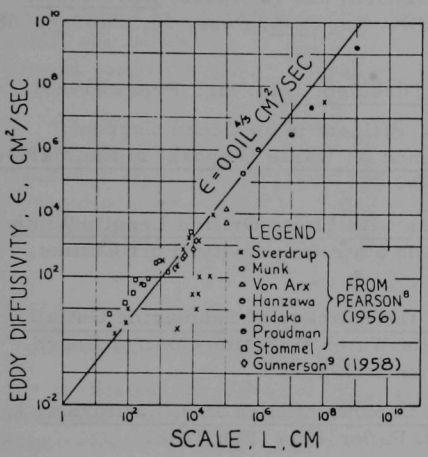

Fig. 12.16. Measured Values of Eddy Diffusivity in the Horizontal Direction in the Ocean, Showing Increase with Scale[6]

There is no apparent reason for the plume to be three-dimensional when the lake is stagnant and two-dimensional when crosscurrents exist. Tsai, however, considers his two diffuser models the best that could be derived with the limited state-of-the-art at the time of the model development and the relatively short time he had been allotted to develop them. Only after the FitzPatrick Plant is constructed and field surveys are taken can these models be fully evaluated.

References

1. Engineering and Ecological Studies for Design of Intake and Discharge Structures, James A. FitzPatrick Nuclear Power Plant, Power Authority of the State of New York, Stone and Webster Engineering Corporation (Jan 1970).

2. N. Tamai, R. L. Wiegel, and G. F. Tornberg, Horizontal Surface Discharge of Warm Water Jets, J. Power Division, ASCE 95, No. PO2, Proc. Paper 6847, pp. 253-276 (Oct 1969).

3. Y. Jen, R. L. Wiegel, I. Mobarek, Surface Discharge of Horizontal Warm-Water Jet, J. Power Division, ASCE 92, No. PO2, Proc. Paper 4801, pp. 1-30 (Apr 1966).

4. M. L. Albertson, Y. B. Dai, R. A. Jensen, and H. Rouse, Diffusion of Submerged Jets, Trans. Am. Soc. Civ. Eng. 115, Paper No. 2407, pp. 689-697 (1950).

5. G. N. Abromovich, The Theory of Turbulent Jets, MIT Press (1963).

6. N. H. Brooks, "Diffusion of Sewage Effluent in an Ocean Current," Proceedings, International Conference on Waste Disposal in the Marine Environment, Pergamon Press (1960).

7. V. Yevdjevich, Diffusion of Slot Jets with Finite Orifice Length-Width Ratios, Hydraulics Papers, Colorado State University, Fort Collins, Colorado (Mar 1966).

8. E. A. Pearson, An Investigation of the Efficacy of Submarine Outfall Disposal of Sewage and Sludge, State Water Pollution Control Board, Publication 14, Sacramento, California (1956).

9. C. G. Gunnerson, Sewage Disposal in Santa Monica Bay, California, J. Sanitary Eng. Div., ASCE 84 (SA1), Paper 1534 (Feb 1958).

IV. MODEL SUMMARIES

This chapter briefly highlights and compares the models reviewed on issues considered by us to be important for model development. Not all models within any one group, say, for instance, jet models, singly consider all the issues. The rationale for model-issue omissions has already been elaborated upon in the previous sections and therefore will not be repeated here. Suffice to say that model acceptance or indictment, based solely on whether the models do or do not consider various issues, is not founded because the true test of any model is whether it can reasonably predict real-world prototype situations within the specified limitations acclaimed for them. For the models reviewed within this report, it is our opinion that none of the models has been objectively and sufficiently validated with prototype field data to enable them to be used "comfortably" in a predictive sense. This is a rather subjective comment on our behalf, and really the suitability of any model for a particular need must in final analysis be judged by the individual model user.

At the end of each section within this chapter listings are presented specifying the input parameters needed for model utilization. In addition, figures are presented in Appendix A yielding schematic representations of the model predictions. Appendix B presents a table summarizing the individual model characteristics.

A. Near-field Regime

1. Method of Approach

Except for the semiempirical methods of Sundaram et al. and Tsai (see Secs. III.C.11 and III.C.12), each jet model reviewed treats the initial dispersion of a heated effluent by integral (as opposed to differential-numerical) approaches. In general, two basic approaches exist in the derivation of plume models--one based on a differential analysis, and the other on an integral analysis. The differential method involves solving the general partial differential equations of motion and heat diffusion to arrive at velocity and temperature distributions. The problem of jet dispersion lies in gaining the solution to those equations once having established such requirements as boundary conditions, eddy-transport coefficients, etc. The equations are impossible to solve analytically while retaining all terms of the equations describing the motion and dilution of the heated jet. For the collective class of plume problems, the very few analytical solutions to the general set of governing equations that do exist have been derived by assuming gross simplifications of the physical phenomena. Differential-numerical modeling has an advantage in that many complexities associated with real physical phenomena do not have to be ignored as is required in the development of analytical solutions.

Numerically solving the problem of the dispersion of a heated jet involves the solution of the coupled flow and energy partial differential equations. The usual assumption made in modeling the jet regime is that the often large initial Froude number indicates that inertial forces dominate the buoyancy forces within the jet and that, to a fair approximation, density-induced pressure gradients can be neglected in the equations of flow. (In some instances, interaction between flow field and density distribution can be very important during initial jet dilution, generally requiring three space dimensions to be considered unless symmetry occurs in a space dimension.) This results in an uncoupling of the flow and energy equations, which clearly simplifies any numerical solution. However, uncertainty as to the proper form of the generally unknown eddy diffusion coefficients (momentum and energy) and the precise flow and pressure boundary conditions has led many investigators to seek a simpler approach. In addition, problems such as computation time and numerical stability have often negated the attractiveness of a numerical method (at least for the jet regime).

The integral analysis, on the other hand, involves a sacrifice of the microscopic characteristics of the flow and temperature fields in favor of a solution for the macroscopic quantities. More specifically, the precise shape of the lateral and vertical temperature and velocity profiles must be assumed, based upon intuition, experiment, or (quite often) both. The integral analysis involves several further simplifications and assumptions about the flow field for the purpose of disregarding a number of terms in the governing equations in addition to the main one uncoupling the flow and energy. Among the additional assumptions often used in the various models are: (1) steady flow, (2) hydrostatic pressure field, (3) a fully turbulent jet, (4) a density difference between jet and ambient fluid which is small compared to the density at any point in the field, (5) an eddy transport of heat which is only effective in the lateral direction (normal to jet axis), and (6) a negligible molecular heat conduction and viscosity. Problems such as the lack of a recognized general form for the eddy-transport properties and the complexity of the boundary conditions in the numerical approach translate to similar uncertainties in the form of the entrainment function and pressure drag in the integral method.

In short, then, the integral technique is a "whittling and fashioning" method in which small terms are dropped from the governing equations and the dependent variables are assumed to have a fixed general form.

The assumptions made on the dependent variables also depend upon the model in question. Each model, however, must make assumptions on the lateral (also vertical) profiles, the entrainment function, and the pressure drag. For the five jet models reviewed the assumptions are:

Hoopes et al. assume lateral velocity and temperature distributions to be similar and Gaussian in form. No vertical variation within the jet is

considered. The jet is assumed to grow linearly with centerline distance from the outfall for the variable-entrainment-coefficient case only. The rate of lateral entrainment through the edges of an orthogonal slice of the jet is defined to be proportional to the centerline velocity, with the constant of proportionality defined as the entrainment coefficient. No influence of the jet-crosscurrent interaction on the pressure distributions around the jet is considered.

Carter assumes an "equivalent" top-hat form for the lateral velocity and temperature distributions within the jet; no vertical variations are considered. Hydraulic-model studies are used to acquire jet-centerline temperature formulas, which are then inputted into the momentum equations to estimate the fraction of entrained ambient fluid at each longitudinal position along the jet. The pressure distribution on the jet resulting from the jet interaction with the crosscurrent is assumed locally to be of the same form as the drag force on a solid body obstruction in a uniform stream. The assumption that the component of the centerline velocity in the direction of the shore-parallel crosscurrent is equal to the ambient current replaces the need for using a continuity relationship within the model.

For the no-bottom-case situation, Stolzenbach and Harleman assume similarity forms for the lateral, longitudinal, and vertical velocity and temperature profiles. For the velocity distribution, there is an additional term to handle the component of the ambient current along the jet axis. The distributions are assumed to be separable functions of the dimensional coordinates and are obtained or inferred from previous studies of plane, submerged, nonbuoyant jets. The lateral and vertical profiles are non-Gaussian in form. An additional component, the lateral spreading velocity, is added to the lateral velocity obtained from nonbuoyant jet theory to account for the increased spreading beyond a linear one due to buoyancy forces. This spreading velocity is assumed to be proportional to the axial velocity along the jet. Experimental relationships for lateral and vertical spread from nonbuoyant jet theory are used to first determine the entrainment coefficients for nonbuoyant jet conditions using the model. The lateral-entrainment coefficients obtained in this manner are then assumed to be applicable in the buoyant-jet case. A special form is assumed for the vertical-entrainment coefficient based on the local Richardson number to account for jet buoyancy. The nonconstant vertical-entrainment coefficient is chosen in such a way that it will reduce to the calculated nonbuoyant value when no temperature differences occur. The actual normal inflow velocity of ambient fluid into the jet both laterally and vertically is then the product of the appropriate coefficient of entrainment and the surface axial velocity. The pressure field established by ambient crosscurrent interactions with the jet are not considered.

After accounting for a region of flow development, Motz and Benedict assume equal Gaussian forms for the lateral velocity and temperature distributions. Vertical variations are not considered. A lateral inflow velocity

is used to account for entrainment. The inflow velocity is assumed to be proportional to the excess of the jet axial velocity over the component of the ambient current in the direction of the centerline. The modification of the local pressure distribution about the jet due to the interaction of the jet with an ambient crossflow was accounted for by treating the jet as a solid obstruction in the crossflow.

Pritchard assumes "equivalent" top-hat lateral distributions for velocity and temperature within the jet regime of his model. A rate-of-spread coefficient is assumed yielding the jet lateral width as a function of the centerline distance. Vertical spread of the jet is assumed to be linear until the jet reaches a "critical mixing depth" intrinsic to the particular receiving body of water.

The model developed by Sundaram et al. determines the jet trajectory by using semiempirical results from the theory of dispersion of chimney-stack effluents into the atmosphere. The trajectory is determined from three empirical constants (fixed for a given site) and from the ratio of the initial jet velocity to the crossflow velocity. The velocity and temperature distribution about that centerline is determined from two-dimensional slot-jet analysis in which the receiving fluid is assumed stagnant. The distributions are then simply "bent" over to fit the deflected centerline.

Tsai handles the problem of jet dispersion from a submerged diffuser system. Hydraulic modeling is employed within the first 300 ft of the line of orifices. For zero lake currents, three-dimensional empirical results on surface jets are used for further predictions. When crosscurrents are significant, a semiempirical formula is used for the prediction of the centerline trajectory further downstream than 300 ft and a far-field model is used to yield the temperature distribution about that centerline.

2. Dimensionality and Buoyancy Considerations

Most surface-jet models considered in this report are strictly two-dimensional. Their authors, Hoopes et al., Carter, Motz and Benedict, and Sundaram et al., freely recognize, however, that a region of vertical entrainment often exists near the orifice, due mainly to the large-velocity gradients between the jet and the ambient current. Vertical spreading is generally somewhat restricted due to the density difference between the warm jet and cooler underlying fluid. However, these investigators expect that this region of initial vertical entrainment is small and its neglect will not have significant effects on the jet trajectory or dilution.

With this assumption made, Hoopes et al. and Motz and Benedict handle jet dispersion in approximately the same manner. They assume that the advection of the heated jet fluid in the longitudinal direction, combined with the interaction of the jet and ambient crosscurrent (resulting in an inflow of cooler ambient fluid laterally), are balanced by lateral turbulent

diffusion and surface heat loss. Buoyant convective motions are not considered, since the secondary currents they induce require a three-dimensional structure. Longitudinal turbulent diffusion is ignored due to the predominance of advection in that direction. The jet is assumed to have a constant depth from the point of discharge with a vertically uniform temperature distribution from the surface to that depth. Although the temperature of the plume water varies longitudinally and laterally, its density is taken to be essentially constant as a simplifying assumption. Conservation equations for mass, momentum, and heat are then written (with the proper input of the entrainment function, pressure drag, and lateral temperature and velocity profiles). A solution to these equations yields the lateral spread, jet deflection, and longitudinal temperature and velocity decay.

Carter follows the same philosophy with some new twists. He derives two momentum-conservation equations and solves for the jet trajectory, using entrainment (dilution) curves as input from his hydraulic studies. He does not solve for the lateral spread and defines only "equivalent" top-hat distributions for velocity and temperature, sidestepping the similarity question. (Carter did this mainly from his observation that inshore entrainment was partially cut off in his associated physical modeling studies. This led to completely nonsimilar functions for velocity and temperature. Lateral temperature measurements revealed a bell-shaped or Gaussian-type distribution from the centerline in the offshore direction; the lateral temperature from the centerline toward the inshore boundary dropped off continuously to a nearly constant value. The velocity appeared to start at zero at the inshore wall and increase in a bell-shaped pattern to the centerline; in the offshore direction from the centerline, the velocity was determined to be nearly constant. This mirror-image identity precluded any similarity.) Heat loss and buoyancy were not considered, which seemed justified in Carter's problem.

Hoopes et al., with Motz and Benedict, use mass and momentum conservation to derive the trajectory and the velocity distribution. The velocity distribution in turn was used to solve for the temperature decay. Carter, on the other hand, used his observed centerline-temperature-decay formula to predict the jet trajectory, and from that the velocity distribution could be evaluated.

Sundaram et al. derive the lateral spread of velocity and temperature along the predetermined centerline trajectory using Prandtl's second mixing-length hypothesis. They employ classical two-dimensional slot-jet theory (for a stagnant receiving fluid) in which a mixing-length hypothesis is used to relate turbulent shear stress to the lateral velocity gradient. With the input of an experimental coefficient, the longitudinal-momentum equation is solved with the aid of the continuity equation to yield the lateral spread of velocity. Horizontal similarity of the transfer of heat and momentum was used to yield the lateral temperature profile. Here, advection

of jet fluid longitudinally and laterally is assumed to balance lateral turbulent diffusion. Sundaram et al. neglect surface heat loss in the jet regime.

Pritchard derives a pseudo two-dimensional model. A top-hat distribution is assumed for the lateral and vertical distributions of velocity and temperature with a total jet width growing symmetrically and linearly with a slope of one on six. The vertical depth is also assumed to grow linearly from the initial jet depth to the "critical mixing depth," supposedly characteristic of each body of water under consideration. The jet is assumed to remain at constant depth from that point, entraining new dilution water only laterally. If the initial plume depth is equal to or greater than the critical mixing depth, Pritchard assumes no vertical entrainment. Buoyant convective motions are not considered. Conservation equations of momentum and heat are solved (neglecting vertical spread) to yield the velocity and temperature decays. A linear correction is applied to account for the additional dilution resulting from any vertical spread. Finally, corrections are made to allow for possible reentrainment of old dilution water as well as a correction for surface heat loss.

Stolzenbach and Harleman consider buoyancy and (hence) three-dimensionality in their model. They begin their analysis from a set of partial differential equations representing mass, momentum, and energy conservation in three dimensions. They then simplify the equations somewhat by dropping negligible terms. The resulting equations show the interaction between the flow and heat transfer through the horizontal pressure terms, written in terms of the lateral and longitudinal temperature gradients. Pseudo similarity forms (which reduce to similarity forms in the no-crosscurrent case) are then assumed for the three-dimensional velocity and temperature, entrainment coefficients are postulated for the lateral and vertical directions (the vertical coefficient is based in part on the local Richardson number and is written to handle the self-induced stratification of the jet), and a lateral-spreading velocity is postulated to aid in predicting the additional spreading caused by the buoyancy. By integrating the reduced set of partial differential equations over four characteristic prechosen regions of an arbitrary jet cross section with the assumed forms for the dependent variables substituted, they obtain a system of ordinary differential equations which are then solved to yield the three-dimensional velocity and temperature distribution along with the jet's lateral- and vertical-spreading characteristics. No drag force is assumed (in the crosscurrent case). Surface heat loss is included.

Tsai uses hydraulic modeling in his submerged jet diffuser problem for the first 300 ft. Velocity and temperature distributions are measured at various cross sections normal to the flow in the zero- and nonzero-crosscurrent cases. For the zero-lake-current case, he then uses empirical results from flume studies of heated surface jets to predict the lateral and longitudinal temperature and velocity fields beyond 300 ft from

the diffuser. When crossflows exist, Tsai considers the region beyond 300 ft to be in the far field and uses the Brooks far-field temperature distribution there. This will be discussed in more detail in Sec. B of this summary chapter.

3. Crosscurrent and Entrainment Effects

One of the main difficulties in modeling a heated discharge with or without the presence of a crosscurrent is an accurate mathematical simulation of the entrainment of ambient fluid. Very few investigators have looked, by experimental means, at the form of the entrainment function in the case of buoyant deflected jets. Efforts are now being made to synthesize various effects such as buoyancy and ambient currents into one single function encompassing the semiempirical results obtained from a variety of previous experiments on buoyant nondeflected jets, nonbuoyant deflected jets, etc. The danger of such forms, however, is in their adequacy for the combination of effects not actually experimentally tested.

Each jet model reviewed uses a form of entrainment generally defined for submerged nonbuoyant jets. Considering a surface jet in a flowing environment as half a submerged jet in half a flowing environment seems legitimate only for a nonbuoyant problem. In addition, each investigator considers entrainment equal on the offshore and inshore sides of the jet. In reality, there is a sheltering effect on the lee side of the jet which reduces entrainment there due to the smaller momentum of fluid in that protected region of the jet. Furthermore, the entrainment coefficient as usually defined is not constant for larger crossflow velocities, as is generally assumed. Recognizing these difficulties in the many present methods of defining entrainment, the methods of approach indicated in the models reviewed will now be summarized.

Entrainment of lateral crossflow momentum is considered in these models to result in a force per unit length on the jet in the direction of the crossflow given by

$$F_e = \rho V q_e,$$

where V is the crossflow velocity and q_e is the total entrainment per unit length of jet.

Motz and Benedict handle entrainment by defining an inflow velocity

$$v_i = E(U - U_a \cos \beta),$$

where

U = jet centerline velocity at centerline position s,

$U_a \cos \beta$ = the parallel component of the ambient velocity U_a, at s,

β = the angle between the jet centerline and the ambient current at s,

and

E = the entrainment coefficient (assumed constant).

This entrainment velocity is assumed to be the same on both sides of the jet. Note that v_i is proportional to the jet velocity relative to the lake. Relative velocity is used since the shear stresses causing the jet to incorporate ambient fluid depend on the change or increment in velocity.

Hoopes et al. assume entrainment is related only to the jet velocity,

$$dQ = 2(u_e z\, ds) = \alpha v_{sm}(2z\, ds),$$

where

dQ = rate of lateral entrainment,

$u_e = \alpha v_{sm}$,

u_e = local entrainment velocity,

v_{sm} = centerline velocity,

α = lateral-entrainment coefficient,

ds = element of length along the jet centerline,

and

z_0 = depth of plume.

Hoopes et al. also define a vertical-entrainment coefficient, but discover its effect to be negligible in comparison with Lake Monona field data.

Carter treats the force downcurrent induced by the entrainment of crossflow momentum as the rate of change of

$$\rho_a u_a f[q(\xi)b(\xi)D],$$

where

ρ_a = density of the ambient water,

u_a = ambient velocity,

$q(\xi)b(\xi)D$ = volumetric discharge through a plume cross section at longitudinal centerline distance ξ,

and

f = fraction of a cross-sectional control volume that is ambient fluid.

Carter then measures the centerline temperature decay (entrainment curve) from which he determines f. The above entrainment term is presently undergoing revision by Carter. Carter does not permit vertical entrainment by having a fixed horizontal bottom in his physical problem to which the plume is attached.

Stolzenbach and Harleman use nonbuoyant jet theory to yield lateral-entrainment coefficients for their deflected buoyant-jet model. Solving the set of mass- and momentum-conservation equations for a nonbuoyant jet (turbulent shear-flow equations) with the well-known experimental relationships for the lateral and vertical spreads of nonbuoyant jets yielded lateral- and vertical-entrainment coefficients. The values are constants, yet the constants change in each of two regions of the jet. These coefficients are defined from

$$v_e = \alpha_y(x)u_c(x)$$

and

$$w_e = \alpha_z(x)u_c(x),$$

where

v_e, w_e = lateral and vertical velocities of the entrained flow at the jet boundary,

u_c = surface centerline velocity,

x = longitudinal distance,

and

α_y, α_z = lateral- and vertical-entrainment coefficients in nonbuoyant jets.

The lateral coefficient is maintained in the cases of buoyancy and crossflow; the vertical coefficient is altered in the case of buoyancy and is based upon the local Richardson number so that it will simulate to some degree the self-induced stratification (or buoyancy) of the jet discharge. The vertical-entrainment coefficient (variable) was derived to be

$$\alpha_{sz}(x) = \alpha_z(x) \exp\left[-5.0 \frac{agh(x)\Delta T(x)}{\rho_a u_c^2(x)}\right]$$

where

x = longitudinal distance downcurrent,

a = coefficient of thermal expansion,

g = acceleration of gravity,

h = vertical height of the turbulent region of the jet,

ΔT = excess temperature,

ρ_a = density of ambient water,

and

u_c = centerline velocity.

These entrainment coefficients are assumed to be the same for crossflow deflection of a buoyant jet.

Pritchard includes lateral entrainment by defining an "inverse-spreading rate" $n = 6$, by which the jet width grows at a rate of one on six. Vertical entrainment is assumed to be linear also from the initial jet depth to the "critical mixing depth" of the body of water under consideration. If the initial depth of the jet is equal to or larger than the critical depth, no vertical entrainment is assumed to occur. Pritchard does not consider ambient crosscurrents in his model, yet he expects that the predicted centerline temperature decay and areas within isotherms are still accurate in the presence of a shore-parallel current less than 10% of the initial discharge velocity.

Sundaram et al. assume no vertical entrainment. Horizontal dispersion of momentum is defined using Prandtl's second mixing-length hypothesis

$$\tau = \rho K_{m_{jet}} \frac{\partial u}{\partial y},$$

where

τ = turbulent shear stress,

ρ = jet fluid density,

$K_{m_{jet}}$ = eddy diffusivity of momentum,

and

u = velocity in longitudinal direction x.

$K_{m_{jet}}$ is determined from

$$K_{m_{jet}} = 0.037 b_{1/2} U,$$

where

U = centerline velocity

and

$b_{1/2}$ = jet half-width at half-depth.

The coefficient 0.037 was determined experimentally from the work of Reichardt. Temperature dispersion was defined from similarity considerations to be

$$\frac{u}{u_{max}} = \frac{T}{T_{max}},$$

where T refers to temperature and the subscript max represents the centerline value. Sundaram et al. uses this two-dimensional slot jet analysis for a jet in a stagnant medium to determine dispersion laterally from a centerline bent due to ambient current effects. The centerline is evaluated from semiempirical relations often used to predict the dispersion of chimney-stack effluents into the atmosphere.

Entrainment is implicitly handled by Tsai in the zero-current and crosscurrent cases by physical modeling within the first 300 ft of the diffuser. In the no-current case he uses an empirical jet model in the region beyond 300 ft. The crosscurrent case for distances greater than 300 ft from the diffuser will be discussed in the far field section (Sec. B) of this summary chapter.

4. Discharge Configuration and Discharge Angle

Each model considers a shoreline surface-canal discharge, except for Tsai who modeled a submerged diffuser system. Hoopes et al., Motz and Benedict, and Stolzenbach and Harleman can handle an arbitrary angle of discharge with respect to shore. Carter, Sundaram et al., and Pritchard treat only a strictly normal discharge (90° to the shore). Tsai, again as a special case, is working with a submerged diffuser design in which the jets are discharged at 90° with respect to the ambient current.

5. Bottom Effects

A bottom slope is generally known to inhibit vertical entrainment and increase buoyant lateral spreading. The only jet model that attempts to simulate the effects of a bottom slope directly in the analysis is that of Stolzenbach and Harleman. They assume that as long as the jet hugged the bottom, all buoyant terms would have no effect on the jet. The vertical entrainment would then be zero, and the bottom boundary of the jet would be confined by the lake-bottom geometry. This required the dropping of one of the governing equations, which the authors chose to be the y-momentum equation mainly due to the difficulty in determining the bottom-wall pressures in that relationship. Adjusting the set of equations they derived for the no-bottom-slope case in the above manner, this new set was then applied in the preseparation region as long as the jet hugged the bottom. The original set (no-bottom-slope equation) was used after the jet separated from the bottom.

Comparisons of their model with hydraulic data revealed an order-of-magnitude discrepancy between theoretical and experimental results in the prediction of lateral spreading. The hydraulic data were found to be much closer to the calculated curve for no slope than for the very small spread the theory predicts when a slope is present. Centerline temperature is also better predicted with a no-slope assumption than with the sloping-bottom analysis of the authors. Clearly, the difficulty resided in that the y-momentum equation should not have been dropped completely, in spite of the apparent impossibility to calculate the unknown bottom-wall pressure.

Carter has a flat bottom boundary in his theoretical model and plume studies and assumes complete two-dimensionality in his physical situation. Any initial region of vertical entrainment is not treated in Carter's analysis. Consequently, his measured dilution curves cannot be extrapolated directly to the situation of a deep receiving basin or the problem of an actual sloping bottom.

Hoopes et al. assume a constant-depth jet from the point of discharge in deriving their model for two Lake Monona outfalls. In their prototype, the average lake depth within 200 ft of the shore is 1 m or less which stimulates significant initial vertical mixing of the jet by bottom effects not considered in the model. Consequently, the existence of the bottom is considered only indirectly by fitting the model to the data in nine of their Lake Monona field surveys. In this way, their initial jet velocity and constant-entrainment coefficient are correlated with wind speed; these correlations are used to predict the jet characteristics in the rest of their 22 surveys. In this way, the vertical mixing induced by the bottom and, in fact, the lack of an inflow establishment region in their model can be considered indirectly. Still, using the specific correlations made in the model (designed specifically for the two Lake Monona outfalls) is a matter of some concern.

Pritchard considers the effect of a bottom only indirectly. He claims that the slope and contours of the lake bottom affect the "critical mixing depth" for that body of water. This depth varies with the lake under consideration and is best determined from previous field studies. Bottom contours also affect the possible recirculation of new ambient dilution water and determine whether a background temperature correction need be made in the model for the temperature distribution derived from its consideration. Finally, Pritchard assumes an approximately level bottom in his rough calculations of the longitudinal distance from the orifice at which vertical entrainment ceases. The calculation is quite crude and is made to estimate the influence and extent of vertical entrainment on dilution.

The models of Sundaram et al. and Motz and Benedict do not consider the influence of a bottom and essentially consider a discharge into an infinite-depth receiving basin. Tsai, in his hydraulic and mathematical modeling of the FitzPatrick Power Plant diffuser discharge, considers the bottom contours

of the Lake to have significance only within the region modeled hydraulically, i.e., within 300 ft of the diffuser in both the zero-current and crosscurrent cases. The bottom contours are physically modeled in their proper relative dimensions to the rest of the geometry. Beyond the 300-ft distance from the diffuser, the flow field is found to be well established and characterized as surface flow. Two-dimensionality is assumed, and no lake-bottom effects are considered.

6. Shoreline Considerations

Sundaram et al., Pritchard, Stolzenbach and Harleman, and Hoopes et al., consider a straight shoreline boundary with no far-bank effects. Carter with Motz and Benedict also develop their models on the basis of the existence of a straight shoreline; however, based upon hydraulic and field studies, they notice a change in jet characteristics depending upon the position of the far bank. Carter, for instance, notices a greater penetration of the jet into the ambient crosscurrent in addition to a near-shore return of the plume at greater downcurrent distance when a larger flume (i.e., greater far-bank distance) is used. Tsai's submerged diffuser model handles a special discharge situation in which no near- or far-shore boundaries are considered significant to be included in the analysis.

7. Pressure Drag

A net pressure force occurs across the jet and is caused by the separation and eddying of the ambient fluid in the near-shore side of the jet and by the distortion of the jet boundaries. The ambient flow is being retarded by the jet at its offshore edge, creating an increased pressure, while a rarefaction occurs at the rear side. The pressure difference creates the centripetal force necessary to deform the jet. Because of the inflow of fluid to the jet, the increase in pressure at its forward edge is somewhat less than it would be at the wall of a solid body of the same form as the curved jet. The main difficulty in modeling the pressure distribution across a jet in a crossflow is that no one to our knowledge has successfully been able to measure total pressure hydraulically (or in the field) to the precision required. (Static pressure, however, can be measured accurately.) The best direct pressure measurements available have come from gas jets of fairly high velocity. Measuring both static and total pressure for high-velocity air jets is fairly standard. Pressure has to be reflected in the elevation of the free surface. However, most often the elevations involve very small differences that cannot be measured with any precision in water, especially in the presence of surface waves.

Of the models considered, only Carter and Motz and Benedict consider pressure drag in the mathematical analysis. The now-classical way of including it is to consider the jet stream as an obstruction in a uniform stream. The rationale for this assumption might be seen from hydraulic

experiments in which some of the ambient current is accepted by the jet while the rest of the oncoming stream is deflected around the jet, much the same as fluid reflected by a solid body.

Carter, for instance, defines this force across the jet as

$$\text{drag force} = \frac{\rho_a C_d A u_a^2}{2}\, ds,$$

where

C_d = coefficient of drag,

A = cross-sectional area normal to the jet centerline,

u_a = velocity of the flow,

ρ_a = density of ambient current,

and

ds = element of arc length along the jet centerline.

This form for the pressure force is analogous to the measure of total drag of solid bodies in a uniform crossflow, usually used in fluid mechanics or hydraulics. The usual drag coefficient C_d measures the relative total resistance of solid bodies of the same cross-sectional area under the same flow conditions. Employed in the liquid-jet case, the above form for the drag is assumed to act pointwise where C_d is variable and defined locally. The precise value of C_d must be determined experimentally. Carter, for instance, evaluates C_d using Rouse's wind-tunnel pressure measurements along the near-shore wall by balancing the integral of the pressure distribution there to the initial offshore momentum. Since Rouse's wall-pressure distribution was approximately constant from the orifice to the wall position corresponding to the point of maximum penetration, Carter expected C_d to be approximately constant. This is a standard assumption. Evaluating C_d for a number of values of R in

$$R = u_0/u_a,$$

where

u_0 = initial jet velocity

and

u_a = ambient current velocity,

determines a curve from which interpolated values of C_d can be evaluated for different R.

Motz and Benedict define their pressure force from

$$\text{drag force} = \frac{\rho_a C_D U_a^2 z \sin \beta}{2} \, ds,$$

where

U_a = ambient velocity,

z = jet depth,

β = angle between the jet and ambient current,

ρ_a = ambient density,

and

ds = element of arc along the jet centerline.

The Motz formula differs from Carter's in that it uses the projected area normal to the flow in its basic definition adding the sin β term in the above expression. The force acts, like Carter's, normal to the jet centerline. The Motz choice is based on their argument that "pressure drag depends more on the form of the body and on separation at the rear of the body than on the conditions at the front of the body." Motz and Benedict determine their drag coefficient C_D from hydraulic experiments relating C_D solely to the ratio of the initial jet velocity to the ambient velocity.

To illustrate the diversity in definitions, Fan (see section on Motz and Benedict, Sec. III.A.3) uses the form

$$\text{pressure drag} = \frac{\rho_a C_D U_a^2 \sin^2 \beta k \sqrt{2}\, r}{2} \, ds$$

for the normal drag force on a submerged axisymmetric buoyant jet. The above form acts normal to the jet where r = radius of the axisymmetric jet (other symbols defined above). The term $U_a^2 \sin^2 \beta$ is the square of the ambient-velocity component normal to the projected area.

The above forms for the drag force are not equivalent. They actually are artificialities set up to attempt to account for the total pressure force across the jet. They represent only a crude approximation to the pressure force across the jet.

As stated above, the other models neglect pressure forces. (They appear in Tsai's hydraulic modeling in the vicinity of the diffuser.) Stolzenbach and Harleman do not consider pressure drag in their cross-flow model, stating that they feel it to be unimportant, at least for their assumed parabolic distribution (see section on Stolzenbach-Harleman model, Sec. III.A.4), as long as the peak velocity divided by the initial jet velocity is less than about 0.4 or 0.5.

It is apparent to us that part of the problem in mathematically modeling a heated jet in a crossflow is hiding in the entrainment difficulties and part is involved with pressure drag. It is seldom clear when a discrepancy between theoretical and experimental data may be due to an imprecise definition of entrainment or an imprecise relationship for pressure drag.

Carter has found in his flume experiments and from the wind-tunnel experiments of Rouse that a second pressure distribution is set up due to the presence of a not-too-distant far-shore boundary. This pressure distribution dissipates the initial offshore momentum and then remains to cause the jet trajectory to curve back toward the near shore until such time as the pressure gradient normal to the shore boundary is balanced by water piling up on the near shore. This effect seems to disappear as the far shore is placed further away. The precise effect of a not-too-distant far-shore boundary on the jet penetration and the bending-back phenomenon is presently being investigated by Carter and Benedict. No models as yet simulate these latter effects.

8. Wind Stress

The only model reviewed in this report that considers the direct effects of wind shear is the jet analysis of Hoopes et al. The authors used a classical relationship between wind speed and wind shear stress encompassing the effects of wind on solid bodies,

$$\tau_w = \rho_a C_D W^2,$$

where

τ_w = wind stress,

ρ_a = density of overlying air,

C_D = drag coefficient,

and

W = wind speed.

The justification for the use of such a formula in a water-plume case is quite meager, especially since the authors could find no way to accurately assess the magnitude of C_D. They chose three representations from the literature, which yielded high, medium, and low wind stresses at a given wind speed. Using these three different formulas for wind stress in their model, the authors assessed the relative effects a given wind speed would have on the jet. They showed from this crude analysis that their measured field data were in reasonable agreement with the theoretical model with no wind shear included. Consequently Hoopes et al. concluded that the effects on the jet characteristics for the near-shore region (for their Lake Monona application) are negligible.

The entire method of approach carried out by Hoopes et al. raises some doubts. As stated by Sundaram, wind-induced shear stresses act not only on the plume but also on the ambient lake waters and therefore should provide no incremental momentum flux to the plume as assumed by Hoopes et al. Hoopes et al., however, envisions the jet to be a layer approximately 1 m thick with wind shear acting on the plume only over this thickness. Outside the jet, wind effects would be felt over a larger depth either to the lake bottom or at least down to the thermocline. Hoopes et al. reason that since the lake bottom or thermocline is generally many times the jet thickness, it would be expected that the wind would cause smaller changes in the ambient lake than on the jet itself.

In reality, wind shear affects plume dispersion by the introduction of wind-induced currents and waves. The mechanism and the division of energy between these two phenomena is not yet understood. No methods are presently available that include these effects in a mathematical model. It is known, however, that these phenomena do occur in a different manner over the plume region and over the ambient lake water and really should be considered in dispersion analyses.

The complexity involved in modeling wind effects is considerable when one recognizes that the ambient-current structure will be generally nonuniform with depth. The top layers of the ambient receiving water typically travel at higher velocities and are strongly influenced by the wind and its variations. A sharp gradient in the current profile is often observed close to the surface. This makes plume dispersion essentially a three-dimensional problem where three-dimensional boundary conditions have to be supplied. Wind may also be a factor in the distribution of interfacial stress at the bottom of a stratified plume. This shear arises from the fact that momentum transfer (affected to some degree by wind) is not inhibited to the same extent as heat transfer. Most models ignore this interfacial friction.

9. Zone of Flow Establishment

The zone of flow establishment refers to the mixing region in the vicinity of the orifice in which turbulent mixing changes the uniform temperature and velocity profiles at the jet origin to fully developed turbulent profiles, which are bell-shaped at the beginning of the established-flow region.

Pritchard assumes a simple representation for this region where no change in the initially top-hat profiles for velocity and temperature occur for a distance of six orifice widths downstream. Only beyond that point does lateral spreading start. Pritchard also assumes top-hat profiles for velocity and temperature in the established-flow region for convenience, yet adjusts one of his later equations for the more accurate bell-shaped lateral

profiles that actually occur there. In this region, vertical spreading occurs in a linear fashion, provided the initial jet depth is less than the "critical mixing depth" of the body of water under consideration.

Stolzenbach and Harleman set up a specific structure in their model to account for a region of flow establishment. Each core cross section at any longitudinal distance x has a half-width s and a depth r. Temperature and velocity maintain their initial top-hat values as long as either r or s is positive. Unlike Pritchard, the authors incorporate lateral spreading right from the orifice in a turbulent region surrounding the potential core just described. Half the width of that turbulent region of the jet is denoted b with its vertical height (located below the potential core) h. Both b and h are functions of x and, like r and s, are monotone-decreasing functions of x and all become zero as the advancing turbulent regions reach the jet centerline. These variables are illustrated in Fig. 4.3 for a nonbuoyant jet (in the chapter on the Stolzenbach-Harleman model). The solution for the variables r, s, b, and h as functions of x is derived from the equations of mass, momentum, and heat conservation as handled by the Stolzenbach-Harleman integral approach.

Carter assumes a zone of flow establishment as defined by the spread of heat as extending in the longitudinal direction $2\frac{1}{2}$ times the initial width for situations in which the ratio of the initial velocity to the ambient velocity is between 1 and 10. This result was based on Carter's hydraulic experiments for R values of approximately 1, 2, 5, and 10. The trajectory of the centerline in the flow-establishment region is circular in Carter's model with no lateral spreading about that centerline.

Actually, the length of the zone of flow establishment is not constant with R, as Carter assumes. Carter expects that more precise measurements would shorten the length of the region of flow establishment as R increases. His most recent (as yet unpublished) hydraulic experiments seem to bear out this statement.

Hoopes <u>et al</u>. do not consider a region of flow establishment. Similarity forms for velocity and temperature are assumed right from the outfall. The authors expect that their wind-speed correlations for the entrainment constant α and the initial jet velocity v_0 do in some indirect way account for the neglect of flow establishment.

Motz and Benedict account for the zone of flow establishment by developing phenomenological relationships for the length, s_e', of the region of flow establishment and the angle, β_0, between the jet and ambient current at the end of that zone. In the laboratory, experiments were carried out in which the ratio of the ambient velocity to initial jet velocity, A, was varied from 0.18 to 0.727 while the initial discharge angle, β_0', was fixed at one of three angles: 90, 60, and 45°. Straight-line curves (on log-log paper) were

fitted to the data for s_e'/b_0 and β_0/β_0' versus A, where b_0 is the width of the jet at the position where the jet becomes fully developed. The width b_0 is calculated by equating the heat fluxes at the immediate jet discharge and at the point s_e'. The zones of momentum and heat development were assumed to be identical and determined from the values of the parameters s_e', β_0, and b_0. No description of the precise form of the temperature (and velocity) profiles was given or deemed necessary for the development of the model in the established-flow regime.

Sundaram et al. use classical two-dimensional slot-jet analysis (for a stagnant receiving body) in deriving the lateral dispersion of heat and momentum about a deflected centerline resulting from a crosscurrent. Similarity assumptions defining the flow to be fully developed are made right from the orifice. Hence no flow-establishment zone is considered.

Tsai's hydraulic modeling experiments obviously include flow-establishment considerations in the scaling of each jet in the diffuser. This is true for the zero-current and crosscurrent cases.

10. Surface Heat Transfer

Carter, Tsai, and Sundaram et al. considered heat loss to the atmosphere to be unimportant in the jet regime and hence neglected it in their analyses. Hoopes et al., with Motz and Benedict, included surface heat transfer in their models, calculating it (i.e., surface loss above ambient) as a constant multiple of the excess temperature above ambient.

Stolzenbach and Harleman use absolute temperatures in their model from which surface heat transfer to the atmosphere is modeled as a constant multiple of the excess of the plume temperature above the equilibrium temperature. They then assume that the equilibrium temperature can be adequately approximated by the ambient receiving-water temperature.

The two-dimensional models of Hoopes et al. and Motz and Benedict include surface heat loss as a term in the differential equation; the three-dimensional analysis undertaken by Stolzenbach and Harleman includes surface heat loss as a boundary condition. Pritchard, however, includes surface heat losses only as a correction to the temperature distribution calculated without its consideration. He basically uses simple intuitive arguments in which the rate of excess heat loss to the atmosphere is considered as a decrease in the initial source strength of the heated effluent.

11. Ambient Stratification

None of the jet models considered accounts for possible ambient lake stratification. The relative effects of stratification are seasonally variable and depend on the stability of the existing lake-temperature structure.

For a large lake in a temperate zone, temperature gradients can develop during certain portions of the year which can oppose the downward spreading of jet- or wind-induced turbulence. This is a boon to the two-dimensional models, since the region above the thermocline may be approximated as fully mixed (vertically uniform). Sundaram et al., for instance, assume their initial discharge to be "supercritical" right from the outfall, the stratification being assumed to be so intense that there is no vertical mixing. The neglect of vertical spreading and the assumption of a fully mixed plume layer form the basis for the two-dimensionality plume assumption.

The ambient stratified lake situation yields a negative effect for a three-dimensional model. The Stolzenbach-Harleman model accounts only for self-induced jet turbulence and assumes the receiving body to be at an initially uniform temperature.

When no lake stratification exists, such as in winter in temperate zones, the lake is at approximately a uniform temperature. This situation benefits the three-dimensional Stolzenbach-Harleman model; yet the additional vertical entrainment expected is not allowed for in the two-dimensional models.

Pritchard includes stratification only in that it combines, as he asserts, with a sloping bottom to maintain a certain stability which keeps the plume at its constant "critical mixing depth." Pritchard states that, in cases void of a great deal of stratification, his evidence shows that the vertical thickness of the jet varies a small amount.

12. Recirculation

Except for Pritchard, none of the investigators treat the possible recirculation of dilution water in his model development. The complexity of such an analysis is handled only crudely by Pritchard himself. He calculates a "background temperature" by estimating the excess temperature that would exist if the heated effluent were completely mixed into the available rate of supply of diluting water to the inshore area where the heated effluent is being discharged. Once this calculation is completed, Pritchard corrects his previously derived temperature distribution to account for the entrainment of water above 0.0°F excess temperature.

Carter noticed in his hydraulic setup that inshore entrainment was being seriously inhibited by the continual reincorporation of warmer plume water into the jet from the large, slowly circulating eddy on the near-shore side. He did not include this fact in his model per se, yet estimated the effect of a partial cutoff of inshore entrainment on the centerline temperature decay.

13. Field and Hydraulic Comparisons

To date, none of the jet models has been objectively compared to good quality field data, mainly due to nonexistence or unavailability of good data for the jet regime.

Hoopes et al. have taken 22 field surveys of two outfalls on Lake Monona. They used the data from nine of their best surveys in obtaining formulas for the rate of entrainment, the ambient lake velocity, and the initial jet velocity based upon the measured wind speed. This was done in each case by fitting their mathematical model to the data. They then used these wind-speed correlations to predict the jet characteristics for all 22 surveys. The authors considered this procedure necessary due to the at-best mediocre quality of the data and the desire to account, in some way, for the neglect of the region of flow establishment and the neglect of bottom effects within the vicinity of the outfall.

Sundaram et al. fit their model to data obtained at the Milliken Power Station on Lake Cayuga. They calculated the lateral eddy thermal diffusivity for six "typical" sets of environmental conditions. They then applied those results predictively to neighboring Bell Station on Lake Cayuga in plume situations when similar environmental conditions prevailed.

Stolzenbach and Harleman carried on 25 hydraulic experiments to compare the predictive results of their three-dimensional model with some data. Parameters varied were: initial Froude number, aspect ratio, surface heat loss, bottom slope, and ambient crosscurrent. Only jet centerline temperature, jet half-depth, and jet half-width were measured. The authors are presently accumulating field data with which to verify their model.

Motz and Benedict also carried on their own hydraulic modeling. However, they fit the data obtained (in addition to other accumulated field and hydraulic-modeling data) to determine curves for their drag and entrainment coefficients. Parameters that were varied were: initial discharge angle, initial Froude number, ratio of initial jet velocity to ambient velocity, and ratio of distance from far bank to initial discharge width. The field data used were from both river and lake situations. The authors are presently collecting more field data with which to better determine the drag and entrainment coefficients by model fitting.

Pritchard has developed a significant portion of his model using field and hydraulic data. This model has been compared to data taken at the Waukegan Power Plant on Lake Michigan. However, the field data were not of sufficiently good quality to verify the model. Pritchard's own hydraulic studies and field data compilations were not available to the writer.

Carter's preliminary report does contain some objective comparisons of theory and hydraulic measurements for the jet-centerline trajectory.

However, the comparisons need to be redone due to an algebraic error and are significant only for river-width to orifice-width ratios of about 12-60. Carter is presently carrying on additional experiments in a larger flume. Carter's measurements include only the centerline-temperature decay and the jet-centerline trajectory.

Tsai used hydraulic modeling within 300 ft of his specially designed submerged diffuser structure for the FitzPatrick Power Plant on Lake Erie. This was a direct part of his model development. No field or hydraulic data have been obtained to verify the analytical portion of his predicted results. The model is unique to the power plant that is now presently under construction.

14. Computer Programs

Computer programs have been written and are available for the models of Hoopes et al. (IBM 1610), Stolzenbach and Harleman (IBM 360), and Motz and Benedict (the computer system used is presently unknown). No programs are available for the models of Sundaram et al., Carter, Pritchard, and Tsai.

15. Input Parameters for Jet Models

a. Hoopes, Zeller, and Rohlich

b_0	outfall width
K	coefficient of surface heat transfer
Q_{0a}	actual outfall discharge (power-plant pumping rate)
T_L	ambient lake temperature
T_0	outfall temperature
v_L	ambient lake velocity (through wind-speed correlation)
v_0	initial jet velocity (through wind-speed correlation)
W	wind speed
z_0	jet thickness at the outfall
α	entrainment coefficient (through wind-speed correlation)

b. Carter

b_0	orifice width
C_d	drag coefficient
Q	initial volumetric flow rate
q_0	initial jet velocity

T_0	initial outfall discharge temperature
u_a	ambient velocity
θ_0	excess temperature across the condensers

c. Motz and Benedict

b_0'	orifice width
C_D	drag coefficient
E	entrainment coefficient
T_0	initial outfall discharge temperature
T_0'	initial excess temperature of jet
U_a	ambient velocity
U_0'	initial jet velocity
z	depth of jet
β_0	angle between jet and ambient current

d. Stolzenbach and Harleman

$2b_0$	width of discharge channel
h_0	depth of discharge channel
K	surface-heat-transfer coefficient
Q_0	volumetric flow rate at discharge
S_x	bottom slope
T_a	uniform lake water temperature
T_0	initial discharge temperature
V	distribution of ambient crossflow velocity with distance offshore

B. Far-field Regime

1. Method of Approach

The philosophy behind the development of far-field models is based on the fact that the plume is drifting along with the prevailing currents, nearly as if it were a part of the ambient velocity field. The three mechanisms that dilute, disperse, and dissipate the excess heat are, first, the turbulent transport or eddy mixing, second, the density difference between the plume temperature field and the ambient, and third, surface heat transfer between the plume and the overlying air. Turbulent mixing and surface heat transfer always exist; dispersion by the action of gravity due to any density disparity may not be significant, depending on the relative density excess.

Significant density gradients, due generally to a large initial excess temperature, require the flow-energy interaction to be treated. If, however, density gradients are small and the plume is essentially drifting with the ambient current, the energy equation may be uncoupled from the hydrodynamic equations with a measured or assumed flow distribution inputted into the heat (convective/diffusion) equation. These two cases provide a dichotomy from which each far-field model can be classified. Wada's Models No. 2 and 3 do not consider the plume to be simply floating with the prevailing current. Model No. 2 solves the coupled flow equations in two dimensions and uses the resultant velocity field to yield the two-dimensional temperature distribution from the energy equation. Model No. 3 considers the actual flow-energy interaction by solving the coupled hydrodynamic and heat equations with spatial variation only longitudinally and vertically. The other investigators--Kolesar, Csanady, Edinger and Polk, Wnek, Sundaram et al., Pritchard, and Tsai (also Wada in his first model)--neglect density differences and their effect on the flow and assume that the plume is dispersing solely by ambient-current advection, turbulent diffusion, and surface heat loss. Their models are based solely on solving the convective-diffusion equation.

The far-field models considered are also divided in their mathematical approach: closed form or numerical. Wada's Models No. 2 and 3 with the Kolesar-Sonnichsen treatment are numerical; the rest yield closed-form solutions.

Two types of input must be handled in the general far-field model: first, a specification of the velocity field and, second, the specification of an expression for the eddy-transport coefficients. Each of these input data categories will be summarized in Sec. 14 below. Suffice it to say that the velocity field of the plume is generally considered to be the ambient flow field, whereas the functional form for the eddy-transport coefficients is not generally known, requiring assumptions to be made based upon semi-empirical results obtained in the literature for each individual case. The only exception to the requirement of this set of input data is in Wada's Models No. 2 and 3. Model No. 2 solves for the flow field from the hydrodynamic equations, and that resultant velocity field is used as input for a numerical solution to the heat equation. Model No. 3 solves the coupled flow and energy equations.

2. Dimensionality

The strictly two-dimensional far-field models are those of Edinger and Polk, Csanady, Sundaram et al., Tsai, and Wada (Models No. 2 and 3). Variations laterally and longitudinally are analyzed in each model, except for Wada's Model No. 3, in which no variations are assumed laterally, but longitudinal and vertical changes are considered to be significant.

The models of Pritchard and Kolesar-Sonnichsen are pseudo-two-dimensional. Pritchard allows for vertical entrainment, which in certain cases can conceivably reach beyond the boundary between his near- and far-field regions. Kolesar and Sonnichsen permit a variable depth in their two-dimensional model; they assume no vertical variation in velocity or temperature with depth.

The three-dimensional far-field models are those of Wnek, Edinger and Polk, and Wada (Model No. 1). Wnek and Wada (all models) start their analysis from the discharge, yet realize their results apply only for distances sufficiently far from the outfall that ambient turbulence will predominate.

3. Diffusivities and Buoyancy

The eddy-diffusion coefficients are fundamental to the solution of the momentum- and heat-conservation equation. Unfortunately, there is presently no general agreement as to the functional form of those coefficients for large lakes.

For homogeneous isotropic turbulence the eddy thermal diffusivities are constant. However, three main factors tend to prevent this from occurring:

a. Density stratification tends to inhibit vertical mixing, so that lateral dispersion greatly dominates vertical dispersion.

b. Wind stresses cause lake turbulence, which decreases in intensity with increasing depth.

c. Larger and larger scales of turbulence take part in the diffusion process as the plume grows in size, increasing the rate of dispersion. Moreover, the lake surface as well as any solid boundaries such as a lake bottom or a shoreline, tend to limit the size of the eddies that cause the dispersion.

These factors complicate any attempt to define a functional form for these coefficients.

Open-sea measurements seem to yield a consensus that the lateral eddy-diffusion coefficient follows the four-thirds-power law; i.e., diffusion is proportional to $L^{4/3}$, where L is the scale size. (L is generally taken as the plume width.) However, in regions off a shoreline in the range of bottom effects, the very large scales of turbulence that exist would be limited by the boundaries. The dye studies of Orlob reveal that lateral dispersion does not grow according to the four-thirds-power law as long as the plume is smaller than the largest eddies. Beyond a small transition zone, the eddy-diffusion coefficient is constant once the plume grows larger

than the largest eddies. For shallow shoreline waters not too far from the outfall, the plume will grow to a size where the maximum possible sized eddies are affecting the diffusion. For such situations a constant-diffusivity model seems reasonable. Since each investigator solves for the temperature distribution using the heat-conservation equation, each defines a functional form for the eddy diffusivities that he feels is applicable for his physical situation.

The consideration of buoyancy (as defined in Appendix B) necessarily involves the inclusion of the interaction of density gradients with the flow field. Only Wada's Model No. 3 solves for flow and temperature simultaneously. Each model will now be summarized as to its treatment of buoyancy and eddy-transport coefficients.

a. Wada's Model No. 1

Wada solves the three-dimensional convective-diffusion equation with constant eddy-thermal diffusivities in the longitudinal, lateral, and vertical directions. No flow-energy interaction is considered.

b. Wada's Model No. 2

Wada solves the coupled horizontal-momentum equations neglecting the inertial terms. The author assumes that ambient turbulence predominates over momentum interactions to permit this simplification. The resulting two-dimensional velocity field is then used as input into the convective-diffusion equation to yield temperature. Again, Wada assumes constant longitudinal and lateral eddy-thermal diffusivities. No buoyant interactions are considered.

c. Wada's Model No. 3

This is the only model that strictly includes buoyancy. The method of inclusion is primarily by the coupling of the flow and heat equations through the ρg term in the vertical-momentum equation.

The density ρ is assumed to vary linearly with temperature. This variation of density with temperature provides the coupling mechanism in this model. Also, in Model No. 3, Wada used the Mamayev form for the vertical eddy coefficients of momentum and heat energy A_z and K_z,

$$A_z = A_1 + A_0 \exp(-mR_i)$$

and

$$K_z = K_1 + K_0 \exp(-nR_i),$$

where A_1, A_0, K_1, K_0, m, and n are empirical coefficients and R_i is the local Richardson number. Wada chooses A_1, A_0, K_1, K_0, m, and n to be constant

in space for the jet application of his model. (This simplifying assumption really implies however, that ambient turbulence controls the diffusion process from the orifice.) These eddy coefficients relate heat and momentum diffusion in the vertical direction to the velocity shear and the plume's self-induced vertical density gradient. They represent the influence of stability due to buoyancy on the vertical mixing process caused by turbulence. The above general forms are semiempirical and represent as good a first approximation to these coefficients for the sea as may be found in the literature. Wada states that these coefficients were obtained under a considerable amount of empiricism and cannot be expected to be valid for all physical frameworks.

d. Edinger and Polk Two-dimensional Model

Buoyancy is not considered in this model. A single lateral eddy-thermal coefficient is chosen to represent turbulent diffusion. A constant value is assumed and is required as input to the model.

e. Edinger and Polk Three-dimensional Model

Here buoyancy is again neglected and constant values of lateral and vertical eddy-thermal diffusivities are assumed. The choice of a constant vertical value implies that the plume's own self-induced stratification is not being modeled.

f. Csanady Offshore Outfall Model

Buoyancy is neglected, and a constant lateral diffusivity is assumed.

g. Csanady Shoreline Surface-discharge Model

Buoyancy is ignored in this model, yet the form for plume dispersion is patterned after methods often used for atmospheric dispersion. Csanady does not use a constant-diffusivity model here, since it is his observation that eddies generated by the shore boundary are more efficient mixers than those 2-3 miles offshore. As an approximation, Csanady uses

$$S_y = px,$$

where S_y is the standard derivation at longitudinal position x of a plume arising from a point source located near shore. Csanady derives his temperature distribution by arranging point-source plumes, each with a Gaussian format at all points of his line source (and allowing for shoreline reflection). This model of plume dispersion yields a faster-growing plume than from a constant-diffusivity model.

h. Kolesar and Sonnichsen

No buoyancy is included since only the convective-diffusion equation is considered. Lateral and longitudinal eddy-thermal coefficients are assumed constant.

i. Wnek

No buoyancy is considered; longitudinal, lateral, and vertical eddy-thermal diffusivities are assumed and are chosen as constant. The constant vertical coefficient does not consider the plume's own self-induced stratification.

j. Pritchard

Pritchard's pseudo two-dimensional model neglects buoyancy and uses a linear rate of spread of the plume width as one on six. This latter assumption sidesteps the need for specifying diffusivities.

k. Sundaram *et al*.

The authors in their two-dimensional model neglect buoyancy, but consider a lateral diffusivity to vary according to the "Richardson four-thirds-power law" in which

$$K_H = k_H b^{4/3},$$

where

K_H = eddy diffusivity of heat,

k_H = constant of proportionality,

and

b = plume width.

The constant k_H depends upon the prevalent environmental conditions and must be determined empirically. The justification for this formulation of diffusivity rests basically on studies in the open sea.

l. Tsai

Tsai also neglects buoyancy and, like Sundaram *et al*., uses the "Richardson four-thirds-power law" to handle lateral diffusivity. The proportionality constant was chosen as an average value $k_H = 0.01\ ft^{2/3}/sec$.

4. Surface Heat Loss

Tsai neglects surface heat loss in the far field based upon his estimates of its effect upon the isotherms. Edinger and Polk neglect surface

heat loss in their three-dimensional model, due primarily to the difficulty in obtaining an analytical solution with surface transfer included.

Wnek formulates his problem with respect to absolute temperatures where surface heat loss is equal to a constant times the difference between the local surface temperature and the equilibrium temperature. Edinger and Polk (two-dimensional case), Csanady, Pritchard, and Sundaram et al. consider excess temperatures above ambient from which the surface heat loss (above that lost by the ambient lake) is calculated. Kolesar and Sonnichsen with Wada also use absolute temperatures, yet treat the total surface heat loss to the atmosphere through an energy balance of incoming and outgoing heat flux.

The "excess temperature above ambient" method is the simplest to use and requires only the wind speed, excess temperature, and the natural temperature of the receiving body as input data. The "equilibrium-temperature" method, as well as the "energy-balance" method, requires information on such receiving-body temperature-independent phenomena as solar radiation, atmospheric radiation, and reflected solar and atmospheric radiation as well as the back radiation, conduction/convection losses, and evaporative transfers required by the "ambient-temperature" method.

Each model that considers heat loss does so in the differential equation if the model is two-dimensional and as a boundary condition if a three-dimensional analysis is given. Pritchard, however, includes surface heat losses only as a correction to the temperature distribution calculated without its consideration. He does it based mainly upon intuitive arguments whereby the rate of excess heat loss to the atmosphere is considered as a decrease in the initial source strength of the heated effluent.

5. Presence of Ambient Currents

Four of the investigations--namely those done by Edinger and Polk, Csanady, Sundaram et al., and Wada (Model No. 1)--assume a uniform shore-parallel current to be advecting the plume. The temperature distribution used by Tsai in his crosscurrent case was also derived using a uniform shore-parallel crosscurrent, yet it was applied about a deflected centerline evaluated from Shandorov's empirical relationship for jets. Tsai's far-field analysis was applied for distances beyond 300 ft of the diffuser.

Wnek's model allows for a constant three-dimensional velocity distribution to be transporting the plume. Kolesar and Sonnichsen require a horizontal (two-dimensional) velocity distribution as input for their model.

Wada's Models No. 2 and 3 solve for the velocity distribution. Model No. 2 uses the coupled hydrodynamic equations in the lateral and longitudinal

directions. Although not expressly stated, it is believed that Model No. 2 can handle not only a stagnant-lake situation in which the dynamic behavior of the cooling water yields a coupling of the hydrodynamic equations, but also the case of a discharge into an ambient lake current. The details are not discussed in Wada's papers. Model No. 3 solves for the velocity and temperature distribution using the coupled hydrodynamic and energy equations, but allowing for variation in longitudinal and vertical directions only. Model No. 2 neglects the inertial terms in the flow equations; Model No. 3 includes all terms.

Pritchard assumes no ambient current, yet considers his centerline temperature decay and isotherm areas to be a fair approximation as long as the ambient current is less than 10% of the initial jet velocity.

6. Bottom Effects

All investigators consider there to be basically an infinite-depth receiving basin in the far field, except for Wada, Kolesar, and Pritchard.

Wada considers depth in Models No. 1 and 3. Model No. 1 envisions an infinitely wide and long receiving basin with a finite depth. The bottom is assumed to have the constant temperature of the lowest layers of the receiving body. Model No. 3 also assumes a flat bottom with the same temperature boundary condition. The bottom and its boundary condition are handled numerically.

Kolesar and Sonnichsen allow for a variable bottom in which bottom contours cause a relocation of the thermal plume due to the resulting transverse flow. The resulting change in the cross-sectional area at each longitudinal position yields a variation in the thermal-energy flux. Variation in depth is incorporated into the heat-energy equation by deriving a new heat balance. Solution is by numerical means.

Bottom effects are considered in Pritchard's far-field development only as they prevent new dilution water from being available for plume entrainment (see Sec. 11 below on Recirculation).

7. Discharge Configuration and Angle of Discharge

The models that consider the initial effluent to be discharged from a channel are those of Wada, Sundaram *et al.*, and Pritchard. The width and height of the discharge are required parameters. Of these models, only Wada's Model No. 2 can handle an arbitrary angle of discharge from the shore. The others assume a strictly 90° initial angle of discharge.

Csanady's Offshore Outfall Model uses a line source to simulate the plume configuration after it has attained a moderately large size and is

drifting at the surface with the prevailing current. Csanady's Shoreline Surface-discharge Model also uses a line source to simulate the beginning of the far-field spreading as a warm-water effluent is discharged at the shoreline into a uniform transverse current. The length of the line source is determined from a heat balance between the actual outlet and the line source. Csanady recommends the use of a rough empirical relationship that he has observed in his fieldwork to yield dilution factors from outfall to virtual source.

Edinger and Polk do not consider the actual geometry of the outfall situation since they simulate the orifice structure with a point source. In their formulation, the initial temperature excess and initial discharge rate are used, however, to evaluate unknown constants.

Wnek can handle an arbitrary discharge configuration in his source term $S(x, y, z, t)$. More complicated simulations than a point or line source can lead to integration difficulties in his closed-form solution. However, his far-field solution is independent of the initial angle of discharge as it is with the models of Edinger and Polk.

Kolesar and Sonnichsen treat the dispersion of a heated effluent between two arbitrary far-field cross sections. The precise nature of the initial discharge and outfall configuration is irrelevant, once the initial temperature and velocity data are given at the two chosen cross sections.

The angle of discharge is irrelevant to the models of Wnek, Edinger and Polk, Csanady, and Kolesar and Sonnichsen.

The Tsai model is a special case in that it was developed for a specific submerged diffuser design. The diffuser jets were placed normal to the transverse current. The flow within 300 ft was modeled hydraulically. A line source was placed at the 300-ft mark from which a deflected centerline was calculated from the Shandorov empirical formula for nonbuoyant deflected jets. The Brooks analysis for the temperature field resulting from a line source in a uniform environment was used to yield the temperature distribution about that centerline. The temperature and velocity distribution measured at 300 ft from the zero-current case was used to give the input parameters for this analysis as well as the ambient crosscurrent velocity.

8. Shoreline Considerations

The models of Wnek, Sundaram *et al.*, Pritchard, Edinger and Polk, and Wada (Model No. 1) assume a straight shoreline with a discharge offshore into an infinitely wide and deep receiving basin. Wada's Model No. 2 can treat an irregular shoreline by numerical means. The integration carried out in Wada's Model No. 3 was done in a vertical section through

the outlet revealing no details of the adjoining shoreline. Csanady's Shoreline Surface-discharge Model assumes a straight shoreline with the plume attached to it as its centerline. Csanady's Offshore Outfall Model predicts dispersion by a uniform current without the presence of any near- or far-shore boundaries. The Kolesar-Sonnichsen code is written for a plume in the environs of a shoreline; however, an option within the code permits a completely offshore plume to be modeled.

9. Wind Stress

Each investigator has assumed wind interaction with the plume to be small and hence negligible. Wind induces relative motions and/or additional mixing between the plume and ambient water. Moreover, vertical dispersion will be influenced by wind effects which will be reflected in the vertical eddy diffusivities of momentum and heat. The comments made in the discussion of wind stress for the near-field models (see Sec. A.8 above) also applies here.

10. Ambient Lake Stratification

Only Wnek and Wada can handle lake-stratified situations. Wnek does it in his initial condition whereby the lake can have an arbitrary temperature distribution initially. Wada's Model No. 1 considers a vertically stratified lake situation as a boundary condition "infinitely far" from the actual outlet.

Ambient lake stratification may well be important at certain portions of the year in inhibiting vertical turbulence and dispersion. A stratified receiving body will require more complicated assumptions for heat transfer and buoyant spreading.

11. Recirculation

No models account for possible recirculation of dilution water except that of Pritchard. Due to the complexity of the analysis, Pritchard can only estimate the temperature excess above ambient of new entraining water into the plume from evidence as to the natural volumetric flow rate into the basin containing the heated discharge and the rate of heat rejection of the power plant. This new background temperature excess (above 0.0°F) is assumed to be constant and is used to develop a set of corrections to the derived temperature distribution.

12. Previous Comparisons with Field and Hydraulic Data

The models of Wnek, Csanady, and Tsai have not been compared with either field or hydraulic data. The Edinger-Polk models have been curve-fitted to some experimental data. These comparisons were made

with temperature fields resulting from selected power-plant discharges into rivers and discharges into open coastal waters. The Kolesar-Sonnichsen code has only been fitted to river data recently obtained by the U.S. Geological Survey. The Sundaram et al. model has been fitted by data taken at Milliken Power Station on Lake Cayuga and the fitted parameters used to predict the temperature distribution from the nearby Bell Station. To date, the model has yet to be used as a predictive device and simultaneously compared with actual field data taken from the site of interest.

Pritchard's model has often been used to predict the temperature distribution and isotherm areas for proposed power-plant sites. However, the model has not been compared with field data of sufficient quality to verify the model.

Except for Wada's Model No. 1, it is presently unknown whether his two other models have been compared with field data. His papers mention no comparisons.

The only hydraulic modeling connected with these far-field models was done by Pritchard at the Chesapeake Bay Institute to verify his centerline temperature-drop formula (temperature inverse with centerline distance) and to aid him in developing empirical formulas for the areas within isotherms under conditions of no surface heat transfer. The details of these hydraulic studies and any comparisons between general hydraulic measurements made at the Chesapeake Bay Institute were unavailable to us.

13. Computer Programs

No computer programs are available from the following authors for the application of their models: Wnek (presently being written), Edinger and Polk, Csanady, Sundaram et al., Tsai, and Pritchard. Kolesar and Sonnichsen have a program available for their code on the UNIVAC 1108. Wada's papers do not mention computer programs available for any of his three diffusion models. However, Wada does state that the numerical equations derived in Models No. 1 and 2 were solved on the IBM System 7090 while the work on Model No. 3 was carried out on the IBM System 360.

14. Input Parameters for Far-field Models

a. Wada

(1) Model No. 1

$2B$	breadth of the outlet
H	height of the outlet
H_w	depth of the plume, or the depth to the thermocline

T_b	constant bottom-water temperature
T_0	initial temperature of the discharge water
K_x, K_y, K_z	longitudinal, lateral, and vertical eddy-diffusion coefficients
U	ambient velocity (shore-parallel)
U_0	initial offshore discharge velocity
z_b	depth to lake bottom

Stratified ambient temperature distribution "infinitely far" from the outlet

(2) Model No. 2

A_x, A_y	constant eddy-momentum diffusivities (in the longitudinal and lateral directions)
$2B$	breadth of the outlet
H	height of the outlet
K_x, K_y	constant eddy-thermal diffusivities (in the longitudinal and lateral directions)
T_0	initial temperature of the discharge water
U_0, V_0	initial offshore and shore-parallel discharge velocity

(3) Model No. 3

A_0, A_1, m	empirical coefficients in the Mamayev form for the vertical eddy-momentum diffusivity
K_0, K_1, n	empirical coefficients in the Mamayev form for the vertical eddy-thermal diffusivity
$2B$	breadth of the outlet
H	height of the outlet
T_b	water temperature in the bottom layer
T_0	initial temperature of the discharge water
U_0	initial discharge velocity directed offshore

In addition to the above, the following parameters are required for each of Wada's models to evaluate Q_0, the net rate of surface heat transfer to the atmosphere:

Q_s'	radiation energy from sun and sky
$\bar{r}$	average reflectance over the integration period
$e(T_a)$	the saturation vapor pressure at the receiving-body surface
K	coefficient depending on the cloud height
n	cloudiness on the scale 1-10
T_a	atmospheric temperature
V	wind speed
k	mass-transfer coefficient
Q_i	intake discharge of cooling water
A	surface area of the bay (or ambient body region influenced)
r	mixing ratio from the upper layer
T_c	rise of water temperature added by condenser of power plant
T_b	water temperature in the bottom layer

b. Edinger and Polk

(1) Two-dimensional Model

d	depth of plume
D_y	lateral thermal diffusivity (constant)
K	coefficient of surface heat transfer
T_0	initial absolute temperature of discharge
u	ambient current velocity
Q_p	volumetric discharge rate
θ_p	initial excess temperature

(2) Three-dimensional Model

D_y	lateral thermal diffusivity (constant)
D_z	vertical thermal diffusivity (constant)

K	coefficient of surface heat transfer
Q_p	volumetric discharge rate
s_p	initial excess temperature
T_0	initial absolute temperature of discharge
u	ambient current velocity

c. Csanady

(1) Offshore Outfall Model

U	ambient crossflow velocity
K	coefficient of surface heat loss
K_y	lateral coefficient of eddy-thermal diffusivity
T_0	temperature of the initial discharge (i.e., at the line source)
h	depth of the plume
b	width of the initial line source
θ_0	initial excess temperature at the line source

(2) Shoreline Surface-discharge Model

p	relative intensity of horizontal lake turbulence
V_e	initial discharge velocity
A_e	cross-sectional area of the outfall
U	ambient current velocity
h	depth of the plume
K	coefficient of surface heat loss
T_0	temperature of the initial discharge (i.e., at the outfall)
$\overline{\theta}_0$	initial excess temperature at discharge

d. Kolesar and Sonnichsen

α_x, α_y horizontal eddy thermal diffusivities

Initial temperature distribution at source and exit cross sections in the far-field (to be translated into nodal temperatures)

Time-dependent inlet temperature distribution (to be translated into nodal temperatures)

Time-independent, two-dimensional velocity distribution at source and at exit cross sections (to be translated into nodal temperatures)

Bottom profiles (to be translated into nodal depth positions)

To evaluate the net rate of surface heat transfer to the atmosphere, the following additional parameters are required:

Q_s	short-wave radiation
Q_r	reflected radiation from the water surface
T_a	mean absolute air temperature
V	wind velocity
e_a	partial vapor pressure of the overlying air
P	average atmospheric pressure on the water surface
β	atmospheric-radiation factor derived from the cloud cover

e. Wnek

K_x, K_y, K_z	constant eddy-thermal diffusivities
v_x, v_y, v_z	constant velocity field
h	coefficient of surface heat exchange
$T_0(x, y, z)$	initial ambient fluid temperature distribution
$T_E(x, y, t)$	equilibrium temperature
$S(x, y, z, t)$	source distribution function

where x, y, z refer to longitudinal (shore-parallel), lateral, and vertical directions, and t refers to time.

C. Complete Models

1. Discussion

The complete near-field, far-field models reviewed were those of Pritchard, Sundaram et al., and Tsai. The development of each was split into jet and far-field analyses, each component of which was discussed in Secs. A and B of this summary.

Their method of linking near- and far-field solutions was not discussed, yet is quite interesting. Pritchard simply assumes that the

longitudinal distance at which the centerline temperature excess decays to 20% of its initial value is the dividing line between jet and far field. Thus, at that position, both solutions must match. Sundaram et al., on the other hand, assume that the demarcation between jet and far field occurs when the eddy diffusivity arising from jet-induced turbulence is equal to the eddy-thermal diffusivity due to ambient turbulence. (The authors assumed that heat and momentum spread horizontally at the same rate.) Tsai, in his submerged diffuser analyses, found from hydraulic studies that, at about 300 ft lakeward, the flow field was well established and could be characterized as surface flow. The temperature and velocity profiles measured at that position were used to yield initial conditions for the far-field predictions.

Clearly, there is a transition between the near- and far-field regions in which buoyancy, residual jet turbulence, and ambient turbulence generally need be analyzed. Much work still remains to be done in investigating the properties of the transition flow and temperature fields.

2. Input Parameters for Complete Models

a. Pritchard

b_0	outfall width
h_0	depth of outfall
K	coefficient of surface heat transfer
Q_H	excess heat-rejection rate of power plant based on θ_0
θ_0	initial excess temperature above ambient

b. Sundaram et al.

b_{0a}	width of outfall
d	depth of plume
K	coefficient of surface loss
k_H	eddy-thermal diffusivity (constant of proportionality in the Richardson 4/3-power law)
T_{0a}	initial excess temperature
u_a	ambient current velocity
u_{0a}	initial jet velocity
α, β, γ	empirical constants required for the evaluation of the jet centerline position

c. Tsai

This model cannot be used in its present form for general predictive purposes. It was included in this state-of-the-art summary as a unique method to model a submerged diffuser discharge.

APPENDIX A

Typical Isotherm Sketches as Predicted by Models Reviewed

1. Jet Models

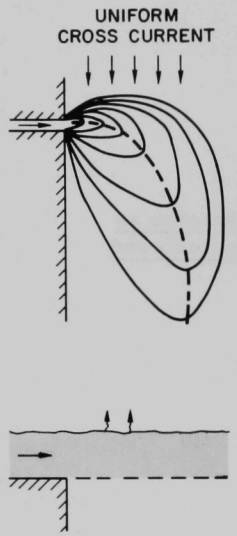

Fig. A.1. Hoopes, Zeller, and Rohlich Model

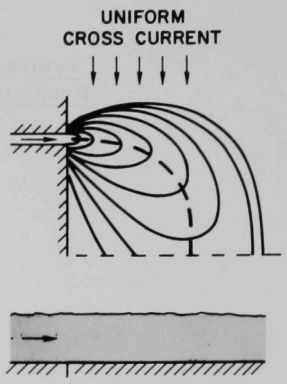

Fig. A.2. Carter Model

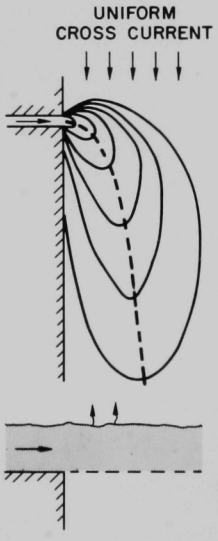

Fig. A.3. Motz and Benedict Model

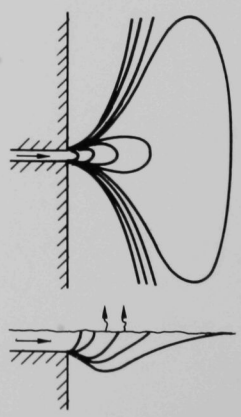

Fig. A.4. Stolzenbach and Harleman Model

2. Far-field Models

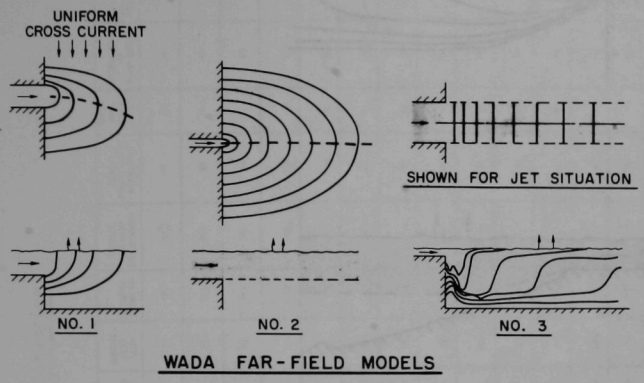

Fig. A.5. Wada Models

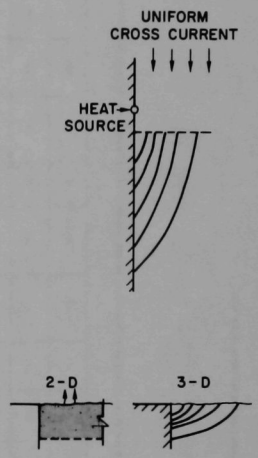

Fig. A.6. Edinger and Polk Models

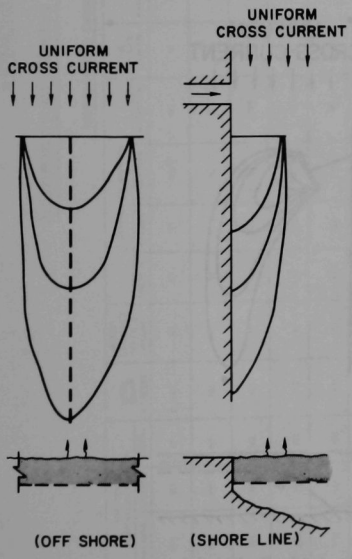

Fig. A.7. Csanady Models

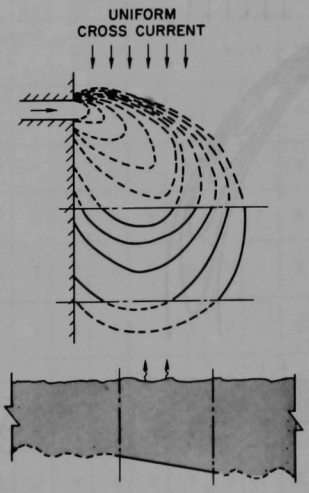

Fig. A.8. Kolesar and Sonnichsen Model

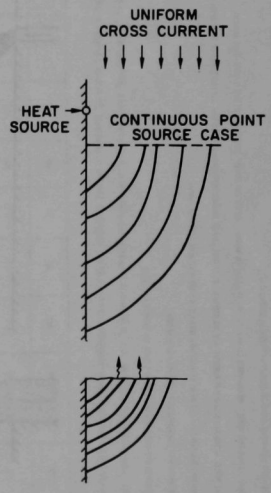

Fig. A.9. Wnek Model

3. Complete Models

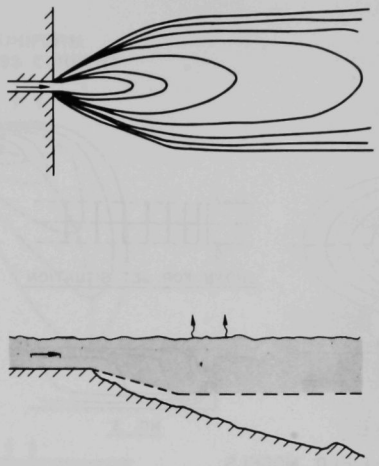

Fig. A.10. Pritchard Model

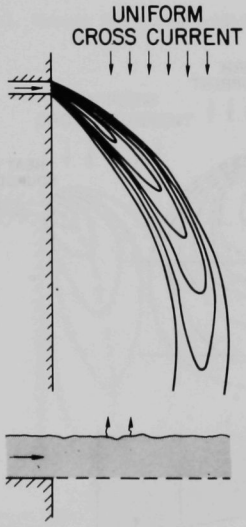

Fig. A.11. Sundaram et al. Model

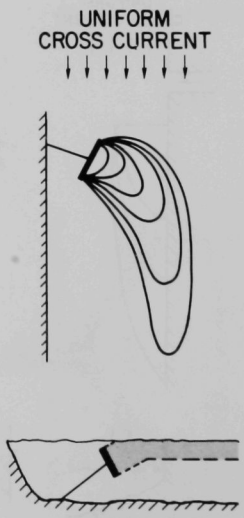

Fig. A.12. Tsai Model

APPENDIX B

Summary of Model Characteristics

SUMMARY OF MODEL CHARACTERISTICS

		DIRECTION OF TEMPERATURE VARIATION			INITIAL MIXING (JET REGIME)	AMBIENT TURBULENCE (FAR FIELD REGION)	MATHEMATICAL APPROACH				TIME DEPENDENT SOLUTION	BUOYANCY	CROSS FLOW	BOTTOM SLOPE	SURFACE HEAT LOSS	DISCHARGE GEOMETRY	PROVIDES FOR FLOW ESTABLISHMENT	AMBIENT STRATIFICATION INTERACTION	DIRECT WIND STRESS EFFECTS	RECIRCULATION OF PLUME WATER	COMPARED OR FITTED WITH		COMPUTER PROGRAM AVAILABLE
		LONGITUDINAL	LATERAL	VERTICAL			NUMERICAL	INTEGRAL	CLOSED FORM	SEMI-EMPIRICAL											FIELD DATA	TANK DATA	
JET MODELS	HOOPES ET AL.	YES	YES	NO	YES	NO	NO	YES	YES(3)	YES	NO	NO	YES	NO(5)	YES	YES	NO(5)	NO	YES	NO	YES	NO	YES
	CARTER	YES	YES	NO	YES	NO	NO	YES	NO	YES	NO	NO	YES	NO	NO	YES	YES	NO	NO	NO	NO	YES	NO
	MOTZ AND BENEDICT	YES	YES	NO	YES	NO	NO	YES	NO	YES	NO	NO	YES	NO	NO	YES	YES	NO	NO	NO	YES	YES	YES
	STOLZENBACH AND HARLEMAN	YES	YES	YES	YES	NO	NO	YES	NO	YES	NO	YES	YES	YES	YES	YES	YES	NO	NO	NO	NO	YES	YES
FAR FIELD MODELS	WADA (MODEL NO. 1)	YES	YES	YES	NO	YES	YES	NO	NO	NO	NO	NO	YES	YES	YES	YES	—	YES	NO	YES	YES	UNKNOWN	WRITTEN BUT NOT AVAILABLE
	WADA (MODEL NO. 2)	YES	YES	NO	NO	YES	YES	NO	NO	NO	NO	NO	NO(7)	YES	YES	YES	—	NO	NO	YES	UNKNOWN	UNKNOWN	
	WADA(8) (MODEL NO. 3)	YES	NO	YES	NO	YES	YES	NO	NO	YES	NO	YES	NO	YES	YES	YES	—	NO	NO	YES	UNKNOWN	UNKNOWN	
	EDINGER AND POLK (2D MODEL)	YES	YES	NO	NO	YES	NO	NO	YES	NO	NO	NO	YES	NO	YES	NO	—	NO	NO	NO	YES	NO	NO
	EDINGER AND POLK (3D MODEL)	YES	YES	YES	NO	YES	NO	NO	YES	NO	NO	NO(2)	YES	NO	NO	NO	—	NO	NO	NO	YES	NO	NO
	CSANADY (OFFSHORE MODEL)	YES	YES	NO	NO	YES	NO	NO	NO	NO	NO	NO	YES	NO	YES	NO	—	NO	NO	NO	NO	NO	NO
	CSANADY (SHORELINE MODEL)	YES	YES	NO	NO	YES	NO	NO	YES	YES	NO	NO	YES	NO	YES	YES	—	NO	NO	NO	NO	NO	NO
	KOLESAR AND SCHMICHSER	YES	YES	NO	NO	YES	YES	NO	YES	NO	YES	NO	YES	YES	YES	NO	—	NO	NO	NO	YES	NO	YES
	WHEK	YES	YES	YES	NO	YES	NO	NO	NO	NO	YES	NO(2)	YES	NO	YES	YES	—	YES	NO	YES	NO	NO	BEING PREPARED
COMPLETE MODELS	PRITCHARD	YES	YES	YES	YES	YES	NO	YES	YES	YES	NO	NO	NO	NO	YES	YES	YES	NO	NO	YES	YES	YES	NO
	SUNDARAM ET AL.	YES	YES	NO	YES	YES	NO	NO	YES	YES	NO	NO	YES	NO	YES(4)	YES	NO	NO	NO	NO	YES	NO	NO
	TSAI(1)	YES	YES	NO(6)	YES	YES	NO	NO	YES	YES	NO	NO	YES	NO	NO	YES	YES	NO	NO	NO	NO	NO	NO

FOOTNOTES:

(1) THE TSAI MODEL HAS BEEN DEVELOPED FOR A UNIQUE SUBMERGED DIFFUSER SITUATION. BECAUSE OF THIS THE GENERAL APPLICABILITY OF THE MODEL IS LIMITED. THE TABLE DESCRIPTION UNDER TSAI APPLIES ONLY TO THE ANALYTICAL PORTION OF HIS MODEL SYNTHESIS. HYDRAULIC MODELING WAS USED IN THE INITIAL REGIME OF FLOW.

(2) A CONSTANT VERTICAL EDDY THERMAL DIFFUSIVITY WAS USED IN THE MODEL. BUOYANCY IS DEFINED HERE AS BEING CONSIDERED IF THE COUPLING OF FLOW AND ENERGY HAS BEEN TREATED.

(3) A CLOSED FORM SOLUTION HAS BEEN DERIVED FOR THE CASE OF ZERO WIND STRESS.

(4) SURFACE HEAT LOSS WAS ONLY CONSIDERED IN THE FAR FIELD REGIME.

(5) FLOW DEVELOPMENT AND BOTTOM EFFECTS WERE CONSIDERED INDIRECTLY VIA WIND SPEED CORRELATIONS.

(6) THE CROSS CURRENT MODEL IS STRICTLY TWO-DIMENSIONAL. THE NO CURRENT CASE USES THREE DIMENSIONAL TANK STUDIES FOR HEATED SURFACE JETS. HOWEVER, ONLY THE SURFACE TEMPERATURE PREDICTIONS WERE UTILIZED IN THE TSAI MODEL.

(7) THERE IS A POSSIBILITY THAT THIS MODEL MAYBE ABLE TO HANDLE THE EFFECTS OF AMBIENT CROSS CURRENTS. THIS IS NOT CLEAR FROM WADA'S PAPERS.

(8) MODEL CAN ALSO BE USED FOR NEAR FIELD OR COMPLETE FIELD APPLICATIONS.

ACKNOWLEDGMENTS

We are grateful for critical comments and suggestions on portions of the initial draft of this report by Prof. B. A. Benedict, Prof. H. H. Carter, Prof. G. T. Csanady, Prof. J. E. Edinger, Prof. J. A. Hoopes, Dr. D. C. Kolesar, Prof. E. M. Polk, Prof. D. W. Pritchard, Prof. L. S. Slotta (for Wada), Dr. J. C. Sonnichsen, Jr., Dr. K. D. Stolzenbach, Dr. T. R. Sundaram, Dr. Y. J. Tsai, and Dr. R. W. Zeller. The bulk of their assistance was generously given through telephone conversations and private correspondence. This acknowledgment does not necessarily imply endorsement by each of the foregoing reviewers/authors of this work.

We would particularly like to acknowledge Dr. K. D. Stolzenbach and Dr. T. R. Sundaram for discussions and insights on plume modeling beyond their own work.

We would also like to thank Mr. B. M. Hoglund for his many helpful suggestions and criticisms throughout the preparation of this draft and to Dr. D. Miller for preliminary efforts relating to this report.

Finally, we would like to thank Miss Linda C. Wood and especially Miss Alice M. Jones for typing the initial draft of this report and would like to express our appreciation to the library staff under Mr. N. P. Zaichick for obtaining the reference material partially utilized in this work.

INTERNATIONAL LAB WEST
3 4444 00032090 3

X

B